High pressure thermophysical behaviour of reference and new lubricants

Mineral, synthetic and vegetable oils and ionic liquids

Memoria presentada por

Teresa Regueira Muñiz

para optar ao grado de Doutora pola

Universidade de Santiago de Compostela

Santiago de Compostela, Xullo 2013

Universidade de Santiago de Compostela
Departamento de Enxeñería Química

Universidade de Santiago de Compostela
Departamento de Física Aplicada
Laboratorio de Propiedades Termofísicas

Dª. JOSEFA FERNÁNDEZ PÉREZ, Catedrática de Física Aplicada da Universidade de Santiago de Compostela e **D. LUIS LUGO LATAS**, Investigador Ramón y Cajal da Universidade de Vigo, directores da presente Tese Doutoral

D. JUAN JOSÉ CASARES LONG, Catedrático de Enxeñaría Química da Universidade de Santiago de Compostela, titor da presente Tese Doutoral

INFORMAN:

Que a presente memoria, titulada '**High pressure thermophysical behaviour of reference and new lubricants. Mineral, synthetic and vegetable oils and ionic liquids**' foi realizada pola Enxeñeira Química Dª Teresa Regueira Muñiz baixo a nosa dirección e constitúe a súa Tese para optar ao grado de Doutora en Enxeñería Química.

Que o traballo que se presenta foi realizado no marco dos seguintes proxectos de investigación: "*Biolubricantes basados en Aceites Vegetales y sus Derivados Sintéticos*" (MICINN, PSE-320100-2006-1 e PSE-420000-2008-4), "*Influencia de la estructura molecular en las propiedades termofísicas y tribológicas de líquidos iónicos en amplios rangos de presión para su uso en lubricación*" (MICINN, CTQ2008-06498-C02-01/PPQ) e "*Nuevos lubricantes nanoestructurados basados en líquidos iónicos para energías renovables*" (MICINN, CTQ2011-23925).

E para que así conste, firman o presente informe en Santiago de Compostela, 30 de Xullo de 2013.

Os directores O titor

Prof. Josefa Fernández Pérez Dr. Luis Lugo Latas Prof. Juan José Casares Long

A doutoranda

Teresa Regueira Muñiz

Nothing in life is to be feared, it is only to be understood.

Now is the time to understand more, so that we may fear less.

Marie Curie

Aos meus pais

Agradecementos

Chega o tempo de clausurar unha etapa, enriquecedora, ardua, estimulante e suxestiva a partes iguais. Son moitos os compañeiros de camiño, e para eles o máis profundo agradecemento:

En primeiro lugar quixera agradecer aos meus directores de Tese, a Prof. Josefa Fernández e o Dr. Luis Lugo por darme a oportunidade de comezar este proxecto no seu equipo, polo saber facer, o apoio e a confianza.

Ao Ministerio de Educación, Cultura e Deporte polo financiamento deste traballo a través do programa FPU.

Ao Prof. João Coutinho, o Dr. Pedro Carvalho e a Dra. Mariana Belo, pola especial acollida na Universidade de Aveiro e por todo o aprendido da vosa man.

A Olivia, por todo o que me ensinaches, pola túa amizade xenerosa, por tódolos instantes.

A tódolos compañeiros do LPT, porque facemos un equipo insuperable en tódalas facetas, non tería atopado outro mellor. Queta, María, Pepi, Xavi, Jujo, Tamara, e por último e imprescindibles, Inés, Fernando e Félix.

Porque os sorrisos sempre son benvidos, a tódolos que pintan os meus momentos de color: Josué, Sei, Ríos, Ague, Sandra, Irais, Vero, Mallegue, Topete, Susana. A Mery e Bea, porque nos sobran as palabras.

E como todo comeza en Gonderande, aos avós porque son un libro de vida, aos irmáns porque formamos un triángulo perfecto. Aos meus pais porque sen eles a meta nunca tería chegado, nin sequera a carreira daría comezo. Sen raíces non se pode voar e as nosas nacen ben profundo.

Grazas

Abstract

This PhD Thesis is devoted to the study of several thermophysical properties, over broad ranges of temperature and pressure, of mineral and semisynthetic reference lubricants, vegetable oils and developed biodegradable lubricants, as well as ionic liquids (ILs) for their use as hydraulic fluids, gear and two stroke lubricants. The reference lubricants, base oils and developed lubricants were supplied by the partners of the BIOVESIN project, a singular and strategic project supported by the Spanish Science and Technology Ministry focused on the development of vegetable based lubricants for their use in different applications, whereas the ILs where kindly supplied by Merck KGaA (Germany) in the framework of two other projects supported by the same Ministry.

The first property studied was the density from 278.15 K to 398.15 K up to 120 MPa. Density was measured by means of two different vibrating tube densimeters from Anton Paar (Graz, Austria). The first is the DMA 512P, which was calibrated in the temperature range from 278.15 K to 353.15 K up to 60 MPa, following the method proposed by Lagourette et al. Density of a high oleic sunflower oil and of six developed biodegradable oils for hydraulic applications was determined with this experimental device. The other densimeter is the DMA HPM, which was used in two different configurations, a manual configuration, and an automated configuration. In the manual configuration the measurements were performed from 298.15 K to 373.15 K up to 60 MPa for three mineral and one semisynthetic reference lubricants, a high oleic sunflower oil and a biodegradable commercial oil. For the automated configuration, the calibration was performed following the method of Lagourette et al. modified by Comuñas et al. in the temperature range from 278.15 K to 398.15 K up to 120 MPa. Three mineral reference lubricants, five biodegradable developed oils and seven ILs were characterized with this last configuration. Density data of all the studied fluids were correlated by means of the Tammann-Tait equation and the density derived properties, i.e. isothermal compressibility, κ_T, and the coefficient of thermal expansivity, α_T, were obtained. Furthermore, density of high oleic sunflower oil and rapeseed oil at atmospheric pressure were used to evaluate the predictive capability of the methods described by Anand et al. and Zong et al. The density values of ILs as a function of temperature and pressure were used to test the prediction methods of Gardas and Coutinho and Jacquemin et al.

The second property studied in this PhD Thesis was the phase equilibria at high pressures. Two different techniques were also employed. The first of them was an isochoric technique in which the solubility of CO_2 and O_2, in a reference and in a biodegradable lubricant for two stroke engines, was measured in the temperature range from 283.15 K to 348.15 K up to

10 MPa. The second is a synthetic technique with a full visibility cell. This last technique was implemented in the Thermophysical Properties Laboratory during this PhD Thesis, and it operates in the temperature range from 298.15 K to 363.15 K and up to 100 MPa. Solubility of CO_2 in a high oleic sunflower oil and in a biodegradable developed oil for being used in two stroke engines was determined with this technique. Moreover, during a three month stay in the research group Process and Product Applied Thermodynamics at the University of Aveiro, the solubility of CO_2 in three vegetable oils, (castor, rapeseed and high oleic sunflower oil) was determined from 298.15 K to 363.15 K and up to 100 MPa. To test the validity of the technique implemented at Thermophysical Properties Laboratory, the solubility of CO_2 in high oleic sunflower oil was compared with that obtained with the group Process and Product Applied Thermodynamics which showed a good agreement. Solubility results of all the studied systems were modeled by means of the PC-SAFT EoS (Perturbed-Chain Statistical Associating Fluid Theory EoS), the SRK EoS (Soave-Redlich-Kwong) or a modified Gordillo et al. correlation. Additionally, the reliability of the Carvalho and Coutinho method for predicting solubility of CO_2 in low volatile solvents was analyzed.

The last property investigated in this PhD Thesis was the rheological behavior and viscosity. Viscosity data at atmospheric pressure for the studied reference, base and developed lubricants was measured by means of an Anton Paar Stabinger SVM 3000 in the temperature range from 278.15 K to 373.15 K. Viscosity index (VI) was also obtained through this last device according to the standard ASTM D2270-04. Concerning the rheological behavior at high pressure, it must be mention that a high pressure concentric cylinder rheometer Reologica StressTech HTHP, which relies on Couette flow, was implemented in the Thermophysical Properties Laboratory during this PhD Thesis to work in the temperature range from 298.15 K to 353.15K up to 75 MPa and shear rates of $1000s^{-1}$. The verification of the equipment was accomplished by studying the rheological behavior of a polyalphaolefin (PAO40) and a polybutene (H8) and comparing the results with those obtained by Bair. Moreover, rheological characterization of two ILs was performed and the viscosity results correlated as a function of temperature and pressure through use of the Comuñas et al. equation. Viscosity derived properties, i.e. the viscosity-temperature coefficient, β, and the local viscosity-pressure coefficient, α, were obtained. Additionally, the universal viscosity-pressure coefficient, α_{film}, was also calculated.

Index

Chapter 1

Introduction

1.1. Historical perspective

The existence of friction led to the development of lubricants along history. A lubricant can be defined as a solid or fluid film inserted between two bodies in relative motion in order to reduce friction or wear. Liquid lubricants present also secondary functions such as cooling of the contacting parts, removing wear particles and providing corrosion resistance, detergency or surface-active layers. The advantages of using a lubricant between moving surfaces have been known for millennia. Thus, Dowson [1] shown an hieroglyph from the old Egypt where a man was pouring liquid in front of a large stone block dragged by hundreds of people in order to reduce friction. Later on, in the Middle Ages, animal fat and vegetable oils were commonly used for lubrication of machines and axes of wagons and chariots [1-7].

Development of lubricants experienced a significant advance with the beginning of the modern petroleum industry in 1859. In this way, from 1850 to 1875 it was attempted to discover different uses to the products available from crude distillation, and it was found that they could substitute pretty well the previously vegetable and animal lubrication oils and become a standard for the emerging industries. The mineral oils had the advantage of not suffering the rapid degradation of fatty oils. Two decades after it began the search for synthetic alternatives to mineral oils, that was successful in synthesising polyalphaolefins (PAOs) and polyalkylene glycols (PAGs), among others. Finally, between 1910 and 1940 chemical additives started to be employed for upgrading and extending the life of petroleum based lubricants, with the objective of meeting new requirements, and the first successful additive was zinc dithiophosphate (ZDDP). More additives were developed to act as antioxidants, corrosion inhibitors, extreme pressure agents, detergents, pour point depressants, viscosity modifiers and antiwear additives [8-10].

From an economical point of view, tribological fails represent a very important cost to every national economy due to energy and material losses, as well as a cause of accidents. Around one-third of the energy resources consumption is somehow due to friction. Therefore, friction reduction and wear control are key factors from the economic perspective. For this reason, the lubricant industry is in continuous evolution in order to develop more suitable lubricants for the different applications [5,11-13].

The global lubricant demand in 2011 was, according to Gosalia [14] of 35.1 million tonnes, whereas the consume of bio-based lubricants was 505.6 kilo tonnes [15]. It is expected for the mineral and synthetic lubricant market to grow at a compound annual growth rate of 2.48 % in the period from 2013 to 2018, whereas for the bio-based lubricant the market it is estimated to grow at a 6.6% in the same period of time. North America is the leader of the bio-based lubricants market followed by Europe, Germany being the main market of this last [15]. Therefore, nowadays, petroleum derived lubricants still comprise a great percentage of total oil

and grease production volume, but in the last three decades, public concern about environmental matters has significantly grown and some biodegradability standards must be met by products. Some factors have determined a turning point in the lubricants field, such as oil spills like the Exxon Valdez in Alaska, the Prestige in Galicia or the BP oil explosion in the Gulf Mexico and also the increasing demand of oil by developing countries. Furthermore, it is estimated that approximately 50 % of the lubricants end up in the environment through evaporation, spills or total loss applications [16-18]. Government incentives and obligatory regulations became necessary to put pressure on the industrial field. Thus, the REACH regulation (EC 1907/2006) on chemicals and their safe use, which promotes the research on the replacement of materials that are persistent, bioaccumulative or toxic by less harmful alternatives, is mandatory since 2007. Additionally, the EU Ecolabel (EEC 880/92, EC 1980/2000, EC 66/2010) is a voluntary award scheme that promotes products with a reduced environmental impact during their entire life cycle, with the aim of reducing the negative effect of consumption and production on the environment, health, climate and natural resources. The latest criteria for the award of the EU Ecolabel to lubricants were established in 2011 (2011/381/EU) and they cover hydraulic fluids and tractor transmission oils, greases and stern tube greases, chainsaw oils, concrete release agents, wire rope lubricants, stern tube oils and other total loss lubricants, two-stroke oils and industrial and marine gear oils. These criteria are based on the low toxicity and biodegradability of the lubricant components, as well as on the prohibitions of some ingredients [4,19,20].

In this context, vegetable oils as biodegradable fluids have arisen as a promising alternative to mineral and synthetic oils in the last two decades, being clear that lubricants of the future must be environmentally adapted with a high level of performance and reduced total life cycle cost compared with those commonly used today. Biodegradability has become one of the most important design parameters in the selection of the base fluid as well as in the formulation of a finished lubricant. The formulation of these new lubricants, less detrimental to the environment when spilled or leaked, involves a deep knowledge of the properties of the base fluids. Besides, from a technical point of view, it is believed that more than 90% of the lubricants could be made rapidly biodegradable [4,10,13,18,21,22].

Additionally, it is expected that great advancements in equipment technology will be performed in the next future. This new equipments will achieve higher production levels and probably more severe operating conditions, which will require stricter demands on lubricants. Therefore, research and development associated to lubricant technology will be a challenge on the next future [10].

1.2. Lubrication regimes

The first distinction that should be made in order to explain the different lubrication regimes is the presence or absence of an external pressure source. Thus, the hydrostatic lubrication occurs when a thick lubricant film is kept between two surfaces with little or no relative motion by means of an external pump. On the other hand, the different lubrication regimes for a hypothetical fluid-lubricated bearing system without external pumping source are well defined by means of the Stribeck curve [23] (see Fig.1.1.). This curve represents the friction coefficient (μ) as a function of a dimensionless number, usually named the Hersey number, given by the following equation [5,7]:

$$Hs = \frac{\eta\omega}{p} \tag{1.1}$$

where η is the shear viscosity in Pa·s, ω is the rotational speed in revolution per second and p is the load by unit of projected bearing area, in Pa.

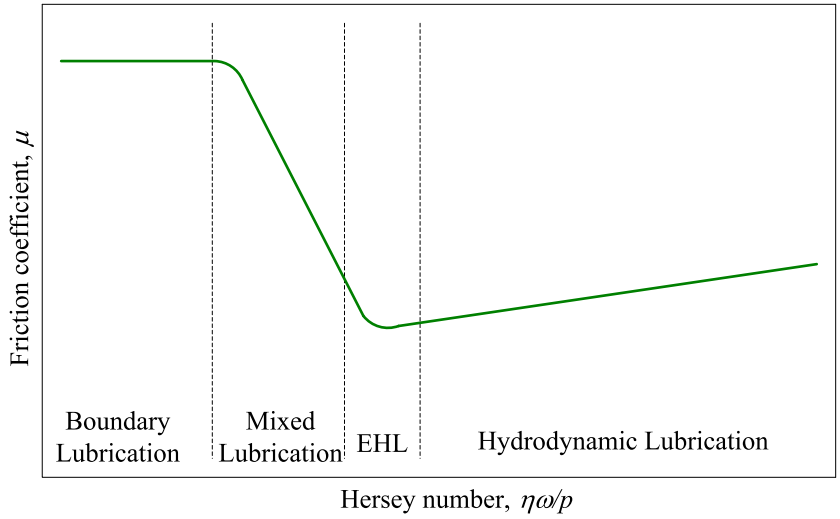

Fig.1.1. Stribeck curve [23]. Lubrication regimes as a function of the Hersey number. (EHL being Elastohydrodynamic lubrication)

In Fig.1.1 four different lubrication regimes are presented according to the Stribeck curve [23]. These lubrication regimes are the following:

- Boundary lubrication: Knowledge of boundary lubrication is attributed to Hardy and Doubleday [24,25]. This lubrication regime occurs when the load increases or the speed decreases as well as when the fluid viscosity decreases, giving rise to a sharply increase of the friction coefficient which reaches very high values. Under these conditions the contact is dominated by the interaction between the thin lubricant film (1–10 nm) and the solid asperities, therefore the physical and chemical properties of the film as well as those of the surface determine the behaviour of the contact, whereas influence of lubricant viscosity is almost negligible [5,7].

- Hydrodynamic lubrication (HDL): Knowledge of hydrodynamic lubrication started with the works of Tower [26] and Petrow [27] and was followed by the work of Reynolds [28]. This type of lubrication occurs in thrust and journal bearings and is due to the flow of a lubricant through a convergent wedge that generates pressure enough to support the load without any external pumping agency. Thickness of the lubricant film is 5-500 μm. Two conditions are required for the existence of this lubrication regime, there must be a relative fast movement among the surfaces that allows the film to be generated and the surfaces must have a convergent shape. In this regime, the behaviour of the contact is controlled by lubricant properties, especially dynamic viscosity [5-7,11].
- Elastohydrodynamic lubrication (EHL): This lubrication regime occurs at high pressures between nonconformal surfaces that are elastically deformed whereas the lubricant viscosity can increase significantly. The lower pressure limit for this lubrication regime to occur is about 500 MPa and a pressure spike is observed near the exit in the pressure distribution of a line EHL contact as depicted in Fig.1.2. Load is mainly supported by the lubricant film that has a thickness between 0.5–5 μm and thermal and shear rate effects are quite important. This lubrication regime is present in ball bearings, rolling bearings, gear teeth and flexible seals, among others. [5,7,29,30].

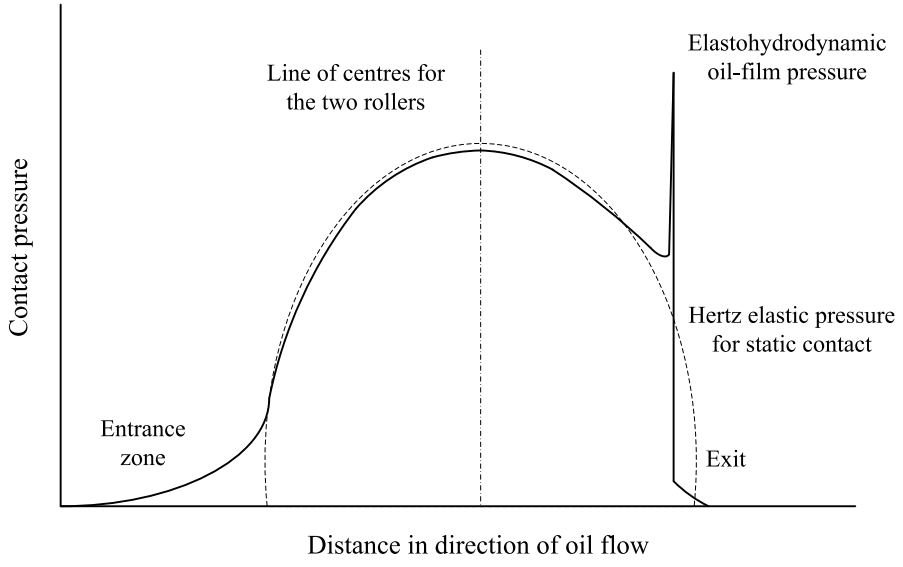

Fig.1.2. Pressure distribution for rolling contact under EHL [6,9,31,32].

- Mixed lubrication: This type of lubrication regime corresponds to the transition between the hydrodynamic or elastohydrodynamic and the boundary lubrication regime, and both lubrication mechanisms are present. As the load increases, a larger part of it is supported by the contact between the asperities of the solids, however a portion of the surface remains supported by a hydrodynamic film [5,7].

1.3. Lubricant formulation and environmental issues

With the aim of meeting performance specifications, lubricants are formulated by blending a base oil with a suitable additive package, the base oil accounting from 70% to 99% of the finished lubricant. Thus, metalworking fluids and automotive engine oils have up to 30% additives, whereas some hydraulic oils contain only 1% additives [9-11,33,34].

The base oil, that is in general chemically inert, removes heat and wear particles and minimizes friction, besides, it contributes significantly to several properties of the finished lubricant, such as thermal stability, viscosity, volatility, solvent capacity, low temperature properties, demulsibility, air release and oxidation stability. Therefore the proper selection of the base oil is a key parameter for the proper performance of the finished lubricant [10,11].

Concerning additives, they are chemical compounds whose purpose in the lubricant formulation is enhancing some properties of the base oil as well as adding some new properties in order to satisfy the requirements of each application and also to extend the durability of the oil. Some of the specific functions of lubricant additives are oxidation, rust and corrosion inhibition, anti-wear, anti-acid, extreme pressure agent, friction modifier, detergent, dispersant, pour-point depressor, antifoaming and viscosity index (VI) improver. Occasionally other additives like dyes and odour improvers are also added [3,6,9-11,34].

Lubricant base stocks have been classified by the American Petroleum Institute (API) into five groups. Groups I, II and III correspond to mineral oils with different amounts of saturates and sulphur content as well as VIs, whereas group IV corresponds to polyalphaolefins and group V includes all other types of base stocks [10,34,35]. Lubricant base oils can also be classified in mineral, synthetic and biological oils.

Mineral lubricants

As it was stated, most of the lubricant base stocks used worldwide are mineral due to their good performance and economic price. These base oils are obtained from petroleum crude oil through refining and extraction processes, as crude oils are complex mixtures of hydrocarbons that contain also other compounds as sulphur, nitrogen, oxygen, nickel, vanadium as well as water. Different types of the crude oil components are shown in Fig.1.3. Thus, crude oils can be classified in paraffinic, naphthenic or aromatic depending on the type of predominant structures. Paraffinic oils contain straight chain hydrocarbons, naphthenic oils contain cyclic carbon molecules with saturated bonds and aromatic ones contain benzene type compounds. The paraffinic chains usually range from 25 to 40 carbons, are stable and have a good viscosity-temperature relationship. Naphthenic lubricants present higher densities and viscosities, for the same molecular weight, compared to paraffinic ones and also better fluidity at low temperatures.

Aromatic oils are not usually employed for obtaining base oils because of their poor viscosity-temperature relationship and thermal and oxidative stability [6,9-11,21,34].

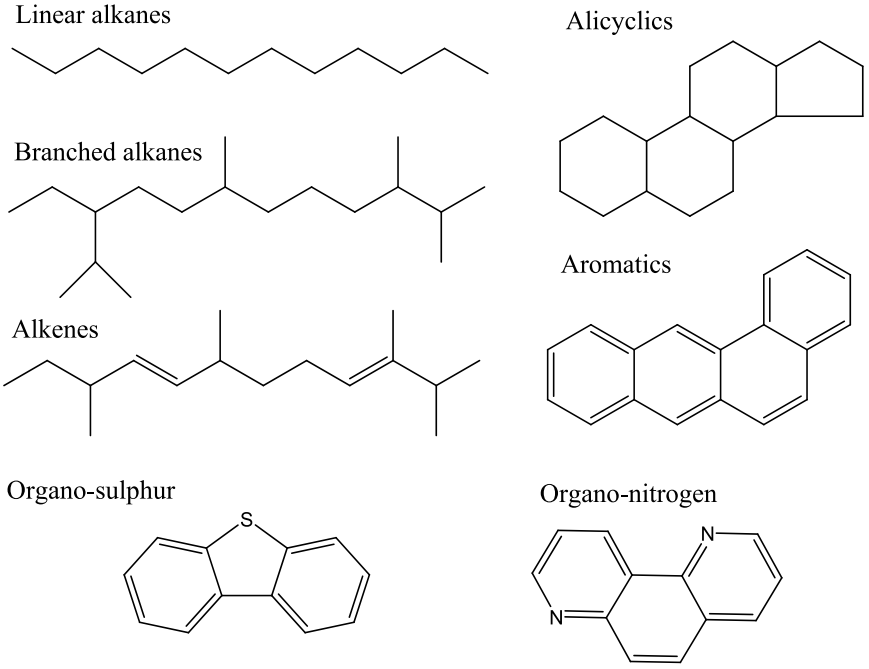

Fig.1.3. Several typical components of a crude oil [34].

Synthetic lubricants

As regard synthetic oils, they are chemically synthesised through the combination of low molecular weight compounds, the starting raw materials being often obtained from petroleum. The advantage of this kind of lubricant base stock is that it can be tailored in order to meet strict requirements, such as water miscibility, fire and extreme temperature resistance, or non-flammability, being successful in fields where mineral oils fail. However, their main disadvantage is the price, which is considerably higher than that of mineral oils and also environmental issues. Synthetic oils can be classified in synthetic hydrocarbon fluids, organic esters, polyglycols, phosphate esters and other synthetic fluids. Polyalphaolefins (PAOs), alkylated aromatics, polybutenes or cycloaliphatics are among the hydrocarbon fluids, whereas among the organic esters, diesters and the polyol esters are found. Polyalkylene glycols (PAGs) belong to the polyglycols group, whereas silicones, silanes and polyphenyl ethers are among the other synthetic fluids [6,7,9,10,36]. In Fig.1.4 structures of several synthetic lubricants are depicted.

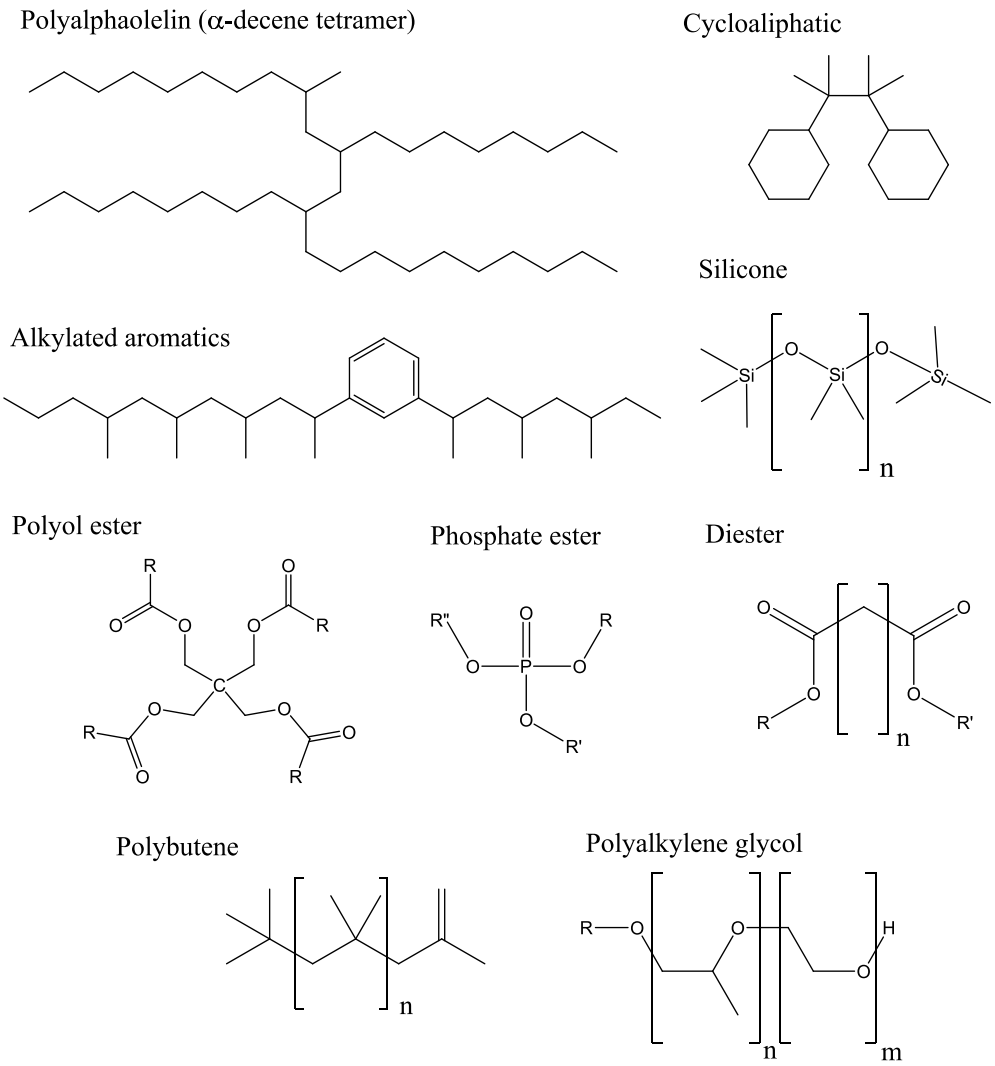

Fig.1.4. Structures of different types of synthetic lubricants [10,11].

Vegetable oils

Biological oils can be obtained from animal and vegetable sources, which are a non-toxic, biodegradable and renewable lubricant base stock. Vegetable oils are triglycerides, i.e. esters derived from glycerol and fatty acids, whose composition is normally characterised in form of fatty acid content. The fatty acids are usually composed by strain hydrocarbon chains with up to 22 carbon atoms, that may be either saturated or mono- or polyunsaturated. In Fig. 1.5 the structure of glycerol, several fatty acids as well as a triglyceride is depicted. The presence of double bonds gives rise to lower melting points and poorer oxidative stability compared to the equivalent saturated fatty acids, thus a compromise between low-temperature properties and oxidative stability must be achieved. Moreover, due to the ester structure of vegetable oils, they can suffer hydrolysis that is detrimental to lubricant properties when a high degree is reached. These properties can be improved through addition of suitable additive packages or through genetic modification, for instance by increasing the high oleic acid content. On the other hand, vegetable oils have several advantages when compared to mineral oils, such as higher viscosity

index, higher flash points, excellent lubricity and low volatility. They also represent a cost advantage in comparison with synthetic biodegradable base stocks. Initially, the main area of application of vegetable oils was hydraulic fluids, but growing areas include cutting and drive chain oils, two stroke engine oils, chain saw bar oils, wire rope oils, outboard engine lubricants, agricultural equipment lubricants, tractor oils, metal cutting oils and several others [10,21,37-40].

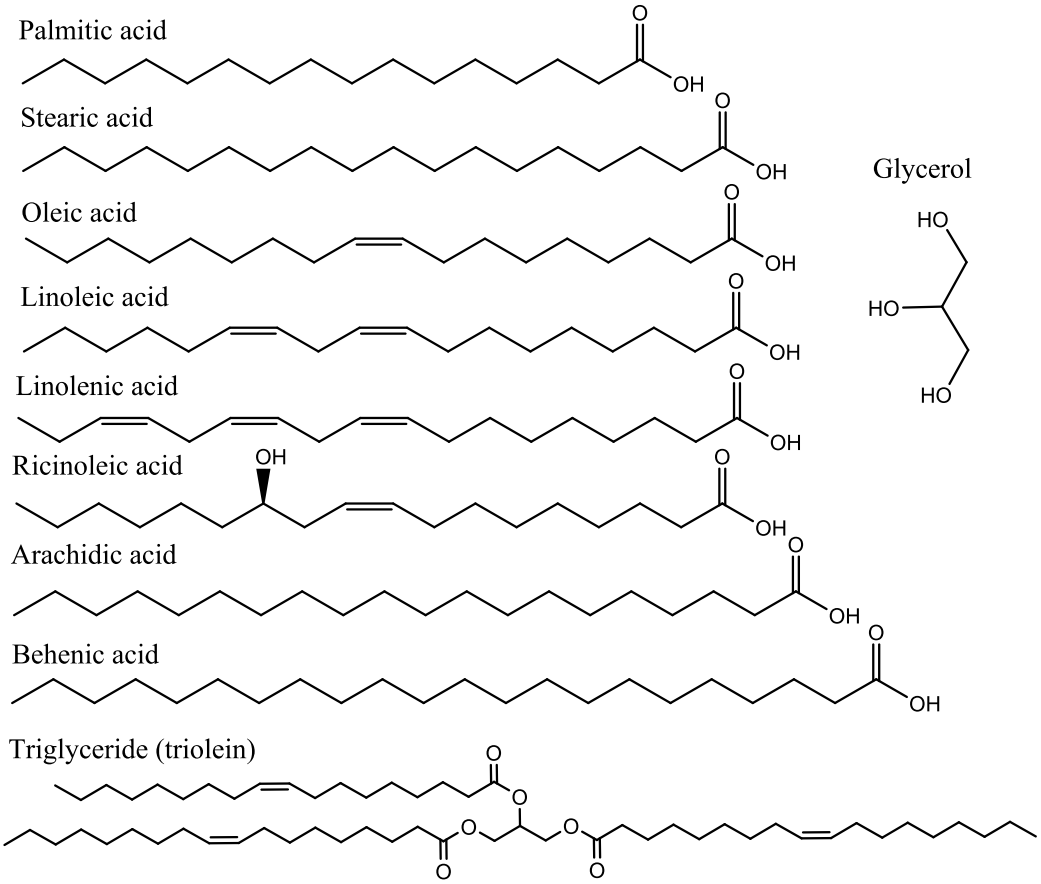

Fig.1.5. Chemical structure of several fatty acids, glycerol and triolein.

These environmentally friendly lubricants have attracted specific scientific attention during the last two decades. Thus, several works have been published concerning the different types of vegetable base stocks and their derivatives as well as their chemical modification and suitable additives for this particular base oil [41-83]. Besides, some other studies have focused on their oxidation, thermal stability and pour point characteristics [84-97] and also on their tribological performance [67,68,70,75,77,86,92,94,96,98-119]. Furthermore, regarding the environmental issues of vegetable oils and their derivatives, some investigations can also be found in literature [51,85,90,120-126].

Ionic liquids (ILs)

Finally, it is important to mention that during the last decade ionic liquids (ILs) were attracting attention for their use as lubricant base fluids or lubricant additives, to be employed in

applications where conventional lubricants fail, such as extreme temperature and pressure or high vacuum applications. ILs are salts with melting points lower than ambient temperature. They are normally composed by ion pairs containing bulky, asymmetric cations and anions, at least one of them being organic. These ions have conformational flexibility, delocalization of electrostatic charge, and interact in complex ways with polar and nonpolar species. ILs exhibit superior tribological behavior because of their polar structure. They can be easily adsorbed on the sliding surface of frictional pairs, forming an effective boundary film which reduces friction and wear. ILs present a set of properties that made them very attractive in lubrication, such as negligible volatility, non-flammability, high thermal stability, low melting point, low temperature fluidity, high thermal and electrical conductivity and high polarity. Besides, their easy tuneability allows creating tailor-made lubricants with the proper combination of cation and anion in order to meet the requirements of each application. On the other hand, the drawbacks of ILs are the toxicity of some of them and their degradation products as well as the tribocorrosion caused by the interaction of high polar ILs with the surface and also the corrosion of the surface caused by some hydrophobic anions when used under humid conditions, therefore additives are required for this issue. The most common cations are based on imidazolium, pyridinium, pyrrolidinium, ammonium and phosphonium, whereas among the anions a great diversity is found. A selection of usual cations and anions is presented in Fig.1.6 [127-134].

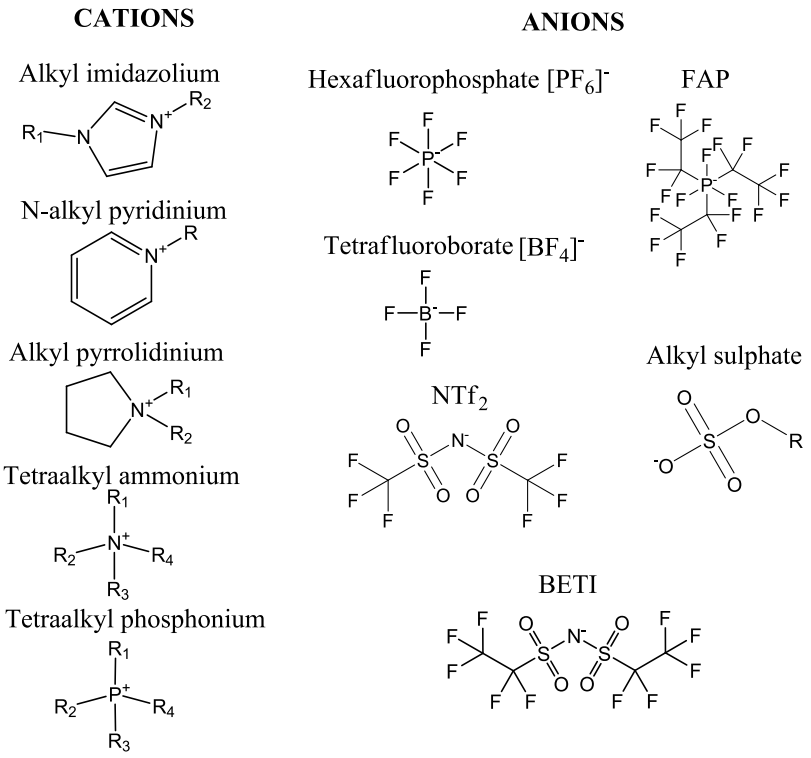

Fig.1.6. Selection of usual ILs cations and anions.

The first article concerning the lubricating ability of ILs dates from 2001 and was published by Ye et al. [135] showing that alkylimidazolium tetrafluoroborates have excellent

friction reduction, antiwear performance and high load carrying capacity. After that, several articles [127,136-181] concerning the tribological performance of ILs as base lubricants and as oil additives of different types of lubricated contacts, as well as the antiwear antioxidant, anticorrosion and friction reduction properties, were published by their research group (Lanzhou Institute of Chemical Physics, China). The studied compounds include alkyl imidazolium, alkyl phosphonium, alkyl phosphates, $[NTf_2]^-$ or $[PF_6]^-$ based ILs, vinyl functionalised ILs, dicationic ILs and crown-type ILs, among others.

Besides, many other research works have been published on the topic of ILs as lubricants [130,132,133,182-244]. Some of them by Bermúdez, from the Polytechnic University of Cartagena, and co-workers [130,132,221-236] deal with friction, wear, corrosion and surface interactions of ILs as neat lubricants and lubricant additives in different contacts. González and co-workers [245-250] have several works on the use of ammonium, imidazolium and pyrrolidinium ILs as lubricants or lubricant additives. Additionally, works from Qu et al. [237-241] on ammonium, imidazolium and phosphonium ILs as well as from Phillips and co-workers [133,242-244] on polyquaternary and dicationic ILs, among others, should be mentioned.

The environmental acceptability of lubricant base stocks comprises numerous aspects such as the use of renewable resources, resource conservation, pollutant source reduction, recycling, reclamation, disposability or degradability, but in a general assessment only three issues are considered, i.e. toxicity, bioaccumulation and biodegradability. Toxicity is specially damaging for aquatic life and is usually evaluated in terms of lethal effect on selected organisms at a given dosage and period of time. The bioaccumulation refers to the accumulation of harmful substances in an organism and is assessed by means of a bioconcentration factor, and finally, the biodegradability refers to the speed at which substances biodegrade and is given by the capacity of a microorganism to decompose a product. When environmental concern is a key factor, readily biodegradable products are required [6,10].

Only some of the previously described lubricant base stocks are considered biodegradable, i.e. PAOs, PAGs, synthetic esters and vegetable oils. Among the PAOs, only those with low viscosity (PAO2 and PAO4) are easily biodegradable, but their low viscosity limits their applicability as lubricant base oils. Concerning the PAGs, only the polyethylene glycols with molar mass lower than 2000 are biodegradable [251]. Among the vegetable oils, the high oleic sunflower oil (HOSO) is highly biodegradable and non toxic, moreover it has a high thermal stability and good low temperature behaviour due to their fatty acid composition, being a promising lubricant base stock. Concerning ILs, their toxicity is currently under study [198,252].

1.4. Framework of this PhD Thesis

This PhD Thesis was carried out within the framework of three funded research projects on the topic of lubrication in which the Thermophysical Properties Laboratory (University of Santiago de Compostela) was involved. These three projects are briefly described in this section.

The first of them is the singular and strategic project 'BIOVESIN' (Biolubricants based on vegetable oils and their synthetic derivatives, PSE- 320100-2006-1 and PSE-420000-2008-4, Ministerio de Ciencia e Innovación). This project was motivated due to the pollution problem caused worldwide by used lubricants. Thus, waste oil can pollute soil severely through waste oils left on the ground, moreover a litre of waste oil can contaminate up to one million litres of water [253]. In this project several companies as well as universities and research centres were involved: Gamesa Eólica, Verkol Lubricantes, Limagrain Ibérica, Abamotor Energía, Agria Hispania, Indra, Instituto de la Grasa, Tekniker, Instituto de Agricultura Sostenible, Instituto de bioquímica vegetal y fotosíntesis, Universidad de Santiago de Compostela, Universidad de Huelva and Universidad de Almería.

The global aim of the BIOVESIN project was the generation of new environmentally friendly lubricants, suitable for different applications, from vegetable oils available in Spain and biodegradable additives selected because of their optimal characteristics for each application and having a good performance/cost relation. The specific objectives of the project were:

- Development of an own technology for the Spanish industry in the field of biodegradable lubricants.
- That Spain could have its own oleaginous cultivation and other special industrial oils.
- Development of an advanced methodology for converting castor in a vegetable biofactory.
- Reducing the biolubricant production costs keeping the performance.
- Development of the technology that allowed biolubricants performance in cold and hot climates.

The BIOVESIN project was divided in four subprojects. The specific aims of the first subproject were to compare the effectiveness of the new high oleic sunflower oils as biolubricant base with those of the different available commercial oils, such as sunflower or rapeseed, and to establish the steps for the oil extraction and refine processes and also the quality control for these oils.

In the second subproject, new varieties of castor with improvements in the fatty acid composition were developed, for instance inserting the high oleic mutant character, or developing new castor oil varieties by means of genetic engineering.

As concern the third subproject, it comprised the formulation and test of biodegradable lubricants for specific applications, i.e. hydraulic fluids, two stroke engines and wind turbine and tractor gearboxes. Vegetable bases from subprojects 1 and 2, as well as biodegradable additives according to the biodegradability criteria of the European Ecolabel were employed in the formulation of environmentally friendly lubricants, which was a hard work due to the lack of technological development. Thus, the most suitable lubricant formulation should allow the modification of the base oil viscosity, low temperature properties, wear resistance, friction coefficient, wettability, and other properties related with the final lubricant use. A complete physico-chemical and tribological characterization of the different properties of the lubricant bases and additives was performed. Thus, the knowledge of properties such as thermal stability, biodegradability, rheology, solubility with gases, among others, was necessary for the selection of the most suitable formulations for their final test in machinery and engines. This subproject, in which was involved the Thermophysical Properties Laboratory, is one of the frameworks of this PhD Thesis.

Finally, the fourth subproject carried out the study of the performance of the formulated lubricants in laboratory and real machinery (wind turbines, agricultural machinery with two stroke engines and tractors).

The other two funded projects that serve as framework for this PhD Thesis deal with the use of ILs as lubricants. One of them is the LUBIONIC project (Molecular structure influence on thermophysical and tribological properties of ionic liquids in broad pressure ranges for their use in lubrication, CTQ2008-06498-C02-01, Ministerio de Ciencia e Innovación), which was carried out by the Thermophysical Properties Laboratory in collaboration with the company Merck KGaA. It aimed to study the molecular structure influence on thermophysical and tribological properties of ILs in broad pressure ranges for their use in lubrication [254-256]. This project tried to broaden the studies on ILs as lubricants and lubricant additives of conventional base oils for their application in EHL, engine and hydraulic oils, among others. The project arose from the needs of new lubricant material with high thermal stabilities and wide liquid range for advance internal combustion engines, aircraft, spacecraft, and nano/microelectromechanical systems. The fundamental properties of ILs are determined by the choice of the cation and the anion as well as the side chain structure. Therefore, their appropriate selection allows creating tailor-made lubricant as well as lubricant additives. Under this framework, knowledge of the influence of the ions structure on the thermophysical properties of the ILs is necessary in their development for lubricant applications. A double approach, experimental and by means of molecular simulation, was performed in order to set the relationship among the macroscopic properties and the molecular structure. The studied properties of this research project were density and viscosity in

broad ranges of temperature and pressure, heat capacities, thermal stability, miscibility of ILs with currently used base fluids, and also tribological properties with different contact pairs.

The last project is the RENELUBIL project (New nanostructured lubricants based on ionic liquids for renewable energies, CTQ2011-23925, Ministerio de Ciencia e Innovación), which has as objective obtaining new nanostructured lubricants based in ILs for their use in renewable energies, mainly as gear lubricants. This project is motivated because the lubricants used nowadays in wind turbines are harmful to the environment. It is intended to develop green lubricants for this application based on biodegradable base oils as well as ILs selected due to their affinity with the base oils, their potential toxicity and biodegradability. In order to do that, several properties of the selected ILs are determined, viscosity and density in broad ranges of temperature and pressure, miscibility of ILs with base oils, wear and friction coefficients of surfaces lubricated with ILs and with mixtures of base oil plus IL, and also degradation, melting and glass transition temperature of the pure ILs. With these results the effectiveness of the new lubricants for boundary and elastohydrodynamic lubrication can be compared with those of the reference oils. Additionally, simulation tools are employed for obtaining a microscopic explanation of the experimental results concerning miscibility and friction [257].

1.5. Lubricant applications and related thermophysical properties

In this PhD Thesis, the studied fluids consist on reference and developed vegetable lubricants for three different applications, i.e. hydraulic fluids, gear lubricants for wind turbines and tractor transmissions and two stroke engine lubricants, as well as ILs as potential fluids for the same purposes. The studied properties include high pressure density and compressibility, high pressure rheology and gas (CO_2, O_2) solubility in lubricant oils.

Hydraulics

Hydraulic systems involve applications where the conversion of mechanical energy into fluid energy and again into mechanical work is required. This kind of systems transmits energy and applies huge forces under high flexibility and control and they constitute a more accurate means of transmitting energy than electrical or mechanical systems. They are composed by a fluid medium under pressure that creates motion in the machine components. In addition, the hydraulic fluid is responsible of other tasks such as sealing, minimizing wear, reducing friction, cooling, preventing rust and corrosion and keeping the system free of deposits [10,258].

The density-pressure behaviour of a hydraulic fluid is a key design factor, because a low compressibility is necessary in order to transmit power effectively and successfully, moreover, pressure losses are proportional to density and the higher the density, the higher the energy to pump. Thus, a low compressibility ratio, i.e. a high bulk modulus, provides fast response time,

high pressure transmission velocity and low power loss. As regards viscosity, it is a property important for lubrication and also for energy transmission. In this way, too low viscosity give rise to excessive metal to metal contact in the moving part, wear and leaking. On the contrary, too high viscosity leads to high energy consumption, too much heating and lower mechanical efficiency, among others [10,258-260].

Some researchers have studied the suitability of using vegetable oils and other biodegradable fluids in hydraulic applications. Reviews dealing with biodegradable lubricants as hydraulic fluids were published by Schneider [261] and by Totten et al. [262]. Additionally, Kassfeldt and Dave [263] maintained that once full film lubrication is achieved there is no disadvantage in using environmentally adapted oils in hydraulic applications and Rhee et al. [264] found environmentally aware hydraulic fluids potentially good candidate for the replacement of some petroleum based military hydraulic fluids, although they did not meet their current military specifications. Different vegetable oils have been studied for this application, i.e. Honary [265] found that soybean oil appears to have sufficient lubricating capability to perform in hydraulic systems, although the performance can be improved through chemical modification, and Oğuz et al. [266] found that this oil can be used as an alternative hydraulic fluid. Moreover, Paeglis et al. [267] studied several biodegradable hydraulic oils based on rapeseed oil finding that they can meet ISO standards for lubricants, whereas Šraj Kladivar et al. [268] found that hydraulic systems can satisfactorily operate with a fluid based in this oil at temperatures up to 353.15 K. On the other hand, Yahaya et al. [269] found peanut oil to be a possible hydraulic brake fluid, Nik et al. [270] carried out an experimental investigation on system performance using palm oil as hydraulic fluid, finding that this vegetable oil could be a potentially useful substitute for mineral-based energy transport media and Mendoza et al. [271] improved the oxidation resistance of HOSO lubricants as tractor hydraulic fluids by means of additivation.

Gears

Gears control motion and transmit mechanical power from a rotating shaft to another or from a rotating shaft to a reciprocating element. Transmission gears are employed for increasing or decreasing torque, changing speed and movement direction. Gear lubricants carry out several functions, as preventing wear and friction between the moving parts, dissipating heat, inhibiting corrosion, removing wear particles, improving power transfer efficiency and reducing noise. The main property to take into account for the formulation of a gear lubricant is the viscosity, because there must be an appropriate oil film between the moving surfaces. For the accurate prediction of EHL parameters, the knowledge of rheological behaviour and lubricant compressibility is also required, this last being a second order effect for the generation of a film

thickness. In fact, the effect of the density-pressure relationship on film thickness and pressure spikes has been studied by several authors, and different results were found depending on the type of relation employed. Thus, Dowson and Higginson [272] proposed a equation of state for the pressure dependence of volume to be employed in the calculation of film thickness for gear conditions, which has been extensively used in EHL, even thought it is not the most accurate for prediction of central film thickness at high temperatures and pressures. On the other hand, Hamrock et al. [273] and Höglund [274] found that an incompressible lubricant originates much higher pressure at the pressure spike than compressible lubricants and that the minimum film thickness is not influenced by compressibility whereas the film thickness at the contact centre is smaller for compressible lubricants. Additionally, Jacobson and Vinet [275] stated that the central film thickness ratio is inversely proportional to the density ratio and Venner and Bos [276] presented EHL film thickness results based on Jacobson and Vinet [275] density-pressure model, whereas Katyal and Kumar [277] and Habchi et al. [278], among others, reported central film thickness calculation by using the Tait equation of state for compressibility description [5,10,260,274,279-285].

Some research on the use of biodegradable lubricants in gear application has been performed by Kržan and Vižintin [286,287] who studied a vegetable based oil for tractor transmission finding that gear protection properties of the vegetable based oils are better or equivalent to that of the mineral ones, although the mineral oil presented better thermal oxidative stability. Moreover, Nagendramma [288] studied a pentaerythritol ester as industrial gear oil finding good response using the conventional commercial mineral base oils additive for this type of fluids. Khairuldean et al. [289] found that refined, bleached and deodorized palm olein has good mild extreme pressure properties, even though film breakdown occurs at higher pressure loads, whereas Arca et al. [290] developed a gear oil based on soybean oil, obtaining comparable or better wear than those of the commercially available gear oils, even though the oxidation onset temperature was lower than those of the commercial products.

Two stroke engines

Two stroke engines are usually used when high specific power, low weight and low price are required, therefore they are often found in motorcycles, boats, lawn mowers, agricultural tractors or chain saws. In this type of engines, the lubricant is added to the fuel, being a large part of it burnt in the combustion process, whereas about one quarter is exhausted as unburned oil mist in every cycle. The tasks that must be carried out by the lubricant in this application are preventing wear and maintaining efficiency, cooling, sealing, avoiding deposits in the system, reducing smoke, and protecting from corrosion. Again viscosity is the main property to take into

account for the selection of a two stroke oil, in fact it is recommended a viscosity above 6.5 $mm^2 \cdot s^{-1}$ at 373.15 K. Additionally, good fuel miscibility and good flowing properties are essential [10,291,292].

Some publications dealt with the use of biodegradable lubricants in two stroke engines, as that from Suhane et al. [293] who presented non edible vegetable oils as potential alternative lubricants for automotive applications or Igartua et al. [294] that studied prototype lubricants based on synthetic esters finding no seizure between piston ring and cylinder liner. Furthermore, Masjuki et al. [119] studied the tribological and emission performance of palm oil and mineral oil based lubricants, reporting that the palm oil lubricant presented better wear performance, whereas the mineral oil presented better friction performance. Fernando and Hanna [295] studied the applicability of soybean oil as two stroke lubricant from the viscosity point of view, whereas Singh [296] found that castor based oil reduces the smoke emission of two stroke engines, without starting problems, piston seizure or other driving problems, suggesting that other oils such as ricebran, neem, karanja, coconut, jotropha or palm oil can be suitable for this application.

Thermophysical properties analyzed

The fluid viscosity is related to its resistance to flow, given by the internal fluid friction, which represents the interaction strength between molecules that opposes motion. Lubricants are classified by means of an ISO standard in viscosity grades, based on the kinematic viscosity at 313.15 K expressed in $mm^2 \cdot s^{-1}$. Viscosity constitutes one of the most important properties of lubrication oils, because it influences film formation, friction, wear, heat generation, sealing, cold starting and energy efficiency. When systems operate over a wide temperature range, it is desired a small viscosity change with temperature, which is given by the viscosity index (VI). This property quantifies the rate of viscosity change with temperature, the higher the VI, the less the effect of temperature on viscosity. Besides, the rheological characterization of lubricating oils as a function of temperature and pressure at different shear rates is basic for the determination of its ability to form an oil layer, the design of a lubricated system and their energetic efficiency [5-7,10,11,34,297]. Among the works concerning the high pressure rheological behaviour of lubricants, it is worth mentioning those from Bair, from the Georgia Institute of Technology, and co-workers [285,298-307], who studied the rheological behaviour of different lubricants up to pressures of 1.5 GPa and shear rates of 10^5 s^{-1}.

As regards the density behaviour with temperature and pressure, it is a necessary property for the calculation of the dynamic viscosity. Moreover volumetric data in broad temperature and pressure ranges is also fundamental for developing equations of state, which are used for the prediction of thermophysical properties with design purposes. Additionally, isothermal

compressibility values can be obtained by differentiation from the experimental density data. This property is useful for the selection of a hydraulic fluid and also for the determination of the central film thickness in EHL, as previously pointed out [9,308].

Data on high pressure density of vegetable oils have been reported by Acosta et al. [309] for castor, linseed, perilla, safflower, sesame, soybean and olive oils up to 144 MPa. Moreover, Safarov et al. published density data of sunflower, corn, olive, cotton seed, sesame and soybean oils up to 49 MPa. Additionally, Werner et al. [310] measured density of olive oil up to 434 MPa and Guignon et al. [311,312] reported values of this property for sunflower, castor and olive oil up to 350 MPa. On the other hand, volumetric properties at high pressure of many different ILs, specially those containing imidazolium cations and $[PF_6]^-$, $[BF_4]^-$ and $[NTf_2]^-$ anions, have been widely determined as is gathered in the review from Aparicio et al. [313].

Finally, as concerns solubility of gases in oils, it is worth mentioning that the majority of gases are soluble in oil to a given extent. This property may affect different lubricant properties such as viscosity, foaming, compressibility, cavitation, heat transfer, oxidation, corrosion and boundary lubrication. In this way the oxygen dissolved in oil may cause lubricant oxidation and surface corrosion. Otsu et al. [314] studied the effect of surrounding gas on cavitation in EHL finding that the cavity length in gas with higher gas solubility is larger than that in gas with lower gas solubility. Regarding hydraulic fluids, the gas bubbles released with pressure drops may cause abrupt compressibility increase which gives rise to poor system performance. In addition, in two stroke engine applications, gases are involved in the combustion process together with the lubricant and the gasoline in the combustion chamber, and knowledge of gas solubility in reference lubricants provide a base for comparison with that in developed lubricants [5,11].

Carbon dioxide solubility in different lubricant oils has been broadly studied in the refrigeration field. An example of these studies is the work from Yokozeki [315] concerning correlation and phase behaviour of carbon dioxide and polyalkylene glycol or polyol ester oils. On the other hand, as regards CO_2 solubility in vegetable oils, it has been mainly studied for supercritical extraction purposes, focusing in the region rich in CO_2. Examples of this kind of systems include castor, corn, olive, soybean and sunflower oils, among others, and are gathered in the solubility reviews by Dohrn and co-workers [316-318].

1.6. Objectives

This PhD Thesis is focused on the experimental determination of several thermodynamic properties of different lubricant fluids, i.e. reference, base and developed biodegradable oils, as well as ILs, with the objective of comparing the values for the reference and the new lubricants,

as well as studying the influence of additivation on the base oils. The different thermodynamic properties determined are density in broad temperature and pressure ranges, viscosity at atmospheric and high pressure and carbon dioxide solubility in different lubricants. The studied ILs are given in table 1.1, whereas the vegetable base oils as well as the reference and developed biodegradable lubricants are presented in table 1.2.

For the determination of high pressure rheology as well as phase equilibria, the implementation of two new apparatus in the Thermophysical Properties Laboratory was performed in this PhD Thesis, one of them is a high pressure rheometer and the other one is a synthetic high pressure phase equilibria apparatus based on a full visibility cell.

Regarding volumetric behaviour, the density of eight reference oils, being currently used in different applications, two high oleic sunflower base oils (HOSO), eleven additivated biodegradable lubricants developed in the BIOVESIN project and also seven ILs is determined in broad temperature and pressure ranges.

As concerns viscosity, this property is measured at atmospheric pressure for the reference, base and developed oils in broad temperature ranges, and the rheological behaviour of two ionic liquids is also studied at high pressure.

Finally, carbon dioxide solubility in a reference oil, three base oils and two oils developed for two stroke engine application is measured.

Table 1.1. Ionic liquids studied in this PhD Thesis.

Ionic Liquid	**Chemical structure**	**Application**	**η /mm^2·s^{-1} 313.15 K [319]**	**VI [319]**
$[C_1OC_2C_1Pyrr][NTf_2]$	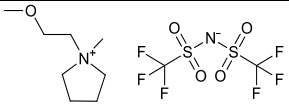	Hydraulic	22	191
$[C_4C_1Pyrr][NTf_2]$	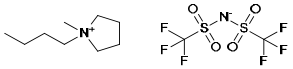	Hydraulic	30	176
$[C_1OC_2C_1Pyrr][(C_2F_5)_3PF_3]$	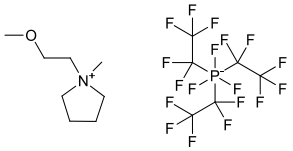	Hydraulic	35	137
$[C_2C_1Im][C_2SO_4]$	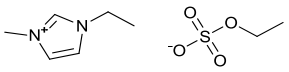	Hydraulic	41	174
$[C_4C_1Pyrr][(C_2F_5)_3PF_3]$	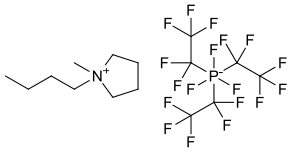	Hydraulic	61	119
$[C_2C_1Im][C_6SO_4]$	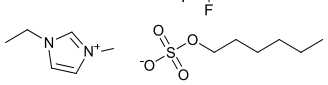	Gear	122	136
$[P_{6,6,6,14}][(C_2F_5)_3PF_3]$	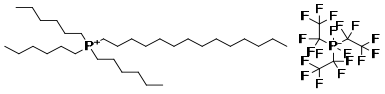	Gear	131	128

Table 1.2. Reference, base and developed biodegradable oils studied in this PhD Thesis.

Name	Application	Description	Final user	η /mm^2·s^{-1} 313.15 K	η /mm^2·s^{-1} 373.15 K	VI
		Reference oils				
MIN-H01	Hydraulic	Mineral	Agria	48.4	8.1	144
MIN-H02	Hydraulic	Mineral	Gamesa	30.6	5.8	138
MIN-H03	Hydraulic	Mineral	Indra	14.4	3.7	146
BIO-H	Hydraulic	Commercial biodegradable	—	58.5	11.5	196
SYN-2T	Two stroke engine	Semi-synthetic	Abamotor	63.0	9.4	118
MIN-G	Gear (wind turbine gearbox)	Mineral	Gamesa	324.0	24.3	96
MIN-G01	Gear (wind turbine gearbox)	Mineral	Indra	329.3	32.4	139
MIN-G02	Gear (tractor transmission)	Mineral	Agria	182.6	16.8	97
		Base oils				
HOSO-B	All	80% oleic	—	39.2	8.5	203
HOSO-B1	All	83% oleic	—	39.6	8.5	204
Castor	All	Castor oil	—	249.6	19.3	87
Rapeseed	All	Rapeseed oil	—	35.8	8.1	214
		Biodegradable developed oils*				
BIO-H01	Hydraulic	HOSO-B1+ AP1	—	39.6	8.5	202
BIO-H02	Hydraulic	HOSO-B1 + AO-1/CI/CP +AW-1	—	40.0	8.4	200
BIO-H03	Hydraulic	HOSO-B1 + AO-2/CI/CP +AW-1	—	40.5	8.5	198
BIO-H04	Hydraulic	HOSO-B1 + Ester-1 + AO-2/CI/CP + AW-2 + PPD	Gamesa	35.7	7.9	204
BIO-H05	Hydraulic	HOSO-B1+ Ester-1+ AO-2/CI/CP +AW-3 + PPD	—	34.8	7.6	201
BIO-H06	Hydraulic	HOSO-B1 + Ester-2+ AO-2/CI/CP +AW-2 + PPD	Agria	41.5	8.7	198
BIO-2T-03	Two stroke engine	60% HOSO-B1 + Ester-1+ Ester-2 + Thickener + M2	Abamotor	46.4	9.0	180
BIO-2T-05	Two stroke engine	50% HOSO-B1 + 50% PAO2 + Thickener + M1	Abamotor	28.2	6.2	182
BIO-G00	Gear (wind turbine gearbox)	25% HOSO-B1 + Synthetic ester+ AP4	Gamesa	244.6	29.0	158
BIO-G01	Gear(wind turbine gearbox)	50% HOSO-B1 + Ester-3+ Thickener 8 + AP4	Indra	221.8	32.0	189
BIO-G02	Gear (tractor transmission)	45% HOSO-B1 + Synthetic ester+ AP4	Agria	148.6	21.0	166
SYN-G01	Gear	Synthetic esters+ AP4	—	254.4	28.8	150

AP: additive package; AO: antioxidants; CI: corrosion inhibitors; CP: cloud point depressants; AW: antiwear additives; PPD: pour point depressant; M: motor package.

*Developed oils were formulated by Verkol Lubricantes.

The specific objectives of this PhD Thesis are:

I. Calibration of a high pressure densimeter Anton Paar DMA 60/512P in the temperature range from 278.15 K to 353.15 K up to 60 MPa and measurement of density with this technique of a high oleic sunflower oil (HOSO-B1) and six biodegradable developed hydraulic oils (BIO-H01, BIO-H02, BIO-H03, BIO-H04, BIO-H05, BIO-H06).

II. Calibration of a high pressure densimeter Anton Paar HPM from 278.15 K to 398.15 K and pressures up to 120 MPa and measurement with this technique of density of four reference hydraulic oils (MIN-H01, MIN-H02, MIN-H03, BIO-H), one base oil (HOSO-B), three reference gear oils (MIN-G, MING-01, MING-02), four developed biodegradable gear oils (BIOG-00, BIOG-01, BIOG-02, SYN-G01), one reference oil for two stroke engines (SYN-2T), one biodegradable oil developed for two stroke engines (BIO-2T-03) and seven ILs (table 1.1).

III. Correlation of the obtained density values as a function of temperature and pressure and calculation of the isothermal compressibility values, κ_T, and the thermal expansion coefficients, α_p. Comparison of the values of these properties among the reference oils, the biodegradable developed oils and ILs.

IV. Review of the literature density and isothermal compressibility values of ILs in order to establish structure-property relationships and to select the best as hydraulic fluids as regards to these properties.

V. Determination of the carbon dioxide solubility in a reference oil for two stroke engines and in a biodegradable oil developed for this application (BIO-2T-03) through an isochoric technique (SOLLPT1) in the temperature range from 283.15 K to 348.15 K and pressures up to 10 MPa. Modelling of the obtained solubility values by means of the PC-SAFT EoS and comparison of the solubility results for the two studied lubricants.

VI. Determination of the carbon dioxide solubility in three base oils (HOSO-B1, Castor, Rapeseed) in a temperature range from 298.15 K to 363.15 K and pressures up to 74 MPa by means of a visual synthetic technique installed in the PATh Laboratory at the University of Aveiro. Modelling of the solubility results by means of the SRK EoS.

VII. Implementation of a high pressure phase equilibria apparatus (SOLLPT2) to operate in a temperature range from 298.15 K to 363.15 K and pressures up to 100 MPa. Determination of the solubility of carbon dioxide in HOSO-B1 by means of this technique and comparison of the results with those obtained at the University of Aveiro, and also determination of the solubility of carbon dioxide in BIO-2T-05.

VIII. Implementation of a high pressure rheometer Reologica HTHP to operate in a temperature range from 298.15 K to 353.15 K, pressures up to 75 MPa and shear rates up to 1000 s^{-1}.

Characterization of the rheological behaviour of PAO40 and polybutene H8 by means of this technique and comparison of the results with literature. Characterization also of the rheological behaviour of two ILs ($[C_2C_1Im][C_6SO_4]$, $[P_{6,6,6,14}][(C_2F_5)_3PF_3]$) in the specified temperature, pressure and shear rate range.

1.7. References

[1] D. Dowson, History of tribology, 2nd ed., John Wiley & sons, Inc., Chichester, 1998.
[2] E. Meyer, T. Gyalog, R.M. Overney, K. Dransfeld, Nanoscience: friction and rheology on the nanometer scale, World Scientific Publishing Company Pte. Ltd., Singapore, 2002.
[3] R.M. Mortier, M.F. Fox, S.T. Orszulik, Chemistry and technology of lubricants, 3rd ed., Springer, New York, 2010.
[4] L.A.T. Honary, E. Richter, Biobased lubricants and greases: Technology and products, 1st ed., John Wiley & Sons, Lt., Chichester, 2011.
[5] B. Bhushan, Principles and applications of tribology, John Wiley & sons, Inc., New York, 1999.
[6] A. Sethuramiah, Lubricated wear. Science and technology, Elsevier, Amsterdam, 2003.
[7] B.J. Hamrock, S.R. Schmid, B.O. Jacobson, Fundamentals of fluid film lubrication, 2nd ed., Marcel Dekker, Inc., New York, 2004.
[8] K. Carnes, R.M. Gresham, N. Canter, M. Anderson, Trib. Lub. Tech. 61 (2005) 38-47.
[9] M.M. Khonsari, E.R. Booser, Applied tribology. Bearing design and lubrication, 2nd ed., John Wiley & Sons, Ltd, Chichester, 2008.
[10] D.M. Pirro, A.A. Wessol, Lubrication fundamentals, 2nd revised and expanded ed., Marcel Dekker, Inc., New York 2001.
[11] G.W. Stachowiak, A.W. Batchelor, Engineering tribology, 3rd ed., Elsevier Butterworth-Heinemann, Burlington, 2005.
[12] K.C. Ludema, Friction, wear, lubrication. A textbook in tribology, CRC Press, Inc., Boca Raton, 1996.
[13] L.R. Rudnick, S.Z. Erhan, Natural oils as lubricants. in: L.R. Rudnick, (Ed.), Synthetic mineral oils and bio-based lubricants: chemistry and technology, CRC Press, Taylor and Francis Group, Boca Raton, 2006, pp. 353-360.
[14] A. Gosalia, Sustainability... and the Global Lubricants Industry, The 16th ICIS World Base Oils & Lubricants Conference, London, 2012.
[15] Synthetic & bio-based lubricants market - global industry analysis, market size, share, trends, analysis, growth and forecast, 2012 - 2018, Transparency Market Research.
[16] T. Mang, Lubricants and their market. in: T. Mang, W. Dresel, (Eds.), Lubricants and lubrication, Wiley-VCH GmbH, Weinheim, 2001.
[17] K. Ludema, Friction. in: E.R. Booser, (Ed.), CRC Handbook of Lubrication: Theory and Practice of Tribology, Volume II: Theory and Design, CRC Press, Boca Raton, 1983, pp. 31-48.
[18] R. Luther, Lubricants in the environment. in: T. Mang, W. Dresel, (Eds.), Lubricants and lubrication, Wiley-VCH, Weinheim, 2001, pp. 115-164.
[19] P. Nagendramma, S. Kaul, Renewable and Sustainable Energy Rev. 16 (2012) 764-774.
[20] C.I. Betton, Lubricants and their environmental impact. in: R.M. Mortier, M.F. Fox, S.T. Orszulik, (Eds.), Chemistry and technology of lubricants, Springer, New York, 2010, pp. 435-457.
[21] S.Z. Erhan, A. Adhwaryu, Vegetable oil-based base stocks. in: S.Z. Erhan, J.M. Perez, (Eds.), Biobased industrial fluids and lubricants, AOCS Press Champaign, 2002, pp. 1-19.
[22] A. Pettersson, Trib. Int. 40 (2007) 638-645.
[23] R. Stribeck, Zeitschrift des Vereines Deutscher Ingenieure 46 (1902) 1341-1348, 1432-1438, 1463-1470.
[24] W.B. Hardy, I. Doubleday, Proceedings of the Royal Society of London. Series A, containing papers of a mathematical and physical character 100 (Mar. 1, 1922) 550-574.
[25] W.B. Hardy, I. Doubleday, Proceedings of the Royal Society of London. Series A, containing papers of a mathematical and physical character 101 (Sep. 1, 1922) 487-492.
[26] B. Tower, Proc. Inst. Mech. Engrs 36 (1885) 58-70.
[27] N.P. Petrov, Inzh. Zh. St. Petersburg 1 71-140, 2 277-279, 3 377-436, 4 535-564 (1883).
[28] O. Reynolds, Phil. Trans. Roy. Soc. 177 (1886) 157-234.

[29] P.M. Lugt, G.E. Morales-Espejel, Tribol. Trans. 54 (2011) 470-496.
[30] D. Berthe, P. Vergne, J. Rheol. 34 (1990) 1387-1414.
[31] D. Dowson, G.R. Higginson, A.V. Whitaker, J. Mech. Eng. Sci. 4 (1962) 121-126.
[32] N.C. Das, Tribol. Trans. 40 (1997) 353-359.
[33] T. Mang, Base oils. in: T. Mang, W. Dresel, (Eds.), Lubricants and lubrication, Wiley-VCH, Weinheim, 2001, pp. 32-60.
[34] R.J. Prince, Base oils from petroleum. in: R.M. Mortier, M.F. Fox, S.T. Orszulik, (Eds.), Chemistry and technology of lubricants, Springer, New York, 2010, pp. 3-33.
[35] Appendix E-API Base Oil Interchangeability Guidelines for Passenger Car Motor Oils and Diesel Engine Oils, API 1509 Engine Oil Licensing and Certification System, 17th Ed. , September 2012.
[36] M. Brown, J.D. Fotheringham, T.J. Hoyes, R.M. Mortier, S.T. Orszulik, S.J. Randles, P.M. Stroud, Synthetic base fluids. in: R.M. Mortier, M.F. Fox, S.T. Orszulik, (Eds.), Chemistry and technology of lubricants, Springer, New York, 2010, pp. 35-74.
[37] H.-S. Hwang, S.Z. Erhan, Lubricant base stocks from modified sooybean oil. in: S.Z. Erhan, J.M. Pérez, (Eds.), Biobased industrial fluids and lubricants, AOCS Press Champaign, 2002, pp. 20-34.
[38] J. Crawford, A. Psaila, S.T. Orszulik, Miscellaneous additives and vegetable oils. in: R.M. Mortier, M.F. Fox, S.T. Orszulik, (Eds.), Chemistry and technology of lubricants, Springer, New York, 2010, pp. 189-211.
[39] A. Srivastava, P. Sahai, Afr. J. Biotechnol. 12 (2013) 880-891.
[40] B. Wilson, Ind. Lubr. Tribol. 50 (1998) 6-15.
[41] A. Adhvaryu, S.Z. Erhan, Ind. Crops Prod. 15 (2002) 247-254.
[42] K. Balamurugan, N. Kanagasabapathy, K. Mayilsamy, J. Sci. Ind. Res. 69 (2010) 794-797.
[43] A. Campanella, E. Rustoy, A. Baldessari, M.A. Baltanás, Bioresour. Technol. 101 (2010) 245-254.
[44] S.C. Cermak, G. Biresaw, T.A. Isbell, R.L. Evangelista, S.F. Vaughn, R. Murray, Ind. Crops Prod. 44 (2013) 232-239.
[45] K.M. Doll, B.K. Sharma, J. Surfactants Deterg. 14 (2011) 131-138.
[46] S.Z. Erhan, S. Asadauskas, Ind. Crops Prod. 11 (2000) 277-282.
[47] S.Z. Erhan, B.K. Sharma, Z. Liu, A. Adhvaryu, J. Agric. Food Chem. 56 (2008) 8919-8925.
[48] R. Garcés, E. Martínez-Force, J.J. Sales, Grasas Aceites 62 (2011) 21-28.
[49] N.H. Jayadas, K.P. Nair, Trib. Int. 39 (2006) 873-878.
[50] N. Ravasio, F. Zaccheria, M. Gargano, S. Recchia, A. Fusi, N. Poli, R. Psaro, Appl. Catal., A 233 (2002) 1-6.
[51] J. Salimon, N. Salih, E. Yousif, Eur. J. Lipid Sci. Technol. 112 (2010) 519-530.
[52] B. Sharma, A. Adhvaryu, Z. Liu, S. Erhan, J. Am. Oil Chem. Soc. 83 (2006) 129-136.
[53] E.O. Aluyor, M. Ori-jesu, Afr. J. Biotechnol. 7 (2008) 4836-4842.
[54] S. Asadauskas, S.Z. Erhan, J. Am. Oil Chem. Soc. 76 (1999) 313-316.
[55] S. Asadauskas, G. Biresaw, T. McClure, Trib. Lett. 37 (2010) 111-121.
[56] P. Baumgart, G. Canzi, T. Hanashiro, L.A. Doezema, M.T. Siniawski, Lubr. Sci. 22 (2010) 393-403.
[57] G. Biresaw, S.J. Asadauskas, T.G. McClure, Ind. Eng. Chem. Res. 51 (2011) 262-273.
[58] H. Chen, J. Yan, T. Ren, Y. Zhao, L. Zheng, Trib. Lett. 45 (2012) 465-476.
[59] U.S. Choi, B.G. Ahn, O.K. Kwon, Y.J. Chun, Trib. Int. 30 (1997) 677-683.
[60] Q. Gong, W. He, W. Liu, Trib. Int. 36 (2003) 733-738.
[61] H.-S. Hwang, S. Erhan, J. Am. Oil Chem. Soc. 78 (2001) 1179-1184.
[62] P.V. Joseph, D.K. Sharma, Lubr. Sci. 22 (2010) 149-161.
[63] I. Minami, K. Mimura, J. Synth. Lubr. 21 (2004) 193-205.
[64] L.A. Quinchia, M.A. Delgado, C. Valencia, J.M. Franco, C. Gallegos, J. Agric. Food Chem. 59 (2011) 12917-12924.
[65] C. Ruger, E. Klinker, E. Hammond, J. Am. Oil Chem. Soc. 79 (2002) 733-736.
[66] B.K. Sharma, J.M. Perez, S.Z. Erhan, Energy Fuels 21 (2007) 2408-2414.
[67] M.V. Thottackkad, R.K. Perikinalil, P.N. Kumarapillai, Int. J. Precis. Eng. Manuf. 13 (2012) 111-116.
[68] J. Padgurskas, R. Kreivaitis, V. Jankauskas, P. Janulis, V. Makareviciene, S. Asadauskas, L. Miknius, Mechanika (2008) 67-72.
[69] S.Z. Erhan, B.K. Sharma, Abstr. Pap. Am. Chem. Soc. 236 (2008).
[70] X.B. Ji, Y.X. Chen, X.B. Wang, W.M. Liu, Ind. Lubr. Tribol. 64 (2012) 315-320.

[71] A.K. Singh, R.K. Singh, J. Surfactants Deterg. 15 (2012) 399-409.
[72] M.A. Maleque, H.H. Masjuki, S.M. Sapuan, Ind. Lubr. Tribol. 55 (2003) 137-143.
[73] O.S. El Kinawy, Energy Sources 26 (2004) 639-645.
[74] R. Becker, A. Knorr, J. Kelm, Oxid. Commun. 19 (1996) 33-43.
[75] S. Asadauskas, J.M. Perez, J.L. Duda, Lubric. Eng. 53 (1997) 35-41.
[76] D.R. Kodali, Ind. Lubr. Tribol. 54 (2002) 165-170.
[77] F.A. Zaher, H.M. Nomany, Grasas Aceites 39 (1988) 235-238.
[78] R.P.S. Bisht, G.A. Sivasankaran, V.K. Bhatia, J. Sci. Ind. Res. 48 (1989) 174-180.
[79] J.S. Aggarwal, S.S. Bhatnagar, L.C. Verman, J. Sci. Ind. Res. 50 (1991) 156-165.
[80] I.G. Fuks, A.Y. Evdokimov, A.A. Dzhamalov, A. Luksa, Chem. Technol. Fuels Oils 28 (1992) 230-237.
[81] R.S. Kuliev, F.R. Shirinov, F.A. Kuliev, Chem. Technol. Fuels Oils 31 (1995) 106-107.
[82] B. Khemchandani, A.K. Jaiswal, E. Sayanna, M. Forsyth, Lubr. Sci. (2013) n/a-n/a.
[83] A. Bírová, A. Pavlovičová, J. Cvenroš, J. Synth. Lubr. 18 (2002) 291-299.
[84] M. Arca, B.K. Sharma, J.M. Pérez, K.M. Doll, Ind. Eng. Chem. Res. 51 (2012) 3550-3555.
[85] L. Bogatu, D. Ciuparu, C. Tanasescu, Rev. Chim. 61 (2010) 1003-1006.
[86] W. Castro, J. Pérez, S.Z. Erhan, F. Caputo, J. Am. Oil Chem. Soc. 83 (2006) 47-52.
[87] S.Z. Erhan, B.K. Sharma, J.M. Pérez, Ind. Crops Prod. 24 (2006) 292-299.
[88] N.J. Fox, G.W. Stachowiak, Trib. Int. 40 (2007) 1035-1046.
[89] A. Govindapillai, N.H. Jayadas, M. Bhasi, Lubr. Sci. 21 (2009) 13-26.
[90] F.M.T. Luna, B.S. Rocha, E.M. Rola Jr, M.C.G. Albuquerque, D.C.S. Azevedo, C.L. Cavalcante Jr, Ind. Crops Prod. 33 (2011) 579-583.
[91] J.R.S. Politi, P.R.R. Matos, M.J.A. Sales, J. Therm. Anal. Calorim. 111 (2013) 1437-1442.
[92] B. Sharma, U. Rashid, F. Anwar, S. Erhan, J. Therm. Anal. Calorim. 96 (2009) 999-1008.
[93] A. Zeman, A. Sprengel, D. Niedermeier, M. Späth, Thermochim. Acta 268 (1995) 9-15.
[94] A.M. Petlyuk, R.J. Adams, Tribol. Trans. 47 (2004) 182-187.
[95] M. Siniawski, N. Saniei, J. Pfaendtner, Thermal degradation of soybean and sunflower oils, Amer. Soc. Mechanical Engineers, New York, 2008.
[96] S. Asadauskas, J.M. Pérez, J.L. Duda, Lubric. Eng. 52 (1996) 877-882.
[97] M. Schneglberger, Lipid / Fett 96 (1994) 294-299.
[98] A. Adhvaryu, G. Biresaw, B.K. Sharma, S.Z. Erhan, Ind. Eng. Chem. Res. 45 (2006) 3735-3740.
[99] A. Adhvaryu, S.Z. Erhan, J.M. Pérez, Wear 257 (2004) 359-367.
[100] S. Arumugam, G. Sriram, Proc. Inst. Mech. Eng., Part J 227 (2013) 3-15.
[101] S. Bhuyan, S. Sundararajan, L. Yao, E.G. Hammond, T. Wang, Trib. Lett. 22 (2006) 167-172.
[102] G. Biresaw, A. Adhvaryu, S.Z. Erhan, J. Am. Oil Chem. Soc. 80 (2003) 697-704.
[103] N.J. Fox, G.W. Stachowiak, Lubric. Eng. 59 (2003) 15-20.
[104] N.H. Jayadas, K.P. Nair, G. Ajithkumar, Trib. Int. 40 (2007) 350-354.
[105] M. Kalin, J. Vižintin, Wear 261 (2006) 22-31.
[106] R. Pai, D.J. Hargreaves, Wear 252 (2002) 970-978.
[107] M.T. Siniawski, N. Saniei, P. Stoyanov, Lubr. Sci. 23 (2011) 301-311.
[108] D.E. Weller, J.M. Perez, Lubric. Eng. 57 (2001) 20-26.
[109] L. Qinghua, T. Dehua, Z. Jianhua, M. Yunhui, Rheological and tribological characteristics of chemically modified rapeseed oil. in: J. Luo, Y. Meng, T. Shao, Q. Zhao, (Eds.), Advanced Tribology, Springer Berlin Heidelberg, 2010, pp. 912-914.
[110] J.K. Mannekote, S.V. Kailas, Asme, Influence of chemical structure on the boundary lubrication properties of vegetable oils, Amer Soc Mechanical Engineers, New York, 2010.
[111] C.V. Ossia, H.G. Han, H. Kong, Ind. Lubr. Tribol. 62 (2010) 26-31.
[112] R. Kreivaitis, J. Padgurskas, M. Gumbytė, V. Makarevičienė, B. Spruogis, Transport 26 (2011) 121-127.
[113] T.C. Ing, A.K. Mohammed Rafiq, Y. Azli, S. Syahrullail, Tribol. Trans. 55 (2012) 539-548.
[114] S. Fernando, M. Hanna, S. Adhikari, Appl. Eng. Agric. 23 (2007) 5-11.
[115] I. Minami, S. Mitsumune, J. Jpn. Soc. Tribol. 45 (2000) 789-794.
[116] K. Lal, V. Carrick, J. Synth. Lubr. 11 (1994) 189-206.
[117] A. Arnšek, J. Vižintin, J. Synth. Lubr. 16 (2000) 281-296.
[118] M. Shahabuddin, H.H. Masjuki, M.A. Kalam, Procedia Engineering 56 (2013) 597-606.
[119] H.H. Masjuki, M.A. Maleque, A. Kubo, T. Nonaka, Trib. Int. 32 (1999) 305-314.
[120] E.O. Aluyor, K.O. Obahiagbon, M. Ori-jesu, Sci. Res. Essays 4 (2009) 543-548.

[121] T. Mang, Lipid / Fett 100 (1998) 524-527.
[122] P. Mercurio, K.A. Burns, J. Cavanagh, Environ. Pollut. 129 (2004) 175-182.
[123] P. Mercurio, K.A. Burns, A. Negri, Environ. Pollut. 129 (2004) 165-173.
[124] P. Mercurio, A.P. Negri, K.A. Burns, A.J. Heyward, Environ. Pollut. 129 (2004) 183-194.
[125] I.S. Tamada, R.N. Montagnolli, P.R.M. Lopes, E.D. Bidoia, Braz. J. Microbiol. 43 (2012) 1576-1581.
[126] I.G. Fuks, A.Y. Evdokimov, A.A. Dzhamalov, Chem. Technol. Fuels Oils 28 (1992) 361-367.
[127] F. Zhou, Y. Liang, W. Liu, Chem. Soc. Rev. 38 (2009) 2590-2599.
[128] M.D. Bermúdez, A.E. Jiménez, J. Sanes, F.J. Carrión, Molecules 14 (2009) 2888-2908.
[129] I. Minami, Molecules 14 (2009) 2286-2305.
[130] A.E. Jiménez, M.D. Bermúdez, Trib. Lett. 37 (2010) 431-443.
[131] M. Palacio, B. Bhushan, Trib. Lett. 40 (2010) 247-268.
[132] A.-E. Jiménez, M.-D. Bermúdez, Trib. Lett. 26 (2007) 53-60.
[133] B.S. Phillips, G. John, J.S. Zabinski, Trib. Lett. 26 (2007) 85-91.
[134] A. Somers, P. Howlett, D. MacFarlane, M. Forsyth, Lubricants 1 (2013) 3-21.
[135] C. Ye, W. Liu, Y. Chen, L. Yu, Chem. Commun. 0 (2001) 2244-2245.
[136] Q. Lu, H. Wang, C. Ye, W. Liu, Q. Xue, Trib. Int. 37 (2004) 547-552.
[137] Z. Mu, F. Zhou, S. Zhang, Y. Liang, W. Liu, Trib. Int. 38 (2005) 725-731.
[138] H. Wang, Q. Lu, C. Ye, W. Liu, Z. Cui, Wear 256 (2004) 44-48.
[139] W. Liu, C. Ye, Q. Gong, H. Wang, P. Wang, Trib. Lett. 13 (2002) 81-85.
[140] Z. Mu, W. Liu, S. Zhang, F. Zhou, Chem. Lett. 33 (2004) 524-525.
[141] M. Cai, Y. Liang, M. Yao, Y. Xia, F. Zhou, W. Liu, ACS Appl. Mater. Interfaces 2 (2010) 870-876.
[142] D. Li, M. Cai, D. Feng, F. Zhou, W. Liu, Trib. Int. 44 (2011) 1111-1117.
[143] M. Cai, Z. Zhao, Y. Liang, F. Zhou, W. Liu, Trib. Lett. 40 (2010) 215-224.
[144] Z. Song, M. Fan, Y. Liang, F. Zhou, W. Liu, Trib. Lett. 49 (2013) 127-133.
[145] Q. Zhao, G. Zhao, M. Zhang, X. Wang, W. Liu, Trib. Lett. 48 (2012) 133-144.
[146] M. Cai, Y. Liang, F. Zhou, W. Liu, ACS Appl. Mater. Interfaces 3 (2011) 4580-4592.
[147] Q. Zhao, G. Zhao, M. Zhang, X. Wang, W. Liu, Lubr. Sci. 25 (2013) 217-230.
[148] B. Yu, F. Zhou, C. Pang, B. Wang, Y. Liang, W. Liu, Trib. Int. 41 (2008) 797-801.
[149] X. Liu, F. Zhou, Y. Liang, W. Liu, Trib. Lett. 23 (2006) 191-196.
[150] B. Yu, F. Zhou, Z. Mu, Y. Liang, W. Liu, Trib. Int. 39 (2006) 879-887.
[151] G.Q. Yu, F. Zhou, W.M. Liu, Y.M. Liang, S.Q. Yan, Wear 260 (2006) 1076-1080.
[152] X.Q. Liu, F. Zhou, Y.M. Liang, W.M. Liu, Wear 261 (2006) 1174-1179.
[153] Y.Q. Xia, S. Sasaki, T. Murakami, M. Nakano, L. Shi, H.Z. Wang, Wear 262 (2007) 765-771.
[154] L.J. Weng, X.Q. Liu, Y.M. Liang, Q.J. Xue, Trib. Lett. 26 (2007) 11-17.
[155] M. Zhu, J. Yan, Y. Mo, M. Bai, Trib. Lett. 29 (2008) 177-183.
[156] Z. Mu, X. Wang, S. Zhang, Y. Liang, M. Bao, W. Liu, J. Tribol.-Trans. ASME 130 (2008) 034501-034501-034505.
[157] Y. Xia, L. Wang, X. Liu, Y. Qiao, Trib. Lett. 31 (2008) 149-158.
[158] M. Yao, Y. Liang, Y. Xia, F. Zhou, X. Liu, Trib. Lett. 32 (2008) 73-79.
[159] Y. Mo, W. Zhao, M. Zhu, M. Bai, Trib. Lett. 32 (2008) 143-151.
[160] Y. Mo, B. Yu, W. Zhao, M. Bai, Appl. Surf. Sci. 255 (2008) 2276-2283.
[161] Y.M. Chen, Z.X. Zeng, S.R. Yang, J.Y. Zhang, Diam. Relat. Mat. 18 (2009) 20-26.
[162] Y. Mo, M. Bai, Nano/micro-tribological properties of ultrathin functionalized imidazolium ionic liquid films on silicon wafer. in: J. Luo, Y. Meng, T. Shao, Q. Zhao, (Eds.), Advanced Tribology, Springer Berlin Heidelberg, 2010, pp. 520-521.
[163] W. Zhao, D. Huang, J. Pu, M. Baia, Effect of heat treatment on the nano-tribological properties of ionic liquid films. in: J. Luo, Y. Meng, T. Shao, Q. Zhao, (Eds.), Advanced Tribology, Springer Berlin Heidelberg, 2010, pp. 505-506.
[164] W. Zhao, M. Zhu, Y. Mo, M. Bai, Colloids Surf., A 332 (2009) 78-83.
[165] M. Yao, Y. Liang, Y. Xia, F. Zhou, ACS Appl. Mater. Interfaces 1 (2009) 467-471.
[166] M. Zhu, Y. Mo, W. Zhao, M. Bai, Surf. Interface Anal. 41 (2009) 205-210.
[167] W. Zhao, Y. Mo, J. Pu, M. Bai, Trib. Int. 42 (2009) 828-835.
[168] H. Zhang, Y. Xia, M. Yao, Z. Jia, Z. Liu, Trib. Lett. 36 (2009) 105-111.
[169] J.L. Li, D.P. Feng, Y.M. Liang, Y.Q. Xia, W.M. Liu, Ind. Lubr. Tribol. 62 (2010) 161-167.
[170] M. Yao, M. Fan, Y. Liang, F. Zhou, Y. Xia, Wear 268 (2010) 67-71.

[171] B. Wang, X. Wang, W. Lou, J. Hao, J. Phys. Chem. C. 114 (2010) 8749-8754.
[172] W. Zhao, Y. Wang, L. Wang, M. Bai, Q. Xue, Colloids Surf., A 361 (2010) 118-125.
[173] D. Jiang, L. Hu, D. Feng, Trib. Lett. 41 (2011) 417-424.
[174] Z. Zhao, Y.W. Shao, T.M. Wang, D.P. Feng, W.M. Liu, Corros. Eng. Sci. Technol. 46 (2011) 330-333.
[175] J. Pu, D. Jiang, Y. Mo, L. Wang, Q. Xue, Surf. Coat. Technol. 205 (2011) 4855-4863.
[176] J. Pu, X. Liu, L. Wang, Q. Xue, Surf. Interface Anal. 43 (2011) 1332-1340.
[177] M. Cai, Y. Liang, F. Zhou, W. Liu, Faraday Discuss. 156 (2012) 147-157.
[178] M. Fan, Y. Liang, F. Zhou, W. Liu, RSC Advances 2 (2012) 6824-6830.
[179] X. Feng, Y. Xia, Appl. Surf. Sci. 258 (2012) 2433-2438.
[180] Z. Wang, Y. Xia, Z. Liu, Lubr. Sci. 24 (2012) 174-187.
[181] X. Liu, L. Wang, J. Pu, Q. Xue, Appl. Surf. Sci. 258 (2012) 8289-8297.
[182] N. Doerr, I.C. Gebeshuber, D. Holzer, H.D. Wanzenboeck, A. Ecker, A. Pauschitz, F. Franek, Journal of microengineering and nanoelectronics 1 (2010) 29-34.
[183] N. Doerr, A. Schneider, Asme, Ionic liquids as lubricants in steel-steel contacts, Amer. Soc. Mechanical Engineers, New York, 2008.
[184] C. Gabler, C. Tomastik, J. Brenner, L. Pisarova, N. Doerr, G. Allmaier, Green Chem. 13 (2011) 2869-2877.
[185] T. Itoh, N. Watanabe, K. Inada, A. Ishioka, S. Hayase, M. Kawatsura, I. Minami, S. Mori, Chem. Lett. 38 (2009) 64-65.
[186] H. Kamimura, T. Chiba, T. Kubo, H. Nanao, I. Minami, S. Mori, J. Jpn. Soc. Tribol. 51 (2006) 826-834.
[187] H. Kamimura, T. Kubo, I. Minami, S. Mori, Trib. Int. 40 (2007) 620-625.
[188] H. Kamimura, I. Minami, S. Mori, J. Jpn. Soc. Tribol. 50 (2005) 208-213.
[189] H. Kondo, Trib. Lett. 31 (2008) 211-218.
[190] Y. Kondo, S. Yagi, T. Koyama, R. Tsuboi, S. Sasaki, Proc. Inst. Mech. Eng. Part J.-J. Eng. Tribol. 226 (2012) 991-1006.
[191] M. Kronberger, V. Pejakovic, C. Gabler, M. Kalin, Proc. Inst. Mech. Eng. Part J.-J. Eng. Tribol. 226 (2012) 933-951.
[192] I. Minami, T. Inada, R. Sasaki, H. Nanao, Trib. Lett. 40 (2010) 225-235.
[193] F. Pagano, C. Gabler, P. Zare, M. Mahrova, N. Dorr, R. Bayon, X. Fernandez, W.H. Binder, M. Hernaiz, E. Tojo, A. Igartua, Proc. Inst. Mech. Eng. Part J.-J. Eng. Tribol. 226 (2012) 952-964.
[194] F.U. Shah, S. Glavatskih, D.R. MacFarlane, A. Somers, M. Forsyth, O.N. Antzutkin, Phys. Chem. Chem. Phys. 13 (2011) 12865-12873.
[195] A.E. Somers, S.M. Biddulph, P.C. Howlett, J. Sun, D.R. MacFarlane, M. Forsyth, Phys. Chem. Chem. Phys. 14 (2012) 8224-8231.
[196] A.E. Somers, P.C. Howlett, J. Sun, D.R. MacFarlane, M. Forsyth, Phosphonium ionic liquids as lubricants for aluminium-steel, Wit Press, Southampton, 2010.
[197] A.E. Somers, P.C. Howlett, J. Sun, D.R. MacFarlane, M. Forsyth, Trib. Lett. 40 (2010) 279-284.
[198] S. Stolte, S. Steudte, O. Areitioaurtena, F. Pagano, J. Thöming, P. Stepnowski, A. Igartua, Chemosphere 89 (2012) 1135-1141.
[199] H. Xiao, D. Guo, S. Liu, G. Pan, X. Lu, Trib. Lett. 41 (2011) 471-477.
[200] G. Xie, Q. Wang, L. Si, S. Liu, G. Li, Trib. Lett. 36 (2009) 247-257.
[201] T. Yagi, S. Sasaki, H. Mano, K. Miyake, M. Nakano, T. Ishida, Proc. Inst. Mech. Eng. Part J.-J. Eng. Tribol. 223 (2009) 1083-1090.
[202] T. Yagi, S. Sasaki, H. Mano, K. Miyake, M. Nakano, T. Ishida, Tribochemical reaction of ionic liquids on sliding metal surfaces. in: J. Luo, Y. Meng, T. Shao, Q. Zhao, (Eds.), Advanced Tribology, Springer Berlin Heidelberg, 2010, pp. 888-889.
[203] H. Arora, P.M. Cann, Trib. Int. 43 (2010) 1908-1916.
[204] T. Ishikawa, M. Kobayashi, A. Takahara, ACS Appl. Mater. Interfaces 2 (2010) 1120-1128.
[205] S.D.A. Lawes, S.V. Hainsworth, P. Blake, K.S. Ryder, A.P. Abbott, Trib. Lett. 37 (2010) 103-110.
[206] R. Lu, S. Mori, K. Kobayashi, H. Nanao, Appl. Surf. Sci. 255 (2009) 8965-8971.
[207] O.A. Mazyar, G.K. Jennings, C. McCabe, Langmuir 25 (2009) 5103-5110.
[208] Y. Mo, F. Huang, F. Zhao, Surf. Interface Anal. 43 (2011) 1006-1014.

[209] W. Morales, K.W. Street, V.R. Koch, R.M. Richard, Asme, Evaluation of vapor pressure and ultra-high vacuum tribological properties of ionic liquids (2) mixtures and additives, Amer. Soc. Mechanical Engineers, New York, 2009.
[210] T. Murakami, K. Kaneda, M. Nakano, A. Korenaga, H. Mano, S. Sasaki, Trib. Int. 41 (2008) 1083-1089.
[211] J.J. Nainaparampil, K.C. Eapen, J.H. Sanders, A.A. Voevodin, J. Microelectromech. Syst. 16 (2007) 836-843.
[212] M. Palacio, B. Bhushan, Adv. Mater. 20 (2008) 1194-1198.
[213] M. Palacio, B. Bhushan, Molecularly thick dicationic ionic liquid films for nanolubrication, AVS, 2009, pp. 986-995.
[214] V. Pejakovic, M. Kronberger, M. Mahrova, M. Vilas, E. Tojo, M. Kalin, Proc. Inst. Mech. Eng. Part J.-J. Eng. Tribol. 226 (2012) 923-932.
[215] R.A. Reich, P.A. Stewart, J. Bohaychick, J.A. Urbanski, Lubric. Eng. 59 (2003) 16-21.
[216] A. Schneider, J. Brenner, C. Tomastik, F. Franek, Lubr. Sci. 22 (2010) 215-223.
[217] A. Suzuki, Y. Shinka, M. Masuko, Trib. Lett. 27 (2007) 307-313.
[218] B. Yu, D.G. Bansal, J. Qu, X. Sun, H. Luo, S. Dai, P.J. Blau, B.G. Bunting, G. Mordukhovich, D.J. Smolenski, Wear 289 (2012) 58-64.
[219] C. Zhang, S. Zhang, L. Yu, P. Zhang, Z. Zhang, Z. Wu, Trib. Lett. 46 (2012) 49-54.
[220] K. Mistry, M.F. Fox, M. Priest, Proc. Inst. Mech. Eng. Part J.-J. Eng. Tribol. 223 (2009) 563-569.
[221] M.D. Bermúdez, A.E. Jiménez, Int. J. Surf. Sci. Eng. 1 (2007) 100-110.
[222] M.D. Bermúdez, A.E. Jiménez, Proc. Inst. Mech. Eng. Part J.-J. Eng. Tribol. 226 (2012) 977-990.
[223] M.D. Bermúdez, A.E. Jiménez, G. Martínez-Nicolás, Appl. Surf. Sci. 253 (2007) 7295-7302.
[224] F.J. Carrión, J. Sanes, M.D. Bermúdez, Mater. Lett. 61 (2007) 4531-4535.
[225] T. Espinosa, J. Sanes, A.-E. Jiménez, M.-D. Bermúdez, Appl. Surf. Sci. 273 (2013) 578-597.
[226] P. Iglesias, M.D. Bermúdez, F.J. Carrión, G. Martínez-Nicolás, Wear 256 (2004) 386-392.
[227] A. Jiménez, M.-D. Bermúdez, Trib. Lett. 33 (2009) 111-126.
[228] A.E. Jiménez, M.D. Bermúdez, Trib. Lett. 40 (2010) 237-246.
[229] A.E. Jiménez, M.D. Bermúdez, F.J. Carrión, G. Martínez-Nicolás, Wear 261 (2006) 347-359.
[230] A.E. Jiménez, M.D. Bermúdez, P. Iglesias, Trib. Int. 42 (2009) 1744-1751.
[231] A.E. Jiménez, M.D. Bermúdez, P. Iglesias, F.J. Carrión, G. Martínez-Nicolás, Wear 260 (2006) 766-782.
[232] A.-E. Jiménez, M.-D. Bermúdez, Wear 265 (2008) 787-798.
[233] J. Sanes, F.J. Carrión, M.D. Bermúdez, Wear 268 (2010) 1295-1302.
[234] J. Sanes, F.J. Carrión, M.D. Bermúdez, G. Martínez-Nicolás, Trib. Lett. 21 (2006) 121-133.
[235] J. Sanes, F.J. Carrión, A.E. Jiménez, M.D. Bermúdez, Wear 263 (2007) 658-662.
[236] J. Sanes, F.J. Carrión-Vilches, M.D. Bermúdez, e-Polymers 5 (2007).
[237] J. Qu, D.G. Bansal, B. Yu, J.Y. Howe, H. Luo, S. Dai, H. Li, P.J. Blau, B.G. Bunting, G. Mordukhovich, D.J. Smolenski, ACS Appl. Mater. Interfaces 4 (2012) 997-1002.
[238] J. Qu, P. Blau, S. Dai, H. Luo, H. Meyer, III, Trib. Lett. 35 (2009) 181-189.
[239] J. Qu, P.J. Blau, S. Dai, H. Luo, H.M. Meyer Iii, J.J. Truhan, Wear 267 (2009) 1226-1231.
[240] J. Qu, M. Chi, H. Meyer, III, P. Blau, S. Dai, H. Luo, Trib. Lett. 43 (2011) 205-211.
[241] J. Qu, J.J. Truhan, S. Dai, H. Luo, P.J. Blau, Trib. Lett. 22 (2006) 207-214.
[242] B.A. Omotowa, B.S. Phillips, J.S. Zabinski, J.M. Shreeve, Inorg. Chem. 43 (2004) 5466-5471.
[243] B.S. Phillips, J.S. Zabinski, Trib. Lett. 17 (2004) 533-541.
[244] Z. Zeng, B.S. Phillips, J.C. Xiao, J.M. Shreeve, Chem. Mat. 20 (2008) 2719-2726.
[245] D. Blanco, A.H. Battez, J.L. Viesca, R. González, A. Fernández-González, Trib. Lett. 41 (2011) 295-302.
[246] D. Blanco, R. González, A. Hernández Battez, J.L. Viesca, A. Fernández-González, Trib. Int. 44 (2011) 645-650.
[247] R. González, A. Hernández Battez, D. Blanco, J.L. Viesca, A. Fernández-González, Trib. Lett. 40 (2010) 269-277.
[248] A. Hernández Battez, R. González, J.L. Viesca, D. Blanco, E. Asedegbega, A. Osorio, Wear 266 (2009) 1224-1228.
[249] A. Hernández Battez, R. González, J.L. Viesca, A. Fernández-González, M. Hadfield, Trib. Int. 58 (2013) 71-78.
[250] J.L. Viesca, A. Hernández Battez, R. González, T. Reddyhoff, A.T. Pérez, H.A. Spikes, Wear 269 (2010) 112-117.

[251] H. Ridderikhoff, Safety, health and environmental considerations in the selection and development of base-fluids for industrial lubricants, 15th Annual General Meeting of the ELGI, Vienna, April 2003.
[252] M. Markiewicz, M. Piszora, N. Caicedo, C. Jungnickel, S. Stolte, Water Res. 47 (2013) 2921-2928.
[253] J. Redmond, E. Walker, C. Wang, J. Environ. Manage. 88 (2008) 275-285.
[254] F.M. Gaciño, X. Paredes, M.J.P. Comuñas, J. Fernández, J. Chem. Thermodyn. 62 (2013) 162-169.
[255] F.M. Gaciño, X. Paredes, M.J.P. Comuñas, J. Fernández, J. Chem. Thermodyn. 54 (2012) 302-309.
[256] J. Fernández, X. Paredes, F.M. Gaciño, M.J.P. Comuñas, A.S. Pensado, Lubr. Sci. (2013) DOI: 10.1002/ls.1236.
[257] X. Paredes, J. Fernández, A.A.H. Pádua, P. Malfreyt, F. Malberg, B. Kirchner, A.S. Pensado, J. Phys. Chem. B. 116 (2012) 14159-14170.
[258] D.G. Placek, Hydraulics. in: L.R. Rudnick, (Ed.), Synthetics, mineral oils, and bio-based lubricants. Chemistry and technology, CRC Press, Boca Raton, FL, 2006, pp. 517-540.
[259] W. Bock, Hydraulic oils. in: T. Mang, W. Dresel, (Eds.), Lubricants and lubrication, Wiley-VCH, Weinheim, 2001, pp. 246-300.
[260] C. Kajdas, A. Karpinska, A. Kulczycki, Industrial lubricants. in: R.M. Mortier, M.F. Fox, S.T. Orszulik, (Eds.), Chemistry and technology of lubricants, Springer, New York, 2010, pp. 239-292.
[261] M.P. Schneider, J. Sci. Food Agric. 86 (2006) 1769-1780.
[262] G.E. Totten, G.H. Kling, J. Reichel, Biodegradable hydraulic fluids: A review, Tampere Univ Technology, Tampere, 1999.
[263] E. Kassfeldt, G. Dave, Wear 207 (1997) 41-45.
[264] I.-S. Rhee, C. Velez, K. Von Bernewitz, Evaluation of environmentally acceptable hydraulic fluids, TACOM Research Development and Engineering Center, DTIC Document, TARDEC-TR-13640, Warren MI, 1995.
[265] L.A.T. Honary, Bioresour. Technol. 56 (1996) 41-47.
[266] H. Oğuz, M. Acaroğlu, H. Öğüt, B. İlban, Energ. Source. Part A 31 (2009) 1487-1493.
[267] T. Paeglis, P. Karabesko, I. Mierina, R. Serzane, M. Strele, V. Tupureina, M. Jure, Compositions of hydraulic fluids based on rapeseed oil and its derivatives. in: L. Malinovska, A. Mezote, E. Kronbergs, I. Nulle, (Eds.), International Scientific Conference: Engineering for Rural Development, Latvia Univ Agriculture, Faculty Engineering, Inst Mechanics, Jelgava, 2009, pp. 171-175.
[268] R. Šraj Kladivar, M. Svoljšak, M. Feldin, J. Vižintin, Goriva i maziva 39 (2000) 11-23.
[269] S.M. Yahaya, I.L. Ibrahim, Journal of Science, Technology, Mathematics and Education 9 (2012) 2-6.
[270] W.B.W. Nik, M.A. Maleque, F.N. Ani, H.H. Masjuki, Ind. Lubr. Tribol. 59 (2007) 200-208.
[271] G. Mendoza, A. Igartua, B. Fernandez-Diaz, F. Urquiola, S. Vivanco, R. Arguizoniz, Grasas Aceites 62 (2011) 29-38.
[272] D. Dowson, G.R. Higginson, Elasto-hydrodynamic lubrication: The fundamentals of roller and gear lubrication, Pergamon press, Oxford, 1966.
[273] B.J. Hamrock, P. Pan, R.-T. Lee, J. Tribol. 110 (1988) 279-284.
[274] E. Höglund, Wear 232 (1999) 176-184.
[275] B.O. Jacobson, P. Vinet, Trans. ASME, J. Tribol. 109 (1987) 709-714.
[276] C.H. Venner, J. Bos, Wear 173 (1994) 151-165.
[277] P. Katyal, P. Kumar, Trib. Int. 48 (2012) 113-121.
[278] W. Habchi, P. Vergne, S. Bair, O. Andersson, D. Eyheramendy, G.E. Morales-Espejel, Trib. Int. 43 (2010) 1842-1850.
[279] P. Kumar, M.M. Khonsari, Trib. Int. 42 (2009) 1522-1530.
[280] W. Habchi, S. Bair, J. Tribol. 135 (2012) 011502-011501-011502-011510.
[281] D.A. Lauer, Industrial gear lubricants. in: L.R. Rudnick, (Ed.), Synthetics, mineral oils, and bio-based lubricants. Chemistry and technology, CRC Press, Boca Raton, FL, 2006, pp. 441-458.
[282] I. Joseph, Driveline fundamentals and lubrication. in: R.M. Mortier, M.F. Fox, S.T. Orszulik, (Eds.), Chemistry and technology of lubricants, Springer, New York, 2010, pp. 325-344.
[283] S.C. Lakes, Automotive gear lubricants. in: L.R. Rudnick, (Ed.), Synthetics, mineral oils, and bio-based lubricants. Chemistry and technology, CRC Press, Boca Raton, FL, 2006, pp. 425-439.

[284] T. Bartels, Gear lubrication oils. in: T. Mang, W. Dresel, (Eds.), Lubricants and lubrication, Wiley-VCH, Weinheim, 2001, pp. 207-245.
[285] S. Bair, High pressure rheology for quantitative elastohydrodynamics, Elsevier Science, Oxford, 2007.
[286] B. Kržan, J. Vižintin, Vegetable based oil as a gear lubricant, International Conference on Gears, Vols 1 and 2, V D I-V D E - Verlag Gmbh, Dusseldorf, 2002, pp. 465-478.
[287] B. Kržan, J. Vižintin, Trib. Int. 36 (2003) 827-833.
[288] P. Nagendramma, Lubr. Sci. 23 (2011) 355-362.
[289] A.K. Khairuldean, T.C. Ing, M.S.C. Kob, A. Budianto, S. Bambang, T.K. Baharin, S. Ariyono, S. Syahrullail, Extreme pressure properties investigation of palm olein using four ball tribotester. in: M.A. Wahid, S. Samion, J.M. Sheriff, N.A.C. Sidik, (Eds.), 4th International Meeting of Advances in Thermofluids, Amer Inst Physics, Melville, 2012, pp. 920-927.
[290] M. Arca, B.K. Sharma, J.M. Pérez, K.M. Doll, International Journal of Sustainable Engineering (2012) 1-6.
[291] J. Omeis, M. Harperscheid, Lubricants for internal combustion engines. in: T. Mang, W. Dresel, (Eds.), Lubricants and lubrication, Wiley-VCH, Weinheim, 2001, pp. 173-206.
[292] D. Atkinson, A.J. Brown, D. Jilbert, G. Lamb, Formulation of automotive lubricants. in: R.M. Mortier, M.F. Fox, S.T. Orszulik, (Eds.), Chemistry and technology of lubricants, Springer, New York, 2010, pp. 293-324.
[293] A. Suhane, A. Rehman, H.K. Khaira, Int. J. Eng. Res. Ind. Appl. 2 (2012) 1330-1335.
[294] A. Igartua, R. Nevshupa, X. Fernandez, M. Conte, R. Zabala, J. Bernaola, P. Zabala, R. Luther, J. Rausch, Trib. Int. 44 (2011) 727-736.
[295] S. Fernando, M. Hanna, Trans. ASABE 44 (2001) 1403-1407.
[296] A.K. Singh, Ind. Crops Prod. 33 (2011) 287-295.
[297] A.R. Lansdown, Lubrication and lubricant selection. A practical guide, 3rd ed., Professional engineering publishing limited London and Bury St Edmunds, UK, 2004.
[298] S. Bair, J. Tribol. 123 (2000) 433-436.
[299] S. Bair, J. Non-Newtonian Fluid Mech. 97 (2001) 53-65.
[300] S. Bair, J. Jarzynski, W.O. Winer, Trib. Int. 34 (2001) 461-468.
[301] S. Bair, M. Khonsari, W.O. Winer, Trib. Int. 31 (1998) 573-586.
[302] S. Bair, F. Qureshi, Tribol. Trans. 45 (2002) 390-396.
[303] S. Bair, P. Vergne, M. Marchetti, Tribol. Trans. 45 (2002) 330-333.
[304] S. Bair, W.O. Winer, J. Tribol. 104 (1982) 357-364.
[305] S. Bair, W.O. Winer, J. Tribol. 112 (1990) 246-252.
[306] S. Bair, W.O. Winer, Trans. ASME, J. Tribol. 114 (1992) 1-9.
[307] S. Bair, W.O. Winer, Tribol. Trans. 36 (1993) 721-725.
[308] F.A.M.M. Gonçalves, C.S.M.F. Costa, C.E. Ferreira, J.C.S. Bernardo, I. Johnson, I.M.A. Fonseca, A.G.M. Ferreira, J. Chem. Thermodyn. 43 (2011) 914-929.
[309] G.M. Acosta, R.L. Smith, K. Arai, J. Chem. Eng. Data 41 (1996) 961-969.
[310] M. Werner, A. Baars, C. Eder, A. Delgado, J. Chem. Eng. Data 53 (2008) 1444-1452.
[311] B. Guignon, C. Aparicio, P.D. Sanz, High Pressure Research 29 (2009) 38-45.
[312] B.r.r. Guignon, C. Aparicio, P.D. Sanz, J. Chem. Eng. Data 55 (2010) 3017-3023.
[313] S. Aparicio, M. Atilhan, F. Karadas, Ind. Eng. Chem. Res. 49 (2010) 9580-9595.
[314] T. Otsu, H. Tanaka, N. Izumi, J. Sugimura, Tribology Online 4 (2009) 50-54.
[315] A. Yokozeki, Appl. Energy 84 (2007) 159-175.
[316] M. Christov, R. Dohrn, Fluid Phase Equilib. 202 (2002) 153-218.
[317] R. Dohrn, S. Peper, J.M.S. Fonseca, Fluid Phase Equilib. 288 (2010) 1-54.
[318] J.M.S. Fonseca, R. Dohrn, S. Peper, Fluid Phase Equilib. 300 (2011) 1-69.
[319] F.M. Gaciño, T. Regueira, L. Lugo, M.J.P. Comuñas, J. Fernández, J. Chem. Eng. Data 56 (2011) 4984-4999.

Chapter 2

High pressure densimetry Experimental and modelling

2.1. Introduction

Density is one of the fundamental thermodynamic properties of materials and provides valuable and practical information on the behaviour of pure fluids or mixtures for the understanding of the molecular interactions. Furthermore, accurate values of density, ρ, as a function of temperature, T, and pressure, p, are necessary in many industrial applications such as the design of several industrial processes including storage, transport and separation and mixing processes. Density is employed for the calculation of tower heights, pipe design, capacity of storage tanks, pressure corrections to liquid fugacities, compressor loads and optimization of operation conditions of industrial processes such us commercial distribution of petroleum products, among others. This property is also required in the design of equipment such as condensers, reboilers, liquid/liquid two phase mixer–settler units, material and energy balances involving liquids as well as the measurements of phase equilibrium, heat capacity and viscosity with several techniques. It is also useful to estimate other physical properties such as surface tension.

Furthermore, density is used in the identification of oils, for the calculation of temperature increase in oil layers, in the determination of Reynolds number, or the heat transfer coefficients. Moreover, $p\rho T$ values are fundamental data for developing and testing models involving equations of state, which are the main tool used for thermophysical properties prediction. Several important properties can be determined from density data. One of them is the isothermal compressibility κ_T (inverse of the bulk modulus) and another is the isobaric thermal expansion coefficient, α_p.

There are several experimental techniques for determining high pressure density values accurately, the bellows volumometer is a technique employed by Woolf and co-workers [1-12] and Uematsu and co-workers [13-19], among others. It consists on a particular type of piezometer where the fluid to be measured is fully contained within the measuring cell, preventing it from being contaminated by the pressurising medium. The entire cell, or a part of it, is a flexible bellows, which transmits the applied pressure to the fluid with a minimal loss in pressure. The linear movement of the bellows is measured to determine the compression of the fluid in the measuring cell caused by the applied pressure. [20]

The single-sinker densimeter was developed by Brachthäuser et al. [21] in the early 1990s; a brief description was also given by Wagner et al. [22] Several improvements of the densimeter were performed by Klimeck et al. [23] in subsequent years. This technique was also employed by Claus et al. [24], Chamorro et al. [25], Schilling et al. [26], Seibt et al. [27,28] and Sommer et al. [29], among others. This densimeter is based on Archimedes' buoyancy principle,

where a sinker is contained in a pressure-proof measuring cell. The sinker is connected with an analytical balance via a magnetic suspension coupling. By means of this coupling, the suspension force is contactlessly transmitted from the pressurized measuring cell to the balance at ambient atmosphere. Thus, the density of a sample fluid in the measuring cell can be determined. [30]

The vibrating wire densimeter is based on the buoyancy force exerted on a mass immersed in the test fluid to alter the resonant frequency of a thin wire from which the mass is suspended. It can be viewed as being a hydrostatic weighing method in which a vibrating-wire sensor is used to measure the buoyancy force. The sinker is suspended vertically from a thin, metallic wire, whose axial tension will depend upon the apparent weight of the sinker. The tension of the wire can be related to its resonant frequency of transverse oscillations, which can be very accurately determined under a forced mode of vibration. The difference between the resonant frequencies observed in a fluid and under vacuum permits the measurement of the density. Thus, the tension of the wire is related to its resonant frequency under steady-state transverse vibrations through a rigorous theoretical model which includes a complete analysis of the hydrodynamic effect of the fluid surrounding the wire. [31-33] This type of densimeter was employed by Wakeham and co-workers [31-39], Audonnet and Pádua [40,41], Pensado et al. [42] and Meng et al. [43,44], among others.

Other method for high pressure density determination is the vibrating tube densimeter. Density measurements of this PhD thesis were performed in this kind of densimeters. Measurements are based on the dependence between the period of oscillation of a fixed U-tube and its mass. Mechanical oscillators have proven to be one of the most versatile and accurate instruments for relative density measurements. More details about this technique will be given in next section.

2.2. Vibrating tube densimeter

The vibrating tube densimeter is a reliable, accurate and versatile method, as well as rugged and of easy operation. The vibration period τ of the U-shape tube completely filled with the sample liquid is measured and then the densities ρ of the sample liquid are computed through a relation between ρ and τ. The liquid sample is a part of the vibrating system affecting directly to its mass and thus also its resonant frequency. [45]

This type of densimeter is of common use in many laboratories. Many works have been published based in this technique, such as those of Defibaugh and co-workers [46-49], Cibulka and co-workers [50-74], Galicia-Luna and co-workers [75-94], Seitz et al. [95-98], Xiao et al. [99-102], Banipal et al. [103,104], Garg et al. [105,106], Abdulagatov et al. [45,107-111], Bobbo

and co-workers [112-117], Boned and co-workers [118-129], Gmehling and co-workers [130-137], Marsh and co-workers [138-141], Hofman and co-workers [142-146], Legido and co-workers [147-150], Morávková et al. [147-157], Outcalt and co-workers [158-161], Pečar and Doleček [162-166], Rebelo and co-workers [167-170], Richon and co-workers [171-176], Romaní and co-workers [177-179], as well as several other authors [180-202], among others.

The Thermophysical Properties Laboratory has broad experience with this type of densimeters. Many works have been published regarding measurements with the high pressure vibrating tube densimeter [203-221].

2.2.1. Measurement principle

A typical mechanical oscillator densimeter measures the frequency of vibration of an excited oscillator and its dependence on the mass of the oscillator. The oscillator consists usually of an U-shaped tube fused into a dual-wall cylinder. Direction of oscillation is perpendicular to the plane of the U-shaped sample tube. The space between the U-shaped tube and the inner wall of the dual-wall cylinder is filled with a gas of high thermal conductivity, to aid a rapid temperature equilibration of the sample inside the oscillator, and of low density, to avoid additional damping in the vibrating move. Through the dual-wall cylinder a thermostatic liquid flows.

The U-shaped tube is forced to oscillate by two magnetic dynamic converters in connection with an electronic control and amplifier circuit which guarantees constant amplitude of the oscillator tube. Under this type of geometry the system executes a simple harmonic oscillation, if the time duration of an oscillation can be made short, in order to minimize the small damping introduced by the restriction of the U-shaped connection to the support and by the gas in the inner wall of the dual-wall cylinder. This is the case when the time of response is of the order of l s. There is, in fact, a microscopic flow of fluid inside and outside during the vibration that might induce secondary flows, making the measurements dependent on the viscosity of the fluid. However the time scale of the event and the velocity of the fluid make the effect negligible, from a macroscopic point of view, or amendable by empirical means. The primary variable is the period of vibration, which is measured by a system coupled to the cell [188].

Therefore, the behaviour of the vibrating tube can be described by the simple mathematical–physical model of the undamped spring-mass system.

The basic relationship allowing derivation of the main working equations is an expression for the period of vibration, τ, at the resonance frequency in the fundamental harmonic mode:

$$\tau = 2\pi\left(\frac{m_0 + \rho V}{k}\right)^{1/2} \Rightarrow \tau^2 = 4\pi^2 \frac{m_0}{k} + 4\pi^2 \frac{\rho V}{k} \tag{2.1}$$

where m_0 is the mass of the empty U-tube (in kg), V is the inner volume of the vibrating tube (in m^3), ρ is the density of the fluid contained in the tube (in $kg \cdot m^{-3}$), and k is the vibrator constant (in $N \cdot m^{-1}$) which depends on the size and shape of the tube and is proportional to Young's modulus of the tube material.

Rearrangement of the equation (2.1) leads to the following equation:

$$\rho = \frac{k\,\tau^2}{4\pi^2 V} - \frac{m_0}{V} \tag{2.1'}$$

Definition of constants A and B as follows,

$$A = \frac{k}{4\pi^2 V} \qquad\qquad B = \frac{m_0}{V} \tag{2.2}$$

and substitution in Eq.(2.1') lead to the classical equation for vibrating tube densimeters:

$$\rho(T,p) = A(T,p)\,\tau^2(T,p) - B(T,p) \tag{2.3}$$

Parameters A and B can be determined by calibration measuring the period of oscillation of at least two substances of known density in the same conditions of temperature, T and pressure, p [20,45,132] .

2.2.2. Experimental set up, procedure and calibration

Nowadays, there are three different vibrating tube densimeters installed in the Thermophysical Properties Laboratory. Two of the densimeters, from Anton Paar, provide high pressure density measurements with high accuracy. In these densimeters the measuring and the electronic units are separated which allows a better thermostating of the sample cell. This fact also offers a greater flexibility of the system configuration. Both densimeters, named DMA 60/512P and DMA HPM are described next. The other densimeter is for measurements at atmospheric pressure and performs simultaneously measurements of density and viscosity. It is an Anton Paar SVM 3000 Stabinger Viscometer.

DMA 60/512P densimeter

The vibrating tube densimeter Anton Paar DMA 60/512P can operate between 253.15 K and 423.15 K and up to 70 MPa and consists of two different units, the electronic and interface unit named DMA 60 and the high pressure measuring cell named DMA 512P. The interface module excites the U-tube at constant amplitude, activating and sustaining a continuous vibration with natural frequency by means of the electromagnet fixed to the cell and the permanent magnet

on the tube. This module comprises also the electronics which assure an interference-free transmission of the period signal to this unit. Oscillation periods are displayed with seven significant digits. Regarding the measurement cell (DMA 512P), it contains the vibrating tube and the sensor and excitation coils and transmits into the DMA 60 the frequency signal. This signal is fed through an optical isolator for the purpose of electrical separation and then through a noise filter. The U-tube is located in a brass housing which is thermostated by the thermostat liquid. The vibration of the tube is detected with a photo-detector, by counting the blinking of light from a light source located in the same plane as the U-tube.

Experimental set up

The experimental setup of this densimeter (Fig.2.1 and 2.2) comprises, besides the aforementioned units, a pressure line connected to the densimeter and composed of a piston screw pump HiP 50-5.75-30 and a digital pressure transducer HBM PE300 calibrated with an accuracy of ± 0.02 MPa in the pressure range from 0 to 60 MPa. This pressure line is also composed of HiP ¼" stainless steel pipes and HiP valves which can operate up to 200 MPa. The experimental setup includes a temperature control system made up of a thermostatic bath Polyscience PS9110, that regulates temperature with fluctuations lower than ± 0.003 K, and a thermometer Anton Paar CKT100 located inside the measurement cell with a resolution of ± 0.001 K and an accuracy of ± 0.02 K.

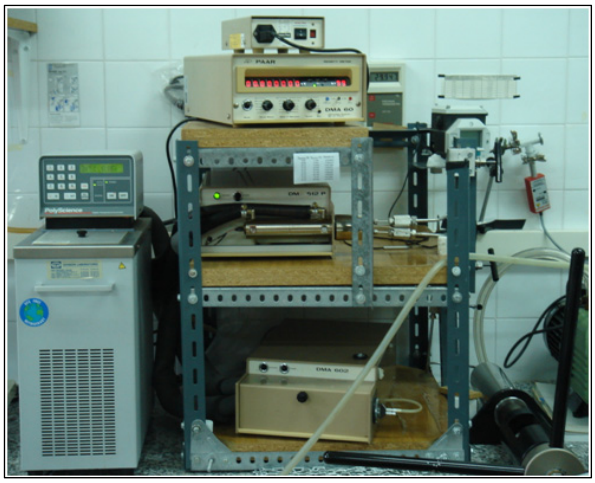

Fig.2.1. Picture of the experimental densimeter DMA 60/512P.

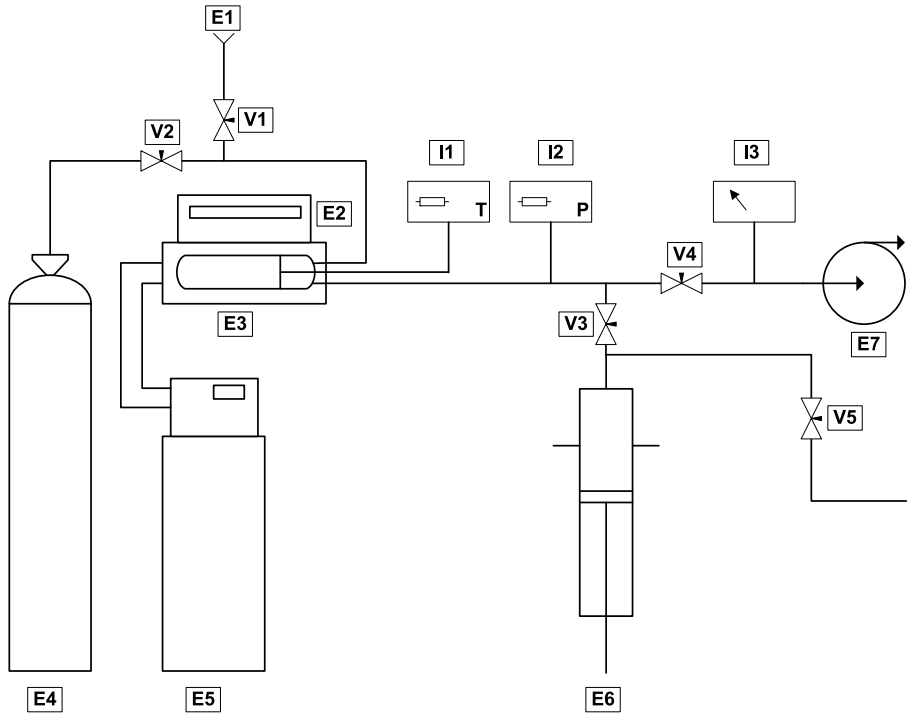

Fig.2.2. Diagram of the densimeter DMA 60/512P experimental setup. (E1) loading funnel, (E2) DMA 60 unit, (E3) DMA 512P measurement cell, (E4) nitrogen bottle, (E5) thermostatic bath, (E6) piston screw pump HiP, (E7) vacuum pump, (V1 a V5) HiP valves, (I1) thermometer CKT 100, (I2) pressure transducer HBM PE300, (I3) vacuometer.

Experimental procedure

Prior to the densimeter loading, all the system is evacuated for at least one hour by means of a rotary vacuum pump Edwards RV3 connected to the pressure line by means of a high vacuum tube Tygon R-3603. The vacuum level is checked during the evacuation process with a vacuometer Edwards Pirani 501, being the final vacuum level achieved around 8 Pa.

As soon as the system is evacuated, the oil sample, previously degassed through an ultrasonic bath Branson 2210 (DTH model), is loaded into the pressure circuit by suction through the funnel connected to the inlet valve, until a stable liquid level is observed. Then this valve is closed and the thermostatic bath is switched on.

When the thermal equilibrium is reached, the oscillation period of the measurement cell is read for the different pressures between 0.1 and 60 MPa. The pressure increase is provided by the piston screw pump HiP which reduces the total volume of the system. After measurements are finished for one isotherm, temperature set point of the thermostatic bath is increased and the described procedure is repeated. Measurements were performed from 278.15 K to 353.15 K and pressures up to 60 MPa.

Once measurements are finished for every oil, an exhaustive cleaning of the system is performed by means of a volatile solvent followed by a continuous nitrogen flow to eliminate the

remainder solvent. Afterwards, the vacuum pump is connected again to the system for a complete evacuation and density measurements of a new oil can be initiated.

Calibration

Vibrating tube densimeters are usually calibrated through the measurement of the oscillation period of two reference fluids whose densities are known with high accuracy at the working temperatures and pressures. It is necessary to make a carefully selection of these reference fluids because they have a dominant influence on the final uncertainty.

Applying Eq. (2.3) to two liquids, named 1 and 2, with known density in the temperature, T, and pressure, p, of the measurement it is possible to determine the functions $A(T, p)$ and $B(T, p)$ from this equation. The following equations are obtained:

$$\rho_1(T,p) = A(T,p)\cdot \tau_1^{\,2}(T,p) - B(T,p) \tag{2.3'}$$

$$\rho_2(T,p) = A(T,p)\cdot \tau_2^{\,2}(T,p) - B(T,p) \tag{2.3''}$$

where ρ_1 and ρ_2 are the known densities of fluids 1 and 2, and τ_1 and τ_2 the measured oscillation periods of these fluids, in the specified T and p conditions. Eqs. (2.3') and (2.3'') compose a system with two equations and two variables, whose solution can be written as follows:

$$A(T,p) = \frac{\rho_1(T,p) - \rho_2(T,p)}{\tau_1^2(T,p) - \tau_2^2(T,p)} \tag{2.4}$$

$$B(T,p) = A(T,p)\cdot\tau_2^2(T,p) - \rho_2(T,p) \tag{2.5}$$

Density of any fluid at conditions T and p can be easily determined substituting values $A(T, p)$ and $B(T, p)$ given by these last equations in Eq. 2.3.

The main problem presented by the aforementioned method is that it is necessary the knowledge of accurate density values of two fluids in a broad temperature and pressure range, and the availability of this kind of data is extremely limited. Therefore, calibration of the densimeter DMA 60/512P was performed following a method that implies only the knowledge of accurate density data in all the temperature and pressure range for one fluid whereas for the second fluid only dependence of density with temperature is needed, not with pressure. This is the method proposed by Lagourette et al. [222]. In this method it is considered that only the coefficient $B(T,p)$ varies significantly with pressure, whereas the coefficient $A(T,p)$ depends only on temperature, that is, k and V (Eq. 2.2) vary in the same manner with pressure, therefore it is possible to write $A(T,p) = A(T)$. Moreover, as the variation of the measurement cell volume between 0 MPa and 0.1 MPa is almost negligible, it is also considered in this method that $B(T,0) = B(T, 0.1\ \text{MPa})$.

Lagourette et al. [222] propose water as the first reference fluid for the density calibration because it is available at very high purity and accurate density data are published in the literature in a broad range of temperature and pressure. Thus, Wagner and Pruβ [223] have published density data with an uncertainty of 0.0001% at 0.1 MPa in the liquid phase, and 0.001% at liquid states up to 10 MPa and temperatures up to 423 K. The uncertainties rise at higher temperatures and/or pressures, but are generally lower than 0.1% except at extreme conditions. Lagourette et al. [222] propose to use the tube under vacuum instead of a second reference fluid. It should be noted that the density of air at 0.1 MPa is of the order of 10^{-3} g·cm^{-3}, whereas at a pressure of less than 100 Pa is around three orders of magnitude lower.

Therefore, following the procedure indicated by Lagourette et al. [222] it is only necessary to measure the oscillation period of the cell under vacuum in all the temperature range as well as that of water in all the required range of temperature and pressure. According to this procedure, Eq. (2.3') and (2.3'') can be written as follows for water and for vacuum:

$$\rho_w(T,p) = A(T)\tau_w^2(T,p) - B(T,p) \tag{2.6}$$

$$\rho_v(T,0) = A(T)\tau_v^2(T,0) - B(T,0) \approx 0 \tag{2.7}$$

where the subscript *w* refers to water and the subscript *v* refers to vacuum.

Hence, $B(T, p)$ can be easily calculated rewriting Eq. (2.6) as follows:

$$B(T,p) = A(T)\tau_w^2(T,p) - \rho_w(T,p) \tag{2.6'}$$

Moreover, applying Eq. (2.6) to atmospheric pressure conditions, taking into account the hypothesis of Lagourette et al. [222] ($B(T,0) = B(T,$ 0.1 MPa)), the following expression is obtained:

$$\rho_w(T,\ 0.1\,\mathrm{MPa}) = A(T)\tau_w^2(T,0.1\,\mathrm{MPa}) - B(T,0) \tag{2.8}$$

Solving the system composed by Eqs. (2.7) and (2.8) for $A(T)$, it is possible to obtain an expression for calculating this parameter as a function of temperature:

$$A(T) = \frac{\rho_w(T,0.1\mathrm{MPa})}{\tau_w^2(T,0.1MPa) - \tau_v^2(T,0)} \tag{2.9}$$

Thus, from Eq. (2.3) density of any fluid as a function of temperature and pressure, $\rho(T, p)$, can be calculated by means of the following expression:

$$\rho(T,p) = \rho_w(T,p) + \rho_w(T,0.1)\frac{\tau^2(T,p) - \tau_w^2(T,p)}{\tau_w^2(T,0.1MPa) - \tau_v^2(T,0)} \tag{2.10}$$

where τ is the oscillation period of the measured fluid.

After measuring water and vacuum periods of oscillation in the densimeter DMA 60/512P in the temperature range from 278.15 K to 353.15 K and pressures up to 60 MPa for water, it was obtained the ratio $A(T)/B(T, p)$ depicted in Fig. 2.3 (a) as a function of pressure. It is observed that this ratio diminishes very slightly with pressure. Moreover, in Fig. 2.3 (b) a linear decrease of $A(T)$ with temperature is observed. This behaviour of the vibrating tube parameters agrees with the previously reported in literature. [76,202]

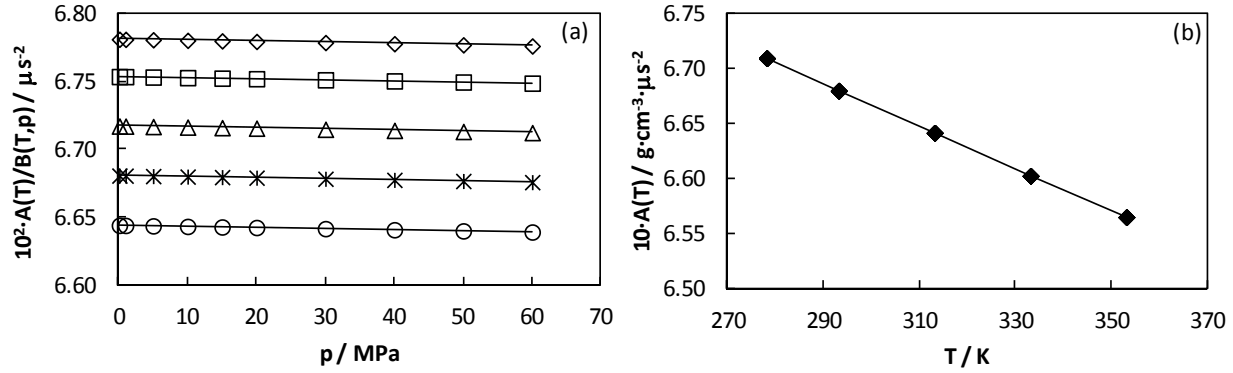

Fig.2.3. (a) Ratio between the calibration parameters $A(T)$ and $B(T, p)$ of the densimeter DMA 60/512P as a function of pressure at 278.15 K (◇), 293.15 K (□), 313.15 K (△), 333.15 K (✳) and 353.15 K (○); (b) Dependence of the parameter $A(T)$ of the densimeter DMA 60/512P with temperature.

DMA HPM densimeter

The densimeter DMA HPM can operate from 263.15 K to 473.15 K and pressures up to 140 MPa, therefore the experimental range is broader than those of the previously described DMA 60/512P. This densimeter consists also in two units, the evaluation unit mPDS 2000V3, that excites the U-tube at constant amplitude and indicates the vibration period with seven significant digits, and the measurement cell that contains the vibrating tube and is connected to the evaluation unit. This measurement cell is analogous to those of the densimeter DMA 60/512P.

Experimental set up

During the course of this PhD Thesis, the experimental set up of the densimeter DMA HPM was changed from manual operation to automated operation. Density measurements were carried out using both configurations, therefore both of them will be detailed.

Regarding the manual configuration of the DMA HPM (Fig.2.4 and 2.5), it consists of the two aforementioned units, as well as a pressure line connected to the densimeter and composed by a piston screw pump HiP model 50-5.75-30 and a pressure transducer Druck PMP4070 connected to a data acquisition unit Agilent 34970A, which can operate up to 70 MPa and is calibrated with an uncertainty of ±0.002 MPa. The pressure line is also made up of ¼" stainless steel pipes and valves HiP that can withstand up to 200 MPa. This technique also includes a temperature control system comprised by a thermostatic bath Polyscience PS9110, which

regulates temperature within ± 0.003 K. Temperature is measured with a Pt100 calibrated with an uncertainty of ± 0.02 K connected to the data acquisition unit Agilent 34970A.

Fig. 2.4. Picture of the manual configuration of the densimeter DMA HPM.

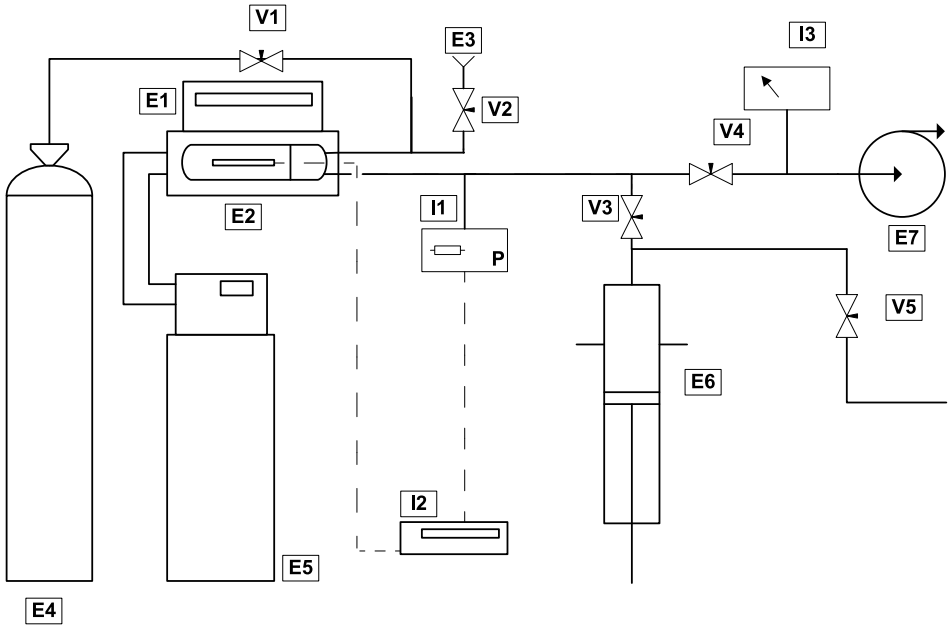

Fig.2.5. Diagram of the manual densimeter DMA HPM experimental set up. (E1) mPDS 2000V3 unit, (E2) DMA HPM measurement cell, (E3) loading funnel, (E4) nitrogen bottle, (E5) thermostatic bath, (E6) piston screw pump HiP, (E7) vacuum pump, (V1 to V5) HiP valves, (I1) pressure transducer Druck PMP4070, (I2) Agilent 34970A, (I3) vacuometer.

As concerns the automated configuration of the DMA HPM (Fig. 2.6 and 2.7), it is worth mentioning that the automation of the instrument was performed by Segovia et al. [218], who performed the following modifications to the manual configuration:

- Addition of a step by step motor (ACP&D limited type 6530-24 with a gearbox) to the mentioned HiP compressor.
- Substitution of the pressure transducer Druck PMP4070 by a digital manometer HBM Digibar II K-PE300 with a working range up to 200 MPa, calibrated with an uncertainty of ±0.02 MPa.
- The control system and data acquisition are performed by means of Agilent VEE Pro 7.0 software. The Agilent 34970A temperature and pressure data acquisition unit is remotely

controlled via IEEE 488 with a PC, whereas the rest of the apparatus is controlled via RS232 interfaces.

- The control program has three chained loops, corresponding to the temperature, pressure, and period, respectively.

Moreover, the inlet funnel was changed for a glass syringe connected to a Hamilton valve, HV Standard PTFE, in this automated configuration, when ionic liquids or other hydrophilic liquids were studied, in order to avoid the contact between these samples and the atmosphere during the densimeter filling procedure.

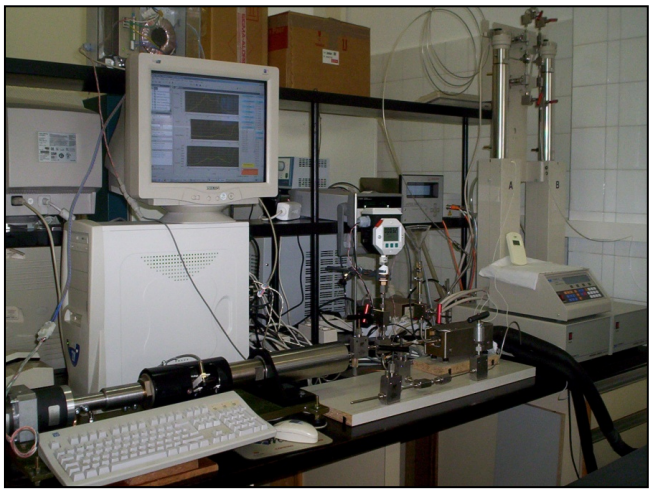

Fig.2.6. Picture of the automated configuration of the densimeter DMA HPM.

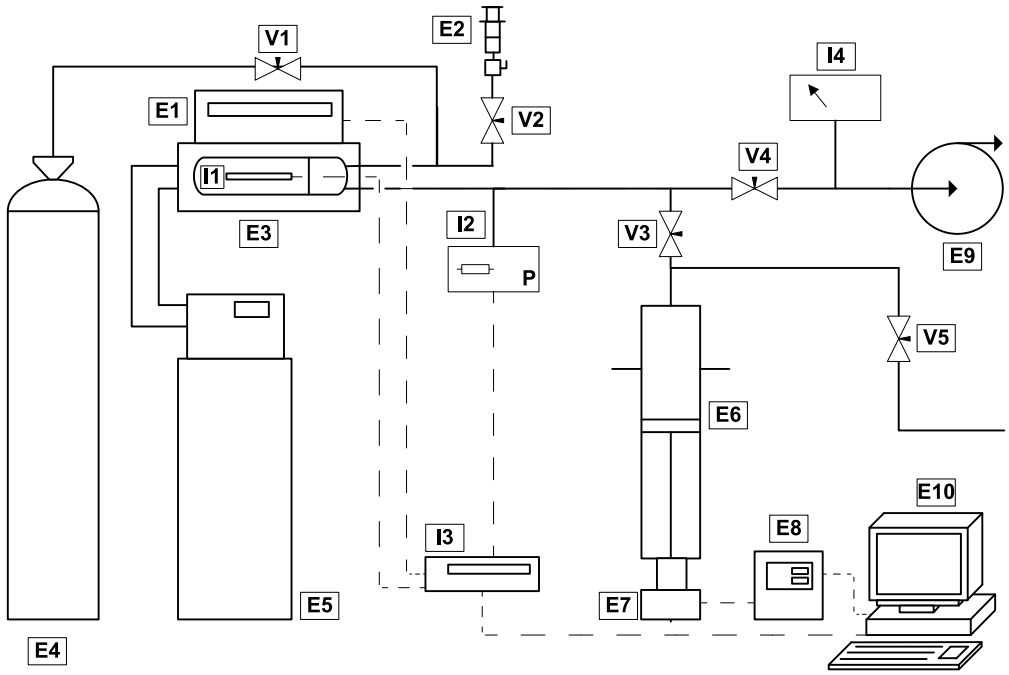

Fig.2.7. Diagram of the automated densimeter DMA HPM experimental set up. (E1) mPDS 2000V3 unit, (E2) glass syringe connected to Hamilton valve, (E3) measurement cell DMA HPM, (E4) nitrogen bottle, (E5) thermostatic bath Polyscience, (E6) piston screw pump HiP, (E7) motor, (E8) electric controls, (E9) vacuum pump, (E10) computer, (V1-V5) HiP valves, (I1) Pt100, (I2) HBM PE300 manometer, (I3) data acquisition unit, (I4) vacuometer.

Experimental procedure

As concern the manual set up, measurements were performed in the temperature range from 298.15 K to 373.15 K and up to 60 MPa. The experimental procedure is analogous to those of the densimeter DMA 60/512P. Thus, the reader is referred to that section for further details**.**

Regarding the automated set up, measurements were carried from 278.15 K to 398.15 K and up to 120 MPa. The degasification of oils and filling procedure are comparable to those of the manual set up, except for ILs. The procedure for treating ILs before filling in the apparatus is described in Appendix A.

For starting the density measurements, the operator has to insert the temperature/pressure set points in a matrix form. Thus, the program starts the first loop sending the first temperature set point to the thermostatic bath, then the piston of the screw pump is moved until the pressure set point is achieved by means of the step by step motor. The established criterion for the pressure stabilization is the standard deviation of the last ten measurements, when it is achieved, the program starts with the next loop that is the measurement of the oscillation period, checking the pressure stability in each measurement. Once the standard deviation of the last ten values of the oscillation period is lower than $1 \cdot 10^{-3}$ μs, the values of mean, maximum and minimum temperature, pressure and oscillation period are stored in an excel data sheet. Afterwards, the program starts again with the following pressure set point of this temperature. As soon as all the oscillation periods corresponding to all the pressure data points of one temperature have been stored, the program repeats the process with the next temperature set point and so forth until the last isotherm is completed. [218] Finally, cleaning of the densimeter is carried out in the same way as in the manual set up.

Calibration

Calibration of the densimeter DMA HPM for manual operation was performed in the temperature range from 298.15 K to 373.15 K and up to 60 MPa following the method of Lagourette et al. [222], in an analogous way as for the densimeter DMA 60/512P. For details of this method the reader is referred to that previous section. The only difference with the calibration of DMA 60/512P is due to the temperature range in which calibration is performed, in this case calibration being performed up to 373.15 K. As water is not liquid at this temperature and atmospheric pressure, it was used for this isotherm as hypothesis that $B(T, 0\ \text{MPa}) = B(T, 0.2\ \text{MPa})$, similarly to Boned et al. [129], instead of the one proposed by Lagourette et al. [222], $B(T, 0\ \text{MPa}) = B(T, 0.1\ \text{MPa})$.

Regarding the calibration of the densimeter DMA HPM for automated operation, it was performed in the temperature range from 278.15 K to 398.15 K and up to 120 MPa. The

calibration was performed following the modification of the Lagourete et al. [222] method proposed by Comuñas et al. [122], in order to take into account the fact that the water is not in the liquid state at temperatures higher or equal to 373.15 K at 0.1 MPa. Thus, this method can be summarised as follows:

- For temperatures between 278.15 K and 348.15 K and all the pressure range, i.e. from 0.1 to 120 MPa, the original Lagourette et al method can be applied, therefore water and vacuum are the fluids employed for calibration and Eqs. (2.6) to (2.10) apply to this temperature and pressure range.
- For temperatures $T \geq 373.15$ K at atmospheric pressure, other reference fluid different from water must be employed in the calibration at these conditions. Comuñas et al. [122] propose as alternative fluid n-decane, because its density is extensively and accurately determined at atmospheric pressure in this temperature range [224,225].

  Therefore, Eqs. (2.6'), (2.9) and (2.10) are replaced, respectively, at these conditions, by:

$$B(T,0.1\text{MPa}) = A(T)\cdot\tau_d^2(T,0.1\text{MPa}) - \rho_d(T,0.1\text{MPa}) \tag{2.11}$$

$$A(T) = \frac{\rho_d(T,0.1\text{MPa})}{\tau_d^2(T,0.1MPa) - \tau_v^2(T,0)} \tag{2.12}$$

$$\rho(T,0.1\text{MPa}) = \rho_d(T,0.1\text{MPa})\left[1 + \frac{\tau^2(T,0.1\text{MPa}) - \tau_d^2(T,0.1\text{MPa})}{\tau_d^2(T,0.1\text{MPa}) - \tau_v^2(T,0)}\right] \tag{2.13}$$

  where τ_d and ρ_d are the n-decane oscillation period and density, respectively.

- Finally, for temperatures $T \geq 373.15$ K and pressures $p > 0.1$ MPa, water is in the liquid state, thus, Eq.(2.6') applies for $B(T, p)$, whereas $A(T)$ and $\rho(T, p)$ are given by the following equations:

$$A(T) = \frac{\rho_d(T,0.1\text{MPa})}{\tau_d^2(T,0.1MPa) - \tau_v^2(T,0)} \tag{2.14}$$

$$\rho(T,p) = \rho_w(T,p) + \rho_d(T,0.1)\frac{\tau^2(T,p) - \tau_w^2(T,p)}{\tau_d^2(T,0.1MPa) - \tau_v^2(T,0)} \tag{2.15}$$

As well as in the case of the densimeter DMA 60/512P, the characteristic parameters of the densimeter DMA HPM, obtained after calibration are presented in Fig. 2.8. The same trends of the ratio $A(T)/B(T, p)$ with pressure and of $A(T)$ with temperature as in the densimeter DMA 60/512P are found, that is $A(T)/B(T, p)$ decreases slightly with pressure and $A(T)$ decreases linearly with temperature.

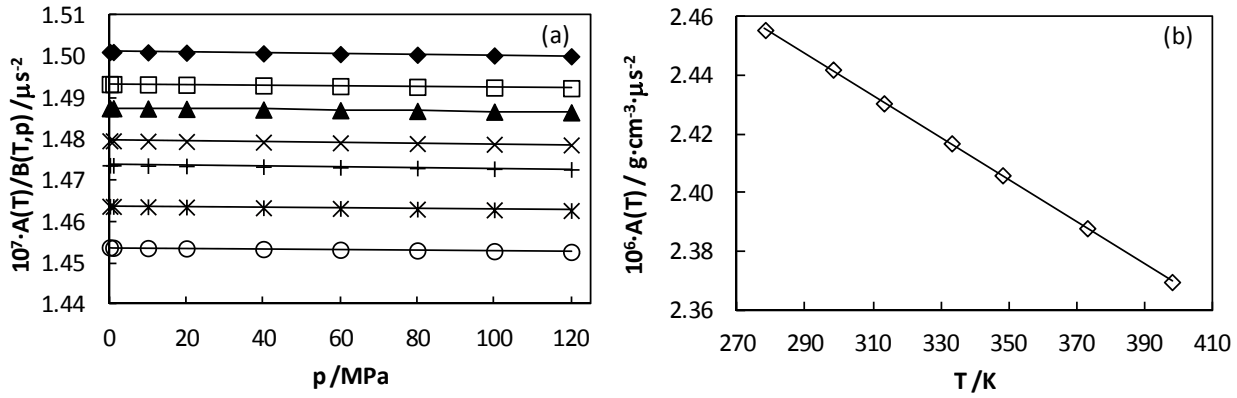

Fig.2.8. (a) Ratio between the calibration parameters $A(T)$ and $B(T, p)$ of the densimeter DMA HPM as a function of pressure at 278.15 K (◆), 298.15 K (□), 313.15 K (▲), 333.15 K (×), 348.15 K (+), 373.15 K (✳) and 398.15 K (○); (b) Dependence of the parameter $A(T)$ of the densimeter DMA HPM with temperature.

SVM 3000 Stabinger densimeter

This atmospheric pressure densimeter from Anton Paar combines the accuracy of conventional capillary viscometers with the speed and ease of use of digital densimeters (Fig.2.9). The SVM 3000 fulfills all requirements of the ASTM Standard D7042. This standard covers and specifies a procedure for the concurrent measurement of both the dynamic viscosity and the density of liquid petroleum products and crude oils.

The required determination of the sample density is undertaken by the integrated density measuring cell which works on the proven principle of the oscillating U-tube (the same used in Anton Paar's DMA series of densimeters). Density cell is a glass U-tube, which is excited to produce mechanical resonant vibrations according to DIN 51757. The measuring results can be displayed on the programmable display and transferred to the internal data memory. Data can also be sent to a printer or computer via the serial interfaces.

It also consist of a integrated thermostat with cascaded Peltier elements and Pt-100 thermometer that, along with the low thermal mass of the measuring cell, enable rapid changes and exact adjustments to the measuring temperature. This apparatus can measure in the temperature range from 233.15 K to 378.15 K. Since the lowest temperature can be only 20 K lower than the thermostatic temperature, a thermostatic bath is employed for refrigerating the measuring cell in order to achieve temperatures down to 273.15 K. The Pt-100 temperature probe is adjusted at the factory over the specified temperature range using a calibrated high-precision thermometer.

Fig.2.9. Picture of the SVM 3000 Stabinger densimeter.

Prior to density measurements oil samples were degassed for one hour through a ultrasonic bath Branson 2210 (DTH model). Measurements are performed automatically in the temperature range scan mode, which measures a specific number of points between two user-defined temperatures. The required sample volume is small, 2.5 cm^3. Cleaning is performed immediately after measurements with the suitable solvent for each sample, usually n-hexane or acetone.

Density of all the oil samples of this PhD Thesis was measured at atmospheric pressure in the SVM 3000. Density was measured in a temperature range from 278.15 K to 373.15 K whereas mixtures were measured between 253.15 K and 373.15 K

2.2.3. Uncertainties

Uncertainty of the experimental density measurements in a high pressure vibrating tube densimeter was evaluated following the rigorous procedure of the EA-4/02 guide [226] by Segovia et al. [218] taking into account uncertainties in the determination of periods of oscillation of vacuum, water and n-decane, and densities of the reference fluids (water and n-decane).

Segovia et al. [218] observed that the main contributions to this uncertainty come from the calibration procedure, through $u(A(T))$ and $u(B(T, p))$. Hence, they stand that the only way to reduce the density uncertainty is to have more reference fluids, for which precise density measurements are needed as a function of pressure and temperature.

For the DMA HPM densimeter, the expanded (k = 2) uncertainty, that corresponds to a coverage probability of approximately 95%, of the density with this technique is, according to this authors, $0.7 \cdot 10^{-3}$ g·cm^{-3} for temperatures below 373.15 K, $5 \cdot 10^{-3}$ g·cm^{-3} at p = 0.1 MPa and T = (373.15 and 398.15) K, and, finally $3 \cdot 10^{-3}$ g·cm^{-3} in the other cases, i.e. at $T \geq 373.15$ K and $p > 0.1$ MPa.

Regarding density measurements with the SVM 3000 Stabinger densimeter, repeatability based on repeated measurements performed on the same filling of the sample is ±0.0001 g/cm³, whereas this value increases to ±0.0002 g/cm³ when it is based on experience with several samples and different operators. The uncertainty of density measurements is ±0.0005 g/cm³, according to the instrument specifications.

2.2.4. Damping effect

In the previous sections it was assumed, to deduce the reported equations for the vibrating tube densimeter, that the fluid within the tube does not flow and thus the viscosity of the fluid is neglected. However, several authors have checked the influence of sample viscosity in density measurements through vibrating tube densimeter.

Thus, Bernhardt and Pauly [227] performed measurements of the specific volume of viscous samples, by using simultaneously pycnometric and densimetric methods, yielding the result that the densimeter measures higher density values. They found the same relative systematic error for different Newtonian substances depending only on the sample viscosity, and stand that this deviation is characteristic for a definite densimeter. They present, for the densimeter DMA 02 C, a quantitative relationship between the densimeter error and the sample viscosity.

Besides, Ashcroft et al. [228] have also studied the effect of the viscosity of the samples on the density readings, founding that it is significant when the viscosity is greater than 1 mPa·s. They propose a correction procedure for the densimeter DMA 602. In addition, Sanmamed et al. [229] devised a procedure for correcting the viscosity-induced errors when measuring the density of RTILs by means of vibrating tube densimeter DSA 48. Several other authors [139,141,207,211,221] have studied influence of sample viscosity on vibrating tube densimeters measurements.Anton Paar provides the following correction factor for the densimeter DMA 512 P, that can be applied in the pressure range from 0.1 to 70 MPa:

$$\frac{\rho_{512P} - \rho}{\rho_{512P}} = \left(-0.5 + 0.45\sqrt{\eta}\right)\cdot 10^{-4} \quad \text{for } \eta \leq 100 \text{ mPa·s} \tag{2.16}$$

$$\frac{\rho_{512P} - \rho}{\rho_{512P}} = 5\cdot 10^{-4} \quad \text{for } \eta \geq 400 \text{ mPa·s} \tag{2.17}$$

where η is the dynamic viscosity in mPa·s, ρ_{512P} is the direct density value obtained from the densimeter and ρ is the corrected density value. For viscosity values between 100 and 400 mPa·s an intermediate behavior of the correction factor is proposed.

For the densimeter DMA HPM, Anton Paar provided us some experimental values of the correction factor for different viscosity values. These values were correlated by Segovia et al. [218] by means of the following equations:

$$\frac{\rho_{HPM}-\rho}{\rho_{HPM}} = \left(-0.1627+0.4482\sqrt{\eta}\right)\cdot 10^{-4} \qquad \text{for } \eta \le 289 \text{ mPa·s} \tag{2.18}$$

$$\frac{\rho_{HPM}-\rho}{\rho_{HPM}} = 7.5\cdot 10^{-4} \qquad \text{for } \eta \ge 289 \text{ mPa·s} \tag{2.19}$$

where η is the dynamic viscosity in mPa·s, ρ_{HPM} is the direct density value obtained from the densimeter and ρ is the corrected density value.

These viscosity corrections, Eqs. (2.16) to (2.19), were applied in this PhD Thesis when viscosity data of the studied samples was available and the correction was higher than the measurement uncertainty.

2.2.5. Verification of the technique

Verification of the densimeter calibrations was performed by measuring different reference fluids and comparing the obtained values with literature. In order to perform this comparison, the absolute average percentage deviation (*AAD%*), the average percentage deviation (*Bias%*) and the percentage maximum deviation (*MD%*) were employed. These statisticals are defined as follows:

$$AAD(\%) = \frac{100}{N}\sum_{i=1}^{N}\left|\frac{Y_i^{\exp}-Y_i^{ref}}{Y_i^{ref}}\right| \tag{2.20}$$

$$Bias(\%) = \frac{100}{N}\sum_{i=1}^{N}\frac{Y_i^{\exp}-Y_i^{ref}}{Y_i^{ref}} \tag{2.21}$$

$$MD(\%) = \max\left(100\cdot\left|\frac{Y_i^{\exp}-Y_i^{ref}}{Y_i^{ref}}\right|\right) \tag{2.22}$$

where $Y_i^{\exp}$ is the experimental property and Y_i^{ref} is its literature value.

Densimeter DMA 60/512P

In order to check the calibration of the densimeter DMA 60/512P, density of n-hexane and toluene were measured and compared with literature values. Regarding n-hexane, experimental density values are presented in table B.1 of appendix B in the temperature range from 278.15 to 353.15 K and up to 50 MPa. These data were compared with data from the correlation proposed by Cibulka and Hnědkovský [224] and also with data from the equation proposed by Span and Wagner [230]. In the first article a correlation is proposed for n-hexane

density based on 1640 experimental points, whereas the second ones propose an equation that is based on 292 experimental points. Deviations obtained are summarised in table 2.1 and depicted as a function of pressure and temperature in Fig. 2.10. Both positive and negative values of the *Bias* are found and the experimental data agree better with data from Cibulka and Hnědkovský [224], being the *AAD* = 0.06 %. Maximum deviations found are in agreement with the combined uncertainty of our experimental technique and literature correlations.

Table 2.1 Deviations between n-hexane experimental and literature density data.

	Cibulka and Hnědkovský [224]	Span and Wagner [230]
Bias %	0.01	-0.07
AAD %	0.06	0.09
MD %	0.16	0.28

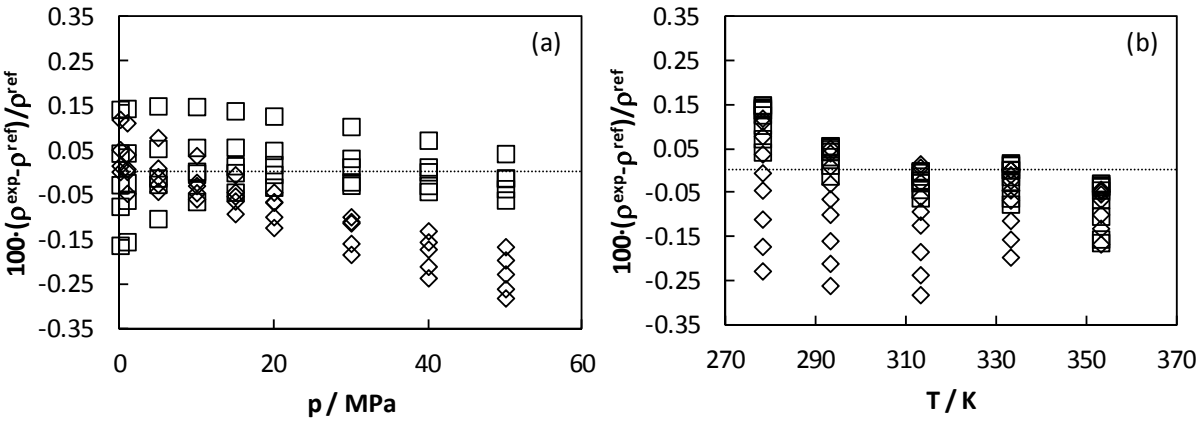

Fig.2.10. Percent deviations between experimental and literature density values of n-hexane (a) as a function of pressure and (b) as a function of temperature. (□) Cibulka and Hnědkovský [224] and (◇) Span and Wagner. [230]

As concerns toluene, experimental density values are presented in table B.2 of appendix B in the temperature range from 278.15 to 353.15 K and up to 60 MPa. These values were compared with experimental data measured by Zéberg- Mikkelsen et al. [220] and also with data obtained from the correlations proposed by Lemmon and Span [225], Assael et al. [231] and Cibulka and Takagi [232]. Zéberg- Mikkelsen et al. [220] measured toluene density from 283.15 to 353.15K and up to 45 MPa with an uncertainty of $1 \cdot 10^{-4} g \cdot cm^{-3}$. The correlation proposed by Lemmon and Span [225] has an uncertainty of 0.05% in the liquid phase up to 540 K, whereas that proposed by Assael et al. [231], taking into account 619 experimental density data, presents an standard deviation of 0.05 %. Finally, Cibulka and Takagi [232] correlation presents an standard deviation of $4 \cdot 10^{-4} g \cdot cm^{-3}$.

Deviations between the experimental density data for toluene and those from literature are presented in table 2.2 and also plotted in Fig. 2.11. The best agreement is found with data

from Zéberg- Mikkelsen et al. [220] with an *AAD* of 0.02%, although all the deviations are within the combined uncertainty of our experimental technique and literature data.

Table 2.2 Deviations between toluene experimental and literature density data.

	Zéberg- Mikkelsen et al. [220]	Lemmon and Span [225]	Assael et al. [231]	Cibulka and Takagi [232]
Bias %	-0.01	-0.04	-0.07	-0.02
AAD %	0.02	0.05	0.08	0.04
MD %	0.05	0.09	0.15	0.08

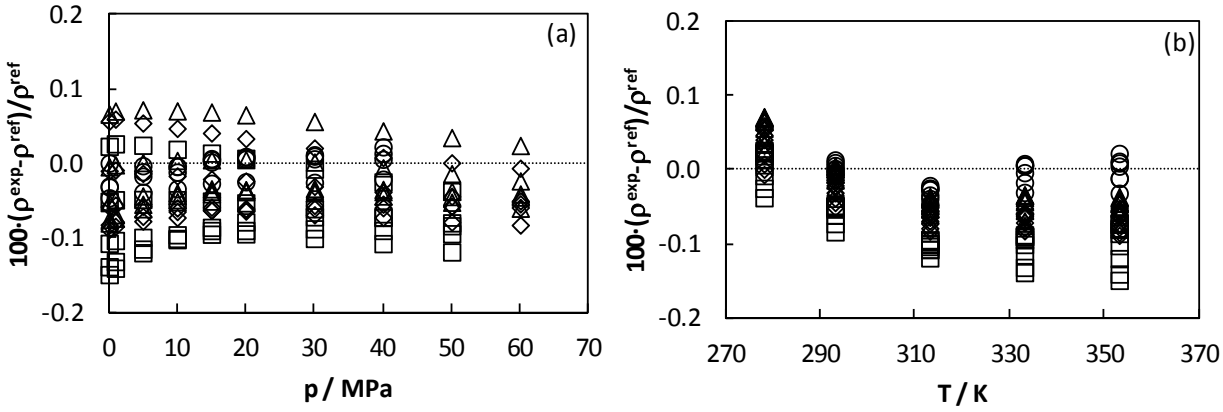

Fig.2.11. Percent deviations between experimental and literature density values of toluene (a) as a function of pressure and (b) as a function of temperature. (△) Cibulka and Takagi [232] (◇) Lemmon and Span [225], (□) Assael et al.[231] and (○) Zéberg- Mikkelsen et al. [220].

Densimeter DMA HPM

Calibration of the densimeter DMA HPM was checked by measuring density of n-decane in the experimental temperature and pressure range where these density values are not needed for calibration, i.e. from 278.15 K to 298.15 K and up to 120 MPa except the points at 278.15 K and 298.15 K and atmospheric pressure. These density data are presented in table B.3 of appendix B and were compared with literature values from the correlations proposed for n-decane by Lemmon and Span [225] and by Cibulka and Hnědkovský [224]. Deviations are summarised in table 2.3 and shown in Fig. 2.12. Both positive and negative deviations with literature are found although negative deviations are slightly more important, giving rise to negative *Bias* in both comparisons, however, the maximum deviations are within the combined uncertainty of the experimental technique and the correlations.

Table 2.3 Deviations between n-decane experimental and literature density data.

	Lemmon and Span [225]	Cibulka and Hnědkovský [224]
Bias %	-0.05	-0.01
AAD %	0.07	0.05
MD %	0.30	0.23

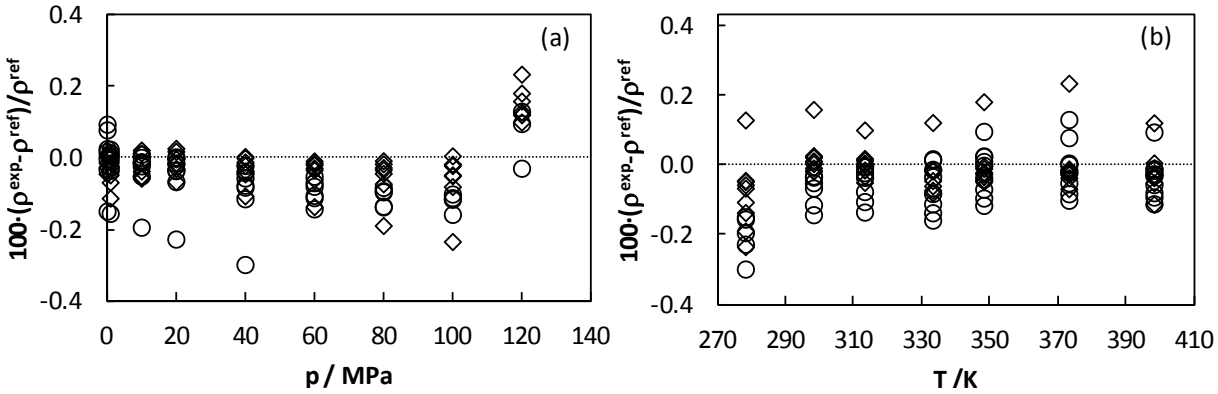

Fig.2.12. Percent deviations between experimental and literature density values of n-decane (a) as a function of pressure and (b) as a function of temperature. (○) Lemmon and Span [225] and (◇) Cibulka and Hnědkovský [224].

Additionally, Schilling et al. [26] have published a comprehensive (p,ρ,T) data of several fluids (n-heptane, n-nonane, 2,4-dichlorotoluene and bromobenzene) with the aim of providing accurate correlation equations for the densities and that these liquids can be used as density reference liquids for the calibration of densimeters. Taking this work into account, it was decided to measure also the density of bromobenzene and compare the results with Schilling et al. [26] data. Density values are presented in table B.4 of appendix B, whereas the comparison between these data and literature values is shown in Fig. 2.13. In this figure other literature data at atmospheric pressure were included. Deviations with values from Schilling et al. [26] are always positive being the AAD 0.09%, which is inside the combined uncertainty of both experimental techniques. These positive deviations are in contrast to those found for n-decane that were mainly negative.

It is important to notice that the deviation with the highly accurate density datum measured by Kuramoto et al. [233] with a magnetic suspension balance is 0.02% whereas Schilling et al. found a deviation of 0.07% with this datum.

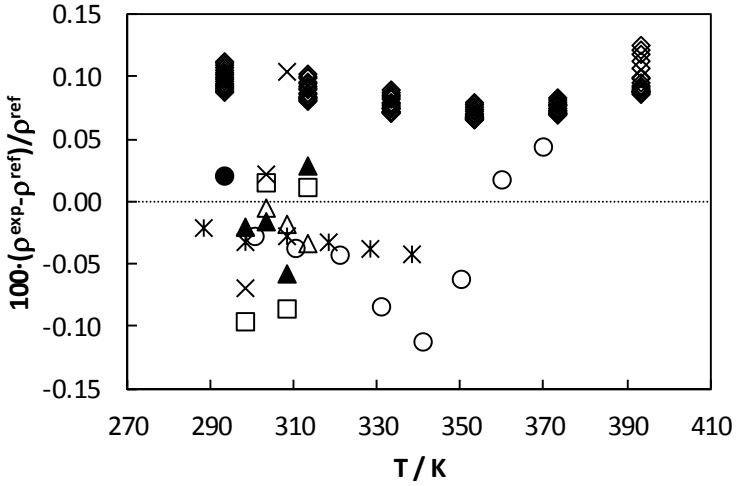

Fig.2.13. Percent deviations between experimental and literature density values of bromobenzene as function of temperature and pressures up to 30 MPa. (○) Nayard and Kudchadker [234], (×) Nayak et al. [235], (□) Ni et al. [236], (△) Rathnam et al. [237], (●) Kuramoto et al. [233], (✳) Góralski and Piekarski [238], (▲) Sastry et al. [239] and (◇) Schilling et al. [26].

Densimeter SVM 3000 Stabinger

Accuracy of the atmospheric pressure densimeter was checked by measuring density of a CANNON certified viscosity reference standard, the CANNON N350, obtaining and *AAD* of 0.03% in the temperature range from 293.15 to 373.15 K.

2.3. Density correlation and derived properties

Tait [240] published the following equation for the pressure dependence of the volume in 1988:

$$\frac{v_0 - v}{p v_0} = \frac{A}{B + p} \tag{2.23}$$

where p is the pressure, v_0 the specific volume at atmospheric pressure, v is the specific volume at pressure p and finally A and B are temperature dependent and pressure independent parameters.

Besides, in 1895 Tammann [241] published the Tammann-Tait equation as a modification of the previous Tait:

$$\frac{v_0 - v}{v_0} = C \ln\left(\frac{B + p}{B}\right) \tag{2.24}$$

where C is a pressure and temperature independent parameter and B is a temperature dependent and pressure independent parameter.

In this PhD Thesis density data as a function of temperature and pressure was correlated by means of a modified Tammann-Tait equation (Eq. 2.25). The modified Tammann-Tait equation can be applied for correlating experimental density data in broad ranges of temperature and pressure and also for performing extrapolations [224,232,242].

$$\rho(T, p) = \frac{\rho(T, 0.1\text{MPa})}{1 - C \cdot \ln\left(\frac{B(T) + p}{B(T) + 0.1\text{MPa}}\right)} \tag{2.25}$$

where $\rho(T, p)$ is the density as a function of temperature and pressure, $\rho(T, 0.1\ \text{MPa})$ is the density as a function of temperature at atmospheric pressure, given by de following equation:

$$\rho(T, 0.1\text{MPa}) = \sum_{i=0}^{m} A_i T^i \tag{2.26}$$

C is a parameter independent of temperature and pressure and $B(T)$ is a temperature dependent parameter given by the following polynomial equation:

$$B(T) = \sum_{j=0}^{n} B_j T^j \tag{2.27}$$

Isothermal compressibility, κ_T, is a density derived property defined by the following equation:

$$\kappa_T(T,p) = \frac{1}{\rho}\cdot\left(\frac{\partial\rho}{\partial p}\right)_T \tag{2.28}$$

It is possible to obtain the isothermal compressibility values of a fluid by differentiation from the Tammann-Tait equation, as follows:

$$\kappa_T(T,p) = \frac{C}{\big(B(T)+p\big)\left(1-C\ln\dfrac{B(T)+p}{B(T)+p_0}\right)} \tag{2.29}$$

As regards the thermal expansion coefficient, α_p, it is defined by this equation:

$$\alpha_p(T,p) = -\frac{1}{\rho}\cdot\left(\frac{\partial\rho}{\partial T}\right)_p \tag{2.30}$$

This property can be obtained from experimental density data either through differentiation from the Tammann-Tait equation or by differentiation from the isobaric density adjustment. Concerning the first option, the equation obtained is the following:

$$\alpha_p(T,p) = \frac{\sum_{i=1}^{n} i\cdot A_i\cdot T^{i-1}}{\sum_{i=0}^{n} A_i\cdot T^i} - \frac{C\big(0.1\text{MPa}-p\big)}{\big(B(T)+p\big)\big(B(T)+0.1\text{MPa}\big)}\cdot\frac{\sum_{j=1}^{m} j\cdot B_j\cdot T^{j-1}}{1-C\ln\left(\dfrac{B(T)+p}{B(T)+0.1\text{MPa}}\right)} \tag{2.31}$$

However, several authors [119,243,244] mentioned that the isobaric thermal expansivities determined from the Tammann–Tait equation depend strongly on the form of $\rho(T, 0.1\text{ MPa})$ and $B(T)$ functions, and they recommend to calculate this property from the isobaric density adjustment. This fact is especially important for ILs which can present non-monotonous $\alpha_p(T)$ curves.

Therefore, in this PhD Thesis, isobaric densities of ILs are also fitted by the following logarithmic equation:

$$ln(\rho) = A + BT + CT^2 + DT^3 \tag{2.32}$$

This type of equation is also employed for ILs by Nieto de Castro et al. [245] Accordingly, the isobaric thermal pressure coefficient is given by ($\alpha_p = -(\partial \ln\rho/\partial T)_p$):

$$\alpha_p = -\big(B + 2CT + 3DT^2\big) \tag{2.33}$$

and the derivative of α_p with temperature:

$$\frac{d\ln\alpha_p}{dT} = 2C + 6DT \tag{2.34}$$

Thus, the Eq. 2.32 can reproduce a non-monotonous behaviour of α_p with a minimum or maximum at T_m given by:

$$T_m = -\frac{C}{3D} \tag{2.35}$$

2.4. Methods of density prediction

2.4.1. Vegetable oils

Anand et al. [246] proposed a group contribution method for prediction the density of vegetable oils at atmospheric pressure from their fatty acid composition.

According to this method, the density of every fatty acid constituent is calculated as follows:

$$\rho_i = \frac{MW_i}{Vs_i} \tag{2.36}$$

where MW_i is the molar mass of the constituent and Vs_i is its saturated molar volume, which is calculated according to the following equation:

$$Vs_i = -\frac{RT_{ci}}{p_{ci}} Z_{RAi}^{\left[1+\left(1-Tr_i\right)^n\right]} \tag{2.37}$$

where T_{ci}, p_{ci} and T_{ri} are the critical temperature, critical pressure and reduced temperature of the constituent, respectively, and Z_{RAi} is the Racket parameter, which is defined as a function of the normal boiling point of every constituent (T_{nbi}) as follows:

$$Z_{RAi} = 0.272 - \left(3.9\cdot 10^{-5}\right) T_{nbi} \tag{2.38}$$

Thus, density of the oil is finally calculated according to this equation:

$$\rho = \sum x_i \rho_i + F_g \tag{2.39}$$

where x_i is the molar fraction of each fatty acid constituent in the oil and F_g is a correction factor due to the glycerol fragment.

On the other hand, Zong et al. [247,248] have recently proposed a fragment based approach for calculating several thermodynamic properties of fats and vegetable oils. According to this method, the liquid molar volume of triglycerides is obtained by means of the following equation:

$$V^{l} = \sum_{A} N_{frag,A} V_{A}^{l}(T) \tag{2.40}$$

where V_A^l is the liquid molar volume contribution of fragment A and $N_{frag,A}$ is the number of fragment A in the component. The temperature dependency for the liquid molar volume of fragment A is given by:

$$V_{A}^{l} = \frac{1 + B_{2,A} T}{B_{1,A}} \tag{2.41}$$

where $B_{1,A}$ and $B_{2,A}$ are the temperature dependency correlation parameters of fragment A.

2.4.2. Ionic liquids

Two group contribution methods for prediction of ILs density in broad ranges of temperature and pressure were applied in this PhD Thesis.

One of the methods was proposed by Gardas and Coutinho [249] as an extension of the Ye and Shreeve [250] group contribution method and is based on the following equation:

$$\rho = \frac{MW_i}{NV_0(a + bT + cp)} \tag{2.42}$$

where, ρ is the density in kg·m^{-3}, N is the Avogadro constant, MW_i is the molar mass in kg·mol^{-1}, T is the temperature in K, p is the pressure in MPa, V_0 is the molecular volume at the reference temperature (T_0) and pressure (p_0) in m^3·molecule^{-1} of the IL and a, b and c are fitting coefficients.

Eq. 2.42, according to these authors [249], covers the density range between 0.9867 and 1.5471 g·cm^{-3}, in a temperature range between 273.15 and 393.15 K and a pressure range between 0.10 and 100 MPa. In this range the coefficient values are a = 8.005·10^{-1}, b = 6.652·10^{-4} K^{-1} and c = −5.919·10^{-4} MPa^{-1}, at 95% level of confidence. Coefficients of the proposed density correlation were estimated using experimental densities of nine imidazolium-based ionic liquids, using a circa 800 density data points.

The other method employed was proposed by Jacquemin et al. [187] for predicting ILs density from 298.15 K to 423.15 K and up to 207 MPa. These authors assume that the IL molar volume results from the addition of the cation and anion molar volumes and they fit the effective molar volumes by means of the following equation:

$$V_{\alpha}^{*}(\delta T, p, G, H) = \frac{V_{\alpha}^{*}(\delta T, 0.1\ MPa)}{1 - G \cdot ln\left(\frac{H(\delta T) + p}{H(\delta T) + 0.1\ MPa}\right)} \tag{2.43}$$

where α stands for the cation or anion constituting an IL or for an extra -CH_2- group in the alkyl chain length of an 1-alkyl-3-methylimidazolium based IL, $V_\alpha^*(\delta T, p_{ref})$ is the reference effective molar volume and $H(\delta T)$ is a second-order polynomial. Coefficients of this method were obtained by Jacquemin et al. by using more than 5080 available density data that correspond to 38 ILs composed by 9 different anions and 15 different cations.

2.5. References

[1] A.J. Easteal, L.A. Woolf, J. Chem. Thermodyn. 17 (1985) 49-62.
[2] R. Malhotra, L.A. Woolf, J. Chem. Thermodyn. 23 (1991) 49-57.
[3] A.J. Easteal, P.J. Back, L.A. Woolf, J. Chem. Eng. Data 42 (1997) 1261-1265.
[4] R. Malhotra, L.A. Woolf, Int. J. Thermophys. 14 (1993) 1021-1038.
[5] R. Malhotra, L.A. Woolf, Fluid Phase Equilib. 92 (1994) 195-213.
[6] P.K. Kipkemboi, L.A. Woolf, J. Chem. Eng. Data 40 (1995) 943-947.
[7] R. Malhotra, L.A. Woolf, J. Chem. Thermodyn. 27 (1995) 833-845.
[8] R. Malhotra, L.A. Woolf, J. Chem. Eng. Data 41 (1996) 254-257.
[9] R. Malhotra, L.A. Woolf, J. Chem. Thermodyn. 28 (1996) 701-715.
[10] R. Malhotra, L.A. Woolf, J. Chem. Eng. Data 41 (1996) 1371-1374.
[11] R. Malhotra, L.A. Woolf, J. Chem. Thermodyn. 28 (1996) 1411-1421.
[12] P.J. Back, A.J. Easteal, R.L. Hurle, L.A. Woolf, J. Phys. E: Sci. Instrum. 15 (1982) 360.
[13] T. Ichihara, M. Uematsu, J. Chem. Thermodyn. 26 (1994) 1129-1136.
[14] M. Kamiya, K. Muroki, M. Uematsu, J. Chem. Thermodyn. 27 (1995) 337-345.
[15] Y. Suehiro, M. Nakajima, K. Yamada, M. Uematsu, J. Chem. Thermodyn. 28 (1996) 1153-1164.
[16] Y. Takiguchi, O. Osada, M. Uematsu, J. Chem. Thermodyn. 28 (1996) 1375-1385.
[17] O. Osada, M. Sato, M. Uematsu, J. Chem. Thermodyn. 31 (1999) 451-463.
[18] T. Munakata, K. Kasahara, M. Uematsu, J. Chem. Thermodyn. 34 (2002) 807-819.
[19] Y. Kabata, S. Yamaguchi, M. Takada, M. Uematsu, J. Chem. Thermodyn. 24 (1992) 1019-1026.
[20] A.R.H. Goodwin, K.N. Marsh, W.A. Wakeham, Measurement of the Thermodynamic Properties of Single Phases, Elsevier, Amsterdam, 2003.
[21] K. Brachthäuser, R. Kleinrahm, H.W. Lösch, W. Wagner, Entwicklung eines neuen Dichtemeßverfahrens und Aufbau einer Hochtemperatur-Hochdruck-Dichtemeßanlage, Fortschr.-Ber. VDI, Reihe 8, Nr. 371. VDI-Verlag: Düsseldorf, 1993.
[22] W. Wagner, K. Brachthäuser, R. Kleinrahm, H.W. Lösch, Int. J. Thermophys. 16 (1995) 399-411.
[23] J. Klimeck, R. Kleinrahm, W. Wagner, J. Chem. Thermodyn. 30 (1998) 1571-1588.
[24] P. Claus, R. Kleinrahm, W. Wagner, J. Chem. Thermodyn. 35 (2003) 159-175.
[25] C.R. Chamorro, J.J. Segovia, M.C. Martín, M.A. Villamañan, J.F. Estela-Uribe, J.P.M. Trusler, J. Chem. Thermodyn. 38 (2006) 916-922.
[26] G. Schilling, R. Kleinrahm, W. Wagner, J. Chem. Thermodyn. 40 (2008) 1095-1105.
[27] D. Seibt, S. Herrmann, E. Vogel, E. Bich, E. Hassel, J. Chem. Eng. Data 54 (2009) 2626-2637.
[28] D. Seibt, K. Vob, S. Herrmann, E. Vogel, E. Hassel, J. Chem. Eng. Data 56 (2011) 1476-1493.
[29] D. Sommer, R. Kleinrahm, R. Span, W. Wagner, J. Chem. Thermodyn. 43 (2011) 117-132.
[30] J. Klimeck, R. Kleinrahm, W. Wagner, J. Chem. Thermodyn. 33 (2001) 251-267.
[31] M. Dix, J.M.N.A. Fareleira, Y. Takaishi, W.A. Wakeham, Int. J. Thermophys. 12 (1991) 357-370.
[32] A.A.H. Pádua, J.M.N.A. Fareleira, J.C.G. Calado, W.A. Wakeham, Int. J. Thermophys. 15 (1994) 229-243.
[33] A.A.H. Pádua, J.M.N.A. Fareleira, J.C.G. Calado, W.A. Wakeham, J. Chem. Eng. Data 41 (1996) 1488-1494.
[34] H.M.T. Avelino, J.M.N.A. Fareleira, W.A. Wakeham, Int. J. Thermophys. 24 (2003) 323-336.
[35] D.R. Caudwell, J.P.M. Trusler, V. Vesovic, W.A. Wakeham, Int. J. Thermophys. 25 (2004) 1339-1352.
[36] J.L.G.C. da Mata, J.M.N.A. Fareleira, C.M.B.P. Oliveira, F.J.P. Caetano, W.A. Wakeham, High Temp.-High Press. 33 (2001) 669-676.
[37] C. Len, J. Trusler, V. Vesovic, W. Wakeham, Int. J. Thermophys. 27 (2006) 48-65.
[38] A.A.H. Pádua, J. Fareleira, J.C.G. Calado, W.A. Wakeham, Int. J. Thermophys. 17 (1996) 781-802.

[39] A.A.H. Pádua, J.M.N.A. Fareleira, J.C.G. Calado, W.A. Wakeham, J. Chem. Eng. Data 41 (1996) 731-735.
[40] F. Audonnet, A.A.H. Pádua, Fluid Phase Equilib. 181 (2001) 147-161.
[41] F. Audonnet, A.A.H. Pádua, Fluid Phase Equilib. 216 (2004) 235-244.
[42] A.S. Pensado, A.A.H. Padua, M.J.P. Comuñas, J. Fernández, J. Supercrit. Fluids 44 (2008) 172-185.
[43] X. Meng, P. Zheng, J. Wu, Z. Liu, J. Chem. Eng. Data 53 (2008) 1474-1478.
[44] X. Meng, P. Zheng, J. Wu, Z. Liu, Fluid Phase Equilib. 271 (2008) 1-5.
[45] I.M. Abdulagatov, J.T. Safarov, F.S. Aliyev, M.A. Talibov, A.N. Shahverdiyev, E.P. Hassel, Fluid Phase Equilib. 268 (2008) 21-33.
[46] D.R. Defibaugh, A.R.H. Goodwin, G. Morrison, L.A. Weber, Fluid Phase Equilib. 85 (1993) 271-284.
[47] D.R. Defibaugh, M.R. Moldover, J. Chem. Eng. Data 42 (1997) 160-168.
[48] D.R. Defibaugh, G. Morrison, J. Chem. Eng. Data 37 (1992) 107-110.
[49] D.R. Defibaugh, G. Morrison, J. Chem. Eng. Data 41 (1996) 376-381.
[50] I. Cibulka, J. Chem. Thermodyn. 42 (2010) 502-512.
[51] I. Cibulka, L. Hnědkovský, J. Chem. Thermodyn. 41 (2009) 489-498.
[52] I. Cibulka, L. Hnedkovsky, P. Hyncica, J. Mol. Liq. 131 (2007) 206-215.
[53] I. Cibulka, L. Hnedkovský, T. Marek, J. Chem. Thermodyn. 39 (2007) 1292-1299.
[54] I. Cibulka, L. Hnedkovský, T. Marek, J. Chem. Thermodyn. 39 (2007) 1286-1291.
[55] I. Cibulka, L. Hnědkovský, J. Šedlbauer, J. Chem. Thermodyn. 42 (2010) 198-207.
[56] I. Cibulka, L. Šimurka, L. Hnědkovský, A. Bolotov, J. Chem. Thermodyn. 43 (2011) 1028-1035.
[57] L. Hnedkovský, I. Cibulka, J. Chem. Thermodyn. 35 (2003) 1185-1197.
[58] L. Hnedkovský, I. Cibulka, J. Chem. Thermodyn. 39 (2007) 833-840.
[59] L. Hnedkovský, I. Cibulka, V. Hynek, J. Chem. Thermodyn. 33 (2001) 1049-1057.
[60] P. Hyncica, L. Hnedkovský, I. Cibulka, J. Chem. Thermodyn. 34 (2002) 861-873.
[61] P. Hyncica, L. Hnedkovský, I. Cibulka, J. Chem. Thermodyn. 35 (2003) 1905-1915.
[62] P. Hyncica, L. Hnedkovský, I. Cibulka, J. Chem. Thermodyn. 36 (2004) 1095-1103.
[63] P. Hyncica, L. Hnedkovský, I. Cibulka, J. Chem. Thermodyn. 38 (2006) 418-426.
[64] P. Hyncica, L. Hnedkovský, I. Cibulka, J. Chem. Thermodyn. 38 (2006) 1085-1091.
[65] P. Hyncica, L. Hnedkovský, I. Cibulka, J. Chem. Thermodyn. 38 (2006) 801-809.
[66] V. Hynek, L. Hnedkovský, I. Cibulka, J. Chem. Thermodyn. 29 (1997) 1237-1252.
[67] J. Jedelský, L. Hnedkovský, I. Cibulka, J. Chem. Thermodyn. 31 (1999) 27-42.
[68] J. Jedelský, L. Hnedkovský, P. Hyncica, I. Cibulka, J. Chem. Thermodyn. 32 (2000) 1299-1310.
[69] K. Ruzicka, L. Hnedkovský, I. Cibulka, J. Chem. Thermodyn. 32 (2000) 1221-1227.
[70] K. Ruzicka, L. Hnedkovský, I. Cibulka, J. Chem. Thermodyn. 32 (2000) 1657-1668.
[71] L. Šimurka, I. Cibulka, L. Hnědkovský, J. Chem. Eng. Data 56 (2011) 4564-4576.
[72] L. Striteská, L. Hnedkovský, I. Cibulka, J. Chem. Thermodyn. 35 (2003) 1199-1212.
[73] L. Striteská, L. Hnedkovský, I. Cibulka, J. Chem. Thermodyn. 36 (2004) 401-407.
[74] L. Stříteská, L. Hnědkovský, I. Cibulka, J. Solution Chem. 35 (2006) 1029-1036.
[75] J. de la Cruz de Dios, C. Bouchot, L.A. Galicia Luna, Fluid Phase Equilib. 210 (2003) 175-197.
[76] L.A. Galicia-Luna, D. Richon, H. Renon, J. Chem. Eng. Data 39 (1994) 424-431.
[77] R. Quevedo-Nolasco, L.A. de la Cruz-Hernández, L.A. Galicia-Luna, O. Elizalde-Solis, J. Chem. Eng. Data 56 (2011) 4226-4234.
[78] A. Zúñiga-Moreno, L. Galicia-Luna, Int. J. Thermophys. 28 (2007) 146-162.
[79] A. Zúñiga-Moreno, L.A. Galicia-Luna, J. Chem. Eng. Data 47 (2001) 155-160.
[80] A. Zúñiga-Moreno, L.A. Galicia-Luna, J. Chem. Eng. Data 47 (2001) 149-154.
[81] A. Zúñiga-Moreno, L.A. Galicia-Luna, J. Chem. Eng. Data 50 (2005) 1224-1233.
[82] A. Zúñiga-Moreno, L.A. Galicia-Luna, J. Chem. Eng. Data 52 (2007) 1773-1783.
[83] A. Zúñiga-Moreno, L.A. Galicia-Luna, J.M. Bernal-García, G.A. Iglesias-Silva, J. Chem. Eng. Data 52 (2007) 1988-1995.
[84] A. Zúñiga-Moreno, L.A. Galicia-Luna, J.M. Bernal-García, G.A. Iglesias-Silva, J. Chem. Eng. Data 53 (2007) 100-107.
[85] A. Zúñiga-Moreno, L.A. Galicia-Luna, F.F. Betancourt-Cárdenas, Fluid Phase Equilib. 236 (2005) 193-204.
[86] A. Zúñiga-Moreno, L.A. Galicia-Luna, F.F. Betancourt-Cárdenas, J. Chem. Thermodyn. 40 (2008) 96-106.

[87] A. Zúñiga-Moreno, L.A. Galicia-Luna, F.F. Betancourt-Cárdenas, J.M. Bernal-García, J. Chem. Eng. Data 51 (2006) 1723-1730.
[88] A. Zúñiga-Moreno, L.A. Galicia-Luna, L.E. Camacho-Camacho, J. Chem. Eng. Data 50 (2005) 1030-1037.
[89] A. Zúñiga-Moreno, L.A. Galicia-Luna, L.E. Camacho-Camacho, J. Chem. Thermodyn. 39 (2007) 254-260.
[90] A. Zúñiga-Moreno, L.A. Galicia-Luna, S. Horstmann, C. Ihmels, K. Fischer, J. Chem. Eng. Data 47 (2002) 1418-1424.
[91] A. Zúñiga-Moreno, L.A. Galicia-Luna, S.I. Sandler, J. Chem. Eng. Data 52 (2007) 1960-1969.
[92] A. Zúñiga-Moreno, L.A. Galicia-Luna, S.I. Sandler, J. Chem. Thermodyn. 40 (2008) 180-192.
[93] L.E. Camacho-Camacho, L.A. Galicia-Luna, J. Chem. Eng. Data 52 (2007) 2455-2461.
[94] M.S. Durán-Zenteno, H.I. Pérez-López, L.A. Galicia-Luna, O. Elizalde-Solis, J. Chem. Thermodyn. 51 (2012) 126-131.
[95] J.C. Seitz, J.G. Blencoe, J. Chem. Thermodyn. 28 (1996) 1207-1213.
[96] J.C. Seitz, J.G. Blencoe, Geochim. Cosmochim. Acta 63 (1999) 1559-1569.
[97] J.C. Seitz, J.G. Blencoe, R.J. Bodnar, J. Chem. Thermodyn. 28 (1996) 521-538.
[98] J.C. Seitz, J.G. Blencoe, Geochim. Cosmochim. Acta 63 (1999) 1559-1569.
[99] C. Xiao, H. Bianchi, P.R. Tremaine, J. Chem. Thermodyn. 29 (1997) 261-286.
[100] C. Xiao, J.M. Simonson, P.R. Tremaine, J. Chem. Thermodyn. 31 (1999) 1055-1065.
[101] C. Xiao, P.R. Tremaine, J.M. Simonson, J. Chem. Eng. Data 41 (1996) 1075-1078.
[102] C. Xiao, P. Trentaine, J. Solution Chem. 26 (1997) 277-294.
[103] T.S. Banipal, S.K. Garg, J.C. Ahluwalia, J. Chem. Thermodyn. 23 (1991) 923-931.
[104] T.S. Banipal, S.K. Garg, J.C. Ahluwalia, J. Chem. Thermodyn. 24 (1992) 729-735.
[105] S.K. Garg, J.C. Ahluwalia, J. Solution Chem. 24 (1995) 153-170.
[106] S.K. Garg, T.S. Banipal, J.C. Ahluwalia, J. Chem. Eng. Data 38 (1993) 227-230.
[107] I. Abdulagatov, A. Tekin, J. Safarov, A. Shahverdiyev, E. Hassel, Int. J. Thermophys. 29 (2008) 505-533.
[108] I. Abdulagatov, A. Tekin, J. Safarov, A. Shahverdiyev, E. Hassel, J. Solution Chem. 37 (2008) 801-833.
[109] I.M. Abdulagatov, F.S. Aliyev, M.A. Talibov, J.T. Safarov, A.N. Shahverdiyev, E.P. Hassel, Thermochim. Acta 476 (2008) 51-62.
[110] I.M. Abdulagatov, J. Safarov, T. Guliyev, A. Shahverdiyev, E. Hassel, Phys. Chem. Liq. 47 (2009) 9-34.
[111] I.M. Abdulagatov, A. Tekin, J. Safarov, A. Shahverdiyev, E. Hassel, J. Chem. Thermodyn. 40 (2008) 1386-1401.
[112] S. Bobbo, L. Fedele, M. Scattolini, R. Camporese, J. Chem. Eng. Data 47 (2002) 179-182.
[113] S. Bobbo, M. Scattolini, L. Fedele, R. Camporese, Fluid Phase Equilib. 222-223 (2004) 291-296.
[114] S. Bobbo, M. Scattolini, L. Fedele, R. Camporese, V. De Stefani, J. Chem. Eng. Data 50 (2005) 1667-1671.
[115] L. Fedele, S. Marinetti, F. Pernechele, S. Bobbo, M. Scattolini, J. Chem. Eng. Data 53 (2008) 1779-1784.
[116] L. Fedele, F. Pernechele, S. Bobbo, M. Scattolini, J. Chem. Eng. Data 52 (2007) 1955-1959.
[117] G. Scalabrin, S. Bobbo, A. Chouai, J. Chem. Eng. Data 47 (2002) 258-261.
[118] F. Alaoui, E. Montero, J.P. Bazile, M.J.P. Comuñas, C. Boned, Fluid Phase Equilib. 320 (2012) 43-48.
[119] F. Alaoui, E. Montero, J.P. Bazile, M.J.P. Comuñas, G. Galliero, C. Boned, Fluid Phase Equilib. 301 (2011) 131-136.
[120] F.E.M. Alaoui, E.A. Montero, J.-P. Bazile, F. Aguilar, C. Boned, J. Chem. Eng. Data 56 (2011) 595-600.
[121] F.E.M. Alaoui, E.A. Montero, J.-P. Bazile, F. Aguilar, C. Boned, J. Chem. Thermodyn. 43 (2011) 1768-1774.
[122] M.J.P. Comuñas, J.-P. Bazile, A. Baylaucq, C. Boned, J. Chem. Eng. Data 53 (2008) 986-994.
[123] Y. Miyake, A. Baylaucq, F. Plantier, D. Bessières, H. Ushiki, C. Boned, J. Chem. Thermodyn. 40 (2008) 836-845.
[124] Y. Miyake, A. Baylaucq, C.K. Zeberg-Mikkelsen, G. Galliero, H. Ushiki, C. Boned, Fluid Phase Equilib. 252 (2007) 79-87.

[125] Y.A. Sanmamed, D. González-Salgado, J. Troncoso, L. Romani, A. Baylaucq, C. Boned, J. Chem. Thermodyn. 42 (2010) 553-563.
[126] G. Watson, T. Lafitte, C.K. Zeberg-Mikkelsen, A. Baylaucq, D. Bessieres, C. Boned, Fluid Phase Equilib. 247 (2006) 121-134.
[127] G. Watson, C.K. Zeberg-Mikkelsen, A. Baylaucq, C. Boned, J. Chem. Eng. Data 51 (2005) 112-118.
[128] M. Yoshimura, A. Baylaucq, J.-P. Bazile, H. Ushiki, C. Boned, J. Chem. Eng. Data 54 (2009) 1702-1709.
[129] C. Boned, A. Baylaucq, J.P. Bazile, Fluid Phase Equilib. 270 (2008) 69-74.
[130] J. Berje, A. Schedemann, J. Gmehling, Fluid Phase Equilib. 300 (2011) 110-115.
[131] E.C. Ihmels, J. Gmehling, Ind. Eng. Chem. Res. 40 (2001) 4470-4477.
[132] E.C. Ihmels, J. Gmehling, Int. J. Thermophys. 23 (2002) 709-743.
[133] E.C. Ihmels, J. Gmehling, J. Chem. Eng. Data 47 (2002) 1314-1319.
[134] E.C. Ihmels, J. Gmehling, J. Chem. Eng. Data 47 (2002) 1547-1552.
[135] E.C. Ihmels, S. Horstmann, K. Fischer, G. Scalabrin, J. Gmehling, Int. J. Thermophys. 23 (2002) 1571-1585.
[136] P. Marchi, G. Scalabrin, E.C. Ihmels, K. Fischer, J. Gmehling, J. Chem. Eng. Data 51 (2006) 992-996.
[137] A. Schedemann, E.C. Ihmels, J. Gmehling, Fluid Phase Equilib. 295 (2010) 201-207.
[138] M.M. Al Motari, M.E. Kandil, K.N. Marsh, A.R.H. Goodwin, J. Chem. Eng. Data 52 (2007) 1233-1239.
[139] M.E. Kandil, K.R. Harris, A.R.H. Goodwin, K. Hsu, K.N. Marsh, J. Chem. Eng. Data 51 (2006) 2185-2196.
[140] M.E. Kandil, K.N. Marsh, A.R.H. Goodwin, J. Chem. Eng. Data 52 (2007) 2382-2387.
[141] R. Lundstrum, A.R.H. Goodwin, K. Hsu, M. Frels, D.R. Caudwell, J.P.M. Trusler, K.N. Marsh, J. Chem. Eng. Data 50 (2005) 1377-1388.
[142] A. Goldon, K. Dabrowska, T. Hofman, J. Chem. Eng. Data 52 (2007) 1830-1837.
[143] A. Goldon, I. Malka, T. Hofman, J. Chem. Eng. Data 53 (2008) 1039-1045.
[144] D. Matkowska, A. Gołdon, T. Hofman, J. Chem. Eng. Data 55 (2009) 685-693.
[145] D. Matkowska, T. Hofman, J. Mol. Liq. 165 (2012) 161-167.
[146] T. Hofman, A. Goldon, A. Nevines, T.M. Letcher, J. Chem. Thermodyn. 40 (2008) 580-591.
[147] D. Cabaleiro, M.J. Pastoriza-Gallego, M.M. Piñeiro, J.L. Legido, L. Lugo, J. Chem. Thermodyn. 50 (2012) 80-88.
[148] J. Cendón, M.M. Piñeiro, D. Bessieres, J. Vijande, J.L. Legido, J. Chem. Eng. Data 49 (2004) 1368-1372.
[149] M.M. Piñeiro, D. Bessieres, J.M. Gacio, H. Saint-Guirons, J.L. Legido, Fluid Phase Equilib. 220 (2004) 125-134.
[150] M.M. Piñeiro, D. Bessières, J.L. Legido, H. Saint-Guirons, Int. J. Thermophys. 24 (2003) 1265-1276.
[151] L. Moravkova, K. Aim, J. Linek, J. Chem. Thermodyn. 34 (2002) 1377-1386.
[152] L. Moravkova, J. Linek, J. Chem. Thermodyn. 34 (2002) 1397-1405.
[153] L. Moravkova, J. Linek, J. Chem. Thermodyn. 35 (2003) 113-121.
[154] L. Moravkova, J. Linek, J. Chem. Thermodyn. 35 (2003) 1119-1127.
[155] L. Moravkova, Z. Wagner, K. Aim, J. Linek, J. Chem. Thermodyn. 38 (2006) 861-870.
[156] L. Moravkova, Z. Wagner, J. Linek, Fluid Phase Equilib. 209 (2003) 81-94.
[157] L. Moravkova, Z. Wagner, J. Linek, J. Chem. Thermodyn. 37 (2005) 658-666.
[158] A. Laesecke, S.L. Outcalt, K.J. Brumback, Energy Fuels 22 (2008) 2629-2636.
[159] S.L. Outcalt, J. Chem. Eng. Data 56 (2011) 4239-4243.
[160] S.L. Outcalt, A. Laesecke, Energy Fuels 25 (2011) 1132-1139.
[161] S.L. Outcalt, A. Laesecke, K.J. Brumback, Energy Fuels 24 (2010) 5573-5578.
[162] D. Pecar, V. Dolecek, Fluid Phase Equilib. 211 (2003) 109-127.
[163] D. Pecar, V. Dolecek, Fluid Phase Equilib. 230 (2005) 36-44.
[164] D. Pecar, V. Dolecek, Acta Chim. Slov. 54 (2007) 538-544.
[165] D. Pecar, V. Dolecek, J. Chem. Eng. Data 52 (2007) 2442-2445.
[166] D. Pecar, V. Dolecek, J. Chem. Eng. Data 53 (2008) 929-932.
[167] J.M.S.S. Esperança, H.J.R. Guedes, M. Blesic, L.P.N. Rebelo, J. Chem. Eng. Data 51 (2005) 237-242.

[168] J.M.S.S. Esperança, Z.P. Visak, N.V. Plechkova, K.R. Seddon, H.J.R. Guedes, L.P.N. Rebelo, J. Chem. Eng. Data 51 (2006) 2009-2015.
[169] R. Gomes de Azevedo, J.M.S.S. Esperança, V. Najdanovic-Visak, Z.P. Visak, H.J.R. Guedes, M. Nunes da Ponte, L.P.N. Rebelo, J. Chem. Eng. Data 50 (2005) 997-1008.
[170] R. Gomes de Azevedo, J.M.S.S. Esperança, J. Szydlowski, Z.P. Visak, P.F. Pires, H.J.R. Guedes, L.P.N. Rebelo, J. Chem. Thermodyn. 37 (2005) 888-899.
[171] C. Jarne, F. Rivollet, D. Richon, J. Chem. Eng. Data 56 (2010) 84-88.
[172] F. Rivollet, C. Jarne, D. Richon, J. Chem. Eng. Data 50 (2005) 1883-1890.
[173] P. Stringari, G. Scalabrin, D. Richon, J. Chem. Eng. Data 53 (2008) 1789-1795.
[174] P. Stringari, G. Scalabrin, D. Richon, J. Chem. Eng. Data 54 (2009) 2285-2290.
[175] P. Stringari, G. Scalabrin, D. Richon, C. Coquelet, J. Chem. Eng. Data 53 (2008) 1167-1174.
[176] P. Stringari, G. Scalabrin, A. Valtz, D. Richon, J. Chem. Thermodyn. 41 (2009) 683-688.
[177] Y.A. Sanmamed, A. Dopazo-Paz, D. González-Salgado, J. Troncoso, L. Romaní, J. Chem. Thermodyn. 41 (2009) 1060-1068.
[178] J. Troncoso, D. Bessieres, C.A. Cerdeiriña, E. Carballo, L. Romaní, Fluid Phase Equilib. 208 (2003) 141-154.
[179] J.L. Valencia, D. González-Salgado, J. Troncoso, J. Peleteiro, E. Carballo, L. Romaní, J. Chem. Eng. Data 54 (2009) 904-915.
[180] S.T. Blanco, L. Gil, P. García-Giménez, M. Artal, S. Otín, I. Velasco, J. Phys. Chem. B. 113 (2009) 7243-7256.
[181] S. Brito e Abreu, H.M.N.T. Avelino, F.J.P. Caetano, J.o.M.N.A. Fareleira, J. Chem. Eng. Data 55 (2010) 3525-3531.
[182] C.-M.J. Chang, C.-C. Chen, Fluid Phase Equilib. 163 (1999) 119-126.
[183] H.F. Costa, R.L. Gardas, I. Johnson, I.M.A. Fonseca, A.G.M. Ferreira, J. Chem. Eng. Data 54 (2009) 256-262.
[184] R.L. Gardas, I. Johnson, D.M.D. Vaz, I.M.A. Fonseca, A.G.M. Ferreira, J. Chem. Eng. Data 52 (2007) 737-751.
[185] H. Guerrero, C. Lafuente, F.l. Royo, L. Lomba, B. Giner, Energy Fuels 25 (2011) 3009-3013.
[186] A. Inglese, P. Robert, R. De Lisi, S. Milioto, J. Chem. Thermodyn. 28 (1996) 873-886.
[187] J. Jacquemin, P. Nancarrow, D.W. Rooney, M.F. Costa Gomes, P. Husson, V. Majer, A.A.H. Pádua, C. Hardacre, J. Chem. Eng. Data 53 (2008) 2133-2143.
[188] I.M.S. Lampreia, C.A. Nieto de Castro, J. Chem. Thermodyn. 43 (2011) 537-545.
[189] S. Matsuo, W.A. Van Hook, J. Phys. Chem. 88 (1984) 1032-1040.
[190] M. Torcal, M.I. Teruel, J. García, J.S. Urieta, A.M. Mainar, J. Chem. Eng. Data 55 (2010) 5332-5339.
[191] G.A. Torín-Ollarves, J.J. Segovia, M.C. Martín, M.A. Villamañán, J. Chem. Thermodyn. 44 (2012) 75-83.
[192] W.-T. Vong, F.-N. Tsai, J. Chem. Eng. Data 42 (1997) 1116-1120.
[193] J. Yin, J. Wu, Fluid Phase Equilib. 307 (2011) 1-5.
[194] J. Yin, J. Wu, X. Meng, I. Abdulagatov, J. Chem. Thermodyn. 43 (2011) 1371-1374.
[195] C.K. Zeberg-Mikkelsen, S.I. Andersen, J. Chem. Eng. Data 50 (2005) 524-528.
[196] J. Zhou, R. Zhu, H. Xu, Y. Tian, J. Chem. Eng. Data 55 (2010) 5569-5575.
[197] C. Bouchot, D. Richon, Ind. Eng. Chem. Res. 37 (1998) 3295-3304.
[198] R. Crovetto, R.H. Wood, Fluid Phase Equilib. 65 (1991) 253-261.
[199] G. Morrison, D.K. Ward, Fluid Phase Equilib. 62 (1991) 65-86.
[200] A.T. Sousa, C.A.N.d. Castro, R. Tufeu, B.L. Neindre, High Temp.-High Press 24 (1992) 185-194.
[201] A. Petek, D. Pecar, V. Dolecek, Acta Chim. Slov. 48 (2001) 317-324.
[202] M.-J. Lee, C.-K. Lo, H.-m. Lin, J. Chem. Eng. Data 44 (1999) 1379-1385.
[203] I.L. Acevedo, L. Lugo, M.J.P. Comuñas, E.L. Arancibia, J. Fernández, J. Chem. Eng. Data 48 (2003) 1271-1278.
[204] M.J.P. Comuñas, A. Baylaucq, C. Boned, J. Fernández, J. Chem. Eng. Data 48 (2003) 1044-1049.
[205] M.J.P. Comuñas, E.R. López, P. Pires, J. García, J. Fernández, Int. J. Thermophys. 21 (2000) 831-851.
[206] M.J.P. Comuñas, P. Reghem, A. Baylaucq, C. Boned, J. Fernández, J. Chem. Eng. Data 49 (2004) 1344-1349.
[207] O. Fandiño, M.J.P. Comuñas, L. Lugo, E.R. López, J. Fernández, J. Chem. Eng. Data 52 (2007) 1429-1436.

[208] O. Fandiño, J. Garcéa, M.J.P. Comuñas, E.R. López, J. Fernández, Ind. Eng. Chem. Res. 45 (2006) 1172-1182.
[209] O. Fandiño, E.R. López, L. Lugo, J. Fernández, Fluid Phase Equilib. 296 (2010) 30-36.
[210] O. Fandiño, L. Lugo, M.J.P. Comuñas, E.R. López, J. Fernández, J. Chem. Thermodyn. 42 (2010) 84-89.
[211] O. Fandiño, A.S. Pensado, L. Lugo, M.J.P. Comuñas, J. Fernández, J. Chem. Eng. Data 50 (2005) 939-946.
[212] E.R. López, L. Lugo, M.J.P. Comuñas, J. García, J. Fernández, J. Chem. Eng. Data 49 (2004) 376-379.
[213] L. Lugo, M.J.P. Comuñas, E.R. López, J. Fernández, Fluid Phase Equilib. 186 (2001) 235-255.
[214] L. Lugo, E.R. López, M.J.P. Comuñas, J. García, J. Fernández, J. Chem. Eng. Data 49 (2004) 1400-1405.
[215] X. Paredes, O. Fandino, A.S. Pensado, M.J.P. Comunas, J. Fernandez, Trib. Lett. 45 (2012) 89-100.
[216] X. Paredes, O. Fandiño, M.J.P. Comuñas, A.S. Pensado, J. Fernández, J. Chem. Thermodyn. 41 (2009) 1007-1015.
[217] X. Paredes, O. Fandiño, A.S. Pensado, M.J.P. Comuñas, J. Fernández, J. Chem. Thermodyn. 44 (2012) 38-43.
[218] J.J. Segovia, O. Fandiño, E.R. López, L. Lugo, M. Carmen Martín, J. Fernández, J. Chem. Thermodyn. 41 (2009) 632-638.
[219] C.K. Zeberg-Mikkelsen, L. Lugo, J. Fernández, J. Chem. Thermodyn. 37 (2005) 1294-1304.
[220] C.K. Zeberg-Mikkelsen, L. Lugo, J. García, J. Fernández, Fluid Phase Equilib. 235 (2005) 139-151.
[221] O. Fandiño, A.S. Pensado, L. Lugo, E.R. López, J. Fernández, Green Chem. 7 (2005) 775-783.
[222] B. Lagourette, C. Boned, H. Saint-Guirons, P. Xans, H. Zhou, Meas. Sci. Technol. 3 (1992) 699-703.
[223] W. Wagner, A. Pruß, J. Phys. Chem. Ref. Data 31 (2002) 387-535.
[224] I. Cibulka, L. Hnědkovský, J. Chem. Eng. Data 41 (1996) 657-668.
[225] E.W. Lemmon, R. Span, J. Chem. Eng. Data 51 (2006) 785-850.
[226] Expression of the Uncertainty of Measurement in Calibration, European Cooperation for Accreditation, EA-4/02, 1999.
[227] J. Bernhardt, H. Pauly, J. Phys. Chem. 84 (1980) 158-162.
[228] S.J. Ashcroft, D.R. Booker, J.C.R. Turner, J. Chem. Soc., Faraday Trans. 86 (1990) 145-149.
[229] Y.A. Sanmamed, D. González-Salgado, J. Troncoso, C.A. Cerdeiriña, L. Romaní, Fluid Phase Equilib. 252 (2007) 96-102.
[230] R. Span, W. Wagner, Int. J. Thermophys. 24 (2003) 41-109.
[231] M.J. Assael, H.M.T. Avelino, N.K. Dalaouti, J.M.N.A. Fareleira, K.R. Harris, Int. J. Thermophys. 22 (2001) 789-799.
[232] I. Cibulka, T. Takagi, J. Chem. Eng. Data 44 (1999) 411-429.
[233] N. Kuramoto, K. Fujii, A. Waseda, Metrologia 41 (2004) S84-S94.
[234] S. Nayar, A.P. Kudchadker, J. Chem. Eng. Data 18 (1973) 356-357.
[235] J.N. Nayak, M.I. Aralaguppi, T.M. Aminabhavi, J. Chem. Eng. Data 48 (2003) 628-631.
[236] B. Ni, L. Su, H. Wang, H. Qiu, J. Chem. Eng. Data 55 (2010) 4541-4545.
[237] M.V. Rathnam, R.K.R. Singh, M.S. Kumar, J. Chem. Eng. Data 53 (2008) 265-270.
[238] P. Góralski, H. Piekarski, J. Chem. Eng. Data 52 (2007) 655-659.
[239] N.V. Sastry, R.R. Thakor, M.C. Patel, Int. J. Thermophys. 29 (2008) 610-618.
[240] P.G. Tait, Physics and Chemistry of the Voyage of H.M.S. Challenger Part IV (1888).
[241] G. Tammann, Z. Phys. Chem. 17 (1895) 620-637.
[242] I. Cibulka, L. Hnedkovsky, T. Takagi, J. Chem. Eng. Data 42 (1997) 415-433.
[243] C.A. Cerdeiriña, C.A. Tovar, D. Gonzalez-Salgado, E. Carballo, L. Romani, Phys. Chem. Chem. Phys. 3 (2001) 5230-5236.
[244] J. Troncoso, D. Bessières, C.A. Cerdeiriña, E. Carballo, L. RomanI, Fluid Phase Equilib. 208 (2003) 141-154.
[245] C.A. Nieto de Castro, E. Langa, A.L. Morais, M.L.M. Lopes, M.J.V. Lourenço, F.J.V. Santos, M.S.C.S. Santos, J.N.C. Lopes, H.I.M. Veiga, M. Macatrão, J.M.S.S. Esperança, C.S. Marques, L.P.N. Rebelo, C.A.M. Afonso, Fluid Phase Equilib. 294 (2010) 157-179.
[246] K. Anand, A. Ranjan, P.S. Mehta, Energy Fuels 24 (2010) 3262-3266.
[247] L. Zong, S. Ramanathan, C.-C. Chen, Ind. Eng. Chem. Res. 49 (2009) 876-886.
[248] L. Zong, S. Ramanathan, C.-C. Chen, Ind. Eng. Chem. Res. 49 (2010) 3022-3023.

[249] R.L. Gardas, J.A.P. Coutinho, Fluid Phase Equilib. 263 (2008) 26-32.
[250] C. Ye, J.n.M. Shreeve, J. Phys. Chem. A 111 (2007) 1456-1461.

Chapter 3

High pressure phase equilibria
Experimental and modelling

3.1. Introduction

Knowledge of the phase behaviour at high pressures is essential to understand many technical and natural processes. Pressure is one of the state variables that determine thermodynamic equilibrium and influences strongly the composition of the coexisting phases. Thus, to design and optimize high pressure chemical and separation processes such as high pressure reactions, gas processing, supercritical fluid applications and polymer processing, it is necessary to know how pressure affects the phase equilibrium. Moreover these data are needed as well in the petroleum an natural gas industries (exploitation, separation, purification, storage, transport, enhanced oil recovery, oil shales), carbon capture and storage, hydrate formation, refrigeration and heat-pump cycles, applications of ionic liquids or the study of geological processes (formation and migration of minerals, geysers, volcanoes, geothermal energy, hydrothermal synthesis…). Particularly, supercritical fluid phase behaviour, which changes greatly with small changes in temperature, pressure or composition, decides important design factors such as solvent-feed ratio, extractor and separator size and operating conditions. Thus, supercritical fluid technology and supercritical chromatography have attracted growing interest in fields as extraction, particle formation, impregnation, leather, paper and textile treatment, dyeing, cleaning and reaction in supercritical fluids. As regards near-critical conditions or gas-expanded liquids, some of the applications are chromatography, drying of aerogels, injection molding and extrusion, electronic chip manufacturing and design of drug delivery systems [1-4].

Even though computational methods for prediction of phase equilibrium have made considerable progress in the past decades, the experimental determination of phase equilibrium remains an indispensable source of data. Theoretical treatment is necessary for interpolating and extrapolating the data to new conditions and for correlating phase behaviour from the minimum amount of experimental data. In fact, many models need at least some experimental data points in order to adjust the interaction parameters. An additional challenge is the desirability of developing methods that can be used not only to correlate but also to predict data, preferably from basic fundamental parameters [2,5].

Several reviews have been published on high pressure phase equilibrium data, such as those of Hicks [6], Knapp et al. [7] and Wisniak and M. Herskowitz [8] that cover the period 1900-1983, Fornari et al. [9] for the period 1978-1987 and Dohrn and co-workers [1,10-12] for 1988-2008. Additionally, the 18 volumes of the IUPAC Solubility Data Series compile over 67,500 solubility measurements.

Regarding the techniques employed for the determination of high pressure phase equilibrium, they are classified according to several criteria. Richon and de Loos [13] as well as

Bogatu et al. [14] classify them in static and dynamic methods taking into account the working regime. Moreover, Dohrn and co-workers [1,2,10-12] classify them in analytical and synthetic methods depending on how the compositions of the two coexisting phases are determined. In this PhD Thesis the criterion employed for this classification is the same as Dohrn and co-workers:

- In the *analytical methods* (or direct sampling methods), the analysis of the composition of the coexisting phases is required. This can be done either on withdrawn samples (by refractometry, chromatography or pressure drop) or directly *in situ* (by spectroscopy or gravimetry). Samples must be representative for the equilibrium phases and the withdrawal of samples must not disturb the equilibrium studied [13,14]. Between the analytical methods the following can be distinguished:

  1. *Analytical-Isothermal Methods*: Equilibration is attained at a constant temperature, whereas the other equilibrium properties such as pressure and phase composition adjust themselves depending on the temperature, the total composition and the volume of the equilibrium cell. When equilibrium is achieved, samples from the coexisting phases are taken to analyse [2,11].

  2. *Analytical-Isobaric Methods*: One or more fluid streams are pumped continuously into a thermostated equilibrium cell and the pressure is kept constant during the experiment by controlling an effluent stream. Typically, isobaric experiments are performed in an ebulliometer. The boiling temperature of the mixture is measured under isobaric conditions and the phase compositions are determined through sampling and analysis [2,11].

  3. *Analytical-Isobaric-Isothermal Methods* (or dynamic methods): As in the analytical-isobaric methods, one or more fluid streams are pumped continuously into a thermostated equilibrium cell and the pressure is kept constant during the experiment by controlling an effluent stream. This methods can be divided in three groups [2,11]:

  - Continuous-Flow Methods: High-pressure metering pumps feed the preheated components into a mixer, where the desired temperature and phase equilibrium is attained. The feed stream from the mixer is separated in an equilibrium cell into a vapour and a liquid phase. Effluents from both phases are withdrawn continuously, depressurized, accumulated and analyzed [2,11].
  - Semiflow Methods: Only one phase is flowing while the other phase stays in an equilibrium cell. A fluid stream is passed through two cells in series containing the solute. The first cell is a presaturator and the second cell is the equilibrium cell. Upon equilibration, the effluent of the vapour phase is reduced in pressure and directed to a trap where the condensed liquid is collected. The quantity of the gas coming out of the trap can

be determined volumetrically. Most often, only the composition of the vapour phase is analyzed [2,11].

- Chromatographic Methods: Solute retention is measured in a chromatographic column and related with the Gibbs energy of solute transfer between the stationary and the mobile phase [2,11].

4. *Analytical-Spectroscopic Methods*: The spectroscopic methods allow fast analysis of phase compositions at high pressures without the need to withdraw samples [2,11].

5. *Analytical-Gravimetric Methods*: The mass of a nonvolatile condensed phase in equilibrium with a fluid phase is monitored and by using additional information, such as the density of the phases, the phase compositions can be determined [2,11].

- In the *synthetic methods* (or indirect methods) sampling is not necessary, the mixture is prepared with precisely known composition, either by weighing or pressure-volume measurements. Then pressure and temperature are measured in the equilibrium state [1,2,10-13]. Synthetic methods can be divided in the following groups:

1. *Synthetic-Visual Methods*: The appearance of a new phase is detected by visual observation, for instance, the appearance or disappearance of a meniscus or turbidity. The visual observation is not possible in isooptic systems in which the coexisting phases have approximately the same refractive index [2,11].

2. *Synthetic-Nonvisual Methods*: Instead of visual observation, other physical properties are monitored to detect the occurrence of phase transitions, for instance, measurements of relative dielectric permittivity or the use of transmitted X-rays as the basis of phase detection. The appearance of a new phase can also be obtained from the abrupt change in slope on the pressure-volume plot more accurately than by visual observation. As an alternative *pVT* measurements can be performed and the intersection of isochors can be used to determine points on the coexistence curve [11].

3. *Synthetic-Material Balance Methods*: The phase compositions at equilibrium conditions are calculated through a material balance. By application of the phase rule, at a given temperature and pressure, the density and composition of the liquid and vapour phases in equilibrium are set for a binary mixture, while the mass of each phase depends on the overall composition of the mixture. Among these methods are the isothermal one, where the pressure of a synthesized multiphase mixture is measured at isothermal conditions, the isobaric one, where the boiling temperature of a synthesized mixture is measured at isobaric conditions or the isochoric one, that is similar to the isothermal method, except that the cell has a fixed volume and pressure is measured as a function of temperature [13].

Determination of solubility in this PhD Thesis was performed by means of two different synthetic techniques, one of them uses a material balance at isochoric conditions and the other one is a visual method. Both techniques are described in the following sections.

3.2. Synthetic isochoric technique

This technique, based on an isochoric saturation technique, is similar to that employed by Wahlström and Vamling [15-18]. The base of this technique is the calculation of the quantity of gas absorbed in a known quantity of liquid solvent by means of the pressure drop observed during the gas absorption process inside a system of known volume. This apparatus is suitable for performing solubility measurements in solvents with negligible vapour pressure.

3.2.1. Experimental setup

The installation of this technique in the Thermophysical Properties Laboratory was performed by Fandiño et al. [19-21]. It can be observed in Fig.3.1.

Fig.3.1. Picture of the iscochoric apparatus for high pressure solubility measurements.

This technique comprises a temperature test chamber DYCOMETAL, CETM-40/300, inside of which it is placed the measurement system, that consists of a stainless steel pressure line (HiP OD ¼'') that connects the gas bottle with the equilibrium cell (Fig.3.2). The temperature inside the chamber is kept constant within ±0.1K. The gas cell is a commercial one (Hoke, SPUN, DOT3E1800) made of stainless steel with a volume of approximately 330 cm^3, whereas the equilibrium cell is also of stainless steel with an inner diameter of 29.8 mm and a volume of around 16 cm^3. A magnetic stirrer with a remote control is placed under the equilibrium cell. The equilibrium cell is connected through the needle valve (V4) (HiP) and the ball valve (V5) (Hoke, 71 Series) to the gas cell (E7). We have named this last configuration '*measurement system*', whereas the system consisting on the gas cell until V4 is named '*gas*

system'. Both, the gas cell and the equilibrium cell are placed inside jacketed glasses that are thermostated through a thermostatic bath (Polyscience PS9512) located outside the temperature test chamber, which controls the temperature with fluctuations lower than ±0.01 K. Moreover, a pressure transducer Paroscientific 42K-HT-101, I1, is located in the pressure line and the system temperature is measured by means of two temperature probes Pt-100 placed inside the jacketed glasses and connected to a thermometer ASL F250, with an accuracy of ±0.02 K. Both the pressure transducer and the thermometer are connected to a computer where the values of temperature and pressure are recorded and plotted.

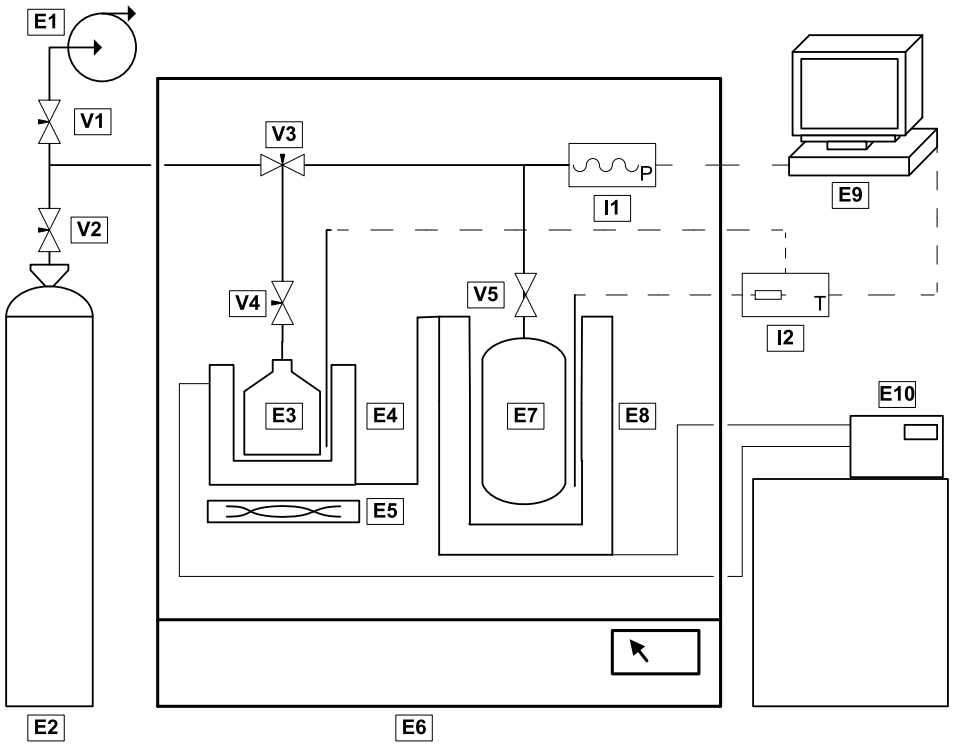

Fig.3.2. Solubility apparatus diagram. (E1) Vacuum pump, (E2) gas cylinder, (E3) equilibrium cell, (E4, E8) jacketed glasses, (E5) magnetic stirrer, (E6) temperature test chamber, (E7) gas cell, (E9) computer, (E10) thermostatic bath, (V1 to V5) valves, (I1) pressure transducer, (I2) thermometer.

Additionally, this experimental technique comprises a vacuum pump for evacuation of the system, a precision balance (Mettler Toledo, XP5003S) for determining the initial quantities of solute and solvent employed and a vacuum line analogous to those of Fig. A.1 (appendix A) for degasification of the solvent.

This technique operates in the temperature range from 283 K to 348 K and pressures up to 10 MPa, its main specifications being presented in table 3.1.

Table 3.1. Specifications of the isochoric technique for solubility measurements.

Device	Measurement range	Resolution	Uncertainty
Temperature test chamber DYCOMETAL CETM-40/300	233.15-423.15 K	±0.01 K	±0.1 K
Thermometer ASL F250	233.15-423.15 K	±0.001K	±0.02 K
Transducer Paroscientific 42K-HT-101	0.01-0.3 MPa	±0.0001 MPa	0.01%
	0.3-1.4 MPa	±0.0001 MPa	$1.4 \cdot 10^{-4}$ MPa
	1.4-13.8 MPa	±0.0001 MPa	0.01 %
Balance Mettler Toledo XP5003S	0-1000 g	±0.001 g	±0.001 g
	1000-5000 g	±0.01 g	±0.01 g

3.2.2. Experimental procedure

The solvent is introduced in the equilibrium cell along with the magnetic bar and is degassed in the vacuum line, after that, the amount of solvent is weighted in the high precision balance. The gas cell is evacuated with the vacuum pump and filled with gas from the gas cylinder. The quantity of gas filled in this cell is also accurately determined by using the high precision balance.

Afterwards, both cells are placed inside the temperature test chamber and connected to the pressure line. Valves V4 and V5 remain closed while the pressure line is evacuated through V3. Once the vacuum achieved is adequate, V3 is closed and the desired temperature set point is fixed for both, the test chamber and the thermostatic bath. Once temperature is stable, V4 and V5 are opened, thus the solute comes in contact with the solvent. Then, the magnetic stirred is switched on and pressure starts to decrease due to solubilisation. Pressure drop is recorded in the computer as well as temperature. After one or two hours the equilibrium is achieved and pressure remains constant. At this moment the magnetic stirred is switched off and an additional time is waited. Finally the values of pressure and temperature in the equilibrium are annotated and measurements at the next temperature can start. In this PhD Thesis solubility measurements through this technique were performed at 283.15 K, 298.15 K, 323.15 K and 348.15 K. Once equilibrium values at all the desired temperatures are measured, the above described procedure is repeated with different gas quantities.

3.2.3. Volume calibration

Knowledge of the volumes of the gas system and of the equilibrium cell is necessary to perform the mass balance for the solubility calculations. Thus, volumes of the gas system ($V_{gas\ s.}$) and of the measurement system ($V_{mes\ s.}$) have been determined as a function of temperature by Fandiño [22]. The system was filled with a precise quantity of N_2, and the values of the pressure of this system as a function of temperature were annotated. By evaluation of the density of N_2 at these temperature and pressure conditions, by means of the reference equation of state of Span et al. [23], the volume of the system was obtained for the different temperatures. The obtained volume values were correlated [22] as a function of temperature according to polynomial Eqs. (3.1) and (3.2) and parameters of these correlations are presented in table 3.2.

$$V_{gas\ s.}(T) = A + BT + CT^2 \tag{3.1}$$

$$V_{mes\ s.}(T) = A + BT + CT^2 \tag{3.2}$$

where T is the temperature in K and volumes are expressed in cm^3.

Table 3.2. Parameters of Eqs. (3.1) and (3.2) along with standard deviation (σ).

	A /cm^3	B /cm^3K^{-1}	C /cm^3K^{-2}	σ / cm^3
$V_{gas\ s.}$	336.548	13.35	4.92	0.10
$V_{mes\ s.}$	354.1014	9.344	6.32	0.06

From these correlations the volume of the equilibrium cell as a function of temperature ($V_{cell(T)}$) can be easily calculated by means of the following equation (Eq. (3.3)):

$$V_{cell}(T) = V_{mes\ s.}(T) - V_{gas\ s.}(T) \tag{3.3}$$

3.2.4. Solubility calculation

The quantity of gas initially introduced in the gas cell is referred as m_1 whereas the quantity of degassed lubricant in the equilibrium cell is referred as m_2. Therefore, the quantity of gas absorbed by the lubricant (m_1^{ab}) is given by the following equation:

$$m_1^{ab} = m_1 - m_1^g \tag{3.4}$$

where m_1^g is the quantity of gas not absorbed by the lubricant, given by the following expression:

$$m_1^g = \rho_1(T_{gas\ s.}, p) V_{gas\ s.}(T_{gas\ s.}) + \rho_1(T_{cell}, p)\left[V_{cell}(T_{cell}) - \left(\frac{m_2}{\rho_2(T_{cell}, p)} + V_{abs\ g.}(T_{cell}, p)\right)\right] \tag{3.5}$$

where $\rho_1(T_{gas\ s.}, p)$ is the gas density at equilibrium temperature of the gas system and equilibrium pressure, $V_{gas\ s.}(T_{gas\ s.})$ the volume of the gas system at the equilibrium temperature of the gas system, $\rho_1(T_{cell}, p)$ the gas density at the equilibrium cell temperature and equilibrium pressure, $\rho_2(T_{cell}, p)$ the lubricant density at the equilibrium cell temperature and equilibrium pressure, $V_{cell}(T_{cell})$ the equilibrium cell volume at the equilibrium cell temperature and $V_{abs\ g.}(T_{cell}, p)$ the volume of the absorbed gas at the equilibrium cell temperature and equilibrium pressure.

Furthermore, the volume of absorbed gas at the equilibrium cell temperature and equilibrium pressure can be written as the product of the partial specific volume in the liquid phase $\bar{v}_{abs\ g.}$ by the mass of absorbed gas:

$$V_{abs\ g.}(T_{cell}, p) = \bar{v}_{abs\ g.}(T_{cell}, p) \cdot m_1^{ab} \tag{3.6}$$

When experimental data of the partial specific volume of the solute in the liquid phase are not available, they should be estimated. Thus, according to Wahlström and Vamling [17], the following two situations are distinguished in order to estimate the partial specific volume in the liquid phase:

(1) $T_{cell} < T_{sat,gas}$, then $\bar{v}_{absg.}(T_{cell}, p)$ is calculated as the liquid specific volume at the equilibrium conditions, T_{cell}, p. $T_{sat,gas}$ being the saturation temperature of the gas.

(2) $T_{cell} > T_{sat,gas}$, then $\bar{v}_{absg.}(T_{cell}, p)$ is calculated as the liquid specific volume at the bubble point if $T_{cell} < T_{c,gas}$, and as the specific volume at infinite dilution in liquid phase following the method proposed by Zellner et al. [24] if $T_{cell} > T_{c,gas}$, $T_{c,gas}$ being the critical temperature.

The method proposed by Zellner et al. [24] stands that in the absence of sufficient experimental information, the partial molar liquid volumes are assumed to be independent of the solution pressure and composition and are equal to the volume of the pure-component saturated liquid at the system temperature. Thus, the liquid volumes can be obtained from the Lyckman et al. [25] generalized correlation, Eqs. (3.7)-(3.11), who obtained useful extrapolations for this property at temperatures greater than critical:

$$V_r = V_r^0 + \omega V_r^1 + \omega^2 V_r^2 \tag{3.7}$$

$$V_r^0 = 0.383252 \qquad \text{if} \qquad T_r \le 0.558 \tag{3.8}$$

$$V_r^0 = 1.151829 - \frac{0.8579705}{T_r} + \frac{0.2394401}{T_r^2} \quad \text{if} \qquad T_r > 0.558 \tag{3.9}$$

$$V_r^1 = 0.0719319 - 0.1112 \arctan\left[\frac{0.56245 \cdot \frac{0.610601}{T_r}}{1 - \left(\frac{0.610601}{T_r}\right)^2}\right] \tag{3.10}$$

$$V_r^2 = -0.202516 + 0.1112 \arctan\left[\frac{0.1620136 \cdot \frac{0.657466}{T_r}}{1 - \left(\frac{0.657466}{T_r}\right)^2}\right] \tag{3.11}$$

where V_r is the reduced molar volume and T_r the reduced temperature.

Finally, in order to obtain the value of m_1^{ab} we replace in Eq. (3.4) the value of m_1^g given by Eq. (3.5), and we substitute in Eq. (3.5) the value of $V_{abs\,g.}(T_{cell}, p)$ given by Eq. (3.6). Thus, we obtain the following expression:

$$m_1^{ab} = \frac{m_1 - \rho_1(T_{gas\,s.}, p) \cdot V_{gas\,s.}(T_{gas\,s.}) - \rho_1(T_{cell}, p)\left(V_{cell}(T_{cell}) - \frac{m_2}{\rho_2(T_{cell}, p)}\right)}{1 - \rho_1(T_{cell}, p) \cdot \bar{v}_{abs\,g.}(T_{cell}, p)} \tag{3.12}$$

Therefore, it is possible to calculate the mass fraction of the gas absorbed by the lubricant by means of:

$$w_1 = \frac{m_1^{ab}}{m_1^{ab} + m_2} \tag{3.13}$$

3.2.5. Uncertainty

In the calculation of the uncertainty of isochoric techniques for gas-liquid solubility measurements several variables, such as the purity of the materials, pressure, volume and temperature [26] can be statistically determined. However, we must take into account, as stood by Cook and Hanson [27], that uncertainty of these techniques is most probably due to other factors such as the failure to attain equilibrium, to completely degas the solvent, to ascertain the true amount of gas dissolved and to make certain that the transfer of gas from a primary container to the apparatus does not involve contamination.

In this PhD Thesis the uncertainty of solubility measurements through the isochoric technique was calculated following the rigorous procedure of the EA-4/02 guide [28] with an expanded uncertainty of measurement given by a coverage factor k =2. The uncertainty of the mass fraction of absorbed gas (w_1) was considered to depend on the uncertainty of the following variables: temperature (T) and pressure (p), mass and density of both components (m_1, m_2, ρ_1,

ρ_2), volume of the gas system and the measurement cell ($V_{gas\ s.}$, V_{cell}) as well as the partial specific volume of absorbed gas ($\bar{v}_{abs\ g.}$). Thus, equation (3.13) was rewritten as a function of these variables as follows:

$$w_1 = \frac{m_1 - \rho_1(T_{gas\ s.},p)V_{gas\ s.}(T_{gas\ s.}) - \rho_1(T_{cell},p)\left(V_{cell}(T_{cell}) - \dfrac{m_2}{\rho_2(T_{cell},p)}\right)}{m_1 - \rho_1(T_{gas\ s.},p)V_{gas\ s.}(T_{gas\ s.}) - \rho_1(T_{cell},p)\left(V_{cell}(T_{cell}) - \dfrac{m_2}{\rho_2(T_{cell},p)}\right) + m_2\left(1-\rho_1(T_{cell},p)\bar{v}_{abs\,g.}(T_{cell},p)\right)} \qquad (3.13')$$

Consequently, the expanded uncertainty (k=2) for w_1, $U(w_1)$, is obtained from the uncertainty of the different dependent variables (u) by means of the following equation:

$$U(w_1) = 2\left[\left(\frac{\partial w_1}{\partial m_1}\right)^2 u^2(m_1) + \left(\frac{\partial w_1}{\partial m_2}\right)^2 u^2(m_2) + \left(\frac{\partial w_1}{\partial \rho_1}\right)^2 u^2(\rho_1) + \left(\frac{\partial w_1}{\partial \rho_2}\right)^2 u^2(\rho_2) + \left(\frac{\partial w_1}{\partial V_{gas\,s.}}\right)^2 u^2(V_{gas\,s.}) + \left(\frac{\partial w_1}{\partial V_{cell}}\right)^2 u^2(V_{cell}) + \left(\frac{\partial w_1}{\partial \bar{v}_{abs\,g.}}\right)^2 u^2(\bar{v}_{abs\,g.})\right]^{1/2} \qquad (3.14)$$

Thus, the uncertainty budget of the isochoric technique is presented in table 3.3. Due to the approximations performed in the calculation of the partial specific volume of absorbed gas, the uncertainty of this property was estimated to be 50%. It can be observed that the uncertainty in the mass fraction of the absorbed gas varies between $2\cdot10^{-3}$ and $5\cdot10^{-2}$ for the different CO_2 + oil systems studied.

Table 3.3. Uncertainty budget for w_1, in the isochoric solubility technique, according to EA-4/02.

$u(x_i)$	Estimate	Units	$\lvert(\partial w_1/\partial x_i)\cdot u(x_i)\rvert$
$u(T)$	0.02	K	$1\cdot10^{-6}$ - $1\cdot10^{-4}$
$u(p)$	$1.4\cdot10^{-4}$/0.01%	MPa	$1\cdot10^{-8}$ - $3\cdot10^{-3}$
$u(m_1)$	0.001	g	$2\cdot10^{-3}$
$u(m_2)$	0.001	g	$3\cdot10^{-8}$ - $3\cdot10^{-5}$
$u(\rho_1)$	0.0007	g·cm^{-3}	$7\cdot10^{-4}$ - $7\cdot10^{-3}$
$u(\rho_2)$	0.05%	g·cm^{-3}	$1\cdot10^{-5}$ - $2\cdot10^{-4}$
$u(V_{gas\,s.})$	0.1	cm^3	$3\cdot10^{-4}$ - $4\cdot10^{-3}$
$u(V_{cell})$	0.2	cm^3	$6\cdot10^{-4}$ - $8\cdot10^{-3}$
$u(\bar{v}_{abs\,g.})$	50%	cm^3	$5\cdot10^{-8}$ - $2\cdot10^{-2}$
$U(w_1)$	k=2		$2\cdot10^{-3}$ - $5\cdot10^{-2}$

3.3. Synthetic visual technique

This technique can be used not only for the determination of vapour-liquid equilibrium, but also for complicated phase behaviour, as multiphase equilibrium, solid-liquid and solid-fluid equilibrium, critical curves of mixtures, gas hydrate formation, cloud point determination, among others [10].

The measurement principle is based on the visual observation of the appearance of a new phase in a mixture of known composition, which avoids the sampling and analyses of liquid and vapour phases. This technique has been extensively employed in literature for determination of high pressure phase equilibrium data. Thus, for instance, the Cailletet apparatus has been frequently used by Peters and co-workers [29-113]. Dariva, Oliveira, Corazza and co-workers [114-146] have published numerous data on the phase equilibrium of binary and multicomponent systems composed by vegetable oils, hydrocarbons, biodiesel, alcohols and CO_2, among others; Jaubert, Daridon, Coutinho and co-workers [147-166] have articles dealing with high pressure phase equilibrium involving methane, CO_2, esters, alkanes, waxy systems, alcohols and ionic liquids; Byun, Lee, Lim and co-workers [167-187] have determined by means of this technique solubility data involving amides, organic acids, CO_2, polymers and haloalkanes, among others.

In this PhD Thesis high pressure solubility measurements through synthetic visual apparatuses were performed both in the Process and Product Applied Thermodynamics research group in the University of Aveiro (PATh-UA) and in the Thermophysical Properties Laboratory (LPT-USC). Both experimental techniques can operate at temperatures up to 423.15 K and pressures up to 100 MPa and are described in the following sections.

3.3.1. PATh-UA apparatus

Experimental setup

The experimental setup (Fig.3.3) comprises a high pressure variable volume cell based on a design of Daridon et al. [148,188], which is the core of the equipment. This cell is made up of a horizontal hollow stainless steel cylinder, closed at one end by a movable piston and at the other end by a sapphire window that allows a visual observation of the interior of the pressure cell. The interior of this cell is illuminated by an optical fibre through a second sapphire window located in the wall of the cell and a video acquisition system, consisting of an endoscope and a video camera connected to a computer, which allows observing what is happening inside the pressure cell. An external magnetic stirrer (IKA KMO 2 basic) located beneath the cell is employed for controlling the magnetic bar which homogenizes the system [160,161].

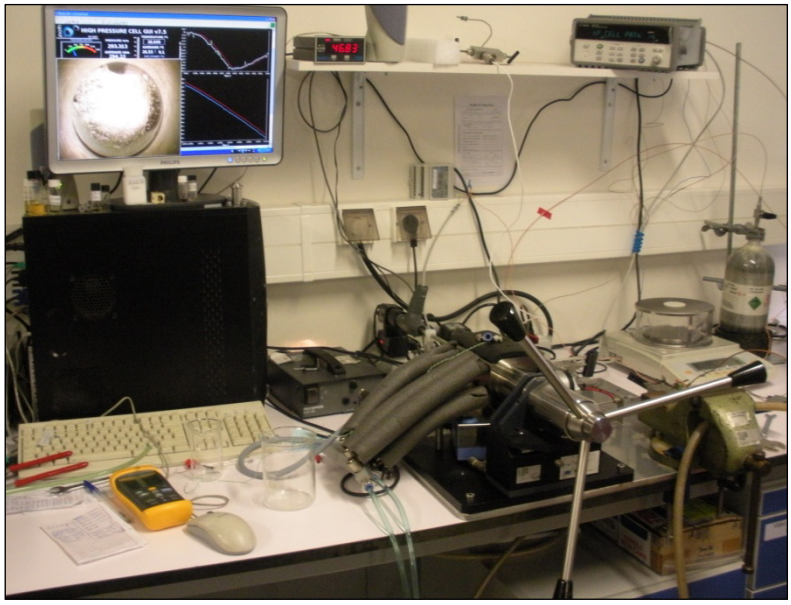

Fig.3.3. Picture of the PATh-UA high pressure phase equilibrium apparatus.

The exact quantities of solvent and solute introduced in the cell are determined by weighting with a balance (Sartorius LA2000P) with an accuracy of $1 \cdot 10^{-3}$g. The internal temperature is kept constant by means of a thermostatic bath circulator (Julabo MC) with a temperature stability of ±0.01K. The thermostatic fluid circulates through three flow lines located in the wall of the cell and a high precision thermometer, model PN 5207 with an accuracy of ±0.02K, connected to a calibrated platinum resistance inserted inside the cell close to the sample, measures the temperature. The pressure in the cell is measured with a piezoresistive silicon pressure transducer (Kulite HEM 375) fixed directly inside to reduce dead volumes, that was previously calibrated and certified by an independent laboratory with IPAC accreditation, following the EN 837-1 standard and with an accuracy better than 0.2%. Both the thermometer and the pressure transducer are connected to a data acquisition unit Agilent 34970A connected to the computer [160,161].

The equipment also comprises a stainless steel and peek pressure line that connects, by means of high pressure valves, the cell with the gas reservoir tank and with the vacuum pump. This line includes a pressure transducer to check that pressure is constant and no leaking occurs. A scheme of the experimental setup can be observed in Fig. 3.4, whereas specifications of the apparatus are presented in table 3.4.

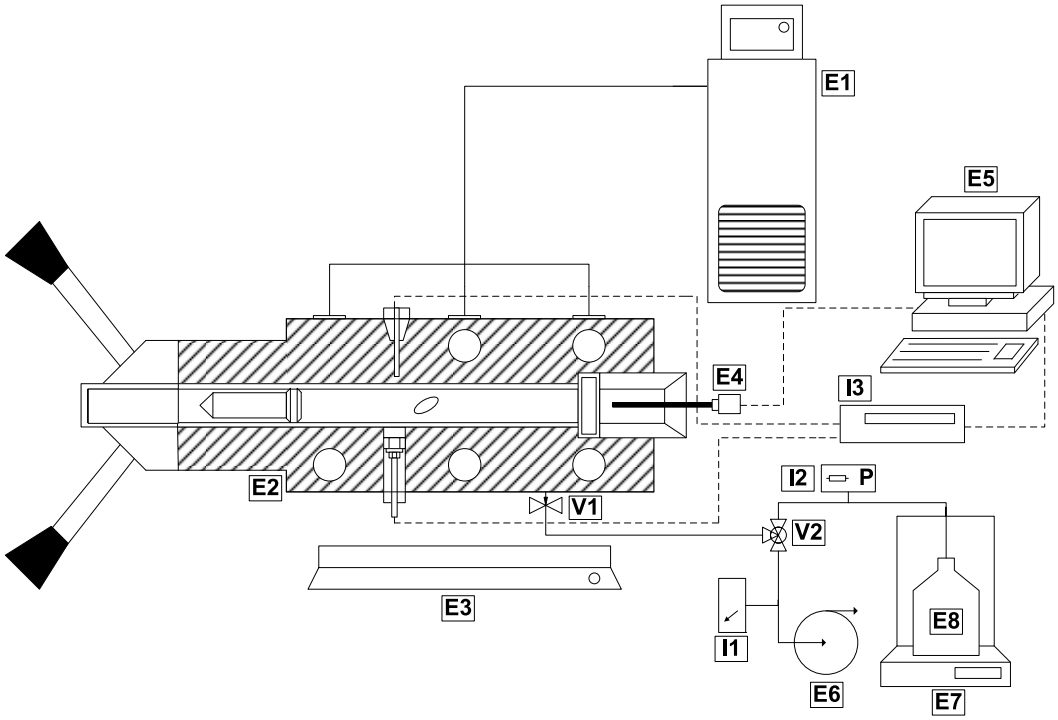

Fig.3.4. Schematic experimental set-up of the PATh-UA and LPT-USC phase equilibrium equipments. (E1) Thermostatic bath, (E2) high pressure cell, (E3) magnetic stirrer, (E4) endoscope and video camera, (E5) computer, (E6) vacuum pump, (E7) high precision balance, (E8) gas cylinder, (V1 and V2) valves, (I1) vacuometer, (I2) pressure transducer and (I3) data acquisition unit.

Table 3.4. Specifications of the visual synthetic technique of PATh-UA.

Device	Measurement range	Resolution	Uncertainty
Thermometer PN 5207	163.15- 387.1 K	±0.01K	±0.02K
Transducer Kulite HEM 375	0-140 MPa		0.2%
Balance	0-1010 g	±0.001 g	±0.001 g
Sartorius LA2000P	1010-2000g	±0.01 g	±0.01 g

Experimental procedure

Measurements were performed in this PhD Thesis in the temperature range from 298.15 K to 363.15 K und up to 74 MPa, according to the subsequent procedure. The solvent is degassed during several hours by using a vacuum line analogous to that of Fig.A.1 (appendix A), and then is introduced in the high pressure cell by means of a syringe. By weighting the syringe before and after this process it is possible to know the exact quantity of solvent in the system. After that, the high pressure cell and the portion of the pressure line until the entrance of the gas cylinder are degassed through the vacuum pump. Once the vacuum level achieved is around 8 Pa, the vacuum pump is stopped and the pressure line is filled with the gas from the gas cylinder. When pressure in the line is stable, the valve in the entrance of the cell is opened and the desired quantity of gas is filled, the balance indicates the quantity of gas introduced during this procedure. At this moment a mixture of the desired composition is inside the high pressure cell,

and phase equilibrium measurements can start. Thus, the thermostat is started up with a set point and it is necessary to wait until temperature is stable. Subsequently, pressure in the cell is increased until the system is homogeneous. After, pressure is smoothly decreased until small vapour bubbles appear (bubble point) followed by a slight increase in pressure until the system become homogeneous again. This is considered the equilibrium pressure, because phase boundaries are evaluated by determining the disappearance conditions of one phase instead of its appearance due to supersaturation effects.

Uncertainties

The expanded uncertainty (k=2) on the solute mass fraction $U(w_1)$ is calculated according to the following equation:

$$U(w_1) = 2\left[\left(\frac{\partial w_1}{\partial m_1}\right)^2 u^2(m_1) + \left(\frac{\partial w_1}{\partial m_2}\right)^2 u^2(m_2)\right]^{1/2} \tag{3.15}$$

where w_1 is the solute mass fraction, m_1 is the mass of the solute, m_2 is the mass of the solvent and u the uncertainty of the dependent variables.

For the studied systems it was found an uncertainty $U(w_1) \leq 2 \cdot 10^{-3}$, whereas for the pressure measurements of equilibrium points through visualization, the reproducibility is estimated to be 0.02 MPa.

3.3.2. LPT-USC equipment

Experimental setup

Installation of the high pressure equilibrium cell in the Thermophysical Properties Laboratory was performed during this PhD Thesis, in an analogous way to that of the PATh-UA equipment. A picture of this installation can be observed in Fig.3.5. The equipment comprises a high pressure cell composed of a horizontal hollow stainless steel cylinder, closed at one end by a sapphire window and in the other by a movable piston, which allows changing the volume of the cell from 8 to 30 cm^3. An optical fibre (OLYMPUS ILK-7B) lights the cell through a second sapphire window that is located in the wall of the cell in an orthogonal position to the first window, in order to avoid parasitic reflections and improve the observation in comparison to axial lighting. A video system comprised by rigid boroscope (OLYMPUS 5 Series) and a video camera (Moticam 2000) connected to a computer allows observing the phase behaviour of the mixture inside the cell.

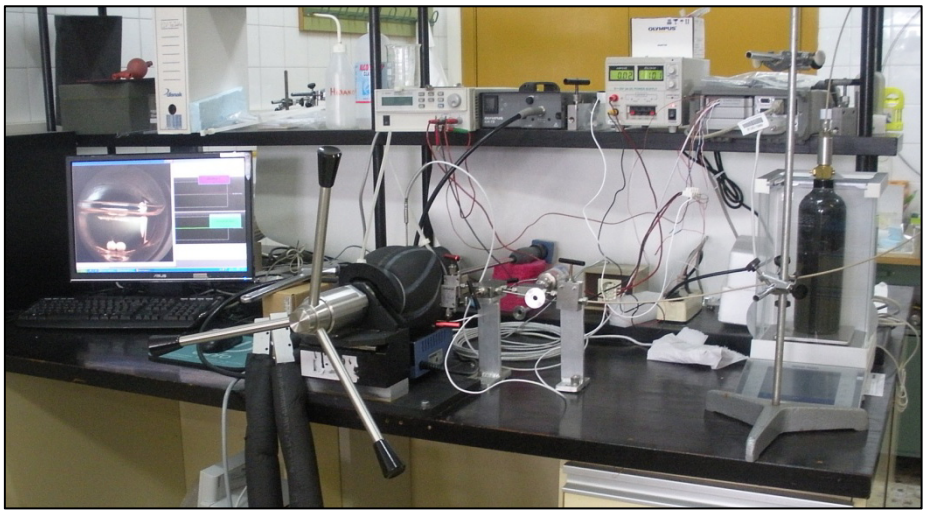

Fig.3.5. Picture of the LPT-USC high pressure phase equilibrium equipment.

The cell is thermostated by using a thermostatic bath (Lauda Proline RP 845) that pumps the thermostatic fluid through three flow lines located in the wall of the cell. Temperature is measured with a Pt100 placed in the upper wall of the cell whereas pressure is measured through a pressure transducer (Kulite HEM-375) fixed in the bottom wall of the cell and fed with a power source HQ Power PS613. Both sensors are connected to a data acquisition unit (Agilent 34970A) connected to the computer. Temperature probe was calibrated and measures temperature within ±0.02 K, whereas the pressure transducer was calibrated in the temperature range (283.15 – 363.15) K with a certified transducer Druck that has an uncertainty of $1.5 \cdot 10^{-2}$ % + $6 \cdot 10^{-4}$ MPa. The uncertainty of the Kulite HEM-375 transducer is ±0.02 MPa.

Two different digital balances were employed to weight the exact quantity of solute and solvent introduced in the cell. The solute was weighted with a Mettler Toledo XP5003S within $\pm 1.10^{-3}$ g, whereas the solvent was weighted with a Sartorius MC210P within $\pm 1.10^{-5}$ g. Homogenization of the mixtures was achieved through a magnetic bar placed inside the cell and controlled by means of a magnetic stirred (IKA KMO 2 basic) located beneath the cell.

This equipment consist also of a pressure line composed by stainless steel and peek tubes and high pressure valves that connect the high pressure cell with the gas cylinder and with the vacuum pump. A pressure transducer (Heise DXD) placed in this line serves to assure that no gas leaking is happening.

An overall scheme of this equipment is depicted in Fig.3.4, whereas the specifications of this apparatus are presented in table 3.5.

Table 3.5. Specifications of the visual synthetic technique of LPT-USC.

Device	Measurement range	Resolution	Uncertainty
Pt-100	273.15-423.15 K	±0.01K	±0.02K
Transducer Kulite HEM 375	0-140 MPa		±0.02 MPa
Balance	0-1000 g	±0.001 g	±0.001 g
Mettler Toledo XP5003S	1000-5000 g	±0.01 g	±0.01 g

Experimental procedure

Measurements were performed in this PhD Thesis in the temperature range from 298.15 K to 363.15 K and up to 72 MPa. The experimental procedure is analogous to that carried out in the PATh-UA equipment, thus readers are referred to that section for details. The only difference is that in the LPT-USC measurements, cloud points were determined in addition to bubble points. LLE was determined by decreasing the pressure from the homogeneous system until the appearance of a cloud, instead of bubbles. For these points, pressure was slightly decreased without agitation until the observance of three phases, which corresponds to a VLLE point.

Uncertainties

The expanded uncertainty (k=2) of the solute mass fraction $U(w_1)$ was calculated according to Eq. (3.15) and an uncertainty $U(w_1) \leq 2 \cdot 10^{-3}$ was obtained for the studied systems.

As regards pressure measurements of equilibrium points through visualization, the reproducibility is estimated to be 0.02 MPa for bubble points and 0.05 MPa for cloud points.

Technique verification

As this technique was implemented in the Thermophysical Properties Laboratory during this PhD Thesis, determination of the phase equilibrium of the binary system CO_2+high oleic sunflower oil (HOSO-B1) was employed to verify the correct operation of this equipment. This system had been previously measured in the PATh-UA equipment and thus comparisons among both results are performed. Measurements were carried out in the temperature range from 283.15 K to 363.15 K and up to 72 MPa. The agreement between both data series can be observed in Fig. 3.6.

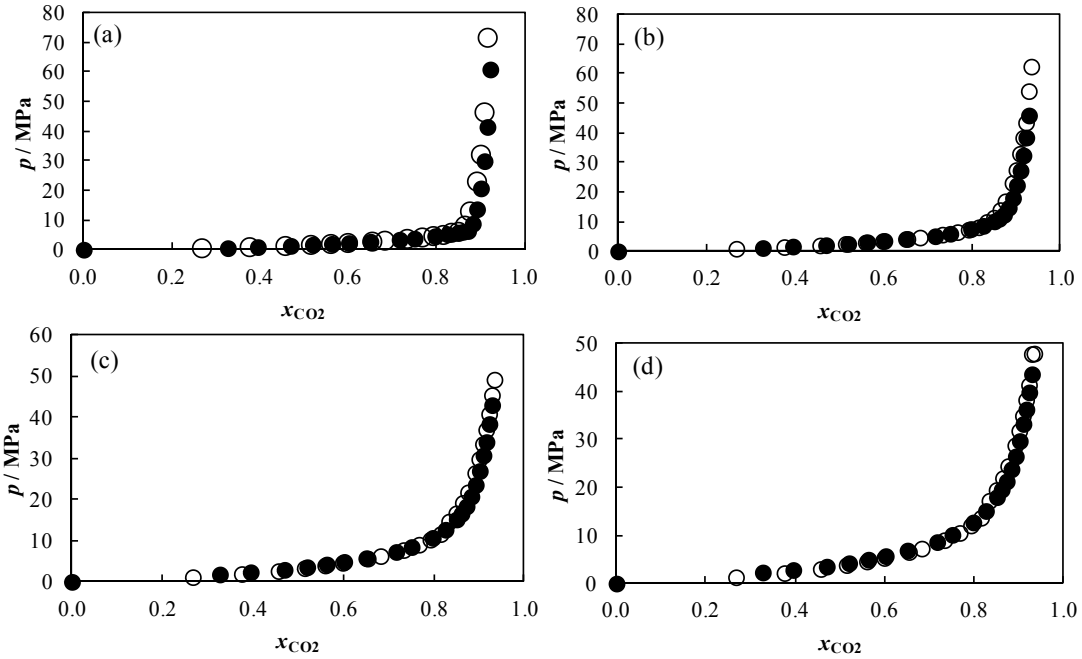

Fig.3.6. Comparison between the solubility values of CO_2 in HOSO-B1 measured in LPT-USC device (empty symbols) and those measured in the PATh-UA device (filled symbols). 298 K, (b) 323 K, (c) 348 K and (d) 363 K.

Moreover, data obtained in the PATh-UA equipment were correlated as a function of pressure for each isotherm by means of a polynomial expression, in order to perform the comparison presented in Fig. 3.7. It can be observed that the highest deviations between both data series are obtained at low pressures, where the relative uncertainty of pressure measurements is higher. The absolute average deviation (AAD%) between both data series, expressed in CO_2 mole fraction, is 2.2%.

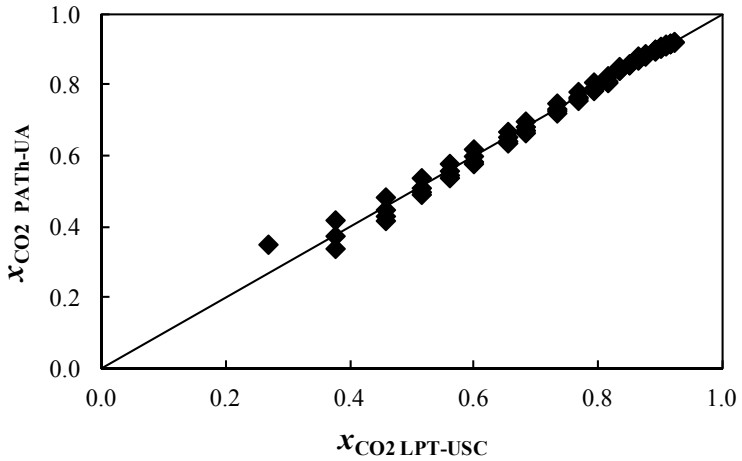

Fig.3.7. Comparison between the solubility data of the system CO_2/HOSO-B1 measured in the PATh-UA equipment and in the LPT-USC equipment.

3.4. Solubility modelling and prediction

Modelling of solubility data was performed either by means of Soave-Redlich-Kwong EoS or Perturbed-Chain Statistical Associating Fluid Theory (PC-SAFT EoS). Moreover, the

experimental solubility data were predicted by using the Carvalho and Coutinho model. All these models are described in the following sections.

3.4.1. Soave-Redlich-Kwong EoS

The Soave-Redlich-Kwong EoS (SRK-EoS) [189], in terms of the compressibility factor, *Z*, is given by:

$$Z = \frac{1}{1-b\rho} - \frac{a(T)\rho}{RT(1+b\rho)} \tag{3.16}$$

where T is the temperature, R is the gas constant, ρ is the mole density, $a(T)$ is a Soave-type temperature dependency of the pure component energy parameter and b is the co-volume, these last two parameters are given by the two following equations:

$$a = a_c\left[1 + m\left(1 - \sqrt{T_r}\right)\right]^2 \tag{3.17}$$

$$b = 0.08664\frac{RT_c}{p_c} \tag{3.18}$$

where T_c is the critical temperature, p_c is the critical pressure, T_r is the reduced temperature (T/T_c) and a_c and m are given by the following expressions:

$$a_c = 0.42747\frac{R^2T_c^2}{p_c} \tag{3.19}$$

$$m = 0.48 + 1.574\omega - 0.176\omega^2 \tag{3.20}$$

where ω is the acentric factor.

When dealing with mixtures, the energy and co-volume parameters are calculated employing the conventional van der Waals one-fluid mixing rules,

$$a = \sum_i \sum_j x_i x_j a_{ij} \tag{3.22}$$

$$a_{ij} = \sqrt{a_i a_j}\left(1 - k_{ij}\right) \tag{3.23}$$

$$b = \sum_i \sum_j x_i x_j b_{ij} \tag{3.24}$$

$$b_{ij} = \sqrt{b_i b_j}\left(1 - l_{ij}\right) \tag{3.25}$$

There are two adjustable parameters, i.e. k_{ij} and l_{ij}. The objective function employed for their estimation is the following:

$$\mathrm{OF} = \sqrt{\frac{1}{n}\sum_i^n \left(x_i^{exp.} - x_i^{cal.}\right)^2} \tag{3.26}$$

where n is the number of experimental points and x_i is the mole fraction of component "i" in the phases selected for the optimization.

3.4.2. PC-SAFT EoS

The PC-SAFT EoS is based on the statistical associating fluid theory (SAFT), applying Barker and Henderson's [190,191] second-order perturbation theory. PC-SAFT uses the same chain term and association term as the previous SAFT equations, but a hard-chain fluid serves as a reference for the perturbation theory [192]. PC-SAFT model is applicable to mixtures of gases, solvents and polymers. This model [192] characterizes non-associating molecules by three pure-component parameters: the temperature-independent segment diameter σ, the depth of the potential ε, and the number of segments per chain m. The parameters for a pair of unlike segments are obtained by conventional Berthelot-Lorentz combining rules:

$$\sigma_{ij} = \frac{1}{2}\left(\sigma_i + \sigma_j\right) \tag{3.27}$$

$$\varepsilon_{ij} = \sqrt{\varepsilon_i \varepsilon_j (1 - k_{ij})} \tag{3.28}$$

where one binary interaction parameter, k_{ij}, is introduced to correct the segment-segment interactions of unlike chains [192]. k_{ij} values are determined by fitting the experimental solubility data by means of Phase Equilibria software (PE2000) [193].

The k_{ij} parameters are calculated for each isotherm and binary system, taking into account the experimental solubility data and using as objective function the Mean Absolute Deviation:

$$MAD_{xCO_2} = \frac{1}{n}\sum_{i=1}^{n}\left|x_i^{exp.} - x_i^{calc.}\right| \tag{3.29}$$

where n is the number of experimental points.

3.4.3. Carvalho and Coutinho model

Carvalho and Coutinho [194] have proposed a general correlation, Eq. (3.30), for predicting the solubility of CO_2 in non-volatile solvents, these last are defined as solvents with a vapour pressure at room temperature inferior to 100 Pa.

$$\frac{p/\mathrm{MPa}}{1\,\mathrm{MPa}} = \frac{m_{CO2}/\mathrm{mol\cdot kg^{-1}}}{1\,\mathrm{mol\cdot kg^{-1}}} e^{\left(6.8591 - \frac{2004.3}{T/\mathrm{K}}\right)} \tag{3.30}$$

where m_{CO2} is the CO_2 solubility. This equation is valid, according to authors, for pressures up to 5 MPa, for temperatures ranging from room temperature up to 363 K and molalities up to 3 $mol\cdot kg^{-1}$. Carvalho and Coutinho stands that when the molecular weight effect is removed from the solubility analysis by comparing the solubilities in molalities instead of mole fractions, the differences in solubilities, among different systems, are minimized, and the solubility of CO_2 in nonvolatile solvents seems to be essentially solvent independent. They have analyzed with the

Flory-Huggins model that the deviations of Raoult's law at low CO_2 concentration are mainly due to entropic effects for most of the non-volatile solvents.

Eq. (3.30) can be written as a function of mass fraction as follows:

$$\frac{p/\mathrm{MPa}}{1\,\mathrm{MPa\cdot g\cdot mol^{-1}}} = \frac{w_{CO2}}{(1-w_{CO2})\cdot 10^{-3}\cdot M_{wCO_2}/\mathrm{g\cdot mol^{-1}}}\cdot e^{\left(6.8591-\frac{2004.3}{T/\mathrm{K}}\right)} \tag{3.31}$$

3.5. References

[1] R. Dohrn, G. Brunner, Fluid Phase Equilib. 106 (1995) 213-282.
[2] R. Dohrn, J.M.S. Fonseca, S. Peper, Annual Review of Chemical and Biomolecular Engineering 3 (2012) 343-367.
[3] G.M. Schneider, Pure Appl. Chem. 63 (1991) 1313-1326.
[4] S. Saito, J. Supercrit. Fluids 8 (1995) 177-204.
[5] A.L. Mühlbauer, J.D. Raal, Chem. Eng. J. 60 (1995) 1-29.
[6] C.P. Hicks, A bibliography of thermodynamic quantities for binary fluid mixtures, Chemical Thermodynamics, 2, Royal Society of Chemistry, London, 1978.
[7] H. Knapp, R. Döring, L. Oellrich, U. Plöcker, J.M. Prausnitz, Vapor-liquid equilibria for mixtures of low boiling substances, DECHEMA Chemistry Data Series, Volume VI, 1981.
[8] J. Wisniak, M. Herskowitz, Solubility of gases and solids: a literature source book, Elsevier, Amsterdam ; New York, 1984.
[9] R.E. Fornari, P. Alessi, I. Kikic, Fluid Phase Equilib. 57 (1990) 1-33.
[10] M. Christov, R. Dohrn, Fluid Phase Equilib. 202 (2002) 153-218.
[11] R. Dohrn, S. Peper, J.M.S. Fonseca, Fluid Phase Equilib. 288 (2010) 1-54.
[12] J.M.S. Fonseca, R. Dohrn, S. Peper, Fluid Phase Equilib. 300 (2011) 1-69.
[13] D. Richon, T.W. de Loos, Vapour-liquid equilibrium at high pressure. in: R.D. Weir, T.W. de Loos, (Eds.), Measurement of the thermodynamic properties of multiple phases, experimental thermodynamics, Volume VII, Elsevier Science, Amsterdam, 2005, pp. 89-136.
[14] C. Bogatu, R. Vîlcu, A. Dută, Analele Universitătii din Bucuresti – Chimie, Anul XIV (serie nouă) I-II (2005) 193-203.
[15] A. Wahlstrom, L. Vamling, Can. J. Chem. Eng. 74 (1996) 426-428.
[16] A. Wahlstrom, L. Vamling, Can. J. Chem. Eng. 75 (1997) 544-550.
[17] A. Wahlstrom, L. Vamling, J. Chem. Eng. Data 44 (1999) 823-828.
[18] A. Wahlstrom, L. Vamling, J. Chem. Eng. Data 45 (2000) 97-103.
[19] O. Fandiño, E.R. López, L. Lugo, J. Fernández, J. Chem. Eng. Data 55 (2010) 5483-5488.
[20] O. Fandiño, E.R. López, L. Lugo, M. Teodorescu, A.M. Mainar, J. Fernández, J. Chem. Eng. Data 53 (2008) 1854-1861.
[21] O. Fandiño, E.R. López, L. Lugo, J. García, J. Fernández, J. Supercrit. Fluids 55 (2010) 62-70.
[22] O. Fandiño, Propiedades termofísicas de lubricantes tipo éster. Densidad y solubilidad del CO_2, Departamento de Física Aplicada, Universidad de Santiago de Compostela, Santiago de Compostela, 2009.
[23] R. Span, E.W. Lemmon, R.T. Jacobsen, W. Wagner, A. Yokozeki, J. Phys. Chem. Ref. Data 29 (2000) 1361-1433.
[24] M.G. Zellner, L.C. Claitor, J.M. Prausnitz, Ind. Eng. Chem. Fundam. 9 (1970) 549-564.
[25] E.W. Lyckman, C.A. Eckert, J.M. Prausnitz, Chem. Eng. Sci. 20 (1965) 703-706.
[26] R. Battino, H.L. Clever, Chemical Reviews 66 (1966) 395-463.
[27] M.W. Cook, D.N. Hanson, Rev. Sci. Instrum. 28 (1957) 370-374.
[28] Expression of the uncertainty of measurement in calibration, European Cooperation for Accreditation, EA-4/02, 1999.
[29] M. Althuluth, M.C. Kroon, C.J. Peters, Ind. Eng. Chem. Res. 51 (2012) 16709-16712.
[30] M. Althuluth, M.T. Mota-Martinez, M.C. Kroon, C.J. Peters, J. Chem. Eng. Data 57 (2012) 3422-3425.
[31] A.E. Andreatta, S.B. Bottini, L.J. Florusse, C.J. Peters, J. Supercrit. Fluids 38 (2006) 306-311.
[32] A.E. Andreatta, L.J. Florusse, S.B. Bottini, C.J. Peters, J. Supercrit. Fluids 42 (2007) 60-68.

[33] S. Arnó, S. Lucas, A. Shariati, C.J. Peters, J. Solution Chem. 41 (2012) 2173-2185.
[34] M. Banaei, L.J. Florusse, S. Raeissi, C.J. Peters, J. Supercrit. Fluids 63 (2012) 25-30.
[35] M.D. Bermejo, A. Martín, L.J. Florusse, C.J. Peters, M.J. Cocero, Fluid Phase Equilib. 244 (2006) 78-85.
[36] M.D. Bermejo, A.J. Kotlewska, L.J. Florusse, M.J. Cocero, F. van Rantwijk, C.J. Peters, Green Chem. 10 (2008) 1049-1054.
[37] M.D. Bermejo, M. Montero, E. Saez, L.J. Florusse, A.J. Kotlewska, M.J. Cocero, F. van Rantwijk, C.J. Peters, J. Phys. Chem. B. 112 (2008) 13532-13541.
[38] B. Breure, E.J.M. Straver, L.J. Florusse, M.P.W.M. Rijkers, I.G. Economou, F.M. Vargas, C.J. Peters, J. Chem. Eng. Data 56 (2011) 1407-1413.
[39] M. Costantini, V.A. Toussaint, A. Shariati, C.J. Peters, I. Kikic, J. Chem. Eng. Data 50 (2004) 52-55.
[40] A.R. Cruz Duarte, M.M. Mooijer-van den Heuvel, C.M.M. Duarte, C.J. Peters, Fluid Phase Equilib. 214 (2003) 121-136.
[41] J.C. de la Fuente, S.B. Bottini, C.J. Peters, J. Chem. Eng. Data 51 (2005) 2-6.
[42] A.R.C. Duarte, A. Shariati, C.J. Peters, J. Chem. Eng. Data 54 (2009) 1628-1632.
[43] A.R.C. Duarte, A. Shariati, L.J. Rovetto, C.J. Peters, J. Phys. Chem. B. 112 (2008) 1888-1889.
[44] I.G. Economou, C.J. Peters, L.J. Florusse, J. De Swaan Arons, Fluid Phase Equilib. 111 (1995) 239-252.
[45] L.J. Florusse, C.J. Peters, Fluid Phase Equilib. 202 (2002) 1-11.
[46] L.J. Florusse, C.J. Peters, J.C. Pàmies, L.F. Vega, H. Meijer, AIChE J. 49 (2003) 3260-3269.
[47] L.J. Florusse, S. Raeissi, C.J. Peters, J. Chem. Eng. Data 53 (2008) 1283-1285.
[48] L.J. Florusse, S. Raeissi, C.J. Peters, J. Chem. Eng. Data 56 (2011) 4797-4799.
[49] L.J. Florusse, T. Fornari, S.B. Bottini, C.J. Peters, J. Supercrit. Fluids 22 (2002) 1-13.
[50] L.J. Florusse, T. Fornari, S.B. Bottini, C.J. Peters, J. Supercrit. Fluids 31 (2004) 123-132.
[51] K. Gauter, C.J. Peters, Fluid Phase Equilib. 150–151 (1998) 501-514.
[52] K. Gauter, L.J. Florusse, J.C. Smits, C.J. Peters, J. Chem. Thermodyn. 30 (1998) 1617-1631.
[53] K.I. Gutkowski, A. Shariati, C.J. Peters, J. Supercrit. Fluids 39 (2006) 187-191.
[54] M.D. Jager, R.M. de Deugd, C.J. Peters, J. de Swaan Arons, E.D. Sloan, Fluid Phase Equilib. 165 (1999) 209-223.
[55] M.D. Jager, C.J. Peters, E.D. Sloan, Fluid Phase Equilib. 193 (2002) 17-28.
[56] S. Kazemi, C.J. Peters, M.C. Kroon, J. Supercrit. Fluids 69 (2012) 8-12.
[57] M.C. Kroon, L.J. Florusse, C.J. Peters, Fluid Phase Equilib. 294 (2010) 84-88.
[58] M.C. Kroon, V.A. Toussaint, A. Shariati, L.J. Florusse, J. van Spronsen, G.-J. Witkamp, C.J. Peters, Green Chem. 10 (2008) 333-336.
[59] M.C. Kroon, A. Shariati, M. Costantini, J. van Spronsen, G.-J. Witkamp, R.A. Sheldon, C.J. Peters, J. Chem. Eng. Data 50 (2004) 173-176.
[60] E. Kühne, C.J. Peters, J. van Spronsen, G.-J. Witkamp, Green Chem. 8 (2006) 287-291.
[61] E. Kühne, S. Santarossa, G.-J. Witkamp, C.J. Peters, Green Chem. 10 (2008) 762-766.
[62] E. Kühne, G.-J. Witkamp, C.J. Peters, Green Chem. 10 (2008) 929-933.
[63] E. Kühne, E. Perez, G.J. Witkamp, C.J. Peters, J. Supercrit. Fluids 45 (2008) 27-31.
[64] E. Kühne, S. Santarossa, E. Perez, G.J. Witkamp, C.J. Peters, J. Supercrit. Fluids 46 (2008) 93-98.
[65] E. Kühne, E.S. Calvo, G.J. Witkamp, C.J. Peters, J. Supercrit. Fluids 45 (2008) 293-297.
[66] F. Llovell, L.J. Florusse, C.J. Peters, L.F. Vega, J. Phys. Chem. B. 111 (2007) 10180-10188.
[67] S. Mainusch, C.J. Peters, J. de Swaan Arons, J. Javanmardi, M. Moshfeghian, J. Chem. Eng. Data 42 (1997) 948-950.
[68] V. Margon, U.S. Agarwal, C.J. Peters, G. de Wit, J.M.N. van Kasteren, P.J. Lemstra, J. Supercrit. Fluids 27 (2003) 25-30.
[69] V. Margon, U.S. Agarwal, C.J. Peters, G. de Wit, C. Bailly, J.M.N. van Kasteren, P.J. Lemstra, J. Supercrit. Fluids 34 (2005) 309-321.
[70] F. Mattea, C.J. Peters, M.C. Kroon, J. Chem. Eng. Data 56 (2011) 2960-2963.
[71] M.M. Mooijer-van den Heuvel, C.J. Peters, J. de Swaan Arons, Fluid Phase Equilib. 172 (2000) 73-91.
[72] M.M. Mooijer-van den Heuvel, R. Witteman, C.J. Peters, Fluid Phase Equilib. 182 (2001) 97-110.
[73] M.M.M.-v. den Heuvel, C.J. Peters, J. de Swaan Arons, Fluid Phase Equilib. 193 (2002) 245-259.

[74] M.M. Mooijer-van den Heuvel, N.M. Sawirjo, C.J. Peters, Fluid Phase Equilib. 241 (2006) 124-137.
[75] M.T. Mota-Martinez, M. Althuluth, M.C. Kroon, C.J. Peters, Fluid Phase Equilib. 332 (2012) 35-39.
[76] K. Nasrifar, M.M. Mooijer-van den Heuvel, C.J. Peters, S. Ayatollahi, M. Moshfeghian, Fluid Phase Equilib. 204 (2003) 1-14.
[77] K. Nasrifar, M.M. Mooijer-van den Heuvel, C.J. Peters, J. Chem. Eng. Data 53 (2008) 2328-2332.
[78] C.J. Peters, L.J. Florusse, J. Chem. Eng. Data 40 (1995) 948-949.
[79] C.J. Peters, J.L. de Roo, J. de Swaan Arons, Fluid Phase Equilib. 109 (1995) 99-111.
[80] C.J. Peters, L.J. Florusse, S. Hähre, J. Supercrit. Fluids 9 (1996) 135-140.
[81] S. Raeissi, C.J. Peters, AIChE J. 58 (2012) 3553-3559.
[82] S. Raeissi, C.J. Peters, Fluid Phase Equilib. 294 (2010) 67-71.
[83] S. Raeissi, C.J. Peters, J. Chem. Eng. Data 54 (2008) 382-386.
[84] S. Raeissi, C.J. Peters, J. Supercrit. Fluids 20 (2001) 221-228.
[85] S. Raeissi, C.J. Peters, J. Supercrit. Fluids 22 (2002) 93-102.
[86] S. Raeissi, C.J. Peters, J. Supercrit. Fluids 35 (2005) 10-17.
[87] S. Raeissi, C.J. Peters, J. Supercrit. Fluids 33 (2005) 201-208.
[88] S. Raeissi, K. Gauter, C.J. Peters, Fluid Phase Equilib. 147 (1998) 239-249.
[89] S. Raeissi, L.J. Florusse, C.J. Peters, J. Chem. Eng. Data 56 (2011) 1105-1107.
[90] S. Raeissi, J.C. Asensi, C.J. Peters, J. Supercrit. Fluids 24 (2002) 111-121.
[91] S. Raeissi, L. Florusse, C.J. Peters, J. Supercrit. Fluids 55 (2010) 825-832.
[92] L.J. Rovetto, S.B. Bottini, E.A. Brignole, C.J. Peters, J. Supercrit. Fluids 25 (2003) 165-176.
[93] L.J. Rovetto, S.B. Bottini, C.J. Peters, J. Supercrit. Fluids 31 (2004) 111-121.
[94] L.J. Rovetto, S.B. Bottini, E.A. Brignole, C.J. Peters, J. Supercrit. Fluids 35 (2005) 182-196.
[95] L.J. Rovetto, C.J. Peters, E.A. Brignole, J. Supercrit. Fluids 34 (2005) 183-187.
[96] K.M. Sabil, G.-J. Witkamp, C.J. Peters, Fluid Phase Equilib. 284 (2009) 38-43.
[97] K.M. Sabil, G.-J. Witkamp, C.J. Peters, J. Chem. Eng. Data 55 (2009) 813-818.
[98] K.M. Sabil, V.R. Román, G.-J. Witkamp, C.J. Peters, J. Chem. Thermodyn. 42 (2010) 400-408.
[99] K.M. Sabil, G.-J. Witkamp, C.J. Peters, J. Chem. Thermodyn. 42 (2010) 8-16.
[100] A.R.S. de Sousa, S. Raeissi, A. Aguiar-Ricardo, C.M. M. Duarte, C.J. Peters, J. Supercrit. Fluids 29 (2004) 59-67.
[101] T.E. Sandoval, M.P. Gárate, J. Scavia, L.J. Florusse, C.J. Peters, J. Chem. Thermodyn. 57 (2013) 224-229.
[102] A.M. Schilderman, S. Raeissi, C.J. Peters, Fluid Phase Equilib. 260 (2007) 19-22.
[103] A. Shariati, C.J. Peters, J. Supercrit. Fluids 23 (2002) 195-208.
[104] A. Shariati, C.J. Peters, J. Supercrit. Fluids 25 (2003) 109-117.
[105] A. Shariati, C.J. Peters, J. Supercrit. Fluids 34 (2005) 171-176.
[106] A. Shariati, K. Gutkowski, C.J. Peters, AIChE J. 51 (2005) 1532-1540.
[107] A. Shariati, C.J. Peters, M. Moshfeghian, J. Chem. Eng. Data 43 (1998) 785-788.
[108] A. Shariati, C.J. Peters, M. Moshfeghian, J. Chem. Eng. Data 43 (1998) 280-282.
[109] A. Shariati, C.J. Peters, M. Moshfeghian, J. Chem. Eng. Data 43 (1998) 789-790.
[110] A. Shariati, L.J. Florusse, C.J. Peters, J. Chem. Eng. Data 56 (2011) 920-922.
[111] A. Shariati, C. Tesauro, E. Reverchon, C.J. Peters, J. Supercrit. Fluids 71 (2012) 110-113.
[112] E.J.M. Straver, J.L. de Roo, C.J. Peters, J. de Swaan Arons, J. Supercrit. Fluids 11 (1998) 139-150.
[113] A.T. Trueba, L.J. Rovetto, L.J. Florusse, M.C. Kroon, C.J. Peters, Fluid Phase Equilib. 307 (2011) 6-10.
[114] O.A.S. Araújo, F.R. Silva, L.P. Ramos, M.K. Lenzi, P.M. Ndiaye, M.L. Corazza, J. Chem. Thermodyn. 47 (2012) 412-419.
[115] O.A.S. Araújo, P.M. Ndiaye, L.P. Ramos, M.L. Corazza, J. Supercrit. Fluids 62 (2012) 41-46.
[116] T. Benazzi, E. Franceschi, M.L. Corazza, J. Vladimir Oliveira, C. Dariva, Fluid Phase Equilib. 244 (2006) 128-136.
[117] J.P. Bender, A. Junges, E. Franceschi, F.C. Corazza, C. Dariva, J.V. Oliveira, M.L. Corazza, Brazilian Journal of Chemical Engineering 25 (2008) 563-570.
[118] J.P. Bender, M. Feitein, M.A. Mazutti, E. Franceschi, M.L. Corazza, J.V. Oliveira, J. Chem. Thermodyn. 42 (2010) 229-233.

[119] J.P. Bender, M. Feitein, E. Franceschi, M.L. Corazza, J.V. Oliveira, J. Chem. Thermodyn. 42 (2010) 48-53.
[120] G.R. Borges, A. Junges, E. Franceschi, F.C. Corazza, M.L. Corazza, J.V. Oliveira, C. Dariva, J. Chem. Eng. Data 52 (2007) 1437-1441.
[121] D. Canziani, P.M. Ndiaye, E. Franceschi, M.L. Corazza, J. Vladimir Oliveira, J. Chem. Thermodyn. 41 (2009) 966-972.
[122] R.M. Charin, M.L. Corazza, P.M. Ndiaye, A.A. Rigo, M.A. Mazutti, J. Vladimir Oliveira, J. Chem. Thermodyn. 43 (2011) 413-419.
[123] R.M. Charin, M.L. Corazza, P.M. Ndiaye, M.A. Mazutti, J.V. Oliveira, J. Supercrit. Fluids 55 (2010) 23-31.
[124] M.L. Corazza, L. Cardozo-Filho, O.A.C. Antunes, C. Dariva, Ind. Eng. Chem. Res. 42 (2003) 3150-3155.
[125] M.L. Corazza, L.C. Filho, O.A.C. Antunes, C. Dariva, J. Chem. Eng. Data 48 (2003) 354-358.
[126] F.V. Corrêa, S.R.R. Comim, A.M. de Cesaro, A.A. Rigo, M.A. Mazutti, H. Hense, J.V. Oliveira, J. Chem. Thermodyn. 43 (2011) 34-38.
[127] I. Dalmolin, M.A. Mazutti, E.A.C. Batista, M.A.A. Meireles, J.V. Oliveira, J. Chem. Thermodyn. 42 (2010) 797-801.
[128] C. Dariva, J.V. Oliveira, F.W. Tavares, J.C. Pinto, J. Appl. Polym. Sci. 81 (2001) 3044-3055.
[129] M.C. Esmelindro, O.v.A.C. Antunes, E. Franceschi, G.R. Borges, M.L. Corazza, J.V. Oliveira, W. Linhares, C.u. Dariva, J. Chem. Eng. Data 53 (2008) 2050-2055.
[130] E. Franceschi, M.B. Grings, C.D. Frizzo, J.V. Oliveira, C. Dariva, Fluid Phase Equilib. 226 (2004) 1-8.
[131] E. Franceschi, M.H. Kunita, A.F. Rubira, E.C. Muniz, M.L. Corazza, J.V. Oliveira, C. Dariva, J. Chem. Eng. Data 51 (2006) 686-690.
[132] P.S. Gaschi, M.R. Mafra, P.M. Ndiaye, M.L. Corazza, J. Chem. Thermodyn. 57 (2013) 14-21.
[133] M. Lanza, P.M. Ndiaye, F.W. Tavares, D. Oliveira, C. Dariva, J.V. Oliveira, J. Supercrit. Fluids 34 (2005) 215-221.
[134] E.M.Z. Michielin, S.R. Rosso, E. Franceschi, G.R. Borges, M.L. Corazza, J.V. Oliveira, S.R.S. Ferreira, J. Chem. Thermodyn. 41 (2009) 130-137.
[135] L.S. Moura, M.L. Corazza, L. Cardozo-Filho, M.A.A. Meireles, J. Chem. Eng. Data 50 (2005) 1657-1661.
[136] L.S. Moura, R. Favareto, P.F. Leal, M.L. Corazza, L. Cardozo-Filho, M.A.A. Meireles, J. Supercrit. Fluids 48 (2009) 126-130.
[137] P.M. Ndiaye, M. Lanza, F.W. Tavares, C. Dariva, D. Oliveira, J. Vladimir Oliveira, Braz. J. Chem. Eng. 23 (2006) 405-415.
[138] P.M. Ndiaye, C. Dariva, J. Vladimir Oliveira, F.W. Tavares, J. Supercrit. Fluids 21 (2001) 93-103.
[139] P.M. Ndiaye, E. Franceschi, D. Oliveira, C. Dariva, F.W. Tavares, J.V. Oliveira, J. Supercrit. Fluids 37 (2006) 29-37.
[140] J.V. Oliveira, C. Dariva, J.C. Pinto, Ind. Eng. Chem. Res. 39 (2000) 4627-4633.
[141] L.F. Pinto, D.I.S. da Silva, F. Rosa da Silva, L.P. Ramos, P.M. Ndiaye, M.L. Corazza, J. Chem. Thermodyn. 44 (2012) 57-65.
[142] L.F. Pinto, P.M. Ndiaye, L.P. Ramos, M.L. Corazza, J. Supercrit. Fluids 59 (2011) 1-7.
[143] S.B. Rodriguez-Reartes, M. Cismondi, E. Franceschi, M.L. Corazza, J.V. Oliveira, M.S. Zabaloy, J. Supercrit. Fluids 50 (2009) 193-202.
[144] S.R. Rosso Comim, E. Franceschi, G.R. Borges, M.L. Corazza, J. Vladimir Oliveira, S.R.S. Ferreira, J. Chem. Thermodyn. 42 (2010) 348-354.
[145] S.R. Rosso, E. Franceschi, G.R. Borges, M.L. Corazza, J.V. Oliveira, S.R.S. Ferreira, J. Chem. Thermodyn. 41 (2009) 1254-1258.
[146] A.T. Souza, M.L. Corazza, L. Cardozo-Filho, R. Guirardello, M.A.A. Meireles, J. Chem. Eng. Data 49 (2004) 352-356.
[147] P. Borg, J.-N. Jaubert, F. Denet, Fluid Phase Equilib. 191 (2001) 59-69.
[148] A.M.A. Dias, H. Carrier, J.L. Daridon, J.C. Pàmies, L.F. Vega, J.A.P. Coutinho, I.M. Marrucho, Ind. Eng. Chem. Res. 45 (2006) 2341-2350.
[149] J.-N. Jaubert, P. Borg, L. Coniglio, D. Barth, J. Supercrit. Fluids 20 (2001) 145-155.
[150] F. Mutelet, S. Vitu, R. Privat, J.-N. Jaubert, Fluid Phase Equilib. 238 (2005) 157-168.
[151] J. Pauly, J.A.P. Coutinho, J.-L. Daridon, Fluid Phase Equilib. 297 (2010) 149-153.

[152] J. Pauly, J.A.P. Coutinho, J.-L. Daridon, Fluid Phase Equilib. 313 (2012) 32-37.
[153] J. Pauly, J. Coutinho, J.-L. Daridon, Fluid Phase Equilib. 255 (2007) 193-199.
[154] E. Petrova, C. Crampon, E. Ali, E. Neau, E. Badens, G. Charbit, J.N. Jaubert, Fluid Phase Equilib. 213 (2003) 153-162.
[155] A.-L. Revelli, F. Mutelet, J.-N.l. Jaubert, J. Phys. Chem. B. 114 (2010) 12908-12913.
[156] S. Vitu, J.-N. Jaubert, J. Pauly, J.-L. Daridon, D. Barth, J. Chem. Eng. Data 52 (2007) 1851-1855.
[157] S. Vitu, J.-N. Jaubert, J. Pauly, J.-L. Daridon, J. Chem. Thermodyn. 40 (2008) 1358-1363.
[158] S. Vitu, J.-N. Jaubert, J. Pauly, J.-L. Daridon, D. Barth, J. Supercrit. Fluids 44 (2008) 155-163.
[159] P.J. Carvalho, V.H. Álvarez, B. Schröder, A.M. Gil, I.M. Marrucho, M. Aznar, L.M.N.B.F. Santos, J.A.P. Coutinho, J. Phys. Chem. B. 113 (2009) 6803-6812.
[160] P.J. Carvalho, V.H. Álvarez, I.M. Marrucho, M. Aznar, J.A.P. Coutinho, J. Supercrit. Fluids 50 (2009) 105-111.
[161] P.J. Carvalho, V.H. Álvarez, J.J.B. Machado, J. Pauly, J.-L. Daridon, I.M. Marrucho, M. Aznar, J.A.P. Coutinho, J. Supercrit. Fluids 48 (2009) 99-107.
[162] P.J. Carvalho, V.H. Álvarez, I.M. Marrucho, M. Aznar, J.A.P. Coutinho, J. Supercrit. Fluids 52 (2010) 258-265.
[163] P.J. Carvalho, A.R. Ferreira, M.B. Oliveira, M. Besnard, M.I. Cabaço, J.A.P. Coutinho, J. Chem. Eng. Data 56 (2011) 2786-2792.
[164] S. Mattedi, P.J. Carvalho, J.A.P. Coutinho, V.H. Alvarez, M. Iglesias, J. Supercrit. Fluids 56 (2011) 224-230.
[165] S.P.M. Ventura, J. Pauly, J.L. Daridon, J.A. Lopes da Silva, I.M. Marrucho, A.M.A. Dias, J.A.P. Coutinho, J. Chem. Thermodyn. 40 (2008) 1187-1192.
[166] S.P.M. Ventura, J. Pauly, J.L. Daridon, I.M. Marrucho, A.M.A. Dias, J.A.P. Coutinho, J. Chem. Eng. Data 52 (2007) 1100-1102.
[167] J.-Y. Ahn, B.-C. Lee, J.S. Lim, K.-P. Yoo, J.W. Kang, Fluid Phase Equilib. 290 (2010) 75-79.
[168] H.-S. Byun, J.-S. Shin, J. Chem. Eng. Data 48 (2002) 97-101.
[169] H.-S. Byun, J.-G. Kim, J.-S. Yang, Ind. Eng. Chem. Res. 43 (2004) 1543-1552.
[170] H.-S. Byun, Fluid Phase Equilib. 198 (2002) 299-312.
[171] H.-S. Byun, J. Chem. Eng. Data 47 (2002) 359-362.
[172] H.-S. Byun, N.-S. Jeon, Fluid Phase Equilib. 167 (2000) 113-122.
[173] H.S. Byun, B.M. Hasch, M.A. McHugh, Fluid Phase Equilib. 115 (1996) 179-192.
[174] H.-S. Byun, N.-H. Kim, C. Kwak, Fluid Phase Equilib. 208 (2003) 53-68.
[175] H.-S. Byun, K. Kim, M.A. McHugh, Ind. Eng. Chem. Res. 39 (2000) 4580-4587.
[176] H.-S. Byun, M.-Y. Choi, J. Chem. Thermodyn. 39 (2007) 855-861.
[177] Y.-M. Kuk, B.-C. Lee, Y.-W. Lee, J.S. Lim, J. Chem. Eng. Data 47 (2002) 575-581.
[178] J.M. Lee, B.-C. Lee, S.-J. Hwang, J. Chem. Eng. Data 45 (2000) 1162-1166.
[179] J.M. Lee, B.-C. Lee, S.-H. Lee, J. Chem. Eng. Data 45 (2000) 851-856.
[180] B.-C. Lee, J.S. Lim, Y.-W. Lee, J. Chem. Eng. Data 48 (2002) 774-777.
[181] J.S. Lim, J.-Y. Park, C.H. Yoon, Y.-W. Lee, K.-P. Yoo, J. Chem. Eng. Data 49 (2004) 1622-1627.
[182] D.-J. Oh, B.-C. Lee, Korean J. Chem. Eng. 23 (2006) 800-805.
[183] D.-J. Oh, B.-C. Lee, S.-J. Hwang, J. Chem. Eng. Data 52 (2007) 1273-1279.
[184] J.-Y. Park, S.Y. Kim, H.-S. Byun, K.-P. Yoo, J.S. Lim, Ind. Eng. Chem. Res. 45 (2005) 3381-3387.
[185] H.N. Song, B.-C. Lee, J.S. Lim, J. Chem. Eng. Data 55 (2009) 891-896.
[186] J.-H. Yim, H.N. Song, B.-C. Lee, J.S. Lim, Fluid Phase Equilib. 308 (2011) 147-152.
[187] E.-K. Shin, B.-C. Lee, J.S. Lim, J. Supercrit. Fluids 45 (2008) 282-292.
[188] J. Pauly, J. Coutinho, J.-L. Daridon, Fluid Phase Equilib. 255 (2007) 193-199.
[189] G. Soave, Chem. Eng. Sci. 27 (1972) 1197-1203.
[190] J.A. Barker, D. Henderson, J. Chem. Phys. 47 (1967) 2856-2861.
[191] J.A. Barker, D. Henderson, J. Chem. Phys. 47 (1967) 4714-4721.
[192] J. Gross, G. Sadowski, Ind. Eng. Chem. Res. 40 (2001) 1244-1260.
[193] O. Pfohl, S. Petkow, G. Brunner, Usage of PE A Program to Calculate Phase Equilibria, ISBN: 3-89675-410-6, 1998.
[194] P.J. Carvalho, J.A.P. Coutinho, J. Phys. Chem. Lett. 1 (2010) 774-780.

Chapter 4

High pressure rheology
Experimental and modelling

4.1. Introduction

Rheology is the science of deformation and flow of materials. Rheology applications can be divided into three categories: characterization, processing and design. Thus, motion and forces are linked to describe the flow processes, which may be applied to solve engineering problems arising in biological systems, slurries, suspensions, emulsions, pastes, polymer processing, lubrication, food technology, printing and many other technologies [1-3].

A rheometer is an instrument that measures both stress and deformation history on a material for which the constitutive relation is not known. Shear rheometers can be divided into two groups, drag flow rheometers in which shear is generated between a moving and a fixed solid surface (concentric cylinder, sliding plates, parallel discs and cone-plate rheometers) and pressure-driven rheometers, in which shear is generated by a pressure difference over a closed channel (capillary, slit flow and axial annulus flow rheometers) [3].

Most of the rheological measurements at atmospheric pressure are performed, due to the ease of experimentation in one of the following four shear geometries, capillary flow, parallel-plate and cone and plate torsional flow and Couette flow [3].

High pressure rheometry is an important issue in the crude oil extraction, polymer and lubrication fields because it allows an accurate determination of the pressure-temperature-viscosity relationship. Furthermore, high pressure rheometry is gaining growing interest in other areas such as high-pressure treatment and processing of foods, basic research in chemistry, physics and geophysics, fuels for diesel engines, high-pressure extraction processes using supercritical fluids, high-pressure impregnation and coating, innovative solvent technology based on ionic liquids and semiconductor and nanoparticle industries [4,5].

High pressure rheometers can be classified into three groups, capillary, rotational (cone and plate, parallel plate and concentric cylinder geometries) and sliding plate rheometers. The first practical rotational rheometer was the concentric cylinder instrument of Maurice Couette (1890). The advantages of rotational rheometers are that the viscosity measurements are made under steady-state conditions and there is negligible variation of shear rate and shear stress throughout the sample [6,7]. However, rotational rheometers present some disadvantages, such as shear-induced dissipative conversion of mechanical energy into thermal energy, secondary flow caused by inertial forces (so-called Taylor vortices), slip on the shear surfaces, separation effects in suspensions and end effects [3,4].

The earliest pressurized Couette viscometer appears to have been constructed by Thomas et al. [8] who placed an electric motor within the pressure vessel to drive the rotation. They experienced many problems with this arrangement and the heat generated by the motor was

significant. Hutton and Phillips [9] overcame the problem of driving the rotation by passing a shaft through a high-pressure seal and situating the motor outside of the pressure vessel [10]. Literature on high pressure Couette rheometry is scarce even thought several authors have worked on this topic [4,5,10-12]. Among others, it is worth mentioning the following works: Garrat et al. [7] designed and built a rheometer measuring system that operated up to 3.5 MPa. Khandare et al. [6,13] have designed and developed a high-temperature-high-pressure rheometer to measure viscosity of pitch material at elevated temperatures. Hamilton and Bottomley [12] characterised the high pressure rheology behaviour of polymer-oil blends up to stresses of $5 \cdot 10^{-4}$ Pa through a high pressure Couette rheometer. Parris et al. [14] performed high pressure steady-shear rheological measurements in a Couette rheometer designed for pressures up to 238 MPa. Hwang et al. [15] determined rheological properties by means of a rotational viscometer adapted to measure the viscosity of polymer under high temperature and pressure conditions. Martínez-Boza and co-workers [16-18] have performed rheological studies on used motor oil/vacuum residue blends, bitumens and heavy oils with a controlled stress rheometer, RheoStress RS600 from Haake Gbr., using conventional coaxial cylinder geometry and coaxial cylinder-pressure cell. Larsson et al. [19] and Petterson [20,21] have determined the pressure–viscosity relationship of lubricants by means of a Couette rheometer whose pressure can be raised to 500 MPa. Bair and Winer [22] developed a rotational Couette high-pressure, high-shear stress viscometer with a pressure capability of 300 MPa. Subsequently, Bair [23] built a similar rheometer that can be used up to 1 GPa. Briscoe et al. [24] have measured rheological properties of poly(ethylene oxide) in aqueous salt solutions by a modified Haake Searle-type viscometer, which was incorporated into a high temperature and pressure chamber, with a maximum operating pressure of 100 MPa.

Often rheometers are used to measure the viscosity of Newtonian fluids, this task being also carried out with viscometers. High pressure viscometers can be classified into three groups, falling body, rolling ball and vibrating wire viscometers. The problems that experience most of the falling ball and falling body viscometers are that velocity is not recorded continuously and fluctuations can occur caused by partial contacts on the tube wall or by phase transition phenomena, and also that if the falling cylinders are guided the shear flow is modified due to partial wear between the tube and the guides. As regards the rolling ball viscometers, problems are due to the simultaneous slip, spin and rolling velocity components that give poor reproducibility results, and when they are used for measuring low viscosities, the ball diameter must be very close to the tube diameter and the result become too sensitive to geometrical defaults [11].

4.2. Couette rheometer

4.2.1. Basic principles

The concentric cylinder rheometer is a very common instrument where the sample is sheared between two concentric cylinders, the inner cylinder is called bob and the outer cup. The shear stress is obtained from measurement of the torque, M, to drive the rotating cylinder and the shear rate is obtained from the rotation rate Ω, and the gap between cylinders [10].

Couette rheometers, as well as the other drag flow rheometers, can be designed as controlled strain rheometers, with stress measurement or as controlled stress rheometers with strain measurement. As regards controlled strain rheometers, the most versatile design is direct coupling of a dc motor to the rotating shaft. A tachometer is used to control angular velocity and a capacitance transducer is used to control angular position. Combined with a servo control system, this design has a fast response and can deliver a wide range of shear deformations to the test sample. On the other hand, the most versatile design of controlled stress Couette rheometers consists of a magnetic field, which rotates around a copper or aluminium cup, which is supported by an air bearing. The field induces eddy currents in the cup, which tries to follow the rotating fields. The torque on the cup is proportional to the square of the voltage on the stators. The device is called a drag cup motor and is not very efficient. It takes a high voltage to generate high torques. This high voltage can cause heating of the motor and a transient decrease in the resulting torque. Cooling and compensating circuits can extend the upper torque range. The lowest torque is limited by imperfections in the air bearing and eccentricities in the rotating shaft. Angular displacement of the shaft can be measured by a variety of methods. The optical encoders have a great advantage because they divide 360º into uniform steps. A major limitation in controlled stress rheometers is instrument inertia. The torque imposed on the drag cup must overcome reluctance torque, air bearing friction, and rotor inertia as well as the sample viscosity. With proper inertia correction controlled stress rheometers are very versatile and may replace controlled strain instruments for many applications [3].

Several assumptions are made in order to develop the working equation of Couette rheometers, the flow is assumed laminar and steady, end effects are negligible, test fluid is incompressible, properties are not a function of pressure, temperature is constant, there is no slip at the walls of the instrument and radial and axial velocity components are zero [25].

For Couette rheometers with stationary cup, R_i and R_o being the bob and cup radius, respectively, the measured torque is that required to maintain a constant angular velocity of the bob, the opposite torque coming from the shear stress exerted on the bob by the fluid. A force balance yields:

$$M = 2\pi L r^2 \sigma \tag{4.1}$$

where M is the torque, L is the length of the bob, r is any location in the fluid ($R_i < r < R_o$) and σ is the shear stress.

Moreover, the shear rate may be defined in terms of ω:

$$\dot{\gamma} = -\frac{du}{dr} = -\frac{r d\omega}{dr} \tag{4.2}$$

where u and ω are the linear and the angular velocities, respectively.

In order to relate velocity to shear stress, r is written as a function of σ in Eq. (4.1) and then differentiated with respect to this last variable, obtaining:

$$\frac{dr}{d\sigma} = -\frac{1}{2}\left(\frac{M}{2\pi L}\right)^{1/2} \sigma^{-3/2} \tag{4.3}$$

Substituting the value of torque defined by Eq. (4.1) into Eq. (4.3) gives:

$$\frac{dr}{r} = -\frac{d\sigma}{2\sigma} \tag{4.4}$$

Taking into account that the shear rate is some function of the shear stress, the following equation can be written from Eq. (4.2):

$$d\omega = -\frac{dr}{r} f(\sigma) \tag{4.5}$$

This last equation can be written as a function of $d\sigma$ as follows:

$$d\omega = \frac{1}{2} f(\sigma) \frac{d\sigma}{\sigma} \tag{4.6}$$

Integrating Eq. (4.6) over the fluid present in the annulus result in a general expression for the angular velocity of the bob (Ω) as a function of the shear stress:

$$\Omega = -\frac{1}{2} \int_{\sigma_i}^{\sigma_o} f(\sigma) \frac{d\sigma}{\sigma} \tag{4.7}$$

When dealing with Newtonian fluids, the relationship between shear stress and shear rate is:

$$\dot{\gamma} = f(\sigma) = \frac{\sigma}{\eta} \tag{4.8}$$

Using the expression for $f(\sigma)$ given by Eq. (4.8) and substituting the value of σ for that obtained from Eq. (4.1), the integration of Eq. (4.7) yields the Margules equation:

$$\Omega = \frac{M}{4\pi L\eta}\left(\frac{1}{R_i^2} - \frac{1}{R_o^2}\right) \tag{4.9}$$

The substitution of the value of σ given by Eq. (4.1), as well as the value of η given by the Margules equation in Eq. (4.8) yields:

$$\dot{\gamma} = \frac{2}{r^2}\left(\frac{1}{R_i^2} - \frac{1}{R_o^2}\right)^{-1}\Omega \tag{4.10}$$

In a typical Couette rheometer, velocity or displacement of the moving surface and the force on one of the surfaces are the variables measured. By using Eq. (4.1) and Eq. (4.10) it is possible to relate the torque with the shear stress and the angular velocity with the shear rate, respectively. Both equations can be rewritten as follows:

$$\sigma = C_\sigma \cdot M \tag{4.11}$$

$$\dot{\gamma} = C_\gamma \cdot \Omega \tag{4.12}$$

where C_σ and C_γ are geometrical constants defined according to the following equations:

$$C_\sigma = \frac{1}{2\pi r^2 L} \tag{4.13}$$

$$C_\gamma = \frac{2}{r^2}\left(\frac{1}{R_i^2} - \frac{1}{R_o^2}\right)^{-1} \tag{4.14}$$

There are some aspects that should be considered when measuring with concentric cylinder rheometers. One of them is the viscous heating, which is the temperature increase during rheological testing due to viscous generation of heat. Most viscometers are designed with effective temperature control systems that minimize viscous heating problems by rapidly removing the excess heat generated during testing [3]. End effects can also influence rheological measurements, thus, it is important to account for the influence of the bottom of the cylinder on the torque response of the system. This surface is in contact with the fluid but not taken into account in the force balance given by Eq. (4.1). Various bob designs have been developed to minimize end effects. They can be made with a reservoir at the top and a recessed bottom or designing the bottom with a slight angle in an effort to make the shear rate at the bottom equivalent to the shear rate in the annulus [25]. See Fig. 4.1. Moreover, wall effects should also be avoided, they occur when the adherence between the moving surface and the liquid is insufficient to transmit the shear stress and the surface slips above the non-moving liquid sample [26].

Other aspect to take into account is the secondary flow in the Couette geometry, because equations developed for the analysis of rheological data assume that flow is laminar. When an inner cylinder rotates in a concentric cylinder system, the fluid near the inner surface tries to move outward due to centrifugal forces. However, in a Couette type system where the outer surface is rotated, the inertial forces have a stabilizing effect and flow is laminar at much higher shear rates [25].

Secondary flow have been well studied following Taylor's classic work [27]. With the inner cylinder rotating at some speed, inertial forces cause a small axisymmetric cellular secondary motion known as Taylor vortices. These phenomena dissipate energy and cause an increase in the measured torque. For Newtonian fluids and narrow gaps, the criterion for stability is [3,28]:

$$Ta = \frac{\rho^2 \Omega^2 (R_o - R_i) 3R_i}{\eta \dot{\gamma}^2} < 3400 \tag{4.15}$$

where Ta is the Taylor number and ρ the density of the fluid.

Other criterion for stability of Newtonian fluids is the following [25,29]:

$$\frac{\rho \Omega (R_o - R_i) R_i}{\eta} > 41.3 \sqrt{\frac{R_o}{R_o - R_i}} \tag{4.16}$$

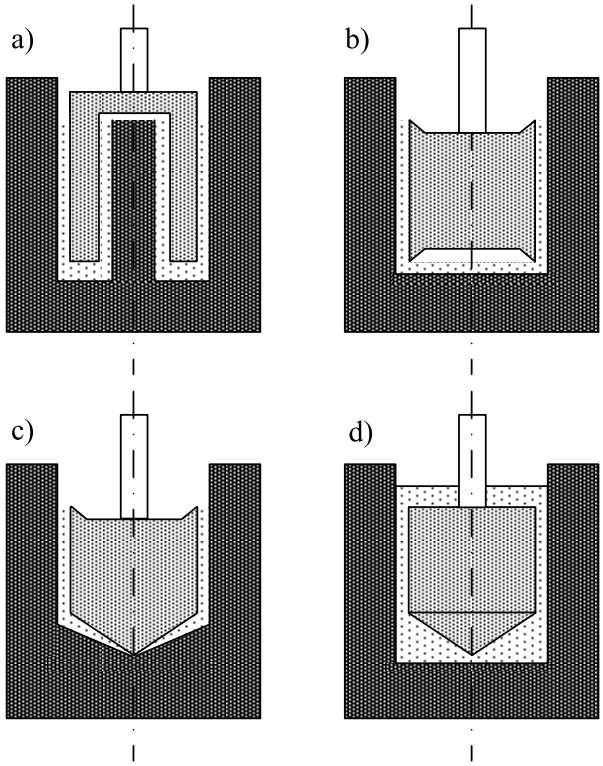

Fig. 4.1. Types of coaxial cylinder designs [26]: (a) Double-gap system (DIN 54453), (b) Traditional system (DIN 53018), (c) Mooney-Ewart system (DIN 53018) and (d) This work, conicylinder system (ISO 3219 / DIN 53019).

Finally, eccentricity is other problem that can appear in Couette rheometers. It changes the assumed velocity profile and can leads to decrease torque. For cylinders with parallel axis displaced an amount a, the reduction ratio in torque (M/M_0) is the following for a Newtonian fluid [3]:

$$\frac{M}{M_0} = \frac{2\left[1-\left(a/(R_o-R_i)\right)^2\right]^{1/2}}{2+\left(1/(R_o-R_i)\right)^2} \tag{4.17}$$

4.2.2. SVM 3000 Stabinger viscometer

In the Thermophysical Properties Laboratory there are several apparatus for viscosity determinations at atmospheric and high pressure. In this PhD Thesis, viscosity values at atmospheric pressure were determined with a viscometer based on a modified Couette principle, SVM 3000 Stabinger. This apparatus from Anton Paar includes a rotational viscometer with cylinder geometry, based on a modified Couette principle. It can perform measurements at atmospheric pressure in the temperature range from 233.15 to 373.15 K, aided by an external cooling at 253.15 K. It can measure viscosities from 0.2 to 10000 mPa·s. This viscometer is a flexible, precise and easy to operate instrument whose basic operating principles and schematic set up are described in a European Patent [30,31]. This apparatus also measures the viscosity index according to ASTM D2270/ ISO 2909. The operation principle of this device is based on a rotating magnet that produces an eddy current field with an exact speed-dependent brake torque. A scheme of the measurement cell is presented in Fig. 4.2. It is important to mention that the viscosity measurement can be traced back to a single speed measurement and it fulfils the required repeatability, reproducibility and comparability of the kinematic viscosity values according to ASTM D 445.

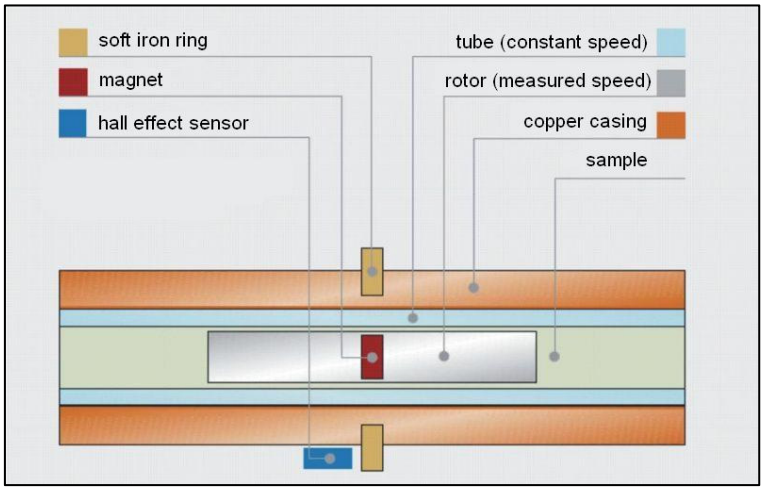

Fig.4.2. Scheme of the viscosity measurement cell of the SVM 3000 Stabinger viscometer.

The small measuring cell contains a tube which rotates at a constant speed and is filled with the sample. Floating in the sample is a hollow titanium measuring rotor with a built-in

magnet. Due to its low density, this rotor is centred in the sample by the buoyancy forces and a measuring gap is formed between the rotor and the tube. It is worth mentioning that this freely swimming rotor requires no bearing, and as it is no bearing, there is no friction. The rotor is forced to rotate by shear stresses in the liquid and is guided axially by a built-in permanent magnet, which interacts with a soft iron ring. The rotating magnetic field delivers the speed signal and induces eddy currents in the surrounding copper casing. These eddy currents are proportional to the speed of the rotor and exert a retarding torque on the rotor, which is measured with extremely high resolution (50 pNm). Shortly after the start of the measurement the rotor reaches a stable speed, determined by the equilibrium between the viscosity-dependent driving torque, which is proportional to the speed difference between the outer tube and the inner rotor, and the retarding torque caused by eddy currents, which is proportional to the inner rotor speed [31]. This rotational speed is measured by an electronic system (hall effect sensor) that counts the frequency of the rotating magnetic field. A diagram concerning the operation of this device is presented in Fig. 4.3.

Thus, two different torques influence the speed of the measuring rotor, the driving torque given by Eq. (4.18) and the retarding torque given by Eq. (4.19) [31]:

$$T_d = \eta A \dot{\gamma} r_1 = K_d \eta (n_2 - n_1) \tag{4.18}$$

$$T_r = K_r n_1 \tag{4.19}$$

where $\dot{\gamma}$ is the shear rate, η the dynamic viscosity, A the area of the measuring rotor, n_1 the speed of the measuring rotor, n_2 the speed of the measuring tube and K_d and K_r are constants.

At the equilibrium the two torques are equal ($T_d = T_r$) and the viscosity is given by the following equation [31]:

$$\eta = \frac{K}{\frac{n_2}{n_1} - 1} \tag{4.20}$$

where K is the ratio between the constants K_r and K_d.

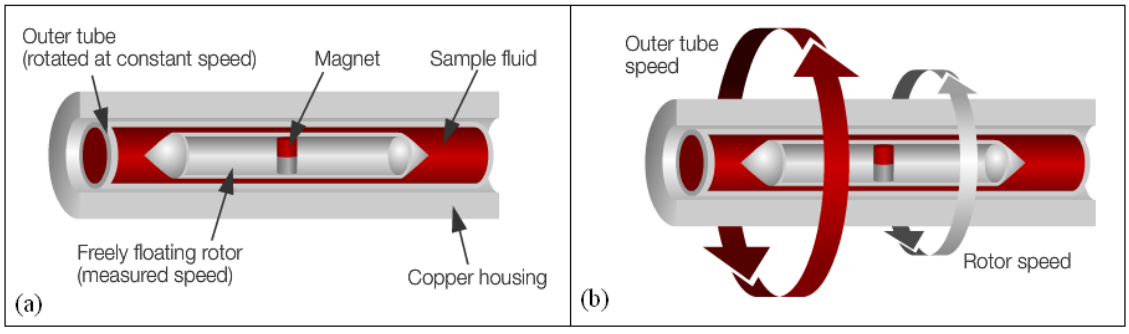

Fig.4.3. Operation principle of the SVM 3000 Stabinger viscometer. Device (a) and rotation (b) diagrams.

Temperature control and measurements are performed through an integrated thermostat with cascaded Peltier elements and Pt-100 thermometer that enable rapid changes, exact adjustments of the measuring temperature and very short equilibrium times.

Experimental setup and procedure

The experimental setup comprises the above described measurement cell along with a density measuring cell that compose the Anton Paar commercial instrument. Additionally, an external thermostatic bath LAUDA PROLINE RP845 is connected to the instrument in order to refrigerate it for performing the low temperature measurements. A photograph of the experimental device was presented in Fig. 2.9. Regarding the experimental procedure, it consists in introducing 2.5 ml of degassed sample in the apparatus by means of a syringe and then measurements are carried out automatically following a temperature ramp. When finished, the device is cleaned through suitable solvents. The temperature range performed in this PhD Thesis was from 278.15 K to 373.15 K.

Calibration and uncertainty

Viscosity calibration is performed in an automated way after introducing in the cell two samples of certified viscosity standards provided by Anton Paar. The temperature uncertainty is 0.02 K from 288.15 K to 378.15 K and 0.05 K outside this range. As regards dynamic viscosity uncertainty of the measurements is ±1% of the measured viscosity value.

The viscometer accuracy was checked by means of the certified viscosity standard oil CANNON N350, in the temperature range from 293.15 K to 373.15 K, obtaining an AAD% of 1.1% for dynamic viscosity values.

4.2.3. High pressure rheometer Reologica StressTech HTHP

The implementation of a high pressure rheometer Reologica StressTech HTHP was performed during this PhD Thesis. This rheometer consists of a CC25 DIN53019 concentric cylinder geometry and relies on Couette flow, involving confinement of the sample between a stationary cup and a rotating bob, with a 1 mm gap (Fig.4.1 (d)). The inner cylinder has a diameter of 25 mm and a length of 37.67 mm. It can perform controlled stress and controlled rate measurements. The rheometer can operate in a torque range between $1 \cdot 10^{-4}$ N·m and $4 \cdot 10^{-2}$ N·m, which entails a maximum shear stress around 350 Pa.

This rheometer works along with the RheoExplorer software, which has been designed to provide flexibility for configuring and using the instrument. It enables a computer to be used as the interface to allow the user to control the instrument, collect and analyze the resulting data.

Reologica StressTech HTHP can operate in a temperature range from ambient temperature to 493.15 K. The cell can be heated or cooled at programmed rates. The temperature control is performed through a Joule/Thomson approach, utilizing a single temperature control system. In addition, a separate water circulator is required to act as the cold side heat sink for the thermoelectric device. The temperature control system consists also of a thermocouple sensor and an electronic box.

The rheometer can operate at pressures up to 100 MPa. The high pressure cell is equipped with inlet and outlet ports for sample loading. The cell is suitable for self purging and does not have to be opened after each measurement. The pressure in the cell is increased externally through a high pressure source. To be able to close the cell completely from the environment, the torque is applied using a magnetic coupling. The structure of the instrument is composed by a motor module, in which the drag cup motor applies a torque to the rotor and the position sensor measures the angular deflection during rotation. The whole system is running in a maintenance free air bearing to avoid friction between rotating and static parts. This type of bearing requires a clean supply of dry oil-free air of 5 l/min and ensures frictionless measurements.

As regards the motor, it is an AC asynchronous one, extremely linear from low to high torque with a smooth and continuous response around 360 degrees. The rotor is light, high strength aluminium alloy, and has low inertia allowing fast transient and excellent high frequency response. Concerning motor temperature, it is maintained constant by using an external heat exchanger (motor cooler) that is coupled with the air form the air bearing allowing the rheometer to run at full power continuously without any change in motor temperature and thus change in torque output.

Experimental setup

In this PhD Thesis, it was undertaken the implementation of a technique for rheological characterization at high pressure whose core is a Reologica StressTech Couette HTHP rheometer. The rheometer, connected to a computer, comprises the high pressure measurement cell equipped with inlet and outlet ports, an electronic box, a motor module and a motor cooler, a water circulator (Huber CC505) and a thermocouple sensor. A picture of the equipment is presented in Fig. 4.4.

Fig.4.4. Picture of the high pressure rheometer apparatus.

In order to supply clean and dry air to the rheometer bearing, an additional compressed air line was installed through four SMC air filters (AMG 150C, AW20, AFM20 and AFD20). In addition, a high pressure line consisting of a piston screw pump HiP model 50-6-15, a pressure transducer Digibar II K-PE-300, as well as high pressure tubes and valves was connected to one of the inlet ports of the measurement cell. Moreover, the other ports were connected to high pressure valves. A syringe coupled to a Hamilton valve is connected to the high pressure line for sample loading.

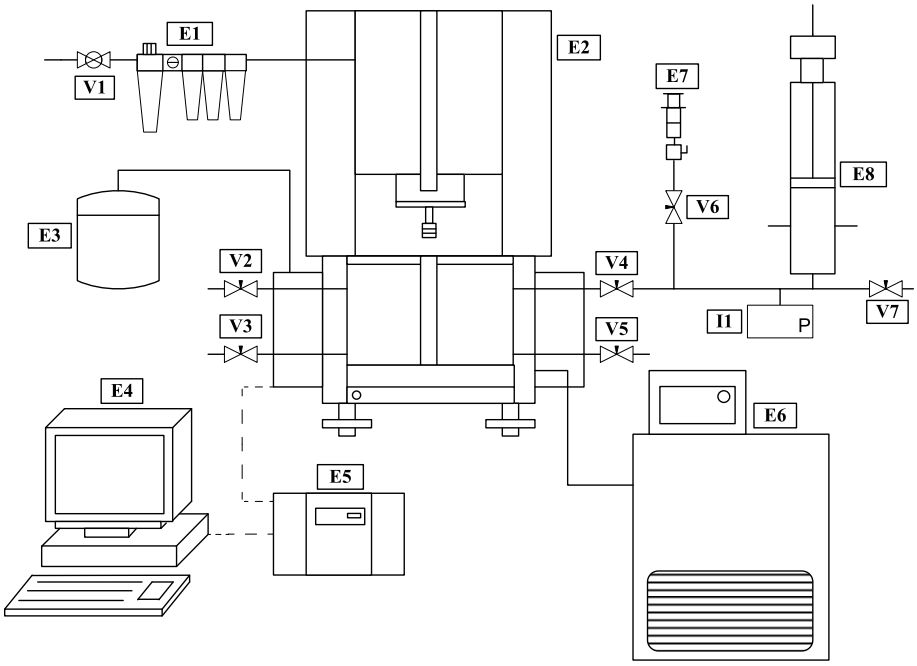

Fig.4.5. Schematic set-up of the high pressure rheometric technique. (E1) air filters; (E2) rheometer; (E3) motor cooler; (E4) computer; (E5) control box; (E6) thermostatic bath; (E7) glass syringe connected to Hamilton valve; (E8) piston screw pump; (V1 to V7) valves; (I1) pressure transducer.

The thermocouple reading was corrected from 288.15 K to 363.15 K through a calibrated Pt-100 probe inserted inside the rheometer cup. The final uncertainty of the temperature readings is estimated to be ±0.5 K, whereas the pressure transducer has a working range up to 200 MPa

and is calibrated with an uncertainty of ±0.02 MPa. The rheometric technique was used from 298.15 K to 353.15 K and up to 75 MPa. A scheme of this experimental technique is presented in Fig. 4.5.

Experimental procedure

Prior to the loading of the samples by means of a syringe coupled to a Hamilton valve and connected to V6, all the system is evacuated through a vacuum pump connected to V7. Once the system is loaded V6 is closed. The temperature set point for the measurements is selected in the RheoExplorer software and the thermostatic bath temperature is automatically fixed 5 K lower. Once the temperature is stable, the magnetic coupling gap of the rheometer is fixed to zero.

The first tests that are performed to the sample are stress-time tests in order to know the minimum and maximum stress limits which give right results for our sample. Afterwards the flow curves at atmospheric pressure under controlled stress tests are performed in an automated way following the stress ramp imposed to the software. A delay time of 10 s and an integration time of 20 s for each measurement are usually selected. When finished, pressure is increased by means of the piston screw pump and the measurement procedure is repeated. As soon as all the desired pressures are measured, the temperature set point is changed and the next isotherm measurements are carried out. Finally all the system must be cleaned with suitable solvents.

Calibration and uncertainty

The rheometer is calibrated for each sample and temperature taking into account the viscosity values at atmospheric pressure measured in the high precision rotational SVM 3000 Stabinger viscometer. The correction of viscosity values performed at atmospheric pressure is maintained in all the pressure range.

As the uncertainty of this rheometric technique is not established in the equipment specifications, it was checked in this PhD Thesis by comparison of the results obtained with those of the literature. In order to do that, two oligomers were selected as reference samples. One of them is a polyalphaolefin (PAO40) provided by Repsol YPF and the other is a polybutene (H8) provided by Ineos Oligomers. Polybutene H8 has a molecular weight of 490 $g \cdot mol^{-1}$ and a polydispersity index of 1.85.

Both of them had been previously rheometrically characterised by Bair [32,33]. PAO40 was characterised by this author [32] in the temperature range from 293.15 K to 373.15 K and pressures up to 1.3 GPa, whereas the polybutene was characterised [32,33] in a temperature range from 303.15 K to 373.15 K, pressures up to 1.0 GPa and shear rates up to $1 \cdot 10^5$ s^{-1}.

The flow tests of PAO40 and polybutene H8 were performed in the temperature range from 298.15 K to 353.15 K and pressures up to 75 MPa. In Figs. 4.6 and 4.7 a Newtonian behaviour for both fluids can be observed.

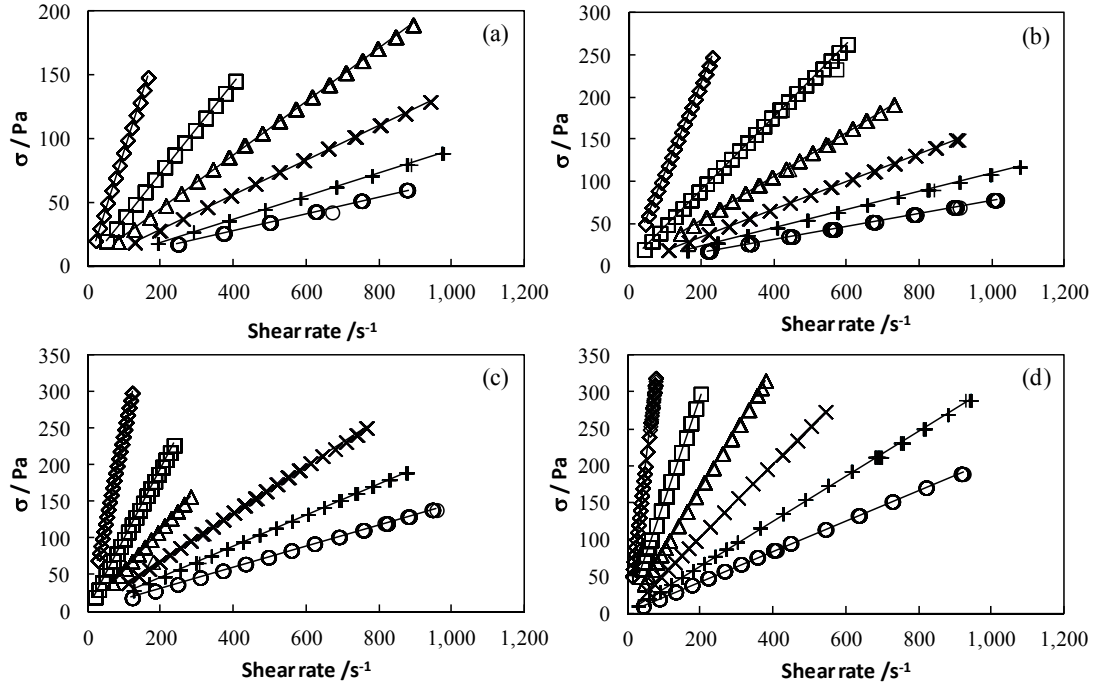

Fig.4.6. Flow tests of PAO40 at (a) 0.1 MPa, (b) 10 MPa, (c) 50 MPa and (c) 75 MPa. 297.91 K (◇), 315.19 K (□), 326.70 K (△), 338.22 K (×), 349.73 K (+) and 361.25 K (○).

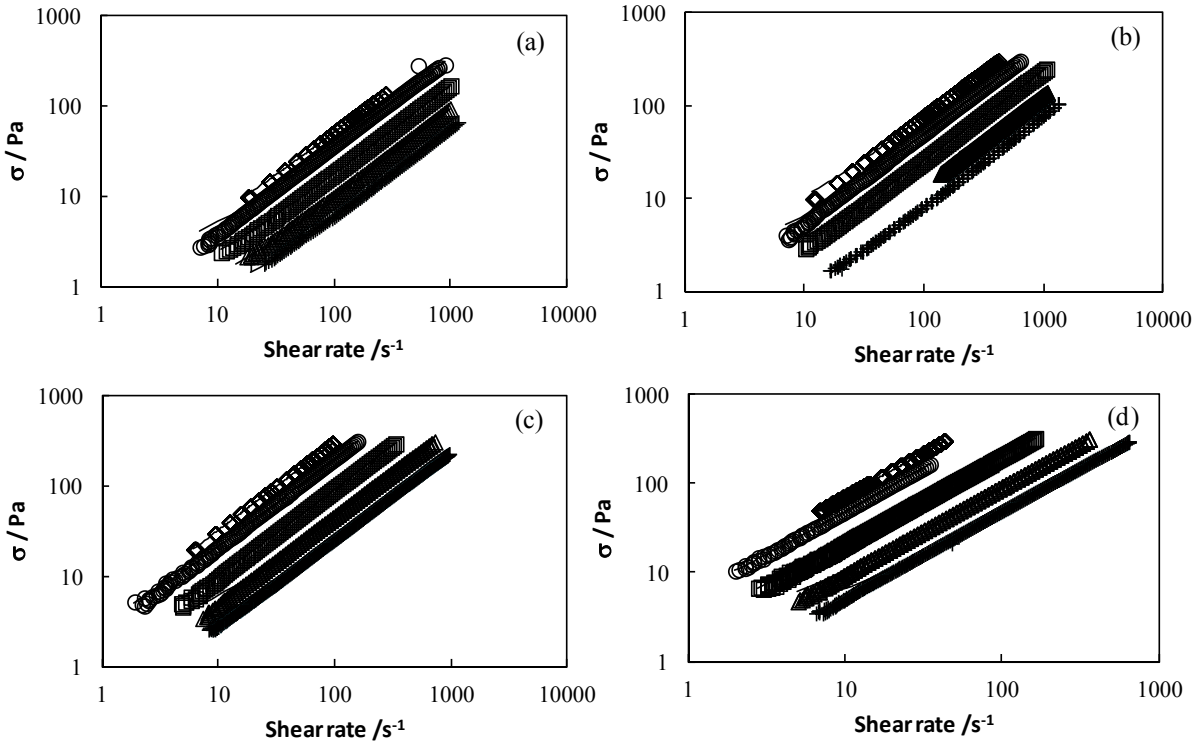

Fig.4.7. Flow tests of polybutene H8 at (a) 0.1 MPa, (b) 10 MPa, (c) 50 MPa and (c) 75 MPa. 297.91 K (◇), 303.67 K (○), 315.19 K (□), 326.70 K (△) and 338.22 K (+).

A comparison between the measured viscosity values for these oligomers and the values published by Bair [32,33] was performed (see deviation plot in Fig. 4.8). The AAD% obtained for PAO40 with the values from Bair correlation [32] was 6.0 %, whereas the AAD% obtained for polybutene H8 was 8.3 % with values from one of the correlations published by Bair [32] and 7.8 % with values from other of his correlations [33].

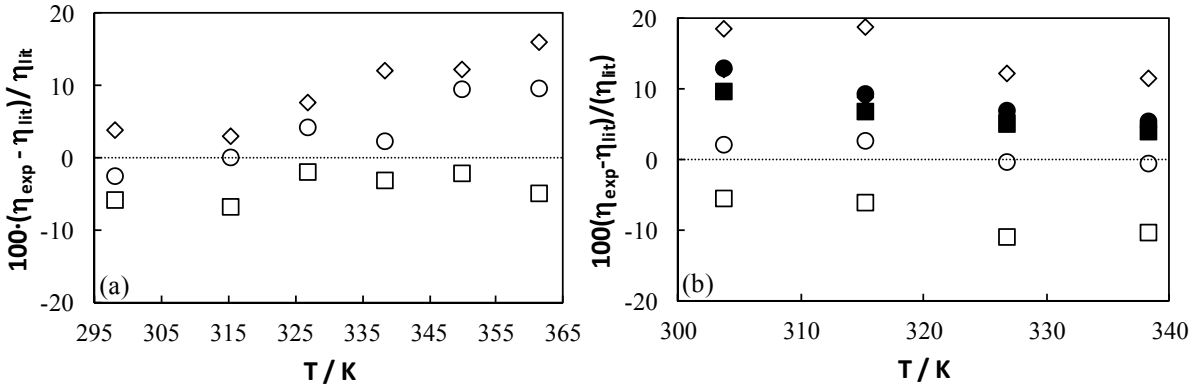

Fig.4.8. Relative deviations between viscosity data obtained in this PhD Thesis and those from Bair [32,33] for (a) PAO40 and (b) polybutene H8 at 10MPa (□, ■), 50 MPa (○, ●) and 75 MPa (◇, ◆). Empty symbols represent comparison with reference [32] and filled symbols with reference [33].

4.3. Viscosity correlations and prediction methods

Viscosity data at atmospheric pressure were correlated by means of the Vogel-Fulcher-Tammann (VFT) equation [34-36]**:**

$$\ln(\eta) = A + \frac{B}{T - T_0} \tag{4.21}$$

where η is the dynamic viscosity, T is the temperature in K and A, B and T_0 are constants.

As regards viscosity data as a function of temperature and pressure, it was correlated by means of the Comuñas et al. equation [37]:

$$\eta(p,T) = A\left(\frac{p+E}{p_{ref}+E}\right)^{F} \exp\left(\frac{B}{T-C}\right) \tag{4.22}$$

where p_{ref} is the reference pressure, B and C are constants and E has the following polynomial dependence on temperature:

$$E = E_0 + E_1 T + E_2 T^2 \tag{4.23}$$

where E_0, E_1 and E_2 are constants.

Moreover, viscosity of the vegetable oils at atmospheric pressure was predicted through the fragment based approach for estimating thermophysical properties of triglycerides, fats and

vegetable oils [38,39]. Thus, the triglycerides liquid viscosities can be calculated from the viscosity fragment composition and fragment-specific parameters according to the equation:

$$\ln \eta = \sum_{A} N_{frag,A} \ln \eta_A(T) \tag{4.24}$$

where $\ln \eta_A$ represents the liquid viscosity contribution of the fragment A (expressed in units of Pa·s) and $N_{frag,A}$ is the number of fragment A in the component.

The expression for the liquid viscosity of fragment A, as a function of temperature is the following:

$$\ln \eta_A = C_{1,A} + \frac{C_{2,A}}{T} + C_{3,A} \ln T \tag{4.25}$$

where $C_{1,A}$, $C_{2,A}$ and $C_{3,A}$ represent temperature dependency correlation parameters for viscosity.

4.4. References

[1] R.I. Tanner, Engineering rheology, 2nd ed., Oxford University Press, Oxford, 2000.
[2] F.A. Morrison, Understanding rheology, Oxford University Press, New York, 2001.
[3] C.W. Macosko, Rheology : principles, measurements and applications, Wiley-VCH, New York, 1994.
[4] L. Kulisiewicz, A. Delgado, Applied Rheology 20 (2010) 13018-13011-13018-13015.
[5] F.J.M. Boza, C. Gallegos, Rheology. in: C. Gallegos, K. Walters, (Eds.), Rheology, Encyclopedia of chemical sciences, engineering and technology resources (Encyclopedia of life support systems), 2009.
[6] P.M. Khandare, J.W. Zondlo, P.B. Stansberry, A.H. Stiller, Carbon 38 (2000) 881-887.
[7] G.W. Garratt, B. Rand, S. Whitehouse, Fuel 67 (1988) 238-241.
[8] B.W. Thomas, W.R. Ham, R.B. Dow, Ind. Eng. Chem. 31 (1939) 1267-1270.
[9] J.F. Hutton, P. M.C., Nature Physical Science 245 (1973) 15-16.
[10] S.S. Bair, High-pressure rheology for quantitative elastohydrodynamics 1st ed., Elsevier, Amsterdam, 2007.
[11] D. Berthe, P. Vergne, Journal of Rheology 34 (1990) 1387-1414.
[12] G.M. Hamilton, L. Bottomley, Trib. Int. 20 (1987) 41-48.
[13] P.M. Khandare, J.W. Zondlo, P.B. Stansberry, A.H. Stiller, Carbon 38 (2000) 889-897.
[14] M.D. Parris, B.A. MacKay, J.W. Rathke, R.J. Klingler, R.E. Gerald, Macromolecules 41 (2008) 8181-8186.
[15] T. Hwang, M. Kim, Y. Ahn, J. Lee, The high pressure rheology of polymer nanocomposites containing supercritical carbon dioxide, 68th Annual technical conference of the society of plastics engineers (ANTEC 2010), Curran Associates, Inc, Orlando, Florida, 2010, pp. 1095-1098.
[16] F. Martínez-Boza, F. Fernández-Latorre, C. Gallegos, Fuel 88 (2009) 1595-1601.
[17] M.J. Martín-Alfonso, F.J. Martínez-Boza, F.J. Navarro, M. Fernández, C. Gallegos, Fuel 86 (2007) 227-233.
[18] M. Martín-Alfonso, F. Martínez-Boza, P. Partal, C. Gallegos, Rheol. Acta 45 (2006) 357-365.
[19] R. Larsson, P.O. Larsson, E. Eriksson, M. Sjöberg, E. Höglund, Proc. Inst. Mech. Eng., Part J: J. Eng. Tribol. 214 (2000) 17-27.
[20] A. Pettersson, Trib. Int. 36 (2003) 815-820.
[21] A. Pettersson, Trib. Int. 40 (2007) 638-645.
[22] S. Bair, W.O. Winer, Tribol. Trans. 36 (1993) 721-725.
[23] S. Bair, Proc. Inst. Mech. Eng., Part J: J. Eng. Tribol. 216 (2002) 139-149.
[24] B. Briscoe, P. Luckham, S. Zhu, Macromolecules 29 (1996) 6208-6211.
[25] J.F. Steffe, Rheological methods in food process engineering, 2nd ed., Freeman Press, East Lansing, MI, 1996.
[26] G. Schramm, A practical approach to rheology and rheometry, 2nd ed., Thermo electron (Karlsruhe) GmbH, Karlsruhe, 2004.

[27] G.I. Taylor, Philosophical Transactions of the Royal Society of London Series a-Containing Papers of a Mathematical or Physical Character 223 (1923) 289-343.
[28] S. Chandrasekhar, Hydrodynamic and hydromagnetic stability, Dover, New York 1981.
[29] R.W. Whorlow, Rheological techniques, Ellis Horwood, New York, 1992.
[30] European Patent EP 0 926 481 A2.
[31] F. Novotny-Farkas, W. Böhme, H. Stabinger, W. Belitsch, Anton Paar GmbH.
[32] S. Bair, Tribol. Trans. 43 (2000) 91-99.
[33] S. Bair, J. Non-Newtonian Fluid Mech. 97 (2001) 53-65.
[34] H. Vogel, Phys. Z. 22 (1921) 645.
[35] G.S. Fulcher, J. Am. Ceram. Soc., 8 (1925) 339.
[36] G. Tammann, W. Hesse, Z. Anorg. Allg. Chem. 156 (1926) 245.
[37] M.J.P. Comuñas, A. Baylaucq, C. Boned, J. Fernández, Int. J. Thermophys. 22 (2001) 749-768.
[38] L. Zong, S. Ramanathan, C.-C. Chen, Ind. Eng. Chem. Res. 49 (2010) 876-886.
[39] L. Zong, S. Ramanathan, C.-C. Chen, Ind. Eng. Chem. Res. 49 (2010) 3022-3023.

Chapter 5

High pressure densimetry
Results and discussion

In this chapter results dealing with high pressure densimetry are presented. Thus, density behavior over a wide temperature and pressure range of eight reference oils for two stroke engines, hydraulic and gear applications (SYN-2T, MIN-H01, MIN-H02, MIN-H03, BIO-H MIN-G, MIN-G01 and MIN-G02) up to 120 MPa is analyzed. Additionaly, density data of two vegetable base oils (HOSO-B and HOSO-B1) and ten biodegradable developed and comercial lubricants for hydraulic and gear applications (BIO-H01, BIO-H02, BIO-H03, BIO-H04, BIO-H05, BIO-H06, BIO-G00, BIO-G01, BIO-G02 and SYN-G01) are provided and a comparison with results for reference fluids is performed. All the studied lubricants were presented in table 1.2. Density derived properties for these oils were also calculated by differenciation from the correlation of this property with temperature and pressure through the Tammann-Tait equation. Finally, viscosity values of these oils at atmospheric pressure, as well as the viscosity index (VI) are also reported.

It was observed that density of the biodegradable lubricants is higher than that of the mineral and synthetic reference oils for the different applications. Besides, among the vegetable based oils, density decreases with the high oleic sunflower oil content. Regarding compressibility, it was found that vegetable base oils and also the biodegradable developed oils based on high oleic sunflower oil present lower compressibility than reference oils for hydraulic and gear applications. In addition, as concerns viscosity index, as expected, a better behaviour was found for the vegetable base oils and the biodegradable developed oils, i.e. they present higher viscosity index than the reference mineral oils.

Results concerning densimetry of ILs up to 120 MPa are also presented in this chapter. The studied ILs are the following, 1-ethyl-3-methylimidazolium ethylsulfate, 1-ethyl-3-methylimidazolium n-hexylsulfate, 1-(2-methoxyethyl)-1-methyl-pyrrolidinium bis(trifluoro-methylsulfonyl)imide, 1-butyl-1-methylpyrrolidinium bis(trifluoromethylsulfonyl)imide, 1-(2-methoxyethyl)-1-methyl-pyrrolidinium tris(pentafluoroethyl)trifluorophosphate, 1-butyl-1-methylpyrrolidinium tris(pentafluoroethyl) trifluorophosphate and trihexyl(tetradecyl)-phosphonium tris(pentafluoroethyl)trifluorophosphate. All the studied ILs were presented in table 1.1. The method proposed by Gardas and Coutinho and also that proposed by Jacquemin et al. were employed for predicting the experimental density values. Furthermore, from experimental density results isothermal compressibility and isobaric thermal expansivity were calculated, finding a non-monotonous behaviour of this last property with temperature. Additionally, a bibliographic search was performed to establish sequences of the studied properties as a function of the IL cations and anions. Finally, the obtained results for the studied properties were compared with those of synthetic, mineral and vegetable lubricants.

All these results are further explained and discussed in the following sections:

1. Compressibilities and viscosities of reference and vegetable oils for their use as hydraulic fluids and lubricants. *T. Regueira, L. Lugo, O. Fandiño, E.R. López, J. Fernández, Green Chem. 13 (2011) 1293–1302*.
2. Compressibility and viscosity of new biodegradable lubricants based on high oleic sunflower oil for their use as hydraulic fluids. *T. Regueira, L. Lugo, J. Fernández, to be submitted.*
3. Compressibilities and viscosities of reference, vegetable and synthetic gear lubricants. *T. Regueira, L. Lugo, J. Fernández, submitted.*
4. High pressure volumetric properties of 1-ethyl-3-methylimidazolium ethylsulfate and 1-(2-methoxyethyl)-1-methyl-pyrrolidinium bis(trifluoromethylsulfonyl)imide. *T. Regueira, L. Lugo, J. Fernández, J. Chem. Thermodyn. 48 (2012) 213–220.*
5. Influence of the pressure, temperature, cation and anion on the volumetric properties of ionic liquids: new experimental values for two salts. *T. Regueira, L. Lugo, J. Fernández, J. Chem. Thermodyn. 58 (2013) 440–448.*
6. Ionic liquids as hydraulic fluids: Comparison of several properties with those of conventional oils. *T. Regueira, L. Lugo, J. Fernández, Lub. Sci., 2013, DOI: 10.1002/ls.1235.*

5.1. Compressibilities and viscosities of reference and vegetable oils for their use as hydraulic fluids and lubricants*

*T. Regueira, L. Lugo, O. Fandiño, E.R. López, J. Fernández, Green Chem. 13 (2011) 1293–1302. Reproduced by permission of The Royal Society of Chemistry. http://pubs.rsc.org/en/Content/ArticleLanding/2011/GC/c0gc00597e.

Abstract

The use of biodegradable lubricants based on vegetable oils is receiving increasing attention, being an important area of research, in order to promote products with a reduced environmental impact during their entire life cycle. Compressibility is one of the key properties that should be taking into account to develop efficient hydraulic fluids and gear oils. The isothermal compressibility of four reference fluids, a sunflower base oil and a biodegradable oil up to 50 MPa and from 298.15 K to 373.15 K has been determined. For this aim an experimental device based on a vibrating-tube densimeter was used to obtain the density values. The density values at atmospheric pressure were correlated within an absolute average deviation of 0.07% with the Rackett equation whereas a modified Tait equation was used to correlate the experimental data over all temperatures and at higher pressures. The sunflower base oil analyzed in this work has a slightly lower compressibility than those of the reference oils for hydraulic and two stroke engines applications. Moreover, viscosities from 278.15 K to 373.15 K and Viscosity Index (VI) were determined for all the analyzed oils using a SVM 3000 Anton Paar rotational Stabinger viscometer.

Introduction

The EU Ecolabel is part of a broader action plan on sustainable consumption and production and sustainable industrial policy adopted in 2008 by the European Commission. The objective of the EU Ecolabel is to promote products with a reduced environmental impact during their entire life cycle and to provide consumers accurate information on the environmental impact of products. The Eco-label is given to the products which have the potential to reduce certain negative environmental impacts, in comparison with other products in the same product group. The product group 'lubricants' is included in the Ecolabel and comprises up to now hydraulic oils, greases, chainsaw oils, two stroke engine oils, concrete release agents and other total loss lubricants.[1]

Fortunately in the last decade, there has had a slow but steady worldwide move toward the use of "environmentally friendly" or more readily biodegradable lubricant fluids[2] and greases[3]. Biodegradability has become one of the most important design parameters both in the selection of the base fluid and in the overall formulation of the finished lubricant due to new environmental regulations. This demand for biodegradable lubricants is due to a growing concern for the impact that our technology is making to our environment. This concern is occurring both, as the result of a combination of local and national regulations, and as a result of consumer influence. The environmentally friendly nature of vegetable oil-based lubricants and the marketing benefits of having such products have prompted several companies to become involved.[4] Vegetable oils are considered a key class of renewable raw materials and base stock

for a new "Green Chemistry" as well as carbohydrates, lignin, natural fibers and natural rubber[5]. The biodegradability of the vegetable oils is better than those of conventional mineral oils, polyalphaolefins or polyalkylene glycols[5-7].

The benefits of vegetable oils being both renewable and biodegradable have provided an incentive to find applications for these fluids as oils for two stroke engines, gears, drilling fluids, metalworking, outboard engine lubricants and greases, as well as hydraulic fluids, chainsaw oils and mould release oils, among others[8, 9]. Apart from the biodegradability, the advantages of vegetable oil-based fluids are their low toxicity, low volatility, high shear stability, high flash point and viscosity index, as well as low health and safety risks and easy disposable.[10] Vegetable oils are preferred not only because of these properties, but also because they are renewable raw materials.[11-13] Besides, their polar ester groups are able to adhere to metal surfaces and, therefore, possess good boundary lubrication properties.[14] Nowadays, vegetable oils present some disadvantages as their higher cost than mineral oils, their poor low-temperature properties, reduced operating temperature ranges, moderate oxidative stability and their availability in limited viscosity ranges[4]. The higher polyunsaturation, the poorer oxidative performance; thus, saturated vegetable oils show better oxidative stability.[15,16] Antioxidants, chemical additives, diluents and high-oleic vegetable oils can be effectively used to improve the oxidative stability and low temperature fluidity of vegetable oil derivatives.[15,16] Vegetable oil-based lubricants formulated using these methods exhibit superior oxidative stability, and improved low temperature properties such as pour points compared to commercially available industrial oils such as bio-based hydraulic fluids.[16] Joseph and Sharma[17] found that the mixture of phenolic and aminic antioxidants may be applied to boost the thermo-oxidative stability of vegetable oils when used as lubricant base oils at temperatures around 120ºC. Another approach used to improve the oxidative stability of vegetable oils is to modify the fatty acid structure either chemically or genetically.[18-20] Thus, Vinci et al.[21] have proposed a thermo-oxidatively stable base lubricant based in methyl-12-hydroxystearate, a derivative of the castor oil with 70% renewable carbon content (instead 100% for the vegetable oils). Nevertheless, Scherer et al.[22] and Rettemeyer et al.[23] concluded that EU-Ecolable biohydraulic oils based in saturated branched esters give better efficiency than vegetable oils. Hence, new research is needed in additives for vegetable oils in order to improve their oxidative stability and low temperature fluidity. As this regard, we should point out that Mendoza et al.[24] have recently developed a formulated sunflower base oil for hydraulic systems of agricultural tractors with a biodegradability of 89%, an improved pour point of -27ºC (being -3ºC for the sunflower base oil) and an improved oxidation stability (its oxidation induction time is 71 minutes instead of 8 min for the base oil). This formulated oil avoids the formation of microweldings and fulfils the

requirements of the reference mineral oil for extreme pressure tribological tests. Mendoza et al.[24] indicated that the new oil has worked in an agricultural tractor without problems at least for 800 hours.

In Spain, several research groups and companies have joined their effort to develop new formulation based on vegetable oils in the framework of the project entitled "Biolubricants based on vegetable oils and their synthetic derivatives" (BIOVESIN)[24,25]. In the framework of this project one of the tasks is to evaluate the density-pressure behavior of vegetable oils because it should also be included in a hydrostatic evaluation since the compressibility of fluids affects their dynamic performance.[26] Thus, compressibility is one of the properties that should be considered when a hydraulic fluid is selected for a determined application. A low compressibility translates into fast response time, high pressure transmission velocity, and low power loss. In hydraulic systems that operate at high pressure, oils with low compressibility are required to transmit power efficiently. Nevertheless, certain compressibility can be convenient because it dampens pressure surges caused by switching and thus provides smoother operation[27]. In general, the potential for energy loss and heat production of a lubricant decreases with its compressibility.

Materials with high compressibility i.e. low bulk modulus act as damping fluids[28]. The issues caused by a high compressibility are: servos fail to maintain static rigidity and present undesirable effects in system amplification, loss in efficiency, and cavitation, which may cause metal fracture, corrosive fatigue, and stress corrosion[29].

Tribological contacts are considered to be elastohydrodynamic if the deformation of the solid bodies in the contact region is not negligible compared to the film thickness. Two of the three critical tribosystems in automobile engines have full elastohydrodynamic lubrication (EHL): the cam/follower system and the crank shaft. The isothermal compressibility is also used in various calculations of the oil film thickness[30,31], as well as to estimate the ratio of the pressure-viscosity and of the temperature-viscosity coefficients[4,32]. Film thickness in the high-pressure region is usually determined by the conditions in the inlet EHL region where the lubricant is not compressed. Nevertheless, for the modeling of the EHL one of the fundamental equations that should be used is the density-pressure relationship of the lubricant. Compression will decrease the film thickness further as the lubricant is entrained into the high-pressure region and the more compressible the lubricant is, the thinner will be the lubricant film[33]. Thus, from numerical EHL analysis, Höglund[34] found that the central film thickness becomes thinner as the oil compressibility increases, whereas the minimum film thickness remains unaffected. Moreover from a theoretical point of view the isothermal compressibilities are used to check

molecular simulations studies[3, 35] of biodegradable compounds, for several industrial applications.

In the last decade, our research group has performed experimental and theoretical studies in broad pressure ranges of the viscosity and density of lubricants (PAGs and esters) and their mixtures with HFC134a and with CO_2.[36-46] In this work, the isothermal compressibility of four reference oils, a sunflower base oil and a biodegradable oil up to 50 MPa and from 298.15 K to 373.15 K has been determined from density measurements. Moreover, using a SVM 3000 Anton Paar rotational Stabinger viscometer, the Viscosity Index (VI) was measured for all the analyzed oils, as well as atmospheric density and viscosity from 278.15 K to 373.15 K. The values of these properties are also of interest in the development of vegetable-oil based fuels.[47-49] Density and compressibility are relevant because injection systems, pumps and injectors must deliver the amount of fuel precisely adjusted to provide proper combustion.[50] Compressibility and densities should be taken into account in the design of the injection systems.[51, 52] Rackett and Tammann-Tait equations were used to correlate atmospheric and pressure density data respectively.

Results and discussion

Studied lubricants

In Table 1 the density at 293.15 K and kinematic viscosity at 313.15 K as well as the viscosity index (VI) of a high-oleic sunflower oil, HOSO-B, a biodegradable oil, BIO-H, three reference mineral oils, MIN-H01, MIN-H02, and MIN-G, as well as a synthetic oil, SYN-2T, are presented. According to this table, the trend found for the viscosity index of the lubricants studied is HOSO-B> BIO-H> MIN-H01> MIN-H02> SYN-2T> MIN-G. Therefore, as expected, the VI of the high-oleic sunflower oil and biodegradable oil are higher than those of the reference mineral and synthetic oils, i.e., their viscosity change less with changes in temperature, what is a desirable requirement for lubricants. This is one of the known advantages of the vegetable oils.

Table 1 Viscosity Index (VI), kinematic viscosity (ν), and density (ρ) of the analyzed oils.

Name	Description	Application	ρ/g·cm^{-3} (293.15 K)	ν/mm^2·s^{-1} (313.15 K)	*VI*
		Reference oils			
MIN-H01	Mineral oil	Hydraulic	0.8745	48.36	144
MIN-H02	Mineral oil	Hydraulic	0.8655	30.62	138
SYN-2T	Synthetic oil	Two Stroke Engine	0.8758	60.32	118
MIN-G	Mineral oil	Gearbox	0.8969	324.0	96.2
		High Oleic Sunflower Base Oil (HOSO)			
HOSO-B	Refined 85% oleic	—	0.9128	39.23	203
		Biodegradable lubricant			
BIO-H	Biodegradable	Hydraulic	0.9180	58.45	196

In Table 2 the experimental viscosity values are presented for the different oils measured in this work from 278.15 K to 373.15 K.

Table 2 Experimental dynamic viscosities at atmospheric pressure, η/mPa·s, for the lubricants studied in this work.

T /K	MINH-01	MIN-H02	SYN-2T	MIN-G	HOSO-B	BIO-H
278.15	297	165	466	4564	181	293
283.15	210	119	319	2805	136	218
288.15	152	88.0	225	1793	104	165
293.15	113	66.6	162	1181	81.3	128
298.15	85.7	51.4	120	799	64.6	100
303.15	66.3	40.3	90.4	555	52.1	79.9
308.15	52.1	32.2	69.5	395	42.6	64.6
313.15	41.7	26.1	54.3	287	35.3	52.9
318.15	33.8	21.5	43.2	212	29.6	43.8
323.15	27.8	17.9	34.9	160	25.1	36.8
328.15	23.1	15.1	28.5	123	21.4	31.1
333.15	19.5	12.8	23.6	95.4	18.5	26.6
338.15	16.5	11.0	19.8	75.6	16.1	23.0
343.15	14.2	9.56	16.8	60.7	14.1	20.0
348.15	12.3	8.35	14.4	49.4	12.5	17.5
353.15	10.7	7.35	12.5	40.7	11.1	15.4
358.15	9.43	6.51	10.9	33.9	9.88	13.7
363.15	8.35	5.81	9.61	28.4	8.88	12.2
368.15	7.43	5.21	8.59	24.1	8.01	11.0
373.15	6.66	4.70	7.76	20.6	7.27	9.91

Viscosity data were correlated using a Vogel-Fulcher-Tamman (VFT) equation (eqn 1), being the AAD 0.79%. Fitting parameters are presented along with the standard deviation σ in Table 3.

$$Ln(\eta) = A + \frac{B}{T - T_0} \tag{1}$$

where η is the dynamic viscosity in mPa·s, T is the temperature in K and A, B and T_0 are adjustable parameters. The behaviour of the dynamic viscosity with temperature is shown in Fig. 1, where it can be observed that the highest viscosity values correspond to the gearbox oil, as expected.

Table 3 Parameters of the VFT correlation, eqn (1), and standard deviation, σ

	MIN-H01	MIN-H02	SYN-2T	MIN-G	HOSO-B	BIO-H
A	-2.85	-2.93	-3.277	-4.251	-2.2658	-2.426
B /K	1004	948.4	1120.5	1591.2	933.35	1061.8
T_0/K	160.6	160.1	159.2	152.62	153.09	147.2
σ/mPa·s	0.12	0.14	0.35	1.31	0.07	0.18

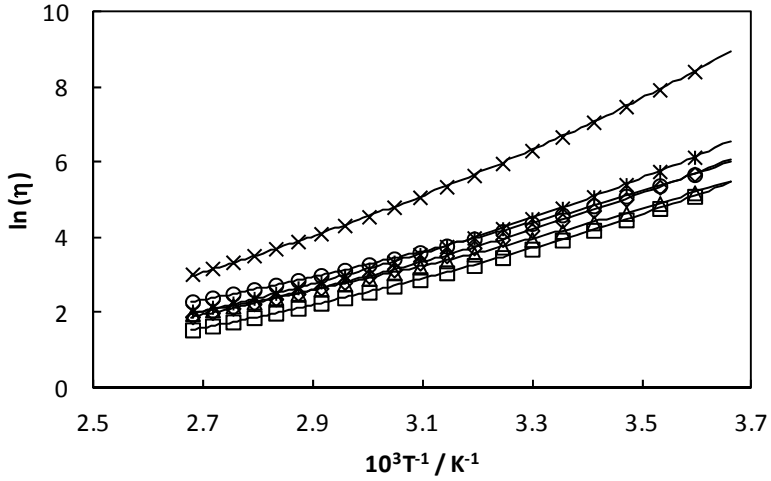

Fig.1 Experimental viscosity values. MIN-G (×), SYN-2T (∗), BIO-H (○), MINH-01 (◇), HOSO-B (△), MINH-02 (□), VFT correlation (—)

Density and derived properties

The experimental density values measured in this work at atmospheric pressure with the Stabinger viscometer are presented in Table 4. Density measurements at ambient pressure were correlated with the Rackett equation[53] to provide an extrapolation method[54] to determine the density at lower pressures than atmospheric and the isothermal compressibility at atmospheric pressure. The Rackett equation is written as following[55-57]:

$$\rho = a_1 \cdot a_2^{-\left(1+\left(1-\frac{T}{a_3}\right)^{a_4}\right)} \tag{2}$$

where T is the temperature and ρ the density at atmospheric pressure. Although the equation was developed to represent saturated liquid densities, it adequately serves as a baseline to compare our data sets to one another as well as to literature data, particularly at low reduced temperatures. It is common practice when the Rackett equation is used, to constrain a_3 to the critical temperature of the fluid for which the correlation is being performed.[56] This method was recently used for fuels and rocket propellants components[55, 56] Table 5 lists the Rackett correlation parameters for the oil samples.

Table 4 Experimental densities at atmospheric pressure, ρ/g·cm^{-3}, for the lubricants studied in this work.

T /K	MIN-H01	MIN-H02	SYN-2T	MIN-G	HOSO-B	BIO-H
278.15	0.8841	0.8751	0.8853	0.9061	0.9229	0.9280
283.15	0.8809	0.8718	0.8821	0.9030	0.9195	0.9247
288.15	0.8777	0.8687	0.8790	0.8999	0.9161	0.9213
293.15	0.8745	0.8655	0.8758	0.8969	0.9128	0.9180
298.15	0.8714	0.8623	0.8726	0.8938	0.9094	0.9147
303.15	0.8682	0.8591	0.8695	0.8907	0.9060	0.9114
308.15	0.8651	0.8559	0.8664	0.8876	0.9027	0.9081
313.15	0.8619	0.8527	0.8632	0.8845	0.8993	0.9048
318.15	0.8588	0.8495	0.8600	0.8815	0.8960	0.9014
323.15	0.8556	0.8463	0.8568	0.8784	0.8926	0.8981
328.15	0.8524	0.8430	0.8536	0.8754	0.8893	0.8948
333.15	0.8493	0.8398	0.8504	0.8724	0.8860	0.8915
338.15	0.8461	0.8366	0.8472	0.8694	0.8826	0.8882
343.15	0.8429	0.8335	0.8441	0.8664	0.8793	0.8849
348.15	0.8398	0.8303	0.8410	0.8634	0.8760	0.8816
353.15	0.8366	0.8271	0.8380	0.8603	0.8727	0.8784
358.15	0.8335	0.8239	0.8350	0.8573	0.8694	0.8751
363.15	0.8303	0.8208	0.8320	0.8543	0.8661	0.8718
368.15	0.8272	0.8176	0.8290	0.8514	0.8628	0.8685
373.15	0.8241	0.8145	0.8261	0.8484	0.8596	0.8653

Table 5 Parameters of the Rackett Correlation from eqn (2) and standard deviations, σ

	MIN-H01	MIN-H02	SYN-2T	MIN-G	HOSO-B	BIO-H
a_1 /kg·m^{-3}	125.468	179.95	211.55	182.52	140.87	128.48
a_2	0.34337	0.41203	0.44213	0.40906	0.3544	0.33854
a_3 /K	982.5	901	1062	1120.3	1077	1062.3
a_4	0.5724	0.6596	0.929	0.815	0.69716	0.6314
σ /kg·m^{-3}	0.04	0.05	0.13	0.04	0.03	0.04

Furthermore we have used the method proposed by Anand et al.[58] to estimate the density of the high oleic sunflower oil from its fatty acid composition to verify the goodness of this procedure with our density data. The critical parameters for the fatty acids were taken from Anand et al.[58], except for behenic acid for which they were estimated with the method of Joback[59]. It can be observed, in Table 6, that the proposed correlation predicts density values within ±0.85%.

Table 6 Predicted and measured densities at atmospheric pressure for HOSO-B

T /K	$\rho_{predicted}$ /g·cm^{-3}	$\rho_{measured}$ /g·cm^{-3}	$(\rho_{measured}-\rho_{predicted})/\rho_{measured}$ %
298.15	0.9016	0.9093	0.85
323.15	0.8898	0.8925	0.31
348.15	0.8776	0.8757	-0.22
373.15	0.8650	0.8593	-0.66

The experimental density values measured with the HPM densimeter up to 60 MPa are presented in Table 7, as a function of temperature and pressure. In Fig. 2 it is shown the density deviations values at atmospheric pressure measured with the Stabinger viscometer and those from the HPM densimeter, being the AAD 0.03%.

Table 7 Experimental densities, ρ/g·cm^{-3}, for the lubricants studied in this work

	***p*/MPa**										
***T*/K**	0.1	1	5	10	15	20	30	40	45	50	60
						MIN-H01					
298.15	0.8715	0.8720	0.8742	0.8769	0.8795	0.8820	0.8868	0.8913	0.8935	0.8957	0.8999
323.15	0.8556	0.8562	0.8586	0.8616	0.8645	0.8672	0.8725	0.8774	0.8798	0.8821	0.8865
348.15	0.8396	0.8402	0.8429	0.8462	0.8494	0.8525	0.8583	0.8637	0.8663	0.8688	0.8736
373.15	0.8239	0.8245	0.8275	0.8312	0.8347	0.8380	0.8443	0.8502	0.8530	0.8557	0.8610
						MIN-H02					
298.15	0.8621	0.8626	0.8648	0.8675	0.8702	0.8728	0.8777	0.8824	0.8846	0.8867	0.8908
323.15	0.8462	0.8468	0.8493	0.8524	0.8553	0.8581	0.8634	0.8684	0.8708	0.8731	0.8776
348.15	0.8302	0.8308	0.8336	0.8369	0.8401	0.8433	0.8491	0.8546	0.8573	0.8598	0.8647
373.15	0.8144	0.8150	0.8181	0.8219	0.8254	0.8288	0.8352	0.8412	0.8440	0.8467	0.8520
						SYN-2T					
298.15	0.8714	0.8719	0.8741	0.8768	0.8794	0.8818	0.8866	0.8911	0.8933	0.8954	0.8996
323.15	0.8557	0.8563	0.8587	0.8617	0.8645	0.8673	0.8725	0.8774	0.8798	0.8821	0.8865
348.15	0.8398	0.8405	0.8432	0.8464	0.8496	0.8526	0.8584	0.8638	0.8664	0.8689	0.8737
373.15	0.8242	0.8248	0.8279	0.8315	0.8350	0.8383	0.8446	0.8505	0.8532	0.8559	0.8611
						MIN-G					
298.15	0.8941	0.8946	0.8966	0.8991	0.9016	0.9039	0.9084	0.9128	0.9148	0.9169	0.9208
323.15	0.8788	0.8794	0.8817	0.8845	0.8872	0.8898	0.8947	0.8994	0.9017	0.9038	0.9081
348.15	0.8633	0.8638	0.8664	0.8694	0.8724	0.8753	0.8808	0.8860	0.8884	0.8908	0.8954
373.15	0.8483	0.8489	0.8517	0.8550	0.8583	0.8614	0.8673	0.8729	0.8755	0.8781	0.8830
						HOSO-B					
298.15	0.9093	0.9098	0.9120	0.9147	0.9173	0.9198	0.9246	0.9292	0.9315	0.9337	0.9379
323.15	0.8925	0.8931	0.8955	0.8985	0.9013	0.9041	0.9094	0.9143	0.9167	0.9191	0.9236
348.15	0.8757	0.8763	0.8790	0.8822	0.8854	0.8884	0.8942	0.8997	0.9023	0.9049	0.9097
373.15	0.8593	0.8599	0.8629	0.8664	0.8699	0.8732	0.8795	0.8854	0.8882	0.8910	0.8962
						BIO-H					
298.15	0.9144	0.9149	0.9171	0.9198	0.9224	0.9249	0.9297	0.9343	0.9366	0.9387	0.9430
323.15	0.8979	0.8984	0.9008	0.9038	0.9066	0.9094	0.9147	0.9196	0.9220	0.9244	0.9289
348.15	0.8812	0.8819	0.8845	0.8878	0.8909	0.8940	0.8998	0.9052	0.9078	0.9103	0.9152
373.15	0.8650	0.8656	0.8685	0.8721	0.8756	0.8789	0.8851	0.8910	0.8938	0.8965	0.9018

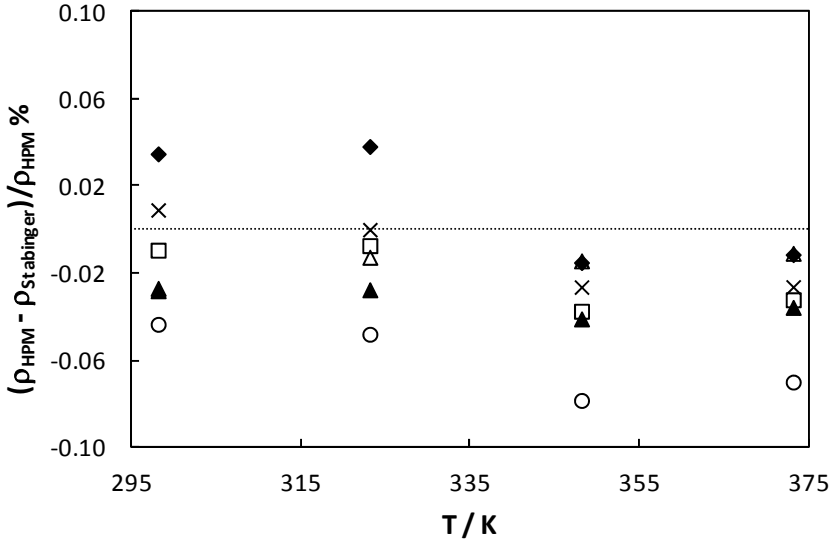

Fig.2 Comparison between density values from Stabinger, $\rho_{Stabinger}$, and from HPM, ρ_{HPM}. (◆) MIN-G, (×) MIN-H01, (□) HOSO-B, (△) MIN-H02, (▲) BIO-H, (○) SYN-2T.

In the field of Tribology, Dowson and Higginson[60] relationship for density–pressure–temperature dependence has been used for a long time although it is recognized that it does not

always describe the real physical behavior of lubricants. In more recent studies on EHL models several authors use Tait-type equations for a more realistic representation of the density–pressure–temperature behavior of the lubricants[61]. Thus, in this work the coefficients in the following modified Tammann-Tait equation were also fitted to the experimental density values:

$$\rho(T, p) = \frac{\rho(T, p_{ref}(T))}{1 - C \ln\left(\frac{B(T) + p}{B(T) + p_{ref}(T)}\right)} \tag{3}$$

where $\rho(T,p_{\mathrm{ref}}(T))$ is the temperature dependence of the fluid density at the reference pressure $p_{\mathrm{ref}}(T)$= 0.1 MPa. Polynomial functions of temperature were used to $\rho(T,p_{\mathrm{ref}}(T))$ and $B(T)$:

$$\rho(T, 0.1\,MPa) = \sum_{i=0}^{m} A_i T^i \tag{4}$$

and

$$B(T) = \sum_{j=0}^{n} B_j T^j \tag{5}$$

The set of fitting coefficient values (A_i, B_j, C) and the standard deviations σ and σ^* are listed in Table 8. Several of the experimental densities, ρ, for the six oils studied are plotted in Fig. 3a against pressure at 323 K and in Fig. 3b against temperature at 30 MPa. It can be seen how, as usual, ρ increases when the temperature decreases at constant pressure or the pressure increases. In the range studied, the variation between the maximum and the minimum density values for these lubricants is around 10%.

Table 8 A_i, B_i, C coefficients and standard deviations, σ and σ* for eqns (3-5).

	MIN-H01	**MIN-H02**	**SYN-2T**	**MIN-G**	**HOSO-B**	**BIO-H**
A_0/g·cm^{-3}	1.060866	1.05167	1.05919	1.076551	1.108222	1.111137
-10^3·A_1 /g·cm$^-$	0.63524	0.63593	0.62977	0.61197	0.66735	0.6599
10^4·σ/g·cm^{-3}	1	0.7	0.7	2	2	1
C	0.0826	0.081525	0.08119	0.0819	0.086944	0.0849
B_0 /MPa	408.31	405.27	437.316	463.2	379.76	397.16
-B_1 /MPa·K^{-1}	1.249	1.285042	1.43251	1.48385	0.971	1.1
10^3·B_2 /MPa·K^{-2}	1.04184	1.13196	1.31671	1.345	0.581	0.79
10^4·σ^* / g·cm^{-3}	0.5	0.7	0.5	0.9	0.7	0.6

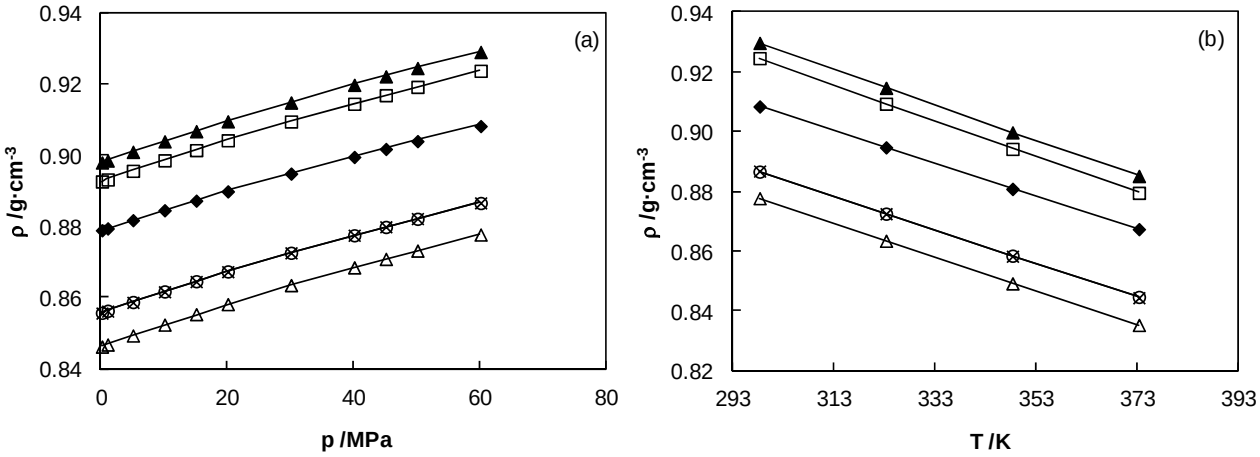

Fig.3 Density values, ρ, (a) vs. pressure at 323.15 K (b) vs. temperature at 30 MPa. (▲) BIO-H, (□) HOSO-B, (◆) MIN-G, (○) SYN-2T, (×) MIN-H01, (△) MIN-H02.

Under the same *p, T* conditions, the following trend for density values was obtained: BIO-H> HOSO-B> MIN-G > SYN-2T ~ MIN-H01 > MIN-H02, i.e. BIO-H presents the highest density values. That is, the densities of the high oleic sunflower oil and the biodegradable lubricant are higher than those of the reference oils. This is because the ester functional groups of the vegetable oils increase the packing of the molecules due to the attractive dipole intermolecular forces. These values are also higher than typical data of other mineral oils[30,62,63]. The higher density of the vegetable lubricant base contributes to more efficient oil separation and lower carry-over. In addition, according to the simplified Sieder-Tate equation, the higher the density value, the better the heat-transfer coefficient[64]. On the other hand, losses in the pipe work and elements of a hydraulic system are directly proportional to the density of the fluid[26]. Besides, in hydrostatic applications, the density of the oils is usually measured at 15°C, but density depends on temperature and pressure because the volume of a fluid expands as its temperature increases and this causes the change in density (Fig. 3).

We have compared in Fig. 4 the density values reported in this work with those of the following natural oils: castor, menhaden, linseed, and olive oils, determined by Acosta et al.[65]and also with the data of sunflower and olive oils measured by Guignon et al.[66] Acosta et al.[65] have also determined the *pVT* behavior of triolein. As can be seen in Fig. 4, the castor oil presents the highest density values, whereas the lowest values correspond to reference mineral and synthetic oils measured in this work. Density values for triolein and olive oil measured by Acosta et al.[65] as well as density values for sunflower oil measured by Guignon et al.[66] are similar to those of the vegetable lubricant base (HOSO-B) and the biodegradable oil (BIO-H). The similarity of HOSO-B and triolein could be expected because of the high composition of oleic branches in their glycerides 85%. Furthermore, we have compared in Fig. 5 the density values reported in this work with those determined by Acosta et al.[65] for the following natural fats at temperatures

higher than the melting points, beef shank, beef tallow, coconut, palm and palm kernel oil fats. As can be seen in Fig.5, density values for coconut oil fat and palm oil fat are very similar to the developed biodegradable oil BIO-H and density values for the high oleic sunflower base oil HOSO-B are very similar to the beef tallow fat; the lowest values correspond to the reference oils measured in this work. This is due to the fact that in mineral oils there are no strong molecular interactions, consequently, the packing is less important.

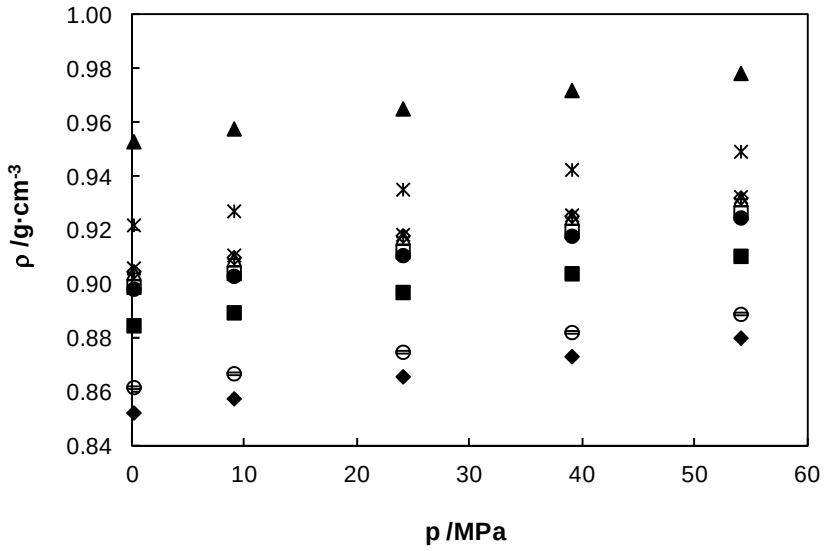

Fig.4 Density values, ρ, vs. pressure at 313.15 K. Oils measured in this work: (△) BIO-H, (□) HOSO-B, (■) MIN-G, (○) SYN-2T, (−) MIN-H01, (◆) MIN-H02. Fluids measured in literature: (▲) castor oil[65], (∗) linseed oil[65], (+) triolein[65], (◇) olive oil[65], (×) sunflower oil[66], (●) olive oil[66].

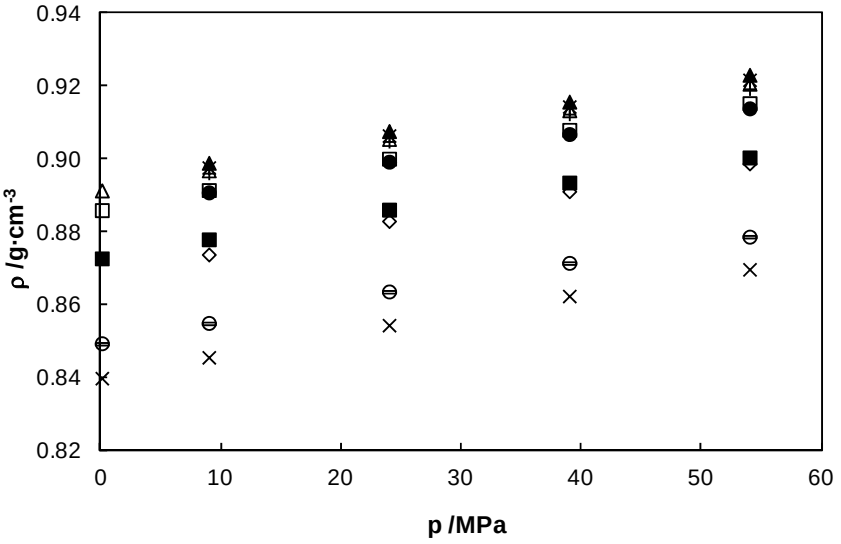

Fig.5 Density values, ρ, vs. pressure at 333 K. Oils measured in this work: (−) MIN-H01, (△) BIO-H, (□) HOSO-B, (○) SYN-2T, (×) MIN-H02, (■) MIN-G. Fluids measured in literature[65]: (▲) coconut oil fat, (∗) palm oil fat, (+) beef shank fat, (●) beef tallow fat, (◇) palm kernel oil fat.

From the $p\rho T$ relations (eqns 3-5), it is easy to determine[67] different thermophysical properties as isobaric thermal expansivities, $\alpha_p = (1/V_m)(\partial V_m/\partial T)_p = -(1/\rho)(\partial\rho/\partial T)_p$ or isothermal compressibilities, $\kappa_T = -(1/V_m)(\partial V_m/\partial p)_T = (1/\rho)(\partial\rho/\partial p)_T$. In the range studied, the variation of the

isobaric thermal expansivities for each oil analyzed in this work is around 30%. In Fig. 6 the α_P values are presented for several oils against pressure and it can be seen how this property decreases when the pressure increases at constant temperature. The isobaric thermal expansivity, α_p, is useful to determine the size of a container in which the oil is heated. In Hydrodynamic Lubrication (HDL), the thermal expansion of the oil in the clearance of a bearing increases the hydraulic pressure. Besides, several authors have suggested that a pressure film is generated in a parallel slider bearing as a result of thermal expansion of the fluid as it passes through the bearing. This phenomenon is named as "Thermal Wedge" or "Density Wedge"[68].

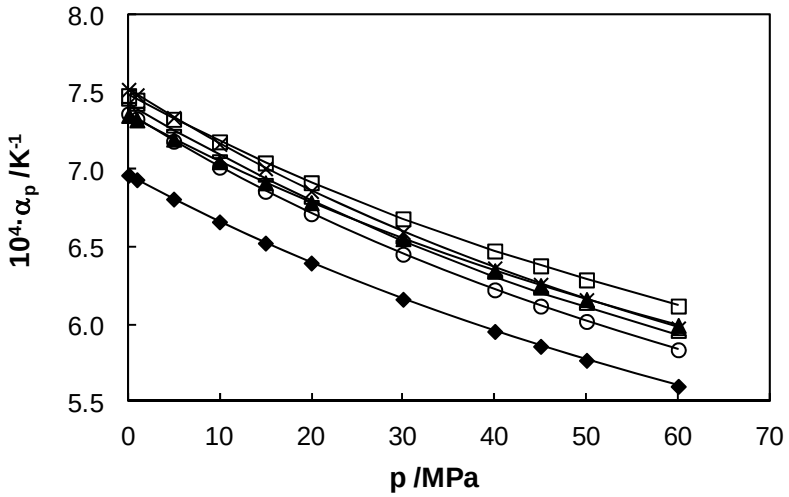

Fig.6 Isobaric thermal expansivities, α_P, against pressure for several oils at 323.15 K. (□) HOSO-B, (×) MIN-H02, (▲) BIO-H, (−) MIN-H01, (○) SYN-2T, (◆) MIN-G.

Isothermal compressibility values are summarized in Table 9. The isothermal compressibility, κ_T, increases with the temperature at constant pressure for all studied oils, whereas it decreases when the pressure rises at constant temperature (see Fig. 7).

The trend found for this property is the following: MIN-H02> MIN-H01> SYN-2T> HOSO-B> BIO-H> MIN-G. The maximum differences among the κ_T values for the oils analyzed at the same temperature and pressure are around 15%. The vegetable base oil has a slightly lower compressibility than those of the reference oils for hydraulic and two stroke engines applications, therefore it presents better properties for power transfer and control medium, this means that with this oil lower both line sizes and actuator cross-sectional areas could be used, i.e. lower fluid volumes and slighter systems[28]. However the compressibility of the sunflower base oil is higher than that of the reference oil for gearbox applications. Usually, film thickness in the high-pressure region is determined by the conditions in the inlet where the lubricant is not compressed. Compression will decrease the film thickness and the more compressible the lubricant is, the thinner will be the lubricant film[33]. Therefore the vegetable oil could form thinner films by a few percent in high-pressure regions. Nevertheless, the outlet

pressure spikes and the sub-surface stress concentrations will be smaller than for a less compressible lubricant[33]. This indicates that vegetable oils may increase operational life of real EHL surfaces.

Table 9 Isothermal compressibility $10^4 \cdot \kappa_T$/MPa^{-1}, of the lubricants studied in this work.

	***p*/MPa**								
***T*/K**	1.00	5.00	10.00	15.00	20.00	30.00	40.00	45.00	50.00
				MIN-H01					
298.15	6.38	6.20	6.00	5.81	5.63	5.30	5.01	4.88	4.76
323.15	7.22	7.00	6.74	6.49	6.27	5.87	5.52	5.36	5.21
348.15	8.20	7.92	7.59	7.28	7.00	6.51	6.08	5.89	5.71
373.15	9.36	8.99	8.56	8.18	7.83	7.22	6.70	6.46	6.25
				MIN-H02					
298.15	6.59	6.40	6.18	5.97	5.78	5.43	5.13	4.99	4.85
323.15	7.47	7.23	6.95	6.69	6.45	6.02	5.64	5.48	5.32
348.15	8.49	8.18	7.82	7.49	7.20	6.67	6.21	6.01	5.82
373.15	9.67	9.27	8.81	8.40	8.03	7.38	6.83	6.58	6.36
				SYN-2T					
298.15	6.33	6.16	5.95	5.76	5.58	5.25	4.96	4.83	4.71
323.15	7.20	6.97	6.71	6.46	6.24	5.83	5.48	5.32	5.17
348.15	8.19	7.90	7.56	7.26	6.97	6.47	6.04	5.85	5.67
373.15	9.33	8.95	8.52	8.13	7.78	7.17	6.64	6.41	6.19
				MIN-G					
298.15	5.80	5.65	5.48	5.32	5.16	4.88	4.64	4.52	4.41
323.15	6.55	6.36	6.14	5.94	5.75	5.41	5.11	4.97	4.84
348.15	7.41	7.17	6.90	6.64	6.41	5.98	5.62	5.45	5.29
373.15	8.38	8.08	7.73	7.41	7.12	6.61	6.16	5.96	5.78
				HOSO-B					
298.15	6.09	5.94	5.76	5.59	5.43	5.14	4.88	4.77	4.65
323.15	6.82	6.63	6.40	6.20	6.00	5.65	5.34	5.20	5.07
348.15	7.69	7.45	7.17	6.91	6.67	6.25	5.87	5.70	5.54
373.15	8.76	8.45	8.09	7.77	7.47	6.93	6.48	6.27	6.08
				BIO-H					
298.15	6.05	5.90	5.72	5.55	5.39	5.10	4.84	4.72	4.60
323.15	6.79	6.59	6.37	6.16	5.96	5.61	5.30	5.15	5.02
348.15	7.66	7.41	7.13	6.87	6.63	6.19	5.81	5.64	5.48
373.15	8.70	8.38	8.02	7.69	7.39	6.86	6.40	6.19	6.00

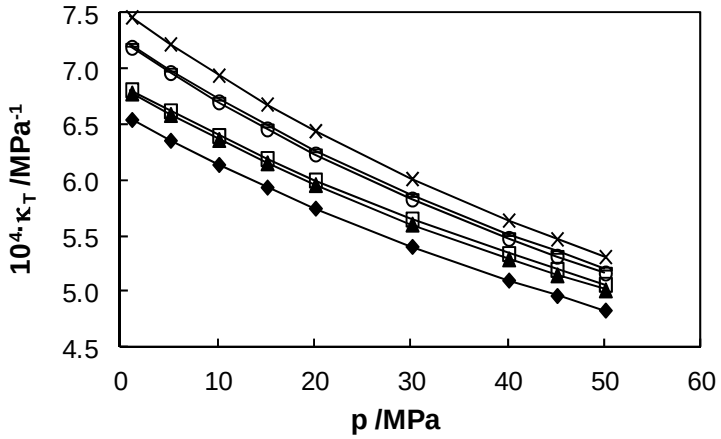

Fig.7 Isothermal compressibility, κ_T, against pressure for several oils at 323.15 K. (×) MIN-H02, (−) MIN-H01, (○) SYN-2T, (□) HOSO-B, (▲) BIO-H, (◆) MIN-G.

In Fig. 8 we present the maximum and minimum isothermal compressibility values for the studied oils. This figure shows that for each of the six oils analyzed in this work, the variation of κ_T in the range studied is around 70%, i.e. it could not be considered constant, as usual in design engineering estimations. The variation of this property for the high-oleic sunflower oil is less pronounced in the analyzed range than for reference oils for hydraulic and two stroke engines applications.

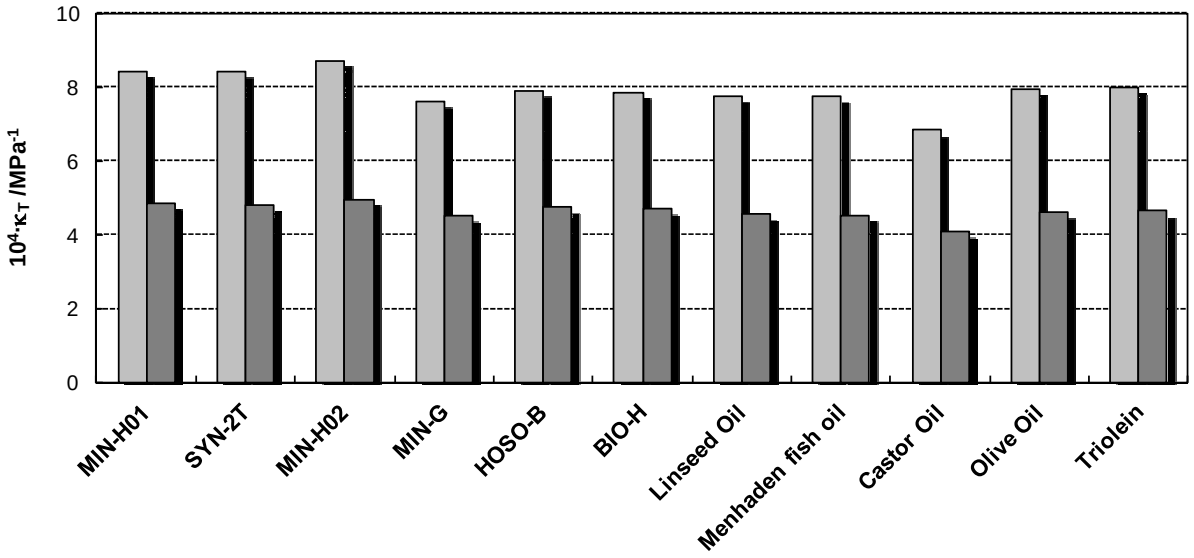

Fig.8 Minimum and maximum isothermal compressibility, κ_T, in the range (303.15 to 353.15) K and (1 to 50) MPa, for the different oils studied in this work and for fluids reported in literature[65].

Experimental

Materials

The oils studied in this work are presented together with their applications in Table 1. These lubricants have been provided by some of the Spanish companies involved in the BIOVESIN project: Abamotor Energía, Verkol Lubricantes and Gamesa as well as by the Instituto de la Grasa (CSIC). The High Oleic Sunflower Base Oil has the following composition, expressed in mass fraction: palmitic acid ($C_{16:0}$) 4.17%, stearic acid ($C_{18:0}$) 3.30%, oleic acid ($C_{18:1}$) 85.55%, linoleic acid ($C_{18:2}$) 5.43%, arachidic acid ($C_{20:0}$) 0.78% and behenic acid ($C_{22:0}$) 0.77%. BIO-H is a lubricant oil formulation composed by trimethylolpropane trioleate as base oil. All the oils, as well as water (purified using a Milli-Q Plus system, with a resistivity of 18.2 MΩ·cm at 298.15 K) were partially degassed, before use, using a Branson 2210 ultrasonic bath.

Apparatus and Procedure

Firstly, the Viscosity Index (VI) and the atmospheric density and viscosity values between 278.15 and 373.15 K were measured for all the analyzed oils using an automated SVM 3000 Anton Paar rotational Stabinger viscometer[69]. The SVM 3000 uses Peltier elements for fast

and efficient thermostatting. The temperature uncertainty is 0.02 K from 288.15 K to 378.15 K and 0.05 K outside this range. The uncertainty of the dynamic viscosity is 1%. This equipment has also a vibrating-tube that permits to measure the densities with an uncertainty of 0.0005 g/cm^3.

Density values of lubricants at high pressure were determined using an Anton Paar HPM vibrating tube densimeter. Density measurements are based on the dependence between the period of oscillation of a fixed U-tube and its mass. Both the complete experimental equipment and the experimental procedure have been previously described in detail[39, 41-44, 46, 70, 71]. In order to obtain the density, it is necessary to know two characteristic parameters. In this work these parameters were determined following the method developed by Lagourette et al.[72] and modified slightly by Comuñas et al.[38] to determine densities at temperatures equal to or higher than 373.15 K. This procedure has been recently applied by Fandiño et al.[42] Taking into account the uncertainties of the temperature, the pressure, the period of oscillation measurements for water, vacuum, and the studied liquid (seven-digit frequency counter), and the water density we have estimated that the expanded, k =2, density uncertainty[42, 71] is $7 \cdot 10^{-4}$ g·cm^{-3}.

Conclusion and outlook

As expected, the vegetable lubricant base has a higher Viscosity Index than the reference mineral and synthetic oils, therefore its viscosity changes less with temperature. It was measured the density of six different lubricants from 298.15 to 373.15 K and from 0.1 to 60 MPa. It was found that density is higher for the biodegradable lubricant and for the high oleic sunflower base oil than for the mineral and synthetic reference oils for the different applications. Density data were compared with literature density values for other different types of natural oils measured by Acosta et al.[65] Density data were correlated by means of a Tammann-Tait type equation and the standard deviation was lower than 0.1·kg·m^{-3}. Density derived properties, isobaric thermal expansivity and isothermal compressibility, were calculated from these correlations. For each fluid analyzed, the change in the isobaric thermal expansivity is around 30% in the studied temperature and pressure range. The trend found for isothermal compressibility is the following MIN-H02> MIN-H01> SYN-2T > HOSO-B> BIO-H> MIN-G, that means that the vegetable base oil presents better properties for power transfer and control medium than those of the reference oils for hydraulic and two stroke engines applications. The reference oil for gearbox applications would form thicker lubricant films than the sunflower base oil because its compressibility is lower. Nevertheless, the outlet pressure spikes and the sub-surface stress concentrations will be smaller for the HOSO base oil, which could lead to an increase in operational life of real EHL surfaces.

Apart from vegetable oil-lubricants, ionic liquids (ILs) have been investigated over the last decade for lubrication applications[73-76]. Some ILs can match or even exceed the tribological behaviour of high-performance lubricants due to their polar nature.[77, 78] Nevertheless, in comparison to vegetable oils, classification of ILs as renewable and biodegradable would be questionable. The registration and systematic toxicological testing of ionic liquids is absolutely necessary prior to any open-access use of ionic liquid lubricants. There are some restrictions for the usage of chemicals such as the European Eco-label, which have to be considered along with all the technical requirements[79] to develop ILs as base oils. However, there are fewer restrictions for the use of ILs as additives of the lubricants. Although miscibility of ILs with base oils is the first concern; however, in polar base oils, it is less difficult to find miscible ILs.[76] Authors think that studies of the ability of the ILs as antiwear additives of vegetable and other biodegradable oils should be encouraged.

Acknowledgements

This work was carried out within the framework of the strategically and singular project "Biolubricants based on vegetable oils and their synthetic derivatives", which is funding by Spanish Science and Innovation Ministry and the EU FEDER program (PSE-320100-2006-1, PSE-420000-2008-4). We are very grateful to the companies Abamotor Energía, Verkol Lubricantes and Gamesa as well as to the Instituto de la Grasa (CSIC, Seville) and Tekniker Foundation for their excellent advice and for providing us the samples of the products. L. L. acknowledges the financial support from the Ramon y Cajal Program (Ministerio de Ciencia e Innovación, Spain). T.R. acknowledges financial support provided by the Spanish Ministry of Education under the FPU program.

References

1. The commission of the European communities. Establishing ecological criteria and the related assessment and verification requirements for the award of the Community eco-label to lubricants. Official Journal of the European Union 2005, L 118/ 126-134.
2. S. Boyde, *Green Chem.*, 2002, **4**, 293-307.
3. R. Sánchez, J. M. Franco, M. A. Delgado, C. Valencia and C. Gallegos, *Green Chem.*, 2009, **11**, 686-693.
4. W. G. Johnston, *ASLE Trans.*, 1981, **24**, 232-238.
5. R. Höfer and J. Bigorra, *Green Chem.*, 2007, **9**, 203-212.
6. R. Höfer and J. Bigorra, *Green Chem. Lett. Rev.*, 2008, **1**, 79-97.
7. K. Hill and R. Höfer, in *Sustainable Solutions For Modern Economies*, R. Höfer, Royal Society Of Chemistry, Cambridge, 2009, pp. 164-166.
8. L. R. Rudnick and W. J. Bartz, in *Synthetic Mineral Oils and Bio-Based Lubricants: Chemistry and Technology*, Taylor and Francis Ed.: Boca Raton, 2006, 331-349.
9. L. R. Rudnick and S. Z. Erhan, in *Synthetic Mineral Oils and Bio-Based Lubricants: Chemistry and Technology*, Taylor and Francis Ed.: Boca Raton, 2006, 353-360.
10. B. N. Rhodes and D. Johnson, eds., *Vegetable-based Motor Oils in Biobased Industrial Fluids and Lubricants*, Aocs Press, Champaign, Illinois, USA, 2002, 85-109.
11. P. S. Lathi and B. Mattiasson, *Appl. Catal. B-Environ.* , 2007, **69**, 207-212.

12. L. A. Quinchia, M. A. Delgado, C. Valencia, J. M. Franco and C. Gallegos, *Environ. Sci. Technol.* , 2009, **43**, 2060-2065.
13. L. A. García-Zapateiro, M. A. Delgado, J. M. Franco, C. Valencia, M. V. Ruiz-Méndez, R. Garcés and C. Gallegos, *Grasas y Aceites*, 2010, **61**, 171-174.
14. B. K. Sharma, J. M. Perez and S. Z. Erhan, *Energy Fuels*, 2007, **21**, 2408-2414.
15. N. H. Jayadas, *J. Synthetic Lubrication*, 2008, **25**, 105-113.
16. S. Z. Erhan, B. K. Sharma and J. M. Perez, *Industrial Crops and Products*, 2006, **24**, 292-299.
17. P. V. Joseph and D. K. Sharma, *Lubrication Science* 2010, **22**, 149-161.
18. A. Adhvaryu and S. Z. Erhan, *Industrial Crops and Products*, 2002, **15**, 247-254.
19. S. Z. Erhan, A. Adhvaryu and B. K. Sharma, in *Chemical Industries*, CRC Press, Boca Raton, FL, U. S., 2006, pp. 361-387.
20. M. A. Schmidt, C. R. Dietrich and E. B. Cahoon, in *Chemical Industries*, CRC Press, Boca Raton, FL, U. S., 2006, pp. 389-397.
21. D. Vinci, J. Kersbulck, M. R. Greaves and N. Khelidj, *High Performance Renewable Base Fluids Derived from Caster Oil for Industrial Applications, Solving Friction and Wear Problems, Synopsis 17th International Colloquium Tribology*, 2010, 88.
22. M. Scherer, D. Rettemeyer, R. Rinklieb and R. Patel, *Latest Trends in Biohydraulic Fluids, Solving Friction and Wear Problems, Synopsis 17th International Colloquium Tribology,* , 2010, 90.
23. D. Rettemeyer, M. Scherer and R. Rinklieb, *Power Fluid Journal*, 2009, 22-24.
24. G. Mendoza, A. Igartua, B. Fernandez-Diaz, F. Urquiola, S. Vivanco and R. Arguizoniz, *Grasas y Aceites*, 2011, **62**, 29-38.
25. B. Fernández-Díaz, A. Igartua, J. Barriga, F. Urquiola, R. Garces, J. Fernández, C. D. d. Cerio, E. Llamazares and R. Arguinzoniz, in *Vegetable and Biodegradable Lubricants: formulation development and testing, LUBMAT*, San Sebastian, Spain, 2008.
26. T. Mang and W. Dresel, *Lubricants and Lubrication*, Wiley-VCH, 2001.
27. L. Bronshteyn and J. H. Kreiner, *Tribology Trans.* , 1999, **42**, 771-776.
28. D. G. Placek, in *Synthetic Mineral Oils and Bio-Based Lubricants: Chemistry and Technology*, Taylor and Francis Ed.: Boca Raton, 2006, 517-540.
29. Engineering and Design, lubricants and hydraulic fluids. Department of the army U.S. Army Corps of Engineers, Washington, DC, Manual No. 1110-1112-1424, 1128 February 1999.
30. D. Godfrey and W. R. Herguth, *Lubrication Eng.*, 1995, **51**, 493-496.
31. S. Bair, *Elsevier, Amsterdam*, 2007.
32. J. W. P. Schmelzer, E. D. Zanotto and V. M. Fokin, *J. Chem. Phys.*, 2005, **122**, 1-11.
33. R. Larsson, E. Kassfeldt, A. Byheden and T. Norrby, *J. Synth. Lubr.*, 2001, **18**, 183-198.
34. E. Höglund, *Wear*, 1999, **232**, 176-184.
35. J. K. Shah, J. F. Brennecke and E. J. Maginn, *Green Chem.*, 2002, **4**, 112-118.
36. M. J. P. Comuñas, A. Baylaucq, C. Boned and J. Fernández, *Ind. Eng. Chem. Res.*, 2004, **43**, 804-814.
37. M. J. P. Comuñas, A. Baylaucq, C.Boned and J. Fernández, *J. Chem. Eng. Data*, 2003, **48**, 1044-1049.
38. M. J. P. Comuñas, J. P. Bazile, A. Baylaucq and C. Boned, *J. Chem. Eng. Data*, 2008, **53**, 986-994.
39. O. Fandiño, M. J. P. Comuñas, L. Lugo, E. R. López and J. Fernández, *J. Chem. Eng. Data*, 2007, **52**, 1429-1436.
40. O. Fandiño, J. García, M. J. P.Comuñas, E. R. López and J. Fernández, *Ind. Eng. Chem. Res.*, 2006, **45**, 1172-1182.
41. O. Fandiño, E. R. López, L. Lugo and J. Fernández, *Fluid Phase Equilib.*, 2010, **296**, 30-36.
42. O. Fandiño, L. Lugo, M. J. P. Comuñas, E. R. López and J. Fernández, *J. Chem. Thermodyn.*, 2010, **42**, 84-89.
43. L. Lugo, X. Canet, M. J. P. Comuñas, A. S. Pensado and J. Fernández, *Ind. Eng. Chem. Res.*, 2007, **46**, 1826.
44. L. Lugo, E. R. López, M. J. P. Comuñas, J. García and J. Fernández, *J. Chem. Eng. Data*, 2004, **49**, 1400-1405.
45. A. S. Pensado, M. J. P. Comuñas and J.Fernández, *Ind. Eng. Chem. Res.*, 2006, **45**, 9171-9183.
46. A. S. Pensado, M. J. P. Comuñas, L. Lugo and J. Fernández, *Ind. Eng. Chem. Res.*, 2006, **45**, 2394-2404.
47. K. Anand, A. Ranjan and P. S. Mehta, *Energy Fuels*, 2010, **24**, 664-672.
48. S. M. P. Meneghetti, M. R. Meneghetti, T. M. Serra, D. C. Barbosa and C. R. Wolf, *Energy Fuels*, 2007, **21**, 3746-3747.
49. G. Vicente, M. Martínez and J. Aracil, *Energy Fuels*, 2006, **20**, 394-398.

50. M. Dzida and P. Prusakiewiez, *Fuel*, 2008, **87**, 1941-1948.
51. M. E. Tat, J. H. Van Gerpen, S. Soylu, M. Canakci, A. Monyem and S. Wormley, *J. Am. Oil Chem. Soc.*, 2000, **77**, 285-289.
52. F. Boudy and P. Seers, *Energy Convers. Manage.*, 2009, **50**, 2905-2912.
53. H. G. Rackett, *J. Chem. Eng. Data*, 1970, **15**, 514-517.
54. N. A. Lai, M. Wendland and J. Fischer, *Fluid Phase Equilib.*, 2009, **280**, 30-34.
55. A. Laesecke, S. L. Outcalt and K. J. Brumback, *Energy Fuels*, 2008, **22**, 2629-2636.
56. S. Outcalt, A. Laesecke and M. B. Freund, *Energy Fuels*, 2009, **23**, 1626-1633.
57. S. L. Outcalt, A. Laesecke and T. J. Fortin, *J. Mol. Liq.*, 2010, **151**, 50-59.
58. K. Anand, A. Ranjan and P. S. Mehta, *Energy Fuels*, 2010, **24**, 3262-3266.
59. B. E. Poling, J. M. Prausnitz and J. P. O'Connell, *The Properties of Gases and Liquids, 5th ed.*, McGraw-Hill, New York, 2001.
60. D. Dowson and G. R. Higginson, *Elastohydrodynamic Lubrication,*, Pergamon Press, Oxford, 1966.
61. W. Habchi, D. Eyheramendy, S. Bair, P. Vergne and G. Morales-Espejel, *Tribol. Lett.*, 2008, **30**, 41-52.
62. L. R. Rudnick and R. L. Shubkin, *Synthetic Lubricants and High-Performance Functional Fluids.*, M. Dekker, New York, 2nd edn, 1999.
63. N. Manring, *Hydraulic Control Systems*, Wiley, New York, 2005.
64. S. J. Randles, in *Lubricants of the Future and Environment, 6th International Congress*, Brussels, 1999.
65. G. M. Acosta, R. L. SmithJr and K. Arai, *J. Chem. Eng. Data*, 1996, **41**, 961-969.
66. B. Guignon, C. Aparicio and P. D. Sanz, *High Pressure Res.*, 2009, **29**, 38-45.
67. O. Fandiño, A. S. Pensado, L. Lugo, E. R. López and J. Fernández, *Green Chem.*, 2005, **7**, 775-783.
68. P. Sinha and G. Adamu, in *Society of Tribologists and Lubrication Engineers (STLE) ANNUAL MEETING 2007, 2006-2010*, Philadelphia, Pennsylvania, May 2007.
69. F. Novotny-Farkas, W. Böhme, H. Stabinger and W. Belitsch, *Anton Paar*, World Tribology Congress II, 2001.
70. L. Lugo, M. J. P. Comuñas, E. R. López and J. Fernández, *Fluid Phase Equilib.*, 2001, **186**, 235-255.
71. J. J. Segovia, O. Fandiño, E. R. López, L. Lugo, M. C. Martín and J. Fernández, *J. Chem. Thermodyn.*, 2009, **41**, 632-638.
72. B. Lagourette, C. Boned, H. Saint-Guirons, P. Xans and H. Zhou, *Meas. Sci. Technol.*, 1992, **3**, 699-703.
73. M.-D. Bermúdez, A.-E. Jiménez, J. Sanes and F.-J. Carrión, *Molecules*, 2009, **14**, 2888-2908.
74. I. Minami, *Molecules*, 2009, **14**, 2286-2305.
75. M. Palacio and B. Bhushan, *Tribol. Lett.*, 2010, **40**, 247-268.
76. F. Zhou, Y. Liang and W. Liu, *Chem. Soc. Rev.*, 2009, **38**, 2590-2599.
77. A. S. Pensado, M. J. P. Comuñas and J. Fernández, *Tribol. Lett.*, 2008, **31**, 107-118.
78. J. Qu, J. J. Truhan, S. Dai, H. Luo and P. J. Blau, *Tribol. Lett.*, 2006, **22**, 207-214.
79. M. Uerdingen, in *Handbook of Green Chemistry*, ed. P. T. Anastas, Wiley-VCH, 2010, pp. 203-219.

5.2. Compressibility and viscosity of new biodegradable lubricants based on high oleic sunflower oil for their use as hydraulic fluids*

*T. Regueira, L. Lugo, J. Fernández, to be submitted.

Abstract

Density data over a wide temperature range and up to 60 MPa of a high oleic sunflower oil (HOSO) and six biodegradable developed oils based on HOSO for hydraulic applications are presented. In order to evaluate the viability of these new biodegradable lubricants, density values up to 120 MPa are also reported for a mineral reference hydraulic lubricant. Isothermal compressibility is a key performance parameter of this type of applications, therefore compressibility values are calculated for reference and developed lubricants and a comparison among the obtained results is also performed. Furthermore, viscosity values at atmospheric pressure of the lubricants in a broad temperature range and viscosity index are also provided.

Introduction

In the last two decades, environmental concern has significantly grown and several factors such as toxicity or biodegradability have gained great importance when designing a new product. Thus, the search for more environmentally friendly fluids to be used as lubricants, which allows the substitution of commonly used synthetic and mineral lubricants, has strengthened in last two decades. A voluntary award scheme that promotes products with a reduced environmental impact during their entire life cycle was established in Europe, the EU Ecolabel (EEC 880/92, EC 1980/2000, EC 66/2010). The latest criteria for the award of the EU Ecolabel to lubricants were established in 2011 (2011/381/EU) and they cover hydraulic fluids and tractor transmission oils, greases and stern tube greases, chainsaw oils, concrete release agents, wire rope lubricants, stern tube oils and other total loss lubricants, two-stroke oils and industrial and marine gear oils.

In the present work we focus on hydraulic lubricants. A hydraulic system constitutes a very accurate and adjustable method to transmit energy. These systems are, in general, reliable, efficient and cost effective, which makes them very suitable for industrial work [1]. Hydraulic fluids are responsible of several functions, apart from that of power transfer, such as sealing, minimizing wear, reducing friction, cooling, preventing rust and corrosion and keeping the system free of deposits [2-4].

Several properties are important for selecting a hydraulic lubricant, such as viscosity, viscosity index, oxidation resistance, tribological and anti-corrosion properties and also compatibility with seals and compressibility, among others [5]. Compressibility is a key parameter, because a fluid with low compressibility transmits power more efficiently and several problems can be caused due to a high compressibility, such as adverse effects in system amplification, the servos fail to maintain static rigidity, loss in efficiency due to the volume reduction than cannot be recovered and also cavitation [6]. A low compressibility ratio translates

into fast response time, high pressure transmission velocity and low power loss. A high compressibility requires increase line sizes and actuator cross-sectional areas to compensate for the lower stiffness or higher compressibility of the fluid [3,7].

In this work we present high pressure density values of a reference hydraulic mineral oil, a vegetable base oil, as well as six biodegradable oils developed for their use as hydraulic fluids. We have calculated the isothermal compressibility values of these lubricants and viscosity data at atmospheric pressure as well as the viscosity index (VI) are also reported.

Materials and methods

The mineral reference hydraulic oil studied in this work was provided by Indra, whereas the high oleic sunflower oil as well as the developed biodegradable oils were kindly provided by Verkol Lubricantes. Their main characteristics are gathered in table 1.

Table 1. Characteristics of the hydraulic lubricants studied in this work.

Lubricant	Description	ρ /g·cm^{-3} (313.15 K)	η / mm^2·s^{-1} (313.15 K)	Viscosity Index (VI)
Reference Lubricants				
MIN-H03	Mineral	0.8422	14.4	146
Base oil				
HOSO-B1	83% HOSO	0.8992	39.6	204
Developed Biodegradable Lubricants				
BIO-H01	HOSO-B1 + AP1[a]	0.8992	39.6	202
BIO-H02	HOSO-B1 + AP2[a]	0.8999	40.0	200
BIO-H03	HOSO-B1 + AP3[a]	0.9010	40.5	198
BIO-H04	HOSO-B1 + Ester[b] + AP4[a]	0.9031	35.7	204
BIO-H05	HOSO-B1 + Ester[b] + AP5[a]	0.9036	34.8	201
BIO-H06	HOSO-B1 + Ester'[b]+ AP4[a]	0.9006	41.5	198

[a]AP1-AP5 are additive packages
[b]Ester and ester' are synthetic esters

Density and viscosity of the studied oils were measured at atmospheric pressure in the temperature range from 278.15 K to 373.15 K by using a Stabinger Anton Paar SVM 3000 viscometer. This apparatus performs density and viscosity measurements simultaneously in two different cells, a vibrating glass tube for density and a modified Couette cell for viscosity. The apparatus calculates also the viscosity index (VI) according to the ASTM standard D2270-04. The basic operating principles and schematic set up of the Stabinger Viscometer are described in a European Patent [8]. Thermostating is performed through Peltier elements, the temperature uncertainty being 0.02 K from 288.15 K to 378.15 K and 0.05 K outside this range. The uncertainty of the dynamic viscosity is 1% whereas density is measured with an uncertainty of 0.0005 g·cm^{-3}. More details on this technique have been previously given [9].

Density values of the mineral oil, MIN-H03, were measured through a fully automated vibrating tube densimeter Anton Paar HPM in the temperature range from 278.15 K to 398.15 K

and up to 120 MPa. Temperature probe Pt-100 is calibrated with an uncertainty of 0.02 K whereas uncertainty of the calibration of the pressure transducer is 0.02 MPa. More details on this experimental setup have been previously given [10,11]. This densimeter was calibrated [10] following the procedure described by Lagourette et al. [12] and modified by Comuñas et al. [13] using vacuum, Milli-Q water and decane as reference fluids. The expanded (k=2) uncertainty of the density with this technique was calculated by Segovia et al. [11] finding that it is $0.7 \cdot 10^{-3}$ g·cm^{-3} for temperatures below T = 373.15 K, $5 \cdot 10^{-3}$ g·cm^{-3} at T = (373.15 and 398.15) K and p = 0.1 MPa, and $3 \cdot 10^{-3}$ g·cm^{-3} in other cases, i.e. at $T \geq 373.15$ K and $p > 0.1$ MPa.

Our initial measurements about the density values of the vegetable based oil, HOSO-B1, and of the biodegrable developed oils of table 1, were performed in the temperature range from 278.15 K to 353.15 K and up to 60 MPa by means of a high pressure vibrating tube densimeter Anton Paar DMA512P. This densimeter consists of two different units, the electronic and interface unit named DMA 60 and the high pressure measuring cell named DMA 512P. The oscillation periods are displayed with seven significant digits. Pressure is measured with an accuracy of 0.02 MPa, whereas temperature is measured with a thermometer Anton Paar CKT100 with an uncertainty of 0.02 K. Calibration was performed following the method proposed by Lagourette et al. [12], using vacuum and Milli-Q water as reference fluids. The accuracy of this calibration was checked by measuring density of hexane and toluene and comparing in Fig. 1 the results with literature values.

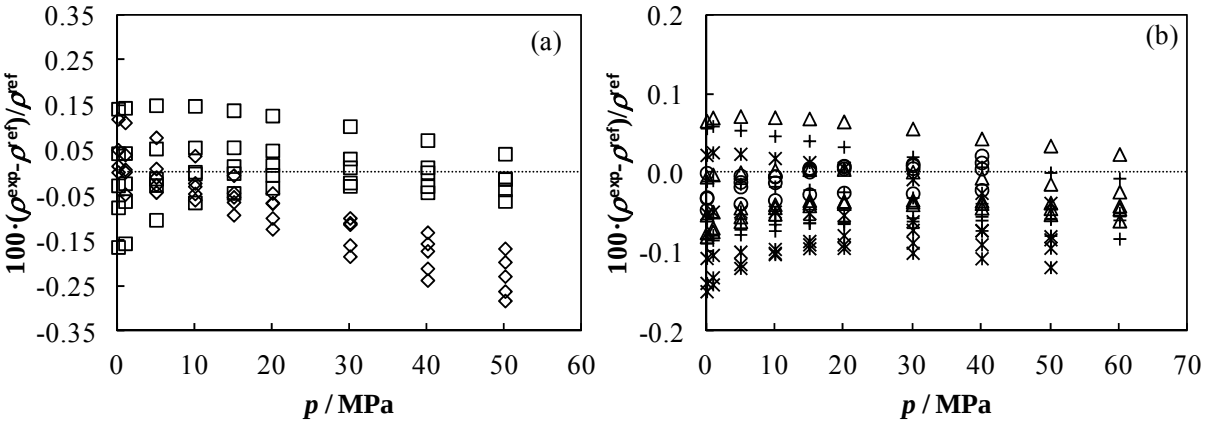

Fig.1. Percent deviations between experimental and literature density values of (a) hexane and (b) toluene. Cibulka and Hnědkovský [14] (□), Span and Wagner [15] (◇), Zéberg- Mikkelsen et al. [16] (○), Lemmon and Span [17] (+), Assael et al. [18] (∗) and Cibulka and Takagi [19] (△).

The reference values used for hexane were taken from the correlation proposed by Cibulka and Hnědkovský [14] and by the equation proposed by Span and Wagner [15]. As concern toluene, the reference density values from Zéberg- Mikkelsen [16], Lemmon and Span [17], Assael et al. [18] and Cibulka and Takagi [19] were used. The AAD% are lower than 0.1% for every data series.

Results

Experimental density and viscosity values at atmospheric pressure of the oils are depicted in Fig. 2.

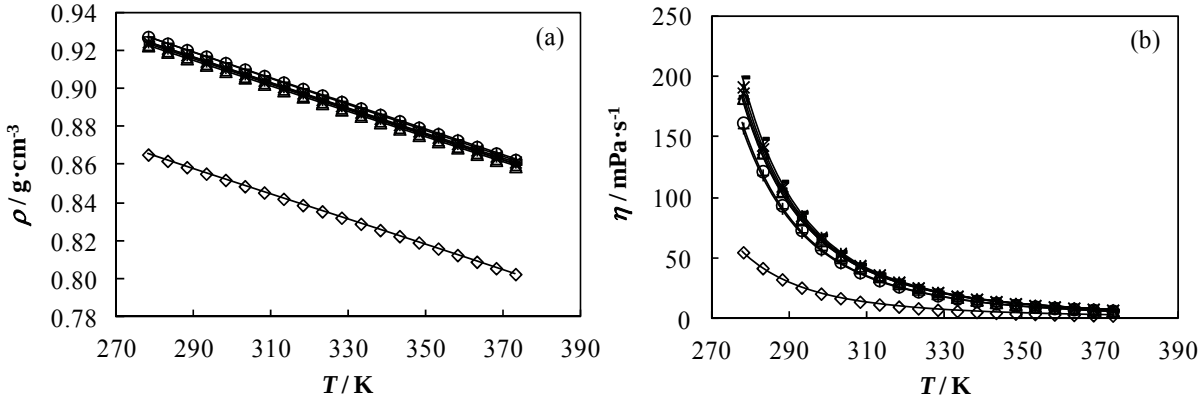

Fig.2. (a) Density and (b) viscosity values of the lubricants at atmospheric pressure. MIN-H03 (◇), HOSO-B1 (□), BIO-H01 (△), BIO-H02 (×), BIO-H03 (✳), BIO-H04 (○), BIO-H05 (+), BIO-H06 (–), solid lines represent correlations through polynomial equation and VFT for (a) and (b), respectively.

It can be observed that density values of the vegetable base oil and the biodegradable oils are higher than those of the reference mineral oil. A similar behavior is observed for viscosity, this last property being between 2.2 and 3.6 times that of the reference oil. Experimental data are gathered in Tables S1 and S2 of the supporting info. Density data were correlated as a function of temperature by means of a third degree polynomial finding standard deviations lower than $1 \cdot 10^{-4}$ g·cm^{-3}. On the other hand, the dependence of viscosity on temperature was correlated by means of the Vogel-Fulcher-Tammann equation (VFT):

$$\ln(\eta) = A + \frac{B}{T - T_0} \tag{1}$$

where η is the dynamic viscosity in mPa·s, T is the temperature in K and A, B and T_0 are fitting constants. The correlation parameters as well as the standard deviations and the average absolute deviation, AAD % are gathered in Table 2.

Table 2. Coefficients of the VFT correlation (Eq.1), standard deviation, σ, and AAD%.

	MIN-G03	HOSO-B1	BIO-H01	BIO-H02	BIO-H03	BIO-H04	BIO-H05	BIO-H06
A	-2.4156	-2.1815	-2.1802	-2.3547	-2.1851	-2.1160	-2.2841	-2.2121
B /K	725.14	911.38	907.91	956.01	906.32	871.84	914.98	913.85
T_0 /K	165.33	154.74	155.34	152.15	156.41	157.16	153.56	156.51
$10^3 \cdot \sigma$	8.3	2.2	2.4	2.4	2.5	1.6	1.3	1.9
AAD %	0.4	0.2	0.2	0.2	0.2	0.1	0.1	0.1

Viscosity indexes (VIs) of the lubricants were presented in Table 1. The higher values of this property for the vegetable based lubricants are a desirable fact, because their viscosity will change less with temperature in comparison with the mineral oil.

The experimental density values measured with the high pressure densimeters are presented in table 3.

Table 3. Experimental densities, ρ, in g·cm^{-3} at high pressure of the oils measured in this work.

	p/MPa									
T/K	0.10	1.00	10.00	20.00	40.00	60.00	80.00	100.00	120.00	
	MIN-H03									
278.15	0.8665	0.8671	0.8718	0.8768	0.8859	0.8941	0.9016	0.9086	0.9144	
298.15	0.8528	0.8532	0.8583	0.8636	0.8734	0.8821	0.8902	0.8977	0.9044	
313.15	0.8427	0.8432	0.8487	0.8544	0.8648	0.8740	0.8824	0.8900	0.8970	
333.15	0.8292	0.8298	0.8357	0.8419	0.8530	0.8628	0.8717	0.8799	0.8875	
348.15	0.8191	0.8198	0.8261	0.8327	0.8445	0.8549	0.8642	0.8726	0.8806	
373.15	0.8031	0.8029	0.8101	0.8175	0.8305	0.8418	0.8518	0.8608	0.8694	
398.15	0.7866	0.7877	0.7957	0.8039	0.8180	0.8301	0.8407	0.8502	0.8601	
	p/MPa									
	0.10	1.00	5.00	10.00	15.00	20.00	30.00	40.00	50.00	60.00
	HOSO-B1									
278.15	0.9229	0.9234	0.9254	0.9278	0.9302	0.9325	0.9369	0.9412	0.9453	0.9492
293.15	0.9120	0.9125	0.9147	0.9173	0.9198	0.9223	0.9271	0.9316	0.9359	0.9400
313.15	0.8982	0.8987	0.9011	0.9039	0.9067	0.9093	0.9144	0.9193	0.9239	0.9283
333.15	0.8846	0.8852	0.8878	0.8909	0.8939	0.8968	0.9023	0.9075	0.9124	0.9171
353.15	0.8718	0.8725	0.8753	0.8786	0.8818	0.8850	0.8909	0.8964	0.9017	0.9067
	BIO-H01									
278.15	0.9231	0.9236	0.9256	0.9281	0.9304	0.9327	0.9372	0.9414	0.9456	0.9494
293.15	0.9123	0.9128	0.9150	0.9176	0.9201	0.9226	0.9274	0.9319	0.9362	0.9403
313.15	0.8984	0.8989	0.9013	0.9041	0.9069	0.9095	0.9146	0.9195	0.9241	0.9285
333.15	0.8851	0.8857	0.8883	0.8914	0.8944	0.8973	0.9028	0.9080	0.9129	0.9176
353.15	0.8720	0.8727	0.8755	0.8788	0.8820	0.8852	0.8911	0.8967	0.9019	0.9069
	BIO-H02									
278.15	0.9239	0.9244	0.9264	0.9288	0.9312	0.9335	0.9380	0.9421	0.9462	0.9501
293.15	0.9131	0.9136	0.9157	0.9183	0.9209	0.9233	0.9281	0.9326	0.9370	0.9411
313.15	0.8992	0.8997	0.9020	0.9049	0.9076	0.9103	0.9154	0.9203	0.9249	0.9293
333.15	0.8859	0.8865	0.8891	0.8922	0.8952	0.8981	0.9036	0.9088	0.9138	0.9184
353.15	0.8728	0.8735	0.8763	0.8796	0.8829	0.8860	0.8919	0.8975	0.9027	0.9077
	BIO-H03									
278.15	0.9253	0.9258	0.9278	0.9303	0.9326	0.9349	0.9394	0.9436	0.9477	0.9516
293.15	0.9146	0.9151	0.9172	0.9198	0.9223	0.9248	0.9296	0.9341	0.9384	0.9425
313.15	0.9008	0.9013	0.9036	0.9065	0.9092	0.9119	0.9170	0.9218	0.9264	0.9309
333.15	0.8874	0.8880	0.8905	0.8937	0.8967	0.8996	0.9050	0.9102	0.9152	0.9199
353.15	0.8742	0.8748	0.8776	0.8810	0.8842	0.8874	0.8933	0.8988	0.9040	0.9090
	BIO-H04									
278.15	0.9285	0.9289	0.9309	0.9334	0.9359	0.9382	0.9428	0.9471	0.9513	0.9552
293.15	0.9173	0.9178	0.9200	0.9226	0.9252	0.9277	0.9325	0.9371	0.9415	0.9457
313.15	0.9032	0.9037	0.9061	0.9090	0.9118	0.9145	0.9197	0.9246	0.9293	0.9338
333.15	0.8894	0.8900	0.8926	0.8957	0.8988	0.9017	0.9073	0.9126	0.9176	0.9224
353.15	0.8759	0.8765	0.8794	0.8828	0.8860	0.8891	0.8951	0.9008	0.9061	0.9109
	BIO-H05									
278.15	0.9282	0.9287	0.9308	0.9333	0.9357	0.9380	0.9426	0.9469	0.9510	0.9550
293.15	0.9174	0.9178	0.9200	0.9227	0.9253	0.9278	0.9327	0.9373	0.9417	0.9459
313.15	0.9033	0.9039	0.9063	0.9092	0.9120	0.9147	0.9200	0.9249	0.9296	0.9341
333.15	0.8899	0.8905	0.8931	0.8963	0.8994	0.9023	0.9079	0.9132	0.9183	0.9230
353.15	0.8771	0.8778	0.8807	0.8842	0.8875	0.8907	0.8968	0.9025	0.9079	0.9130
	BIO-H06									
278.15	0.9246	0.9251	0.9271	0.9296	0.9320	0.9343	0.9389	0.9432	0.9473	0.9513
293.15	0.9140	0.9145	0.9167	0.9193	0.9219	0.9244	0.9293	0.9339	0.9383	0.9424
313.15	0.9004	0.9009	0.9033	0.9062	0.9089	0.9117	0.9169	0.9218	0.9264	0.9309
333.15	0.8869	0.8875	0.8901	0.8932	0.8962	0.8991	0.9047	0.9100	0.9149	0.9197
353.15	0.8735	0.8742	0.8770	0.8804	0.8837	0.8869	0.8929	0.8985	0.9039	0.9089

These experimental density values were correlated by means of a modified Tammann-Tait equation:

$$\rho(T/\mathrm{K}, p/\mathrm{MPa}) = \frac{\rho(T/\mathrm{K}, 0.1\mathrm{MPa})}{1 - C\cdot\ln\left(\frac{B(T/\mathrm{K}) + p/\mathrm{MPa}}{B(T/\mathrm{K}) + 0.1\mathrm{MPa}}\right)} \quad (2)$$

where ρ(T/K, 0.1MPa) is the density as a function of temperature at a reference pressure 0.1 MPa, following this polynomial expression:

$$\rho(T/\mathrm{K}, 0.1\mathrm{MPa}) = \sum_{i=0}^{2} A_i (T/\mathrm{K})^i \quad (3)$$

C is a parameter independent of temperature and pressure and $B(T)$ is a parameter depending on temperature as a polynomial function:

$$B(T/\mathrm{K}) = \sum_{j=0}^{2} B_j (T/\mathrm{K})^j \quad (4)$$

Parameters obtained for Tammann-Tait correlation are presented in Table 4, along with standard deviations, σ, for ρ(T/K, 0.1MPa) and σ^* for $\rho(T/\mathrm{K}, p/\mathrm{MPa})$, as well as the AAD%.

Table 4. Coefficients of the Tammann-Tait correlation.

	MIN-H03	HOSO-B1	BIO-H01	BIO-H02	BIO-H03	BIO-H04	BIO-H05	BIO-H06
A_0/g·cm^{-3}	1.0727	1.1772	1.1712	1.1727	1.1628	1.1743	1.1929	1.1403
-10^3·A_1/g·cm^{-3}·K^{-1}	0.7945	1.0978	1.058	1.063	0.991	1.029	1.1638	0.8514
10^7·A_2/g·cm^{-3}·K^{-2}	1.920	6.60	5.990	6.06	4.912	5.200	7.630	2.72
10^4·σ/ g·cm^{-3}	1.5691	0.7067	0.9024	0.9412	0.6934	1.3638	0.3863	0.9812
C	0.0856	0.0824	0.082	0.08	0.0803	0.0812	0.0792	0.084
B_0/ MPa	411.4	529	532	546	528	547.8	469	487
-B_1/MPaK^{-1}	1.267	1.926	1.94	2.06	1.96	2.091	1.62	1.65
10^3·B_2/MPa·K^{-2}	1.034	2.02	2.05	2.24	2.1	2.316	1.56	1.6
10^4·σ^* / g·cm^{-3}	2.5	0.5	0.7	0.8	0.6	0.9	0.5	0.5
10^2·AAD%	2.4	0.4	1.7	1.0	0.6	1.3	1.7	2.1

As an example, values of density are depicted in Fig. 3 as a function of pressure at 313.15 K and as a function of temperature at 40 MPa, along with values of two other reference mineral oils for hydraulic applications measured in a previous work [6]. As it was found at atmospheric pressure, density values of the vegetable base oil as well as those of the developed oils based in high oleic sunflower oil are considerably higher than those of the mineral reference oil. This fact may imply that the use of the developed lubricant as hydraulic fluids will require higher diameter of the suction line and/or a more elevated tank to provide positive inlet pressure [20]. Additionally, according to the simplified Sieder-Tate equation, the higher the density value, the better the heat-transfer coefficient [21]. Besides, density of the mineral reference oil measured in

this work, MIN-H03, is lower than those previously measured [6] for two other mineral oils, MIN-H01 and MIN-H02.

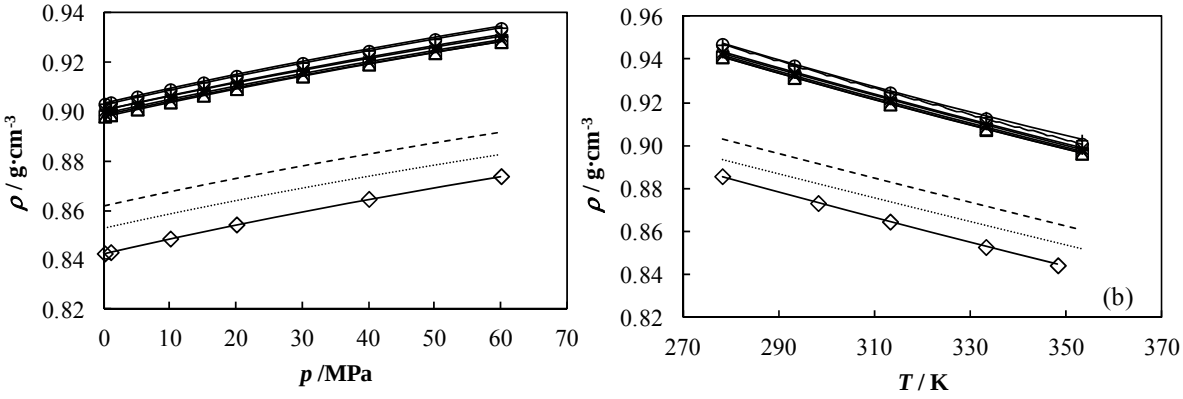

Fig.3. High pressure density values (a) as a function of pressure at 313.15 K and (b) as function of temperature at 40 MPa. MIN-H01 [6] (---), MIN-H02 [6] (···), MIN-H03 (◇), HOSO-B1 (□), BIO-H01 (△), BIO-H02 (×), BIO-H03 (✳), BIO-H04 (○), BIO-H05 (+), BIO-H06 (–), solid lines represent the Tammann-Tait correlation.

We have compared in Fig. 4 the results obtained for density at atmospheric pressure measured by means of the densimeter Stabinger Anton Paar SVM 3000 and by means of the high pressure densimeters. Both positive and negative deviations among the techniques were found, furthermore, the results obtained are within the combined uncertainty of both experimental techniques, the overall AAD% being 0.05%.

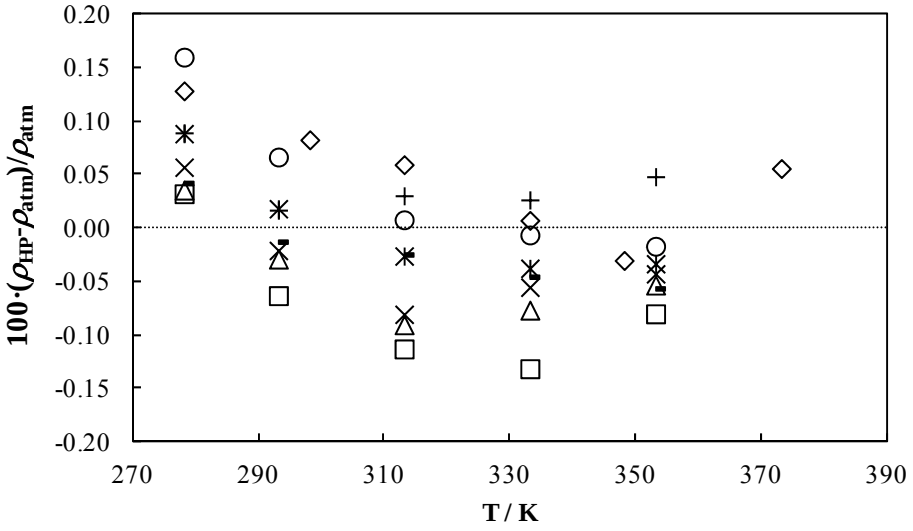

Fig.4. Comparison between the experimental density values at atmospheric pressure obtained through the high pressure densimeters (HP) and through the Stabinger Anton Paar SVM 3000 densimeter (atm). MIN-H03 (◇), HOSO-B1 (□), BIO-H01 (△), BIO-H02 (×), BIO-H03 (✳), BIO-H04 (○), BIO-H05 (+), BIO-H06 (–).

Isothermal compressibility values, κ_T, were obtained by differentiation from the Tammann-Tait equation, taking into account the coefficient values of table 4. Thus, this property is defined by means of the following equation:

$$\kappa_T(T,p) = \frac{1}{\rho}\left(\frac{\partial \rho}{\partial p}\right)_T \tag{5}$$

This property is plotted against pressure at 313.15 K in Fig.5, it can be observed, as usual, that it decreases with pressure increase. Additionally, compressibility values of the reference mineral oil (MIN-H03) are higher than those of the vegetable based and developed lubricants. This fact indicates us that the vegetable lubricants are more efficient than the mineral reference oil for transmitting power in a hydraulic system. Besides, among the vegetable based oils, that with the highest compressibility is BIO-H05, which contains HOSO and ester as base fluid, whereas that with the lowest one is BIO-H01, which is based only in HOSO. Furthermore, in this Fig.5 compressibility values of two reference mineral oils for hydraulic applications measured in a previous work [6] were also plotted. It can be seen that the compressibility values of these reference fluids (MIN-H01 and MIN-H02) is also higher to those of the vegetable based fluids, even though the values are lower than those of MIN-H03. It is important to note that the values obtained for the developed oil BIO-H05 are very close to those of MIN-H01.

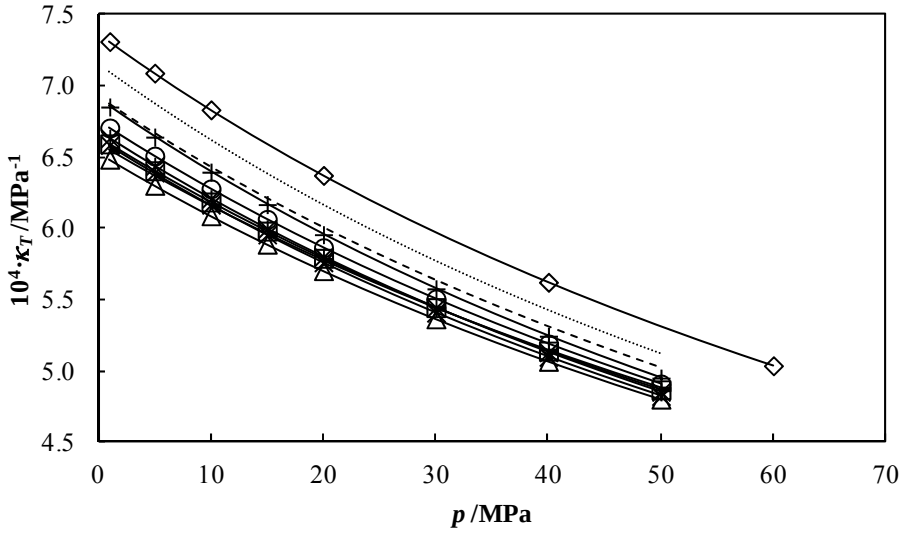

Fig.5. Isothermal compressibility values, κ_T, as a function of pressure at 313.15 K. MIN-H01 [6] (---), MIN-H02 [6] (···), MIN-H03 (◇), HOSO-B1 (□), BIO-H01 (△), BIO-H02 (×), BIO-H03 (✳), BIO-H04 (○), BIO-H05 (+), BIO-H06 (–).

In Fig. 6, the maximum and minimum values of κ_T in the temperature range from 278.15 K to 353.15 K and the pressure range from 1 to 50 MPa are presented. As it can be observed, the ratio between the maximum and minimum values for every oil is around two, which indicates that this property should not be considered as constant in the design of a hydraulic system.

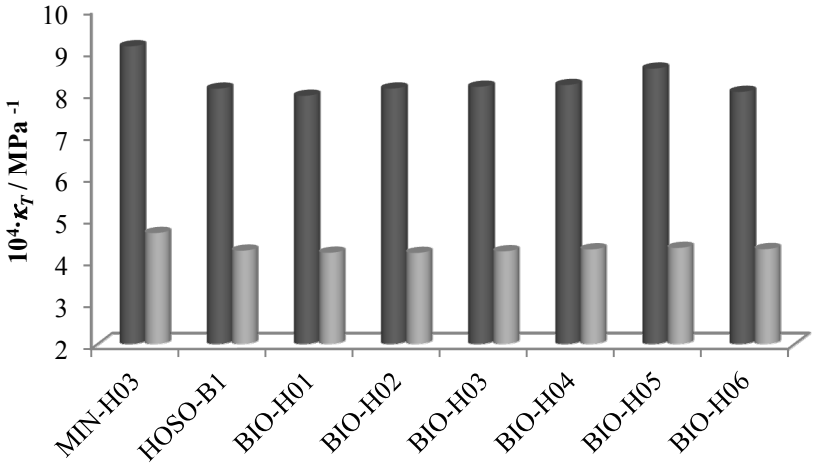

Fig.6. Maximum (dark grey) and minimum (light grey) compressibility values, κ_T, of the studied oils in the temperature range from 278.15 K to 353.15 K and pressure range from 1 MPa to 50 MPa.

Finally, the values of the thermal expansion coefficient were also obtained by differentiation from the Tammann-Tait equation, according to the following expression:

$$\alpha_p(T,p) = -\frac{1}{\rho}\left(\frac{\partial \rho}{\partial T}\right)_p \tag{6}$$

This property is plotted as a function of pressure at 313.15 K in Fig. 7. It decreases with pressure and the highest values are those of the mineral reference oils. In order to get adequate heat transfer properties for a hydraulic fluid, a low coefficient of thermal expansion is preferred [3], i.e., that of the vegetable based oils.

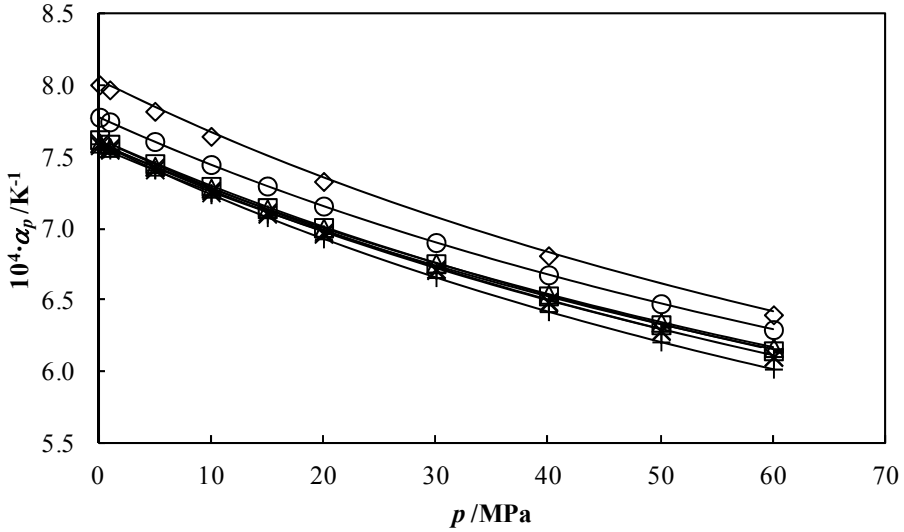

Fig.7. Thermal expansion coefficient, α_p, as a function of pressure at 313.15 K. MIN-H03 (◇), HOSO-B1 (□), BIO-H01 (△), BIO-H02 (×), BIO-H03 (✳), BIO-H04 (○), BIO-H05 (+), BIO-H06 (–).

Conclusions

In this work new density data at high pressure of a reference mineral oil, a vegetable base oil and six biodegradable base oils for their use as hydraulic fluids are presented. The values of this property for vegetable based lubricants are higher than those of the reference mineral

lubricant, which indicates that the firsts could require higher diameter of the suction line and/or a more elevated tank to provide positive inlet pressure with comparison to the mineral lubricant. Additionally, according to the simplified Sieder-Tate equation, they will have a better the heat-transfer coefficient.

Concerning compressibility, it was found that the value of this property is lower for the vegetable based oils than for the reference mineral oils, therefore, they will be more efficient in transmitting power.

Finally, concerning viscosity, it was found that viscosity of the developed oils is higher than that of the reference mineral oil, whereas viscosity index for the latter is also lower.

Acknowledgements

This work was carried out within the framework of the strategic and singular project "Biolubricants based on vegetable oils and their synthetic derivatives", which was funded by Spanish Science and Innovation Ministry and the EU FEDER program (PSE- 320100-2006-1, PSE-420000-2008-4). We are very grateful to the BIOVESIN partners for their excellent advice and for providing us the samples of the products. L.L and T.R. acknowledge financial support under the Ramon y Cajal Program and the FPU program, respectively.

Supplementary information

This supplementary information includes the experimental density and viscosity values measured with the Stabinger Anton Paar SVM 3000 viscometer.

Table S1. Experimental density values, in $g \cdot cm^{-3}$, at atmospheric pressure measured with Stabinger Anton Paar SVM 3000.

T/K	MIN-H03	HOSO-B1	BIO-H01	BIO-H02	BIO-H03	BIO-H04	BIO-H05	BIO-H06
278.15	0.8654	0.9226	0.9228	0.9234	0.9245	0.9270	0.9274	0.9242
283.15	0.8621	0.9193	0.9194	0.9201	0.9212	0.9235	0.9240	0.9208
288.15	0.8588	0.9160	0.9160	0.9167	0.9178	0.9201	0.9206	0.9174
293.15	0.8554	0.9126	0.9126	0.9133	0.9144	0.9167	0.9172	0.9141
298.15	0.8521	0.9093	0.9093	0.9100	0.9111	0.9133	0.9138	0.9107
303.15	0.8488	0.9059	0.9059	0.9066	0.9077	0.9099	0.9104	0.9073
308.15	0.8455	0.9025	0.9026	0.9032	0.9044	0.9065	0.9070	0.9040
313.15	0.8422	0.8992	0.8992	0.8999	0.9010	0.9031	0.9036	0.9006
318.15	0.8389	0.8958	0.8959	0.8965	0.8977	0.8997	0.9002	0.8973
323.15	0.8356	0.8925	0.8925	0.8931	0.8943	0.8963	0.8968	0.8939
328.15	0.8323	0.8892	0.8891	0.8898	0.8910	0.8929	0.8935	0.8906
333.15	0.8291	0.8858	0.8858	0.8864	0.8877	0.8895	0.8901	0.8873
338.15	0.8258	0.8825	0.8824	0.8831	0.8844	0.8861	0.8867	0.8840
343.15	0.8226	0.8791	0.8791	0.8798	0.8811	0.8828	0.8834	0.8806
348.15	0.8193	0.8758	0.8758	0.8764	0.8778	0.8794	0.8800	0.8773
353.15	0.8161	0.8725	0.8725	0.8732	0.8745	0.8760	0.8767	0.8740
358.15	0.8127	0.8692	0.8692	0.8699	0.8712	0.8727	0.8734	0.8707
363.15	0.8092	0.8659	0.8659	0.8666	0.8678	0.8693	0.8699	0.8674
368.15	0.8058	0.8627	0.8627	0.8634	0.8646	0.8659	0.8664	0.8640
373.15	0.8027	0.8596	0.8594	0.8602	0.8615	0.8625	0.8631	0.8607

Table S2. Experimental viscosity values, in mPa·s^{-1}, at atmospheric pressure measured with Stabinger Anton Paar SVM 3000.

T/K	MIN-G03	HOSO-B1	BIO-H01	BIO-H02	BIO-H03	BIO-H04	BIO-H05	BIO-H06
278.15	55.1	181	183	186	191	162	158	200
283.15	42.0	136	138	140	143	122	119	149
288.15	32.8	105	106	108	110	93.9	91.3	114
293.15	25.9	82.0	82.4	83.8	85.4	73.5	71.5	88.1
298.15	21.0	65.1	65.3	66.3	67.5	58.6	57.0	69.6
303.15	17.2	52.5	52.6	53.3	54.2	47.3	46.3	55.8
308.15	14.4	42.9	43.0	43.5	44.2	38.8	37.9	45.4
313.15	12.1	35.6	35.6	36.0	36.5	32.2	31.4	37.4
318.15	10.3	29.8	29.8	30.1	30.5	27.1	26.4	31.2
323.15	8.87	25.2	25.3	25.4	25.8	23.0	22.4	26.3
328.15	7.70	21.6	21.6	21.7	22.0	19.7	19.2	22.4
333.15	6.74	18.6	18.6	18.7	18.9	17.1	16.6	19.3
338.15	5.91	16.2	16.2	16.2	16.4	14.9	14.5	16.7
343.15	5.23	14.2	14.2	14.1	14.4	13.1	12.7	14.6
348.15	4.58	12.5	12.5	12.4	12.7	11.6	11.2	12.9
353.15	4.26	11.2	11.1	11.0	11.3	10.3	10.0	11.4
358.15	3.87	9.97	9.94	9.83	10.1	9.23	8.91	10.2
363.15	3.52	8.96	8.93	8.82	9.02	8.31	8.01	9.13
368.15	3.20	8.09	8.07	7.95	8.14	7.52	7.23	8.23
373.15	2.93	7.34	7.32	7.20	7.38	6.84	6.58	7.45

References

[1] S. Lawate, Environmentally friendly hydraulic fluids. in: L.R. Rudnick, (Ed.), Synthetics, mineral oils, and bio-based lubricants. Chemistry and technology, CRC Press, Boca Raton, FL, 2006, pp. 541-550.

[2] D.M. Pirro, A.A. Wessol, Lubrication fundamentals, 2nd revised and expanded ed., Marcel Dekker, Inc., New York 2001.

[3] D.G. Placek, Hydraulics. in: L.R. Rudnick, (Ed.), Synthetics, mineral oils, and bio-based lubricants. Chemistry and technology, CRC Press, Boca Raton, FL, 2006, pp. 517-540.

[4] S. Boyde, Green Chem. 4 (2002) 293-307.

[5] C. Kajdas, A. Karpinska, A. Kulczycki, Industrial lubricants. in: R.M. Mortier, M.F. Fox, S.T. Orszulik, (Eds.), Chemistry and technology of lubricants, Springer, New York, 2010, pp. 239-292.

[6] T. Regueira, L. Lugo, O. Fandiño, E.R. López, J. Fernández, Green Chem. 13 (2011) 1293-1302.

[7] R. Navette, F. De Clercq, The development of hydraulic fluids for earthmoving machines complying with ecolabel requirements, SAE Technical Paper, 981490, 1998.

[8] F. Novotny-Farkas, W. Böhme, H. Stabinger, W. Belitsch, Anton Paar World Tribology Congress II, 2001.

[9] F.M. Gaciño, T. Regueira, L. Lugo, M.J.P. Comuñas, J. Fernández, J. Chem. Eng. Data 56 (2011) 4984-4999.

[10] T. Regueira, L. Lugo, J. Fernández, J. Chem. Thermodyn. 48 (2012) 213-220.

[11] J.J. Segovia, O. Fandiño, E.R. López, L. Lugo, M.C. Martín, J. Fernández, J. Chem. Thermodyn. 41 (2009) 632-638.

[12] B. Lagourette, C. Boned, H. Saint-Guirons, P. Xans, H. Zhou, Meas. Sci. Technol. 3 (1992) 699-703.

[13] M.J.P. Comuñas, J.P. Bazile, A. Baylaucq, C. Boned, J. Chem. Eng. Data 53 (2008) 986-994.

[14] I. Cibulka, L. Hnědkovský, J. Chem. Eng. Data 41 (1996) 657-668.

[15] R. Span, W. Wagner, Int. J. Thermophys. 24 (2003) 41-109.

[16] C.K. Zeberg-Mikkelsen, L. Lugo, J. García, J. Fernández, Fluid Phase Equilib. 235 (2005) 139-151.

[17] E.W. Lemmon, R. Span, J. Chem. Eng. Data 51 (2006) 785-850.

[18] M.J. Assael, H.M.T. Avelino, N.K. Dalaouti, J.M.N.A. Fareleira, K.R. Harris, Int. J. Thermophys. 22 (2001) 789-799.

[19] I. Cibulka, T. Takagi, J. Chem. Eng. Data 44 (1999) 411-429.

[20] Sauer-Danfoss, Hydraulic fluids and lubricants technical information, 2010.

[21] S.J. Randles, Value Creation from a Technology Viewpoint (How Esters Can Save You Money), Lubricants of the Future and Environment, 6th International Congress, Brussels, 1999.

5.3. Compressibilities and viscosities of reference, vegetable and synthetic gear lubricants*

*T. Regueira, L. Lugo, J. Fernández, submitted.

ABSTRACT

Nowadays, one of the primary choices of base oils for environmentally aware lubricants is vegetable oils. This is due to their good natural biodegradability and very low toxicity in combination with very good lubricity characteristics. Development of new vegetable-base lubricants requires the knowledge of their thermophysical properties such as viscosity or density, among others. Regarding this issue, in this work, we have carried out density measurements over a wide temperature and pressure range and calculated the isothermal compressibility values of six gear lubricants, two of them reference mineral oils and the other four developed biodegradable oils based in high oleic sunflower oil or in synthetic esters. Moreover, the viscosities were measured for these oils covering a broad range of temperatures and the viscosity index was also determined.

INTRODUCTION

Despite the impact of recession that gave rise to a minimum in the world lubricants demand in 2009, Gosalia[1] stands that the regional lube market dynamics of the past ten years in terms of quantity and quality will continue in the future. Thus, the global lubricant demand in 2011 was, according to Gosalia[1], of 35.1 million tonnes, and it has increased an 1.9% compared with the previous year 2010. In the past 10 years overall, in volume terms, Europe and America together lost what Asia-Pacific and rest of world gained, and these latter regions now share close to 4% of the global lubricant market[2].

Under this frame of market dynamics, the global environmental awareness is also growing. The environment must be protected against pollution caused by lubricants based on petroleum oils. The pollution problem is so severe that approximately 50% of all lubricants sold worldwide end up in the environment via volatility, spills or total loss applications. This threat to the environment can be avoided by either preventing undesirable losses, reclaiming and recycling mineral oil lubricants, or using environmentally friendly lubricants[3]. To initiate and boost the use of biodegradable products, government incentives and mandatory regulations are needed to put pressure on the industries that release lubricants into the environment[2]. Thus, the EU Ecolabel is a voluntary award scheme intended to promote products with a reduced environmental impact during their entire life cycle. This scheme is part of the sustainable consumption and production policy of the Community, which aims at reducing the negative impact of consumption and production on the environment, health, climate and natural resources. It is intended to promote those products which have a high level of environmental performance. Therefore, the EU Ecolabel should aim at substituting hazardous substances by safer ones, wherever technically possible[4]. The EU established in 2011 the latest ecological criteria for the

award of the EU Ecolabel to lubricants. This product group comprises five categories which include hydraulic fluids and tractor transmission oils, greases and stern tube greases, chainsaw oils, concrete release agents, wire rope lubricants, stern tube oils and other total loss lubricants, two-stroke oils and industrial and marine gear oils[5].

In this context, one of the primary choices of base oils for environmentally aware lubricants is vegetable oils. This is due to their good natural biodegradability and very low toxicity in combination with very good lubricity characteristics[6, 7]. The triglyceride structure gives these esters a high natural viscosity and viscosity index and is also responsible for structural stability over reasonably operating temperature ranges. However, they have poor oxidative stability as compared to mineral oils and in general they cannot withstand reservoir temperatures over 80ºC, even thought the use of appropriate antioxidants can combat this fact[2]. These renewable resources also provide a cost advantage over other base materials such as synthetic base stocks. Furthermore, genetically modified high oleic sunflower oil (HOSO) contains 87.4 % oleic acid (about 70% more than regular oil) and 5.45% linoleic acid (which is about 66% less than regular sunflower oil), this could increase the oxidative stability during storage, which would make high oleic sunflower oil a good candidate for preparing biolubricant basestock oil[8].

Gear lubrication oils are a machine component of particular significance for the transmission, i.e. in gearboxes of wind turbines or in agricultural tractors. Apart from the important function of lubricating the sliding rolling contacts, the oil also fulfils the task of cooling and removing the friction heat generated. Elastohydrodynamic lubrication (EHL) prevails in lubricated contacts where the external load per unit area is high compared to the stiffness of the material and the contacting surface are non-conformal, i.e., they do not fit well together. Gears are a typical example of highly loaded EHL contacts[9]. In EHL, for severe operating conditions the temperature increase in conjunctions may not be ignored. Neglecting the heat generation in EHD contacts operating under severe conditions leads to an overestimation of both film thicknesses and friction coefficients. Temperature variations lead to both viscosity, η, and density, ρ, changes throughout the lubricant film[10].

The effect of the density-pressure relation on EHL parameters such as film thickness and pressure spikes has been studied by several authors. It has been shown that compressibility has a very small effect on the minimum film thickness, whereas the film thickness at the centre of the contact becomes minor in case of high compressible lubricants[9]. Kweh et al.[11] demonstrate that in a circular contact the reduction in central film thickness due to compressibility can be correlated with the increase in density at the local pressure in the centre of the contact.

Moreover, Venner and Bos[12] shown that, although compressibility is not one of the predominant effects accounting for film formation, it does determine to a great extend the shape of the lubricant film in the central region of the contact. Hamrock et al.[13] studied the influence of compressibility on the pressure spike and found that an incompressible lubricant gives rise to much higher pressure at the pressure spike than lubricants that are compressible. Furthermore, the risk of surface fatigue is much greater for a lubricant with low compressibility than for more compressible lubricants[9].

In EHL more effort has been directed toward a better understanding of shear response than into the study of compressibility of EHL lubricants, however, the pursuing of higher precision is necessary to enable the theory to cope with film thicknesses of the order of nanometers, which are encountered in the mixed lubrication and partial EHL regimes. Consequently, it is appropriate to give more attention to descriptions of the density, pressure and temperature relations for fluid lubricants[14].

In the present work, we have carried out density measurements in a temperature range between 278.15 and 398.15K and pressures up to 120 MPa of two mineral gear oils, three biodegradable oils based in high oleic sunflower oil and a synthetic biodegradable oil. The mineral oils are considered reference lubricants because one of them is currently used in wind turbines and the other in agricultural tractors, whereas the biodegradable oils were specifically developed to replace them. Besides, the correlation ability of two different equations for fitting experimental density values as a function of temperature and pressure was checked. Additionally, density predictive capacity of the EoS from Dowson and Higginson[15], Zhu and Wen[16] and Jacobson and Vinet[17] was also analysed for the studied lubricants. Furthermore, compressibility values of the lubricants were calculated from the correlation of the experimental density data. Moreover, viscosity data for these oils were determined under a temperature range from 278.15 to 373.15 K and their corresponding viscosity indexes are also reported. This work was carried out in the framework of a Spanish singular and strategic project, BIOVESIN, aiming to develop formulation of a new range of environment-friendly biodegradable lubricants from vegetable oils[18-24] for wind energy and agricultural sectors.

EXPERIMENTAL SECTION

Materials

The gear lubricants have been provided by some of the Spanish companies involved in the BIOVESIN project: Verkol Lubricantes, Agria Hispania and Indra. All of them are presented in Table 1, along with their density and kinematic viscosity at 313.15 K and their viscosity index. Three of the biodegradable oils, BIO-G00, BIO-G01 and BIO-G02 are based in high oleic

sunflower oil (HOSO) and the last one, SYN-G01, is composed by synthetic esters. These biodegradable lubricants were developed by Verkol Lubricantes to substitute the reference mineral oils.

Table 1. Characteristics of the gear lubricants studied in this work.

Lubricant	**Description**	**Application**	**ρ /g·cm^{-3} (313.15 K)**	**ν/ mm^2·s^{-1} (313.15 K)**	**Viscosity Index (VI)**
Reference Lubricants					
MIN-G01	Mineral	Wind turbine	0.8600	329.29	139.4
MIN-G02	Mineral	Tractor transmission	0.8838	182.64	96.7
Developed Biodegradable Lubricants					
BIO-G00	25% HOSO*	Wind turbine	0.9261	244.56	158.2
BIO-G01	50% HOSO*	Wind turbine	0.9207	221.80	189.3
BIO-G02	45% HOSO*	Tractor transmission	0.9203	148.56	165.8
SYN-G01	Synthetic esters	Wind turbine	0.9269	254.35	149.6

*HOSO is High Oleic Sunflower Oil

Experimental procedure

The viscosity index (VI) and viscosity values between 278.15 and 373.15 K were measured with an automated SVM 3000 Anton Paar rotational Stabinger device[25]. The basic operating principles and schematic set up of this equipment are described in a European Patent[25]. This apparatus has also a glass vibrating-tube, which allows density measurements, which was used to measure the densities of the studied oils at atmospheric pressure. The SVM 3000 uses Peltier elements for fast and efficient thermostating. The temperature uncertainty is 0.02 K from 288.15 K to 378.15 K and 0.05 K outside this range. The uncertainty of the dynamic viscosity is 1% whereas density is measured with an uncertainty of 0.0005 g·cm^{-3} [26, 27].

Density measurements up to 120 MPa in the temperature range from 278.15 K to 398.15 K were performed in a fully automated vibrating tube densimeter Anton Paar HPM[28-31]. Temperature is measured by a Pt100 probe calibrated with an uncertainty of 0.02 K whereas pressure transducer was calibrated with an uncertainty of 0.02 MPa. Water, decane and vacuum were used as reference fluids for density calibration, following the procedure described by Comuñas et al.[32] Taking into account the uncertainties of the temperature, pressure, water and decane density and oscillation period measurements for water, decane, vacuum and the studied liquid, it was estimated[29] that the expanded (k=2) density uncertainty is $0.7\cdot10^{-3}$ g·cm^{-3} for temperatures below T = 373.15 K, $5\cdot10^{-3}$ g·cm^{-3} at T = (373.15 and 398.15) K and p = 0.1 MPa, and $3\cdot10^{-3}$ g·cm^{-3} in other cases, i.e. at $T \geq 373.15$ K and $p > 0.1$ MPa. More details about the experimental setup were previously given[29].

RESULTS AND DISCUSSION

Table 1 shows the viscosity index (VI) of the lubricants studied in this work. These values were obtained according to ASTM D2270 and ISO 2909 by means of the automated Anton Paar Stabinger SVM 3000 viscometer. It can be observed that the developed biodegradable lubricants present VI higher than the reference mineral oils, indicating that their viscosity suffers lower changes with temperature, which is a desirable property for lubricant applications. It should be highlighted that among the vegetable based lubricants, the higher the HOSO content, the higher the VI. The synthetic oil composed by a mixture of biodegradable synthetic esters has a VI slightly lower than the HOSO based lubricants.

The viscosity values at atmospheric pressure of the studied lubricants were also obtained with the automated Anton Paar Stabinger SVM 3000 device and are presented in Table 2. It can be seen that the developed oil BIO-G01 have similar viscosities to that of the reference oil MIN-G01 from 343.15 to 363.15 K, because the biodegradable oil was developed to have similar viscosities to the reference oil at the working wind turbine temperatures (343.15-353.15 K). Similarly, the developed oil for tractor transmission, BIO-G02, presents similar viscosity values to the reference oil MIN-G02 at temperatures higher than 353.15 K.

Table 2. Viscosity values, η (mPa·s), at atmospheric pressure of the gear lubricants.

T/K	MIN-G01	MIN-G02	BIO-G00	BIO-G01	BIO-G02	SYN-G01
278.15	3265	2121	2144	1584	1086	2472
283.15	2140	1348	1455	1110	756	1637
288.15	1439	890	1013	796	541	1118
293.15	994	603	721	584	397	786
298.15	704	419	524	438	296	563
303.15	510	299	389	334	225	413
308.15	376	217	294	259	174	309
313.15	283	161	226	204	137	236
318.15	217	122	177	163	109	183
323.15	169	94.1	140	133	88.2	144
328.15	134	73.6	113	109	72.2	116
333.15	107	58.5	92.1	90.3	59.9	93.8
338.15	86.7	47.3	76.0	75.8	50.2	77.0
343.15	71.2	38.6	63.4	64.3	42.4	64.0
348.15	59.0	31.8	53.4	55.0	36.3	53.7
353.15	49.5	26.6	45.4	47.4	31.2	45.5
358.15	41.9	22.4	39.0	41.2	27.1	38.9
363.15	35.7	19.1	33.7	36.1	23.7	33.6
368.15	30.7	16.4	29.3	31.8	20.9	29.2
373.15	26.6	14.2	25.7	28.2	18.5	25.5

In Table 2 and Figure 1a it can be observed that the developed oils, BIO-G01 and BIO-G02 reach up to half viscosity values (at 278.15 K) compared to that of the corresponding reference oils, MIN-G01 and MIN-G02. This fact is an important advantage of the vegetable developed oils, because in cold starts, the lubricant film is too robust at low temperatures, and it will change in a noticeable way when the temperature rises, leading to a nonlinear power transmission[33].

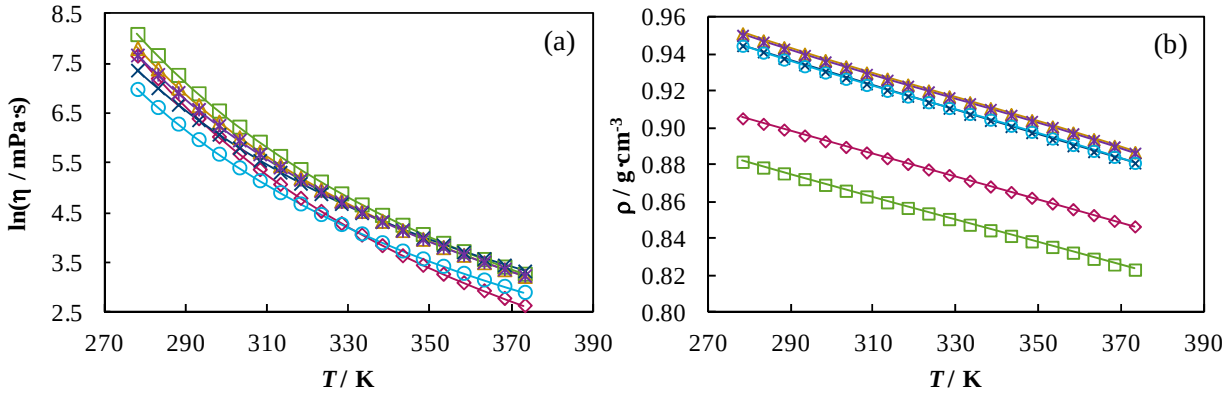

Figure 1. (a) Experimental dynamic viscosity values, η, and (b) density values, ρ, at atmospheric pressure from Anton Paar Stabinger SVM 3000. MIN-G02 (◇), MIN-G01 (□). SYN-G01 (△), BIO-G01 (×), BIO-G00 (✳), BIO-G02 (○). Solid line is (a) the VFT correlation and (b) a third order polynomial correlation.

Viscosity values were correlated (Figure 1a) as a function of temperature by means of the Vogel-Fulcher-Tammann equation (VFT):

$$\ln(\eta) = A + \frac{B}{T - T_0} \tag{1}$$

where η is the dynamic viscosity in mPa·s, T is the temperature in K and A, B and T_0 are fit constants. The correlation parameters as well as the standard deviations and the average absolute deviation, AAD% are gathered in Table 3.

Table 3. Coefficients of the VFT correlation (eq 1), standard deviation, σ, and AAD%.

	MIN-G01	MIN-G02	BIO-G00	BIO-G01	BIO-G02	SYN-G01
A	-2.9559	-3.5062	-2.4919	-1.8850	-2.3471	-2.4157
B /K	1355.6	1297.3	1246.0	1135.4	1141.9	1196.4
T_0 /K	155.55	162.09	155.69	155.54	155.96	161.30
$10^3 \cdot \sigma$	5.2	7.7	6.3	3.8	5.1	5.4
AAD %	0.4	0.6	0.5	0.3	0.4	0.4

In this apparatus we have also measured the density data at atmospheric pressure, which are depicted in Figure 1b. Density values measured in the high pressure densimeter are gathered in Table 4. The values at atmospheric pressure measured in this last device, were compared with

those obtained in the Stabinger SVM 3000, finding an agreement (AAD%) between both data sets of 0.08%, which is within the combined uncertainty of both apparatus.

Table 4. Experimental density values, ρ (g·cm^{-3}), of the studied lubricants at different temperatures and pressures.

	p/MPa								
T/K	0.10	1.00	10.00	20.00	40.00	60.00	80.00	100.00	120.00
	MIN-G01								
278.15	0.8828	0.8833	0.8878	0.8924	0.9008	0.9085	0.9156	0.9222	0.9277
298.15	0.8703	0.8707	0.8753	0.8803	0.8893	0.8975	0.9050	0.9120	0.9185
313.15	0.8606	0.8611	0.8660	0.8713	0.8809	0.8895	0.8974	0.9047	0.9115
333.15	0.8480	0.8486	0.8540	0.8597	0.8701	0.8793	0.8877	0.8954	0.9025
348.15	0.8388	0.8394	0.8452	0.8512	0.8622	0.8719	0.8806	0.8886	0.8960
373.15	0.8236	0.8240	0.8302	0.8369	0.8489	0.8593	0.8687	0.8773	0.8854
398.15	0.8082	0.8093	0.8164	0.8237	0.8366	0.8478	0.8577	0.8666	0.8750
	MIN-G02								
283.15	0.9031	0.9035	0.9078	0.9124	0.9208	0.9287	0.9359	0.9427	0.9494
298.15	0.8937	0.8942	0.8988	0.9036	0.9126	0.9207	0.9282	0.9351	0.9417
313.15	0.8841	0.8846	0.8895	0.8947	0.9041	0.9127	0.9205	0.9276	0.9344
323.15	0.8777	0.8782	0.8833	0.8887	0.8985	0.9074	0.9155	0.9228	0.9297
348.15	0.8619	0.8625	0.8682	0.8741	0.8848	0.8944	0.9031	0.9110	0.9184
373.15	0.8464	0.8469	0.8532	0.8597	0.8713	0.8816	0.8908	0.8993	0.9071
398.15	0.8315	0.8316	0.8387	0.8458	0.8585	0.8695	0.8793	0.8882	0.8964
	BIO-G00								
278.15	0.9504	0.9504	0.9548	0.9595	0.9681	0.9760	0.9834	0.9902	0.9965
298.15	0.9367	0.9368	0.9416	0.9466	0.9558	0.9643	0.9722	0.9795	0.9865
313.15	0.9268	0.9270	0.9321	0.9373	0.9471	0.9560	0.9642	0.9717	0.9788
333.15	0.9132	0.9135	0.9190	0.9247	0.9352	0.9448	0.9534	0.9614	0.9689
348.15	0.9032	0.9036	0.9095	0.9156	0.9266	0.9366	0.9456	0.9539	0.9616
373.15	0.8863	0.8873	0.8938	0.9005	0.9124	0.9230	0.9327	0.9414	0.9497
398.15	0.8693	0.8704	0.8777	0.8850	0.8980	0.9094	0.9197	0.9291	0.9388
	BIO-G01								
278.15	0.9455	0.9459	0.9503	0.9550	0.9636	0.9716	0.9790	0.9858	0.9922
298.15	0.9308	0.9313	0.9361	0.9412	0.9505	0.9590	0.9668	0.9741	0.9809
313.15	0.9206	0.9212	0.9262	0.9316	0.9415	0.9504	0.9586	0.9662	0.9732
333.15	0.9071	0.9076	0.9131	0.9189	0.9294	0.9390	0.9477	0.9557	0.9633
348.15	0.8972	0.8978	0.9037	0.9098	0.9209	0.9309	0.9399	0.9482	0.9561
373.15	0.8812	0.8814	0.8879	0.8946	0.9067	0.9173	0.9269	0.9358	0.9441
398.15	0.8651	0.8652	0.8723	0.8796	0.8928	0.9042	0.9145	0.9239	0.9326
	BIO-G02								
278.15	0.9465	0.9465	0.9510	0.9556	0.9643	0.9723	0.9797	0.9864	0.9929
298.15	0.9325	0.9326	0.9375	0.9425	0.9519	0.9605	0.9684	0.9757	0.9826
313.15	0.9224	0.9225	0.9277	0.9330	0.9428	0.9518	0.9600	0.9676	0.9747
333.15	0.9087	0.9090	0.9146	0.9204	0.9309	0.9405	0.9492	0.9572	0.9647
348.15	0.8987	0.8991	0.9050	0.9111	0.9222	0.9322	0.9413	0.9496	0.9574
373.15	0.8815	0.8826	0.8892	0.8959	0.9079	0.9185	0.9282	0.9370	0.9452
398.15	0.8651	0.8663	0.8735	0.8809	0.8939	0.9053	0.9156	0.9250	0.9336
	SYN-G01								
278.15	0.9527	0.9527	0.9572	0.9618	0.9706	0.9786	0.9860	0.9928	0.9993
298.15	0.9388	0.9389	0.9438	0.9488	0.9582	0.9668	0.9748	0.9821	0.9891
313.15	0.9285	0.9287	0.9339	0.9392	0.9491	0.9581	0.9663	0.9740	0.9811
333.15	0.9150	0.9153	0.9209	0.9267	0.9373	0.9469	0.9556	0.9636	0.9711
348.15	0.9049	0.9053	0.9113	0.9175	0.9287	0.9387	0.9478	0.9560	0.9637
373.15	0.8879	0.8889	0.8955	0.9023	0.9145	0.9252	0.9349	0.9436	0.9517
398.15	0.8716	0.8727	0.8801	0.8875	0.9006	0.9121	0.9225	0.9318	0.9403

The $p\rho T$ values were correlated as a function of temperature and pressure by means of the Tammann-Tait equation:

$$\rho(T/\mathrm{K}, p/\mathrm{MPa}) = \frac{\rho(T/\mathrm{K}, 0.1\mathrm{MPa})}{1 - C\cdot\ln\left(\frac{B(T/\mathrm{K}) + p/\mathrm{MPa}}{B(T/\mathrm{K}) + 0.1\mathrm{MPa}}\right)} \tag{2}$$

where ρ(T/K, 0.1MPa) is the density as a function of temperature at a reference pressure 0.1 MPa, following this polynomial expression:

$$\rho(T/\mathrm{K}, 0.1\mathrm{MPa}) = \sum_{i=0}^{3} A_i (T/\mathrm{K})^i \tag{3}$$

C is a parameter independent of temperature and pressure and *B(T)* is a parameter depending on temperature as a polynomial function:

$$B(T/\mathrm{K}) = \sum_{j=0}^{2} B_j (T/\mathrm{K})^j \tag{4}$$

Parameters obtained for Tammann-Tait correlation are presented in Table 5, along with standard deviations, σ, for ρ(T/K, 0.1MPa) and σ^* for $\rho(T/\mathrm{K}, p/\mathrm{MPa})$, as well as the AAD%.

Table 5. Ai, Bi, C, standard deviations, σ and σ*, and AAD% from Tammann-Tait equation.

	MIN-G01	MIN-G02	BIO-G00	BIO-G01	BIO-G02	SYN-G01
A_0 /g·cm^{-3}	1.1513	0.9922	1.1797	1.3169	1.137	1.1443
-10^3·A_1 /g·cm^{-3}·K^{-1}	1.441	-0.23	1.056	2.2077	0.6557	0.657
10^6·A_2 /g·cm^{-3}·K^{-2}	2.307	-2.742	1.152	4.1573	-0.192	-0.218
-10^9·A_3 /g·cm^{-3}·K^{-1}	2.14	-2.89	1.15	3.672	-0.31	-0.37
10^4·σ/g·cm^{-3}	2.9	0.4	0.9	1.1	1.8	1.3
10^2·C	8.4	8.4	8.6	8.78	8.4	8.25
B_0 /MPa	454.8	508.9	510.2	550.3	512.17	501.3
-B_1 /MPa·K^{-1}	1.438	1.732	1.63	1.913	1.706	1.668
10^3·B_2 /MPa·K^{-2}	1.26	1.69	1.44	1.928	1.595	1.555
10^4·σ^* / g·cm^{-3}	2.3	1.5	2.2	2.1	2.0	1.9
10^2·AAD%	1.9	1.2	2.2	1.5	1.5	1.5

Additionally, density values as a function of temperature and pressure were also correlated using the following modification of the Tait equation[34-36]:

$$\rho(T/\mathrm{K}, p/\mathrm{MPa}) = \frac{\rho(T/\mathrm{K}, 0.1\,\mathrm{MPa})}{1 - \frac{1}{1+K_0'}\ln\left[1 + \frac{p/\mathrm{MPa}}{K_{00}\exp(-\beta_K T)}\left(1+K_0'\right)\right]} \tag{5}$$

where K_0' is the pressure derivative of the bulk modulus at ambient pressure[37], K_{00} and β_K are the constants that define the exponential dependence of the bulk modulus at ambient pressure on the temperature[36] and, finally, $\rho(T/\mathrm{K}, 0.1\ \mathrm{MPa})$ is the dependence of density on temperature at atmospheric pressure given by the following expression[34]:

$$\rho(T/\mathrm{K}, 0.1\,\mathrm{MPa}) = \rho_R\left(1 - a_p\left(T/\mathrm{K} - T_R/\mathrm{K}\right)\right) \quad (6)$$

where T_R is a reference temperature and ρ_R is the density at T_R and atmospheric pressure. In this fit the reference temperature was considered as the lowest experimental temperature for each of the oils, i.e. 283.15 K for MIN-G02 and 278.15 K for the other oils. Fitting coefficients as well as standard deviations are presented in Table 6. The obtained standard deviations with this fit are lower than the uncertainty of the experimental density measurements but slightly higher than those of the fit with the Tammann-Tait equation.

Table 6. Fitting parameters of the modified Tait equation[34-36], a_p, K_0', K_{00} and β_K, standard deviations, σ (eq. 6) and σ* (eq. 5), and AAD%.

	MIN-G01	MIN-G02	BIO-G00	BIO-G01	BIO-G02	SYN-G01
$10^4 \cdot a_p/\mathrm{K}^{-1}$	7.0755	6.9481	7.1065	7.1856	7.2063	7.1406
$10^4 \cdot \sigma/\mathrm{g\cdot cm}^{-3}$	3.0	3.3	0.9	9.7	2.9	0.0
K_0'	10.888	10.696	10.445	9.864	10.658	10.869
K_{00} /MPa	8168.4	7672.6	8627.5	8560.4	8695.4	8821.2
$10^3 \cdot \beta_K/\ \mathrm{K}^{-1}$	5.3695	5.0089	5.3036	5.2295	5.3706	5.4183
$10^4 \cdot \sigma^*/\ \mathrm{g\cdot cm}^{-3}$	3.3	2.4	2.4	6.1	3.5	3.9
$10^2 \cdot$AAD%	3.2	2.1	1.9	5.1	3.1	3.4

Density of the mineral lubricant MIN-G02 compares well with those previously published of a mineral lubricant for gear application, MIN-G[18], the AAD% at T = 313.15 K and pressures up to 60 MPa being 0.08%.

Moreover, density values from the Anton Paar HPM densimeter are plotted as a function of pressure at 313.15 K and as a function of temperature at 40 MPa in Figure 2. It can be observed that the lubricants with the lowest densities are the reference mineral ones, whereas density of the vegetable based lubricant as well as the synthetic lubricant are similar to each other and higher than those of the mineral oils, the highest density values being those of the synthetic lubricant SYN-G01. This is due to the ester groups of the molecules of the four biodegradable oils which increase the packing of the molecules due to the attractive dipole intermolecular forces. Among the vegetable based oils the density sequence is the following: BIO-G00 > BIO-G02 > BIO-G01, therefore the density of these oils decreases with the HOSO content. We have also found previously[18] that HOSO is denser than mineral hydraulic oils. According to the Sieder-Tate equation, the higher the density value, the better the heat-transfer coefficient.

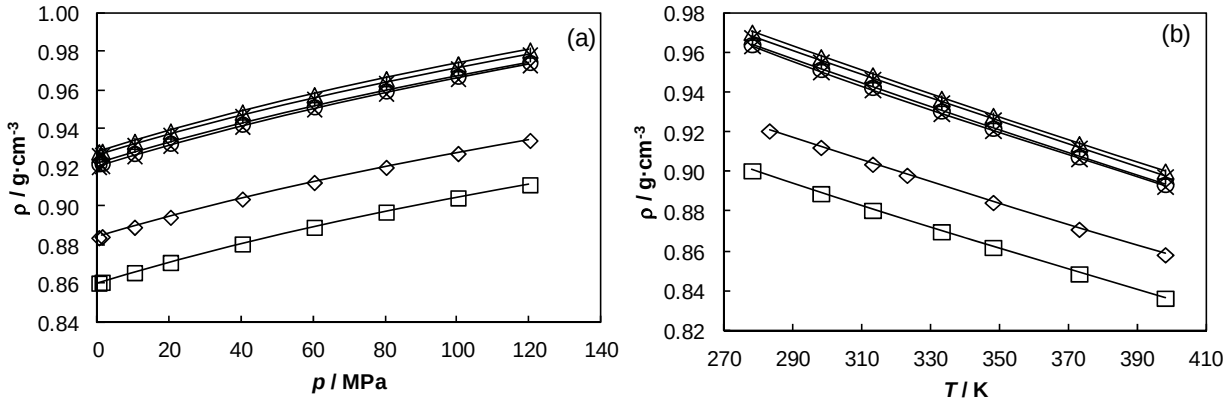

Figure 2. Experimental density values, ρ, from Anton Paar HPM of the lubricants measured in this work, (a) as a function of pressure at T = 313.15 K and (b) as a function of temperature at p = 40 MPa. SYN-G01 (△), BIO-G00 (✳), BIO-G02 (○), BIO-G01 (×), MIN-G02 (◇), MIN-G01 (□). Solid line is the Tammann-Tait correlation.

Density values as a function of temperature and pressure for the studied oils have been predicted by means of two methods. The first of them was the Dowson and Higginson[15] EoS:

$$\rho(T/\mathrm{K},\, p/\mathrm{GPa}) = \rho\left(T/\mathrm{K},\, 0.1\ \mathrm{MPa}\right)\left(1+\frac{0.6\,p/\mathrm{GPa}}{1+1.7\,p/\mathrm{GPa}}\right) \tag{7}$$

In this last expression, eq 3 was used for obtaining ρ(T/K,0.1 MPa).

The other method consists in the use of the EoS from Zhu and Wen[16], which is defined as follows:

$$\rho(T/\mathrm{K},\, p/\mathrm{GPa}) = \rho\left(T_{\mathrm{R}}/\mathrm{K},\, 0.1\ \mathrm{MPa}\right)\left(1+\frac{0.6\,p/\mathrm{GPa}}{1+1.7\,p/\mathrm{GPa}}-0.65\cdot10^{-3}\left(T-T_R\right)\right) \tag{8}$$

where T_R is a reference temperature.

Finally the relation proposed by Jacobson and Vinet[17] and employed by Venner and Bos[12] in numerical EHL simulations was employed for prediction of the experimental pressure values as a function of density as follows:

$$p = 3B_0\left(\frac{\rho_0}{\rho}\right)^{-2/3}\left[1-\left(\frac{\rho_0}{\rho}\right)^{1/3}\right]\exp\left[\eta'\left[1-\left(\frac{\rho_0}{\rho}\right)^{1/3}\right]\right] \tag{9}$$

where B_0 and η' are characteristic parameters with values of $1.7\cdot10^{-9}$ Pa and 10.0 for a mineral oil[12], respectively.

Dowson and Higgison[15] EoS predicts density values of each oil with an AAD%≤0.4%, whereas the prediction from the Zhu and Wen EoS[16] gives rise to similar results, the AAD% being lower or equal to 0.3%. Finally, the prediction method from Jacobson and Vinet[17] predicts pressure values for each of the oils with and AAD%<29%. Additionally, these prediction methods as well as the Tammann-Tait and the modified Tait [34-36] correlations of the experimental density data were employed to predict density values at pressures higher than the experimental ones, up to typical pressure values of EHL, as it can be observed in Figure 3. All the equations

predict similar density values up to 0.3 GPa, whereas at high pressures the values predicted by means of the Jacobson and Vinet EoS[17] are higher than those obtained through the other EoS, the lowest values being those of Dowson and Higginson[15] as well as those of Zhu and Wen[16]. Moreover, an asymptotic behavior is observed as pressure increases for the EoS of Dowson and Higginson[15] and Zhu and Wen[16]. These results agree with those previously published by Habchi and Bair[12], Venner and Bos[12], Martini and Vadakkepatt[38] and by Ramesh[39].

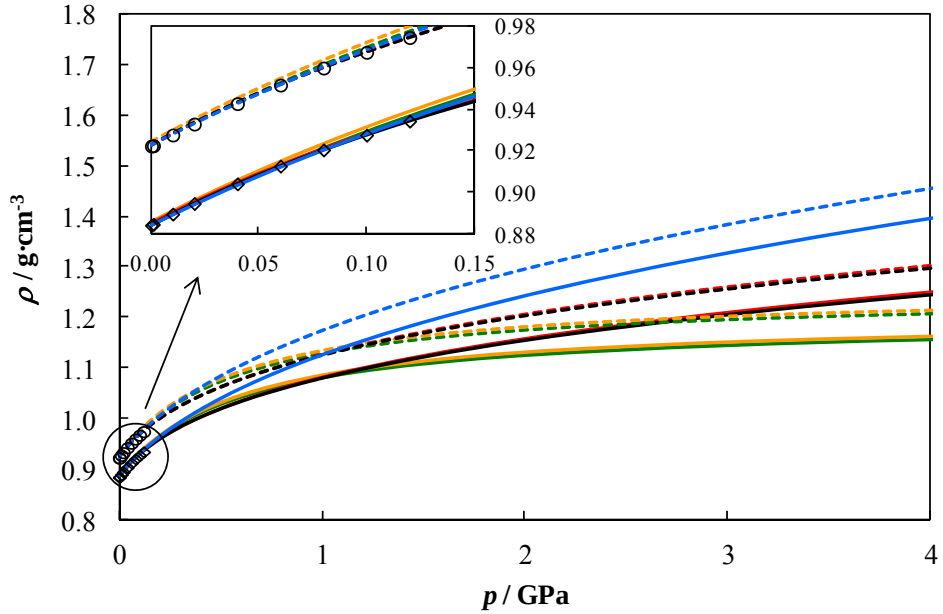

Figure 3. Experimental density values of MIN-G02 (◇) and BIO-G02 (○) at 313.15 K. Solid and dashed lines represent the prediction and correlation EoS for MIN-G02 and BIO-G02, respectively. Tammann-Tait (—), modified Tait[34-36] (—), Dowson and Higinsson[15] (—), Zhu and Wen[16] (—) and Jacobson and Vinet[17] (—) equations.

We have calculated the density derived property isothermal compressibility (κ_T) by differentiation from the Tammann-Tait equation taking into account the following equation:

$$\kappa_T(T,p) = \frac{1}{\rho}\left(\frac{\partial \rho}{\partial p}\right)_T \tag{10}$$

This property is the inverse of the bulk modulus[40]. Compressibility values are presented in Table 7 for the lubricants studied in this work. In Figure 4a we present the pressure dependence of the compressibility values at 313.15 K of the vegetable based lubricants. It can be observed that κ_T values and its pressure dependence are very similar. We can establish the following sequence for temperatures lower or equal to 333.15K: BIO-G01 > BIO-G02 > BIO-G00, as it can be observed. However, at the highest temperature the trend found is BIO-G02 > BIO-G00 > BIO-G01. Therefore, it is not possible to establish a relation between the high oleic sunflower oil (HOSO) content in these lubricants and their compressibility. The maximum deviation between κ_T of these vegetable developed oils is $0.5 \cdot 10^{-4}$ MPa^{-1} (5%) at this temperature. In Figure 4b, we have plotted the compressibility values of the reference mineral

lubricants along with those of the vegetable based lubricant BIO-G01 and the synthetic based lubricant SYN-G01, in order to perform a comparison between the behaviour of a biodegradable vegetable oil, the biodegradable synthetic lubricant and the reference lubricants. It can be observed that the compressibility of MIN-G01 is slightly higher than those of the other lubricants (up to 4.7% at this temperature). Thus, MIN-G01, due to its higher compressibility, could form thinner films by a few percent in the high-pressure regions.

Table 7. Isothermal compressibility values, $10^4 \cdot \kappa_T$ (MPa^{-1}), of the lubricants studied in this work.

	p /MPa						
T/K	1.00	10.00	20.00	40.00	60.00	80.00	100.00
	MIN-G01						
278.15	5.50	5.22	4.95	4.47	4.09	3.76	3.49
298.15	6.07	5.73	5.40	4.84	4.39	4.02	3.71
313.15	6.54	6.15	5.77	5.14	4.64	4.23	3.89
333.15	7.25	6.77	6.31	5.56	4.98	4.51	4.13
348.15	7.83	7.28	6.75	5.90	5.25	4.74	4.32
373.15	8.94	8.22	7.56	6.51	5.73	5.13	4.64
398.15	10.20	9.28	8.44	7.17	6.24	5.53	4.97
	MIN-G02						
283.15	5.42	5.15	4.88	4.42	4.04	3.72	3.45
298.15	5.85	5.53	5.22	4.69	4.27	3.92	3.62
313.15	6.31	5.94	5.58	4.99	4.51	4.12	3.80
323.15	6.63	6.23	5.84	5.19	4.68	4.26	3.91
348.15	7.52	7.01	6.52	5.72	5.10	4.61	4.21
373.15	8.50	7.85	7.24	6.27	5.54	4.97	4.51
398.15	9.53	8.72	7.97	6.82	5.97	5.31	4.79
	BIO-G00						
278.15	5.08	4.85	4.61	4.21	3.87	3.58	3.34
298.15	5.62	5.33	5.05	4.57	4.17	3.84	3.56
313.15	6.06	5.73	5.40	4.86	4.41	4.05	3.74
333.15	6.72	6.32	5.92	5.27	4.76	4.34	3.99
348.15	7.28	6.81	6.35	5.61	5.03	4.56	4.18
373.15	8.32	7.71	7.13	6.21	5.51	4.96	4.51
398.15	9.51	8.72	7.99	6.86	6.02	5.37	4.85
	BIO-G01						
278.15	5.22	4.98	4.73	4.32	3.97	3.68	3.42
298.15	5.77	5.47	5.18	4.69	4.28	3.94	3.66
313.15	6.22	5.88	5.54	4.98	4.52	4.15	3.83
333.15	6.87	6.45	6.05	5.39	4.86	4.43	4.08
348.15	7.38	6.91	6.45	5.70	5.12	4.65	4.26
373.15	8.30	7.70	7.14	6.23	5.54	5.00	4.55
398.15	9.22	8.49	7.81	6.75	5.95	5.32	4.83
	BIO-G02						
278.15	5.19	4.94	4.69	4.26	3.90	3.61	3.35
298.15	5.74	5.44	5.14	4.63	4.21	3.87	3.58
313.15	6.21	5.85	5.51	4.93	4.46	4.08	3.76
333.15	6.90	6.46	6.04	5.35	4.81	4.37	4.01
348.15	7.47	6.96	6.47	5.69	5.08	4.59	4.20
373.15	8.52	7.87	7.25	6.28	5.55	4.98	4.52
398.15	9.69	8.85	8.08	6.90	6.03	5.36	4.84
	SYN-G01						
278.15	5.20	4.95	4.69	4.25	3.89	3.59	3.34
298.15	5.76	5.45	5.14	4.62	4.20	3.85	3.56
313.15	6.23	5.87	5.51	4.92	4.45	4.06	3.74
333.15	6.93	6.48	6.05	5.34	4.79	4.35	3.98
348.15	7.50	6.98	6.48	5.68	5.06	4.57	4.17
373.15	8.56	7.89	7.26	6.27	5.53	4.95	4.49
398.15	9.75	8.89	8.10	6.89	6.01	5.33	4.80

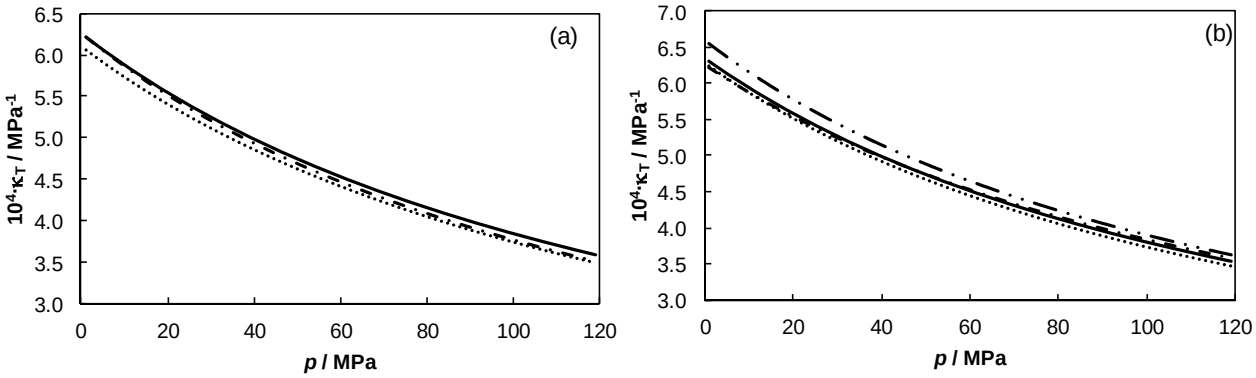

Figure 4. Isothermal compressibility values, κ_T, as a function of pressure at T = 313.15 K. (a) BIO-G01 (—), BIO-G02 (–·–) and BIO-G00 (···); (b) MIN-G01 (–··), MIN-G02 (—), SYN-G01 (···) and BIO-G01 (–·–).

An AAD% of 0.2% was found in the comparison of the compressibility values of BIO-G02 with the reference mineral lubricant MIN-G[18], at 313.15 K and pressures up to 59 MPa, which indicates that, taking into account this property, the vegetable developed oils of this work are suitable for gear applications.

Compressibility values have also been calculated from differentiation from the modified Tait equation[34-36] according to the following expression:

$$\kappa_T = \frac{1}{\left(1-\frac{1}{1+K_0'}\ln\left[1+\frac{p}{K_{00}\exp\left(-\beta_K T\right)}\left(1+K_0'\right)\right]\right)\left(K_{00}\exp\left(-\beta_K T\right)+p\left(1+K_0'\right)\right)} \tag{11}$$

A global AAD% among the compressibility values obtained from the Tammann-Tait equation and those obtained through the modified Tait[34-36] equation of 0.8 % was found.

Compressibility values of the studied oils were also predicted by means of differentiation form the Dowson and Higginson[15] and the Zhu and Wen[16] EoS. It is important to notice that this compressibility values are fluid independent.

$$\kappa_T = \frac{0.6}{\left(1+4p+3.91p^2\right)} \tag{12}$$

$$\kappa_T = \frac{0.6}{\left(1+4p+3.91p^2\right)-0.65\cdot 10^{-3}\left(T-T_R\right)\left(1+1.7p\right)^2} \tag{13}$$

The compressibility predictions along with values obtained from the Tammann-Tait and the modified Tait[34-36] equations are depicted in Figure 5. It can be observed that at the highest and the lowest pressures (p<0.01 GPa and p> 0.5 GPa) the compressibility values predicted by means of the Dowson and Higginson[15] and the Zhu and Wen[16] EoS are lower than those obtained through the Tammann-Tait and the modified Tait[34-36] equations. The contrary occurs at intermediate pressures.

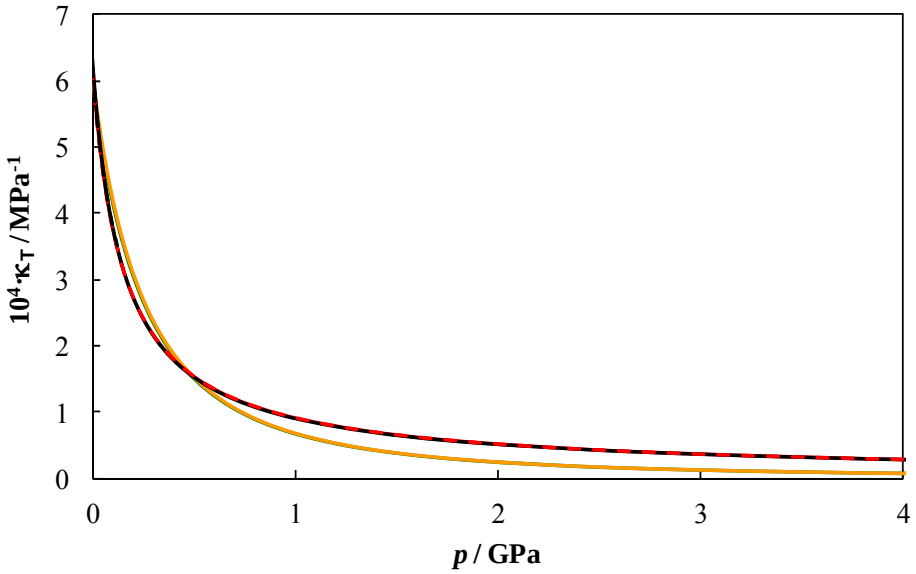

Figure 5. Compressibility values of MIN-G02 (solid lines) and BIO-G02 (dashed lines) at 313.15 K. Tamman-Tait (—), modified Tait[34-36] (—), Dowson and Higinsson[15] (—), and Zhu and Wen[16] (—).

Thermal wedge is a pressure generation action brought about by changes in density and viscosity due to temperature rise in a bearing film[41]. Besides, it is shown that film lubrication is possible if, and only if, either the distance between the surfaces decreases in the direction of motion (the geometric wedge), or the density of the fluid decreases in the same direction (the thermal wedge)[42]. For these reasons, we have calculated the thermal expansion coefficient (α_p) by differentiation from the isobaric fit of the density dependence with temperature, $\alpha_p = -(\partial \ln\rho/\partial T)_p$. Thus, we have previously fit the isobaric densities by means of the following equation:

$$\ln(\rho) = a_0 + a_1 T + a_2 T^2 + a_3 T^3 \tag{14}$$

The obtained thermal expansion coefficient values are presented in Table 8. Furthermore, in Figure 6, it can be observed the behaviour of α_p with pressure at different temperatures for the studied lubricants. This property decreases when pressure increases, whereas a crossover is found between the isotherms for all the lubricants except for BIO-G01. This crossing point is related to a minimum of the isobaric heat capacity[43].

Table 8. Thermal expansion coefficient, $10^4 \cdot \alpha_p$ (K^{-1}), of the lubricants studied in this work.

	p /MPa								
T/K	0.10	1.00	10.00	20.00	40.00	60.00	80.00	100.00	120.00
MIN-G01									
298.15	7.30	7.25	7.06	6.80	6.34	5.98	5.68	5.42	5.03
313.15	7.26	7.37	7.07	6.79	6.28	5.90	5.57	5.29	4.97
333.15	7.26	7.43	7.05	6.75	6.19	5.79	5.45	5.15	4.90
348.15	7.30	7.42	7.01	6.69	6.13	5.71	5.36	5.07	4.84
373.15	7.43	7.29	6.91	6.55	6.01	5.58	5.25	4.99	4.74
MIN-G02									
298.15	7.10	7.06	6.80	6.55	6.11	5.79	5.51	5.36	5.28
313.15	7.21	7.16	6.89	6.62	6.17	5.82	5.52	5.28	5.12
323.15	7.26	7.21	6.93	6.65	6.20	5.82	5.52	5.24	5.04
348.15	7.29	7.29	6.97	6.66	6.18	5.78	5.46	5.14	4.88
373.15	7.20	7.30	6.92	6.59	6.04	5.65	5.34	5.05	4.81
BIO-G00									
298.15	7.21	7.17	6.92	6.71	6.29	5.92	5.64	5.38	5.12
313.15	7.26	7.17	6.91	6.65	6.23	5.86	5.57	5.33	5.14
333.15	7.35	7.22	6.94	6.63	6.19	5.82	5.52	5.28	5.11
348.15	7.44	7.30	6.99	6.66	6.19	5.82	5.51	5.26	5.03
373.15	7.64	7.49	7.11	6.78	6.26	5.88	5.54	5.26	4.81
BIO-G01									
298.15	7.60	7.55	7.31	7.06	6.62	6.27	5.98	5.71	5.46
313.15	7.43	7.41	7.14	6.88	6.44	6.08	5.79	5.52	5.25
333.15	7.28	7.31	7.00	6.73	6.27	5.90	5.60	5.33	5.06
348.15	7.23	7.29	6.97	6.68	6.20	5.82	5.51	5.24	4.97
373.15	7.25	7.39	7.03	6.72	6.17	5.79	5.45	5.17	4.94
BIO-G02									
298.15	7.37	7.34	7.10	6.84	6.43	6.07	5.78	5.48	5.26
313.15	7.43	7.33	7.07	6.80	6.37	6.02	5.72	5.45	5.22
333.15	7.49	7.33	7.05	6.76	6.31	5.96	5.65	5.40	5.17
348.15	7.53	7.35	7.05	6.74	6.27	5.92	5.60	5.35	5.12
373.15	7.60	7.42	7.08	6.74	6.23	5.85	5.52	5.24	5.02
SYN-G01									
298.15	7.33	7.28	7.04	6.78	6.38	6.02	5.73	5.45	5.23
313.15	7.37	7.28	7.02	6.74	6.29	5.94	5.65	5.42	5.21
333.15	7.42	7.29	7.01	6.69	6.21	5.86	5.56	5.35	5.16
348.15	7.45	7.30	6.99	6.67	6.17	5.80	5.50	5.28	5.09
373.15	7.49	7.34	6.96	6.64	6.13	5.74	5.40	5.13	4.92

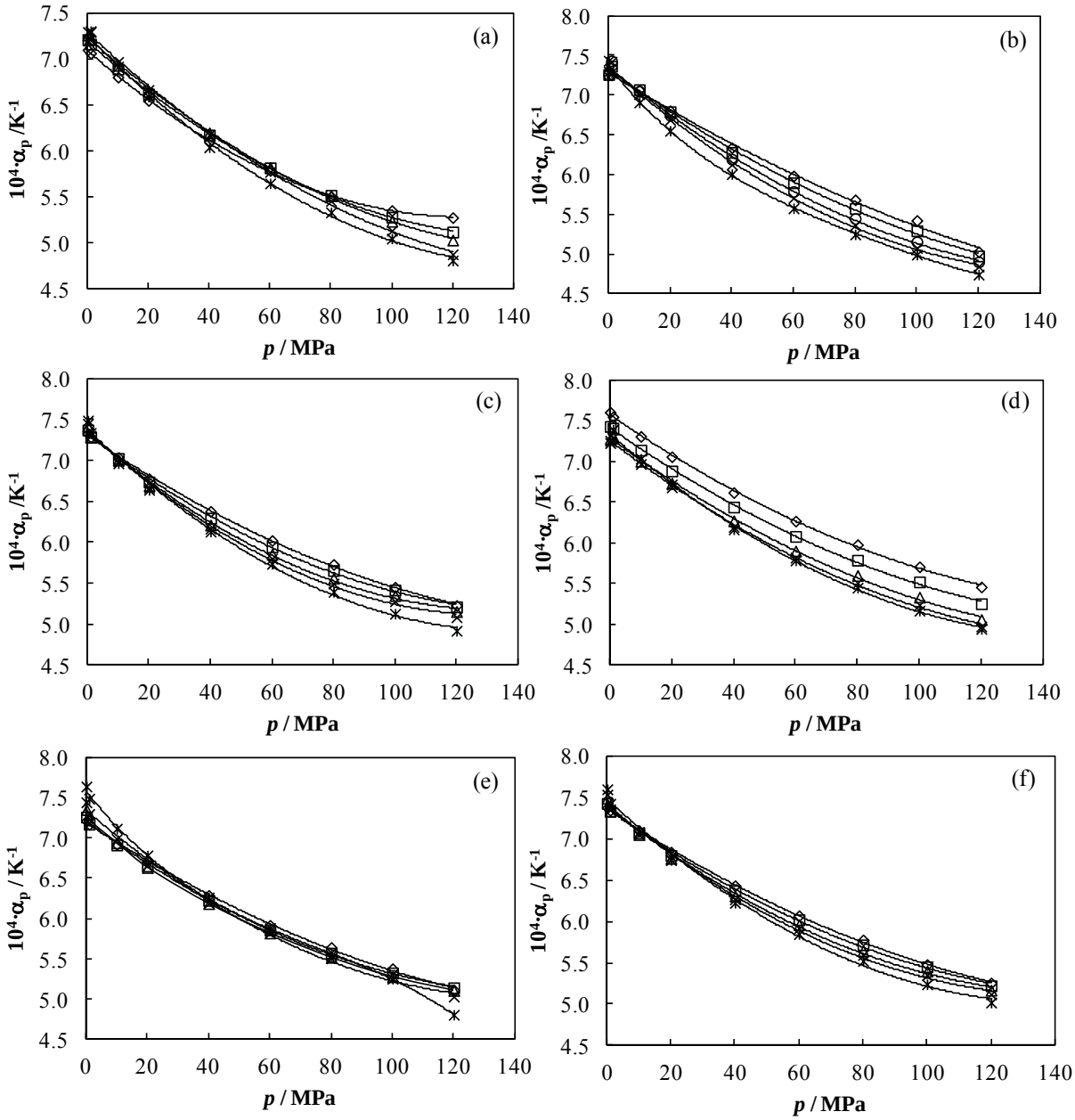

Figure 6. Thermal expansion coefficient values (α_p) as a function of pressure for different temperatures: 298.15 K (◇), 313.15 K (□), 323.15 K (△), 333.15 K (○), 348.15 K (×), 373.15 K (✳). (a) MIN-G01, (b) MIN-G02, (c) SYN-G01, (d) BIO-G01, (e) BIO-G00 and (f) BIO-G02.

CONCLUSIONS

Viscosity data of new biodegradable developed oils and reference mineral oils for wind turbine and tractor transmission were reported. The new formulated oils present the highest viscosity indexes and the lowest viscosity data at low temperatures, therefore they become the most suitable for machinery cold start.

Regarding $p\rho T$ data, it was found that the highest values are those of the synthetic lubricant, whereas the lowest are those of the mineral lubricants. Among the vegetable based oils the density decreases with the HOSO content. Several empirical EoS were used to evaluate the

$p\rho T$ curves. Thus, Dowson and Higgison[15] and Zhu and Wen[16] EoS predict density values with an AAD%≤0.4%and the method from Jacobson and Vinet[17] predicts pressure values with and AAD%<29%, whereas Tammann-Tait and the modified Tait[34-36] equations correlate experimental density values with AADs% of 0.02% and 0.06%, respectively. Moreover, when using these equations for prediction of density values up to pressures of 4 GPa, the lowest values are those of Dowson and Higginson[15] and Zhu and Wen[16].

The studied lubricants have a similar compressibility, being the highest differences below 5%. Thus, with regard to this property, the developed vegetable lubricants are suitable for their use as gear lubricants. The mineral lubricant MIN-G01 presents the highest compressibility and therefore, according to this property, could form thinner films by a few percent in the high-pressure regions. At pressures higher than 0.5 GPa, compressibility values predicted by means the Dowson and Higginson[15] and the Zhu and Wen[16] EoS are lower than those obtained through the Tammann-Tait and the modified Tait[34-36] equations.

ACKNOWLEDGMENTS

This work was carried out within the framework of the strategic and singular project "Biolubricants based on vegetable oils and their synthetic derivatives", which is funded by Spanish Science and Innovation Ministry and the EU FEDER program (PSE- 320100-2006-1, PSE-420000-2008-4). We are very grateful to the BIOVESIN partners for their excellent advice and for providing us the samples of the products. L.L and T.R. acknowledge financial support under the Ramon y Cajal Program and the FPU program, respectively.

References

1. Gosalia, A., Sustainability... and the Global Lubricants Industry. In *The 16th ICIS World Base Oils & Lubricants Conference*, London, 2012.
2. Nagendramma, P.; Kaul, S. *Renewable Sustainable Energy Rev.* **2012,** 16, 764-774.
3. Erhan, S. Z.; Sharma, B. K.; Liu, Z.; Adhvaryu, A. *J. Agric. Food Chem.* **2008,** 56, 8919-8925.
4. Regulation (EC) No 66/2010 of the European Parliament and of the Council of 25 November 2009 on the EU Ecolabel. In Official Journal of the European Union: 2010; pp L 27/01 - L 27/19.
5. Commission decision of 24 June 2011 on establishing the ecological criteria for the award of the EU Ecolabel to lubricants. In Official Journal of the European Union: 2011; Vol. 2011/381/EU, pp L 169/28 - L 169/38.
6. Sharma, B. K.; Perez, J. M.; Erhan, S. Z. *Energy Fuels* **2007,** 21, 2408-2414.
7. Prasad, L.; Das, L. M.; Naik, S. N. *Energy Fuels* **2012,** 26, 5307-5315.
8. Salih, N.; Salimon, J.; Yousif, E. *Ind. Crop. Prod.* **2011,** 34, 1089-1096.
9. Höglund, E. *Wear* **1999,** 232, 176-184.
10. Habchi, W.; Vergne, P.; Bair, S.; Andersson, O.; Eyheramendy, D.; Morales-Espejel, G. E. *Trib. Int.* **2010,** 43, 1842-1850.
11. Kweh, C. C.; Evans, H. P.; Snidle, R. W. *Proc. Inst. Mech. Eng., Part C* **1989,** 203, 133-148.
12. Venner, C. H.; Bos, J. *Wear* **1994,** 173, 151-165.
13. Hamrock, B. J.; Pan, P.; Lee, R.-T. *J. Tribol.* **1988,** 110, 279-284.
14. Wong, P. L.; Wang, R.; Lingard, S. *Wear* **1996,** 201, 58-63.
15. Dowson, D.; Higginson, G. R.; Whitaker, A. V. *J. Mech. Eng. Sci.* **1962,** 4, 121-126.

16. Zhu, D.; Wen, S. Z. *Trans. ASME, J. Tribol.* **1984,** 106, 246-254.
17. Jacobson, B. O.; Vinet, P. *Trans. ASME, J. Tribol.* **1987,** 109, 709-714.
18. Regueira, T.; Lugo, L.; Fandiño, O.; López, E. R.; Fernández, J. *Green Chem.* **2011,** 13,
19. García-Zapateiro, L. A.; Delgado, M. A.; Franco, J. M.; Valencia, C.; Ruiz-Méndez, M. V.; Garcés, R.; Gallegos, C. *Grasas Aceites (Seville)* **2010,** 61, 171-174.
20. Quinchia, L. A.; Delgado, M. A.; Valencia, C.; Franco, J. M.; Gallegos, C. *Environ. Sci. Technol.* **2009,** 43, 2060-2065.
21. Mendoza, G.; Igartua, A.; Fernandez-Diaz, B.; Urquiola, F.; Vivanco, S.; Arguizoniz, R. *Grasas Aceites (Seville)* **2011,** 62, 29-38.
22. Garcés, R.; Martínez-Force, E.; Salas, J. J. *Grasas Aceites (Seville)* **2011,** 62, 21-28.
23. Quinchia, L. A.; Delgado, M. A.; Valencia, C.; Franco, J. M.; Gallegos, C. *J. Agric. Food Chem.* **2011,** 59, 12917-12924.
24. Quinchia, L. A.; Delgado, M. A.; Valencia, C.; Franco, J. M.; Gallegos, C. *Ind. Crop. Prod.* **2010,** 32, 607-612.
25. Novotny-Farkas, F.; Böhme, W.; Stabinger, H.; Belitsch, W. *Anton Paar* World Tribology Congress II, 2001,
26. Gaciño, F. M.; Regueira, T.; Lugo, L.; Comuñas, M. J. P.; Fernández, J. *J. Chem. Eng. Data* **2011,** 56, 4984-4999.
27. Carvalho, P. J.; Regueira, T.; Santos, L. M. N. B. F.; Fernandez, J.; Coutinho, J. A. P. *J. Chem. Eng. Data* **2009,** 55, 645-652.
28. Fandiño, O.; Lugo, L.; Segovia, J. J.; López, E. R.; Comuñas, M. J. P.; Fernández, J. *J. Supercrit. Fluids* **2011,** 58, 189-197.
29. Segovia, J. J.; Fandiño, O.; López, E. R.; Lugo, L.; Martín, M. C.; Fernández, J. *J. Chem. Thermodyn.* **2009,** 41, 632-638.
30. Regueira, T.; Lugo, L.; Fernández, J. *J. Chem. Thermodyn.* **2012,** 48, 213-220.
31. Regueira, T.; Lugo, L.; Fernández, J. *J. Chem. Thermodyn.* **2013,** 58, 440-448.
32. Comuñas, M. J. P.; Bazile, J.-P.; Baylaucq, A.; Boned, C. *J. Chem. Eng. Data* **2008,** 53, 986-994.
33. Paredes, X.; Fandiño, O.; Pensado, A. S.; Comuñas, M. J. P.; Fernández, J. *Trib. Lett.* **2012,** 45, 89-100.
34. Habchi, W.; Bair, S. *Trans. ASME, J. Tribol.* **2013,** 135, 011502-1-011502-10.
35. Dymond, J. H.; Malhotra, R. *Int. J. Thermophys.* **1988,** 9, 941-951.
36. Fakhreddine, Y. A.; Zoller, P. *J. Appl. Polym. Sci.* **1990,** 41, 1087-1093.
37. Cook, R. L.; King, J. H. E.; Herbst, C. A.; Herschbach, D. R. *J. Chem. Phys.* **1994,** 100, 5178-5189.
38. Martini, A.; Vadakkepatt, A. *Trib. Lett.* **2010,** 38, 33-38.
39. Ramesh, K. T. *Trans. ASME, J. Tribol.* **1991,** 113, 361-371.
40. Lapuerta, M.; Agudelo, J. R.; Prorok, M.; Boehman, A. L. *Energy Fuels* **2011,** 26, 1336-1343.
41. Yang, P.; Kaneta, M., Thermal wedge in lubrication. In *Encyclopedia of Tribology*, Wang, Q. J.; Chung, Y. W., Eds. Springer: http://www.springerreference.com/docs/html/chapterdbid/332800.html, 2013.
42. Cope, W. *Proceedings of the Royal Society of London. Series A. Mathematical and Physical Sciences* **1949,** 197, 201-217.
43. Randzio, S. L.; Grolier, J. P. E.; Quint, J. R.; Eatough, D. J.; Lewis, E. A.; Hansen, L. D. *Int. J. Thermophys.* **1994,** 15, 415-441.

5.4. High pressure volumetric properties of 1-ethyl-3-methylimidazolium ethylsulfate and 1-(2-methoxyethyl)-1-methyl-pyrrolidinium bis(trifluoromethylsulfonyl)imide*

*T. Regueira, L. Lugo, J. Fernández, J. Chem. Thermodynamics 48 (2012) 213–220. http://www.sciencedirect.com/science/article/pii/S0021961411004630

Abstract

In order to select the most suitable ionic liquids (ILs) for certain applications it is necessary to know some of their thermophysical properties, such as density or viscosity. In this work we have performed density measurements of two ILs 1-ethyl-3-methylimidazolium ethylsulfate and 1-(2-methoxyethyl)-1-methyl-pyrrolidinium bis(trifluoromethylsulfonyl)imide in a broad range of temperature and pressure (278.15 K to 398.15 K and up to 120 MPa). From these measurements we have obtained other volumetric properties such as isothermal compressibility and isobaric thermal expansivity. In addition, density values were predicted using the method proposed by Gardas and Coutinho and also that proposed by Jacquemin et al., obtaining a good agreement with experimental values.

Introduction

Ionic Liquids (ILs) possess unique properties, such as negligible volatility, non-flammability, high thermal stability, low melting point, broad liquid range and controlled miscibility with organic compounds, that made them suitable for different technological fields.[1-3] Their structure allows that several of their properties, such as melting point, viscosity, density and hydrophobicity can be easily tailored or tuned through an adequate combination of cation and anion. Thus, ILs are of increasing interest in various applications as: solvents in organic synthesis, separation process, [4-7] lubricants and lubricant additives [8,9], hydraulic fluids, coatings, nano technology [10], lithium-ion batteries, dye-sensitized solar cells [11] as well as in biorefining [12], CO_2-capture [13,14], environmental remediation [15], pharmaceuticals [2] and waste treatment [16].

The development of ILs for several of these applications requires the knowledge of their thermophysical properties, as densities in broad ranges of temperature and pressure. Thus, accurate values of liquid density are required in the design of equipment such as condensers, reboilers, liquid/liquid two phase mixer–settler units, calculation of tower heights, material and energy balances involving liquids as well as the measurements of phase equilibrium, heat capacity and viscosity with several techniques. Moreover, PVT values are fundamental data for developing models involving equations of state, which are the main tool used for thermophysical properties prediction.

Aparicio et al. [11] have recently analyzed the density data at high pressures for liquids available in the open literature. A high number of density data at high pressures corresponds to ILs with tetrafluoroborate and hexafluorophosphate anions ($[BF_4]^-$ and $[PF_6]^-$) which are not reliable for industrial applications [17,18]. These fluorine-based anions have been the subject of several studies about their eventual decomposition into the toxic hydrofluoridric acid [18,19].

Data for new or environmentally friendly ILs are quite scarce [8,11]. In this work, the ILs 1-ethyl-3-methylimidazolium ethylsulfate $[C_2C_1Im][C_2SO_4]$ and 1-(2-methoxyethyl)-1-methyl-pyrrolidinium bis(trifluoromethylsulfonyl)imide $[C_1OC_2C_1Pyrr][NTf_2]$ have been studied. In the last years, the properties and applications of alkyl-sulfate-based salts [20] have been strongly analyzed because they are stable, water soluble, inherently 'chloride-free', present hydrolysis stability and display a large electrochemical window. Thus, the relative non-toxic [21] $[C_2C_1Im][C_2SO_4]$ IL is being studied for several uses as lubricants of microelectromechanical systems (MEMS) [22], in the entrapment of enzymes [23], in hydrogen generation, storage and activation [24], in the extraction of alkaloids [25], or CO_2 capture [26]. Russina et al. [27] have found that $[C_2C_1Im][C_2SO_4]$ is characterised by the occurrence of structural nano-scale heterogeneities which do not occur with the 1-ethyl-3-methylimidazolium salts with a symmetric-small anion (such as $[Cl]^-$, $[BF_4]^-$ and $[PF_6]^-$). Up to now, $[C_1OC_2C_1Pyrr][NTf_2]$ is not very studied in the literature, as in general the pyrrolidinium imide salts with alkyl ether chains, being most of these scarce researches on electrochemical applications. Thus, Ferrari et al. [28] have found that this IL and their mixtures with $[Li][NTf_2]$ have reliable properties for lithium batteries. There are only literature density data for $[C_1OC_2C_1Pyrr][NTf_2]$ at 293.15 K, 295 K and 298.15 K.

In this work the density of $[C_2C_1Im][C_2SO_4]$ and $[C_1OC_2C_1Pyrr][NTf_2]$ was measured in a temperature range from 278.15 K to 398.15 K and pressures up to 120 MPa with a vibrating tube densimeter. Initial experimental density values were corrected as a function of its viscosity and then compared with published literature values. A density description as a function of pressure and temperature was obtained by means of the modified Tamman-Tait equation. Furthermore, density derived properties i.e. isobaric thermal expansivity (α_p) and isothermal compressibility (κ_T) were obtained by differentiation. The pressure effect on the unusual behaviour of the isobaric thermal expansivity of ILs [29-31] was also analyzed.

2. Experimental

2.1. Materials

Samples of 1-ethyl-3-methylimidazolium ethylsulfate, $[C_2C_1Im][C_2SO_4]$ with CAS 342573-75-5 and 1-(2-Methoxyethyl)-1-methyl-pyrrolidinium bis(trifluoromethylsulfonyl)imide $[C_1OC_2C_1Pyrr][NTf_2]$ with CAS 757240-24-7 were kindly provided by Merck with a specified mole-fraction purity higher than 98%. The manufacturer gives the mole-fraction purities by HPLC gas chromatographic analysis (GC) and alkalimetric after ionic exchange, indicated in Table 1. The water used for densimeter calibration was purified using a Milli-Q Plus system. It has a resistivity of 18.2 MΩ·cm and a total organic carbon (TOC) smaller than 5 ng·cm^{-3}, and it

is free of particles greater than 0.22 μm. n-Decane also employed in the calibration was supplied by Sigma-Aldrich with a specified mole-fraction purity higher or equal to 99% and a gas chromatographic analysis given by the manufacturer of 99.9%. Bromobenzene used to verify the densimeter calibration was supplied by Alfa Aesar with a specified mole-fraction purity of 99% and GC of 99.7%.

TABLE 1
Purity and water content (ppm) in ionic liquids samples.

Ionic Liquid	Mole-fraction purity	Water content$_{IN}$	Water content$_{OUT}$
$[C_2C_1Im]$ $[C_2SO_4]$	98.4 %[a]	81.51	229.61
$[C_1OC_2C_1Pyrr][NTf_2]$	99.4%[b]	12.07	86.02

[a]HPLC analysis
[b]Alkalimetry after ionic exchange

2.2. Experimental procedure

In order to eliminate water and volatile components, ILs were dried and degassed under vacuum for at least 48 hours, under agitation and using a vacuum system with a rotary pump Edwards RV3. Vacuum was measured with a vacuometer Edwards Pirani 501 obtaining values around 1 Pa. A Karl-Fischer coulometric titrator (Mettler Toledo DL32) was employed to measure the water content in the samples before and after density measurements. Water contents are presented in Table 1. In order to avoid contact between the ILs and the atmosphere, they were transferred to the densimeter through a Hamilton valve, HV Standard PTFE, connected to a glass syringe.

The experimental device consists of a fully automated vibrating tube densimeter Anton Paar HPM, where density measurements were performed up to 120 MPa and between 278.15 K and 398.15 K. This densimeter consists of two different units, the measurement cell, named DMA HPM, and the electronic processing unit, named mPDS 2000V3. A scheme of the overall experimental device is shown in Figure 1. Temperature control systems consists of a thermostatic bath Polyscience 9102 through inlet/outlet ports, that regulates temperature with fluctuations lower than 0.01 K; temperature is measured by means of a Pt100 probe located inside the cell and connected to an Agilent 34970A data acquisition unit. This probe was calibrated with an uncertainty of 0.02 K. Pressure is automatically generated by means of a step by step engine connected to a compressor HiP 50-5.75-30 and is measured through a pressure transducer HBM Digibar II K-PE300 with a working range up to 200 MPa, calibrated with an uncertainty of 0.02 MPa and connected to the data acquisition unit Agilent 34970A. More details were given previously [32].

The densimeter was calibrated [32] following the procedure described by Lagourette et al. [33] and modified by Comuñas et al. [34] Milli-Q water was employed as reference fluid at temperatures between 278.15 K and 348.15 K and pressures between 0.1 MPa and 120 MPa and also at T = 373.15 K and T = 398.15 K for pressures higher than 0.1 MPa, whereas n-decane was used as reference fluid at T = 373.15 K and T = 398.15 K and at 0.1 MPa. The expanded (k=2) uncertainty of the density with this technique was rigorously calculated by Segovia et al. [32] finding that it is $0.7 \cdot 10^{-3}$ g·cm^{-3} for temperatures below T = 373.15 K, $5 \cdot 10^{-3}$ g·cm^{-3} at T = (373.15 and 398.15) K and p = 0.1 MPa, and $3 \cdot 10^{-3}$ g·cm^{-3} in other cases, i.e. at $T \geq 373.15$ K and $p > 0.1$ MPa.

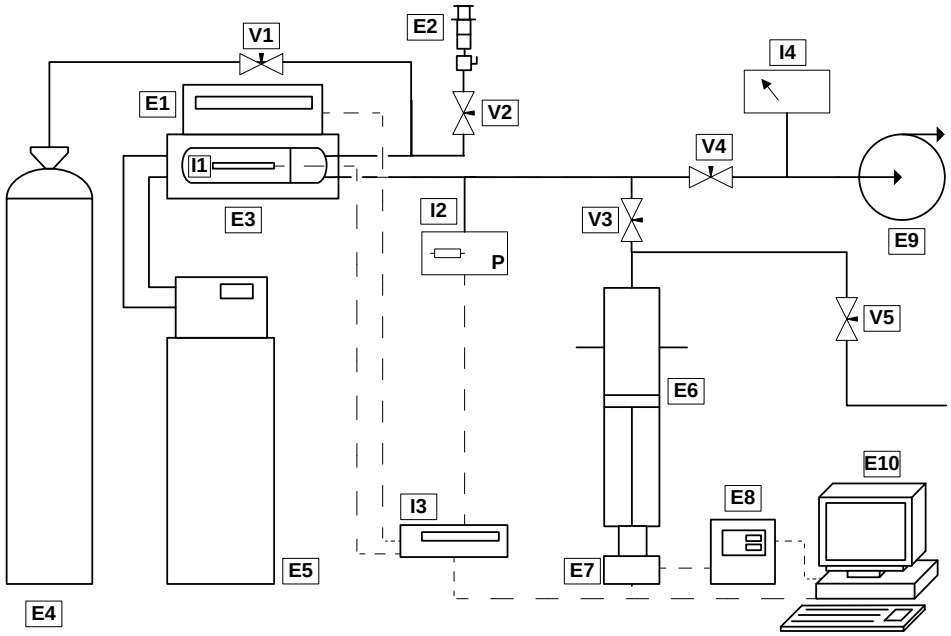

FIGURE 1. Experimental equipment scheme. (E1) mPDS 2000V3 unit; (E2) glass syringe connected to Hamilton valve; (E3) measurement cell DMA HPM; (E4) nitrogen bottle; (E5) thermostatic bath Polyscience; (E6) HiP compressor; (E7) motor; (E8) electric controls; (E9) vacuum pump; (E10) computer; (V1-V5) HiP valves; (I1) Pt100; (I2) HBM PE300 manometer; (I3) data acquisition unit; (I4) vacuometer.

To account the effect of the sample viscosity on the density measurements on mechanical oscillator densimeters, the following correction factor for the DMA HPM model has been considered [32,35]:

$$\frac{\rho_{HPM} - \rho}{\rho_{\mathrm{HPM}}} = \left[0.4482\sqrt{\eta / mPa{\cdot}s} - 0.1627\right]10^{-4} \qquad (1)$$

where ρ_{HPM} represents the density value obtained from the densimeter calibration and the measured periods, ρ is the "corrected" density value due to the effect of viscosity, and η is the dynamic viscosity of the sample. This equation is valid for viscosities lower than 289 mPa·s. For viscosities higher than 289 mPa·s the relative correction factor, i.e. $\Delta\rho/\rho$, becomes constant, taking the value of $7.5 \cdot 10^{-4}$. The viscosity values of the two ILs studied in the present work have

been measured in our laboratory [36] over a wide range of pressure and temperature with a falling body viscometer designed and implemented in our laboratory, which is similar to that reported by Dauge et al. [37] From these values we have calculated the correction factor for the ILs. The density correction ranges from $1.1 \cdot 10^{-4}$ to $1.1 \cdot 10^{-3}$ g·cm^{-3} in the present experimental *pT* conditions, which corresponds to a viscosity range from 4.77 to 1142.10 mPa·s.

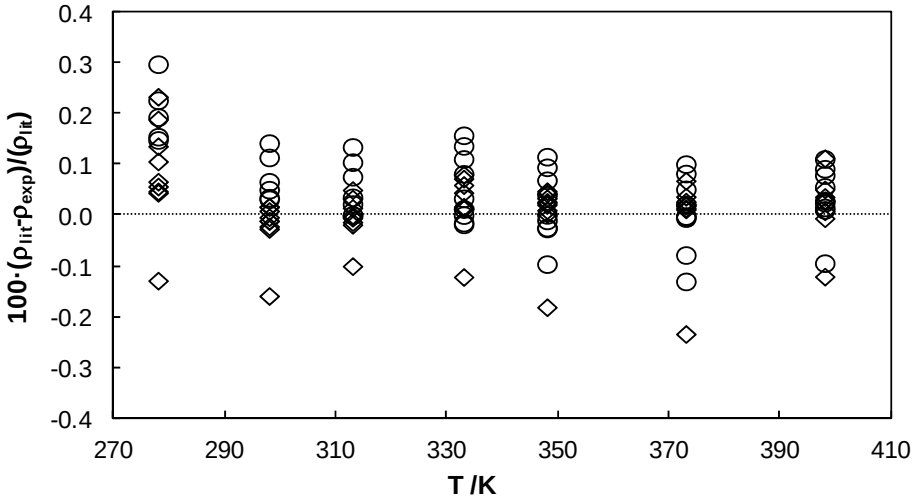

FIGURE 2. Relative deviations for n-decane as a function of temperature for pressures up to 120 MPa. Lemmon and Span [39] (○), Cibulka and Hnedkovsky [38] (◇).

Calibration accuracy was checked through measurement of density data of n-decane (at temperature and pressure conditions different from *T*=373.15 K and *T*=398.15 K and at 0.1 MPa) and bromobenzene. Results for n-decane were compared (Figure 2) with literature correlated densities published by Cibulka and Hnedkovsky [38] and by Lemmon and Span [39] obtaining an AAD% of 0.05% and 0.07%, respectively. In Figure 3, experimental densities of bromobenzene were compared with Schilling et al. [40] data up to 30 MPa obtaining an AAD of 0.09%, and with several literature values at atmospheric pressure [40-47] finding a good agreement. It is important to notice that the deviation with the highly accurate density datum measured by Kuramoto et al. [45] with a magnetic suspension balance is 0.02 % whereas Schilling et al. found a deviation of 0.07%.

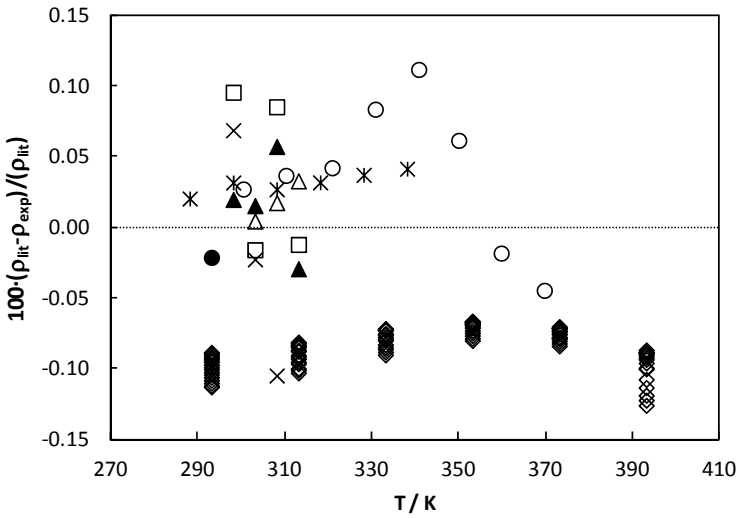

FIGURE 3. Relative deviations with literature density data for bromobenzene as a function of temperature and pressures up to 30 MPa. Nayard and Kudchadker [41] (○), Nayak et al. [42] (×), Ni et al. [43] (□), Rathnam et al. [44] (△), Kuramoto et al. [45] (●), Góralski and Piekarski [46] (∗), Sastry et al. [47] (▲) and Schilling et al. [40] (◇).

3. Results and discussion

Experimental and corrected density values are presented in Table 2 for the ILs measured in this work. Density increases with pressure and decreases with temperature as standard. $[C_1OC_2C_1pyrr][NTf_2]$ has higher densities than $[C_2C_1Im][C_2SO_4]$.

The following modified Tamman-Tait equation [32] was employed to correlate experimental density values with temperature and pressure.

$$\rho(T,p) = \frac{\rho_0(T, 0.1\text{MPa})}{1 - C\cdot\ln\left(\frac{B(T)/MPa + p/MPa}{B(T)/MPa + 0.1\text{MPa}}\right)} \tag{2}$$

where $\rho_0(T,0.1\text{MPa})$ is the density as a function of temperature at a reference pressur, 0.1 MPa, following this polynomial expression:

$$\rho_0(T,0.1\text{MPa})/g\cdot cm^{-3} = \sum_{i=0}^{m} A_i (T/K)^i \tag{3}$$

C is a parameter independent of temperature and pressure [48] and $B(T)$ is a parameter depending on temperature as a polynomial function:

$$B(T)/MPa = \sum_{j=0}^{n} B_j (T/K)^j \tag{4}$$

Parameters obtained for Tammann-Tait correlation are presented in Table 3, along with standard deviations, σ, for $\rho_0(T,0.1\text{MPa})$ and σ^* for $\rho(T,p)$.

TABLE 2
Direct experimental densities* and their corrected values[a] according to eq. 1, in g·cm^{-3}, for the two ILs at different temperatures T^b, and pressures, p^c.

	T /K						
p/MPa	278.15	298.15	313.15	333.15	348.15	373.15	398.15
				$[C_2C_1Im][C_2SO_4]$			
0.1	1.2519	1.2370	1.2266	1.2130	1.2031	1.1873	1.1714
	1.2528*	1.2375*	1.2270*	1.2132*	1.2033*	1.1874*	1.1715*
1	1.2522	1.2373	1.2270	1.2134	1.2036	1.1873	1.1719
	1.2532*	1.2379*	1.2274*	1.2136*	1.2038*	1.1874*	1.1720*
10	1.2557	1.2410	1.2308	1.2174	1.2077	1.1918	1.1759
	1.2567*	1.2415*	1.2312*	1.2176*	1.2079*	1.1920*	1.1760*
20	1.2595	1.2450	1.2350	1.2217	1.2123	1.1966	1.1810
	1.2605*	1.2456*	1.2354*	1.2220*	1.2125*	1.1968*	1.1811*
40	1.2668	1.2526	1.2428	1.2300	1.2209	1.2058	1.1907
	1.2677*	1.2532*	1.2433*	1.2303*	1.2211*	1.2059*	1.1908*
60	1.2737	1.2597	1.2503	1.2378	1.2289	1.2142	1.1997
	1.2746*	1.2604*	1.2508*	1.2382*	1.2292*	1.2144*	1.1998*
80	1.2802	1.2665	1.2573	1.2452	1.2365	1.2222	1.2081
	1.2812*	1.2673*	1.2578*	1.2455*	1.2367*	1.2224*	1.2082*
100	1.2865	1.2731	1.2641	1.2523	1.2438	1.2297	1.2160
	1.2875*	1.2740*	1.2647*	1.2526*	1.2440*	1.2299*	1.2161*
120	1.2922	1.2793	1.2705	1.2591	1.2508	1.2370	1.2234
	1.2932*	1.2802*	1.2712*	1.2595*	1.2511*	1.2372*	1.2236*
				$[C_1OC_2C_1Pyrr][NTf_2]$			
0.1	1.4742	1.4535	1.4391	1.4208	1.4073	1.3853	1.3632
	1.4750*	1.4540*	1.4395*	1.4210*	1.4075*	1.3855*	1.3633*
1	1.4749	1.4541	1.4401	1.4216	1.4080	1.3857	1.3633
	1.4757*	1.4546*	1.4404*	1.4219*	1.4082*	1.3858*	1.3634*
10	1.4808	1.4602	1.4465	1.4285	1.4154	1.3934	1.3720
	1.4816*	1.4607*	1.4469*	1.4288*	1.4156*	1.3936*	1.3721*
20	1.4870	1.4669	1.4535	1.4359	1.4232	1.4018	1.3810
	1.4879*	1.4674*	1.4539*	1.4362*	1.4234*	1.4020*	1.3811*
40	1.4986	1.4792	1.4664	1.4495	1.4375	1.4172	1.3974
	1.4996*	1.4798*	1.4668*	1.4498*	1.4377*	1.4173*	1.3976*
60	1.5095	1.4906	1.4784	1.4622	1.4505	1.4309	1.4120
	1.5106*	1.4913*	1.4788*	1.4625*	1.4508*	1.4310*	1.4122*
80	1.5198	1.5014	1.4894	1.4737	1.4625	1.4435	1.4254
	1.5209*	1.5021*	1.4899*	1.4741*	1.4627*	1.4437*	1.4256*
100	1.5293	1.5114	1.4998	1.4846	1.4736	1.4552	1.4379
	1.5305*	1.5122*	1.5004*	1.4850*	1.4739*	1.4554*	1.4381*
120	1.5383	1.5209	1.5096	1.4948	1.4842	1.4663	1.4496
	1.5394*	1.5218*	1.5103*	1.4953*	1.4846*	1.4665*	1.4498*

[a]Density uncertainties: $0.7\cdot10^{-3}$ g·cm^{-3} for temperatures below T = 373.15 K, $5\cdot10^{-3}$ g·cm^{-3} at T = (373.15 and 398.15) K and p = 0.1 MPa, and $3\cdot10^{-3}$ g·cm^{-3} in other cases, i.e. at $T \geq 373.15$ K and $p > 0.1$ MPa.
[b]Temperature uncertainty: 0.02 K
[c]Pressure uncertainty: 0.02 MPa

TABLE 3
A_i, B_i, C and standard deviations, σ and σ^* from Tammann- Tait equation.

	$[C_2C_1Im][C_2SO_4]$	$[C_1OC_2C_1Pyrr][NTf_2]$
A_0 /g·cm^{-3}	1.65207	2.12764
$-10^3 \cdot A_1$ /g·cm^{-3}·K^{-1}	2.4296	4.2910
$10^6 \cdot A_2$ /g·cm^{-3}·K^{-2}	4.704	9.359
$-10^9 \cdot A_3$ /g·cm^{-3}·K^{-3}	4.10	8.55
$10^4 \cdot \sigma$ /g·cm^{-3}	1.0	1.0
$10^2 \cdot C$	9.82	8.72
B_0 /MPa	809	517
$-B_1$ /MPa·K^{-1}	2.436	1.555
$10^3 \cdot B_2$ /MPa·K^{-2}	2.41	1.42
$10^4 \cdot \sigma^*$ / g·cm^{-3}	2.3	2.9

In Figure 4 our correlated density values at atmospheric pressure are compared with eighteen $\rho(T)$ sets of literature values [30,49-65] for $[C_2C_1Im][C_2SO_4]$ being the overall AAD% 0.12%. Deviations from thirteen sets of the literature data [30,49-52,54,58,59,63,65] are lower than the combined estimated expanded uncertainties. Our values agree very well (AAD%=0.04%) with those of the three batches measured recently by Lehmann et al. [58] who have obtained a maximum relative deviation of 0.08%, which was outside the combined expanded uncertainties of their measurements. The differences among the different literature values can be attributed to both the different and/or undefined impurities as well as the fact that authors usually underestimate the experimental uncertainties.

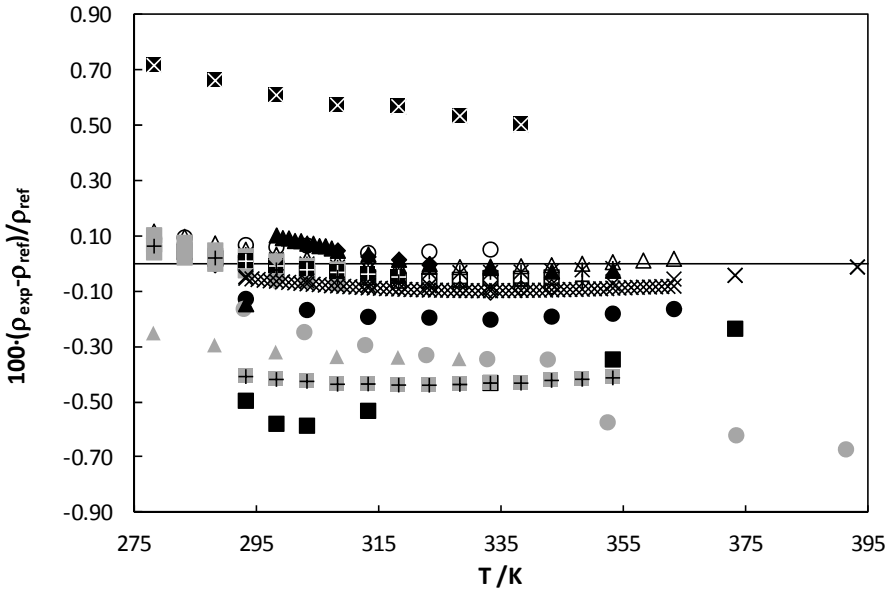

FIGURE 4. Comparison between our atmospheric density data for $[C_2C_1Im][C_2SO_4]$ and those from the literature for different temperatures. Fröba et al. [51] (△), Matkowska et al. [59] (□), Hofman et al. [54] (○), Jacquemin et al. [55] (●), Lehmann et al. [58] (■), García-Miaja et al. [52] ( ),Wandschneider et al. [62] (▲), Wong et al. [63](◆), Jacquemin et al. [80] (●), Fernández et al. [50] (∗), Tomé et al. [61] (■), Gómez et al. [53] (◇), Domanska et al. [49] (◆), Rodríguez et al. [60] (+), Krummen et al. [57] (+), Yang et al. [64] ( ), Nieto de Castro et al. [30] (×), Soriano et al.[65] (▲).

Up to our knowledge, only two rigorous experimental density data, at 293.15 K and 298.15 K, have been published for $[C_1OC_2C_1Pyrr][NTf_2]$. These values were reported by Appetechi et al. [66] and Zhou et al. [67] being the obtained deviations -0.03% in both cases.

As regards literature density data at high pressures for $[C_2C_1Im][C_2SO_4]$, there are four sets of measurements performed in DMA 512P Anton Paar densimeters by Jacquemin et al. [68] from (293 to 415) K and from (0.1 to 40) MPa, by Tome et al. [61] from (293.15 to 393.15) K and from (0.1 to 35) MPa and by Hofman et al. [54] and Matkowska et al. [59] in the same equipment from (283.15 to 343.15) K and up to 35 MPa. In addition, Nieto de Castro et al. [30] have measured in an Anton Paar HP densimeter from (293.15 to 433.15) K and up to 60 MPa. None of these researchers have corrected the effect of the viscosity on the density measurements at high pressures. As the range of our measurements is from 278.15K to 398.15 K and up to 120 MPa, our data complete the available literature sets for pressures between 60 MPa to 120 MPa and for the 278.15 K isotherm. In Figure 5 the correlated density values for $[C_2C_1Im][C_2SO_4]$ are compared with literature values as a function of pressure.

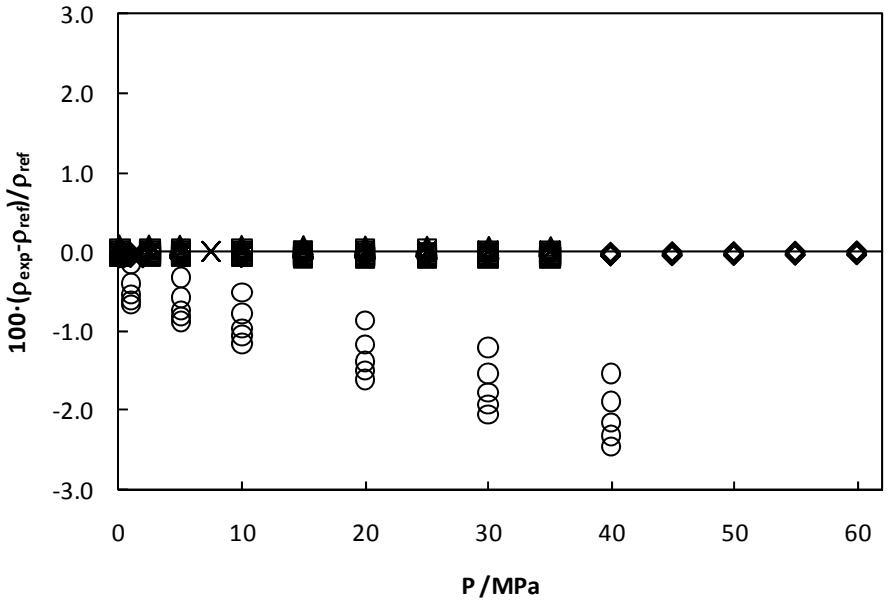

FIGURE 5. Comparison between our density data for $[C_2C_1Im]$ $[C_2SO_4]$ and those from the literature against pressure for different temperatures. Hofman et al. [54] (△), Matkowska et al. [59] (□), Tomé et al. [61] (×), Nieto de Castro et al. [30] (◇), Jacquemin et al. [68] (○).

Both, Hofman et al. [54] and Matkowska et al. [59], reported an expanded uncertainty for their data sets of 0.2 $kg \cdot m^{-3}$, being the AAD% with our data in both cases of 0.05%, which is lower than our uncertainty in density measurements (the density uncertainty 0.7 $kg \cdot m^{-3}$ is equivalent to 0.06% in the density range of this IL). Our high pressure density values also agree very well with those of Nieto de Castro et al. [30] with an AAD% of 0.05% which is quite lower that their estimated expanded uncertainty of ±0.4%. Nevertheless, Tomé et al. [61] data, with uncertainty of 1 $kg.m^{-3}$, deviate from our density data with an AAD% of 0.45%, which is higher

than the combined uncertainty, which is around 0.14%. In the case of Jacquemin et al. [68] data, the uncertainty claimed by the authors is 0.1 $kg.m^{-3}$, but the AAD% with our data is 1.2% and the combined uncertainty is around 0.07%. If we compare the density values without the correction of the viscosity effect (eq. 1) the AAD% decreases with data by Nieto de Castro et al. [30], 0.03%, by Matkowska et al. [59], 0.04%, Tomé et al. [61], 0.43% and Jacquemin et al. [68], 1.2 %, whereas with the Hofman et al. [54] data increases to 0.09%.

Density derived properties can be obtained from the modified Tammann-Tait equation by simple analytical derivation. Isothermal compressibility shows system modification when it is subjected to pressure changes at constant temperature. It is defined by the following expression:

$$\kappa_T(T,p) = \frac{1}{\rho}\left(\frac{\partial\rho}{\partial p}\right)_T \tag{5}$$

Isobaric thermal expansivity, also named thermal expansion coefficient, shows the fractional change in density when temperature increases at constant pressure. It is defined by the following expression:

$$\alpha_p(T,p) = -\frac{1}{\rho}\left(\frac{\partial\rho}{\partial T}\right)_p \tag{6}$$

In the last years, several authors have found that α_p values decrease when temperature increases [29-31,69,70], contrary to what had been found for most of the molecular and polymer liquids [31]. Troncoso et al. [29] have studied this behaviour by using an equation of state based on thermodynamic perturbation theory, which can explain the different behaviour of ILs and molecular liquids as well as predict the existence of regions of positive and negative signs of the $(\partial\alpha/\partial T)$ depending on the temperature and pressure region. Different behaviour of molecular and ILs is explained by these authors by the fact that at ambient conditions ILs are more far below of their critical point than molecular liquids. In 1991, Cibulka et al. [71] reported non-monotonous α_p *(T)* curves for some alcohols at low temperatures. Hofman et al. [54], Matkowska et al. [59], Nieto de Castro et al. [30] and Tariq et al. [72] have reported experimental non-monotonous α_p *(T)* curves for $[C_2C_1Im][C_2SO_4]$ and other three ILs for which density was measured in broad temperatures ranges.

Several authors [73-75] mentioned that the isobaric thermal expansivities determined with the Tamman-Tait equation depends on the form of ρ_0*(T,* 0.1 MPa*)* and *B(T)* functions. This is the reason why it is recommended to derive the isobaric thermal expansivity from the isobaric densities. Concerning the form of the ρ*(T)* function to fit density data for the ILs $[C_2C_1Im][C_2SO_4]$ and $[C_nC_1Im][NTf_2]$, some authors fit the density [54,59] or ln(ρ) [30,72] values with a

third degree polynomial dependence on temperature and found a minima in the curves α_p vs. T; other authors [60-62,68] fit the density dependence on temperature with a second degree polynomial and found α_p both increasing or decreasing with temperature depending on the author; in references [50,55] it is established a linear dependence of density on temperature and found that α_p increases with temperature; finally some authors [53,64] establish a linear dependence of ln(ρ) with temperature, which gives rise to α_p independent from temperature. Similar situation is found for other ILs. Thus, it can be concluded that the trend observed depends strongly on the type of equation used for $\rho(T)$. Therefore, to analyze the dependence of the α_p values on the equation used to fit the densities at each pressure and to compare our results with those previously reported in the literature, we have correlated the density and ln(ρ) values as a third degree polynomial of the temperature. Thus, in the second case, we have used the following equation:

$$ln(\rho / g{\cdot}cm^{-3}) = A + B(T/K) + C(T/K)^2 + D(T/K)^3 \tag{7}$$

Accordingly, the isobaric thermal expansivity is given by ($\alpha_p = -(\partial \ln \rho / \partial T)_p$):

$$\alpha_p / K^{-1} = -\left(B + 2C(T/K) + 3D(T/K)^2\right) \tag{8}$$

and the derivative of α_p with temperature:

$$\frac{d\alpha_p}{dT} = -\left(2C + 6D(T/K)\right) \tag{9}$$

Thus, the eq. 7 can reproduce a non-monotonous behaviour of α_p with a minimum or maximum at T_m given by:

$$T_m / K = -\frac{C}{3D} \tag{10}$$

If T_m is in the temperature range of the experimental density measurements, a non-monotonous behaviour is reproduced, otherwise the experimental $\alpha_p(T)$ curve is monotonous. Nieto de Castro [30] have found $\alpha_p(T)$ with or without extrema (minimum) depending on the IL and the pressure.

In Table 4 we have gathered the values of the A, B, C, D parameters of the eq. 7 at the different pressures for $[C_2C_1Im][C_2SO_4]$ and $[C_1OC_2C_1Pyrr][NTf_2]$. In Table 5 we have indicated the α_p values using the parameters of Table 4 together with eq. 7. We have also calculated the α_p values using third degree polynomial for the densities dependence on temperature. The AADs% between both sets of α_p values are only 0.17% and 0.12% for $[C_2C_1Im][C_2SO_4]$ and $[C_1OC_2C_1Pyrr][NTf_2]$, respectively, i.e. the effect of considering third degree polynomial for ρ

or for ln(ρ) is negligible. Besides, the effect of the viscosity correction in the α_p values was determined for [C_2C_1Im][C_2SO_4] finding that, in general, the α_p values determined from corrected densities are slightly lower, being the AAD% between both sets of α_p of 1.2% and the maximum deviation of 3.1% (at the lowest temperature and pressure, 278.15 K and 0.1 MPa).

TABLE 4
Parameters *A*, *B*, *C* and *D* from eq. 7.

p /MPa	*A*	$-10^3 \cdot B$ / K^{-1}	$10^6 \cdot C$ / K^{-2}	$-10^9 \cdot D$ / K^{-3}
		[C_2C_1Im][C_2SO_4]		
0.1	0.5306	1.835	3.528	3.188
1	0.5507	2.045	4.260	4.023
10	0.5403	1.928	3.899	3.623
20	0.5408	1.919	3.896	3.612
40	0.5697	2.148	4.603	4.274
60	0.5580	2.011	4.219	3.869
80	0.5646	2.046	4.365	4.007
100	0.5525	1.915	4.022	3.676
120	0.5547	1.936	4.191	3.907
		[$C_1OC_2C_1Pyrr$][NTf_2]		
0.1	0.8208	2.841	6.263	5.907
1	0.8056	2.722	5.988	5.720
10	0.8047	2.687	5.877	5.548
20	0.8066	2.690	5.922	5.570
40	0.8083	2.673	5.929	5.536
60	0.8001	2.567	5.674	5.268
80	0.8010	2.533	5.596	5.150
100	0.7864	2.370	5.151	4.695
120	0.7680	2.179	4.638	4.190

In Figure 6 the α_p values are plotted against temperature for several isobars. We can see that $\alpha_p(T)$ presents a minimum located in the range 357 to 368 K for [C_2C_1Im][C_2SO_4] and 353 to 369 K for [$C_1OC_2C_1Pyrr$][NTf_2]. We have compared the α_p values obtained in the present work, using the same procedure (eq. 7 and Table 4), with the values published in literature, this comparison can be observed in Figure 7 for [C_2C_1Im][C_2SO_4], finding the maximum deviation with the data published by Jacquemin et al. [68]. As it can be observed, an excellent agreement, 1.4%, is reached with α_p values of Nieto de Castro et al. [30]. We should take into account that these authors estimate in 4% the uncertainty of their α_p values and that they have not corrected the effect of viscosities. The AAD% between our α_p values (Table 5) and those determined by Hofman et al. [54] and Matkowska et al. [59], determined using a Tammann-Tait equation, are 2.4% and 3.5%, respectively. These authors estimate the uncertainty of their α_p values in 10^{-5} K^{-1}, which is about 2% in terms of relative deviations.

TABLE 5
Isobaric thermal expansivity, $10^4 \cdot \alpha_P(K^{-1})$, obtained from eq. 7 along with the parameters presented in table 4.

	p /MPa								
T/K	0.1	1	10	20	40	60	80	100	120
					$[C_2C_1Im][C_2SO_4]$				
278.15	6.12	6.09	6.00	5.90	5.79	5.62	5.48	5.31	5.11
298.15	5.81	5.78	5.69	5.59	5.43	5.27	5.12	4.97	4.79
313.15	5.63	5.60	5.52	5.42	5.22	5.07	4.91	4.78	4.61
333.15	5.45	5.46	5.36	5.26	5.04	4.88	4.72	4.59	4.45
348.15	5.37	5.42	5.31	5.20	4.97	4.80	4.64	4.51	4.39
373.15	5.33	5.46	5.32	5.20	4.98	4.78	4.62	4.49	4.40
398.15	5.41	5.66	5.46	5.34	5.15	4.91	4.76	4.61	4.57
					$[C_1OC_2C_1Pyrr][NTf_2]$				
278.15	7.28	7.19	7.05	6.88	6.59	6.33	6.15	5.94	5.71
298.15	6.81	6.77	6.62	6.44	6.14	5.88	5.70	5.50	5.31
313.15	6.56	6.55	6.39	6.20	5.88	5.63	5.43	5.25	5.07
333.15	6.34	6.37	6.19	5.99	5.66	5.40	5.19	5.01	4.84
348.15	6.28	6.33	6.12	5.92	5.57	5.32	5.09	4.90	4.73
373.15	6.34	6.43	6.19	5.97	5.60	5.33	5.08	4.87	4.68
398.15	6.63	6.74	6.46	6.23	5.84	5.54	5.26	5.01	4.78

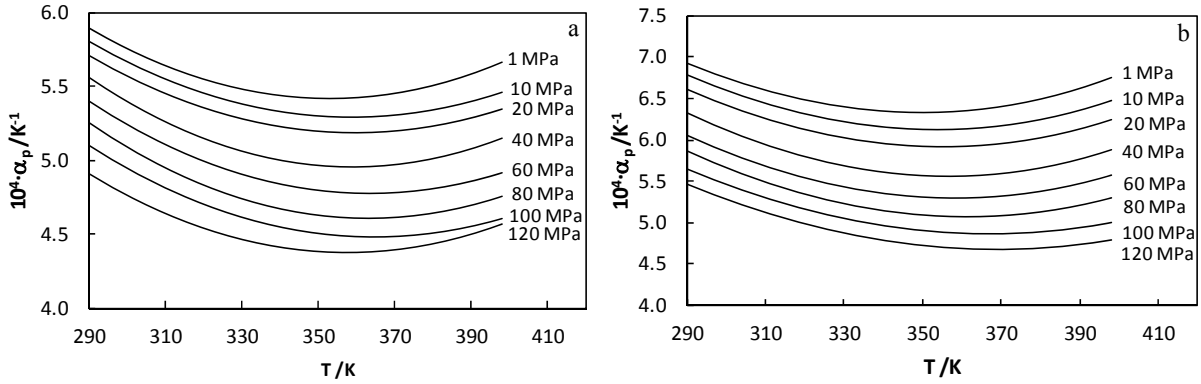

FIGURE 6. Isobaric thermal expansivity, α_P, vs. temperature at different pressures for (a) $[C_2C_1Im][C_2SO_4]$ and (b) $[C_1OC_2C_1Pyrr][NTf_2]$.

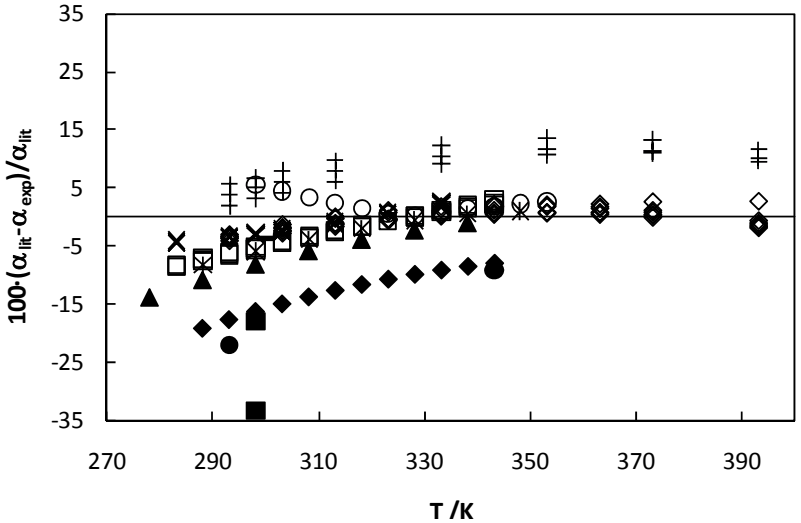

FIGURE 7. Comparison between the isobaric thermal expansivity, α_P, determined in this work and the values published in literature for $[C_2C_1Im][C_2SO_4]$. Nieto de Castro et al. [30] (◇), Fernández et al. [50] (○), Gómez et al. [53] (◆), Jacquemin et al. [68] (■), Rodríguez and Brenecke [60] (∗), Wandschneider et al. [62] (-), Tomé et al. [61] (+), Hofman et al. [54] (×), Yang et al. [64] (▲), Jacquemin et al. [55] (●), Matkowska et al. [59] (□).

The values obtained for κ_T are summarised in Table 6. Figure 8 presents κ_T values vs. pressure at different temperatures; these values diminish when pressure increases and are higher for $[C_1OC_2C_1Pyrr][NTf_2]$ than for $[C_2C_1Im][C_2SO_4]$. The differences in κ_T values for both ILs diminish with pressure. It can also be observed the increase in κ_T with increasing temperature. This behaviour is similar for molecular liquids. It could be explained because when the temperature decreases or the pressure increases, the intermolecular (or interionic) space becomes smaller, that leads to a decrease of the liquids compressibility. The IL $[C_2C_1Im][C_2SO_4]$ has a very small compressibility, which is around a half of that of the normal molecular liquids. This fact makes them appropriate as hydraulic fluids [76].

TABLE 6
Isothermal compressibility values, $10^4 \cdot \kappa_T$ (MPa^{-1}).

	p/MPa							
T/K	1	5	10	20	40	60	80	100
				$[C_2C_1Im][C_2SO_4]$				
278.15	3.09	3.05	3.01	2.93	2.77	2.64	2.51	2.40
298.15	3.30	3.26	3.21	3.12	2.95	2.80	2.67	2.55
313.15	3.46	3.42	3.37	3.27	3.08	2.92	2.78	2.65
333.15	3.69	3.64	3.58	3.47	3.27	3.08	2.92	2.78
348.15	3.87	3.81	3.75	3.62	3.40	3.20	3.03	2.88
373.15	4.15	4.09	4.01	3.87	3.62	3.40	3.20	3.03
398.15	4.42	4.35	4.27	4.11	3.82	3.58	3.36	3.17
				$[C_1OC_2C_1Pyrr][NTf_2]$				
278.15	4.44	4.36	4.27	4.08	3.77	3.50	3.26	3.06
298.15	4.82	4.72	4.61	4.40	4.03	3.72	3.46	3.24
313.15	5.11	5.00	4.88	4.64	4.23	3.90	3.61	3.37
333.15	5.52	5.40	5.25	4.98	4.52	4.13	3.81	3.54
348.15	5.85	5.71	5.55	5.24	4.73	4.32	3.97	3.68
373.15	6.43	6.26	6.06	5.70	5.10	4.62	4.23	3.90
398.15	7.02	6.82	6.59	6.17	5.47	4.92	4.48	4.11

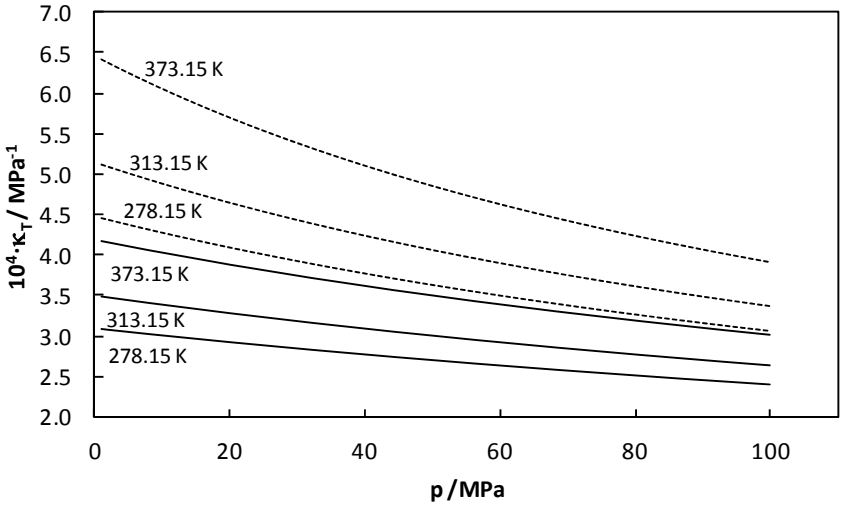

FIGURE 8. Isothermal compressibility, κ_T, vs. pressure. $[C_1OC_2C_1Pyrr][NTf_2]$ (dashed line), $[C_2C_1Im][C_2SO_4]$ (solid line).

Density values, expressed in g·cm^{-3}, were predicted as a function of temperature and pressure using the correlation proposed by Gardas and Coutinho [77] (eq.11).

$$\rho / kg{\cdot}m^{-3} = \frac{W / kg{\cdot}mol^{-1}}{NV_0(a + bT/K + cp/MPa)} \tag{11}$$

where W is the molar mass, N is the Avogadro constant, V_0 is the molecular volume at the reference temperature (T_0) and pressure (p_0) in m^3·molecule^{-1} and a, b and c are fitting coefficients. Molecular volumes employed for calculation are presented in Table 7.

TABLE 7
Molecular volumes (Å^3·molecule^{-1}) employed in the Gardas-Coutinho density prediction.

Ionic Liquid	Cation Volume	Anion Volume	References
$[C_2C_1Im][C_2SO_4]$	182	134	Gardas and Coutinho [77] / Tomé et al. [61]
$[C_1OC_2C_1Pyrr][NTf_2]$	235	248	Gardas and Coutinho [77] / Shreeve and Ye [79]

Eq. (11), according to the authors, covers the density range between 0.9867 and 1.5471 g·cm^{-3}, in a temperature range between 273.15 and 393.15 K and a pressure range between 0.10 and 100 MPa. In this range coefficient values are the following: $a = 8.005{\cdot}10^{-1} \pm 2.333{\times}10^{-4}$, $b = 6.652{\cdot}10^{-4} \pm 6.907{\cdot}10^{-7}$ K^{-1} and $c = -5.919{\cdot}10^{-4} \pm 2.410{\cdot}10^{-6}$ MPa^{-1}, at 95% level of confidence. The AAD% obtained in the prediction of the density values, considering temperature and pressure limits given by the authors, were 1.32 % and 1.02 % for $[C_2C_1Im][C_2SO_4]$ and $[C_1OC_2C_1Pyrr][NTf_2]$, respectively. For the imidazolium based IL, $[C_2C_1Im][C_2SO_4]$, the AAD% obtained is higher than that reported by Gardas and Coutinho [77] for this type of ILs (0.45%); this can be due to the fact that we have predicted more density points at high pressure compared to Gardas and Coutinho [77], who have predicted only one data set up to 100 MPa, meanwhile our whole prediction was extended up to this pressure. Applying the prediction to the whole experimental temperature and pressure range, out of the limits proposed by Gardas and Coutinho [77], i.e., up to 398.15 K and 120 MPa respectively, the AAD% increases slightly to 1.5 % and 1.1 % for $[C_2C_1Im]$ $[C_2SO_4]$ and $[C_1OC_2C_1Pyrr][NTf_2]$, respectively.

Furthermore, we have also predicted the density values of $[C_2C_1Im]$ $[C_2SO_4]$ by means of the method proposed by Jacquemin et al. [78], in the temperature range from 298.15 K to 398.15 K and in the whole pressure range, obtaining an AAD% of 2.5%, being the maximum deviation of 6.4%.

4. Conclusions

Experimental density values were determined for $[C_2C_1Im][C_2SO_4]$ and $[C_1OC_2C_1Pyrr][NTf_2]$ in a temperature range from 273.15 K to 298.15 K and pressures up to 120 MPa obtaining the highest values for $[C_1OC_2C_1Pyrr][NTf_2]$. A correction factor due to the ILs viscosity values has been applied. Isothermal compressibility (κ_T) was obtained by derivation from the Tammann- Tait correlation, meanwhile the isobaric thermal expansivity (α_p) was obtained by differentiation from the isobaric densities. The κ_T sequence obtained was the following $[C_1OC_2C_1Pyrr][NTf_2]$ > $[C_2C_1Im][C_2SO_4]$. The behaviour of α_p with temperature along isobars has been highly discussed in literature, because it seems to depend on the type of equation used to fit density dependence on temperature. In this work we have employed both, a third degree polynomial and a third degree logarithmic function to fit the behaviour of density with temperature, obtaining in both cases a non monotonous behaviour of α_p with temperature and finding a minimum in the studied temperature and pressure range. We have applied the correlation proposed by Gardas and Coutinho [77] for predicting the density values reported in this work in the whole experimental temperature and pressure range obtaining and AAD% lower than 1.5 %. Furthermore, we have applied the method of Jacquemin et al. [78] for predicting the density of $[C_2C_1Im]$ $[C_2SO_4]$ in the temperature range from 298.15 K to 398.15 K and in the whole pressure range obtaining an AAD% of 2.5 %.

Acknowledgments

Authors acknowledge the advices and samples provided by Dr. Uerdingen from Merck KGaA. This work was supported by Spanish Ministry of Science and Innovation and FEDER Program through CTQ2008-06498-C02-01 and CTQ2011-23925 projects. L.L and T.R. acknowledge financial support under the Ramon y Cajal Program and the FPU program, respectively.

References

[1] N.V. Plechkova, K.R. Seddon, Chem. Soc. Rev. 37 (2008) 123-150.
[2] M. Freemantle, Chem. Eng. News 85 (2007) 23-26.
[3] H. Zhao, Chem. Eng. Commun. 193 (2006) 1660 - 1677.
[4] M.G. Freire, C.L.S. Louros, L.P.N. Rebelo, J.A.P. Coutinho, Green Chem. 13 (2011) 1536-1545.
[5] A.R. Ferreira, M.G. Freire, J.C. Ribeiro, F.M. Lopes, J.G. Crespo, J.A.P. Coutinho, Ind. Eng. Chem. Res. 50 (2011) 5279-5294.
[6] C.M.S.S. Neves, J.F.O. Granjo, M.G. Freire, A. Robertson, N.M.C. Oliveira, J.A.P. Coutinho, Green Chem. 13 (2011) 1517-1526.
[7] C.L.S. Louros, A.F.M. Claudio, C.M.S.S. Neves, M.G. Freire, I.M. Marrucho, J. Pauly, J.A.P. Coutinho, Int. J. Mol. Sci 11 (2010) 1777-1791.
[8] M.-D. Bermúdez, A.-E. Jiménez, J. Sanes, F.-J. Carrión, Molecules 14 (2009) 2888-2908.
[9] I. Minami, Molecules 14 (2009) 2286-2305.

[10] K.B. Sidhpuria, A.L. Daniel-da-Silva, T. Trindade, J.A.P. Coutinho, Green Chem. 13 (2011) 340-349.
[11] S. Aparicio, M. Atilhan, F. Karadas, Ind. Eng. Chem. Res. 49 (2010) 9580-9595.
[12] A. Stark, Energy Environ. Sci. 4 (2011) 19-32.
[13] P.J. Carvalho, V.H. Álvarez, I.M. Marrucho, M. Aznar, J.A.P. Coutinho, J. Supercrit. Fluids 50 (2009) 105-111.
[14] N. MacDowell, N. Florin, A. Buchard, J. Hallett, A. Galindo, G. Jackson, C.S. Adjiman, C.K. Williams, N. Shah, P. Fennell, Energy Environ. Sci. 3 (2010) 1645-1669.
[15] H.-L. Huang, H.P. Wang, G.-T. Wei, I.W. Sun, J.-F. Huang, Y.W. Yang, Environ. Sci. Technol. 40 (2006) 4761-4764.
[16] A.P. Abbott, G. Frisch, J. Hartley, K.S. Ryder, Green Chem. 13 (2011) 471-481.
[17] P. Wasserscheid, R.v. Hal, A. Bosmann, Green Chem. 4 (2002) 400-404.
[18] M.G. Freire, C.M.S.S. Neves, I.M. Marrucho, J.A.P. Coutinho, A.M. Fernandes, J. Phys. Chem. A 114 (2009) 3744-3749.
[19] S.P.M. Ventura, R.L. Gardas, F. Gonçalves, J.A.P. Coutinho, J. Chem. Technol. Biotechnol. (2011) n/a-n/a.
[20] J.D. Holbrey, W.M. Reichert, R.P. Swatloski, G.A. Broker, W.R. Pitner, K.R. Seddon, R.D. Rogers, Green Chem. 4 (2002) 407-413.
[21] M. Rebros, H.Q.N. Gunaratne, J. Ferguson, K.R. Seddon, G. Stephens, Green Chem. 11 (2009) 402-408.
[22] J.J. Nainaparampil, K.C. Eapen, J.H. Sanders, A.A. Voevodin, J. Microelectromech. Syst. 16 (2007) 836-843.
[23] N.M.T. Lourenço, J. Österreicher, P. Vidinha, S. Barreiros, C.A.M. Afonso, J.M.S. Cabral, L.P. Fonseca, React. Funct. Polym. 71 (2011) 489-495.
[24] S.S. Mal, F.H. Stephens, R.T. Baker, Chem. Commun. 47 (2011) 2922-2924.
[25] M.G. Freire, C.M.S.S. Neves, I.M. Marrucho, J.N. Canongia Lopes, L.P.N. Rebelo, J.A.P. Coutinho, Green Chem. 12 (2010) 1715-1718.
[26] J. Albo, P. Luis, A. Irabien, Ind. Eng. Chem. Res. 49 (2010) 11045-11051.
[27] O. Russina, L. Gontrani, B. Fazio, D. Lombardo, A. Triolo, R. Caminiti, Chem. Phys. Lett. 493 (2010) 259-262.
[28] S. Ferrari, E. Quartarone, P. Mustarelli, A. Magistris, S. Protti, S. Lazzaroni, M. Fagnoni, A. Albini, J. Power Sources 194 (2009) 45-50.
[29] J. Troncoso, C.A. Cerdeiriña, P. Navia, Y.A. Sanmamed, D. González-Salgado, L. Romaní, J. Phys. Chem. Lett. 1 (2010) 211-214.
[30] C.A. Nieto de Castro, E. Langa, A.L. Morais, M.L. Matos Lopes, M.J.V. Lourenço, F.J.V. Santos, M.S.C.S. Santos, J.N. Canongia Lopes, H.I.M. Veiga, M. Macatrão, J.M.S.S. Esperança, C.S. Marques, L.P.N. Rebelo, C.A.M. Afonso, Fluid Phase Equilib. 294 (2010) 157-179.
[31] J. Troncoso, P. Navia, L. Romaní, D. Bessieres, T. Lafitte, J. Chem. Phys. 134 (2011) 094502.
[32] J.J. Segovia, O. Fandiño, E.R. Lopez, L. Lugo, M.M. Carmen, J. Fernandez, J. Chem. Thermodyn. 41 (2009) 632-638.
[33] B. Lagourette, C. Boned, H. Saint-Guirons, P. Xans, H. Zhou, Meas. Sci. Technol. 3 (1992) 699-703.
[34] M.J.P. Comuñas, J.P. Bazile, A. Baylaucq, C. Boned, J. Chem. Eng. Data 53 (2008) 986-994.
[35] O. Fandiño, L. Lugo, M.J.P. Comunas, E.R. Lopez, J. Fernandez, J. Chem. Thermodyn. 42 (2009) 84-89.
[36] F.M. Gaciño, X. Paredes, M.J.P. Comuñas, J. Fernández, Viscosity behavior of 1-ethyl-3-methylimidazolium ethylsulfate and 1-(2-methoxyethyl)-1-methyl-pyrrolidinium bis(trifloromethylsulfonyl)imide at high pressures, 25th European Symposium on Applied Thermodynamics, Saint Petersburg, Russia, 2011.
[37] P. Daugé, A. Baylaucq, L. Marlin, C. Boned, J. Chem. Eng. Data 46 (2001) 823-830.
[38] I. Cibulka, L. Hnedkovsky, J. Chem. Eng. Data 41 (1996) 657-668.
[39] E.W. Lemmon, R. Span, J. Chem. Eng. Data 51 (2006) 785-850.
[40] G. Schilling, R. Kleinrahm, W. Wagner, J. Chem. Thermodyn. 40 (2008) 1095-1105.
[41] S. Nayar, A.P. Kudchadker, J. Chem. Eng. Data 18 (1973) 356-357.
[42] J.N. Nayak, M.I. Aralaguppi, T.M. Aminabhavi, J. Chem. Eng. Data 48 (2003) 628-631.
[43] B. Ni, L. Su, H. Wang, H. Qiu, J. Chem. Eng. Data 55 (2010) 4541-4545.
[44] M.V. Rathnam, R.K.R. Singh, M.S. Kumar, J. Chem. Eng. Data 53 (2008) 265-270.

[45] N. Kuramoto, K. Fujii, A. Waseda, Metrologia 41 (2004) S84-S94.
[46] P. Góralski, H. Piekarski, J. Chem. Eng. Data 52 (2007) 655-659.
[47] N.V. Sastry, R.R. Thakor, M.C. Patel, Int. J. Thermophys. 29 (2008) 610-618.
[48] L. Lugo, M.J.P. Comuñas, E.R. López, J. Fernández, Fluid Phase Equilib. 186 (2001) 235-255.
[49] U. Domanska, M. Laskowska, J. Solution Chem. 37 (2008) 1271-1287.
[50] A. Fernandez, J. García, J.S. Torrecilla, M. Oliet, F. Rodríguez, J. Chem. Eng. Data 53 (2008) 1518-1522.
[51] A.P. Froba, H. Kremer, A. Leipertz, J. Phys. Chem. B 112 (2008) 12420-12430.
[52] G. García-Miaja, J. Troncoso, L. Romaní, J. Chem. Thermodyn. 41 (2009) 334-341.
[53] E. Gómez, B. González, N. Calvar, E. Tojo, Á. Domínguez, J. Chem. Eng. Data 51 (2006) 2096-2102.
[54] T. Hofman, A. Gołdon, A. Nevines, T.M. Letcher, J. Chem. Thermodyn. 40 (2008) 580-591.
[55] J. Jacquemin, P. Husson, A.A.H. Padua, V. Majer, Green Chem. 8 (2006) 172-180.
[56] J. Jacquemin, P. Nancarrow, D.W. Rooney, M.F. Costa Gomes, P. Husson, V. Majer, A.A.H. Pádua, C. Hardacre, J. Chem. Eng. Data 53 (2008) 2133-2143.
[57] M. Krummen, P. Wasserscheid, J. Gmehling, J. Chem. Eng. Data 47 (2002) 1411-1417.
[58] J. Lehmann, M.H. Rausch, A. Leipertz, A.P. Froba, J. Chem. Eng. Data 55 (2010) 4068-4074.
[59] D. Matkowska, A. Goldon, T. Hofman, J. Chem. Eng. Data 55 (2010) 685-693.
[60] H. Rodríguez, J.F. Brennecke, J. Chem. Eng. Data 51 (2006) 2145-2155.
[61] L.I.N. Tomé, P.J. Carvalho, M.G. Freire, I.M. Marrucho, I.M.A. Fonseca, A.G.M. Ferreira, J.A.P. Coutinho, R.L. Gardas, J. Chem. Eng. Data 53 (2008) 1914-1921.
[62] A. Wandschneider, J.K. Lehmann, A. Heintz, J. Chem. Eng. Data 53 (2008) 596-599.
[63] C.-L. Wong, A.N. Soriano, M.-H. Li, Fluid Phase Equilib. 271 (2008) 43-52.
[64] J.-Z. Yang, X.-M. Lu, J.-S. Guic, W.-G. Xua, Green Chem. 6 (2004) 541-543.
[65] A.N. Soriano, B.T. Doma Jr., M.-H. Li, J. Taiwan Inst. Chem. Eng. 41 (2010) 115-121.
[66] G.B. Appetecchi, M. Montanino, M. Carewska, M. Moreno, F. Alessandrini, S. Passerini, Electrochimica Acta 56 (2011) 1300-1307.
[67] Z.-B. Zhou, H. Matsumoto, K. Tatsumi, Chem. Eur. J. 12 (2006) 2196 - 2212.
[68] J. Jacquemin, P. Husson, V. Mayer, I. Cibulka, J. Chem. Eng. Data 52 (2007) 2204-2211.
[69] R.L. Gardas, M.G. Freire, P.J. Carvalho, I.M. Marrucho, I.M.A. Fonseca, A.G.M. Ferreira, J.A.P. Coutinho, J. Chem. Eng. Data 52 (2007) 1881-1888.
[70] R. Taguchi, H. Machida, Y. Sato, R.L. Smith, J. Chem. Eng. Data 54 (2008) 22-27.
[71] I. Cibulka, Fluid Phase Equilib. 89 (1993) 1-18.
[72] M. Tariq, A.P. Serro, J.L. Matab, B. Saramago, J.M.S.S. Esperanca, J.N.C. Lopes, L.P.N. Rebelo, Fluid Phase Equilib. 294 (2010) 131-138.
[73] F. Alaoui, E. Montero, J.P. Bazile, M.J.P. Comuñas, G. Galliero, C. Boned, Fluid Phase Equilib. 301 (2011) 131-136.
[74] J. Troncoso, D. Bessières, C.A. Cerdeiriña, E. Carballo, L. RomanI, Fluid Phase Equilib. 208 (2003) 141-154.
[75] C.A. Cerdeirina, C.A. Tovar, D. Gonzalez-Salgado, E. Carballo, L. Romani, Phys. Chem. Chem. Phys. 3 (2001) 5230-5236.
[76] M. Uerdingen, Ionic Liquids as Lubricants. in: P. Wasserscheid, A. Stark, (Eds.), Green Solvents, Wiley-VCH Verlag GmbH & Co. KGaA, Weinheim, 2010, pp. 203-219.
[77] R.L. Gardas, J.A.P. Coutinho, Fluid Phase Equilib. 263 (2008) 26-32.
[78] J. Jacquemin, P. Nancarrow, D.W. Rooney, M.F. Costa Gomes, P. Husson, V. Majer, A.A.H. Padua, C. Hardacre, J. Chem. Eng. Data 53 (2008) 2133-2143.
[79] J.M. Shreeve, C. Ye, Personal Communication (2010).
[80] J. Jacquemin, R. Ge, P. Nancarrow, D.W. Rooney, M.F. Costa Gomes, A.A.H. Pádua, C. Hardacre, J. Chem. Eng. Data 53 (2008) 716-726.

5.5. Influence of the pressure, temperature, cation and anion on the volumetric properties of ionic liquids: new experimental values for two salts*

*T. Regueira, L. Lugo, J. Fernández, J. Chem. Thermodynamics 58 (2013) 440–448. http://www.sciencedirect.com/science/article/pii/S0021961412003837

Abstract

Experimental densities of two ionic liquids (ILs), 1-butyl-1-methylpyrrolidinium bis(trifluoromethylsulfonyl)imide ([C_4C_1Pyrr][NTf_2]) and 1-(2-Methoxyethyl)-1-methyl-pyrrolidinium tris(pentafluoroethyl)trifluorophosphate ([$C_1OC_2C_1$Pyrr][$(C_2F_5)_3PF_3$]), were measured in a broad temperature and pressure range, i.e. from 278.15 K to 398.15 K and up to 120 MPa. The isobaric thermal expansion coefficient of the two ILs was determined from these measurements finding a non-monotonous behaviour over the entire pressure range. The obtained density values were used to analyze the prediction ability of the methods proposed by Gardas and Coutinho and by Jacquemin et al. Furthermore, the influence of the cation and anion structure on the densities and the isothermal compressibilities was analyzed, also considering literature values.

1. Introduction

Nowadays, environmental concern is leading to the development of more sustainable materials and processes. Ionic liquids (ILs) are one of the products that are attracting more attention in last years. Their main properties made them interesting for several applications, such as, electrolytic reactions, electrochemistry and electrolyte systems [1-4], battery technology [5], solvents and/or catalysts for chemical reactions and organic synthesis [6-11], functional advanced materials and material processing [12-14], biotechnology applications [15], polymer science [16], extraction, chromatography, and electrophoresis [17], lubricants [18] and heat transfer fluids [19-23], among others.

Precise determination of thermophysical properties of ILs is needed to select those with the most suitable properties for the different applications. Accurate values of liquid density are required in the design of equipment such as condensers, reboilers, liquid/liquid two phase mixer–settler units, calculation of tower heights, material and energy balances involving liquids as well as the measurements of phase equilibrium, heat capacity and viscosity with several techniques. As regards heat transfer, the sensible heat and phase change storage depend on the density of the fluid [24]. Furthermore, in the lubrication area, compressibility is one of the properties that should be considered when a fluid is selected for a hydraulic application. A low compressibility translates into fast response time, high pressure transmission velocity, and low power loss. In hydraulic systems that operate at high pressure, oils with low compressibility are required to transmit power efficiently. Nevertheless, a certain amount of compressibility can be convenient because it dampens pressure surges caused by switching and thus provides a smoother operation [25,26]. Usually, the potential for energy loss and heat production of a lubricant decreases with its compressibility. Materials with high compressibility i.e. low bulk modulus act as damping

fluids [27]. Moreover, pVT values are fundamental data for developing models involving equations of state, which are the main tool used for thermophysical properties prediction.

In this work we have performed density measurements in a broad range of pressure and temperature of two ILs, 1-butyl-1-methylpyrrolidinium bis(trifluoromethylsulfonyl)imide ($[C_4C_1Pyrr][NTf_2]$) and 1-(2-Methoxyethyl)-1-methyl-pyrrolidinium tris(pentafluoroethyl)-trifluorophosphate ($[C_1OC_2C_1Pyrr][(C_2F_5)_3PF_3]$). From these experimental data we have determined their compressibility, as well as their thermal expansion coefficient. Our present results for density trends complement those found previously by several researchers [28-49]. Few works were published on the pressure influence on thermal expansion coefficients [41,43,50-52] of ILs. In the case of isothermal compressibilities, we are also aware of very few previous studies [53,54].

One of the important aspects of ILs is their tuneability, which allows to design tailor made ILs with the proper combination of anion and cation to fulfill the specifications of certain processes and applications. Therefore, we have also analyzed our experimental values and the literature data concerning density and compressibility looking for sequences in terms of the type and side lengths of the cation and the anion.

2. Materials and methods

IL samples were kindly provided by Merck KGaA, the specified mole fraction purity for both $[C_4C_1Pyrr][NTf_2]$ and $[C_1OC_2C_1Pyrr][(C_2F_5)_3PF_3]$ is higher than 98%. Besides, the manufacturer gives the mole-fraction purities by alkalimetry after ionic exchange and electrophoresis indicated in table 1. Prior to density measurements, samples were kept under vacuum and mechanical agitation for at least 48 h in order to eliminate water and other volatile compounds. Table 1 shows the water content of IL samples determined by the Karl Fischer method using a Mettler Toledo DL32 coulometric titrator, before and after the density measurements.

TABLE 1. Purity and water content (ppm) in IL samples prior and after the density measurements.

Ionic Liquid	Mole-fraction purity	Water content$_{IN}$	Water content$_{OUT}$
$[C_4C_1Pyrr][NTf_2]$	99.9 %[a]	57.19	233.5
$[C_1OC_2C_1Pyrr][(C_2F_5)_3PF_3]$	> 99.0%[b]	30.66	97.85

[a]Alkalimetry after ionic exchange
[b]Electrophoresis

In order to avoid contact between the ILs and the atmosphere, they were transferred to the densimeter through a Hamilton valve, HV Standard PTFE, connected to a glass syringe. Density measurements were performed up to 120 MPa and between 278.15 K and 398.15 K in an automated vibrating tube densimeter Anton Paar HPM. This densimeter consists of two different

units, the measurement cell, named DMA HPM, and the electronic processing unit, named mPDS 2000V3. Temperature Pt100 probe was calibrated with an uncertainty of 0.02K whereas pressure transducer with an uncertainty of 0.02 MPa. Calibration of the densimeter was performed according to the method described by Lagourette et al. [55] and modified by Comuñas et al. [56] Milli-Q water was employed as reference fluid in the temperature range from 278.15 to 348.15 K and pressures up to 120 MPa and also at T = 373.15 K and T = 398.15 K for pressures higher than 0.1 MPa. Additionally, n-decane was used as reference fluid at T = 373.15 K and T = 398.15 K at 0.1 MPa. More details of the equipment have been previously reported.[54,57,58]

Because of the high viscosity of both ILs (98.7 and 148 mPa·s at 293.15 K for $[C_4C_1Pyrr][NTf_2]$ and $[C_1OC_2C_1Pyrr][(C_2F_5)_3PF_3]$, respectively), a correction factor for the DMA HPM model has been considered. This factor accounts the effect of the sample viscosity on the density measurements on mechanical oscillator densimeters, and is given by the following equation [57,59]:

$$\frac{\rho_{HPM}-\rho}{\rho_{\mathrm{HPM}}}=\left[0.4482\sqrt{\eta/mPa{\cdot}s}-0.1627\right]10^{-4} \quad (1)$$

where ρ_{HPM} represents the density value obtained from the densimeter calibration and the measured periods, ρ is the "corrected" density value due to the effect of viscosity, and η is the dynamic viscosity of the sample. This equation is valid for viscosities lower than 289 mPa·s. For viscosities higher than 289 mPa·s the relative correction factor, i.e. $\Delta\rho/\rho$, becomes constant, taking the value of $7.5{\cdot}10^{-4}$. For this purpose, we have used viscosity values of $[C_4C_1Pyrr][NTf_2]$ and $[C_1OC_2C_1Pyrr][(C_2F_5)_3PF_3]$ in broad temperature and pressure ranges, measured for both ILs with a falling body viscometer in our laboratory [60,61] and also for $[C_4C_1Pyrr][NTf_2]$ by Harris et al.[62].

The expanded (k=2) uncertainty of the density measurements with this technique was rigorously calculated by Segovia et al. [57] finding that it is $0.7{\cdot}10^{-3}$ g·cm^{-3} for temperatures below T = 373.15 K, $5{\cdot}10^{-3}$ g·cm^{-3} at T = (373.15 and 398.15) K and p = 0.1 MPa, and $3{\cdot}10^{-3}$ g·cm^{-3} in other cases, i.e. at $T \geq 373.15$ K and $p > 0.1$ MPa. For the ILs studied, these uncertainties correspond around to 0.05%, 0.4% and 0.2%, respectively.

3. Results and discussion

3.1. Experimental results

Direct experimental density values are reported in table S1 of the supporting information, whereas those obtained after applying the viscosity correction are presented in tables 2 and 3 for the two ILs studied in this work. Mean relative deviations between both density values, i.e. with

and without viscosity correction, are 0.03% and 0.04% for $[C_4C_1Pyrr][NTf_2]$ and $[C_1OC_2C_1Pyrr][(C_2F_5)_3PF_3]$, respectively. Furthermore, in figure 1, density values of the ILs are plotted against pressure at 278.15 and 398.15 K. Density values of $[C_4C_1Pyrr][NTf_2]$ are around 17% lower than those of $[C_1OC_2C_1Pyrr][(C_2F_5)_3PF_3]$ at the same temperature and pressure conditions.

TABLE 2. Corrected density values[a], according to equation (1), for $[C_4C_1Pyrr][NTf_2]$ at different pressures[b] and temperatures[c].

	T /K						
p /MPa	278.15 K	298.15 K	313.15 K	333.15 K	348.15 K	373.15 K	398.15 K
0.1	1.4142	1.3947	1.3813	1.3637	1.3509	1.3303	1.3076
1	1.4148	1.3953	1.3819	1.3644	1.3516	1.3307	1.3086
10	1.4205	1.4012	1.3884	1.3713	1.3589	1.3385	1.3162
20	1.4269	1.4078	1.3954	1.3787	1.3667	1.3468	1.3252
40	1.4387	1.4200	1.4082	1.3923	1.3808	1.3620	1.3416
60	1.4496	1.4313	1.4202	1.4048	1.3937	1.3756	1.3561
80	1.4597	1.4419	1.4310	1.4162	1.4055	1.3881	1.3695
100	1.4691	1.4518	1.4411	1.4269	1.4165	1.3996	1.3818
120	1.4780	1.4618	1.4510	1.4371	1.4271	1.4106	1.3932

[a]Density uncertainties: $0.7 \cdot 10^{-3}$ g·cm^{-3} for temperatures below T = 373.15 K, $5 \cdot 10^{-3}$ g·cm^{-3} at T = (373.15 and 398.15) K and p = 0.1 MPa, and $3 \cdot 10^{-3}$ g·cm^{-3} in other cases, i.e. at $T \geq 373.15$ K and $p > 0.1$ MPa.
[b]Pressure uncertainty: 0.02 MPa
[c]Temperature uncertainty: 0.02 K

TABLE 3. Corrected density values[a], according to equation (1), for $[C_1OC_2C_1Pyrr][(C_2F_5)_3PF_3]$ at different pressures[b] and temperatures[c].

	T /K	□					
p /MPa	278.15 K	298.15 K	313.15 K	333.15 K	348.15 K	373.15 K	398.15 K
0.1	1.6533	1.6301	1.6135	1.5918	1.5755	1.5491	1.5224
1	1.6541	1.6309	1.6144	1.5927	1.5765	1.5497	1.5226
10	1.6611	1.6387	1.6227	1.6016	1.5859	1.5600	1.5338
20	1.6687	1.6470	1.6315	1.6109	1.5957	1.5706	1.5453
40	1.6832	1.6622	1.6474	1.6278	1.6135	1.5899	1.5661
60	1.6965	1.6761	1.6620	1.6434	1.6297	1.6071	1.5843
80	1.7089	1.6891	1.6753	1.6575	1.6444	1.6226	1.6007
100	1.7202	1.7015	1.6879	1.6706	1.6580	1.6369	1.6159
120	1.7305	1.7129	1.6996	1.6826	1.6704	1.6502	1.6299

[a]Density uncertainties: $0.7 \cdot 10^{-3}$ g·cm^{-3} for temperatures below T = 373.15 K, $5 \cdot 10^{-3}$ g·cm^{-3} at T = (373.15 and 398.15) K and p = 0.1 MPa, and $3 \cdot 10^{-3}$ g·cm^{-3} in other cases, i.e. at $T \geq 373.15$ K and $p > 0.1$ MPa.
[b]Pressure uncertainty: 0.02 MPa
[c]Temperature uncertainty: 0.02 K

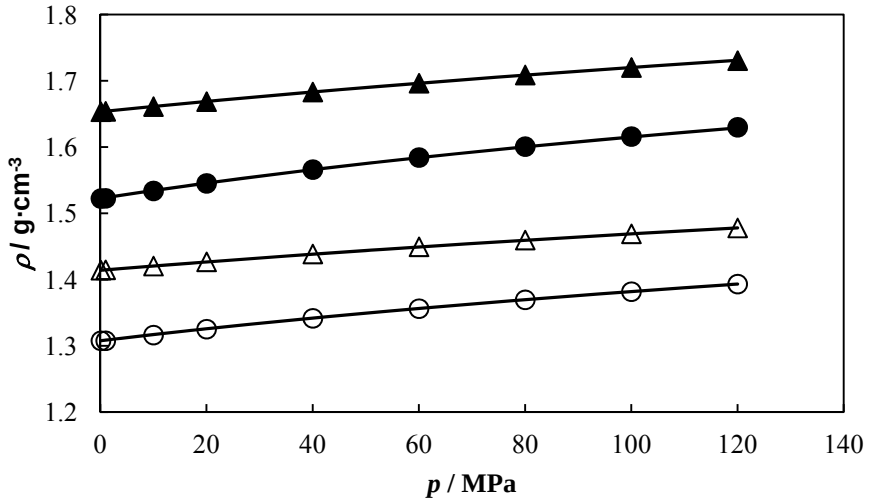

FIGURE 1. Corrected density values of $[C_4C_1Pyrr][NTf_2]$ (empty symbols) and $[C_1OC_2C_1Pyrr][(C_2F_5)_3PF_3]$ (filled symbols) as a function of pressure. T = 278.15 K (▲, △) and T = 398.15 K (●, ○). Tammann-Tait correlation (—).

The following modified Tammann-Tait equation was employed to correlate experimental density values with temperature and pressure:

$$\rho(T/\mathrm{K}, p/\mathrm{MPa}) = \frac{\rho(T/\mathrm{K}, 0.1\mathrm{MPa})}{1 - C \cdot ln\left(\frac{B(T/\mathrm{K}) + p/\mathrm{MPa}}{B(T/\mathrm{K}) + 0.1\mathrm{MPa}}\right)} \tag{2}$$

where $\rho(T/\mathrm{K}, 0.1\mathrm{MPa})$ is the density as a function of temperature at a reference pressure of 0.1 MPa, following this polynomial expression:

$$\rho(T/\mathrm{K}, 0.1\mathrm{MPa}) = \sum_{i=0}^{m} A_i (T/\mathrm{K})^i \tag{3}$$

The parameters A_i were determined with the experimental ρ values at atmospheric pressure, their number being determined by using an F-test with a 0.05 of significance level for both ILs data series.

C is a parameter independent of temperature and pressure and *B(T)* is a parameter depending on temperature as a polynomial function:

$$B(T/\mathrm{K}) = \sum_{j=0}^{n} B_j (T/\mathrm{K})^j \tag{4}$$

The parameters B_i and *C* were determined with the experimental ρ values at pressures higher than 0.1 MPa. All the parameters obtained for Tammann-Tait correlation are presented in table 4, along with standard deviations, σ, for $\rho(T/\mathrm{K}, 0.1\mathrm{MPa})$ and σ^* for $\rho(T/\mathrm{K}, p/\mathrm{MPa})$.

As it can be observed, standard deviations, σ^*, of $1 \cdot 10^{-4}$ and $3 \cdot 10^{-4}$ g·cm^{-3}, obtained respectively for $[C_4C_1Pyrr][NTf_2]$ and $[C_1OC_2C_1Pyrr][(C_2F_5)_3PF_3]$, are lower than the density uncertainty.

TABLE 4. A_i, B_i, C and standard deviations, σ and σ* from Tammann-Tait equation.

	$[C_4C_1Pyrr][NTf_2]$	$[C_1OC_2C_1Pyrr][(C_2F_5)_3PF_3]$
A_0 /g·cm^{-3}	2.1752	2.1948
$-10^3 \cdot A_1$ /g·cm^{-3}·K^{-1}	5.4202	3.1102
$10^5 \cdot A_2$ /g·cm^{-3}·K^{-2}	1.3152	0.56022
$-10^8 \cdot A_3$ /g·cm^{-3}·K^{-3}	1.2585	0.51037
$10^4 \cdot \sigma$ /g·cm^{-3}	2.7	1.2
$10^2 \cdot C$	8.9008	8.5241
B_0 /MPa	485.47	514.96
B_1 /MPa·K^{-1}	-1.3829	-1.6854
$10^3 \cdot B_2$ /MPa·K^{-2}	1.1742	1.6366
$10^4 \cdot \sigma^*$ / g·cm^{-3}	1.2	2.7
10^2·Bias %	0.2	-0.2
10^2·AAD%	1.5	1.5

In figure 2, corrected density values of $[C_4C_1Pyrr][NTf_2]$ are compared with literature values at atmospheric pressure and different temperatures. The Absolute Average Deviations, AADs%, with data from Jacquemin et al. [63], Gaciño et al. [37], Pereiro et al. [64] and Kolbeck et al. [38] as well as from Harris et al. [62] for three samples are within the combined estimated expanded uncertainties, whereas the AADs% with Deng et al. [65] and with Shamsipur et al. [66] are slightly higher. Moreover, AADs% from densities of Katsuta et al. [67], Zarrougui et al. [68] and Gardas et al. [69] are considerably higher than the estimated combined uncertainty. In figure 3, we have plotted the relative density deviations with literature data [63,69] for $[C_4C_1Pyrr][NTf_2]$ up to 40 MPa at different temperatures, finding both positive and negative values. The AAD% with data from Jacquemin et al. [63] is 0.10%, which is within the combined uncertainty whereas that with data from Gardas et al. [69] is 0.54%. Regarding the $[C_1OC_2C_1Pyrr][(C_2F_5)_3PF_3]$ IL, as far as we know, there are only density values at atmospheric pressure previously measured in our laboratory by using an Anton Paar Stabinger SVM 3000 [37], which agree well with the present measurements with an AAD% of 0.03 %.

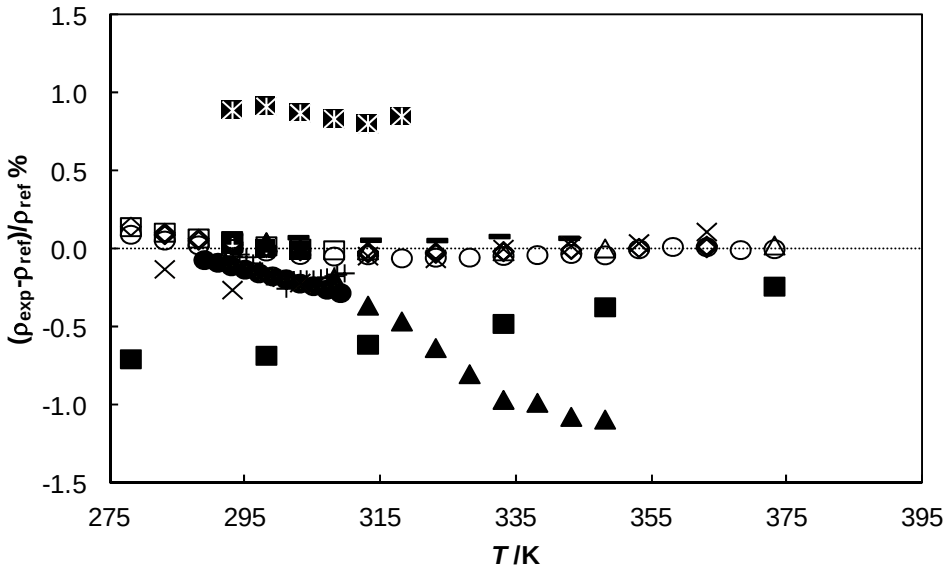

FIGURE 2. Percentage deviations between our density values at atmospheric pressure and literature data for $[C_4C_1Pyrr][NTf_2]$ at different temperatures. (○) Gaciño et al. [37], (▲) Kato and Gmehling[87], (╋) Pereiro et al.[64], (+) Katsuta et al.[88], (□) Kolbeck et al. [38], (◇) Harris et al. [62], (✳) Zarrougui et al. [68], (■) Gardas et al.[69], (△) Jacquemin et al.[63], (●) Kumełan et al.[89], (–) Deng et al.[65], (×) Shamsipur et al.[66].

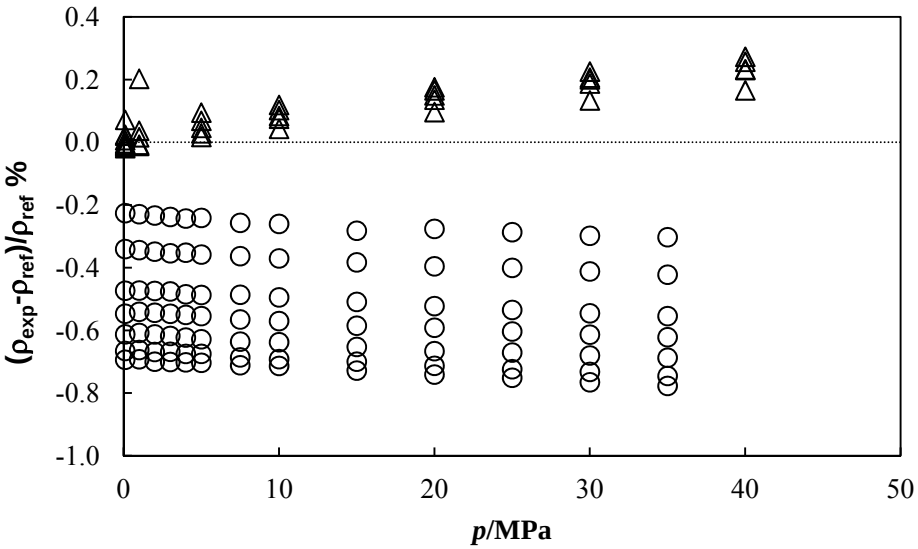

FIGURE 3. Percentage deviations between our density values and literature data for $[C_4C_1Pyrr][NTf_2]$ at high pressures and different temperatures. (△) Jacquemin et al.[63], (○) Gardas et al.[69].

3.2. Influence of the cation and anion on the IL density

Several authors have previously analyzed the trend of density of several ILs with the type of cation, anion and their alkyl chain lengths [28-49]. As a example, in figure 4 we have plotted our density values along with literature values for ILs with the $[NTf_2]^-$ anion at 313.15 K and atmospheric pressure. The same sequence is obtained at 298.15 K. It can be observed that density decreases with the increase of both imidazolium and pyridinium alkyl chain lengths, as it is usual for ILs [38]. The same influence of the alkyl chain length on the density was also found for polar molecular compounds (without hydrogen bonds) with a polar group like ester, ketone or

organic carbonate [70-72]. Thus, in polar molecular liquids as for ILs, increasing dispersive interactions between the aliphatic carbon chains with increasing chain length lead to lower dense packing. Kolbeck et al. [38] have indicated that increasing the chain length, the nonpolar regions grow occupying more space, i.e. a lower overall IL density. In ILs the dispersive interactions also increase with chain length, resulting in a nanostructural separation in polar and nonpolar domains [73]. The packing of the chains within the nonpolar domains of ILs is limited by the existence of the polar regions due to the charged heads groups covalently attached to the chains [38]. Palomar et al. [35] infer that the densities of imidazolium ILs decrease with the cation alkyl chain length because the increase of the molecular weight is less important than the increment produced in the molar volume.

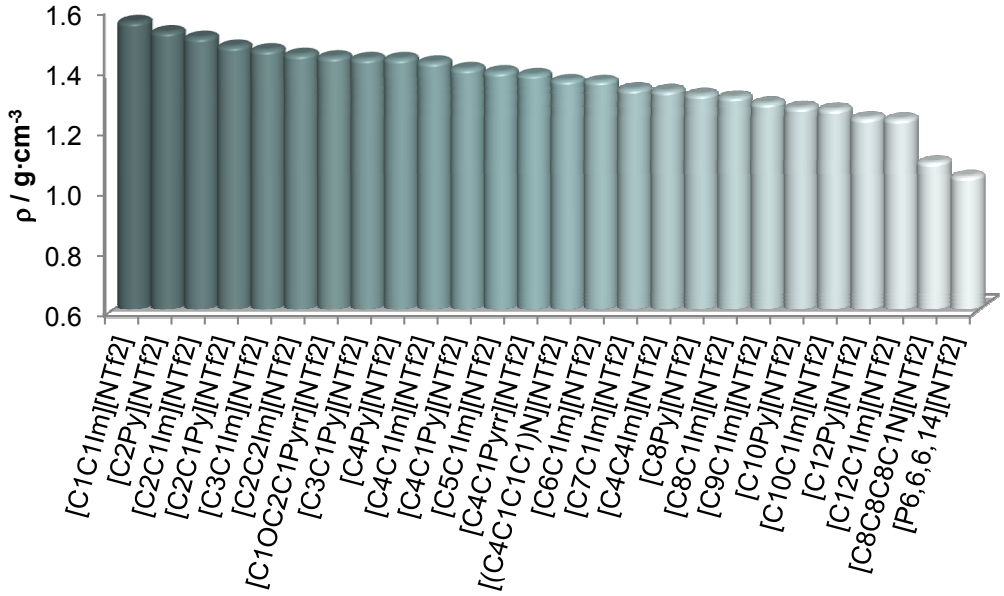

FIGURE 4. Density values for ILs containing the anion $[NTf_2]^-$ at 313.15 K and atmospheric pressure. $[C_1C_1Im][NTf_2]$ [90], $[C_2Py][NTf_2]$ [91], $[C_2C_1Im][NTf_2]$ [77], $[C_2C_1Py][NTf_2]$ [92], $[C_3C_1Im][NTf_2]$ [93], $[C_2C_2Im][NTf_2]$ [94], $[C_1OC_2C_1Pyrr][NTf_2]$ [54], $[C_3C_1Py][NTf_2]$ [92], $[C_4Py][NTf_2]$[44], $[C_4C_1Im][NTf_2]$ [95], $[C_4C_1Py][NTf_2]$ [96], $[C_5C_1Im][NTf_2]$ [93], $[C_4C_1Pyrr][NTf_2]$ (this work), $[(C_4C_1C_1C_1)N][NTf_2]$ [97], $[C_6C_1Im][NTf_2]$ [78], $[C_7C_1Im][NTf_2]$ [77], $[C_4C_4Im][NTf_2]$ [98], $[C_8Py][NTf_2]$ [44], $[C_8C_1Im][NTf_2]$ [77], $[C_9C_1Im][NTf_2]$ [43], $[C_{10}Py][NTf_2]$ [44], $[C_{10}C_1Im][NTf_2]$ [94], $[C_{12}Py][NTf_2]$ [44], $[C_{12}C_1Im][NTf_2]$ [43], $[C_8C_8C_8C_1N][NTf_2]$ [32], $[P_{6,6,6,14}][NTf_2]$ [97].

Besides, for the ILs with $[NTf_2]^-$ anion and $[C_4C_1Py]^+$, $[C_4C_1Pyrr]^+$ or $[C_4C_1Im]^+$ cations, the density follows the sequence imidazolium ≈ pyridinium > pyrrolidinium whereas the sequence for both, the molecular weight and the cation volume is $[C_4C_1Py]^+$>$[C_4C_1Pyrr]^+$>$[C_4C_1Im]^+$. When comparing the pyrrolidinium and imidazolium ILs, the molecular radius decreases and the density increases because the length of a double bond is shorter than that of a single bond. The density sequence can also be explained by the planarization of the cation due to the formation of conjugated structures (as imidazolium and pyridinium), and the resulting decrease in excluded volume due to packing and stacking might

lead to an increase in the density of the ILs [38,48]. In this way, Seki et al.[48] explain that ILs with a conjugated ring structure cation (imidazolium and pyrazolium) have a higher density than those with a quaternary-ammonium (chainlike or cyclic)-cation. Thus, for the ILs with $[NTf_2]^-$ anion (figure 4), the one with lowest density is that with a quaternary-phosphonium: trihexyl(tetradecyl)phosphonium ($[P_{6,6,6,14}]^+$) cation.

Sánchez et al.[39] have found for thiocyanate ILs a similar density trend than that of $[NTf_2]^-$ ILs, but for dicyanamide ILs found a different sequence: pyrrolidinium > imidazolium > pyridinium. These authors claim that the change in the density trends with the cation type is linked to the kind of atomic associations that a given cation exerts on the counteranion.

Regarding the behaviour of density as a function of the anion taking into account literature density data, it can be observed in figure 5 that for the same cation, $[C_4C_1Im]^+$, at 313.15 K and atmospheric pressure, density decreases according to the following trend: $[(C_2F_5SO_2)_2N]^-$ > $[NTf_2]^-$ > $[PF_6]^-$ > $[CF_3SO_3]^-$ > $[ClO_4]^-$ > $[CF_3CO_2]^-$ > $[C_1SO_4]^-$ > $[BF_4]^-$ > $[C_1(OC_2)_2SO_4]^-$ > $[NO_3]^-$ > $[C_8SO_4]^-$ > $[N(CN)_2]^-$ > $[CH_3CO_2]^-$ > $[C_4C_4PO_4]^-$ > $[C(CN)_3]^-$. This trend agrees well with those previously proposed by Tariq et al. [31], Tokuda et al. [28], Gaciño et al. [37], Kolbeck et al. [38], Muhammad et al. [45], Guerrero et al. [46], Seki et al. [48] and Palomar et al. [35].

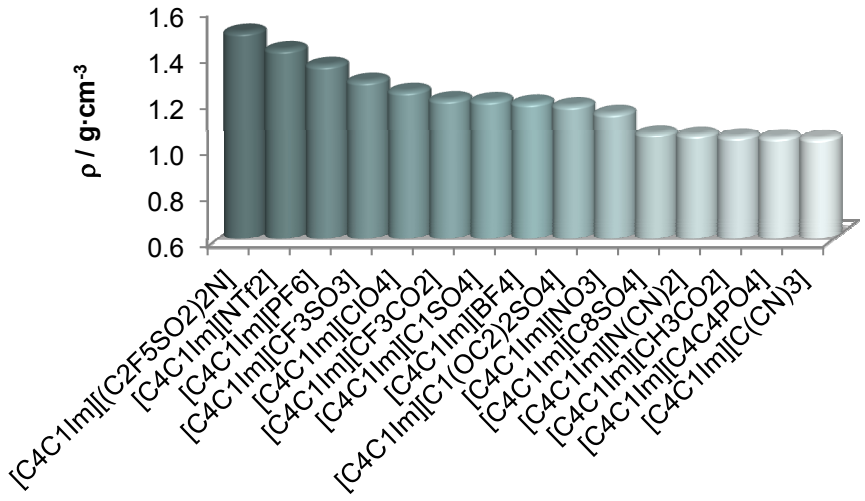

FIGURE 5. Density values for $[C_4C_1Im]^+$ ILs at 313.15 K and atmospheric pressure. $[C_4C_1Im][(C_2F_5SO_2)_2N]$ [99], $[C_4C_1Im][NTf_2]$ [95], $[C_4C_1Im][PF_6]$ [34], $[C_4C_1Im][CF_3SO_3]$ [100], $[C_4C_1Im][ClO_4]$ [101], $[C_4C_1Im][CF_3CO_2]$ [99], $[C_4C_1Im][C_1SO_4]$ [102], $[C_4C_1Im][BF_4]$ [103], $[C_4C_1Im][C_1(OC_2)_2SO_4]$ [104], $[C_4C_1Im][NO_3]$ [105], $[C_4C_1Im][C_8SO_4]$ [106], $[C_4C_1Im][N(CN)_2]$ [33], $[C_4C_1Im][CH_3CO_2]$ [31], $[C_4C_1Im][C_4C_4PO_4]$ [107], $[C_4C_1Im][C(CN)_3]$ [77].

3.3. Comparison of the densities with the predictions of group contribution models

We have used our experimental density values to analyze the group contribution method proposed by Gardas and Coutinho [74] for the prediction of the densities in broad ranges of temperature and pressure. This method is based on the following equation:

$$\rho / kg{\cdot}m^{-3} = \frac{MW_i / kg{\cdot}mol^{-1}}{NV_0(a + bT / K + cp / MPa)} \quad (5)$$

where, N is the Avogadro constant, MW_i is the molar mass, V_0 is the molecular volume at the reference temperature (T_0) and pressure (p_0) in $m^3{\cdot}molecule^{-1}$ of the IL and a, b and c are fitting coefficients. Molecular volumes employed for calculation are presented in table 5.

TABLE 5. Molecular volumes ($Å^3{\cdot}molecule^{-1}$) employed in the Gardas-Coutinho density prediction.

Ionic Liquid	Cation Volume	Anion Volume	References
$[C_4C_1Pyrr][NTf_2]$	253	248	Gardas and Coutinho [74]
$[C_1OC_2C_1Pyrr][(C_2F_5)_3PF_3]$	235	360	Shreeve and Ye [86]

Equation 5, according to these authors [74], covers the density range between 0.9867 and 1.5471 $g{\cdot}cm^{-3}$, in a temperature range between 273.15 and 393.15 K and a pressure range between 0.10 and 100 MPa. In this range the coefficient values are a = $8.005{\cdot}10^{-1}$, b = $6.652{\cdot}10^{-4}$ K^{-1} and c = $-5.919{\cdot}10^{-4}$ MPa^{-1}, at 95% level of confidence. The AAD% obtained among the predicted and experimental density values, considering our whole experimental pT range is 1.0% for $[C_4C_1Pyrr][NTf_2]$ and 1.5% for $[C_1OC_2C_1Pyrr][(C_2F_5)_3PF_3]$. The maximum deviations are obtained at T = 278.15 K and p = 120 MPa for both ILs, being 3.6 % and 3.9% for $[C_4C_1Pyrr][NTf_2]$ and $[C_1OC_2C_1Pyrr][(C_2F_5)_3PF_3]$, respectively. The highest deviations with this prediction method for the densities of $[C_2C_1Im][C_2SO_4]$ and $[C_1OC_2C_1Pyrr][NTf_2]$ were also previously found [54] at these extreme pT conditions. The observed deviations are in good agreement with those reported by Gardas and Coutinho for pyrrolidinium based ILs, between 0.41% and 1.5 %.

Jacquemin et al. [63] have also proposed a method for predicting density of ILs from 298.15 K to 423.15 K and up to 207 MPa. It is a group contribution method, whose parameters were calculated using more than 5080 available density data. Thus, these authors [63] assume that the IL molar volume result from the addition of the cation and anion molar volumes and they fit the effective molar volumes by means of the following equation:

$$V_\alpha^*(\delta T, p, G, H) = \frac{V_\alpha^*(\delta T, 0.1\,MPa)}{1 - G{\cdot}ln\left(\frac{H(\delta T) + p}{H(\delta T) + 0.1\,MPa}\right)} \quad (6)$$

where α stands for the cation or anion constituting an IL or for an extra $-CH_2-$ group in the alkyl chain length of an 1-alkyl-3-methylimidazolium based IL, $V_\alpha^*(\delta T, p_{ref})$ is the reference effective molar volume and $H(\delta T)$ is a second-order polynomial. Coefficients of this method were

obtained by Jacquemin et al.[63] by fitting the density data of 38 ILs composed by 9 different anions and 15 different cations.

Prediction of the density values of $[C_1OC_2C_1Pyrr][(C_2F_5)_3PF_3]$ was not possible with Jacquemin et al. [63] method because authors do not provide parameters for both ions. For $[C_4C_1Pyrr][NTf_2]$, in the temperature range from 298.15 K to 398.15 K and in the whole pressure range, this method predicts the densities with an AAD% of 0.46% and a maximum deviation of 1.5 % (at 120 MPa and 398.15 K). Hence, the Jacquemin et al. predictions which use seven parameters are significantly better than those of Gardas and Coutinho who employ only three parameters.

3.4. Derived Properties

Density derived properties can be obtained from the modified Tammann-Tait equation by simple analytical derivation. Isothermal compressibility, κ_T, shows system modification when it is subjected to pressure changes at constant temperature. It is defined by the following expression:

$$\kappa_T(T,p) = \frac{1}{\rho}\left(\frac{\partial \rho}{\partial p}\right)_T \tag{7}$$

Isothermal compressibility values of $[C_4C_1Pyrr][NTf_2]$ and $[C_1OC_2C_1Pyrr][(C_2F_5)_3PF_3]$ are presented in table 6, whereas in figure 6 they are plotted against pressure for different temperatures. In the whole studied temperature and pressure range, κ_T values of $[C_4C_1Pyrr][NTf_2]$ are in average 6% lower than those of $[C_1OC_2C_1Pyrr][(C_2F_5)_3PF_3]$. We have also indicated in figure 6 the κ_T values obtained by differentiation from Gardas and Coutinho correlation (equation 5), which are fluid independent and also the values obtained by differentiation from the Jacquemin et al method (equation 6) for the IL $[C_4C_1Pyrr][NTf_2]$. The simplicity of equation 5 does not permit to describe both the pressure decrease and the temperature increase of the isothermal compressibility whereas the Jacquemin et al. method underestimates its pressure dependence.

Our κ_T values were also compared with those published by Jacquemin et al. [63] for $[C_4C_1Pyrr][NTf_2]$ at 298.15 K and 373.15 K up to 40 MPa obtaining an AAD% of 10.7% and also with those reported by Gardas et al. [69] from 293.15 K to 393.15 K up to 35 MPa finding an AAD% of 4.3%. The compressibility data shown in the present work are between those from Jacquemin et al. [63] and those from Gardas et al. [69], as it can be observed in figure 7.

TABLE 6. Isothermal compressibility values, $10^4 \cdot \kappa_T$ (MPa^{-1}).

	***p*/MPa**						
***T*/K**	1	10	20	40	60	80	100
			[C_4C_1Pyrr][NTf_2]				
278.15	4.63	4.44	4.25	3.91	3.63	3.39	3.17
298.15	5.00	4.78	4.56	4.17	3.85	3.58	3.34
313.15	5.30	5.05	4.80	4.38	4.03	3.73	3.48
333.15	5.72	5.44	5.15	4.67	4.27	3.94	3.66
348.15	6.06	5.75	5.43	4.89	4.46	4.10	3.80
373.15	6.68	6.29	5.92	5.29	4.79	4.38	4.03
398.15	7.34	6.88	6.43	5.70	5.12	4.65	4.27
			[$C_1OC_2C_1$Pyrr][$(C_2F_5)_3PF_3$]				
278.15	4.89	4.79	4.67	4.45	4.07	3.74	3.47
298.15	5.35	5.09	4.82	4.38	4.01	3.70	3.44
313.15	5.72	5.42	5.12	4.62	4.21	3.87	3.59
333.15	6.24	5.89	5.54	4.96	4.49	4.11	3.79
348.15	6.66	6.26	5.87	5.22	4.71	4.29	3.95
373.15	7.39	6.90	6.43	5.66	5.07	4.59	4.20
398.15	8.14	7.55	6.99	6.09	5.41	4.87	4.43

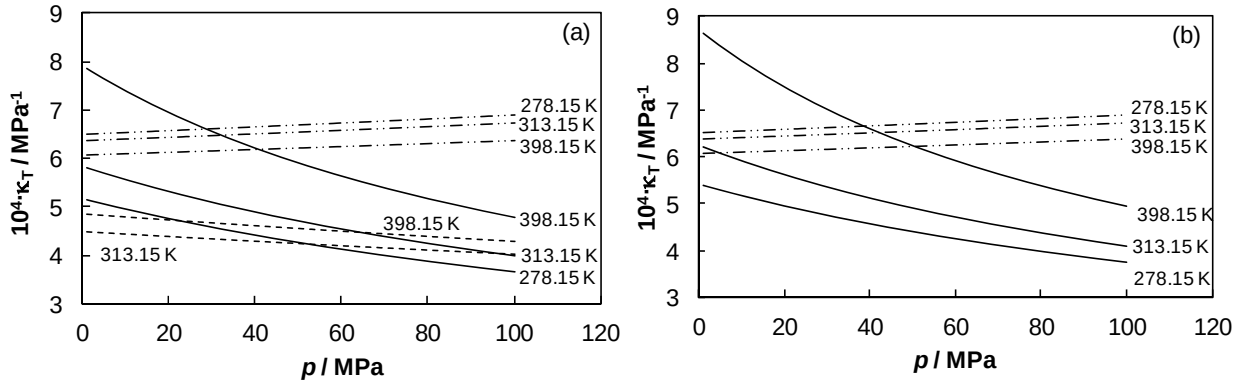

FIGURE 6. Isothermal compressibility values, κ_T, of (a) [C_4C_1Pyrr][NTf_2] and (b) [$C_1OC_2C_1$Pyrr][$(C_2F_5)_3PF_3$]. (—) represent the κ_T values obtained in this work, (---) are the κ_T values obtained from Jacquemin et al [63] model and (–··–) represents κ_T values obtained from Gardas and Coutinho [74] model.

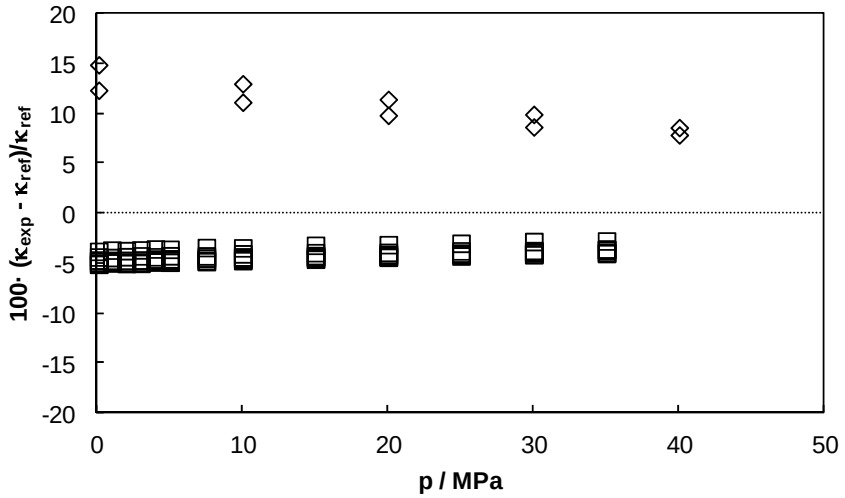

FIGURE 7. Comparison between the κ_T values of this work and those of literature as a function of pressure for different temperatures. (◇) Jacquemin et al. [63] and (□) Gardas et al. [69]

Moreover, we have performed a search on the published isothermal compressibility values of different ILs. We present in figure 8 the κ_T values of ILs containing $[NTf_2]^-$ anion to evaluate the influence of the cation in this property. It can be observed that, in general, κ_T increases with the alkyl chain length of the cation and is slightly higher for the ILs with imidazolium cation than for the pyrrolidinium ILs. For $[C_2C_1Im][NTf_2]$ and $[C_6C_1Im][NTf_2]$ the results from Jacquemin et al.[75] and Gomes de Azevedo et al. [76] follow this general trend but not the data of Gardas et al. [77] and Esperança et al. [78]. Królikowska and Hofman [53] have also found that ILs with longer alkyl chain length and greater molar volumes are generally more compressible.

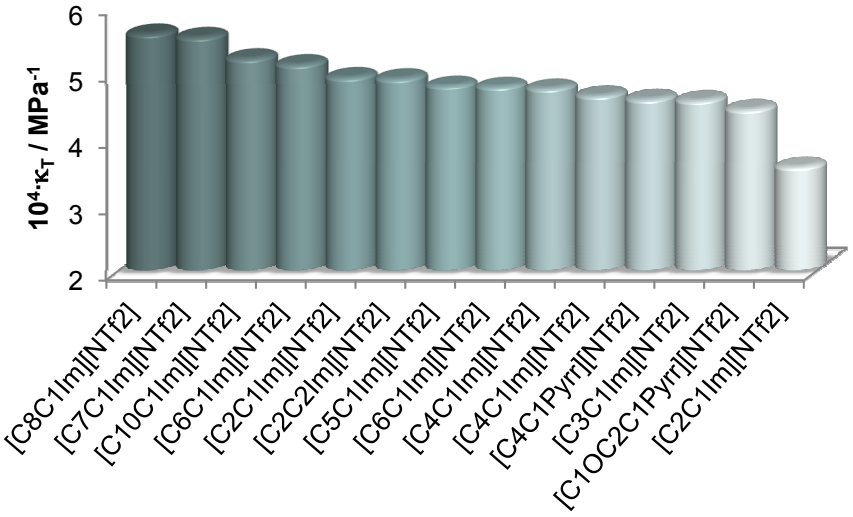

FIGURE 8. Isothermal compressibility values, κ_T, of $[NTf_2]^-$ ILs at 313.15 K and 30 MPa. $[C_8C_1Im][NTf_2]$ [77], $[C_7C_1Im][NTf_2]$ [77], $[C_{10}C_1Im][NTf_2]$ [94], $[C_6C_1Im][NTf_2]$ [76,78], $[C_2C_1Im][NTf_2]$ [75,77], $[C_2C_2Im][NTf_2]$ [94], $[C_5C_1Im][NTf_2]$ [93], $[C_4C_1Im][NTf_2]$ [75,76], $[C_4C_1Pyrr][NTf_2]$ (this work), $[C_3C_1Im][NTf_2]$ [93] and $[C_1OC_2C_1Pyrr][NTf_2]$ [54].

Furthermore, in figure 9 it can be observed the κ_T of several ILs containing $[C_2C_1Im]^+$ cation. We should point out that the results for $[C_2C_1Im][NTf_2]$ and $[C_2C_1Im][BF_4]$ from Gardas et al.[77] do not agree with those of Jacquemin et al. [75] and Taguchi et al. [79] As a general sequence for κ_T of these ILs, taking into account also the trend for $[C_4C_1Im]^+$ ILs, we propose: $[NTf_2]^- > [C(CN)_3]^- > [C_2SO_4]^- > [C_1SO_4]^- > [PF_6]^- \approx [BF_4]^-$. The high compressibility of the $[NTf_2]^-$ anion can be due to the fact that this anion is highly flexible and explores a number of conformations as opposed to $[PF_6]^-$ and $[BF_4]^-$ that are conformationally rigid [80].

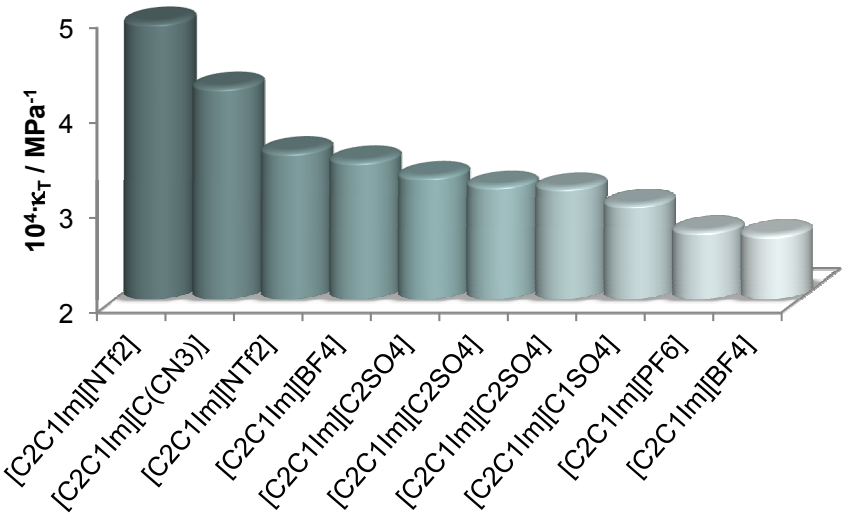

FIGURE 9. Isothermal compressibility values, κ_T, of $[C_2C_1Im]^+$ ILs at 313.15 K and 30 MPa. $[C_2C_1Im][NTf_2]$ [75,77], $[C_2C_1Im][C(CN_3)]$ [77], $[C_2C_1Im][BF_4]$ [77,79], $[C_2C_1Im][C_2SO_4]$ [54,94,108], $[C_2C_1Im][C_1SO_4]$ [94], $[C_2C_1Im][PF_6]$ [79].

Considering figures 8 and 9, it is observed that at 313.15 K and 30 MPa compressibility varies from $5.6 \cdot 10^{-4}$ MPa^{-1} for $[C_8C_1Im][NTf_2]$ to $2.7 \cdot 10^{-4}$ MPa^{-1} for $[C_2C_1Im][BF_4]$, whereas those of the reference lubricants for hydraulic, gears and two stroke engines [26] at the same temperature and pressure conditions vary between $5.8 \cdot 10^{-4}$ MPa^{-1} and 5.2 10^{-4} MPa^{-1}. Therefore among these ILs it is possible to find several of them that present lower compressibilites than those of the reference lubricants [26].

Isobaric thermal expansion coefficient, α_p, indicates the fractional change in density with temperature at constant pressure and it was calculated by differentiation from Tammann-Tait equation by using the parameters from Table 4, according its definition:

$$\alpha_P(T,p) = -\frac{1}{\rho}\left(\frac{\partial \rho}{\partial T}\right)_P \tag{8}$$

The isobaric thermal expansion coefficients for both ILs are presented in table 7 and its temperature dependence is gathered in figure 10 for different pressures. It can be observed a non-monotonous behaviour for both ILs with temperature in all the isobars. The existence of the minimum agrees well with the behaviour previously explained by Troncoso et al. [81] who, using a theoretical model for ILs and molecular liquids, predict the existence of regions of positive and negative signs of the $(\partial \alpha_p / \partial T)$ depending on the temperature and pressure.

TABLE 7. Isobaric thermal expansion coefficient, $10^4 \cdot \alpha_P(K^{-1})$.

	***p*/MPa**								
***T*/K**	0.10	1.00	10.00	20.00	40.00	60.00	80.00	100.00	120.00
					$[C_4C_1Pyrr][NTf_2]$				
298.15	6.70	6.68	6.51	6.35	6.06	5.81	5.60	5.41	5.25
313.15	6.41	6.39	6.22	6.04	5.74	5.48	5.26	5.07	4.91
333.15	6.21	6.19	6.01	5.82	5.50	5.23	5.00	4.80	4.63
348.15	6.21	6.19	5.99	5.79	5.46	5.18	4.95	4.75	4.57
373.15	6.48	6.46	6.25	6.03	5.68	5.39	5.15	4.95	4.78
					$[C_1OC_2C_1Pyrr][(C_2F_5)_3PF_3]$				
298.15	6.94	6.91	6.71	6.50	6.15	5.85	5.60	5.39	5.20
313.15	6.84	6.81	6.60	6.38	6.01	5.70	5.45	5.23	5.04
333.15	6.77	6.74	6.51	6.28	5.89	5.58	5.32	5.09	4.90
348.15	6.76	6.73	6.49	6.26	5.86	5.54	5.28	5.06	4.87
373.15	6.85	6.82	6.57	6.33	5.93	5.61	5.35	5.14	4.96

The different behaviour of molecular and ILs is because ILs are more far below of their critical point than molecular liquids at ambient conditions [81]. In a previous work, we have also found this kind of behaviour for the ILs 1-ethyl-3-methylimidazolium ethylsulfate, $[C_2C_1Im][C_2SO_4]$, and 1-(2-methoxyethyl)-1-methyl-pyrrolidinium bis(trifluoromethylsulfonyl) imide, $[C_1OC_2C_1Pyrr][NTf_2]$ [54]. Moreover, this behaviour has been also found for other ILs by Hofman et al. [82], Matkowska et al. [83], Nieto de Castro et al. [84] and Tariq et al. [85]. In figure 10 it can be also observed that, in general, the temperature of the minima of the α_p(T) curves rise when the pressure increases, from 341.4 K at 0.1 MPa to 347.3 K at 120 MPa for $[C_4C_1Pyrr][NTf_2]$ and from 342.3 K at 0.1 MPa to 348.9 K at 120 MPa for $[C_1OC_2C_1Pyrr][(C_2F_5)_3PF_3]$. This is in agreement with the unusual behaviour of the isobaric thermal expansivity for ILs reported by Troncoso et al. [81].

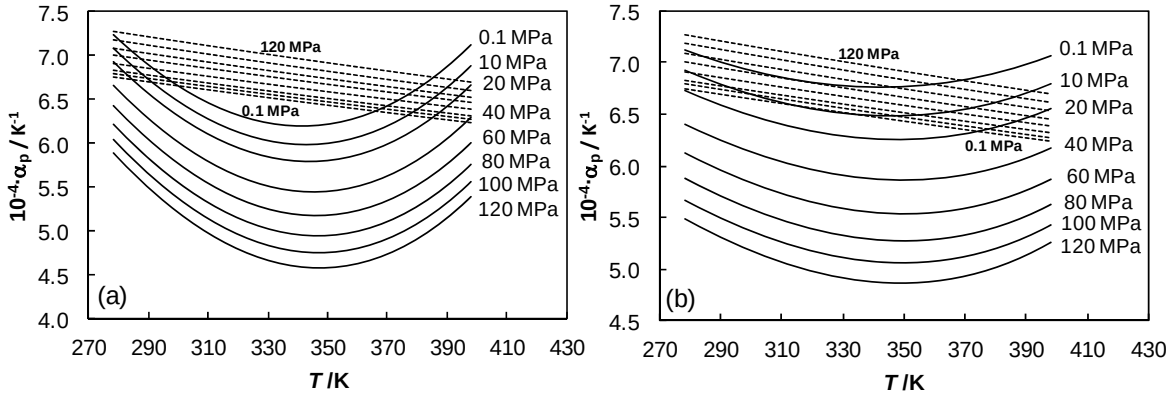

FIGURE 10. Isobaric thermal expansion coefficient, α_p, of (a) $[C_4C_1Pyrr][NTf_2]$ and (b) $[C_1OC_2C_1Pyrr][(C_2F_5)_3PF_3]$ as a function of temperature for different pressures. Dashed lines represent α_p values obtained from Gardas and Coutinho [74] density model.

We have compared our α_p values for $[C_4C_1Pyrr][NTf_2]$ at atmospheric pressure with those from the literature [37,38,62-67,69] finding an overall AAD% of 5.8%. α_p values from Gaciño et al. [37], Pereiro et al. [64] and Kolbeck et al. [38] are almost constant with temperature for this IL whereas Harris et al. [62], Deng et al. [65], Jacquemin et al. [63] and Katsuta et al. [67] show that α_p values increase with temperature. On the contrary, Gardas et al. [69], and Shamsipur et al. [66] density data lead to α_p values decreasing with temperature. Moreover, we have also compared our α_p values at high pressure (up to 40 MPa) with those of the literature [63,69] finding an AAD% of 6.2%. Regarding the IL $[C_1OC_2C_1Pyrr][(C_2F_5)_3PF_3]$, we have compared our α_p values at atmospheric pressure with those published by Gaciño et al.[37], which present also a non-monotonous behaviour and the AAD% is 1.1 %.

The α_p values by differentiation from Gardas and Coutinho method (equation 5) are also shown in figure 10. As in the case of compressibility, the predicted α_p values are fluid independent. The simplicity of equation 5 leads to a monotonically decrease of the isobaric thermal expansion coefficient with temperature, as well as an increase with pressure, contrary to the experimental trends. On the contrary, Jacquemin et al. method (equation 6) predicts a more complex behavior with temperature (figure 11), presenting a crossing point among the isobars around 381 K. Regarding pressure dependence, experimental and predicted α_p values diminish with increasing pressure below this temperature.

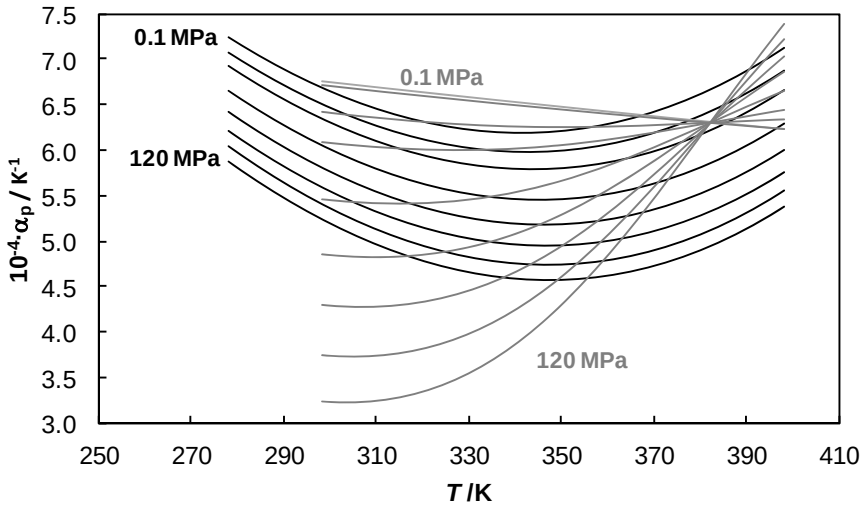

FIGURE 11. Isobaric thermal expansion coefficient, α_p, of $[C_4C_1Pyrr][NTf_2]$ as a function of temperature for different pressures. Grey lines represent α_p values obtained from Jacquemin et al. [63] density model.

Conclusions

Density values of $[C_4C_1Pyrr][NTf_2]$ are around 17% lower than those of $[C_1OC_2C_1Pyrr][(C_2F_5)_3PF_3]$. Gardas and Coutinho [74] group contribution method predicts the density with an AAD% of 0.94% and 1.4% for $[C_4C_1Pyrr][NTf_2]$ and

$[C_1OC_2C_1Pyrr][(C_2F_5)_3PF_3]$, whereas with Jacquemin et al. [63] method the density of $[C_4C_1Pyrr][NTf_2]$ is predicted with an AAD % of 0.46%.

Regarding the density dependence on structure, it was found that density decreases with the increase of the cation alkyl chain length. We have found that for the ILs containing the $[NTf_2]^-$ anion, the one with the lowest density is $[P_{6,6,6,14}][NTf_2]$. Moreover, concerning anion, density decreases according to the following trend: $[(C_2F_5SO_2)_2N]^- > [NTf_2]^- > [PF_6]^- > [CF_3SO_3]^- > [ClO_4]^- > [CF_3CO_2]^- > [C_1SO_4]^- > [BF_4]^- > [C_1(OC_2)_2SO_4]^- > [NO_3]^- > [C_8SO_4]^- > [N(CN)_2]^- > [CH_3CO_2]^- > [C_4C_4PO_4]^- > [C(CN)_3]^-$.

Isothermal compressibility values, κ_T, of $[C_4C_1Pyrr][NTf_2]$ are around 6% lower than κ_T values of $[C_1OC_2C_1Pyrr][(C_2F_5)_3PF_3]$ and κ_T increases with the alkyl chain length of the cation. For ILs with the same cation, κ_T decreases according to the following sequence $[NTf_2]^- > [C(CN)_3]^- > [C_2SO_4]^- > [C_1SO_4]^- > [PF_6]^- \approx [BF_4]^-$. Finally, it was found a non-usual behaviour of α_p values with temperature for $[C_4C_1Pyrr][NTf_2]$ and $[C_1OC_2C_1Pyrr][(C_2F_5)_3PF_3]$ over all the pressure range.

Supplementary information

This supplementary information includes the direct experimental density values of $[C_4C_1Pyrr][NTf_2]$ and $[C_1OC_2C_1Pyrr][(C_2F_5)_3PF_3]$.

TABLE S1. Direct experimental density values[a] ($g \cdot cm^{-3}$) for $[C_4C_1Pyrr][NTf_2]$ at different pressures[b] and temperatures[c].

	T /K						
p /MPa	278.15 K	298.15 K	313.15 K	333.15 K	348.15 K	373.15 K	398.15 K
0.1	1.4151	1.3952	1.3816	1.3640	1.3511	1.3305	1.3078
1	1.4157	1.3958	1.3823	1.3647	1.3518	1.3308	1.3087
10	1.4215	1.4018	1.3888	1.3716	1.3591	1.3386	1.3164
20	1.4280	1.4084	1.3958	1.3790	1.3669	1.3470	1.3253
40	1.4398	1.4207	1.4087	1.3926	1.3811	1.3622	1.3417
60	1.4506	1.4322	1.4207	1.4052	1.3940	1.3759	1.3563
80	1.4608	1.4428	1.4316	1.4166	1.4059	1.3883	1.3697
100	1.4702	1.4529	1.4418	1.4274	1.4169	1.3999	1.3820
120	1.4791	1.4629	1.4518	1.4376	1.4275	1.4109	1.3935

[a]Density uncertainties: $0.7 \cdot 10^{-3}$ $g \cdot cm^{-3}$ for temperatures below T = 373.15 K, $5 \cdot 10^{-3}$ $g \cdot cm^{-3}$ at T = (373.15 and 398.15) K and p = 0.1 MPa, and $3 \cdot 10^{-3}$ $g \cdot cm^{-3}$ in other cases, i.e. at $T \geq 373.15$ K and $p > 0.1$ MPa.
[b]Pressure uncertainty: 0.02 MPa
[c]Temperature uncertainty: 0.02 K

TABLE S2. Direct experimental density values[a] ($g \cdot cm^{-3}$) for $[C_1OC_2C_1Pyrr][(C_2F_5)_3PF_3]$ at different pressures[b] and temperatures[c].

	T /K						
p /MPa	278.15 K	298.15 K	313.15 K	333.15 K	348.15 K	373.15 K	398.15 K
0.1	1.6546	1.6308	1.6140	1.5921	1.5758	1.5492	1.5225
1	1.6553	1.6316	1.6149	1.5931	1.5767	1.5499	1.5228
10	1.6623	1.6396	1.6233	1.6020	1.5862	1.5602	1.5340
20	1.6700	1.6480	1.6321	1.6113	1.5960	1.5708	1.5454
40	1.6844	1.6633	1.6481	1.6283	1.6139	1.5902	1.5663
60	1.6978	1.6773	1.6628	1.6439	1.6301	1.6073	1.5845
80	1.7101	1.6904	1.6764	1.6582	1.6449	1.6229	1.6010
100	1.7215	1.7027	1.6891	1.6714	1.6585	1.6373	1.6162
120	1.7318	1.7142	1.7009	1.6835	1.6710	1.6506	1.6302

[a]Density uncertainties: $0.7 \cdot 10^{-3}$ $g \cdot cm^{-3}$ for temperatures below $T = 373.15$ K, $5 \cdot 10^{-3}$ $g \cdot cm^{-3}$ at $T = (373.15$ and $398.15)$ K and $p = 0.1$ MPa, and $3 \cdot 10^{-3}$ $g \cdot cm^{-3}$ in other cases, i.e. at $T \geq 373.15$ K and $p > 0.1$ MPa.
[b]Pressure uncertainty: 0.02 MPa
[c]Temperature uncertainty: 0.02 K

Acknowledgments

Authors acknowledge the advice and samples provided by Dr. Uerdingen from Merck KGaA. This work was supported by Spanish Ministry of Science and Innovation and FEDER Program through CTQ2008-06498-C02-01 and CTQ2011-23925 projects. L.L and T.R. acknowledge financial support under the Ramon y Cajal Program and the FPU program, respectively.

References

[1] T. Fuchigami, S. Inagi, Electrolytic reactions. in: H. Ohno, (Ed.), Electrochemical Aspects of Ionic Liquids, John Wiley & Sons, Inc., 2011, pp. 101-127.
[2] I.M. AlNashef, M.A. Matthews, J.W. Weidner, ACS Symp. Ser. 856 (2003) 509-525.
[3] W.R. Pitner, P. Kirsch, K. Kawata, H. Shinohara, Applications of ionic liquids in electrolyte systems. in: P.T. Anastas, (Ed.), Handbook of Green Chemistry Wiley-VCH Verlag GmbH & Co. KGaA, 2010, pp. 191-201.
[4] E.A.S. Zein, J. Solid State Electrochem. 16 (2012) 775-783.
[5] A.S. Best, A.I. Bhatt, A.F. Hollenkamp, J. Electrochem. Soc. 157 (2010) A903-A911.
[6] T. Jiang, B. Han, Curr. Org. Chem. 13 (2009) 1278-1299.
[7] H. Olivier-Bourbigou, F. Hugues, NATO Sci. Ser., II 92 (2003) 67-84.
[8] H. Zhao, S.V. Malhotra, Aldrichim. Acta 35 (2002) 75-83.
[9] D. Zhao, M. Wu, Y. Kou, E. Min, Catal. Today 74 (2002) 157-189.
[10] Y. Gu, G. Li, Adv. Synth. Catal. 351 (2009) 817-847.
[11] P.J. Dyson, T.J. Geldbach, Electrochem. Soc. Interface 16 (2007) 50-53.
[12] T. Torimoto, T. Tsuda, K. Okazaki, S. Kuwabata, Adv. Mater. (Weinheim, Ger.) 22 (2010) 1196-1221.
[13] R.G. Reddy, J. Phys.: Conf. Ser. 165 (2009).
[14] O. Green, S. Grubjesic, S. Lee, M.A. Firestone, Polym. Rev. (Philadelphia, PA, U. S.) 49 (2009) 339-360.
[15] G. Quijano, A. Couvert, A. Amrane, Bioresour. Technol. 101 (2010) 8923-8930.
[16] J. Lu, F. Yan, J. Texter, Prog. Polym. Sci. 34 (2009) 431-448.
[17] C.F. Poole, Adv. Chromatogr. (Boca Raton, FL, U. S.) 45 (2007) 89-124.
[18] M.-D. Bermudez, A.-E. Jimenez, J. Sanes, F.-J. Carrion, Molecules 14 (2009) 2888-2908.
[19] V.M.E. Van, R.L. Vaughn, M. Williams, J.S. Wilkes, Thermochim. Acta 425 (2005) 181-188.

[20] V.M.E. Van, R.L. Vaughn, M. Williams, J.S. Wilkes, Proc. - Electrochem. Soc. 2002-19 (2002) 112-123.
[21] J.D. Holbrey, W.M. Reichert, R.G. Reddy, R.D. Rogers, ACS Symp. Ser. 856 (2003) 121-133.
[22] H. Machida, M. Takesue, R.L. Smith, J. Supercrit. Fluid. 60 (2011) 2-15.
[23] X. Zhang, D. Hu, Appl. Therm. Eng. 37 (2012) 129-135.
[24] M.E.V. Valkenburg, R.L. Vaughn, M. Williams, J.S. Wilkes, Thermochim. Acta 425 (2005) 181-188.
[25] L. Bronshteyn, J.H. Kreiner, Tribol. T. 42 (1999) 771–776.
[26] T. Regueira, L. Lugo, O. Fandiño, E.R. López, J. Fernández, Green Chem. 13 (2011) 1293-1302.
[27] D.G. Placek, Hydraulics. in: L.R. Rudnick, (Ed.), Synthetic Mineral Oils and Bio-Based Lubricants:Chemistry and Technology, Taylor and Francis Group, Boca Raton, FL, 2006, pp. 517-540.
[28] H. Tokuda, K. Hayamizu, K. Ishii, M.A.B.H. Susan, M. Watanabe, J. Phys. Chem. B 108 (2004) 16593-16600.
[29] H. Tokuda, K. Hayamizu, K. Ishii, M.A.B.H. Susan, M. Watanabe, J. Phys. Chem. B 109 (2005) 6103-6110.
[30] H. Tokuda, K. Ishii, M.A.B.H. Susan, S. Tsuzuki, K. Hayamizu, M. Watanabe, J. Phys. Chem. B 110 (2006) 2833-2839.
[31] M. Tariq, P.A.S. Forte, C. Gomes, C. Lopes, L.P.N. Rebelo, J. Chem. Thermodyn. 41 (2009) 790-798.
[32] A.P. Fröba, H. Kremer, A. Leipertz, J. Phys. Chem. B 112 (2008) 12420-12430.
[33] C.P. Fredlake, J.M. Crosthwaite, D.G. Hert, S.N.V.K. Aki, J.F. Brennecke, J. Chem. Eng. Data 49 (2004) 954-964.
[34] A.B. Pereiro, J.L. Legido, A. Rodríguez, J. Chem. Thermodyn. 39 (2007) 1168-1175.
[35] J. Palomar, V.R. Ferro, J. Torrecilla, F. Rodríguez, Ind. Eng. Chem. Res. 46 (2007) 6041-6048.
[36] M. Anouti, J. Jacquemin, D. Lemordant, Fluid Phase Equilibr. 297 (2010) 13-22.
[37] F.M. Gaciño, T. Regueira, L. Lugo, M.J.P. Comuñas, J. Fernández, J. Chem. Eng. Data 56 (2011) 4984-4999.
[38] C. Kolbeck, J. Lehmann, K.R.J. Lovelock, T. Cremer, N. Paape, P. Wasserscheid, A.P. Froba, F. Maier, H.P. Steinruck, J. Phys. Chem. B 114 (2010) 17025-17036.
[39] L.G. Sánchez, J.R. Espel, F. Onink, G.W. Meindersma, A.B.d. Haan, J. Chem. Eng. Data 54 (2009) 2803-2812.
[40] R.L. Gardas, M.G. Freire, P.J. Carvalho, I.M. Marrucho, I.M.A. Fonseca, A.G.M. Ferreira, J.A.P. Coutinho, J. Chem. Eng. Data 52 (2007) 80-88.
[41] M.G. Freire, A.R.R. Teles, M.A.A. Rocha, B. Schröder, C.M.S.S. Neves, P.J. Carvalho, D.V. Evtuguin, L.M.N.B.F. Santos, J.A.P. Coutinho, J. Chem. Eng. Data 56 (2011) 4813-4822.
[42] E. Gómez, N. Calvar, Á. Domínguez, E.A. Macedo, J. Chem.Thermodyn. 42 (2010) 1324-1329.
[43] M. Tariq, A.P. Serro, J.L. Mata, B. Saramago, J.M.S.S. Esperança, J.N. Canongia Lopes, L.P.N. Rebelo, Fluid Phase Equilibr. 294 (2010) 131-138.
[44] N.M. Yunus, M.I. Abdul Mutalib, Z. Man, M.A. Bustam, T. Murugesan, J. Chem. Thermodyn. 42 (2010) 491-495.
[45] A. Muhammad, M.I. Abdul Mutalib, C.D. Wilfred, T. Murugesan, A. Shafeeq, J. Chem. Thermodyn. 40 (2008) 1433-1438.
[46] H. Guerrero, S. Martín, V. Pérez-Gregorio, C. Lafuente, I. Bandrés, Fluid Phase Equilibr. 317 (2012) 102-109.
[47] T.-Y. Wu, S.-G. Su, K.-F. Lin, Y.-C. Lin, H.P. Wang, M.-W. Lin, S.-T. Gung, I.W. Sun, Electrochim. Acta 56 (2011) 7278-7287.
[48] S. Seki, T. Kobayashi, Y. Kobayashi, K. Takei, H. Miyashiro, K. Hayamizu, S. Tsuzuki, T. Mitsugi, Y. Umebayashi, J. Mol. Liq. 152 (2010) 9-13.
[49] T.-Y. Wu, I.W. Sun, S.-T. Gung, M.-W. Lin, B.-K. Chen, H.P. Wang, S.-G. Su, J. Taiwan Inst. Chem. E. 42 (2011) 513-522.
[50] A. Kumar, J. Solution Chem. 37 (2008) 203-214.
[51] A.K. Ziyada, C.D. Wilfred, M.A. Bustam, Z. Man, T. Murugesan, J. Chem. Eng. Data 55 (2010) 3886-3890.
[52] K.A. Kurnia, C.D. Wilfred, T. Murugesan, J. Chem. Thermodyn. 41 (2009) 517-521.
[53] M. Królikowska, T. Hofman, Thermochim. Acta 530 (2012) 1-6.
[54] T. Regueira, L. Lugo, J. Fernández, J. Chem. Thermodyn. 48 (2012) 213-220.

[55] B. Lagourette, C. Boned, H. Saint-Guirons, P. Xans, H. Zhou, Meas. Sci. Technol. 3 (1992) 699-703.
[56] M.J.P. Comuñas, J.P. Bazile, A. Baylaucq, C. Boned, Journal of Chemical & Engineering Data 53 (2008) 986-994.
[57] J.J. Segovia, O. Fandiño, E.R. López, L. Lugo, M.C. Martin, J. Fernández, J. Chem. Thermodyn. 41 (2009) 632-638.
[58] O. Fandiño, L. Lugo, J.J. Segovia, E.R. López, M.J.P. Comuñas, J. Fernández, J. Supercrit. Fluid. 58 (2011) 189-197.
[59] O. Fandiño, L. Lugo, M.J.P. Comuñas, E.R. López, J. Fernández, J. Chem. Thermodyn. 42 (2010) 84-89.
[60] M.J.P. Comuñas, X. Paredes, F.M. Gaciño, J. Fernández, Low shear viscosity behaviour of vegetable and ionic lubricants at high pressure. in: M.T. Cidade, I.M.N. Sousa, J.M. Franco, (Eds.), IbeReo 2011: Reology Trends, from nano to macro systems, Caparica, Portugal, 2011, pp. 289-292.
[61] F.M. Gaciño, X. Paredes, M.J.P. Comuñas, J. Fernández, J. Chem. Thermodyn. 54 (2012) 302-309.
[62] K.R. Harris, L.A. Woolf, M. Kanakubo, T. Rüther, J. Chem. Eng. Data 56 (2011) 4672-4685.
[63] J. Jacquemin, P. Nancarrow, D.W. Rooney, M.F. Costa Gomes, P. Husson, V. Majer, A.A.H. Padua, C. Hardacre, J. Chem. Eng. Data 53 (2008) 2133-2143.
[64] A.B. Pereiro, H.I.M. Veiga, J.M.S.S. Esperança, A. Rodríguez, J. Chem. Thermodyn. 41 (2009) 1419-1423.
[65] Y. Deng, P. Husson, A.-M. Delort, P. Besse-Hoggan, M. Sancelme, M.F. Costa Gomes, J. Chem. Eng. Data 56 (2011) 4194-4202.
[66] M. Shamsipur, A.A.M. Beigi, M. Teymouri, S.M. Pourmortazavi, M. Irandoust, J. Mol. Liq. 157 (2010) 43-50.
[67] S. Katsuta, Y. Shiozawa, K. Imai, Y. Kudo, Y. Takeda, J. Chem. Eng. Data 55 (2009) 1588-1593.
[68] R. Zarrougui, M. Dhahbi, D. Lemordant, Ionics 17 (2011) 343-352.
[69] R.L. Gardas, H.F. Costa, M.G. Freire, P.J. Carvalho, I.M. Marrucho, I.M.A. Fonseca, A.G.M. Ferreira, J.A.P. Coutinho, J. Chem. Eng. Data 53 (2008) 805-811.
[70] H.K. Shobha, K. Kishore, J. Chem. Eng. Data 37 (1992) 371-376.
[71] O. Fandiño, A.S. Pensado, L. Lugo, E.R. López, J. Fernández, Green Chem. 7 (2005).
[72] O. Fandiño, E.R. López, L. Lugo, J. Fernández, Fluid Phase Equilibr. 296 (2010) 30-36.
[73] J.N.A. Canongia Lopes, A.A.H. Pádua, J. Phys. Chem. B 110 (2006) 3330-3335.
[74] R.L. Gardas, J.A.P. Coutinho, Fluid Phase Equilibr. 263 (2008) 26-32.
[75] J. Jacquemin, P. Husson, V. Mayer, I. Cibulka, J. Chem. Eng. Data 52 (2007) 2204-2211.
[76] R. Gomes de Azevedo, J.M.S.S. Esperança, J. Szydlowski, Z.P. Visak, P.F. Pires, H.J.R. Guedes, L.P.N. Rebelo, J. Chem.Thermodyn. 37 (2005) 888-899.
[77] R.L. Gardas, M.G. Freire, P.J. Carvalho, I.M. Marrucho, I.M.A. Fonseca, A.G.M. Ferreira, J.A.P. Coutinho, J. Chem. Eng. Data 52 (2007) 1881-1888.
[78] J.M.S.S. Esperança, H.J.R. Guedes, J.N.C. Lopes, L.P.N. Rebelo, J. Chem. Eng. Data 53 (2008) 867-870.
[79] R. Taguchi, H. Machida, Y. Sato, R.L. Smith, J. Chem. Eng. Data 54 (2008) 22-27.
[80] A. Pensado, M.J.P. Comuñas, J. Fernández, Tribol. Lett. 31 (2008) 107-118.
[81] J. Troncoso, C.A. Cerdeiriña, P. Navia, Y.A. Sanmamed, D. González-Salgado, L. Romaní, J. Phys. Chem. Lett. 1 (2010) 211-214.
[82] T. Hofman, A. Gołdon, A. Nevines, T.M. Letcher, J. Chem. Thermodyn. 40 (2008) 580-591.
[83] D. Matkowska, A. Gołdon, T. Hofman, J. Chem. Eng. Data 55 (2010) 685-693.
[84] C.A. Nieto de Castro, E. Langa, A.L. Morais, M.L.M. Lopes, M.J.V. Lourenço, F.J.V. Santos, M.S.C.S. Santos, J.N.C. Lopes, H.I.M. Veiga, M. Macatrão, J.M.S.S. Esperança, C.S. Marques, L.P.N. Rebelo, C.A.M. Afonso, Fluid Phase Equilib. 294 (2010) 157-179.
[85] M. Tariq, A.P. Serro, J.L. Mata, B. Saramago, J.M.S.S. Esperança, J.N. Canongia Lopes, L.P.N. Rebelo, Fluid Phase Equilib. 294 (2010) 131-138.
[86] J.M. Shreeve, C. Ye, Personal Communication, Department of Chemistry, University of Idaho, Moscow, ID, 2010.
[87] R. Kato, J. Gmehling, J. Chem.Thermodyn. 37 (2005) 603-619.
[88] S. Katsuta, Y. Shiozawa, K. Imai, Y. Kudo, Y. Takeda, Journal of Chemical & Engineering Data 55 (2009) 1588-1593.
[89] J. Kumełan, D. Tuma, Á. Pérez-Salado Kamps, G. Maurer, J.Chem. Eng. Data 55 (2009) 165-172.
[90] M. Krummen, P. Wasserscheid, J. Gmehling, J. Chem. Eng. Data 47 (2002) 1411-1417.

[91] R. Kato, J. Gmehling, Fluid Phase Equilibr. 226 (2004) 37-44.
[92] R.G. Seoane, S. Corderí, E. Gómez, N. Calvar, E.J. González, E.A. Macedo, Á. Domínguez, Ind. Eng. Chem. Res. 51 (2012) 2492-2504.
[93] J.M.S.S. Esperança, Z.P. Visak, N.V. Plechkova, K.R. Seddon, H.J.R. Guedes, L.P.N. Rebelo, J. Chem. Eng. Data 51 (2006) 2009-2015.
[94] L.I.N. Tomé, P.J. Carvalho, M.G. Freire, I.M. Marrucho, I.M.A. Fonseca, A.G.M. Ferreira, J.A.P. Coutinho, R.L. Gardas, J. Chem. Eng. Data 53 (2008) 1914-1921.
[95] K.R. Harris, M. Kanakubo, L.A. Woolf, J. Chem. Eng. Data 52 (2007) 1080-1085.
[96] Y. Hou, R.E. Baltus, Ind. Eng. Chem. Res. 46 (2007) 8166-8175.
[97] P. Kilaru, G.A. Baker, P. Scovazzo, J. Chem. Eng. Data 52 (2007) 2306-2314.
[98] B. Hasse, J. Lehmann, D. Assenbaum, P. Wasserscheid, A. Leipertz, A.P. Fröba, J. Chem. Eng. Data 54 (2009) 2576-2583.
[99] H. Tokuda, S. Tsuzuki, M.A.B.H. Susan, K. Hayamizu, M. Watanabe, J. Phys. Chem. B 110 (2006) 19593-19600.
[100] G. García-Miaja, J. Troncoso, L. Romaní, J. Chem. Thermodyn. 41 (2009) 334-341.
[101] B. Mokhtarani, M.M. Mojtahedi, H.R. Mortaheb, M. Mafi, F. Yazdani, F. Sadeghian, J. Chem. Eng. Data 53 (2008) 677-682.
[102] A.B. Pereiro, P. Verdía, E. Tojo, A. Rodríguez, J. Chem. Eng. Data 52 (2007) 377-380.
[103] C. Schreiner, S. Zugmann, R. Hartl, H.J. Gores, J. Chem. Eng. Data 55 (2009) 1784-1788.
[104] P. Bhujrajh, N. Deenadayalu, J. Solution Chem. 36 (2007) 631-642.
[105] K.R. Seddon, A. Stark, M.-J. Torres, Viscosity and Density of 1-Alkyl-3-methylimidazolium Ionic Liquids, Clean Solvents, American Chemical Society, 2002, pp. 34-49.
[106] J. Jacquemin, P. Husson, V. Majer, A.A.H. Padua, M.F. Costa Gomes, Green Chem. 10 (2008) 944-950.
[107] J. Palgunadi, J.E. Kang, D.Q. Nguyen, J.H. Kim, B.K. Min, S.D. Lee, H. Kim, H.S. Kim, Thermochim. Acta 494 (2009) 94-98.

5.6. Ionic liquids as hydraulic fluids: Comparison of several properties with those of conventional oils*

*T. Regueira, L. Lugo, J. Fernández, Lub. Sci., 2013, DOI: 10.1002/ls.1235. http://onlinelibrary.wiley.com/doi/10.1002/ls.1235/pdf

Abstract

Ionic liquids (ILs) possess several remarkable properties, that make them striking for their use as lubricants for different applications. Isothermal compressibility (or bulk modulus) is a fundamental parameter in the hydraulic fluids field. Therefore, an analysis of the compressibility of different ILs, mineral, synthetic and vegetable oils, as well as water is presented in this work. Furthermore, thermal expansion coefficient, viscosity and viscosity index of these fluids are also analysed.

1. Introduction

From the earliest times water has been used in hydraulic engineering. Their limitations to operate at high temperature due to the low boiling point of water were solved in the first decade of the 20th century with the use of refined mineral oil. During the Second World War synthetic hydraulic fluids were developed specially for aviation. Nowadays, the most common synthetic hydraulic fluids are alkylated aromatics, polyalkylene glycols (PAGs), polyphenyl ethers, polyalphaolefines (PAO) perfluorocarbons, silicones, silohydrocarbons, diesters and (polyol, phosphate or silicate) esters.[1] The pollution caused by some of these lubricants is one of the environmental problems that must be solved. It should be noted that about 50% of all lubricants sold worldwide end up in the environment via volatility, spills or total loss applications. This threat to the environment can be avoided by either preventing undesirable losses, reclaiming and recycling mineral oil lubricants, or using environmentally friendly lubricants.[2] Especially to systems with a high leakage rate, non-toxic hydraulic lubricants with adequate levels of biodegradability must be used to avoid polluting the environment. Therefore, in the last years some vegetable hydraulic oils have been developed mainly for agriculture applications[3-5].

Hydraulic systems provide a significantly more accurate and adjustable means to transmit energy than electrical or mechanical systems. In general hydraulic systems are reliable, efficient and cost effective, leading to their use in the industrial work.[1] Hydraulic fluids are one of the most important groups of industrial lubricants with a market share of 15% in Europe and 22% in USA[3,4].

The purpose of a hydraulic fluid is to transmit power to the moving parts of many machines, as wind turbines, tractors, bulldozers, and other heavy equipment used in the building of road and big structures. Hydraulic fluids are also used in land, sea and airborne transport and in brake systems. Greatly differentiated hydraulic systems, operation in various environmental atmospheres and often at extreme temperatures require a multitude of products of consistently varied properties[5]. The transmitted power is used for performing specific functions. Apart from this function of power transfer and control medium the hydraulic fluid should act as heat transfer

and/or sealing medium, lubricant, be compatible as well as provide a good pump efficiency and a long functioning life[5].

The EU Ecolabel is a voluntary–award scheme intended to promote products with a reduced environmental impact during their entire life cycle. This scheme is part of the sustainable consumption and production policy of the Community, which aims at reducing the negative impact of consumption and production on the environment, health, climate and natural resources. It is intended to promote products which have a high level of environmental performance[6]. The latest ecological criteria for the award of the EU Ecolabel to lubricants were established in 2011 by the EU, taking into account the exclusion of specific substances, aquatic toxicity requirements, biodegradability and bioaccumulative potential, use of renewable raw materials and a minimum technical performance[7]. Under this frame of searching for products that have a reduced impact on the environment some ionic liquids (ILs) could be also of great interest. ILs were proposed as high performance lubricants, due to their main properties such as negligible volatility, non-flammability, thermo-oxidative stability, low melting point, broad liquid range and controlled miscibility with organic solvents. They have been investigated over the last decade for different lubrication applications. Different reviews recently published, as those of Minami[8] and Bermúdez et al.[9] present an overview about ILs on this field with a wide literature survey, which is indicative of the efforts done in the last few years.

Regarding the use of new liquids as hydraulic fluids, compressibility is a key parameter. In hydraulic systems that operate at high pressure, fluids with low compressibility (high bulk modulus) are required to transmit power efficiently. ILs are mainly characterized by their low isothermal compressibility, which is usually lower (being in some cases up to the half) than those of the current reference mineral and synthetic hydraulic oils[10,11]. Compressibility has significant effects on high-pressure fluid systems. Problems directly caused by compressibility include the following: servos fail to maintain static rigidity and experience adverse effects in system amplification, loss in efficiency due to the fact that volume reduction cannot be recovered and cavitation, which may cause metal fracture, corrosive fatigue and stress corrosion[10]. Therefore, a low compressibility translates into fast response time, high pressure transmission velocity, and low power loss. Usually, the potential for energy loss and heat production of a lubricant decreases with the increase of its compressibility. Materials with high compressibility i.e. low bulk modulus act as damping fluids [1]. In hydraulic systems that operate at high pressure, oils with low compressibility are required to transmit power efficiently. The importance of low compressibility becomes greater when equipment size and weight are critical, as in aircrafts. Nevertheless, certain compressibility can be convenient because it dampens pressure surges caused by switching and thus provides smoother operation[1].

Hence, the density-pressure behavior of lubricants should also be included in a hydrostatic evaluation because the compressibility of fluids affects their dynamic performance. Besides, the isothermal compressibility is used in various calculations thickness of the oil film[10,12,13], in elastohydrodynamic lubrication (EHL). The temperature increase in elastohydrodynamically lubricated conjunctions may not be ignored. This is more likely to occur when contact conditions combine several factors such as high sliding or entrainment speeds, high viscosity or viscosity–pressure dependence of the lubricant and heavy normal loads. Neglecting the heat generation in EHD contacts operating under severe conditions leads to poor estimations of both film thicknesses and friction coefficients[14]. Compression decrease the film thickness further as the lubricant is entrained into the high-pressure region and the more compressible the lubricant is the thinner will be the lubricant film[15].

In this work we establish comparisons between the isothermal compressibilities of several ILs and several conventional and vegetable oils as well as water. The studied ILs contain relatively new anions, different from the commonly used hexafluorophosphate or tetrafluoroborate that are hydrolytically unstable, especially at elevated temperature. Thus, ILs with the anion tris(pentafluoroethyl)trifluorophosphate $[(C_2F_5)_3PF_3]^-$, also known as $[FAP]^-$, are analysed, among others. ILs containing this anion are immiscible with water and show a low melting point, they also possess high thermal stability (comparable with that of bis(trifluoromethylsulfonyl)imide-based ionic liquids and much better than tetrafluoroborates)[16]. We have analyzed the suitability of seven ILs as hydraulic liquids taking into account compressibility values. Additionally, a comparison between the thermal expansion coefficients of these fluids was performed, as well as an analysis of viscosity and viscosity index.

2. Materials and experimental techniques

ILs studied in our laboratory were kindly provided by Merck KGaA with a purity higher than 98 %[11,17-19]. These seven ILs are based on the following cations 1-ethyl-3-methyl-imidazolium $[C_2C_1Im^+]$, trihexyl(tetradecyl)phosphonium $[P_{6,6,6,14}]^+$, 1-butyl-1-methylpyrrolidinium $[C_4C_1Pyrr]^+$ and 1-(2-methoxyethyl)-1-methylpyrrolidinium $[C_1OC_2C_1Pyrr]^+$ as well as the following anions ethyl sulphate $[C_2SO_4]^-$, n-hexylsulfate $[C_6SO_4]^-$, bis(trifluoromethylsulfonyl)imide $[NTf_2]^-$, and tris(pentafluoroethyl)trifluorophosphate $[(C_2F_5)_3PF_3]^-$, also known as $[FAP]^-$. More information about the purity analysis and the procedure to eliminate the volatile impurities is given elsewhere[11,18,19]. The chemical structures of these ILs are presented in Table 1, whereas other physical properties needed for a full evaluation as the kinematic viscosities (ν), viscosity index (VI), glass transition temperature (Tg), melting points are reported in Table 2.

Table 1: Structure of the ILs studied in the present work.

IONIC LIQUID	CHEMICAL STRUCTURE
$[C_1OC_2C_1Pyrr][NTf_2]$ (IL 1)	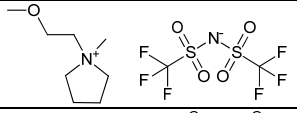
$[C_4C_1Pyrr][NTf_2]$ (IL 2)	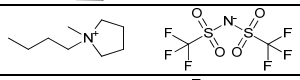
$[C_1OC_2C_1Pyrr][FAP]$ (IL 3)	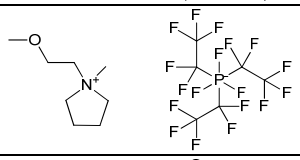
$[C_2C_1Im][C_2SO_4]$ (IL 4)	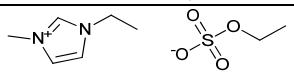
$[C_4C_1Pyrr][FAP]$ (IL 5)	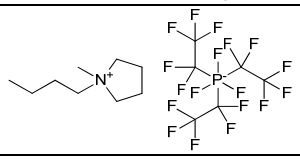
$[C_2C_1Im][C_6SO_4]$ (IL 6)	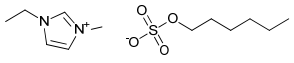
$[P_{6,6,6,14}][FAP]$ (IL 7)	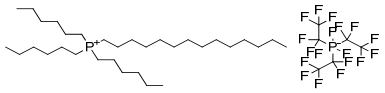

Table 2: Melting point, kinematic viscosity (ν) at 40ºC and 0.1 MPa[18] and viscosity index (VI)[18] of the lubricants investigated in this work .

IL	Melting Point (ºC)	Glass Transition temperature (ºC)	ν at 40ºC $mm^2 \cdot s^{-1}$	VI
$[C_1OC_2C_1Pyrr][NTf_2]$ (IL 1)	*[36]	-95[52], -91[36]	22	191
$[C_4C_1Pyrr][NTf_2]$ (IL 2)	~-7[42,53-56], -13[56], -15[58,59], -18[43,60,61]	-81[57,58], -83[59], -85[54], -87[43,61], -89[60], -92[56]	30	176
$[C_1OC_2C_1Pyrr][FAP]$ (IL 3)	<-50[62]	-79[18]	35	137
$[C_2C_1Im][C_2SO_4]$ (IL 4)	*[37,38]	-78[38], -80[63], -86[37]	41	174
$[C_4C_1Pyrr][FAP]$ (IL 5)	2[42], 4[40], -27[40**]	-116[40]	61	119
$[C_2C_1Im][C_6SO_4]$ (IL 6)	7[62]	-77[18]	122	136
$[P_{6,6,6,14}][[FAP]$ (IL 7)	<-50[62]	-92[18]	131	128

*These ILs have no melting point
**Freezing point

Density measurements for the above ILs were performed previously in our laboratory using an automated vibrating tube densimeter Anton Paar HPM up to 120 MPa and between (278.15 and 398.15) K[11,19]. The densimeter was calibrated following the procedure described by Lagourette et al.[20] and modified by Comuñas et al.[21] Milli-Q water was employed as reference fluid at temperatures between (278.15 and 348.15) K and pressures between (0.1 and 120) MPa and also at T = 373.15 K and T = 398.15 K for pressures higher than 0.1 MPa, whereas n-decane

was used as reference fluid at T = 373.15 K and T = 398.15 K and at 0.1 MPa. The effect of the sample viscosity on this property was taken into account[11,19,22]. More details were previously given[23]. Viscosities and viscosity index were measured in a previous work[18] with an Anton Paar Stabinger SVM3000, which uses the ASTM D2270-04 standard for VI. Calibration of this equipment was performed using two reference fluids provided by Anton Paar. Uncertainty of viscosity measurements was checked with one reference fluid from Cannon Instrument Comp., N35, finding that the average absolute deviation (AAD %) is lower than 1 %[18].

3. Results

Viscosity is also one of the most important properties of any hydraulic fluid or systems and applications of all types. Proper viscosity grade and VI selection is critical for optimizing equipment performance and operating costs. Viscosity is directly related to wear control (elastohydrodynamic lubrication film), liquid frictional losses, leakage, start-up ease, and efficiency. There are three viscosity grades (VG) that represent over 80% of all hydraulic fluids consumed: ISO VG 32, ISO VG 46, and ISO VG 68[1,24]. From table 2, it can be concluded, that four of the seven ILs have these VGs, whereas $[C_1OC_2C_1Pyrr][NTf_2]$ has a VG of 22 and $[C_2C_1Im][C_6SO_4]$ and $[P_{6,6,6,14}][FAP]$ present kinematic viscosities slightly higher than those of a VG100 lubricant. We should point out that the National Fluid Power Association (NFPA) issued a recommended practice in which the acceptable operating viscosity for most pumps and motors was set from 13 to 860 $mm^2 \cdot s^{-1}$. Hydraulic units work under extreme temperature changes, especially in heavy duty vehicles[1,25].

Furthermore, the viscosity range of the hydraulic fluid is extremely important at the working temperatures, i.e. the viscosity index. Most of the current hydraulic fluids have VI around 90-110, especially the mineral lubricants.[26] High VI fluids lead to a good starting up and a minimal loss in performance at low temperatures. At high temperatures, a sufficient sealing effect and protection against wear is achieved by using hydraulic fluids with appropriate viscosity grades. Table 2 shows that VI for the seven ILs range from 119 to 191, being the best VI for ILs with the $[NTf_2]$ anion. Pensado et al.[27] and Gaciño et al.[17] have shown how the VI of the ILs can be tailored with an appropriate selection of the anion and cation, reaching values up to 191 for $[C_1OC_2C_1Pyrr][NTf_2]$. High VI are also found for hydraulic fluids as PAGs or vegetable oils, thus Paredes et al.[28,29] have reported a VI of 220 for a PAG and Regueira et al.[10] a value of 203 for high oleic sunflower base oil.

Other important issue is the low temperature fluidity. If fluid flow is insufficient at low temperature (due to a low VI or the proximity to the pour point), cavitation can occur in the pump intake, or the cylinder operation can be impeded. Pump manufacturers have set limits for

the maximum viscosity at cold start. The general limit recommended for vane pumps is around 860 cSt and for piston pumps, 1600 cSt[1,25]. Start up temperature is recommended to be approximately 15 °C above hydraulic fluid pour point. As regards ILs, Zhou et al.[30] indicate that they have pour points (lowest temperature to keep flow at 45º tilting angle) below -50ºC. Wang et al.[31] reported pour points lower than -30ºC for six alkylimidazolium hexafluorophosphate ILs, without indicating the technique used. Omotowa et al.[32] determined by drop-ball method the pour points of three phosphazene-based ILs obtaining values of 10ºC for two of them and 25ºC for the other one. We have not found more articles on pour points of ILs. Several articles on ILs tribology[33-35] report melting or glass transition temperatures instead of pour points. The glass transition temperature, T_g, is a relevant parameter for low temperature fluidity of amorphous ILs, which have not melting points, as IL 1[36] and IL 4[37,38] (see table 2). At the T_g temperature it is considered[18,39] that the viscosity is 10^{12} Pa·s. However, for crystalline ILs the relevant parameters are the freezing and melting points, for which differences up to 31ºC were reported for IL 5[40], and even up to 200ºC for 1-propyl-3-methyl-imidazolium chloride[41]. In table 2 it can be observed that T_g of some of the studied ILs varies between -77 and -116ºC and that there is some dispersion among the data reported in literature for ILs melting and T_g temperatures, especially in the case of IL 2. These differences can be explained by the use of different techniques, scanning rates, or by the presence of impurities, as water, in the IL samples. Additionally, crystallization points were reported for IL 2 at -39ºC[42] and -53ºC[43] and for IL 5 at -39ºC[42]. Melting points and glass transition temperatures of the seven ionic liquids analysed are quite low, except for IL 5 and IL 6. For mineral oils the pour point ranges from 0ºC to −60ºC and for vegetable oils from −9 to −21ºC. Concerning the synthetic oils, the worst pour temperatures are those of polyphenyl ethers, which range from +20ºC to −20ºC and the best are diesters from −50ºC to −80ºC and silicate esters from −50ºC to −70ºC[44]. There are a quite variety of ILs with low melting points[45], which permits cold starts of the machinery.

Density values of the ILs were correlated as a function of temperature and pressure by means of the Tammann-Tait equation:

$$\rho(T,p) = \frac{\rho(T,0.1\ \text{MPa})}{1 - C\cdot\ln\left(\frac{B(T)+p}{B(T)+0.1\ \text{MPa}}\right)} \tag{1}$$

where p is the pressure in MPa, $\rho(T,0.1\ \text{MPa})$ is the polynomial dependence of density on temperature at a reference pressure 0.1 MPa, $\sum_{i=0}^{m} A_i T^i$, C is parameter independent of temperature and pressure and $B(T)$ is a parameter depending on temperature as a polynomial

function, $\sum_{j=0}^{n} B_j T^j$.

Coefficients of the Tammann-Tait correlation of the different ILs are presented in table 3.

Table 3: A_i, B_i, C coefficients from Tammann-Tait equation

	IL 1[11]	IL 2[19]	IL 3[19]	IL 4[11]	IL 5	IL 6	IL 7
A_0 /g·cm^{-3}	2.12764	2.1752	2.1948	1.65207	1.9284	1.3345	1.3488
-10^3·A_1 /g·cm^{-3}·K^{-1}	4.291	5.4202	3.1102	2.4296	1.213	0.605	0.0433
10^6·A_2 /g·cm^{-3}·K^{-2}	9.359	13.152	5.6022	4.704	0.24	-0.528	-2.4793
-10^9·A_3 /g·cm^{-3}·K^{-3}	8.55	12.585	5.1037	4.102	0.078	-0.87	-2.5628
10^2·C	8.72	8.9008	8.5241	9.82	8.35	8.85	8.069
B_0 /MPa	517	485.47	515.96	809	487.2	547.3	447.4
-B_1 /MPa·K^{-1}	1.555	1.3829	1.6854	2.436	1.529	1.498	1.4975
10^3·B_2 /MPa·K^{-2}	1.42	1.1742	1.6366	2.41	1.384	1.22	1.424

In Figure 1, density values of the ILs are plotted against pressure at T = 313.15 K[11,19]. The following sequence can be inferred for the dependence of density with the cation: $[C_1OC_2C_1Pyrr]^+ > [C_4C_1Pyrr]^+ > [P_{6,6,6,14}]^+$. Regarding the anion, two sequences can be deduced: $[FAP]^- > [NTf_2]^-$ and $[C_2SO_4]^- > [C_6SO_4]^-$. The lightest of the studied ILs is $[C_2C_1Im][C_6SO_4]$. Moreover, we have performed an analysis about the influence of the cation and anion structure on the density for a broad database concluding that also for the $[NTf_2]^-$ ILs, that with the lowest density contains the $[P_{6,6,6,14}]^+$ cation[19].

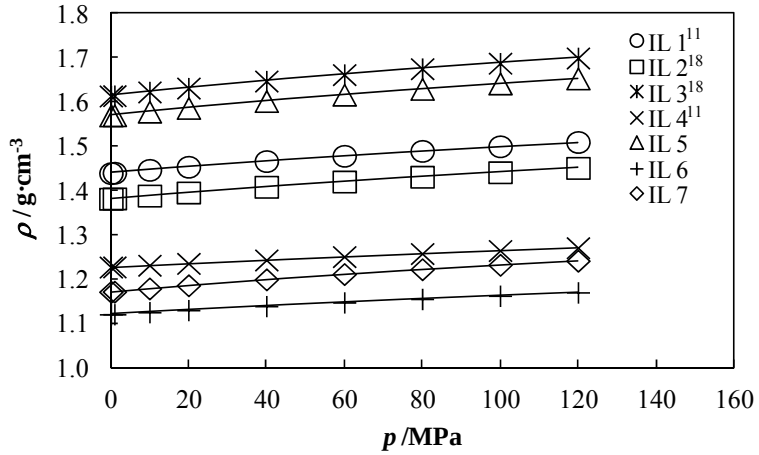

Figure 1: ILs density, ρ, as a function of pressure at 313.15 K. Solid line is the Tammann-Tait correlation.

From these density values and those of the literature[11,18,19,45,46], it can be concluded that densities of ILs are a little higher than those of the current hydraulic fluids[10,26]. At 15ºC densities range from 0.86 g.cm^{-3} for petroleum fluids to 1.13 g.cm^{-3} for synthetic anhydrous fluids composed of phosphate esters (HFDR). Using hydraulic fluids with a high density requires the sufficient diameter of the suction line and/or elevated tank to provide positive inlet pressure[26].

Moreover, according to the simplified Sieder-Tate equation, the higher the density value, the better the heat-transfer coefficient[47].

Isothermal compressibility, κ_T, is a density derived property defined according to equation (2):

$$\kappa_T(T,p) = \frac{1}{\rho}\left(\frac{\partial \rho}{\partial p}\right)_T \tag{2}$$

The isothermal compressibility values of the ILs presented in Table 1 were obtained by differentiation from equation (1)[11,19]. It was found that this property decreases with pressure and increases with temperature. In Figure 2, κ_T values of these ILs as well as those of water are plotted against pressure at 313.15 K. It can be observed that the ILs with the highest compressibility are those with the $[FAP]^-$ anion, whereas those with the lowest compressibility are the alkylimidazolium alkylsulfates (even lower or equal to that of water).

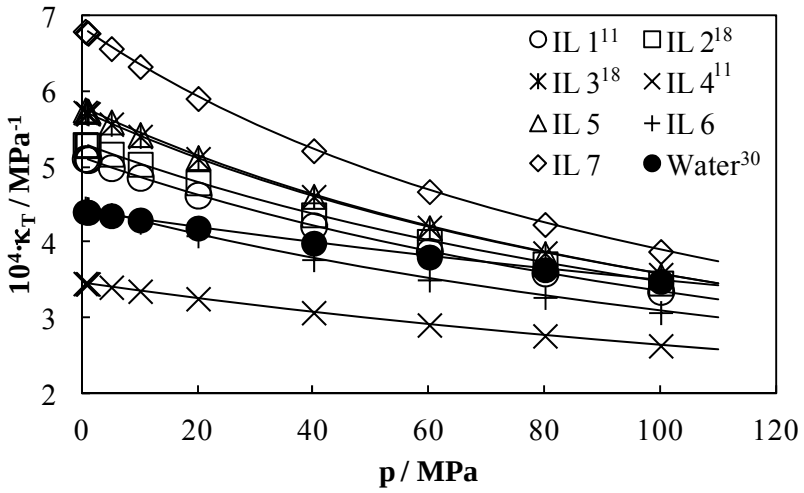

Figure 2: Isothermal compressibility, κ_T, as a function of pressure at 313.15 K.

For the ILs with the anion $[FAP]^-$, κ_T follows this sequence with the cation: $[P_{6,6,6,14}]^+ > [C_1OC_2C_1Pyrr]^+ \approx [C_4C_1Pyrr]^+$, whereas for the ILs with the anion $[NTf_2]^-$, κ_T of the IL with $[C_4C_1Pyrr]^+$ cation is higher or equal to that of the IL with $[C_1OC_2C_1Pyrr]^+$ cation.

Recently we have performed a broader analysis of the dependence of κ_T with the cation and anion of ILs, using high-pressure literature density data[19]. It was observed, as a general trend, that this property increases slightly with the alkyl chain length of the cation for ILs with the $[NTf_2]^-$ anion. Moreover, for ILs with the $[C_2C_1Im]^+$ cation, the trend found for this property, as a function of the anion, was the following: $[NTf_2]^- > [C(CN)_3]^- > [C_nSO_4]^- \approx [PF_6]^- \approx [BF_4]^-$.

We have compared in Figure 3 compressibility values of the ILs from table 1 with water[48] as well as with several hydraulic lubricants, two mineral lubricants MIN-H01 and MIN-H02[10], two synthetic lubricants, a dimethoxy end-capped poly(propylene glycol) PAG1[22] and a

dipentaerythritol hexaheptanoate DiPEC7[49], a vegetable based oil HOSO-B[10] and a developed biodegradable lubricant based in high oleic sunflower oil, BIO-H01[50].

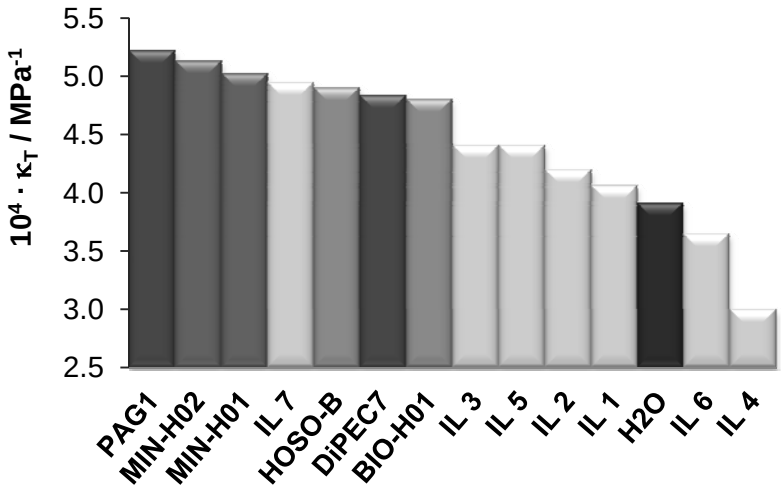

Figure 3: Isothermal compressibility values, κ_T, at 313.15 K and 50 MPa, of the ILs from table 1, water [48] and hydraulic lubricants: PAG1[22], MIN-H01[10], MIN-H02[10], DiPEC7[49], BIO-H01[50] and HOSO-B[10].

Except for the IL $[P_{6,6,6,14}][FAP]$, whose compressibility is between those of the mineral and synthetic lubricants, compressibility of the ILs is lower than those of the mineral and synthetic lubricants and also lower to that of the biodegradable lubricant. Therefore, taking into account the isothermal compressibility, it can be concluded that these ILs are more suitable as hydraulic fluids than the mineral and synthetic oils due to their low compressibility values, that translates into higher power efficiency. Besides, ILs could form thicker films by a few percent in high-pressure regions in EHL regime.

In order to obtain the values of the isobaric thermal expansion coefficient, α_p, we have followed the method described by Nieto de Castro et al.[51] We have correlated ln(ρ) as a third polynomial function of the temperature for each isobar, using the following equation:

$$ln(\rho) = A + BT + CT^2 + DT^3 \tag{3}$$

Therefore, the isobaric thermal pressure coefficient is given by ($\alpha_p = -(\partial \ln \rho / \partial T)_p$):

$$\alpha_p = -\left(B + 2CT + 3DT^2\right) \tag{4}$$

Values of this property for several fluids at 40 MPa are depicted in Figure 4 as a function of temperature. It can be observed that the highest α_p values correspond to synthetic, vegetable and mineral oils. Furthermore, it can be observed a non-monotonous behaviour of this property with temperature for some ILs. This property should be taken into account when the heat associated is not dissipated. Fluids with a low coefficient of thermal expansion are preferred[1].

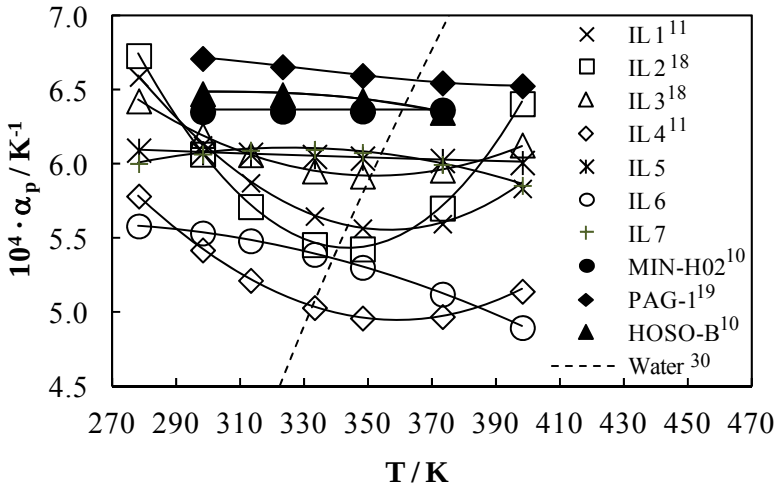

Figure 4: Thermal expansion coefficient, α_p, at 40 MPa.

4. Summary and conclusions

We have compared the density, compressibility and thermal expansion coefficient of seven ILs among them and also with synthetic, mineral and vegetable oils as well as with water. Among the ILs, it was found that those with the $[FAP]^-$ anion present the highest compressibility whereas those with the lowest compressibility are the alkylimidazolium alkylsulfates. Compressibility of these last ILs is even lower than that of water. In addition, $[C_2C_1Im][C_2SO_4]$ present a high viscosity index (174) and excellent low temperature properties (it has not melting point and its glass transition temperature is about -80ºC).The low compressibility of several ILs makes them more suitable as hydraulic fluids than the currently employed hydraulic oils, whereas as EHL lubricants the film thickness suffers a lower decrease.

As regards isobaric thermal expansion coefficient, it was found that values of this property for ILs are lower than those of synthetic, mineral and vegetable oils.

Acknowledgments

Authors acknowledge Merck KGaA for providing the IL samples. This work is being supported by Spanish Ministry of Science and Innovation under CTQ2008-06498-C02-01 and CTQ2011-23925 projects. T.R. and L.L. acknowledge the support provided by FPU and Ramón y Cajal Program, respectively.

References

1. Placek DG, Hydraulics. Rudnick L R, *Synthetics, Mineral Oils, and Bio-Based Lubricants: Chemistry and Technology*, CRC Press, Wilmington, Delaware, USA, 2005, 517-540.
2. Erhan SZ, Sharma BK, Liu Z, Adhvaryu A. Lubricant base stock potential of chemically modified vegetable oils. *Journal of Agricultural and Food Chemistry* 2008; **56**: 8919-8925.
3. Lawate S, Environmentally friendly hydraulic fluids. Rudnick L R, *Synthetics, Mineral Oils, and Bio-Based Lubricants: Chemistry and Technology*, CRC Press, Wilmington, Delaware, USA, 2005, 541-550.
4. Mendoza G, Igartua A, Fernandez-Diaz B, Urquiola F, Vivanco S, Arguizoniz R. Vegetable oils as hydraulic fluids for agricultural applications. *Grasas Aceites* 2011; **62**: 29-38.

5. Kajdas C, Karpinska A, Kulczycki A, Industrial Lubricants. Mortier R M, Fox M F, Orszulik S T, *Chemistry and Technology of Lubricants*, Springer, 2010, 239-292.
6. Regulation (EC) No 66/2010 of the European Parliament and of the Council of 25 November 2009 on the EU Ecolabel, Official Journal of the European Union, 2010, pp. L 27/01 - L 27/19.
7. Commission decision of 24 June 2011 on establishing the ecological criteria for the award of the EU Ecolabel to lubricants, Official Journal of the European Union, 2011, pp. L 169/128 - L 169/138.
8. Minami I. Ionic liquids in tribology. *Molecules* 2009; **14**: 2286-2305.
9. Bermúdez M-D, Jiménez A-E, Sanes J, Carrión F-J. Ionic liquids as advanced lubricant fluids. *Molecules* 2009; **14**: 2888-2908.
10. Regueira T, Lugo L, Fandiño O, López ER, Fernández J. Compressibilities and viscosities of reference and vegetable oils for their use as hydraulic fluids and lubricants. *Green Chemistry* 2011; **13** :1293–1302.
11. Regueira T, Lugo L, Fernández J. High pressure volumetric properties of 1-ethyl-3-methylimidazolium ethylsulfate and 1-(2-methoxyethyl)-1-methyl-pyrrolidinium bis(trifluoromethylsulfonyl)imide. *Journal of Chemical Thermodynamics* 2012; **48**: 213-220.
12. Godfrey D, Herguth WR. Physical and chemical properties of industrial mineral oils affecting lubrication. *Lubrication Engineering* 1995; **51**: 493-496.
13. Bair S. *High-Pressure Rheology for Quantitative Elastohydrodynamics*. Elsevier: Amsterdam, 2007.
14. Habchi W, Vergne P, Bair S, Andersson O, Eyheramendy D, Morales-Espejel GE. Influence of pressure and temperature dependence of thermal properties of a lubricant on the behaviour of circular TEHD contacts. *Tribology International* 2010; **43**: 1842-1850.
15. Larsson R, E.Kassfeldt, Byheden A, Norrby T. Base fluid parameters for elastohydrodynamic lubrication and friction calculations and their influence on lubrication capability. *Journal of Synthetic Lubrication* 2001; **18**: 183-198.
16. Ignat'ev NV, Welz-Biermann U, Kucheryna A, Bissky G, Willner H. New ionic liquids with tris(perfluoroalkyl)trifluorophosphate (FAP) anions. *Journal of Fluorine Chemistry* 2005; **126**: 1150-1159.
17. Gaciño FM, Paredes X, Comuñas MJP, Fernández J. Effect of the pressure on the viscosities of ionic liquids: Experimental values for 1-ethyl-3-methylimidazolium ethylsulfate and two bis(trifluoromethyl-sulfonyl)imide salts. *Journal of Chemical Thermodynamics* 2012; **54**: 302-309.
18. Gaciño FM, Regueira T, Lugo L, Comuñas MJP, Fernández J. Influence of Molecular Structure on Densities and Viscosities of Several Ionic Liquids. *Journal of Chemical and Engineering Data* 2011; **56**: 4984-4999.
19. Regueira T, Lugo L, Fernández J. Influence of the pressure, temperature, cation and anion on the volumetric properties of ionic liquids: new experimental values for two salts. *Journal of Chemical Thermodynamics* 2013; **58**: 440-448.
20. Lagourette B, Boned C, Saint-Guirons H, Xans P, Zhou H. Densimeter calibration method versus temperature and pressure. *Meas. Sci. Technol.* 1992; **3**: 699-703.
21. Comuñas MJP, Bazile JP, Baylaucq A, Boned C. Density of diethyl adipate using a new vibrating tube densimeter from (293.15 to 403.15) K and up to 140 MPa. Calibration and measurements. *Journal of Chemical & Engineering Data* 2008; **53**: 986-994.
22. Fandiño O, Lugo L, Comuñas MJP, López ER, Fernández J. Temperature and pressure dependences of volumetric properties of two poly(propylene glycol) dimethyl ether lubricants. *Journal of Chemical Thermodynamics* 2010; **42**: 84-89.
23. Segovia JJ, Fandiño O, López ER, Lugo L, Martin MC, Fernández J. Automated densimetric system: Measurements and uncertainties for compressed fluids. *Journal of Chemical Thermodynamics* 2009; **41**: 632-638.
24. Wamback WE. Hydraulic systems and fluid. *Lubrication Engineering* 1983; **39**: 483-486.
25. NFPA Recommended Practice T2.13.13-2002. Fluid Viscosity Selection Criteria for Hydraulic Motors and Pumps, www.nfpa.com., 2002.
26. Hydraulic Fluids and Lubricants Technical Information, Sauer-Danfoss, 2010.
27. Pensado A, Comuñas M, Fernández J. The pressure–viscosity coefficient of several ionic liquids. *Tribology Letters* 2008; **31**: 107-118.
28. Paredes X, Fandiño O, Pensado AS, Comuñas MJP, Fernández J. Pressure-viscosity coefficients for polyalkylene glycol oils and other ester or ionic lubricants. *Tribology Letters* 2012; **45**: 89-100.

29. Paredes X, Pensado AS, Comuñas MJP, Fernández J. How pressure affects the dynamic viscosities of two poly(propylene glycol) dimethyl ether lubricants. *Journal of Chemical and Engineering Data* 2010; **55**: 4088-4094.
30. Zhou F, Liang Y, Liu W. Ionic liquid lubricants: designed chemistry for engineering applications. *Chemical Society Reviews* 2009; **38**: 2590-2599.
31. Wang H, Lu Q, Ye C, Liu W, Cui Z. Friction and wear behaviors of ionic liquid of alkylimidazolium hexafluorophosphates as lubricants for steel/steel contact. *Wear* 2004; **256**: 44-48.
32. Omotowa BA, Phillips BS, Zabinski JS, Shreeve JnM. Phosphazene-based ionic liquids: Synthesis, temperature-dependent viscosity, and effect as additives in water lubrication of silicon nitride ceramics. *Inorganic Chemistry* 2004; **43**: 5466-5471.
33. Minami I, Kita M, Kubo T, Nanao H, Mori S. The tribological properties of ionic liquids composed of trifluorotris(pentafluoroethyl) phosphate as a hydrophobic anion. *Tribology Letters* 2008; **30**: 215-223.
34. Minami I, Inada T, Sasaki R, Nanao H. Tribo-chemistry of phosphonium-derived ionic liquids. *Tribology Letters* 2010; **40**: 225-235.
35. Minami I, Kamimura H, Mori S. Thermo-oxidative stability of ionic liquids as lubricating fluids. *Journal of Synthetic Lubrication* 2007; **24**: 135-147.
36. Zhou Z-B, Matsumoto H, Tatsumi K. Cyclic quaternary ammonium ionic liquids with perfluoroalkyltrifluoroborates: synthesis, characterization, and properties. *Chemistry – A European Journal* 2006; **12**: 2196-2212.
37. Domańska U, Żołek-Tryznowska Z, Królikowski M. Thermodynamic phase behavior of ionic liquids. *Journal of Chemical & Engineering Data* 2007; **52**: 1872-1880.
38. Fernández A, Torrecilla JS, García J, Rodríguez F. Thermophysical properties of 1-ethyl-3-methylimidazolium ethylsulfate and 1-butyl-3-methylimidazolium methylsulfate ionic liquids. *Journal of Chemical & Engineering Data* 2007; **52**: 1979-1983.
39. Gupta PK, Mauro JC. Composition dependence of glass transition temperature and fragility. I. A topological model incorporating temperature-dependent constraints. *The Journal of Chemical Physics* 2009; **130**: 094503-094508.
40. Fletcher SI, Sillars FB, Hudson NE, Hall PJ. Physical properties of selected ionic liquids for use as electrolytes and other industrial applications. *Journal of Chemical & Engineering Data* 2009; **55**: 778-782.
41. Ngo HL, LeCompte K, Hargens L, McEwen AB. Thermal properties of imidazolium ionic liquids. *Thermochimica Acta* 2000; **357–358**: 97-102.
42. Wachter P, Schreiner C, Schweiger H-G, Gores HJ. Determination of phase transition points of ionic liquids by combination of thermal analysis and conductivity measurements at very low heating and cooling rates. *The Journal of Chemical Thermodynamics* 2010; **42**: 900-903.
43. Jin H, O'Hare B, Dong J, Arzhantsev S, Baker GA, Wishart JF, Benesi AJ, Maroncelli M. Physical properties of ionic liquids consisting of the 1-butyl-3-methylimidazolium cation with various anions and the bis(trifluoromethylsulfonyl)imide anion with various cations. *The Journal of Physical Chemistry B* 2007; **112**: 81-92.
44. Rudnick LR, Bartz WJ, Comparison of synthetic, mineral oil, and bio-Based lubricant fluids. Rudnick L R, *Synthetics, Mineral Oils, and Bio-Based Lubricants: Chemistry and Technology*, CRC Press, Wilmington, Delaware, USA, 2005, 331-349.
45. Zhang S, Sun N, He X, Lu X, Zhang X. Physical properties of ionic liquids: Database and evaluation. *Journal of Physical and Chemical Reference Data* 2006; **35**: 1475-1517.
46. Gardas RL, Freire MG, Carvalho PJ, Marrucho IM, Fonseca IMA, Ferreira AGM, Coutinho JAP. High-Pressure Densities and Derived Thermodynamic Properties of Imidazolium-Based Ionic Liquids. *Journal of Chemical and Engineering Data* 2007; **52**: 80-88.
47. Randles SJ, Lubricants of the Future and Environment, 6th International Congress, Brussels, 1999.
48. Wagner W, Pruss A. The IAPWS formulation 1995 for the thermodynamic properties of ordinary water substance for general and scientific use. *Journal of Physical and Chemical Reference Data* 2002; **31**: 387-535.
49. Fandiño O, López ER, Lugo L, Fernández J. Compressed liquid densities of two dipentaerythritol esters. *Fluid Phase Equilibria* 2010; **296**: 30-36.
50. T. Regueira, L. Lugo, M.J.P. Comuñas, J. Fernández, Experimental density and viscosity data of some vegetable oils, European Conference on Thermophysical Properties, ECTP-2008, Pau (France), 31 August - 4 September, 2008.

51. Nieto de Castro CA, Langa E, Morais AL, Lopes MLM, Lourenço MJV, Santos FJV, Santos MSCS, Lopes JNC, Veiga HIM, Macatrão M, Esperança JMSS, Marques CS, Rebelo LPN, Afonso CAM. Studies on the density, heat capacity, surface tension and infinite dilution diffusion with the ionic liquids [C4mim][NTf2], [C4mim][dca], [C2mim][EtOSO3] and [Aliquat][dca]. *Fluid Phase Equilibria* 2010; **294**: 157-179.
52. Yuyama K, Masuda G, Yoshida H, Sato T. Ionic liquids containing the tetrafluoroborate anion have the best performance and stability for electric double layer capacitor applications. *Journal of Power Sources* 2006; **162**: 1401-1408.
53. Appetecchi GB, Montanino M, Zane D, Carewska M, Alessandrini F, Passerini S. Effect of the alkyl group on the synthesis and the electrochemical properties of N-alkyl-N-methyl-pyrrolidinium bis(trifluoromethanesulfonyl)imide ionic liquids. *Electrochimica Acta* 2009; **54**: 1325-1332.
54. Furlani M, Albinsson I, Mellander BE, Appetecchi GB, Passerini S. Annealing protocols for pyrrolidinium bis(trifluoromethylsulfonyl)imide type ionic liquids. *Electrochimica Acta* 2011; **57**: 220-227.
55. Paulechka YU, Kabo AG, Blokhin AV, Kabo GJ, Shevelyova MP. Heat capacity of ionic liquids: Experimental determination and correlations with molar volume. *Journal of Chemical & Engineering Data* 2010; **55**: 2719-2724.
56. Shimizu Y, Ohte Y, Yamamura Y, Tsuzuki S, Saito K. Comparative study of imidazolium- and pyrrolidinium-based ionic liquids: Thermodynamic properties. *The Journal of Physical Chemistry B* 2012; **116**: 5406-5413.
57. Martinelli A, Matic A, Jacobsson P, Börjesson L, Fernicola A, Scrosati B. Phase behavior and ionic conductivity in lithium bis(trifluoromethanesulfonyl)imide-doped ionic liquids of the pyrrolidinium cation and bis(trifluoromethanesulfonyl)imide anion. *The Journal of Physical Chemistry B* 2009; **113**: 11247-11251.
58. Abdallah T, Lemordant D, Claude-Montigny B. Are room temperature ionic liquids able to improve the safety of supercapacitors organic electrolytes without degrading the performances? *Journal of Power Sources* 2012; **201**: 353-359.
59. Tokuda H, Ishii K, Susan MABH, Tsuzuki S, Hayamizu K, Watanabe M. Physicochemical properties and structures of room-temperature ionic liquids. 3. Variation of cationic structures. *The Journal of Physical Chemistry B* 2006; **110**: 2833-2839.
60. Funston AM, Fadeeva TA, Wishart JF, Castner EW. Fluorescence probing of temperature-dependent dynamics and friction in ionic liquid local environments. *The Journal of Physical Chemistry B* 2007; **111**: 4963-4977.
61. MacFarlane DR, Meakin P, Sun J, Amini N, Forsyth M. Pyrrolidinium imides: A new family of molten salts and conductive plastic crystal phases. *The Journal of Physical Chemistry B* 1999; **103**: 4164-4170.
62. Ionic liquids product range for your innovations, Merck KGaA.
63. Zhang Z-H, Tan Z-C, Sun L-X, Jia-Zhen Y, Lv X-C, Shi Q. Thermodynamic investigation of room temperature ionic liquid: The heat capacity and standard enthalpy of formation of EMIES. *Thermochimica Acta* 2006; **447**: 141-146.

Chapter 6

High pressure phase equilibria
Results and discussion

In this chapter the results concerning phase equilibrium at high pressure among CO_2 and vegetable oils, as well as biodegradable oils developed for their use in two stroke engines are presented. Firstly, the results obtained with the isochoric technique are reported, i.e. CO_2 solubility in a reference (SYN-2T) and in a biodegradable developed oil (BIO-2T-03) from 283 K to 348 K and pressures up to 9 MPa. It was found that CO_2 solubility is higher in BIO-2T-03 than in SYN-2T. Moreover, the obtained data were successfully modeled through the PC-SAFT EoS, finding average deviations, expressed in CO_2 mass fraction, of 0.006 and 0.015 for CO_2+SYN-2T and CO_2+BIO-2T-03, respectively.

After, results obtained in the PATh (University of Aveiro) laboratory are presented. Thus, data dealing with CO_2 solubility in a high oleic sunflower oil (HOSO-B1), a castor oil and a rapeseed oil are reported for mole fractions of CO_2 ranging from 0.32 to 0.93 in the temperature range from 298 to 363 K and up to 75 MPa. It was found that HOSO-B1 and rapeseed oil present similar CO_2 solubilities in all the composition range, whereas those in castor oil are lower. The obtained data were modelled through the SRK-EoS with global absolute average deviations, expressed in CO_2 mole fraction, lower to 6%.

Finally, the implantation of a new experimental device based on visual cell for determining phase equilibria up to 100 MPa is presented together with the results of the solubility of CO_2 in HOSO-B1 and in a biodegradable developed lubricant (BIO-2T-05) composed by HOSO-B1 and PAO2. Results for the system composed by HOSO-B1 were compared with the previously ones obtained in the University of Aveiro, obtaining an AAD% for the CO_2 mole fraction of 2.2 %. Moreover, vapor-liquid-liquid equilibrium was observed for the system CO_2 + BIO-2T-05. Additionally, the reliability of the Carvalho and Coutinho prediction method was examined for all the studied systems.

These results are further explained in the following sections:

1. Carbon dioxide solubility in reference and vegetable lubricants developed for two stroke engines. *T. Regueira, O. Fandiño, L. Lugo, E.R. López, J. Fernández, J. Supercrit. Fluids 68 (2012) 123–130.*
2. Experimental measurements and modelling of CO_2 solubility in sunflower, castor and rapeseed oils for two stroke engines. *T. Regueira, P.J. Carvalho, M.B. Oliveira, L. Lugo, J.A.P. Coutinho, J. Fernández, J. Supercrit. Fluids, accepted.*
3. A new experimental high pressure device to determine phase equilibria. Measurements of two CO_2+ biodegradable oil systems. *T. Regueira, O. Fandiño, L. Lugo, E.R. López, J. Fernández, to be submitted.*

6.1. Carbon dioxide solubility in reference and vegetable lubricants developed for two stroke engines*

*T. Regueira, O. Fandiño, L. Lugo, E.R. López, J. Fernández, J. Supercrit. Fluids 68 (2012) 123–130. http://www.sciencedirect.com/science/article/pii/S0896844612001532

Abstract

The solubilities of carbon dioxide, CO_2, in a reference semi-synthetic oil and in a developed vegetable-sunflower-based oil for two stroke engines have been measured from 283 K to 348 K and pressures up to 9 MPa in a high pressure gas solubility apparatus that works in isochoric conditions. The densities of the developed vegetable oil from 293 K to 353 K and pressures up to 60 MPa were also measured by using a vibrating tube technique. It was found that the solubility of CO_2 in the vegetable oil is higher than in the reference semi-synthetic oil. The solubility of CO_2 in both lubricants decreases when the temperature increases. In addition, we have found that the solubilities of O_2 in these lubricants are between 7 and 10 times lower than those of CO_2. Furthermore, PC-SAFT EoS was employed to model the solubility behavior of CO_2 in both lubricants and the goodness of Carvalho and Coutinho model for prediction of CO_2 solubility in low volatile solvents was checked for these lubricants.

1. Introduction

Nowadays the searching of new products safe with the environment is a challenge. One of the areas of interest is the field of lubrication. It is estimated [1,2] that approximately 50% of all lubricants sold worldwide end up in the environment via total loss applications, volatility, spills or accidents. The lubricant market is dominated by mineral oils, which have a high ecotoxicity and low biodegradability. The first alternative was turn to synthetics [3], more friendly to the environment and even with superior performance [4] than mineral oils, but with the disadvantage of having a high price. In this scenario, to look back on vegetable oils (really biodegradable and only little more expensive than mineral oils) still comprises a narrow segment; however, they are finding their way replacing mineral oils [5].

Vegetable oils present very interesting properties [6] as their inherent lubricity (polar ester groups being responsible) or low volatility. Nevertheless, vegetable oils show some disadvantages as their poor low-temperature properties, reduced operating temperature ranges, moderate oxidative stability and their availability in limited viscosity ranges [1,2,7-10].

Two-stroke engines are one of the applications where most of the lubricants and their degradation products are released directly into the environment, polluting the soil, water and atmosphere [1,5,11]. The knowledge of the solubility of different gases such as O_2, N_2 and CO_2 in lubricants used for two stroke engines is important because these gases are involved in the combustion process together with the lubricant and the gasoline in the combustion chamber. Besides, it has been claimed [12] that under boundary or mixed lubrication regimes, the solubility of O_2 in non-additivated oils improves their lubricating performance or provides seizure resistance [12,13]. On the other hand, CO_2 is a natural refrigerant that is being considered

as a potential candidate to replace existing refrigerants, especially in small and medium systems [14]. Thus, in applications where the lubricant is in contact with the refrigerant, its solubility in the oil is a key property [15]. Moreover, knowledge of the solubility data of the systems CO_2 + vegetable oil is necessary for the design of supercritical carbon dioxide extraction processes of oils and other compounds from seeds [16-20].

In this work, the solubilities of carbon dioxide, CO_2, in a developed vegetable-sunflower-based oil for two stroke engines and in a reference semi-synthetic oil (currently used in this application) have been measured from 283 K to 348 K and pressures up to 9 MPa in a high pressure gas solubility apparatus [21]. Furthermore, some solubility data of oxygen in these lubricants were roughly determined in order to compare them with CO_2 solubilities. We have correlated CO_2 experimental solubility data using perturbed-chain SAFT (PC-SAFT) EoS [22] and analyzed the reliability of the Carvalho and Coutinho prediction method [23]. This last method can be useful, according to authors [23], for process design and calculations in enhanced oil recovery, purification of vegetable or animal oils or the extraction of value-added compounds from them, Selexol process or CO_2 capture and gas separation purposes.

2. Material and methods

Semi-synthetic and vegetable oils studied in this work were provided by Abamotor and Verkol Lubricantes, respectively. Some of their main characteristics are summarised in table 1. The semi-synthetic oil is composed mainly by a paraffinic mineral oil and a synthetic base. Molecular weight of this semi-synthetic oil (SYN-2T) was estimated to be 505 $g \cdot mol^{-1}$ by means of the ASTM D2502-04 (2009), taking into account its viscosity values [24], whereas molecular weight of the biodegradable formulated oil (BIO-2T-03) was assumed to be the same as its base oil, high oleic sunflower oil, i.e. 882 $g \cdot mol^{-1}$ [25]. Carbon dioxide was provided by Air Liquide, with a purity of 99.998%.

Table 1. Density (ρ), kinematic viscosity (ν), and viscosity index (VI) of the two stroke engine lubricants.

Name	Description	ρ /g cm^{-3} (293.15 K)	ν / mm^2·s^{-1} (313.15 K)	VI
SYN-2T	Semi-synthetic oil	0.8758 [24]	62.96 [24]	118.1 [24]
BIO-2T-03	Biodegradable oil	0.9130	46.35	180.3

A SVM3000 Anton Paar Stabinger device [26] was used to characterize the lubricant BIO-2T-03 in terms of density, viscosity and viscosity index (VI). Uncertainty in density measurements is 0.0005 $g \cdot cm^{-3}$, whereas for the dynamic viscosity is 1%. More details can be found in previous works [27,28].

High pressure density data of the lubricants are necessary to determine the gas solubility, among other properties. Densities of SYN-2T were published in a previous work [24], whereas the densities of BIO-2T-03 up to 60 MPa were determined in the present work by means of an automated Anton Paar HPM vibrating tube densimeter [29]. The density equipment and experimental procedure were explained elsewhere [29]. The uncertainty of density has been estimated [29] to be 0.0007 $g \cdot cm^{-3}$.

The experimental device used for solubility measurements is based on an isochoric saturation technique [15,21,30]. In this technique the solubility is determined by means of the pressure drop, observed during the gas absorption process in a precisely determined quantity of degassed solvent, inside a system of known volume.

The experimental equipment, placed inside a temperature test chamber DYCOMETAL, CETM-40/300, consists of a stainless steel pressure line that connects the gas bottle with the equilibrium cell (Fig.1). The system consisting of the gas cell and the interconnection pipes and valves until the entrance of the equilibrium cell is named as '*gas system*'. Moreover, the gas cell and the equilibrium cell are placed, each of them, inside a jacketed glass. A pressure transducer PAROSCIENTIFIC 42K-HT-101, is placed in the pressure line and the system temperature is measured by means of two temperature probes Pt-100 located inside the jacketed glasses and connected to a thermometer ASL F250. The main characteristics of the experimental equipment are summarised in table 2 and the experimental procedure is fully detailed elsewhere [15,21,30].

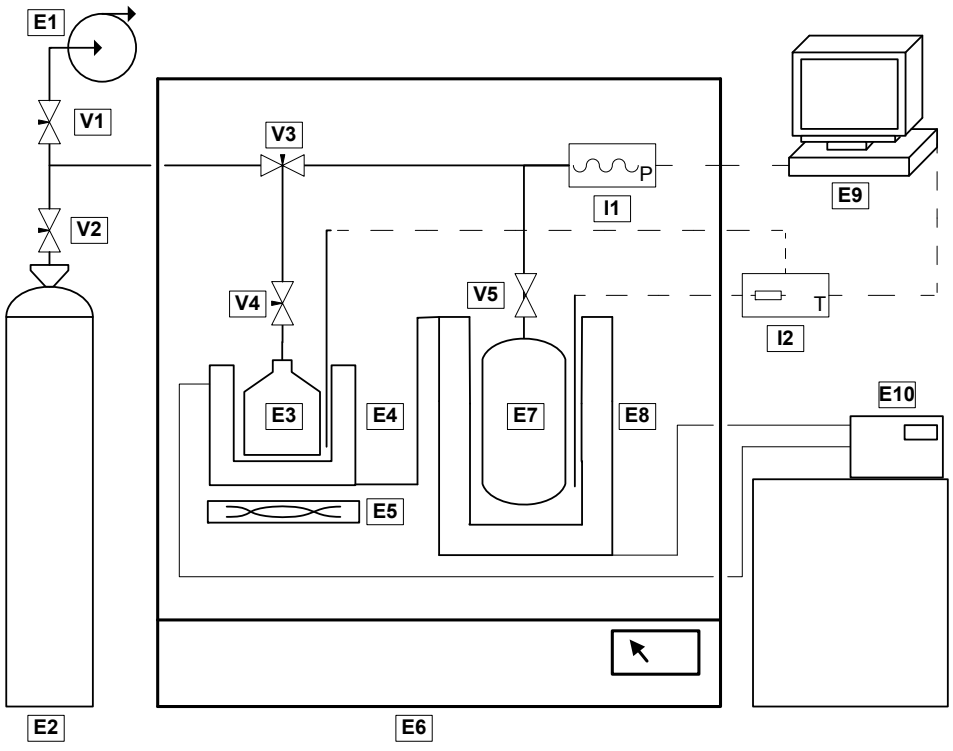

Fig.1. Solubility equipment diagram. (E1) Vacuum pump, (E2) gas bottle, (E3) equilibrium cell, (E4, E8) jacketed glasses, (E5) magnetic stirrer, (E6) temperature test chamber, (E7) gas cell, (E9) computer, (E10) thermostatic bath; (V1 to V5) valves; (I1) pressure transducer, (I2) thermometer.

Table 2. Solubility equipment. Measurement ranges, resolutions and uncertainties.

Device	Measurement range	Resolution	Uncertainty
Temperature test chamber	233.15 – 423.15 K	± 0.01 K	± 0.1 K
Thermometer	233.15 – 423.15 K	± 0.001 K	± 0.02 K
Transducer	0 – 13.8 MPa	± 0.0001 MPa	0.02 % FS
Balance	0 – 1000 g	± 0.001 g	± 0.001 g

The quantity of gas initially introduced in the gas cell is referred as m_1 whereas the quantity of degassed lubricant in the equilibrium cell is referred as m_2. Therefore, the quantity of gas absorbed by the lubricant (m_1^{ab}) is given by the following equation:

$$m_1^{ab} = m_1 - m_1^g \tag{1}$$

where m_1^g is the quantity of gas not absorbed by the lubricant, given by the following expression:

$$m_1^g = \rho_1(T_{gas\,s.}, p)V_{gas\,s.}(T_{gas\,s.}) + \rho_1(T_{cell}, p)\left[V_{cell}(T_{cell}) - \left(\frac{m_2}{\rho_2(T_{cell}, p)} + V_{abs\,g.}(T_{cell}, p)\right)\right] \tag{2}$$

where $\rho_1(T_{gas\,s.}, p)$ is the gas density at equilibrium temperature of the gas system and equilibrium pressure, $V_{gas\,s.}(T_{gas\,s.})$ is the volume at the equilibrium temperature of the gas system**,** $\rho_1(T_{cell}, p)$ is the gas density at the equilibrium cell temperature and equilibrium pressure, $\rho_2(T_{cell}, p)$ is the lubricant density at the equilibrium cell temperature and equilibrium pressure, $V_{cell}(T_{cell})$ is the equilibrium cell volume at the equilibrium cell temperature and finally $V_{abs\,g.}(T_{cell}, p)$ is the volume of the absorbed gas at the equilibrium cell temperature and equilibrium pressure.

Densities of lubricants at the conditions of the equilibrium cell were determined using the Tammann-Tait correlations from Regueira et al. [24] and from this work for SYN-2T and BIO-2T-03, respectively. Besides, CO_2 density data were obtained from the reference equation of state of Span and Wagner [31], using the REFPROP 8 database [32].

Furthermore, the volume of absorbed gas at the equilibrium cell temperature and equilibrium pressure can be written as the product of the partial specific volume in the liquid phase $\bar{v}_{abs\,g.}$ by the mass of absorbed gas:

$$V_{abs\,g.}(T_{cell}, p) = \bar{v}_{abs\,g.}(T_{cell}, p) \cdot m_1^{ab} \tag{3}$$

Taking into account that for the experimental conditions, the temperature T is higher than the saturation temperature of the CO_2 or than its critical temperature, $T_{c,gas}$, we have to distinguish between the following two situations in order to estimate the partial specific volume:

(1) If $T < T_{c,gas}$, then it is calculated as the liquid specific volume at the bubble point at temperature T.

(2) If $T > T_{c,gas}$, the partial specific volume is calculated as the specific volume at infinite dilution in liquid phase, which was obtained following the method proposed by Zellner et al. [33].

In order to obtain the value of m_1^{ab} we replace in Eq. (1) the value of m_1^g given by Eq. (2), while at the same time, we substitute in Eq. (2) the value of $V_{abs\,g.}(T_{cell}, p)$ given by Eq. (3). Thus, we obtain the following expression:

$$m_1^{ab} = \frac{m_1 - \rho_1(T_{gas\,s.}, p)\cdot V_{gas\,s.}(T_{gas\,s.}) - \rho_1(T_{cell}, p)\cdot\left(V_{cell}(T_{cell}) - \dfrac{m_2}{\rho_2(T_{cell}, p)}\right)}{1 - \rho_1(T_{cell}, p)\cdot\bar{v}_{abs\,g.}(T_{cell}, p)} \tag{4}$$

Therefore, it is possible to calculate the mass fraction of the gas absorbed by the lubricant by means of:

$$w_1 = \frac{m_1^{ab}}{m_1^{ab} + m_2} \tag{5}$$

The total uncertainty of the solubilities is determined for each experimental value taken into account the influence of the uncertainties of the volume of the equilibrium cell, total volume of the system, volume of the absorbed gas in the solvent, lubricant and gas masses, and the density of carbon dioxide due to the equation of state, and according to the characteristics reported in Table 2 [30].

3. Results and discussion

3.1 Experimental results

Density values at atmospheric pressure of BIO-2T-03, measured by using a Stabinger Anton Paar SVM 3000, are presented in table 3 along with viscosity values in the temperature range from 278.15 K to 373.15 K. Experimental density values of BIO-2T-03 are reported in table 4, for pressures up to 60 MPa and in the temperature range from 293.17 K to 353.16 K. At atmospheric pressure, both sets of experimental densities agree very well, with an AAD of 0.04%.

Table 3. Experimental density (ρ) and viscosity (η) values of BIO-2T-03 at atmospheric pressure.

T / K	ρ / g·cm^{-3}	η / mPa·s
278.15	0.9231	242.0
283.15	0.9198	177.9
288.15	0.9164	133.8
293.15	0.9130	102.6
298.15	0.9097	80.03
303.15	0.9064	63.47
308.15	0.9030	51.09
313.15	0.8997	41.70
318.15	0.8964	34.48
323.15	0.8930	28.84
328.15	0.8897	24.39
333.15	0.8864	20.83
338.15	0.8831	17.95
343.15	0.8798	15.60
348.15	0.8765	13.65
353.15	0.8732	12.04
358.15	0.8699	10.68
363.15	0.8666	9.530
368.15	0.8633	8.552
373.15	0.8599	7.714

Table 4. Experimental density data (ρ) of BIO-2T-03 at different pressures and temperatures.

T /K	p /MPa	ρ / g·cm^{-3}	T /K	p /MPa	ρ / g·cm^{-3}
293.17	0.10	0.9132	333.21	0.10	0.8861
293.17	1.00	0.9143	333.21	1.00	0.8866
293.17	5.00	0.9165	333.22	5.00	0.8892
293.17	10.00	0.9191	333.22	10.00	0.8923
293.17	15.00	0.9216	333.22	15.00	0.8953
293.17	20.00	0.9241	333.22	20.00	0.8981
293.17	30.00	0.9288	333.22	30.00	0.9037
293.17	40.00	0.9334	333.22	40.00	0.9089
293.17	50.00	0.9378	333.22	50.00	0.9138
293.17	60.00	0.9419	333.22	60.00	0.9185
313.11	0.10	0.8998	353.16	0.10	0.8726
313.12	1.00	0.9003	353.16	1.00	0.8732
313.12	5.00	0.9027	353.16	5.00	0.8760
313.12	10.00	0.9055	353.16	10.00	0.8794
313.12	15.00	0.9083	353.16	15.00	0.8826
313.12	20.00	0.9110	353.16	20.10	0.8857
313.12	30.00	0.9161	353.16	30.00	0.8917
313.13	40.00	0.9210	353.16	40.00	0.8972
313.13	50.00	0.9256	353.16	50.00	0.9024
313.13	60.00	0.9300	353.16	60.00	0.9074

Density data over the entire range of temperature and pressure were correlated by means of the Tammann-Tait equation:

$$\rho(T/\mathrm{K},\ p/\mathrm{MPa}) = \frac{\rho(T/\mathrm{K},\ 0.1\ \mathrm{MPa})}{1 - C\ln\left(\dfrac{B(T/\mathrm{K}) + p/\mathrm{MPa}}{B(T/\mathrm{K}) + 0.1\ \mathrm{MPa}}\right)} \tag{6}$$

where C is a parameter independent of temperature and pressure [34], $\rho(T/\mathrm{K}, 0.1\,\mathrm{MPa})$ is given by the following polynomial expression:

$$\rho(T/\mathrm{K}, 0.1\mathrm{MPa}) = \sum_{i=0}^{m} A_i \left(T/\mathrm{K}\right)^i \tag{7}$$

$B(T/K)$ is a parameter depending on temperature as a polynomial function:

$$B(T/\mathrm{K}) = \sum_{j=0}^{n} B_j \left(T/\mathrm{K}\right)^j \tag{8}$$

Parameters obtained for Tammann-Tait correlation are presented in Table 5, along with standard deviations, σ, for $\rho(T/\mathrm{K}, 0.1\,\mathrm{MPa})$ and σ^* for $\rho(T/\mathrm{K}, p/\mathrm{MPa})$. The obtained AAD% between experimental values and those correlated is 0.014%. Correlated density values of BIO-2T-03 were compared with those of the reference semi-synthetic oil for two stroke engine application, SYN-2T [24], in the temperature range from 298 K to 348 K and in the whole pressure range, observing that density of the biodegradable lubricant is around 4% lower than density of the semi-synthetic lubricant.

Table 5. A_i, B_i, C and standard deviations, σ and σ^* from Tammann- Tait equation for BIO-2T-03.

BIO-2T-03			
A_0 /g·cm^{-3}	1.111792	B_0 /MPa	171.7
-10^3·A_1 /g·cm^{-3}·K^{-1}	0.67727	B_1 /MPa·K^{-1}	0.126
10^4·σ /g·cm^{-3}	0.6	-10^3·B_2 /MPa·K^{-2}	0.97226
10^2·C	7.823	10^4·σ^* / g·cm^{-3}	1.7

Isothermal compressibility values (κ_T) were obtained by differentiation from the Tammann-Tait correlation, according to the definition:

$$\kappa_T = \frac{1}{\rho}\left(\frac{\partial \rho}{\partial p}\right)_T \tag{9}$$

The BIO-2T-03 isothermal compressibility values (κ_T) are plotted in Fig. 2 against pressure for different temperatures, together with the κ_T values of SYN-2T reported in a previous

work [24]. It can be observed that κ_T values are higher (between 2% and 3%) for the reference semi-synthetic oil than for the developed biodegradable oil.

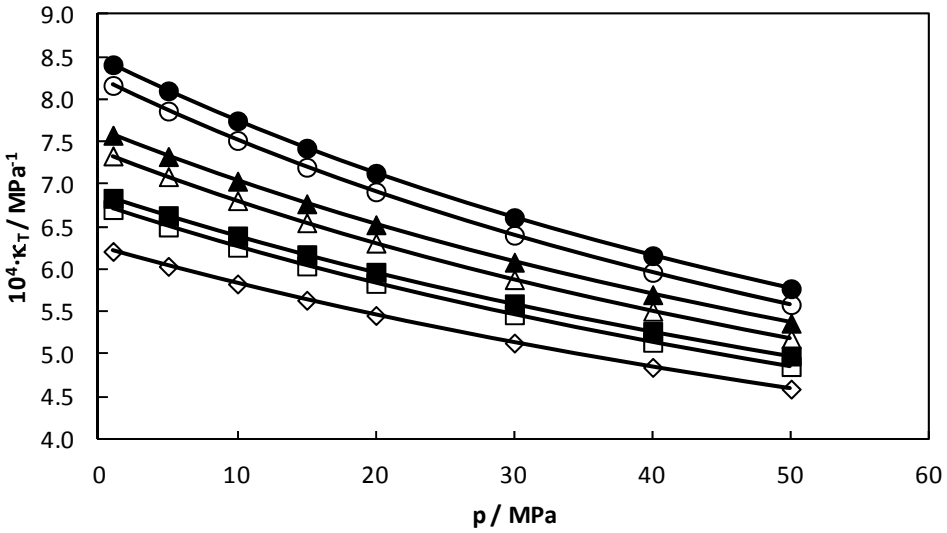

Fig.2. Isothermal compressibilities (κ_T) of BIO-2T-03 (empty symbols) and those of SYN-2T [24] (filled symbols). 353.15K (○, ●), 333.15 K (△, ▲), 313.15 K (□, ■) and 293.15 K (◇).

Carbon dioxide solubility in these oils was measured at 283.15 K, 298.15 K, 323.15 K and 348.15 K and up to 9 MPa. The experimental solubility data for CO_2 + SYN-2T and CO_2 + BIO-2T-03 are summarised in table 6. In this table, the estimated absolute uncertainty of each experimental point is also presented. Fig. 3a and 3b show the *p-x* diagrams for both systems at the different temperatures. For both lubricants, CO_2 solubility decreases with the temperature at constant pressure, and increases with pressure at constant temperature. CO_2 solubility is higher in the vegetable based oil BIO-2T-03 (Fig. 3b) than in the semi-synthetic reference oil SYN-2T (Fig. 3a), which shows that the molecular affinity between the lubricant and CO_2 is higher for the vegetable lubricant.

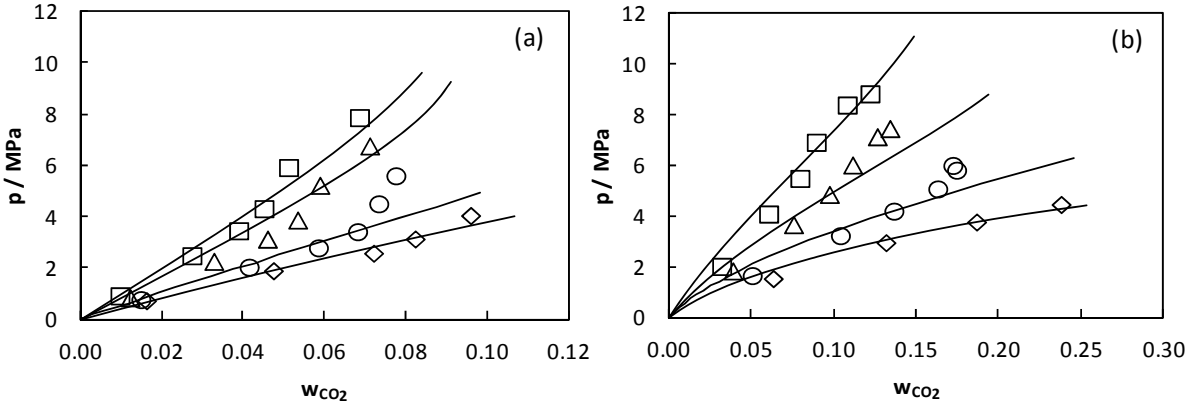

Fig.3. CO_2 solubility at different temperatures: 283.15 K (◇), 298.15 K (○), 323.15 K (△) and 348.15 K (□). PC-SAFT EoS (—). (a) in SYN-2T and (b) in BIO-2T-03.

Table 6. Mass fraction solubility of CO_2 in SYN-2T and in BIO-2T-03.

T/K	p/MPa	w_{CO2}	w_{CO2} *uncertainty*	T/K	p/MPa	w_{CO2}	w_{CO2} *uncertainty*
	SYN-2T				BIO-2T-03		
283.15	0.7459	0.0164	±0.0006	283.15	1.5567	0.064	±0.001
283.15	1.9163	0.048	±0.001	283.15	2.9731	0.132	±0.002
283.15	2.5975	0.072	±0.003	283.15	3.7877	0.187	±0.002
283.15	3.1536	0.083	±0.003	283.15	4.4782	0.238	±0.004
283.15	4.0657	0.096	±0.005	298.15	1.6750	0.051	±0.001
298.15	0.7903	0.0151	±0.0006	298.15	3.2499	0.104	±0.003
298.15	2.0552	0.042	±0.001	298.15	4.2168	0.137	±0.005
298.15	2.8086	0.059	±0.003	298.15	5.0936	0.163	±0.004
298.15	3.4379	0.068	±0.003	298.15	5.8321	0.175	±0.011
298.15	4.5244	0.074	±0.005	298.15	6.0185	0.172	±0.012
298.15	5.6166	0.078	±0.008	323.15	1.8598	0.039	±0.001
323.15	0.8642	0.0124	±0.0006	323.15	3.6851	0.076	±0.003
323.15	2.2816	0.033	±0.001	323.15	4.8767	0.098	±0.006
323.15	3.1469	0.046	±0.003	323.15	6.0365	0.112	±0.009
323.15	3.8931	0.054	±0.004	323.15	7.1531	0.127	±0.013
323.15	5.2456	0.059	±0.006	323.15	7.4742	0.134	±0.015
323.15	6.7805	0.071	±0.009	348.15	2.0383	0.032	±0.001
348.15	0.9376	0.0099	±0.0006	348.15	4.1040	0.061	±0.003
348.15	2.5030	0.028	±0.001	348.15	5.5069	0.080	±0.005
348.15	3.4757	0.039	±0.003	348.15	6.9325	0.090	±0.008
348.15	4.3339	0.045	±0.003	348.15	8.4025	0.109	±0.012
348.15	5.9379	0.051	±0.005	348.15	8.8442	0.122	±0.015
348.15	7.8837	0.069	±0.009				

There are scarce literature data concerning CO_2 solubility in sunflower oil. Soares et al. [35] have published solubility data for the system CO_2 + a sunflower oil from 313.15 K to 353.15 K, but only at high CO_2 mass fractions ($w_{CO_2} > 0.99$). Furthermore, Fernández-Ronco et al. [36] have published CO_2 solubility data in a sunflower oil at 314.4 K and 325.9 K for $w_{CO2} > 0.20$. As BIO-2T-03 is a lubricant based in high oleic sunflower oil (HOSO-B1), in Fig. 4 we have plotted experimental solubility data for CO_2 in BIO-2T-03 at 298.15 and 323.15 K together with data from Fernández-Ronco et al. [36] at 314.4 and 325.9 K. It can be observed a good agreement between both data sets, taking into account that fatty acid composition is slightly different for both oils. The CO_2 solubility values presented here permit a better knowledge of the phase diagram of CO_2 + sunflower oil.

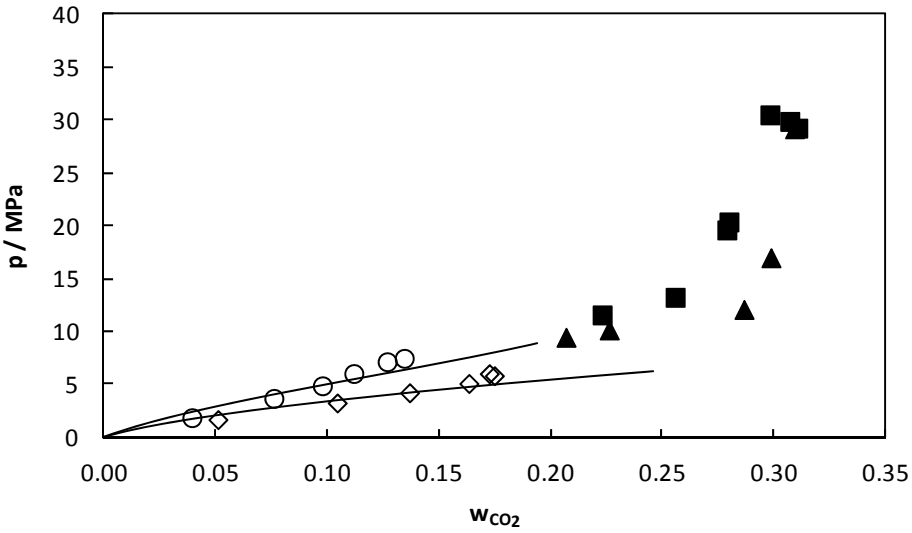

Fig. 4. CO_2 solubility in a sunflower oil [36] at 314.4 K (▲), 325.9 K (■); and in BIO-2T-03 [this work] at 298.15 K (◇), 323.15 K (○). Theoretical results using PC-SAFT EoS for BIO-2T-03 (—).

In Fig. 5a, we have plotted CO_2 solubilities at 298.15 K for SYN-2T and BIO-2T-03 along with other lubricants and oils from literature [15,21,30,37-41]. It can be observed that SYN-2T lubricant presents positive deviations from Raoult's law for x_{CO_2} higher than 0.4, whereas for the polar lubricants negative deviations are found up to mole fractions x_{CO_2} of 0.8 or higher. Fig. 5b shows that the p-x_{CO_2} behaviour in SYN-2T (additivated paraffinic oil) at 323.15 K, is quite similar to those in long chain alkanes, as eicosane [37], docosane [37] and squalane [38].

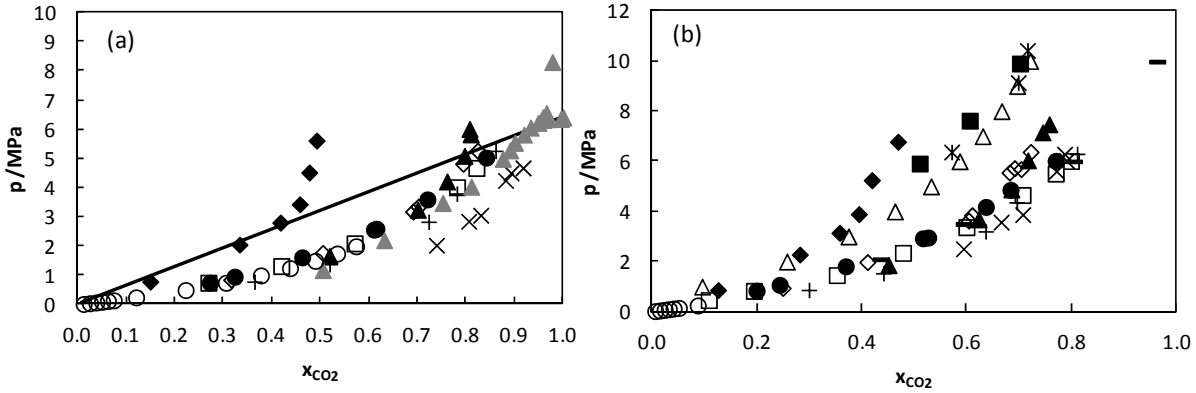

Fig.5. Solubility of CO_2 in: SYN-2T (◆), olive oil [40] (○), BIO-2T-03 (▲), DiPEC7 [30] (+), PAG1 [30] (×), PEC7 [15] (◇), PEBE8 [21] (□), PEC5 [21] (●), POE ISO 56 [39] (▲), eicosane [37] (■), docosane [37] (✳), squalane [38] (△) and PAG0 [41] (–). (a) 298.15 K and (b) 323.15 K. Solid line represents the Raoult's law at 298.15 K.

Recently, Carvalho and Coutinho [23] have proposed the following general correlation for predicting the solubility of CO_2 in nonvolatile solvents, such as ionic liquids, alkanes, alcohols and methyl esters:

$$\frac{p/\mathrm{MPa}}{1\,\mathrm{MPa}} = \frac{m_i/\mathrm{mol\cdot kg^{-1}}}{1\,\mathrm{mol\cdot kg^{-1}}} e^{\left(6.8591-\frac{2004.3}{T/\mathrm{K}}\right)} \tag{10}$$

where m_i is the CO_2 solubility. Eq. (10) is valid for pressures up to 5 MPa, for temperatures ranging from room temperature up to 363 K and molalities up to 3 mol·kg^{-1}. These authors stands that when the molecular weight effect is removed from the solubility analysis by comparing the solubilities in molalities instead of mole fractions, the differences in solubilities, among different systems, are minimized, and the solubility of CO_2 in nonvolatile solvents seems to be essentially solvent independent. They have analyzed with the Flory-Huggins model that the deviations of Raoult's law at low CO_2 concentration are mainly due to entropic effects for most of the non-volatile solvents.

Fig. 6 shows the experimental solubility values expressed in CO_2 molality (m_{CO_2}) for the two lubricants studied in this work. It can be observed that Eq. 10 predicts the equilibrium pressure for the CO_2+ BIO-2T-03 system reasonably well (AAD = 8.3%) but not for the CO_2+ SYN-2T system (AAD = 41.7%). The satisfactory predictions for the vegetable oil contrast with the high underestimations found by Carvalho and Coutinho [23] with their model for fatty acid alkyl esters. These authors have attributed this fact to the energetically favourable CO_2-carbonyl interactions when compared with both the CO_2-CO_2 and the carbonyl-carbonyl interactions.

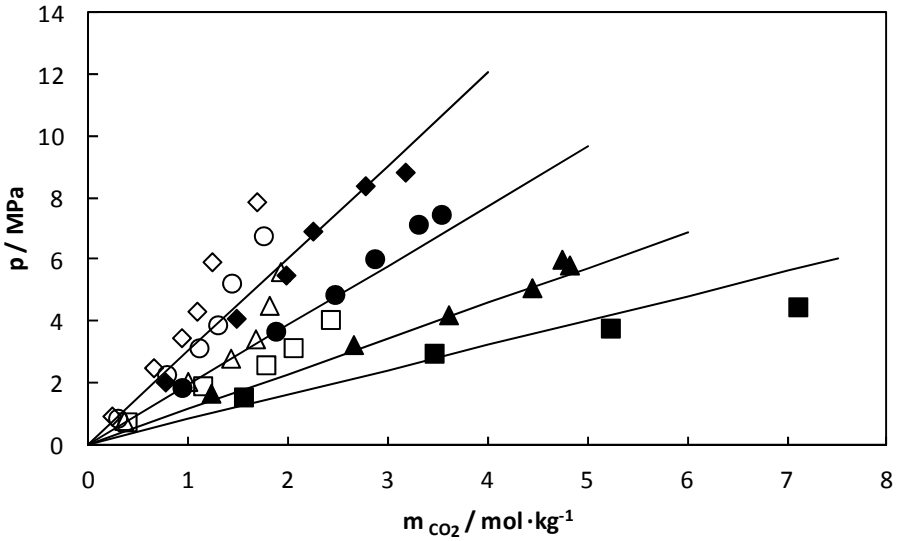

Fig.6. Pressure – molality diagram for CO_2 solubility in SYN-2T (empty symbols) and BIO-2T-03 (filled symbols) at different temperatures: 348.15 K (◇,◆), 323.15 K (○, ●), 298.15 K (△, ▲) and 283.15 K (□, ■). Carvalho-Coutinho general correlation [23] (—).

Eq. (10) can be written as a function of mass fraction as follows:

$$\frac{p/\mathrm{MPa}}{1\,\mathrm{MPa\cdot g\cdot mol^{-1}}} = \frac{w_{CO2}}{(1-w_{CO_2})\cdot 10^{-3}\cdot M_{wCO2}/\mathrm{g\cdot mol^{-1}}} \cdot e^{\left(6.8591-\frac{2004.3}{T/\mathrm{K}}\right)} \tag{11}$$

In Fig. 7 it is plotted the solubility of CO_2 in BIO-2T-03 and in SYN-2T, as well as in different lubricants and oils from literature [15,21,30,39,40,42] at 298.15 K. In this figure, it can be observed that, in the low concentration range, the semi-synthetic oil SYN-2T and the polyalphaolefin (PAO) [42] present positive deviations from the general correlation of Carvalho and Coutinho, whereas slightly negative deviations from this correlation are found for pentaerythritol tetraalkanoates (PEC7 [15] and PEC5 [21]), pentaerythritol tetra-2-ethylhexanoate (PEBE8 [21]), dipentaerythritol heptanoate (DiPEC7 [30]), a polyalkylene glycol (PAG1 [30]) and a formulated polyolester (POE ISO 56 [39]). Positive deviations for the semi-synthetic oil SYN-2T and the polyalphaolefin (PAO) could be explained because CO_2 solubility is not mainly due to entropic effects but also to the fact that interactions between unlike molecules (CO_2 + SYN-2T or CO_2 + PAO) must be weaker than between like molecules.

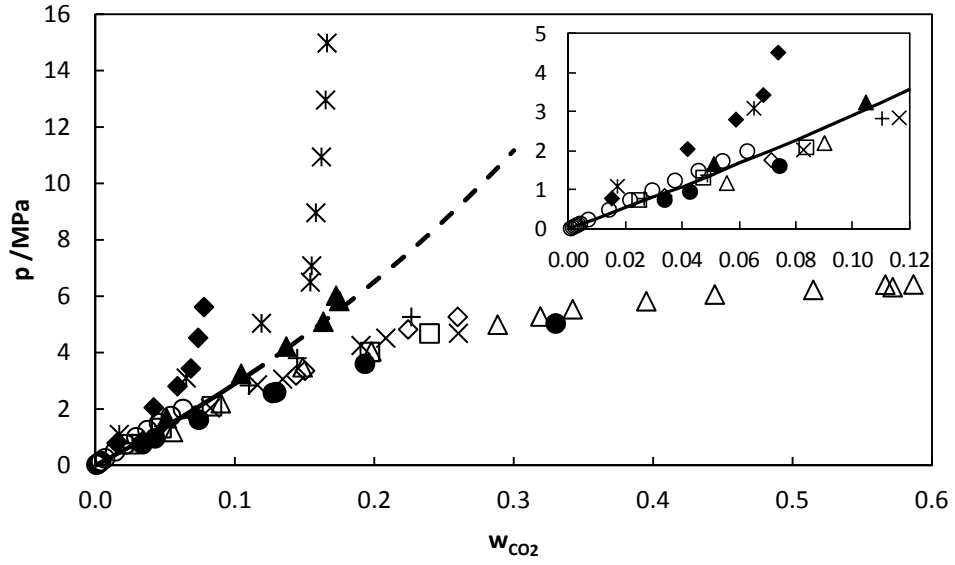

Fig.7. Solubility of CO_2 at 298.15 K in different lubricants: SYN-2T (◆), PAO [42] (✳), olive oil [40] (○), BIO-2T-03 (▲), DiPEC7 [30] (+), PAG1 [30] (×), PEC7 [15] (◇), PEBE8 [21] (□), PEC5 [21] (●), POE ISO 56 [39] (△). Solid line is the Carvalho-Coutinho general correlation and dashed line is an extrapolation of Carvalho-Coutinho general correlation.

As it was pointed out, we have also determined the solubility of O_2 in the same lubricants from 298.15 K to 348.15 K. It was found that the O_2 mass fractions, w_{O_2}, are of the same order of magnitude as their uncertainties. For SYN-2T and BIO-2T-03, the O_2 mass fractions at the equilibrium conditions are between 7 to 10 times lower than the corresponding CO_2 mass fractions. Taking into account the database from Wilhelm and Battino [43] of solubility of gases in different compounds, it can be concluded that the ratio between CO_2 and O_2 mass fractions at 298.15 K and 1 atm partial gas pressure ranges from 4 to 31 for alkanes, perfluoroalkanes, polar and associated compounds. This fact is in agreement with our solubility results. We have also found that the solubility of O_2 in SYN-2T is higher than in BIO-2T-03, the opposite happens with CO_2. This different behaviour for CO_2 and O_2 agrees with the work of Wilhelm and Battino

[43], in which it can be observed that at 298.15 K and 1 atm partial gas pressure, the O_2 solubility is higher in *n*-heptane than in acetone, whereas CO_2 solubility is higher in acetone than in *n*-heptane. Besides, the O_2 solubility in these lubricants increases with temperature, which was also found by Fischer and Wilken [44] and by Li et al. [45] for the system O_2 + toluene, and by Battino et al. [46] for binary systems composed by O_2 and *n*-hexane, *n*-heptane, cyclohexane, benzene, methyl acetate or 2-butanone, among others.

3.2 PC-SAFT modelling

The PC-SAFT EoS is based on the statistical associating fluid theory (SAFT), applying Barker and Henderson's [47,48] second-order perturbation theory. PC-SAFT uses the same chain term and association term as the previous SAFT equations, but a hard-chain fluid serves as a reference for the perturbation theory [22]. PC-SAFT model is applicable to mixtures of gases, solvents and polymers. This model [22] characterizes nonassociating molecules by three pure-component parameters: the temperature-independent segment diameter σ, the depth of the potential $\in$, and the number of segments per chain m. The parameters for a pair of unlike segments are obtained by conventional Berthelot-Lorentz combining rules:

$$\sigma_{ij} = \frac{1}{2}\left(\sigma_i + \sigma_j\right) \tag{12}$$

$$\in_{ij} = \sqrt{\in_i \in_j (1 - k_{ij})} \tag{13}$$

where one binary interaction parameter, $k_{ij,}$ is introduced to correct the segment-segment interactions of unlike chains [22]. k_{ij} values were determined by fitting the experimental solubility data by means of Phase Equilibria software (PE2000) [49].

We have taken the CO_2 pure component parameters from literature [22], meanwhile for SYN-2T and BIO-2T-03 the pure component parameters were calculated taking into account experimental density values of BIO-2T-03 from this work and for SYN-2T from Regueira et al. [24]. For SYN-2T, literature vapour pressures values were also considered [50] using a procedure similar to that used by Razzouk et al. [51] and García et al. [52]. The pure component parameters obtained are presented in table 7. Due to the low vapour pressure of the lubricants and the scarce literature data, it is difficult to provide reliable PC-SAFT parameters. Consequently, the representation of the low vapour pressures and the saturated densities with the same set of parameters is poor. Nevertheless, we have found that the values of the lubricant component parameters do not affect to the quality of the fit of the solubilities when the k_{ij} values are determined.

Table 7. Calculated lubricant parameters of PC-SAFT EoS.

	SYN-2T	BIO-2T-03
σ_{ii} / Å	2.5874	5.9905
$\epsilon_{ii} \cdot k^{-1}$ /K	116.71	334.73
m_i	33.394	6.7048

The k_{ij} parameters were calculated for each isotherm and binary system, taking into account the experimental solubility data and using as objective function the Mean Absolute Deviation:

$$MAD_{xCO2} = \frac{1}{n}\sum_{i=1}^{n}\left|x_{CO2}^{\exp} - x_{CO2}^{calc}\right| \quad (14)$$

where n is the number of experimental points, x_{CO2} is the mole fraction of CO_2 and the superscripts *exp* and *calc* represent experimental and calculated values, respectively. Binary interaction parameters, k_{ij}, are presented in table 8 for the different temperatures; it can be observed a linear dependence between the binary interaction parameters and temperature (Fig.8).

Table 8. Binary interaction parameters, k_{ij}.

T /K	CO_2+SYN-	CO_2+BIO-
283.15	0.1673	0.2934
298.15	0.1809	0.3020
323.15	0.2303	0.3148
348.15	0.2590	0.3364

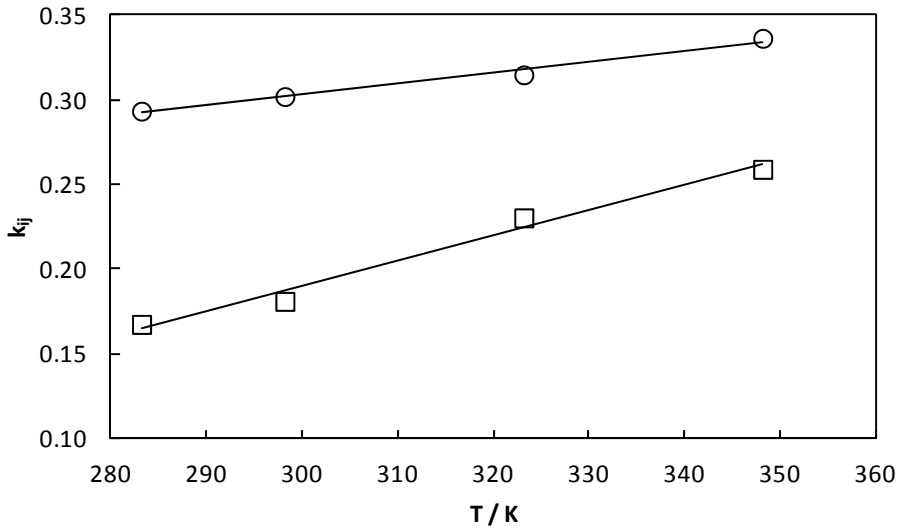

Fig.8. Binary interaction parameters, k_{ij}, against temperature for the mixtures CO_2+SYN-2T (□) and CO_2+BIO-2T-03 (○).

The PC-SAFT calculated solubility values can be observed in Fig. 3a and 3b. The obtained average deviations between experimental and calculated solubility values, expressed in

mass fraction, are 0.006 and 0.015 for SYN-2T and BIO-2T-03, respectively. Moreover, it is worth to mention, that PC-SAFT EoS predicts, for both systems a LLE region for pressures higher than the experimental ones, i.e. for the system CO_2+ SYN-2T, 4.4 MPa, 6.2 MPa, 12.0 MPa and 16.5 MPa, for 283.15 K, 298.15 K, 323.15 K and 348.15 K, respectively; and for the system CO_2+ BIO-2T-03, 4.4 MPa, 6.2 MPa, 18.1 MPa and 26.3 MPa for 283.15 K, 298.15 K, 323.15 K and 348.15 K, respectively.

4. Conclusions

In this work we have performed high pressure density measurements of a biodegradable lubricant for two stroke engine application, finding that its density is around 4% lower than that of the analyzed reference semi-synthetic lubricant. Besides, isothermal compressibility values (κ_T) were calculated from density measurements finding that κ_T values are slightly lower for the biodegradable lubricant than those previously determined for the reference semi-synthetic lubricant [24]. The solubility tests show that CO_2 solubility is higher in the developed vegetable based oil than in the semi-synthetic reference oil, whereas CO_2 solubility is always much higher than O_2 solubility. The agreement between the predictions of the Carvalho and Coutinho method [23] and our data was checked, finding good results for the vegetable based lubricant but not for the semi-synthetic one. The solubility of CO_2 in both lubricants decreases when the temperature increases whereas the opposite occurs for the O_2 solubility. PC-SAFT EoS was used to model the CO_2 solubility in both lubricants obtaining a smooth linear dependence of k_{ij} with temperature. Average deviations, expressed in CO_2 mass fraction, of 0.006 and 0.015 were found for CO_2+SYN-2T and CO_2+BIO-2T-03, respectively.

Acknowledgments

This work was carried out within the framework of the strategic and singular project "Biolubricants based on vegetable oils and their synthetic derivatives", which is funded by Spanish Science and Innovation Ministry and the EU FEDER program (PSE- 320100-2006-1,PSE-420000-2008-4). We are very grateful to the companies Abamotor Energía, Verkol Lubricantes and Gamesa as well as to the Instituto de la Grasa (CSIC, Seville) and Tekniker Foundation for their excellent advice and for providing us the samples of the products. L. L. acknowledges the financial support from the Ramon y Cajal Program (Ministerio de Ciencia e Innovación, Spain). T. R. acknowledges financial support provided by the Spanish Ministry of Education under the FPU program.

References

[1] M.P. Schneider, Plant-oil-based lubricants and hydraulic fluids, J. Science of Food and Agriculture 86 (2006) 1769-1780.
[2] S.Z. Erhan, B.K. Sharma, Z. Liu, A. Adhvaryu, Lubricant base stock potential of chemically modified vegetable oils, J. Agricultural and Food Chemistry 56 (2008) 8919-8925.
[3] L.R. Rudnick, R.L. Shubkin, Synthetic lubricants and high-performance functional liquids, 2nd. ed., Marcel Dekker, New York, 1999.
[4] S. Boyde, Green lubricants. Environmental benefits and impacts of lubrication, Green Chemistry 4 (2002) 293-307.
[5] O.N. Anand, V.K. Chhibber, Vegetable oil derivatives: environment-friendly lubricants and fuels, J. Synthetic Lubrication 23 (2006) 91-107.
[6] S.Z. Erhan, B.K. Sharma, J.M. Perez, Oxidation and low temperature stability of vegetable oil-based lubricants, Industrial Crops and Products 24 (2006) 292-299.
[7] S. Erhan, A. Adhvaryu, B. Sharma, in: Synthetics, mineral oils, and bio-based lubricants, L.R. Rudnick (Ed.) CRC Press, 2006, pp. 361-387.
[8] S. Erhan, L. Rudnick, in: Synthetics, mineral oils, and bio-based lubricants, L.R. Rudnick (Ed.) CRC Press, 2006, pp. 353-360.
[9] R. Garcés, E. Martínez-Force, J.J. Salas, Vegetable oil basestocks for lubricants, Grasas y Aceites 62 (2011) 21-28.
[10] L.A. Quinchia, M.A. Delgado, C. Valencia, J.M. Franco, C. Gallegos, Natural and synthetic antioxidant additives for improving the performance of new biolubricant formulations, J. Agricultural and Food Chemistry (2011)
[11] S.Z. Erhan, S. Asadauskas, Lubricant basestocks from vegetable oils, Industrial Crops and Products 11 (2000) 277-282.
[12] T. Murakami, H. Sakamoto, Effect of dissolved oxygen on lubricating performance of oils containing organic sulfides, Tribology International 32 (1999) 359-366.
[13] T. Murakami, H. Sakamoto, Lubricating properties of vegetable oils and paraffinic oils with unsaturated fatty acids under high-contact-pressure conditions in four-ball tests, J. Synthetic Lubrication 20 (2003) 183-201.
[14] M.-H. Kim, J. Pettersen, C.W. Bullard, Fundamental process and system design issues in CO_2 vapor compression systems, Progress in Energy and Combustion Science 30 (2004) 119-174.
[15] O. Fandiño, E.R. López, L. Lugo, J. García, J. Fernández, Solubility of carbon dioxide in pentaerythritol ester oils. New data and modeling using the PC-SAFT model, J. Supercritical Fluids 55 (2010) 62-70.
[16] W.-H. Chen, C.-H. Chen, C.-M.J. Chang, Y.-H. Chiu, D. Hsiang, Supercritical carbon dioxide extraction of triglycerides from Jatropha curcas L. seeds, J. Supercritical Fluids 51 (2009) 174-180.
[17] E. Jenab, F. Temelli, Viscosity measurement and modeling of canola oil and its blend with canola stearin in equilibrium with high pressure carbon dioxide, J. Supercritical Fluids 58 (2011) 7- 14.
[18] S. Machmudah, M. Kondo, M. Sasaki, M. Goto, J. Munemasa, M. Yamagata, Pressure effect in supercritical CO_2 extraction of plant seeds, J. Supercritical Fluids 44 (2008) 301-307.
[19] H. Sovová, M. Zarevúcka, M. Vacek, K. Stránský, Solubility of two vegetable oils in supercritical CO_2, J. Supercritical Fluids 20 (2001) 15-28.
[20] M.P. Fernández-Ronco, I. Gracia, A.D. Lucas, J.F. Rodríguez, Measurement and modeling of the high-pressure phase equilibria of CO_2-Oleoresin Capsicum, J. Supercritical Fluids 57 (2011) 112-119.
[21] O. Fandiño, E.R. López, L. Lugo, M. Teodorescu, A.M. Mainar, J. Fernández, Solubility of carbon dioxide in two pentaerythritol ester oils between 283 and 333 K J. Chemical and Engineering Data 53 (2008) 1854-1861.
[22] J. Gross, G. Sadowski, Perturbed-Chain SAFT: An equation of state based on a perturbation theory for chain molecules, Industrial and Engineering Chemistry Research 40 (2001) 1244-1260.
[23] P.J. Carvalho, J.A.P. Coutinho, On the nonideality of CO_2 solutions in ionic liquids and other low volatile solvents, J. Physical Chemistry Letters 1 (2010) 774-780.
[24] T. Regueira, L. Lugo, O. Fandiño, E.R. López, J. Fernández, Compressibilities and viscosities of reference and vegetable oils for their use as hydraulic fluids and lubricants, Green Chemistry 13 (2011) 1293-1302.

[25] T. Regueira, P.J. Carvalho, M.B. Oliveira, L. Lugo, J.A.P. Coutinho, J. Fernáandez, Experimental measurements and modelling of CO_2 solubility in castor, sunflower and rapeseed oils, in: 25th European Symposium on Applied Thermodynamics, Saint Petersburg, Russia, 2011.
[26] F. Novotny-Farkas, W. Böhme, H. Stabinger, W. Belitsch, The Stabinger viscometer a new and unique instrument for oil service laboratories, Anton Paar, Graz, Austria, 2001.
[27] F.M. Gaciño, T. Regueira, L. Lugo, M.J.P. Comuñas, J. Fernández, Influence of molecular structure on densities and viscosities of several ionic liquids, J. Chemical and Engineering Data 56 (2011) 4984-4999.
[28] X. Paredes, O. Fandiño, M.J.P. Comuñas, A.S. Pensado, J. Fernández, Study of the effects of pressure on the viscosity and density of diisodecyl phthalate, J. Chemical Thermodynamics 41 (2009) 1007-1015.
[29] J.J. Segovia, O. Fandiño, E.R. López, L. Lugo, M.C. Martín, J. Fernández, Automated densimetric system: Measurements and uncertainties for compressed fluids, J. Chemical Thermodynamics 41 (2009) 632-638.
[30] O. Fandiño, E.R. López, L. Lugo, J. Fernández, Solubilities of carbon dioxide in a dipentaerythritol ester and in a polyether, J. Chemical and Engineering Data 55 (2010) 5483-5488.
[31] R. Span, W. Wagner, A new equation of state for carbon dioxide dovering the fluid region from the triple-point temperature to 1100 K at pressures up to 800 MPa, J. Physical and Chemical Reference Data 25 (1996) 1509-1596.
[32] E.W. Lemmon, M.L. Huber, M.O. McLinden, REFPROP: NIST reference fluid thermodynamic and transport properties, NIST, Gaithersburg, USA, 2007.
[33] M.G. Zellner, L.C. Claitor, J.M. Prausnitz, Prediction of vapor-liquid equilibriums and enthalpies of mixtures at low temperatures, Industrial and Engineering Chemistry Fundamentals 9 (1970) 549-564.
[34] L. Lugo, M.J.P. Comuñas, E.R. López, J. Fernández, (p, V_m, T, x) measurements of dimethyl carbonate+octane binary mixtures. I. Experimental results, isothermal compressibilities, isobaric expansivities and internal pressures, Fluid Phase Equilibria 186 (2001) 235-255.
[35] B.M.C. Soares, F.M.C. Gamarra, L.C. Paviani, L.A.G. Gonçalves, F.A. Cabral, Solubility of triacylglycerols in supercritical carbon dioxide, J. Supercritical Fluids 43 (2007) 25-31.
[36] M.P. Fernández-Ronco, M. Cismondi, I. Gracia, A.D. Lucas, J.F. Rodríguez, High-pressure phase equilibria of binary and ternary mixtures of carbon dioxide, triglycerides and free fatty acids: Measurement and modeling with the GC-EOS, Fluid Phase Equilibria 295 (2010) 1-8.
[37] Y. Sato, Y. Tagashira, D. Maruyama, S. Takishima, H. Masuoka, Solubility of carbon dioxide in eicosane, docosane, tetracosane, and octacosane at temperatures from 323 to 473 K and pressures up to 40 MPa, Fluid Phase Equilibria 147 (1998) 181-193.
[38] E. Kukova, Phasenverhalten und transporteigenschaften binärer systeme aus hochviskosen polyethylenglykolen und kohlendioxid, PhD Thesis, Fakultät für Maschinenbau der Ruhr-Universität Bochum, Bochum, Germany, 2003.
[39] M.A. Marcelino-Neto, Caracterização de propriedades termofísicas de misturas de óleos lubrificantes e fluidos refrigerantes naturais, M. Eng. dissertation, Universidade Federal de Santa Catalina, Florianópolis, Brazil, 2006.
[40] A. Yokozeki, M.B. Shiflett, The solubility of CO_2 and N_2O in olive oil, Fluid Phase Equilibria 305 (2011) 127-131.
[41] J. García, M. Youbi-Idrissi, J. Bonjour, J. Fernández, Experimental and PC-SAFT volumetric and phase behavior of carbon dioxide + PAG or POE lubricant systems, J. Supercritical Fluids 47 (2008) 8-16.
[42] A. Hauk, Thermo- und fluiddynamik von synthetischen schmierstoffen mit kohlendioxid als kältemittel PhD Thesis, Universitaät Bochum, Bochum, Germany, 2001.
[43] E. Wilhelm, R. Battino, Thermodynamic functions of the solubilities of gases in liquids at 25°C, Chemical Reviews 73 (1973) 1-9.
[44] K. Fischer, M. Wilken, Experimental determination of oxygen and nitrogen solubility in organic solvents up to 10 MPa at temperatures between 298 K and 398 K, J. Chemical Thermodynamics 33 (2001) 1285-1308.
[45] A. Li, S. Tang, P. Tan, C. Liu, B. Liang, Measurement and prediction of oxygen solubility in toluene at temperatures from 298.45 K to 393.15 K and pressures up to 1.0 MPa, J. Chemical and Engineering Data 52 (2007) 2339-2344.
[46] R. Battino, T.R. Rettich, T. Tominaga, The solubility of oxygen and ozone in liquids, J. Physical and Chemical Reference Data 12 (1983) 163-178.

[47] J.A. Barker, D. Henderson, Perturbation theory and equation of state for fluids: the square-well potential, J. Chemical Physics 47 (1967) 2856-2861.
[48] J.A. Barker, D. Henderson, Perturbation theory and equation of state for fluids. II. A successful theory of liquids, J. Chemical Physics 47 (1967) 4714-4721.
[49] O. Pfohl, S. Petkow, G. Brunner, Usage of PE A program to calculate phase equilibria, ISBN: 3-89675-410-6, 1998.
[50] Vapor pressure of mineral oil, TOTAL Lubricants USA Southwest, http://www.finalube.com.
[51] A. Razzouk, I. Mokbel, J. García, J. Fernández, N. Msakni, J. Jose, Vapor pressure measurements in the range 10-5 Pa to 1 Pa of four pentaerythritol esters: Density and vapor-liquid equilibria modeling of ester lubricants, Fluid Phase Equilibria 260 (2007) 248-261.
[52] J. García, R.A. Naccoul, J. Fernández, A. Razzouk, I. Mokbel, Vapor-pressure measurements and modeling of dipentaerythritol ester lubricants, Industrial and Engineering Chemistry Research 50 (2011) 4231-4237.

6.2. Experimental measurements and modelling of CO_2 solubility in sunflower, castor and rapeseed oils for two stroke engines*

*T. Regueira, P.J. Carvalho, M.B. Oliveira, L. Lugo, J.A.P. Coutinho, J. Fernández, J. Supercrit. Fluids, accepted.

Abstract

In this work solubility measurements of CO_2 in three vegetable oils, a high oleic sunflower oil (HOSO-B1), a castor oil and a rapeseed oil, for mole fractions ranging from 0.32 to 0.93 in the temperature range (298 to 363) K and up to 75 MPa were performed. Moreover, the densities and viscosities of these oils are reported from (278.15 to 373.15) K at atmospheric pressure. These data were used to evaluate the predictive ability of the fragment based approach. Solubility data were modelled by means of the SRK-EoS and predicted employing the Carvalho and Coutinho correlation. Global average deviations inferior to 6% in CO_2 mole fraction composition were achieved with the SRK-EoS and maximum percentage absolute average deviations of 13% in pressure were obtained using the Carvalho and Coutinho correlation.

1 Introduction

The environmental drive for the use of rapidly biodegradable oils as lubricants has been a gradual process in Europe and niche markets have arisen where mineral oils have been banned by legislation. Vegetable oils are an obvious choice, which can offer an optimum solution, particularly in total-loss systems (drilling muds, chain-saw bar oils and outboard engines) and partial-loss systems (hydraulic oils and greases). With the aid of selective plant breeding and additives, more thermal and oxidative stable vegetable oils can be formulated [1,2]. The commercial use of a vegetable-oil based system would represent a significant environmental improvement in areas where hydrocarbons are still employed [3-5].

The EU Ecolabel is a voluntary award system for the promotion of products with a reduced environmental impact during their life cycle. This scheme is part of the sustainable consumption and production policy of the European Community, which aims at substituting hazardous substances by safer ones, wherever technically possible [6]. The EU established in 2011 the latest ecological criteria for the award of the EU Ecolabel to lubricants. This product group comprises five categories that include hydraulic fluids and tractor transmission oils, greases and stern tube greases, chainsaw oils, concrete release agents, wire rope lubricants, stern tube oils and other total loss lubricants, two-stroke oils and industrial and marine gear oils [7].

Vegetable oils as lubricants are environmentally preferred to petroleum-based oils not only because they are renewable raw materials but also because they are biodegradable and non-toxic [8]. Other advantages include very low volatility due to the high molecular weight of the triglyceride molecule and excellent temperature-viscosity properties. Their polar ester groups are able to adhere to metal surfaces, and therefore, provide good lubricity. In addition, vegetable oils have high solubilising power for polar contaminants and additive molecules [1]. However there are concerns about their oxidative stability and low-temperature performance. Improvements in

oxidative stability can be made through chemical or genetic modifications [2,9-12], as well as adding antioxidant additives. [13,14]

Two-stroke engines are one of the applications where most of the lubricants and their degradation products are released directly into the environment, polluting the soil, water and atmosphere [15-17]. The knowledge of the solubility of different gases, such as O_2, N_2 and CO_2, in lubricants used for two stroke engines is important because these gases are involved in the combustion process together with the lubricant and the gasoline in the combustion chamber and this can provide information on the best lubricant choice. Moreover, CO_2 is a natural refrigerant that is being considered as a potential candidate to replace existing refrigerants, especially in small and medium systems [18]. Thus, in applications where the lubricant is in contact with the refrigerant, its solubility in the oil is a key property [19]. It is well recognized that the surrounding gas affects lubrication performance in any lubrication regimes. In hydrodynamic lubrication the surrounding gas and its pressure affect the dissolution of the gas into the lubricant, which may cause changes in the lubricant viscosity and may further cause degradation of the lubricant. Therefore, investigating the effects of the surrounding gas on lubrication is important to design the lubricant for reliability and safety [20]. Furthermore, the knowledge of the CO_2 + vegetable oil solubility data is necessary for the design of supercritical carbon dioxide oil extraction processes from seeds [21-24].

In this work solubility measurements of CO_2 in three vegetable oils susceptible of being used as lubricant base oils, a high oleic sunflower, a castor oil, and a rapeseed oil, were carried out in the temperature range (298.15 to 363.15) K and for pressures up to 75 MPa. It should be highlighted, that solubilities of CO_2 in a rapeseed oil were previously studied by Klein and Schulz [25] at 313.15 K, 333.15 K, 353.15 K and 373.15 K and pressures up to 85 MPa. The present work is focused on different temperatures and also broadens the range to a lower temperature, i.e. 298.15 K. Data is also presented in a lower CO_2 composition range. Additionally, solubilities of CO_2 in castor oil were studied by Ndiaye et al. [26] in the temperature range from 308.15 K to 343.15 K up to 25.5 MPa. Our experimental data broadens both temperature and pressure ranges up to 363.15 K and 74 MPa, respectively.

Additionally, in the present work, the SRK EoS was used to model the experimental solubility data, which were also used to evaluate the prediction ability of the Carvalho and Coutinho correlation [27]. Moreover, densities and viscosities of these oils were experimentally measured over a wide range of temperatures in order to perform a better characterization of the studied oils and also to analyze the reliability of the fragment based approach [28,29].

2 Materials and Methods

High oleic sunflower oil (HOSO-B1), castor oil and rapeseed oil were kindly provided by Verkol Lubricantes. Fatty acid composition of these oils was determined in the Instituto de la Grasa (CSIC, Seville) and is presented in Table 1, along with the respective standard deviation. Prior to the measurements, oils were dried under high vacuum (0.1 Pa) and at moderate temperature (around 353K) for a period of 48 h. Carbon dioxide (CO_2) was provided by Air Liquide with a purity ≥ 99.998%, their H_2O, O_2, C_nH_m, N_2 and H_2 impurities volume fractions being lower than (3, 2, 2, 8 and 0.5)×10^{-6}, respectively. Molecular weights of the oils were estimated taking into account their fatty acid composition presented in Table 1. The obtained values are 881.77, 920.89 and 878.83 g·mol^{-1} for HOSO-B1, castor oil and rapeseed oil, respectively.

Table 1. Fatty acid composition of high oleic sunflower oil (HOSO-B1), castor oil and rapeseed oil, along with their standard deviations (σ)

	HOSO-B1		Castor oil		Rapeseed oil	
Fatty acid	% Mass fraction	σ	% Mass fraction	σ	% Mass fraction	σ
Palmitic	3.98	0.01	2.25	0.04	4.86	0.01
Estearic	2.99	0.02	2.50	0.06	1.65	0.05
Oleic	82.89	0.20	7.21	0.18	65.28	0.49
Linoleic	9.17	0.11	8.40	0.14	19.49	0.23
Linolenic	-	-	-	-	7.69	0.26
Ricinoleic	-	-	79.64	0.24	-	-
Arachidic	0.26	0.01	-	-	0.79	0.04
Behenic	0.72	0.04	-	-	0.26	0.01

Density and viscosity of the oils were measured at atmospheric pressure in an automated SVM 3000 Anton Paar rotational Stabinger apparatus [30]. The SVM 3000 uses Peltier elements for fast and efficient thermostatization. The temperature uncertainty is 0.02 K from 288.15 K to 378.15 K and 0.05 K outside this range, whereas the uncertainty of the dynamic viscosity is 1%. This equipment has also a vibrating-tube that permits measurements of the densities with an uncertainty of 0.0005 g cm^{-3}. Measurements were performed from (278.15 to 373.15) K.

Solubility measurements were performed in a high pressure equilibrium cell based on the design of Daridon and co-workers [31,32] using the synthetic method which avoid the sampling and analyses of liquid and vapour phases. The high pressure equilibrium cell is a variable volume high pressure cell that consists of a horizontal hollow stainless steel cylinder, closed at one end by a movable piston and at the other end by a sapphire window that allows a visual

observation of the interior of the pressure cell. The volume of this cell varies from 8 to 30 cm^3. Phase behaviour as a function of temperature and pressure is observed by means of a video acquisition system, consisting of an endoscope and a video camera connected to a computer, which permits to follow the phase change inside the cell. The interior of the equilibrium cell is illuminated by an optical fibber through a second sapphire window located in the wall of the cell. A magnetic bar placed inside the cell and controlled by an external magnetic stirrer is used to homogenize the system. The internal temperature is kept constant by means of a thermostatic bath circulator. The temperature is measured with three-wire Pt100 thermometer (Bresimar, Aveiro), with an uncertainty of 0.15 K, connected to a calibrated platinum resistance inserted inside the cell close to the sample. The pressure is measured by a piezoresistive silicon pressure transducer (Kulite HEM 375) directly fixed inside the cell to reduce dead volumes. This transducer was previously calibrated and certified following the EN 837-1 standard and with accuracy better than 0.2% and the reproducibility of the pressure readings was 0.02 MPa. More details can be found in a previous work [33].

Measurements were performed in the temperature range from (298.15 to 363.15) K for the systems CO_2 + HOSO-B1 and CO_2 + rapeseed oil, whereas for the system CO_2 + castor oil measurements were performed in the temperature range from (323.15 to 363.15) K due to the high viscosity of castor oil at 298.15 K that hinders a proper homogenization of the system.

3. Models

3.1 Soave-Redlich-Kwong EoS

The Soave-Redlich-Kwong EoS [34] was used to model the experimental solubility data measured in this work. The SRK EoS, in terms of pressure is given by:

$$p = \frac{RT}{V_m - b} - \frac{a}{V_m (V_m + b)} \tag{1}$$

where p is the pressure, T is the temperature, R is the gas constant, V_m is the molar volume and a is the pure component energy parameter which has a Soave-type temperature dependency given by the following equation:

$$a = a_0 \left[1 + c_1 \left(1 - \sqrt{T_r}\right)\right]^2 \tag{2}$$

where T_r is the reduced temperature (T/T_c, where T_c is the critical temperature). a_0 and c_1 are given by the following expressions:

$$a_0 = 0.42747 \frac{R^2 T_c^2}{p_c} \tag{3}$$

$$c_1 = 0.48 + 1.574\omega - 0.176\omega^2 \tag{4}$$

The pure compound co-volume parameter, b, is given by:

$$b = \frac{0.08664\, RT_c}{p_c} \tag{5}$$

where p_c is the critical pressure and ω is the acentric factor.

When dealing with mixtures, the energy and co-volume parameters are calculated employing the conventional van der Waals one-fluid mixing rules,

$$a = \sum_i \sum_j x_i x_j a_{ij} \tag{6}$$

$$a_{ij} = \sqrt{a_i a_j}\left(1 - k_{ij}\right) \tag{7}$$

$$b = \sum_i \sum_j x_i x_j b_{ij} \tag{8}$$

$$b_{ij} = \sqrt{b_i b_j}\left(1 - l_{ij}\right) \tag{9}$$

There are two adjustable parameters from the solubility data for the studied mixtures, i.e. the binary interaction parameters k_{ij} and l_{ij}. The objective function employed for the binary parameters regression was:

$$\mathrm{OF} = \sqrt{\frac{1}{N}\sum_i^N \left(x_i^{exp.} - x_i^{cal.}\right)^2} \tag{10}$$

where x_i is the mole fraction of component "i" in the phases selected in the optimization.

3.2 Carvalho and Coutinho correlation

Carvalho and Coutinho [27] have proposed the following general correlation for predicting the solubility of CO_2 in nonvolatile solvents:

$$p = m_{CO2} e^{\left(6.8591 - \frac{2004.3}{T}\right)} \tag{11}$$

where p is the pressure in MPa, m_{CO2} is the CO_2 solubility expressed in molality (mol·kg^{-1}) and T is the temperature in K. Eq. (11) is valid for pressures up to 5 MPa, for temperatures ranging from room temperature up to 363 K and molalities up to 3 mol·kg^{-1}. This correlation infers that when the molecular weight effect is removed from the solubility analysis by comparing the solubilities expressed in molalities instead of in mole fractions, the solubility differences, among different systems are minimized and the solubility of CO_2 in nonvolatile solvents becomes essentially solvent independent.

4 Results and discussion

4.1 Density and viscosity of the pure oils

The densities and the dynamic viscosities were measured in the (278.15 to 373.15) K temperature range, at atmospheric pressure. The experimental values are depicted in Fig. 1 and presented in Table S1 in the supplementary data. These results complement those from literature. Thus, in the case of castor oil, up to our knowledge, density has been reported only from 298 to 333 K by Sankarappa et al. [35] and what concerns rapeseed oil, density and viscosity data have not been previously measured at 278.15 K. The rapeseed oil and HOSO-B1 have similar density and viscosity values whereas castor oil is the densest and also the most viscous. This behaviour is due to the additional hydroxyl groups of the ricinoleic chains of the castor oil, which can form hydrogen bonds.

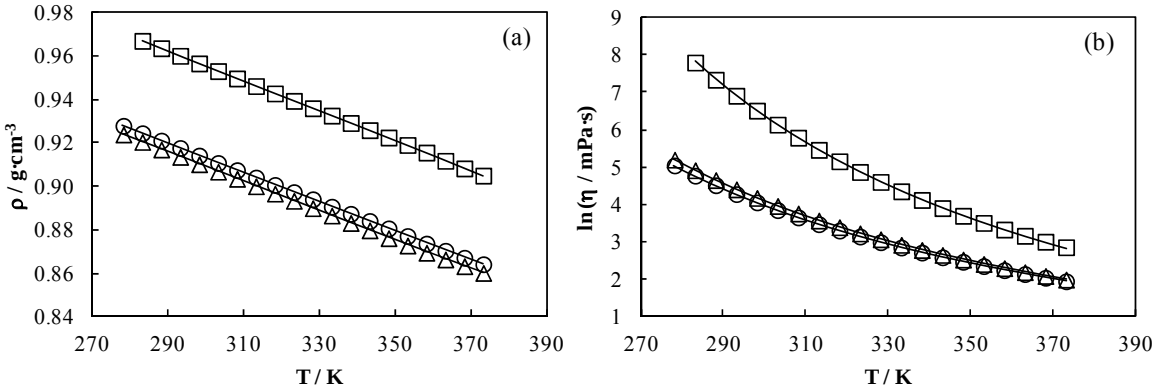

Fig. 1. (a) Experimental density and (b) viscosity values of the oils measured in this work. (□) Castor oil, (○) rapeseed oil and (△) HOSO-B1. Lines represent correlations according to Eqs. 14 and 15 for density and viscosity values, respectively.

The percentage relative deviations between the experimental HOSO-B1 density data and those reported for HOSO-B1 [36,37] and sunflower oil [35,38,39] are presented in Fig. 2a. Agreement between our experimental density and viscosity data and those from literature has been quantified in terms of Absolute Average Deviation (AAD%) which is given by:

$$AAD(\%) = \frac{100}{N}\sum_{i=1}^{N}\left|\frac{Y_i^{\exp} - Y_i^{ref}}{Y_i^{ref}}\right| \tag{12}$$

and the *bias*%:

$$bias(\%) = \frac{100}{N}\sum_{i=1}^{N}\frac{Y_i^{\exp} - Y_i^{ref}}{Y_i^{ref}} \tag{13}$$

where N is the number of experimental data points and $Y_i^{\exp}$ and Y_i^{ref} represent the experimental and literature values, respectively. Concerning the information given by the *bias*%, it should be mentioned that, when AAD% = *bias*%, all the experimental points are higher than the predicted

data and if AAD% = -*bias*%, all the experimental densities are lower than the predicted values [40].

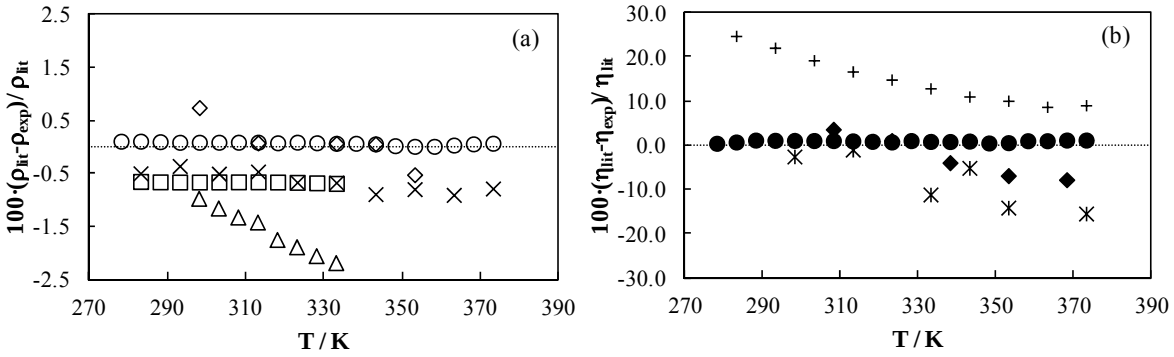

Fig. 2. (a) Comparison between the reported density data of HOSO-B1 and values from literature for HOSO (Quinchia et al. [37] (◇) and Regueira et al. [36] (○)) and for sunflower oil (Esteban et al. [38] (×), Sankarappa et al. [35] (△) and Guignon et al. [39] (□)). (b) Comparison between the reported viscosity data of HOSO-B1 and values from literature for HOSO (Regueira et al. [36] (●) and Quinchia et al. [42] (✳)) and for sunflower oil (Fasina et al. [43] (◆) and Esteban et al. [38] (+)).

Thus, our HOSO density data show an overall AAD% of 0.55 % with literature data for HOSO [36,37] and sunflower oil [35,38,39]. We have found *bias*% values different from AAD% for one data series and *bias*% = |AAD%| for four sets (one of them positive). Furthermore, the density obtained for the castor oil was compared with those published by Sankarappa et al. [35] showing an AAD% of 0.98 %, the AAD% being equal to the *bias*%. Finally, the rapeseed oil density was compared with those of the 48 samples measured at 293 K by Wesołowski and Erecińska [41], showing an AAD% of 0.80%, and with those reported by Esteban et al. [38] in the (283.15 to 373.15) K temperature range, showing an AAD% of 0.19 %. For these last data sets the AAD% are different from the *bias*%.

The viscosity of HOSO-B1 was compared with literature values of HOSO [36,42] and sunflower oil [38,43], as depicted in Fig. 2b, showing an overall *bias*% of 2.6% and an overall AAD% of 5.9%. Besides, the castor oil viscosity values were also compared with those reported in literature [42,44,45], finding an overall *bias*% of 2.9% and an AAD% of 10%. Finally, the rapeseed oil viscosity values were compared with reported literature values [38,43,46] yielding an overall *bias*% of -2.5% and a global AAD% of 8.4%.

The high deviations found with some of the literature data for the oils densities and viscosities can be explained by the different fatty acid composition of the oil samples, particularly in the case of sunflower oil and HOSO. Sunflower oil from Esteban et al. [38] has a composition of only 38.7% in oleic acid whereas our sunflower oil has 83%. Guignon et al. [39] and Sankarappa et al. [35] do not report the sunflower oil compositions.

Density values were correlated as a function of temperature by means of a polynomial, as follows:

$$\rho = a_0 + a_1 T + a_2 \cdot T^2 + a_3 \cdot T^3 \tag{14}$$

where ρ is the density in g·cm^{-3} and T is the temperature in K.

The parameters of the density adjustment are presented in Table 2 along with the standard deviations (σ).

Table 2. Parameters of the polynomial density correlation (Eq. 14) for the vegetable oils.

	a_0 g·cm^{-3}	$10^3 \cdot a_1$ g·cm^{-3}·K^{-1}	$10^7 \cdot a_2$ g·cm^{-3}·K^{-2}	$10^{10} \cdot a_3$ g·cm^{-3}·K^{-3}	$10^4 \cdot \sigma$ g·cm^{-3}
HOSO-B1	0.96336	0.7519	-45.553	48.192	1.4
Castor oil	1.37463	-2.6617	60.723	-61.982	1.0
Rapeseed oil	1.12203	-0.7073	0.0840	0.9028	1.2

The viscosity values were correlated as function of temperature by the Vogel-Fulcher-Tammann (VFT) equation:

$$\ln(\eta) = A + \frac{B}{T - T_0} \tag{15}$$

where η is the dynamic viscosity in mPa·s.

The parameters obtained by fitting the VFT equation against the experimental data are presented in Table 3 along with standard deviations (σ) of the fit.

Table 3. Parameters of the VFT equation (Eq. 15) for the vegetable oils.

	A	B /K	T_0 /K	$10^2 \cdot \sigma$
HOSO-B1	-2.171884	908.218	155.0831	0.2
Castor oil	-3.343743	1247.729	171.3842	1.2
Rapeseed oil	-2.097011	886.062	154.1951	0.1

The fragment based approach for estimating thermophysical properties of fats and vegetable oils [28,29] was tested to predict the density values of the studied oils. This methodology adopts a chemical constituent fragment-based approach to estimate the triglyceride pure component properties from fragment composition and parameters of the fragments. The fragment-specific parameters were obtained by Zong et al. [28,29] by regressing against very limited experimental data for triglycerides. According to this method, the liquid molar volume of triglycerides can be calculated according to the following equation:

$$V^l = \sum_A N_{frag,A} V_A^l(T) \tag{16}$$

where V_A^l is the liquid molar volume contribution of fragment A and $N_{frag,A}$ is the number of fragment A in the component. The temperature dependency for the liquid molar volume of fragment A is given by [28,29]:

$$V_A^l = \frac{1 + B_{2,A}T}{B_{1,A}} \tag{17}$$

where $B_{1,A}$ and $B_{2,A}$ are the temperature dependency correlation parameters of fragment A. This method [28] predicts the density values reported in table S1 with percentage absolute average deviations (AAD%) of 0.8% for HOSO-B1 and 1.1% for rapeseed oil. For the castor oil, the authors [28] do not provide parameters for the ricinoleic fragment. We have calculated the values of these parameters, $B_{1,A}$ and $B_{2,A}$, finding a value of 4.27 kmol·m^{-3} for $B_{1,A}$ and of 1.2485·10^{-04} K^{-1} for $B_{2,A}$ with an AAD% of 0.03%.

Additionally, the fragment based approach [28,29] was also employed to estimate the viscosity of the studied vegetable oils. Through this approach, the triglycerides liquid viscosities can be calculated from the viscosity fragment composition and fragment-specific parameters according to the equation:

$$\ln \eta = \sum_A N_{frag,A} \ln \eta_A(T) \tag{18}$$

where $\ln \eta_A$ represents the liquid viscosity contribution of the fragment A (expressed in units of Pa·s) and $N_{frag,A}$ is the number of fragment A in the component.

The expression for the liquid viscosity of fragment A, as a function of temperature is the following:

$$\ln \eta_A = C_{1,A} + \frac{C_{2,A}}{T} + C_{3,A} \ln T \tag{19}$$

where $C_{1,A}$, $C_{2,A}$ and $C_{3,A}$ represent temperature dependency correlation parameters for viscosity. AADs% of 3.6% and 4.0% for the viscosity prediction of HOSO-B1 and rapeseed oil, respectively, were obtained using this correlation. These uncertainties are quite low, i.e. the values of the parameters are reliable. For the castor oil, parameters for the ricinoleic fragment are not available [28]. Thus, we have calculated the parameters for viscosity prediction for the ricinoleic fragment, using our experimental viscosity data, finding the following values for the parameters: -129.17 Pa·s for $C_{1,A}$, 7269.3 K for $C_{2,A}$ and 32.471K for $C_{3,A}$ with an AAD% of 0.38%.

4.2 Experimental solubility data

Experimental solubility data are presented in Tables 4-6 for the three systems studied whereas the *p-x* diagrams are depicted in Figs. 3-5.

Table 4. Solubility data of the system CO_2 + HOSO-B1.

w_{CO2}	T / K	p /MPa	w_{CO2}	T / K	p /MPa
0.024	298.34	0.519	0.024	348.39	1.800
0.032	298.10	0.879	0.032	348.20	2.338
0.042	298.27	1.294	0.042	347.95	2.934
0.051	298.31	1.681	0.051	348.05	3.570
0.060	297.88	1.978	0.060	347.94	4.226
0.070	298.39	2.247	0.070	347.96	4.858
0.085	298.05	2.699	0.085	347.90	5.749
0.112	298.01	3.378	0.112	348.20	7.271
0.130	298.02	3.722	0.130	348.23	8.470
0.164	298.39	4.579	0.164	348.19	10.70
0.191	297.92	5.189	0.191	348.06	12.68
0.220	298.03	5.800	0.220	348.24	15.18
0.235	298.48	6.046	0.235	348.14	16.57
0.253	297.96	6.310	0.253	348.37	18.36
0.273	298.39	8.762	0.273	348.36	20.75
0.292	298.36	13.67	0.292	348.23	23.57
0.312	298.39	20.71	0.312	348.04	26.96
0.333	298.49	29.93	0.333	348.36	30.76
0.352	298.00	41.48	0.352	348.22	34.00
0.372	298.17	60.92	0.372	348.44	38.38
0.024	323.18	1.130	0.392	348.21	42.98
0.032	323.16	1.630	0.024	362.92	2.310
0.042	323.35	2.090	0.032	362.87	2.824
0.051	323.26	2.523	0.042	363.27	3.528
0.060	323.15	3.077	0.051	363.21	4.236
0.070	323.44	3.532	0.060	363.14	4.976
0.085	323.29	4.175	0.070	362.92	5.716
0.112	323.03	5.115	0.085	363.21	6.880
0.130	323.22	5.958	0.112	362.98	8.636
0.164	323.55	7.555	0.130	363.20	10.15
0.191	323.30	8.631	0.164	363.21	12.73
0.220	323.35	10.14	0.191	363.24	15.11
0.235	323.33	11.01	0.220	363.26	18.00
0.253	323.34	12.37	0.235	363.31	19.57
0.273	323.14	14.75	0.253	363.11	21.28
0.292	323.33	18.00	0.273	363.11	23.81
0.312	323.16	22.31	0.292	363.25	26.48
0.333	323.08	27.28	0.312	363.21	29.68
0.352	323.03	32.42	0.333	363.52	33.24
0.372	323.02	38.47	0.352	363.34	36.26
0.392	323.45	45.93	0.372	363.19	39.82
			0.392	363.14	43.60

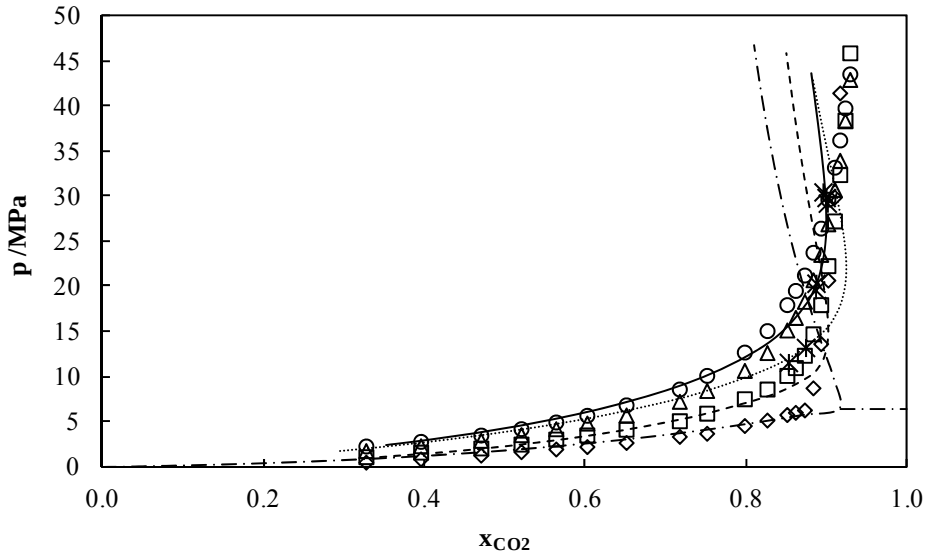

Fig. 3. Experimental solubility data of the system CO_2 + HOSO-B1 at 298 K (◇), 323 K (□), 348 K (△) and 363 K (○). Data from Fernández-Ronco et al. [47] for the system CO_2 + sunflower oil at 325.9 K (✳). Lines represent the SRK EoS with two interaction parameters (k_{ij} and l_{ij}) from table 8 at 298 K (–·–), 323 K (– –), 348 K (…) and 363 K (—).

Table 5. Solubility data of the system CO_2 + castor oil.

w_{CO2}	T / K	p /MPa	w_{CO2}	T / K	p /MPa
0.024	323.46	1.506	0.240	348.45	23.94
0.061	323.30	3.645	0.260	348.31	28.46
0.101	322.93	5.633	0.293	348.30	36.66
0.130	323.45	7.198	0.309	348.45	40.15
0.150	323.31	8.337	0.334	348.29	47.00
0.190	323.20	11.06	0.350	348.00	52.34
0.221	323.22	15.47	0.024	363.39	2.449
0.240	323.28	20.85	0.061	363.41	5.673
0.260	323.32	27.35	0.101	363.15	9.167
0.293	323.39	40.99	0.130	363.30	11.87
0.309	323.16	46.30	0.150	363.12	13.75
0.334	323.46	58.91	0.190	363.06	18.24
0.350	323.27	73.97	0.221	363.29	22.74
0.024	348.23	2.197	0.240	363.17	26.20
0.061	348.25	4.919	0.260	363.35	30.28
0.101	348.19	7.796	0.293	363.36	37.29
0.130	348.45	10.25	0.309	363.14	40.18
0.150	348.38	11.74	0.334	363.23	46.08
0.190	348.22	15.78	0.350	363.31	50.24
0.221	348.35	19.94			

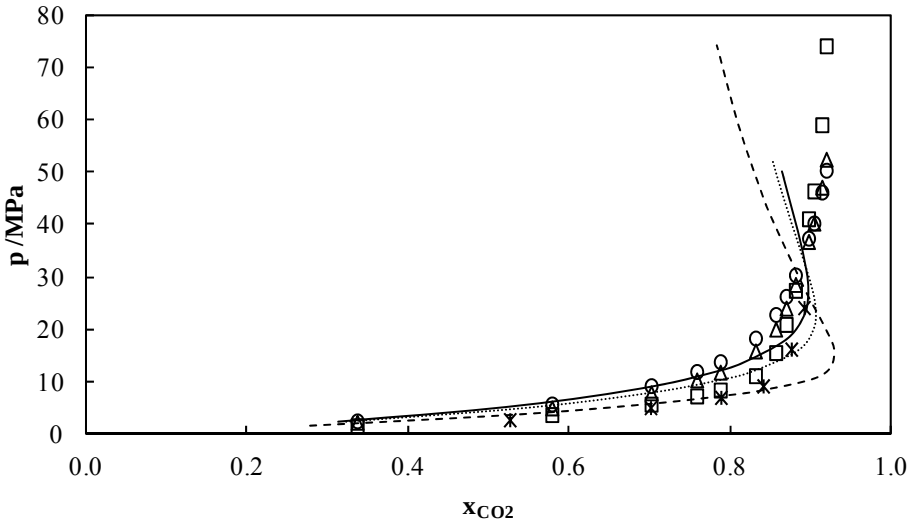

Fig. 4. Experimental solubility data of the system CO_2 + castor oil at 323 K (□), 348 K (△) and 363 K (○). Data from Ndiaye et al.[26] for the system CO_2 + castor oil at 323.15 K (✳). Lines represent the SRK EoS with two interaction parameters (k_{ij} and l_{ij}) from table 8 at 323 K (– –), 348 K (…) and 363 K (—).

Table 6. Solubility data of the system CO_2 + rapeseed oil.

w_{CO2}	T / K	p /MPa	w_{CO2}	T / K	p /MPa
0.024	298.25	0.585	0.024	348.45	1.779
0.062	298.15	1.938	0.062	348.25	4.338
0.104	298.25	3.230	0.104	348.15	7.049
0.131	298.15	3.932	0.131	348.05	8.718
0.161	298.25	4.708	0.161	348.15	10.82
0.200	298.15	5.594	0.200	348.15	13.68
0.246	298.15	6.476	0.246	348.15	18.35
0.280	298.25	11.83	0.280	348.05	22.73
0.301	298.25	17.66	0.301	348.25	26.14
0.320	298.15	25.47	0.320	348.15	29.29
0.345	298.15	36.31	0.345	348.15	33.84
0.372	298.15	58.03	0.372	348.14	39.59
0.024	323.25	1.183	0.390	348.35	44.02
0.062	323.35	3.113	0.024	363.45	2.119
0.104	323.25	5.046	0.062	363.25	5.077
0.131	323.15	6.207	0.104	363.35	8.278
0.161	323.15	7.567	0.131	363.15	10.26
0.200	323.15	9.269	0.161	363.15	12.73
0.246	323.15	12.38	0.200	363.15	16.19
0.280	323.25	17.06	0.246	363.15	21.32
0.301	323.15	21.12	0.280	363.05	25.89
0.320	323.05	25.35	0.301	363.15	29.02
0.345	323.05	31.55	0.320	363.05	31.84
0.372	323.05	39.80	0.345	363.05	35.97
0.390	323.05	47.58	0.372	363.05	40.86
			0.390	363.05	44.60

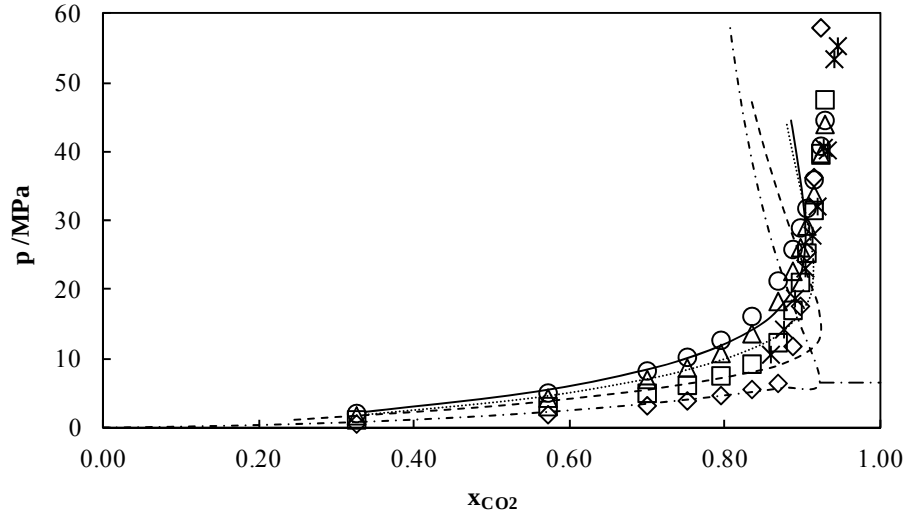

Fig. 5. Experimental solubility data of the system CO_2 + rapeseed oil at 298 K (◇), 323 K (□), 348 K (△) and 363 K (○). Data from Klein and Schulz [25] at 333 K (✳). Lines represent the SRK EoS with two interaction parameters (k_{ij} and l_{ij}) from table 8 at 298 K (–·–), 323 K (– –), 348 K (…) and 363 K (—).

The temperature increase leads to an increase on the equilibrium pressure up to a crossing point that is observed for all the systems. These crossing of isotherms are located at (w_{CO2}, p) around (0.31, 21MPa), (0.26, 28MPa) and (0.32, 25MPa) for the systems CO_2 + HOSO-B1, CO_2 + castor oil and CO_2 + rapeseed oil, respectively. Above this point the temperature dependency of the solubility is inversed, increasing with the temperature increase. Crossovers of the isotherms for these systems have been previously reported by Klein and Schulz [25] for CO_2 + rapeseed oil and also by Ndiaye et al. [26] for CO_2 + castor oil. The solubility data for the CO_2 + HOSO-B1 system were measured for CO_2 mass fractions up to 0.40 and 61 MPa and are depicted in Fig. 3 along with the values for the CO_2 + a sunflower oil system, reported by Fernández-Ronco et al. [47] at 325.9 K. The solubility data for the CO_2 + castor oil system were determined for CO_2 mass fractions up to 0.35 and 74 MPa and are depicted in Fig. 4, along with the literature solubility CO_2 data in other castor oil reported by Ndiaye et al. [26] at 323.15 K. This figure shows that our values at this temperature are in agreement with those from Ndiaye et al. [26] Also, it must be noted that other isotherms (different from the ones studied in the present work, i.e. 313.15 K, 333.15 K and 343.15 K) were reported by Ndiaye et al. [26] for this system but they were not plotted to avoid a misleading figure. The solubility data for the CO_2 + rapeseed oil system measured for CO_2 mass fractions up to 0.39 and 58 MPa are depicted in Fig. 5, along with the solubility data reported by Klein und Schulz [25] at 333.15 K. These last authors have also reported solubility data for this system at 313.15 K, 353.15 K and 373.15 K. A good agreement is found between the experimental data and those available in the literature at a single temperature, taking into account that fatty acid composition of the oils is not the same for the compared samples. In a previous work we have reported the CO_2 solubility in a HOSO-based

lubricant [48], BIO-2T-03. Interestingly, and despite the composition differences inherent to the two oils, the CO_2 solubility in both is remarkably similar, as depicted in Fig. 6.

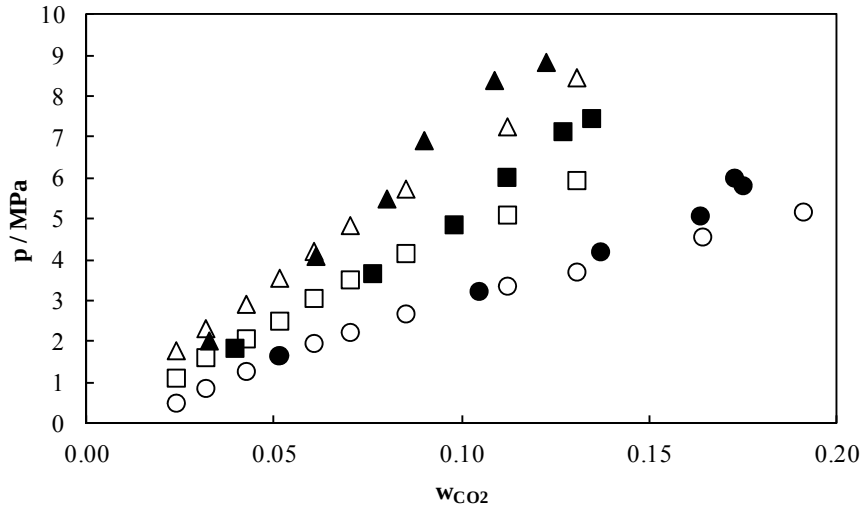

Fig. 6. Solubility of CO_2 in HOSO-B1 (empty symbols) and in BIO-2T-03 [48] (filled symbols) at 298 K (○, ●), 323 K (□, ■) and 348 K (△, ▲).

In Fig. 7 a comparison between the solubility of the CO_2 in the different oils in mole and mass fraction, at 323 K, is presented. The solubilities up to a CO_2 mass fraction of 0.2 are similar in the three of them. Over this composition, CO_2 solubility starts to increase slower for the three oils, keeping similar values in HOSO-B1 and in the rapeseed oil, whereas in the castor oil the CO_2 solubilities are lower. This is likely due to the hydroxyl groups of the ricinolecic chains of the castor molecule, which are not present in the other two oils. However, when solubility is expressed in mass fraction, the solubility curve of the system CO_2 + castor oil is closer to the other systems, but still having lower solubility values. Carvalho and Coutinho [27] have recently investigated the behaviour of the CO_2 solubility in several solvents, among them alcohols, indicating that in spite of the strong CO_2···OH interactions observed spectroscopically [49-53], the alcohol systems are the only ones with positive deviations to ideality (Raoult's Law). According to these authors, for this type of mixtures strong solute-solvent interactions are not enough to guarantee enhanced solubility if the solvent-solvent interactions destroyed during the solvation of the solute are not energetically compensated by that process.

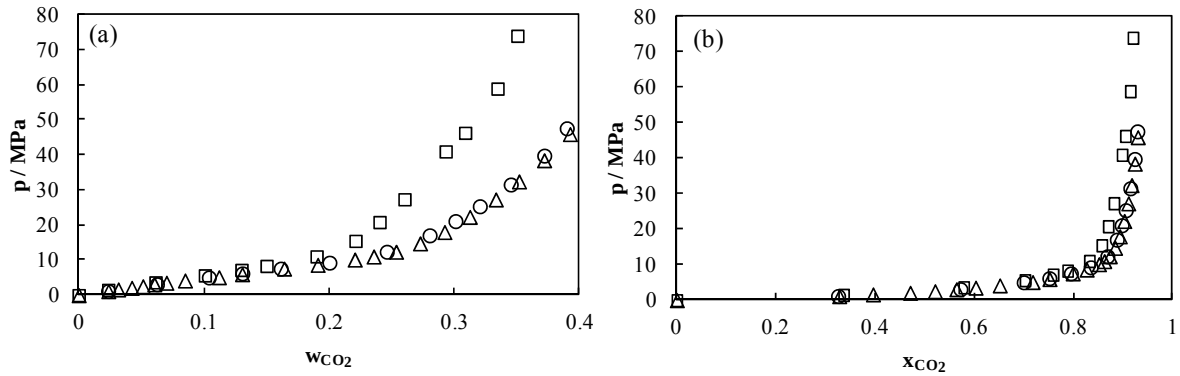

Fig. 7. Experimental solubility values (a) in mass fraction and (b) in mole fraction of the systems CO_2+ castor oil (□), CO_2 + HOSO-B1 (△) and CO_2 + rapeseed oil (○) at 323 K.

4.3 SRK EoS modelling

The SRK EoS was here applied to describe the experimental solubility data and modelling was performed through the PE 2000 software [54]. The critical properties and acentric factor needed to apply the SRK EoS were obtained for the oils by the Constantinou and Gani group contribution method [55,56]. This method uses first and second order group contributions to distinguish special configurations such as isomers and was already previously used to estimate critical properties of triglycerides [57]. The estimated oil critical properties and acentric factors are presented in Table 7.

Table 7. Critical temperatures, pressures and acentric factors for oils estimated using the group contribution method of Constantinou and Gani [55,56].

Oil	T_c/ K	p_c/ MPa	ω
HOSO-B1	974.55	0.33	1.99
Castor oil	961.57	0.35	1.94
Rapeseed oil	973.98	0.34	1.98

Temperature dependent binary interaction parameters (k_{ij} and l_{ij}) were employed for the SRK EoS solubility data description within the equation of state framework. Two different approaches were performed for modelling, one of them consists on adjusting only the k_{ij}, i.e. l_{ij}=0, and the other one on adjusting both parameters. The use of two binary interaction parameters (Table 8) gives rise to better modelling results for all the systems in comparison with the use of only one parameter (Table S2). In Figs. 3 to 5 experimental solubility data together with SRK EoS and parameters of table 8 were plotted for all systems. Global average deviations lower than 6% were obtained in the whole experimental temperature and pressure range using the two binary interaction parameters (Table 8). For all the systems and temperatures, positive binary interaction parameters are obtained. It is important to highlight that the SRK EoS, with the parameters of Table 8, predicts the existence of VLLE at 298.15 K for the system CO_2 + HOSO-B1 at p = 6.45 MPa from x_{CO2}= 0.916 and for the system CO_2 + rapeseed oil at p = 6.45 MPa from x_{CO2}= 0.922. This behaviour was not experimentally investigated.

4.4 Carvalho and Coutinho model

In Fig. 8 experimental solubility values are presented for the three systems along with the predictions obtained from Carvalho and Coutinho correlation [27] for all the temperatures studied and CO_2 molalities (m_{CO2}) up to 5 mol·kg^{-1}. The obtained AAD% in pressure was 11 % for the system CO_2 + HOSO-B1 and 10% for the system CO_2 + rapeseed oil, whereas for the system CO_2 + castor oil the AAD% was 13%. It can be considered that the goodness of these predictions are quite good although we had previously [48] obtained a slightly better prediction result (AAD% = 8.3 %) for the system CO_2+BIO-2T-3 with this model.

Table 8. Values of k_{ij} and l_{ij}, and SRK EoS AAD% in x_{CO2} for the CO_2 + oil systems modeled using two binary interaction parameters.

Oil	T / K	k_{ij}	l_{ij}	AAD %
HOSO-B1	298.15	0.0435	0.0200	7.3
	323.15	0.0598	0.0297	2.5
	348.15	0.0528	0.0115	4.9
	363.15	0.0722	0.0200	2.3
Global AAD %				4.3
Castor oil	323.15	0.0436	0.0059	7.6
	348.15	0.0612	0.0103	4.1
	363.15	0.0710	0.0104	3.6
Global AAD %				5.1
Rapeseed oil	298.15	0.0418	0.0226	5.8
	323.15	0.0449	0.0082	6.5
	348.15	0.0590	0.0182	2.7
	363.15	0.0714	0.0213	2.2
Global AAD %				4.3

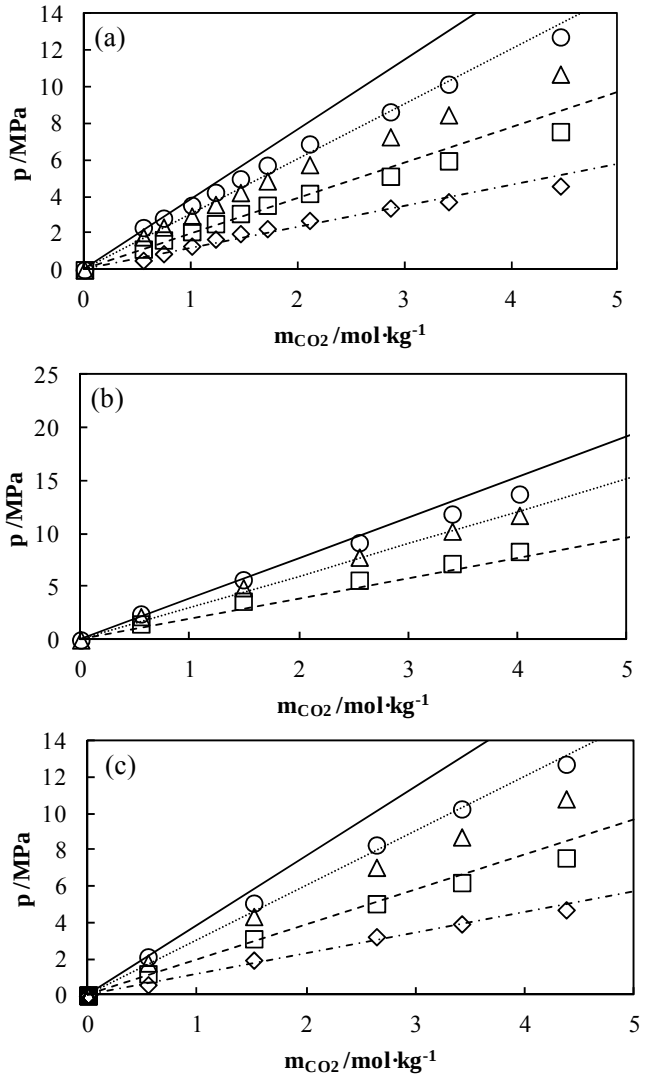

Fig. 8. Experimental solubility values of CO_2 in (a) HOSO-B1, (b) castor oil and (c) rapeseed oil. Lines represent the Carvalho and Coutinho model [27]. 298 K (◇, –·–), 323 K (□, – –), 348 K (△, …) and 363 K (○, —).

5 Conclusions

Density, viscosity and CO_2 solubility were determined for three vegetable oils, a high oleic sunflower oil (HOSO-B1), castor oil and rapeseed oil. The rapeseed oil and HOSO-B1 present similar density and viscosity values whereas castor oil present both higher density as well as viscosity. A fragment based approach was employed for density and viscosity prediction of the oils in the whole experimental temperature range. This approach was able to predict the density of HOSO-B1 and rapeseed oil within an AAD% lower or equal to 1.1%. For the viscosity the fragment approach was able to predict within an AAD% of 3.6% for HOSO-B1 and 4.0 % for rapeseed oil. Additionally, we have proposed parameters for the ricinoleic fragment to be employed in the fragment base approach for density and viscosity predictions.

HOSO-B1 and rapeseed oil present similar CO_2 solubilities in all the composition range. For CO_2 mass fraction higher that 0.2, the solubilities start to increase slower especially for castor oil, because of the hydroxyl groups of the ricinoleic chains of the later.

The experimental solubility data were described with the SRK EoS, with mole fraction global average deviations inferior to 6 %. Furthermore, the Carvalho and Coutinho correlation predicts quite successfully the solubility data, up to molalities of 5 $mol \cdot kg^{-1}$ within an AAD%, in pressure, of 11 % for the CO_2 + HOSO-B1, 10% for the CO_2 + rapeseed oil system and 13% for the CO_2 + castor oil system.

Acknowledgments

This work was carried out within the framework of the strategic and singular project “Biolubricants based on vegetable oils and their synthetic derivatives”, which was funded by Spanish Science and Innovation Ministry and the EU FEDER program (PSE- 320100-2006-1, PSE-420000-2008-4). We are very grateful to Verkol Lubricantes and Instituto de la Grasa (CSIC, Seville) for providing us the oil samples and the analysis of their fatty acid composition. Luis Lugo acknowledges the financial support from the Ramon y Cajal Program (Science and Innovation Ministry, Spain). Teresa Regueira acknowledges financial support provided by the FPU program (Ministry of Education, Culture and Sport, Spain). Part of this work was also funded by FCT- *Fundação para a Ciência e a Tecnologia*, through project Pest-C/CTM/LA0011/2011. Mariana B. Oliveira and Pedro J. Carvalho acknowledge the financial support from FCT- *Fundação para a Ciência e a Tecnologia* through their post-doctoral grants (SFRH/BPD/71200/2010, SFRH/BPD/82264/2011).

Supplementary information

Table S1. Experimental density, ρ, and dynamic viscosity, η, of the vegetable oils.

	HOSO-B1		Castor oil		Rapeseed oil	
T /K	ρ / g·cm^{-3}	η / mPa·s	ρ / g·cm^{-3}	η / mPa·s	ρ / g·cm^{-3}	η / mPa·s
278.15	0.9239	181.8	—	—	0.9279	155.8
283.15	0.9205	137.0	0.9670	2439	0.9245	118.4
288.15	0.9170	105.2	0.9636	1541	0.9211	91.78
293.15	0.9136	82.22	0.9601	1005	0.9177	72.35
298.15	0.9102	65.31	0.9566	674.6	0.9142	57.96
303.15	0.9068	52.67	0.9531	464.2	0.9108	47.11
308.15	0.9035	43.05	0.9497	327.3	0.9075	38.80
313.15	0.9001	35.65	0.9462	236.2	0.9041	32.36
318.15	0.8967	29.87	0.9428	174.0	0.9007	27.29
323.15	0.8934	25.29	0.9394	130.8	0.8974	23.25
328.15	0.8900	21.63	0.9360	100.2	0.8941	20.00
333.15	0.8866	18.66	0.9326	78.10	0.8907	17.34
338.15	0.8832	16.24	0.9292	61.87	0.8874	15.16
343.15	0.8798	14.23	0.9259	49.76	0.8841	13.35
348.15	0.8762	12.57	0.9225	40.58	0.8807	11.83
353.15	0.8728	11.17	0.9191	33.54	0.8772	10.56
358.15	0.8695	9.982	0.9156	28.05	0.8737	9.467
363.15	0.8664	8.972	0.9118	23.72	0.8704	8.534
368.15	0.8633	8.106	0.9083	20.27	0.8672	7.730
373.15	0.8602	7.357	0.9050	17.48	0.8642	7.033

Table S2. k_{ij} values and SRK EoS AAD% in x_{CO2} for the CO_2 + oil systems modelled using only one binary interaction parameter.

Oil	T / K	k_{ij}	AAD %
HOSO-B1			
	323.15	0.0545	13
	348.15	0.0741	12
	363.15	0.0571	8.0
Global AAD %			11
Castor oil			
	323.15	0.0498	9.6
	348.15	0.0651	6.4
	363.15	0.0606	5.7
Global AAD %			7.2
Rapeseed oil			
	323.15	0.0469	9.3
	348.15	0.0509	6.8
	363.15	0.0582	6.0
Global AAD %			7.4

References

[1] S.Z. Erhan, B.K. Sharma, J.M. Perez, Oxidation and low temperature stability of vegetable oil-based lubricants, Industrial Crops and Products 24 (2006) 292-299.
[2] J.M. Fernández-Martínez, M. Mancha, J. Osorio, R. Garcés, Sunflower mutant containing high levels of palmitic acid in high oleic background, Euphytica 97 (1997) 113-116.
[3] P. Miles, Synthetics versus vegetable oils: Applications, options, and performance, J. Synthetic Lubrication 15 (1998) 43-52.
[4] B.J. Bremmer, L. Plonsker, Bio-based lubricants. A market opportunity study update, United Soybean Board, 2008.
[5] L.A.T. Honary, An investigation of the use of soybean oil in hydraulic systems, Bioresource Technology 56 (1996) 41-47.
[6] Regulation (EC) No 66/2010 of the European Parliament and of the Council of 25 November 2009 on the EU Ecolabel, Official Journal of the European Union, 2010, pp. L 27/01 - L 27/19.
[7] Commission decision of 24 June 2011 on establishing the ecological criteria for the award of the EU Ecolabel to lubricants, Official Journal of the European Union, 2011, pp. L 169/128 - L 169/138.
[8] N.S. Battersby, S.E. Pack, R.J. Watkinson, A correlation between the biodegradability of oil products in the CEC L-33-T-82 and modified Sturm tests, Chemosphere 24 (1992) 1989-2000.
[9] W. Castro, J.M. Perez, S.Z. Erhan, F. Caputo, A study of the oxidation and wear properties of vegetable oils: soybean oil without additives, J. American Oil Chemists' Society 83 (2006) 47–52.
[10] R. Garcés, E. Martínez-Force, J.J. Salas, Vegetable oil basestocks for lubricants, Grasas y Aceites 62 (2011) 21-28.
[11] T.A. Isbell, B.A. Lowery, S.S. DeKeyser, M.L. Winchell, S.C. Cermak, Physical properties of triglyceride estolides from lesquerella and castor oils, Industrial Crops and Products 23 (2006) 256-263.
[12] G. Márquez-Ruiz, R. Garcés, M. León-Camacho, M. Mancha, Thermoxidative stability of triacylglycerols from mutant sunflower seeds, J. American Oil Chemists' Society 76 (1999) 1169-1174.
[13] R. Becker, A. Knorr, An evaluation of antioxidants for vegetable oils at elevated temperatures, Lubrication Science 8 (1996) 95-117.
[14] N.J. Fox, G.W. Stachowiak, Vegetable oil-based lubricants—A review of oxidation, Tribology International 40 (2007) 1035-1046.
[15] O.N. Anand, V.K. Chhibber, Vegetable oil derivatives: environment-friendly lubricants and fuels, J. Synthetic Lubrication 23 (2006) 91-107.
[16] S.Z. Erhan, S. Asadauskas, Lubricant basestocks from vegetable oils, Industrial Crops and Products 11 (2000) 277-282.
[17] M.P. Schneider, Plant-oil-based lubricants and hydraulic fluids, J. Science of Food and Agriculture 86 (2006) 1769-1780.
[18] M.-H. Kim, J. Pettersen, C.W. Bullard, Fundamental process and system design issues in CO_2 vapor compression systems, Progress in Energy and Combustion Science 30 (2004) 119-174.
[19] O. Fandiño, E.R. López, L. Lugo, J. García, J. Fernández, Solubility of carbon dioxide in pentaerythritol ester oils. New data and modeling using the PC-SAFT model, J. Supercritical Fluids 55 (2010) 62-70.
[20] T. Otsu, H. Tanaka, N. Izumi, J. Sugimura, Effect of Surrounding Gas on Cavitation in EHL, Tribology Online 4 (2009) 50-54.
[21] W.-H. Chen, C.-H. Chen, C.-M.J. Chang, Y.-H. Chiu, D. Hsiang, Supercritical carbon dioxide extraction of triglycerides from Jatropha curcas L. seeds, J. Supercritical Fluids 51 (2009) 174-180.
[22] E. Jenab, F. Temelli, Viscosity measurement and modeling of canola oil and its blend with canola stearin in equilibrium with high pressure carbon dioxide, J. Supercritical Fluids 58 (2011) 7- 14.
[23] S. Machmudah, M. Kondo, M. Sasaki, M. Goto, J. Munemasa, M. Yamagata, Pressure effect in supercritical CO_2 extraction of plant seeds, J. Supercritical Fluids 44 (2008) 301-307.
[24] H. Sovová, M. Zarevúcka, M. Vacek, K. Stránský, Solubility of two vegetable oils in supercritical CO_2, J. Supercritical Fluids 20 (2001) 15-28.
[25] T. Klein, S. Schulz, Measurement and model prediction of vapor-liquid equilibria of mixtures of rapeseed oil and supercritical carbon dioxide, Industrial & Engineering Chemistry Research 28 (1989) 1073-1081.
[26] P.M. Ndiaye, E. Franceschi, D. Oliveira, C. Dariva, F.W. Tavares, J.V. Oliveira, Phase behavior of soybean oil, castor oil and their fatty acid ethyl esters in carbon dioxide at high pressures, J. Supercritical Fluids 37 (2006) 29-37.

[27] P.J. Carvalho, J.A.P. Coutinho, On the nonideality of CO_2 solutions in ionic liquids and other low volatile solvents, J. Physical Chemistry Letters 1 (2010) 774-780.
[28] L. Zong, S. Ramanathan, C.-C. Chen, Fragment-based approach for estimating thermophysical properties of fats and vegetable oils for modeling biodiesel production processes, Industrial & Engineering Chemistry Research 49 (2010) 876-886.
[29] L. Zong, S. Ramanathan, C.-C. Chen, Fragment-based approach for estimating thermophysical properties of fats and vegetable oils for modeling biodiesel production processes, Industrial & Engineering Chemistry Research 49 (2010) 3022-3023.
[30] F.M. Gaciño, T. Regueira, L. Lugo, M.J.P. Comuñas, J. Fernández, Influence of molecular structure on densities and viscosities of several ionic liquids, J. Chemical & Engineering Data 56 (2011) 4984-4999.
[31] A.M.A. Dias, H. Carrier, J.L. Daridon, J.C. Pàmies, L.F. Vega, J.A.P. Coutinho, I.M. Marrucho, Vapor−liquid equilibrium of carbon dioxide−perfluoroalkane mixtures: Experimental data and SAFT modeling, Industrial & Engineering Chemistry Research 45 (2006) 2341-2350.
[32] J. Pauly, J. Coutinho, J.-L. Daridon, High pressure phase equilibria in methane+waxy systems: 1. Methane+heptadecane, Fluid Phase Equilibria 255 (2007) 193-199.
[33] P.J. Carvalho, V.H. Álvarez, J.J.B. Machado, J. Pauly, J.-L. Daridon, I.M. Marrucho, M. Aznar, J.A.P. Coutinho, High pressure phase behavior of carbon dioxide in 1-alkyl-3-methylimidazolium bis(trifluoromethylsulfonyl)imide ionic liquids, J. Supercritical Fluids 48 (2009) 99-107.
[34] G. Soave, Equilibrium constants from a modified Redlich-Kwong equation of state, Chemical Engineering Science 27 (1972) 1197-1203.
[35] T. Sankarappa, M. Prashant Kumar, A. Ahmad, Ultrasound velocity and density studies in some refined and unrefined edible oils, Physics and Chemistry of Liquids 43 (2005) 507-514.
[36] T. Regueira, L. Lugo, O. Fandiño, E.R. López, J. Fernández, Compressibilities and viscosities of reference and vegetable oils for their use as hydraulic fluids and lubricants, Green Chemistry 13 (2011) 1293-1302.
[37] L.A. Quinchia, M.A. Delgado, C. Valencia, J.M. Franco, C. Gallegos, Viscosity modification of high-oleic sunflower oil with polymeric additives for the design of new biolubricant formulations, Environmental Science & Technology 43 (2009) 2060-2065.
[38] B. Esteban, J.-R. Riba, G. Baquero, A. Rius, R. Puig, Temperature dependence of density and viscosity of vegetable oils, Biomass and Bioenergy 42 (2012) 164-171.
[39] B. Guignon, C. Aparicio, P.D. Sanz, Volumetric properties of sunflower and olive oils at temperatures between 15 and 55°C under pressures up to 350 MPa, High Pressure Research 29 (2009) 38-45.
[40] O. Fandiño, J. García, M.J.P. Comuñas, E.R. López, J. Fernández, PρT Measurements and Equation of State (EoS) Predictions of Ester Lubricants up to 45 MPa, Industrial & Engineering Chemistry Research 45 (2006) 1172-1182.
[41] M. Wesołowski, J. Erecińska, Thermal analysis in quality assessment of rapeseed oils, Thermochimica Acta 323 (1998) 137-143.
[42] L.A. Quinchia, M.A. Delgado, C. Valencia, J.M. Franco, C. Gallegos, Viscosity modification of different vegetable oils with EVA copolymer for lubricant applications, Industrial Crops and Products 32 (2010) 607-612.
[43] O.O. Fasina, Z. Colley, Viscosity and specific heat of vegetable oils as a function of temperature: 35°C to 180°C, International J. Food Properties 11 (2008) 738-746.
[44] J.d.D. Alvarado, Propiedades mecánicas de aceites y grasas vegetales, Grasas y Aceites 46 (1995) 264-269.
[45] M. Kumar, P.N. Shankar, The kinematic viscosities of ethylene-glycol and castor-oil, Current Science 65 (1993) 983-984.
[46] H. Noureddini, B. Teoh, L. Davis Clements, Viscosities of vegetable oils and fatty acids, J. American Oil Chemists' Society 69 (1992) 1189-1191.
[47] M.P. Fernández-Ronco, M. Cismondi, I. Gracia, A. De Lucas, J.F. Rodríguez, High-pressure phase equilibria of binary and ternary mixtures of carbon dioxide, triglycerides and free fatty acids: Measurement and modeling with the GC-EOS, Fluid Phase Equilibria 295 (2010) 1-8.
[48] T. Regueira, O. Fandiño, L. Lugo, E.R. López, J. Fernández, Carbon dioxide solubility in reference and vegetable lubricants developed for two stroke engines, J. Supercritical Fluids 68 (2012) 123-130.

[49] M. Maiwald, H. Li, T. Schnabel, K. Braun, H. Hasse, On-line ^{1}H NMR spectroscopic investigation of hydrogen bonding in supercritical and near critical CO_2–methanol up to 35 MPa and 403 K, J. Supercritical Fluids 43 (2007) 267-275.
[50] S. Bai, C.R. Yonker, Pressure and temperature effects on the hydrogen-bond structures of liquid and supercritical fluid methanol, J. Physical Chemistry A 102 (1998) 8641-8647.
[51] D.S. Bulgarevich, T. Sako, T. Sugeta, K. Otake, Y. Takebayashi, C. Kamizawa, Y. Horikawa, M. Kato, The role of general and hydrogen-bonding Interactions in the solvation processes of organic compounds by supercritical CO_2/n-alcohol mixtures, Industrial & Engineering Chemistry Research 41 (2002) 2074-2081.
[52] M. Kanakubo, T. Aizawa, T. Kawakami, O. Sato, Y. Ikushima, K. Hatakeda, N. Saito, Studies on solute−solvent interactions in gaseous and supercritical carbon dioxide by high-pressure ^{1}H NMR spectroscopy, J. Physical Chemistry B 104 (2000) 2749-2758.
[53] J.C. Dobrowolski, M.H. Jamróz, Infrared evidence for CO_2 electron donor—acceptor complexes, J. Molecular Structure 275 (1992) 211-219.
[54] O. Pfohl, S. Petkow, G. Brunner, Usage of PE A program to calculate phase equilibria, ISBN: 3-89675-410-6, 1998.
[55] B.E. Poling, J.M. Prausnitz, J.P. O'Connell, The properties of gases and liquids, 5th ed., McGraw-Hill New York, 2001.
[56] L. Constantinou, R. Gani, New group contribution method for estimating properties of pure compounds, AIChE J. 40 (1994) 1697-1710.
[57] S. Glisic, D. Skala, The prediction of critical parameters for triolein, diolein, monoolein and methyl esters, Arcachon, France, May 18-20, 2009.

6.3. A new experimental high pressure device to determine phase equilibria. Measurements of two CO_2+ biodegradable oil systems[*]

[*]T. Regueira, O. Fandiño, L. Lugo, E.R. López, J. Fernández, to be submitted.

Abstract

A new experimental device based on visual cell for determining phase equilibria up to 100 MPa is presented. Two carbon dioxide systems with high oleic sunflower oil (HOSO-B1) or an additivated vegetable lubricant (BIO-2T-05) were investigated from 298 to 363 K up to mass compositions of CO_2 of 0.48. Vapour-liquid-liquid equilibrium was found for the CO_2 + BIO-2T-05 system, whereas the existence of three phase equilibria was not investigated for the other system. The experimental device was verified comparing the results for CO_2 + HOSO-B1 system with the values obtained in other laboratory.

The values of CO_2 solubility for both systems show crossing points among the different isotherms. An empirical equation was used to correlate the data, with deviations in x_{CO_2} lower than 1.5%. Carvalho and Coutinho empirical model was tested with experimental data. Furthermore, densities and viscosities at 0.1 MPa of BIO-2T-05 from 278 to 373 K were measured.

1. Introduction

The knowledge of high-pressure phase equilibria is fundamental in several application areas and for the understanding of natural processing [1-5]. Pressure is one of the state variables that determine thermodynamic equilibrium and thereby strongly influences the composition of the coexisting phases [6]. High pressure favors phases of lower volume. Pressure increases the ability of gases to dissolve high-boiling substances; high-density supercritical fluids have a solvent power similar to that of a light hydrocarbon for most solutes. There are a variety of devices and techniques to determine phase equilibria at high pressures [1] and the articles published by Dorhn and coworkers [1,6-9] are a guide which includes a wide literature survey. In our laboratory we have recently implemented a new apparatus based in the visual synthetic method that avoids sampling and analyzing of samples. The apparatus has a full visibility cell, which is similar to those of Dias *et al.* [10] and Pauly *et al.* [11].

The knowledge of the solubility of different gases as CO_2 in lubricants used for two stroke engines is important because this gas is involved in the combustion process together with the lubricant and the gasoline in the combustion chamber [12]. Most of the market of lubricants is dominated by petroleum base stocks which are toxic, no biodegradable and no renewable. Approximately 50% of used lubricants end up in the environment, percentage that increases to 70%-80% in the case of hydraulic fluids [13]. Two-stroke engines are also one of the applications where most of the lubricants and their degradation products are released directly into the environment, polluting the soil, water and atmosphere [12,14,15]. In this scenario, vegetable base oils are shown as environmentally friendly alternatives, even for synthetic oils,

for several applications [16]. Vegetable oils present very interesting advantages [17] such as very low volatility, good viscosity/temperature relationship, and their inherent lubricity (polar ester groups being responsible). However, for their use as lubricants, vegetable oils show some disadvantages, their main drawback the low thermal and oxidative stabilities [17].

On the other hand, supercritical fluid extraction (SFE) has emerged in the last years as a novel technique to extract seed oils or flavors, among others. Carbon dioxide is the most widely used solvent for SFE. Supercritical CO_2 has many benefits like being a clean solvent, cheap, non-flammable and nontoxic. A promising solvent for extraction and fractionation processes of vegetable oils containing unsaturated fatty acids, since these processes can be carried out at low temperatures [18]. Nevertheless supercritical CO_2 presents limited miscibility with vegetable oils, becoming necessary the presence of cosolvents, such as propane or ethanol, to improve the miscibility [19,20]. Knowledge of the solubility of vegetable oils in supercritical CO_2 and its dependence on pressure and temperature is important for the successful application of supercritical fluid technology. Thus for this aim, the phase behavior of systems composed by different natural oils [21-23] or their constituents [24-26], among them sunflower oils [19,27-30], and carbon dioxide has been studied.

In this work, a new experimental device which can be used for measuring phase equilibria at pressures up to 100 MPa over a wide temperature range is presented. Moreover, we show the solubility behavior of CO_2 in a high oleic sunflower oil, namely HOSO-B1, and in an additivated mixture, namely BIO-2T-05, of a polyalphaolefin and HOSO-B1, developed for two stroke engines at four temperatures between 298 and 363 K. In order to validate the apparatus and experimental procedure, the results for the CO_2 + HOSO-B1 system have been compared with previous measurements performed in the University of Aveiro [31]. Experimental data have been correlated using a modified form of Gordillo *et al.* [32] equation. In addition, the temperature dependence of the densities and viscosities for BIO-2T-05 was experimentally determined.

2. Experimental Section

2.1 Materials

Carbon dioxide (CAS 124-38-9, CO_2), with 99.998 % mole purity, was supplied by Air Liquide. In Table 1 the main characteristics of the oils studied in this work are presented. Molecular mass of the HOSO-B1, which is a mixture of triglycerides, was calculated according to its fatty acid composition (Table 2) and it was found to be 881.37 $g \cdot mol^{-1}$. The lubricant BIO-2T-05 was developed by Verkol Lubricantes as candidate to substitute the mineral or

semisynthetic oils currently used in two stroke engines. BIO-2T-05 is composed by a base oil and some additives.

Table 1.Density (ρ), kinematic viscosity (ν), and viscosity index (VI) of the lubricants.

Name	Description	Molar mass $g \cdot mol^{-1}$	ρ/$g \cdot cm^{-3}$ (313.15 K)	ν/$mm^2 \cdot s^{-1}$ (313.15 K)	VI
HOSO-B1	83 % content of oleic acid	881.77	0.9001 [31]	39.606 [31]	202.4
BIO-2T-05	50%HOSO-B1+50%PAO+additives	582.16	0.8576	28.189	181.8

The base oil is composed by 50% of a biodegradable polyalphaolefin (PAO2) and 50% of an aliquot of the HOSO-B1 whose fatty acid composition is indicated in Table 2. Its molecular mass is estimated to be 582.16 $g \cdot mol^{-1}$. Oil samples were degassed under vacuum during 48 hours at room temperature before use.

Table 2. Fatty acid composition of the high oleic sunflower oil (HOSO-B1) and standard deviation of the determination (σ).

	Mass fraction (%)	σ (%)
Palmitic acid	3.98	0.01
Stearic acid	2.99	0.02
Oleic acid	82.89	0.20
Linoleic acid	9.17	0.11
Arachidic acid	0.26	0.01
Behenic acid	0.72	0.04

2.2 Experimental Technique

The phase equilibria measurements have been performed in a new device, the heart of the same being a high pressure cell with full visibility similar to that of Dias *et al.* [10] and Pauly *et al.* [11]. The cell was made by Top Industrie (France) and it is constructed in stainless steel DIN 1.4980, and supports working pressures and temperatures up to 100 MPa and 423 K, respectively. The cell consists of a horizontal cylinder of 2 cm internal diameter with a movable piston at one end. This piston can be displaced a maximum of 6.9 cm changing the volume of the cell from 8 to 30 cm^3. At the other end it has a sapphire window, diameter 1.6 cm, which allows visual observation of the interior of the cell of equilibrium. On the lateral wall of the cylinder is placed a second sapphire window, of 0.6 cm of diameter, which allows lighting up the inside of the cell through an optical fiber. A video acquisition system is located in front of the first sapphire window and consists of an endoscope (Olympus 5 Series) and a video camera (Moticam 2000), connected to a computer for viewing inside the measuring cell. A pressure transducer (Kulite, model HEM375), directly connected to minimize the dead volumes, allows to measure

the pressure with a typical uncertainty less than ±0.03 MPa and the reproducibility of the pressure readings for bubble points was 0.02 MPa whereas for cloud points it was 0.05 MPa. The temperature is kept constant by circulating a fluid from a thermostatic bath through three internal lines in the cell wall, and it is measured with an uncertainty of ±0.02 K by means of a Pt100 probe.

This technique is based on a static visual synthetic method, thus avoiding inconvenient sampling and analyzing the composition of the two phases [10]. The operating procedure is as follows: initially the cell is charged with a known amount of liquid precisely measured with a Sartorius MC210P balance, after, vacuum is performed in the system and then the gas is transferred to the cell from a high pressure reservoir; the amount of gas transferred is determined by weighting in a Mettler Toledo XP5003S balance. The expanded ($k = 2$) uncertainty of the CO_2 mass fraction (w_{CO_2}) for the studied systems is lower or equal to $2 \cdot 10^{-3}$. Under isothermal conditions, the mixture of known composition is compressed to achieve a single phase with continuous stirring. Subsequently, the appearance of a new phase is determined visually (by means of bubbles or turbidity appearance) by slowly decreasing pressure. Again the system is compressed until the disappearance of the second phase. Then, in the case of bubble points (liquid-vapor transitions), the pressure at which the last bubble disappears is recorded. In the case of cloud points (liquid-fluid or liquid-liquid transitions), the pressure at which turbidity disappears was taken as the pressure of the phase transition. For a fixed temperature, several trials have been performed, the lowest value being associated to the experimental equilibrium pressure. After that, a new temperature is set up. When all the selected temperatures are investigated, the composition is changed adding more CO_2. To analyze the existence of vapor-liquid-liquid equilibria, VLLE, when a cloud point is detected the pressure is decreased without agitation until three phases are observed. Fig. 1 shows as an example the cell images for the different types of phase equilibria detected in this work.

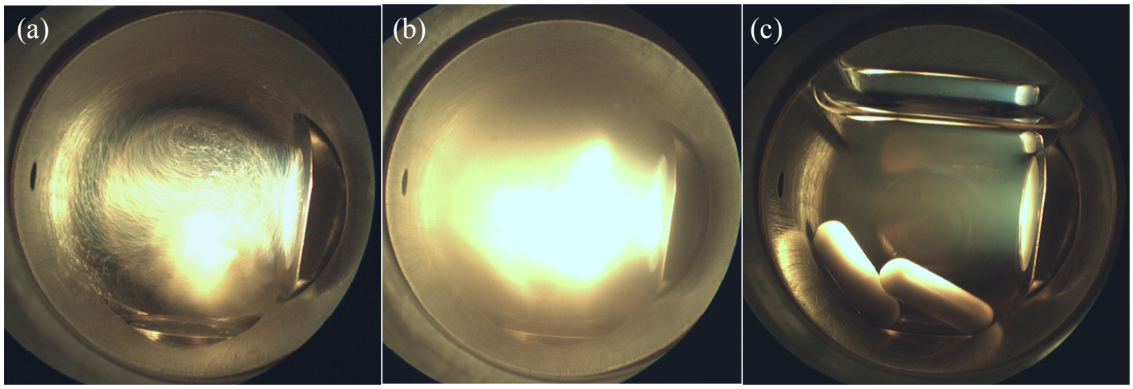

Fig. 1. Images of the high pressure cell corresponding to (a) a pressure slightly lower than the bubble point, (b) 298.17 K and pressure slightly lower than 14.29 MPa (cloud point) and (c) VLLE.

A SVM3000 Anton Paar Stabinger device [33] was also used to characterize the lubricant BIO-2T-05 in terms of density, viscosity and viscosity index (VI). Uncertainty in density measurements is 0.0005 g·cm^{-3}, whereas for the dynamic viscosity is 1%. More details can be found in previous work [34]. Measurements were performed in the temperature range from 278.15 K to 373.15 K. As regards HOSO-B1, density and viscosity behavior with temperature were reported in a previous work [31].

3. Results

Density values at atmospheric pressure of BIO-2T-05 are presented in Table 3 along with viscosity values in the temperature range from 278.15 K to 373.15 K. These density values were correlated as a function of temperature by means of the following equation:

$$\rho / g{\cdot}cm^{-3} = a_0 + a_1{\cdot}(T/K) + a_2(T/K)^2 + a_3(T/K)^3 \quad (1)$$

Table 3. Experimental density (ρ) and dynamic viscosity (η) values of BIO-2T-05 at atmospheric pressure.

T / K	ρ / g·cm^{-3}	η / mPa·s
278.15	0.8804	119
283.15	0.8773	91.4
288.15	0.8740	70.4
293.15	0.8707	55.2
298.15	0.8675	44.0
303.15	0.8642	35.6
308.15	0.8609	29.1
313.15	0.8576	24.2
318.15	0.8544	20.3
323.15	0.8511	17.2
328.15	0.8478	14.8
333.15	0.8446	12.8
338.15	0.8413	11.1
343.15	0.8380	9.76
348.15	0.8347	8.63
353.15	0.8313	7.68
358.15	0.8278	6.87
363.15	0.8246	6.19
368.15	0.8214	5.60
373.15	0.8183	5.08

Parameters of this correlation as well as standard deviation of the fit are presented in Table 4. Moreover, viscosity values were fitted to the Vogel-Fulcher-Tammann (VFT) equation:

$$\ln(\eta / mPa{\cdot}s) = A + \frac{B}{T - T_0} \quad (2)$$

Coefficients of the VFT equation for BIO-2T-05 are also presented in Table 4, along with standard deviation of the fit.

Table 4. Coefficients of the density an viscosity dependence on temperature and standard deviations(σ) for BIO-2T-05 (Eq. 1 and Eq. 2).

Eq. 1		Eq. 2	
a_0 /g·cm^{-3}	1.01029	A	-2.54381
$10^4 a_1$/g·cm^{-3}K^{-1}	-1.8844	B / K	915.807
$10^6 a_2$/g·cm^{-3}K^{-2}	-1.3700	T_0 / K	153.326
$10^9 a_3$/g·cm^{-3}K^{-3}	1.3265	$10^3 \cdot \sigma$	4.2
$10^5 \sigma$ / g·cm^{-3}	9.2		

Solubilities of the systems CO_2 + HOSO-B1 or BIO-2T-05 (Tables 5 and 6) have been measured at temperatures of 298, 323, 348 and 363 K; the saturation pressures were measured at mass compositions of CO_2 from 0.0179 up to 0.4116, and from 0.0204 to 0.4810, respectively for both systems.

The high pressure oil-CO_2 phase equilibrium is plotted in Figs. 2 and 3 where a similar behaviour is shown for both systems. It can be also seen as at constant temperature the solubility increases with pressure, as usual, whereas crossing points are observed between the isotherms in the CO_2-rich area at pressures between 30 and 40 MPa for CO_2 + HOSO-B1 and around 30 MPa for the system CO_2 + BIO-2T-05. Thus, below the crossing points the solubility diminishes when temperature increases whereas at higher pressures the tendency is opposite. This type of crossing point has also been reported by Klein and Schulz [36] for the system CO_2 + rapeseed oil and by Borch-Jensen and Mollerup [37] for the system CO_2 + fish oil. The solubility of CO_2 in both oils is similar at low CO_2 concentration, but for w_{CO2}>0.20, solubility in the developed oil is higher than in HOSO-B1. In Fig. 4, it can be observed as CO_2 solubility in both oils increases with CO_2 density [35]. The abrupt increase of CO_2 density with pressure at constant temperature when CO_2 changes from vapor to liquid state at 298 K could be related to the change in the slope of the curve p-x_{CO_2} for x_{CO_2} found at this temperature around 0.85 and 0.82 for the systems containing HOSO-B1 and BIO-2T-05, respectively.

Table 5. Mass fraction solubility of CO_2 in HOSO-B1.

T/K	p/MPa	w_{CO_2}	T/K	p/MPa	w_{CO_2}
298.16	0.655	0.0179	348.14	2.623	0.0402
298.16	1.033	0.0291	348.17	3.324	0.0502
298.16	1.427	0.0402	348.22	3.982	0.0596
298.18	1.797	0.0502	348.13	4.622	0.0692
298.12	2.101	0.0596	348.15	5.660	0.0860
298.15	2.441	0.0692	348.14	6.268	0.0966
298.18	2.903	0.0860	348.14	7.737	0.1203
298.15	3.211	0.0966	348.10	9.042	0.1410
298.17	3.828	0.1203	348.13	10.261	0.1596
298.17	4.304	0.1410	348.13	11.619	0.1798
298.16	4.777	0.1596	348.14	14.676	0.1994
298.16	5.155	0.1798	348.16	16.674	0.2192
298.15	5.899	0.1994	348.16	19.210	0.2398
298.16	6.211	0.2192	348.14	21.770	0.2589
298.16	8.307	0.2398	348.15	26.471	0.2895
298.16	13.104	0.2589	348.16	29.836	0.3094
298.17	23.211	0.2895	348.13	33.503	0.3298
298.15	32.278	0.3094	348.16	36.989	0.3499
298.14	46.589	0.3298	348.14	40.817	0.3697
298.16	71.808	0.3499	348.16	45.406	0.3907
323.16	0.889	0.0179	348.16	49.176	0.4116
323.12	1.460	0.0291	363.06	1.311	0.0179
323.16	2.000	0.0402	363.10	2.185	0.0291
323.14	2.528	0.0502	363.14	3.033	0.0402
323.17	3.005	0.0596	363.16	3.845	0.0502
323.17	3.477	0.0692	363.11	4.592	0.0596
323.15	4.203	0.0860	363.11	5.324	0.0692
323.15	4.669	0.0966	363.11	6.565	0.0860
323.15	5.660	0.1203	363.17	7.286	0.0966
323.14	6.508	0.1410	363.16	9.034	0.1203
323.17	7.316	0.1596	363.13	10.541	0.1410
323.17	8.138	0.1798	363.17	12.093	0.1596
323.17	9.953	0.1994	363.16	13.705	0.1798
323.17	11.396	0.2192	363.16	17.248	0.1994
323.15	13.955	0.2398	363.17	19.487	0.2192
323.16	16.932	0.2589	363.16	21.948	0.2398
323.16	23.083	0.2895	363.18	24.468	0.2589
323.17	27.493	0.3094	363.20	28.785	0.2895
323.18	32.995	0.3298	363.16	31.808	0.3094
323.16	38.392	0.3499	363.16	34.917	0.3298
323.18	43.494	0.3697	363.19	38.252	0.3499
323.14	54.158	0.3907	363.15	41.344	0.3697
323.17	62.456	0.4116	363.17	47.802	0.3907
348.13	1.152	0.0179	363.15	47.912	0.4116
348.13	1.912	0.0291			

Table 6. Mass fraction solubility of CO_2 in BIO-2T-05.

T/K	p/MPa	w_{CO_2}	T/K	p/MPa	w_{CO_2}
298.15	0.706	0.0204	348.13	2.374	0.0394
298.16	1.045	0.0309	348.15	3.039	0.0496
298.16	1.314	0.0394	348.16	3.685	0.0596
298.17	1.696	0.0496	348.17	4.318	0.0696
298.16	2.038	0.0596	348.17	4.915	0.0799
298.17	2.368	0.0696	348.15	6.118	0.1004
298.16	2.680	0.0799	348.14	7.209	0.1199
298.15	3.280	0.1004	348.16	8.920	0.1499
298.17	3.741	0.1199	348.16	10.608	0.1805
298.15	4.416	0.1499	348.15	12.445	0.2109
298.14	5.045	0.1805	348.16	12.929	0.2195
298.14	5.618	0.2109	348.16	14.318	0.2392
298.14	5.765	0.2195	348.16	15.896	0.2604
298.17	6.041	0.2392	348.16	17.831	0.2803
298.16	6.268	0.2604	348.15	19.921	0.3007
298.15	9.849	0.2803	348.14	22.424	0.3211
298.17	14.292	0.3007	348.14	24.707	0.3416
298.17	21.317	0.3211	348.14	27.217	0.3603
298.14	31.743	0.3416	348.16	29.956	0.3805
298.15	52.732	0.3603	348.16	32.598	0.4007
323.17	0.951	0.0204	348.16	35.898	0.4200
323.17	1.436	0.0309	363.18	1.388	0.0204
323.17	1.835	0.0394	363.17	2.086	0.0309
323.16	2.357	0.0496	363.16	2.710	0.0394
323.18	2.826	0.0596	363.16	3.460	0.0496
323.17	3.316	0.0696	363.15	4.200	0.0596
323.17	3.751	0.0799	363.18	4.898	0.0696
323.18	4.632	0.1004	363.15	5.621	0.0799
323.17	5.394	0.1199	363.17	7.002	0.1004
323.16	6.555	0.1499	363.15	8.323	0.1199
323.17	7.685	0.1805	363.16	10.335	0.1499
323.14	8.828	0.2109	363.17	12.328	0.1805
323.17	9.133	0.2195	363.17	14.480	0.2109
323.14	10.018	0.2392	363.17	15.039	0.2195
323.16	11.198	0.2604	363.17	16.623	0.2392
323.15	13.358	0.2803	363.17	18.456	0.2604
323.16	15.826	0.3007	363.16	20.247	0.2803
323.16	18.874	0.3211	363.15	22.378	0.3007
323.15	22.527	0.3416	363.16	24.548	0.3211
323.16	26.624	0.3603	363.14	26.706	0.3416
323.16	31.173	0.3805	363.15	28.867	0.3603
323.15	35.279	0.4007	363.15	31.183	0.3805
323.16	42.506	0.4200	363.15	33.747	0.4007
348.14	1.244	0.0204	363.16	36.039	0.4200
348.15	1.857	0.0309			

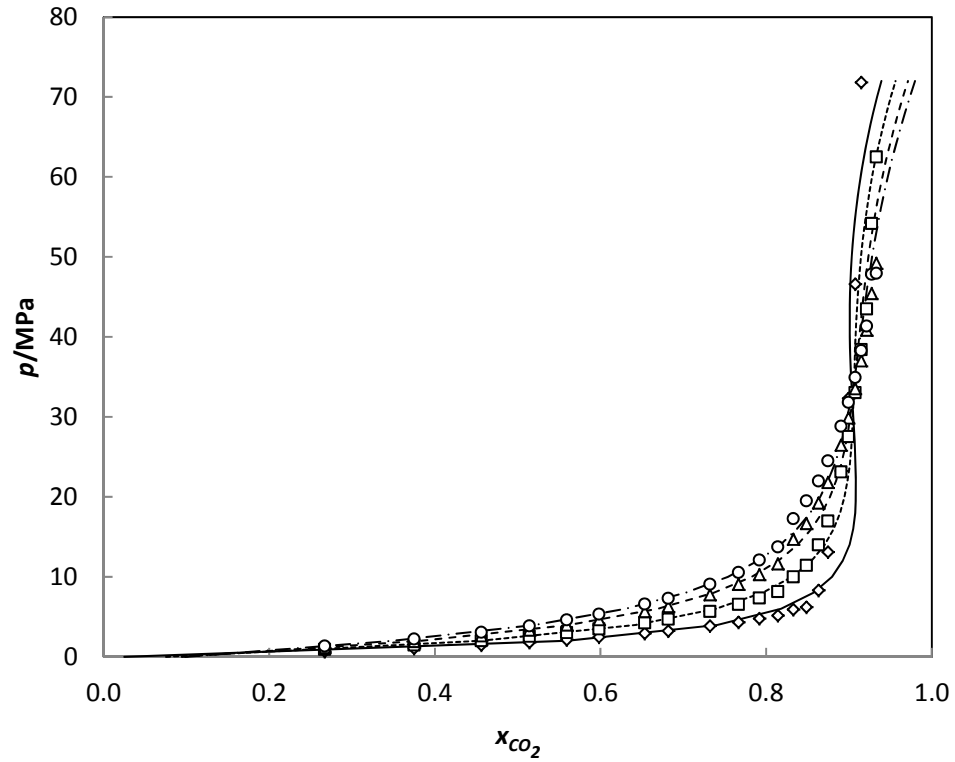

Fig. 2. Experimental solubility values of the system CO_2+HOSO-B1. 298 K (◇, —), 323 K (□, …), 348 K (△, – –) and 363 K (○, –·- –). Lines are the correlation with Eq. (3).

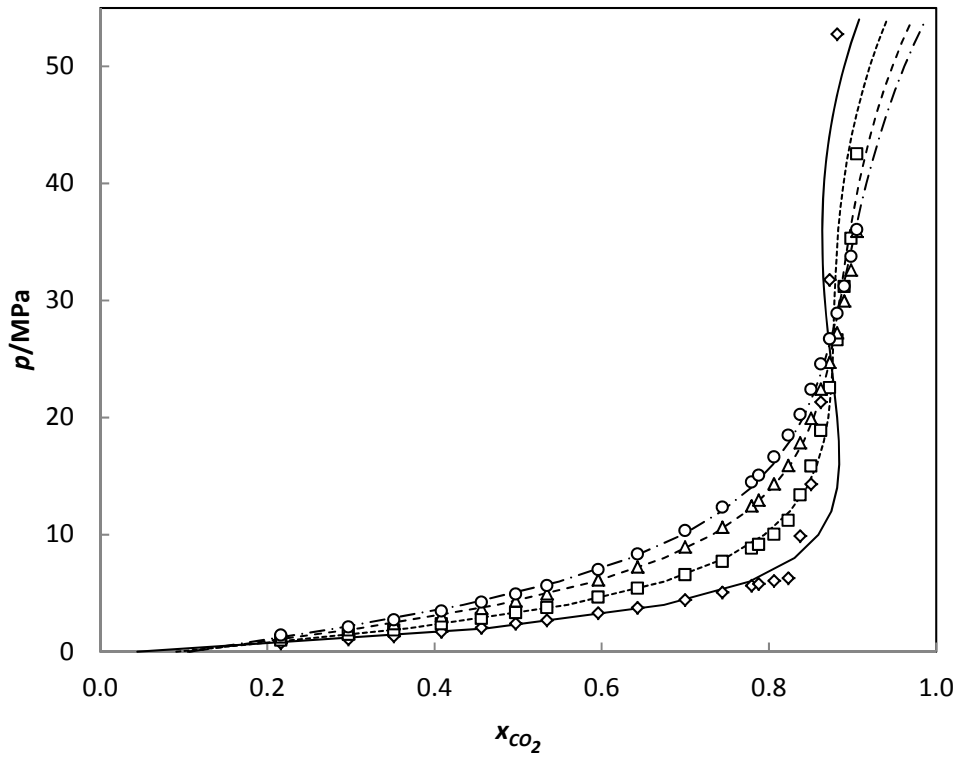

Fig. 3. Experimental solubility values of the system CO_2+ BIO-2T-05. 298 K (◇, —), 323 K (□, …), 348 K (△, – –) and 363 K (○, – - –). Lines are the correlation with Eq. (3).

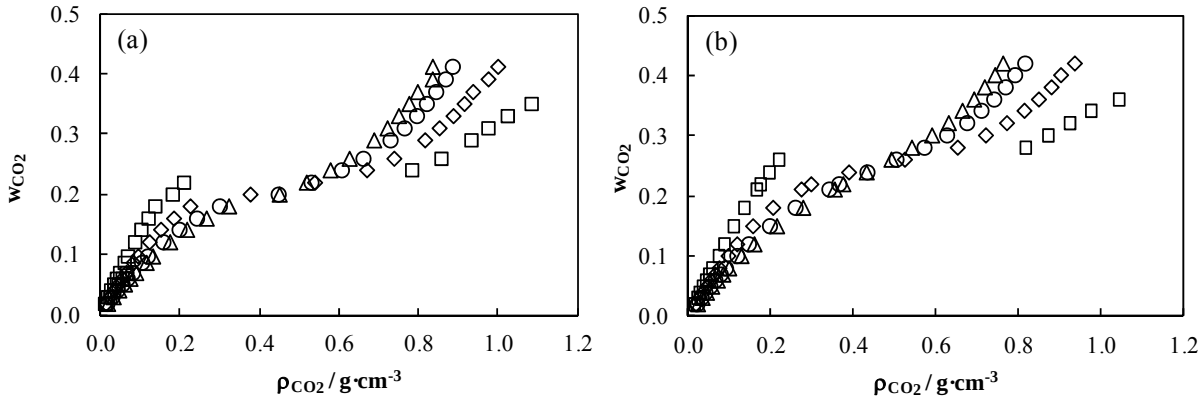

Fig.4. Solubility of CO_2 in (a) HOSO-B1 and (b) BIO-2T-05 as a function of CO_2 density [35]. 298 K (□), 323 K (◇), 348 K (○) and 363 K (△).

The results for the system CO_2+ HOSO-B1 have been compared with those previously determined in a similar apparatus in the Universidade de Aveiro [31]. As can be seen in Fig. 5, both sets of data agree well. To perform the comparison we have correlated the solubility values $w(p)$ of reference [31] along isotherms and then the solubility was evaluated at the pressures of the present work, see Fig. 6. The highest deviations in composition are found at lower pressures where the relative uncertainty of the pressure measurements is greater. The absolute average deviation (AAD%) between both sets of CO_2 mole fraction data is 2.2%.

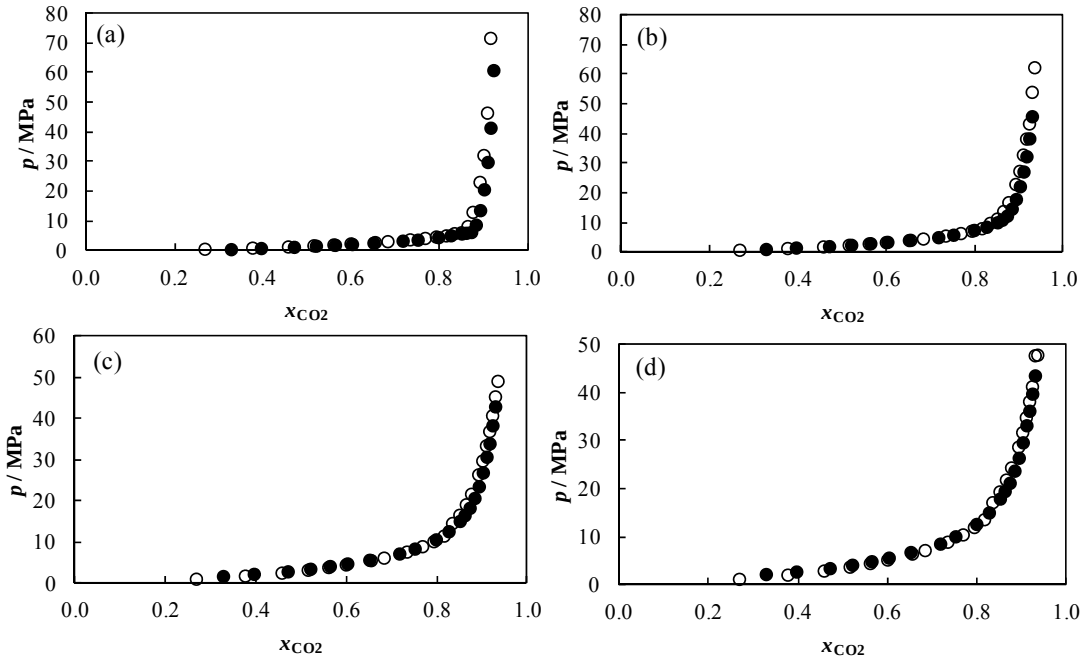

Fig. 5. Comparison between the solubility values of CO_2 in HOSO-B1 measured in this work (empty symbols) and those measured in the high pressure equilibrium cell of the University of Aveiro [31] (filled symbols). (a) 298 K, (b) 323 K, (c) 348 K and (d) 363 K.

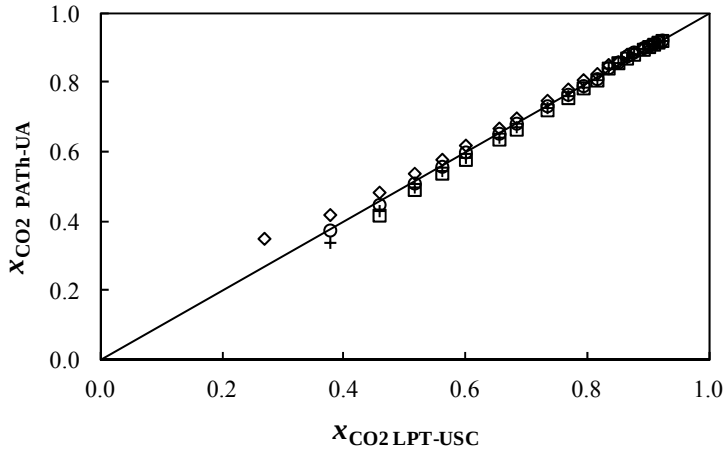

Fig.6. Comparison between the solubility values of CO_2 in HOSO-B1 measured in this work (LPT-USC) and those measured in the high pressure equilibrium cell of the University of Aveiro (PATh-UA) [31]. 298 K (◇), 323 K (○), 348 K (+) and 363 K (□).

Vapor-liquid-liquid equilibrium (VLLE) can occur near the vapour pressure of the pure gas and even extend up to temperatures above its critical point. For the system CO_2+BIO-2T-05, VLLE was observed at T=298 K and p=6.5 MPa for w_{CO2}≥0.36 and also from 288 K (lower temperatures were not investigated) to 306 K for $w_{CO2=}$ 0.481 (Table 7 and Fig. 7). The existence of three phase equilibria was not investigated for the other system.

Table 7. VLLE of CO_2 in BIO-2T-05.

T / K	p/MPa
288.16	4.967
289.14	5.078
291.15	5.326
293.15	5.584
296.15	5.995
298.14	6.308
300.16	6.598
303.17	7.067
305.14	7.364
305.64	7.451

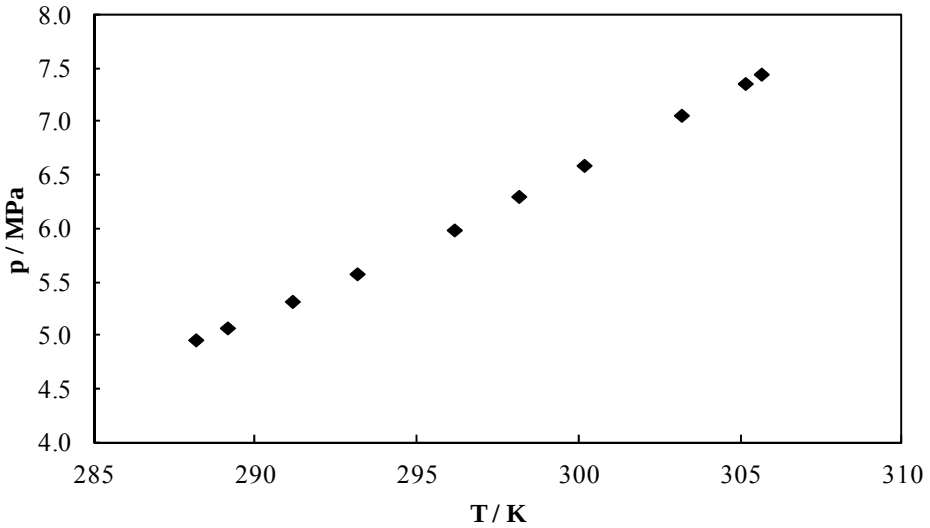

Fig. 7. Vapor-liquid-liquid equilibria (VLLE) of the system CO_2+BIO-2T-05- from 288 K to 306 K at mass fraction of CO_2 of 0.481.

Solubility data have been correlated using an empirical equation obtained modifying that proposed by Gordillo *et al.* [32]:

$$x_{CO_2} = \exp\left(\frac{A + Bp + Cp^2 + Dp^3 + EpT + FT + GT^2}{H + Ip + JT}\right) \quad (3)$$

where *A-I* are fitting parameters. For both systems, the absolute average deviation obtained between experimental and correlated carbon dioxide mole fractions is lower than 1.5 %. As can be seen in Figs. 2 and 3 in both cases the worse results correspond to the lower isotherms. The correlation is able to reproduce the crossing point around 34 MPa for the system CO_2 + HOSO-B1 and 26 MPa for the CO_2 + BIO-2T-05 ones (Figs. 2 and 3).

Vapor–liquid equilibria for a CO_2-sunflower oil system have been determined by Fernández-Ronco *et al.* [29] at 314.4 K and 325.9 K. Their data have been compared with those obtained using the correlation of the system CO_2 + HOSO-B1, with an AAD% of 0.80, a bias% of 0.03 and a maximum deviation of 2.3%.

On the other hand, Carvalho and Coutinho [38] have proposed the following general correlation for predicting the solubility of CO_2 in nonvolatile solvents:

$$\frac{p/\mathrm{MPa}}{1\,\mathrm{MPa}} = \frac{m_i/\mathrm{mol{\cdot}kg^{-1}}}{1\,\mathrm{mol{\cdot}kg^{-1}}} e^{\left(6.8591 - \frac{2004.3}{T/\mathrm{K}}\right)} \quad (4)$$

where m_i is the CO_2 solubility. Eq. (4) is valid for pressures up to 5 MPa, for temperatures ranging from room temperature up to 363 K and molalities up to 3 $mol{\cdot}kg^{-1}$. Carvalho and Coutinho prediction model (Fig.8) predicts our experimental solubility values of CO_2 in HOSO-B1, taking into account the molality and pressure limits given by the authors, with an AAD% in pressure of 14% and those in BIO-2T-05, with an AAD% in pressure of 17 %.

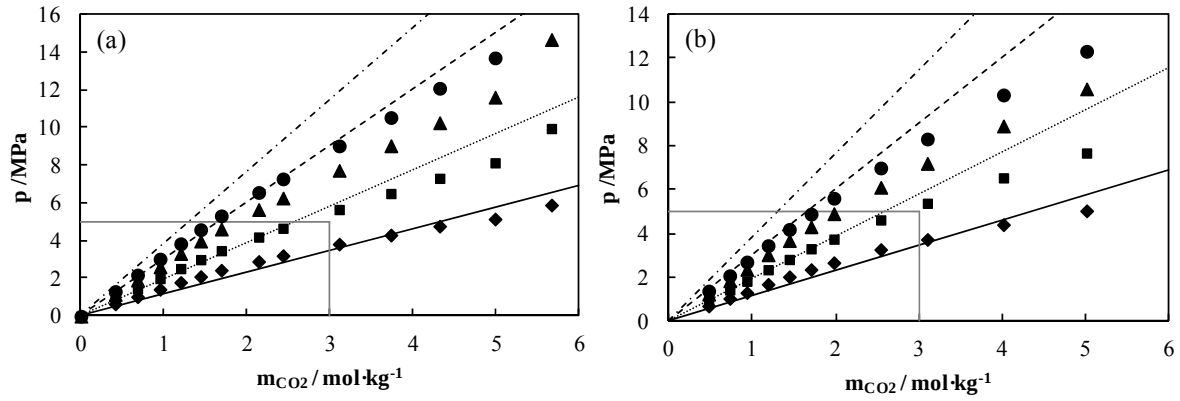

Fig. 8. Pressure-molality diagram for the systems (a) CO_2+HOSO-B1 and (b) CO_2+ BIO-2T-05. T= 298 K (◆, —), 323 K (■, …), 348 K (▲, – –) and 363 K (●, –·–). Black lines represent the Carvalho and Coutinho prediction model [38], whereas grey lines represent the applicability limits of the model given by the authors.

CO_2 solubility in these oils was compared in Fig. 9 with those of other two oils for two stroke engine applications, one of them is a reference semi-synthetic oil (SYN-2T [12]) and the other one is a biodegradable developed oil based in HOSO-B1 (BIO-2T-03 [12]), which differs from BIO-2T-05 in having synthetic esters instead of PAO2.

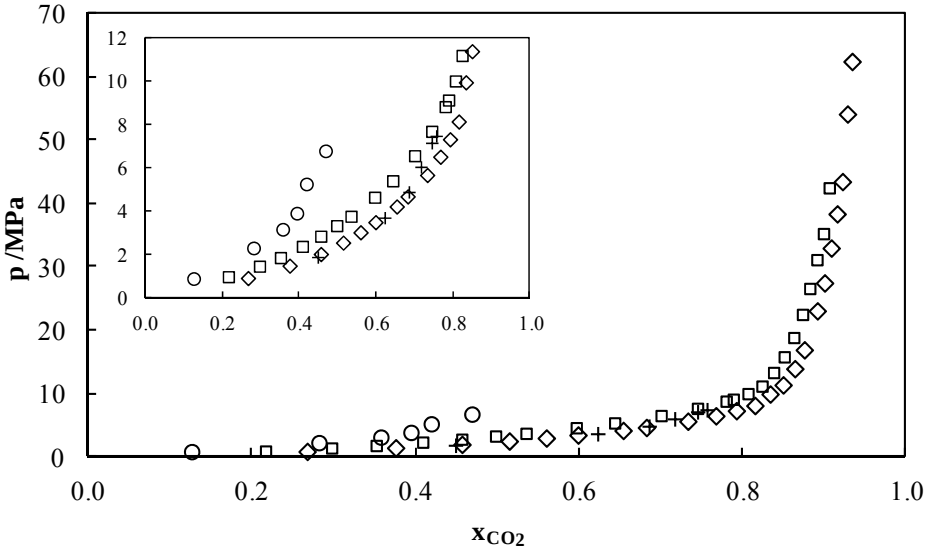

Fig.9. Comparison between the CO_2 solubility in the oils studied in this work and other two measured in a previous work for two stroke engine applications. HOSO-B1 (◇), BIO-2T-05 (□), BIO-2T-03 [12] (＋) and SYN-2T [12] (○).

It can be observed that the lowest CO_2 solubility is in SYN-2T [12] oil, because of its low polarity. Moreover, among the biodegradable oils, both CO_2 solubility in HOSO-B1 and in BIO-2T-03 [12] are the highest, due to the polarity of the ester groups. Finally, concerning CO_2 solubility in BIO-2T-05, it can be observed that its values are close to those of HOSO-B1 but slightly lower due to the PAO2 contain of the base oil that reduces its polarity.

4. Conclusions

A new technique for determining phase equilibria was successfully implemented, the heart being a high pressure cell with full visibility. The bubble points of the system CO_2+ HOSO-B1 have been measured at temperatures of 298, 323, 348 and 363 K; the saturation pressures, ranging from 0.655 to 71.808 MPa, were measured at mass compositions of CO_2 from 0.0179 up to 0.4116. The results agree with the previous ones measured in a similar apparatus in the Universidade de Aveiro with an AAD% of CO_2 mole fraction of 2.2 %.

For the system CO_2+BIO-2T-05, bubble points and cloud points have been measured at temperatures of 298, 323, 348 and 363 K; the saturation pressures, ranging from 0.706 to 52.732 MPa, were measured at mass compositions of CO_2 from 0.0204 up to 0.4200. VLLE equilibrium was observed at T=298 K and p=6.5 MPa for w_{CO2}≥0.36 and also from 288 K (lower temperatures were no investigated) to 306 K for $w_{CO2=}$ 0.481. Under the analyzed conditions, high pressure solubility data showed crossing points for both systems in the pressure-

composition diagram, between 30 and 40 MPa for CO_2+ HOSO-B1 and around 30 MPa for CO_2+BIO-2T-05.

Carvalho and Coutinho model predicts our high-pressure oil-CO_2 phase equilibrium data within the composition and pressure limits given by the authors with an AAD% of 14 % for CO_2+HOSO-B1 and 17 % for CO_2+BIO-2T-05 system.

Acknowledgments

This work was carried out within the framework of the strategic and singular project "Biolubricants based on vegetable oils and their synthetic derivatives", which was funded by Spanish Science and Innovation Ministry and the EU FEDER program (PSE- 320100-2006-1, PSE-420000-2008-4). We are very grateful to Verkol Lubricantes and Instituto de la Grasa (CSIC, Seville) for providing us the oil samples and the analysis of their fatty acid composition. Authors gratefully acknowledge advice from Prof. J.A.P. Coutinho and Dr. P.J. Carvalho (University of Aveiro) as well as from Prof. J.L.Daridon (Pau University). L. L. acknowledges the financial support from the Ramon y Cajal Program (Ministerio de Economía y Competitividad, Spain). T.R. acknowledges financial support provided by the FPU program (Ministerio de Educación, Cultura y Deporte, Spain).

References

[1] J.M.S. Fonseca, R. Dohrn, S. Peper, High-pressure fluid-phase equilibria: experimental methods and systems investigated (2005–2008), Fluid Phase Equilibria 300 (2011) 1-69.

[2] G. Brunner, Supercritical Fluids as Solvents and Reaction Media, Elsevier, Amsterdam, 2004.

[3] D.E. Knox, Solubilities in supercritical fluids, Pure and Applied Chemistry 77 (2005) 513-530.

[4] G. Brunner, in: Annual Review of Chemical and Biomolecular Engineering, J.M. Prausnitz, M.F. Doherty, M.A. Segalman (Ed.) 2010, pp. 321-342.

[5] E. Kiran, G. Brunner, R.L. Smith Jr, The 20th anniversary of the Journal of Supercritical Fluids–A special issue on future directions in supercritical fluid science and technology, The Journal of Supercritical Fluids 47 (2009) 333-335.

[6] R. Dohrn, J.M.S. Fonseca, S. Peper, Experimental methods for phase equilibria at high pressures, Annual Review of Chemical and Biomolecular Engineering 3 (2012) 343-367.

[7] M. Christov, R. Dohrn, High-pressure fluid phase equilibria: Experimental methods and systems investigated (1994–1999), Fluid Phase Equilibria 202 (2002) 153-218.

[8] R. Dohrn, G. Brunner, High-pressure fluid-phase equilibria: experimental methods and systems investigated (1988–1993), Fluid Phase Equilibria 106 (1995) 213-282.

[9] R. Dohrn, S. Peper, J.M.S. Fonseca, High-pressure fluid-phase equilibria: experimental methods and systems investigated (2000–2004), Fluid Phase Equilibria 288 (2010) 1-54.

[10] A.M.A. Dias, H. Carrier, J.L. Daridon, J.C. Pàmies, L.F. Vega, J.A.P. Coutinho, I.M. Marrucho, Vapor−liquid equilibrium of carbon dioxide−perfluoroalkane mixtures: Experimental data and SAFT modeling, Industrial & Engineering Chemistry Research 45 (2006) 2341-2350.

[11] J. Pauly, J. Coutinho, J.-L. Daridon, High pressure phase equilibria in methane+waxy systems: 1. Methane+heptadecane, Fluid Phase Equilibria 255 (2007) 193-199.

[12] T. Regueira, O. Fandiño, L. Lugo, E.R. López, J. Fernández, Carbon dioxide solubility in reference and vegetable lubricants developed for two stroke engines, The Journal of Supercritical Fluids 68 (2012) 123-130.
[13] S.Z. Erhan, B.K. Sharma, Z. Liu, A. Adhvaryu, Lubricant base stock potential of chemically modified vegetable oils, Journal of Agricultural and Food Chemistry 56 (2008) 8919-8925.
[14] O.N. Anand, V.K. Chhibber, Vegetable oil derivatives: environment-friendly lubricants and fuels, Journal of Synthetic Lubrication 23 (2006) 91-107.
[15] S.Z. Erhan, S. Asadauskas, Lubricant basestocks from vegetable oils, Industrial Crops and Products 11 (2000) 277-282.
[16] L.A. Quinchia, M.A. Delgado, C. Valencia, J.M. Franco, C. Gallegos, Viscosity modification of high-oleic sunflower oil with polymeric additives for the design of new biolubricant formulations, Environmental Science & Technology 43 (2009) 2060-2065.
[17] L.A. Quinchia, M.A. Delgado, C. Valencia, J.M. Franco, C. Gallegos, Natural and synthetic antioxidant additives for improving the performance of new biolubricant formulations, Journal of Agricultural and Food Chemistry 59 (2011) 12917-12924.
[18] H. Sovová, M. Zarevúcka, M. Vacek, K. Stránský, Solubility of two vegetable oils in supercritical CO_2, The Journal of Supercritical Fluids 20 (2001) 15-28.
[19] P. Hegel, G. Mabe, M. Zabaloy, S. Pereda, E. A. Brignole, Liquid−liquid−supercritical fluid equilibria for systems containing carbon dioxide, propane, and triglycerides, Journal of Chemical & Engineering Data 54 (2009) 2085-2089.
[20] S.R. Rosso, E. Franceschi, G.R. Borges, M.L. Corazza, J.V. Oliveira, S.R.S. Ferreira, Phase equilibrium measurements of ternary systems formed by linoleic and linolenic acids in carbon dioxide/ethanol mixtures, The Journal of Chemical Thermodynamics 41 (2009) 1254-1258.
[21] A.P.A. Corrêa, C.A. Peixoto, L.A.G. Gonçalves, F.A. Cabral, Fractionation of fish oil with supercritical carbon dioxide, Journal of Food Engineering 88 (2008) 381-387.
[22] I. Prado, W. Giufrida, V. Alvarez, V. Cabral, S. Quispe-Condori, M.A. Saldaña, L. Cardozo-Filho, Phase equilibrium measurements of sacha inchi oil (Plukenetia volubilis) and CO_2 at high pressures, Journal of the American Oil Chemists' Society 88 (2011) 1263-1269.
[23] F. Gironi, M. Maschietti, Phase equilibrium of the system supercritical carbon dioxide–lemon essential oil: New experimental data and thermodynamic modelling, The Journal of Supercritical Fluids 70 (2012) 8-16.
[24] P.L. Penedo, G.L.V. Coelho, M.F. Mendes, Phase equilibria of oleic, palmitic, stearic, linoleic and linolenic acids in supercritical CO_2, Brazilian Journal of Chemical Engineering 26 (2009) 137-142.
[25] R. Davarnejad, K.M. Kassim, Z. Ahmad, S.A. Sata, Solubility of β-carotene from crude palm oil in high-temperature and high-pressure carbon dioxide, Journal of Chemical & Engineering Data 54 (2009) 2200-2207.
[26] R. Davarnejad, Z. Ahmad, S.A. Sata, M.K. Moraveji, F. Ahmadloo, Mutual solubility study in supercritical fluid extraction of tocopherols from crude palm oil using CO_2 solvent, International Journal of Molecular Sciences 11 (2010) 3649-3659.
[27] P.E. Hegel, G.D.B. Mabe, S. Pereda, M.S. Zabaloy, E.A. Brignole, Phase equilibria of near critical CO_2+propane mixtures with fixed oils in the LV, LL and LLV region, The Journal of Supercritical Fluids 37 (2006) 316-322.
[28] P.E. Hegel, M.S. Zabaloy, G.D.B. Mabe, S. Pereda, E.A. Brignole, Phase equilibrium engineering of the extraction of oils from seeds using carbon dioxide+propane solvent mixtures, The Journal of Supercritical Fluids 42 (2007) 318-324.
[29] M.P. Fernández-Ronco, M. Cismondi, I. Gracia, A. De Lucas, J.F. Rodríguez, High-pressure phase equilibria of binary and ternary mixtures of carbon dioxide, triglycerides and free fatty acids: Measurement and modeling with the GC-EOS, Fluid Phase Equilibria 295 (2010) 1-8.
[30] B.M.C. Soares, F.M.C. Gamarra, L.C. Paviani, L.A.G. Gonçalves, F.A. Cabral, Solubility of triacylglycerols in supercritical carbon dioxide, The Journal of Supercritical Fluids 43 (2007) 25-31.

[31] T. Regueira, P.J. Carvalho, M.B. Oliveira, L. Lugo, J.A.P. Coutinho, J. Fernández, Experimental measurements and modelling of CO_2 solubility in sunflower, castor and rapeseed oils, The Journal of Supercritical Fluids submitted (2013)
[32] M.D. Gordillo, M.A. Blanco, A. Molero, E. Martínez de la Ossa, Solubility of the antibiotic penicillin G in supercritical carbon dioxide, The Journal of Supercritical Fluids 15 (1999) 183-190.
[33] F. Novotny-Farkas, W. Böhme, H. Stabinger, W. Belitsch, The Stabinger Viscometer a new and unique instrument for oil service laboratories, Anton Paar, Graz, Austria, 2001.
[34] F.M. Gaciño, T. Regueira, L. Lugo, M.J.P. Comuñas, J. Fernández, Influence of molecular structure on densities and viscosities of several ionic liquids, Journal of Chemical & Engineering Data 56 (2011) 4984-4999.
[35] R. Span, W. Wagner, A new equation of state for carbon dioxide covering the fluid region from the triple-point temperature to 1100 K at pressures up to 800 MPa, Journal of Physical and Chemical Reference Data 25 (1996) 1509-1596.
[36] T. Klein, S. Schulz, Measurement and model prediction of vapor-liquid equilibria of mixtures of rapeseed oil and supercritical carbon dioxide, Industrial & Engineering Chemistry Research 28 (1989) 1073-1081.
[37] C. Borch-Jensen, J. Mollerup, Phase equilibria of fish oil in sub- and supercritical carbon dioxide, Fluid Phase Equilibria 138 (1997) 179-211.
[38] P.J. Carvalho, J.A.P. Coutinho, On the nonideality of CO_2 solutions in ionic liquids and other low volatile solvents, The Journal of Physical Chemistry Letters 1 (2010) 774-780.

Chapter 7

High pressure rheology
Results and discussion

In this chapter results concerning the implementation of the high pressure rheometric technique, based on a Reologica StressTech HTHP concentric cylinder, in the Thermophysical Properties Laboratory during this PhD Thesis, together with a performance test by means of the rheometric characterization of a polybutene in the temperature range from 298.15 K to 333.15 K and pressures up to 75 MPa and comparison with literature values for this lubricant are presented. The flow tests were performed up to shear rate of 1000 s^{-1} or stress of 350 Pa and a Newtonian behaviour was observed for the polybutene in the whole experimental range. A maximum AAD% of 10.6% was obtained in the comparison of shear viscosity values with those from literature.

Furthermore, non-linear viscoelastic tests measuring shear viscosity as a function of shear rate of two ILs susceptible of being used as gear lubricants, $[C_2C_1Im][C_6SO_4]$ and $[P_{6,6,6,14}][(C_2F_5)_3PF_3]$, are presented in the temperature range from 298.15 K to 333.15 K and pressures up to 75 MPa. Calculations of pressure-viscosity (α) and temperature-viscosity (β) coefficients for these two ILs, as well as comparison of the obtained results with those of reference gear lubricants from literature are carried out. It was observed that $\alpha(p)$ values of $[P_{6,6,6,14}][(C_2F_5)_3PF_3]$ are of the same order as those of squalane and higher than those of $[C_2C_1Im][C_6SO_4]$. Additionally, regarding the universal pressure-viscosity coefficient (α_{film}), it was obtained that α_{film} for $[P_{6,6,6,14}][(C_2F_5)_3PF_3]$ doubles the value of that for $[C_2C_1Im][C_6SO_4]$.

All these results are further explained and discussed in the following two sections:

1. High pressure rheometric characterization of a polybutene. *T. Regueira, L. Lugo, M.J.P. Comuñas, J. Fernández, proceeding at Ibereo 2011 Rheology Trends: from Nano to Macro Systems, 7-9 September 2011, Caparica, Portugal, 313-316, ISBN: 978-972-8669-50-8.*
2. Rheometric characterization of 1-ethyl-3-methylimidazolium n-hexylsulfate and trihexyl(tetradecyl) phosphonium tris(pentafluoroethyl)trifluorophosphate up to 75 MPa. *T Regueira, L. Lugo, M.J.P. Comuñas, J. Fernández, to be submitted.*

7.1. High pressure rheometric characterization of a polybutene*

*T. Regueira, L. Lugo, M.J.P. Comuñas, J. Fernández, proceeding at Ibereo 2011 Rheology Trends: from Nano to Macro Systems, 7-9 September 2011, Caparica, Portugal, 313-316, ISBN: 978-972-8669-50-8.

Introduction

Among many applications, high pressure rheometry is an important issue in the field of lubrication in order to characterize lubricants behaviour when subjected to high pressures [1].

The viscometers employed in high pressure determinations can be classified into three groups, capillary, rotational and falling body devices. The advantages of rotational rheometers are: the viscosity measurements are made under steady-state conditions, there is negligible variation of shear rate and shear stress throughout the sample and they allow the study and characterization of Non-Newtonian behaviour [2, 3]. However, rotational rheometers present some disadvantages, such as shear-induced dissipative conversion of mechanical energy into thermal energy, secondary flow caused by inertial forces (so-called Taylor vortices), slip on the shear surfaces, separation effects in suspensions and end effects [1].

Literature on high pressure rheometry is scarce even though several authors have worked on this topic [1, 4]. Regarding rotational rheometers, Khandare et al. [3, 5] have designed and developed a high-temperature, high-pressure rheometer to measure viscosity of pitch material at elevated temperatures. Parris et al. [6] performed high pressure steady-shear rheological measurements in a Couette rheometer designed for pressures up to 2380 bar. Hwang et al. [7] determined rheological properties by means of a rotational viscometer adapted to measure the viscosity of polymer under high temperature and pressure conditions. Martínez-Boza and collaborators [8-10] have performed rheological studies on used motor oil/vacuum residue blends, bitumens and heavy oils with a controlled stress rheometer, RheoStress RS600 from Haake Gbr., using conventional coaxial cylinder geometry and coaxial cylinder-pressure cell. Larsson et al. [11] and Petterson [12, 13] have determined the pressure–viscosity relationship of lubricants by means of a Couette rheometer whose pressure can be raised to 5000 bar. Bair and Winer [14] developed a rotational Couette high-pressure, high-shear stress viscometer with a pressure capability of 3000 bar. Subsequently, Bair [15] built a similar rheometer that can be used up to 1 GPa. Briscoe et al. [16] have measured rheological properties by a modified Haake Searle-type viscometer, which was incorporated into a high temperature and pressure chamber, with a maximum operating pressure of 1000 bar.

In this work we have undertaken the development of a new device for rheological characterization at high pressure. The heart of the setup is a Reologica StressTech Couette HTHP rheometer equipped with a high pressure cell that allows measurements up to 1000 bar. A study on rheological parameters at pressures up to 750 bar for a synthetic base oil that can be used for lubricant applications, polybutene H8, was also performed.

Experimental

Polybutene H8 was provided by Ineos Oligomers with a molecular weight of 490 $g \cdot mol^{-1}$ and a polydispersity index of 1.85.

We have recently installed a rheometric technique based on a Reologica StressTech HTHP concentric cylinder. This instrument consists of a DIN53019 concentric cylinder measurement and relies on Couette flow, involving confinement of the sample between a stationary cup and a rotating bob, with a 1 mm gap. The inner cylinder, with a diameter of 25 mm, is suspended by a magnetic coupling and rotates on low friction air bearing. The rheometer is equipped with a high pressure cell that can be used for liquids at pressures up to 1000 bar. Temperature is controlled by means of electrical resistance heating and a thermostatic bath. We have found that this equipment is appropriate for liquids with viscosities higher than 50 mPa·s. The rheometer can operate in a torque range between $1 \cdot 10^{-4}$ N·m and $4 \cdot 10^{-2}$ N·m, and up to shear rates of 1000 s^{-1}. The maximum shear stress was about 350 Pa. The equipment is calibrated for each liquid and each temperature taking into account viscosities measured with a precise rotational Stabinger viscometer at atmospheric pressure. At present, our rheometric technique can operate from 298.15 to 353.15 K and up to 750 bar. The accuracy of the dynamic viscosity measurements at high pressures was checked [17] by comparison with experimental data correlation of PAO40 previously published by Bair [18], obtaining an average absolute deviation around 7% in the whole pressure and temperature ranges. These values were obtained from the flow curves performed under controlled stress tests up to stresses of 350 Pa.

In the present work, we have performed controlled stress tests of a low molecular weight liquid, polybutene H8. The experimental tests were carried out from 298.15 K to 333.15 K and up to 750 bar, determining the flow curves at torques between $1 \cdot 10^{-4}$ N·m and $4 \cdot 10^{-2}$ N·m. We have studied whether the non-Newtonian behaviour found at high shear stress and pressure [19] happens also at low shear rates. Besides, we have compared the limiting low shear viscosity with that published by Bair [19].

Results and discussion

As example, in Figure 1 the results of the steady state tests for different shear stress from 40 Pa to 150 Pa at 303.15 K and 750 bar are presented. In figure 1 it can be observed how the dispersion of the data is higher at 40 Pa and the viscosity decreases less than 3.5 % with increasing stress due to the inertia of the equipment. We found that with increasing pressure, the minimum stress at which the results show a reliable response is higher.

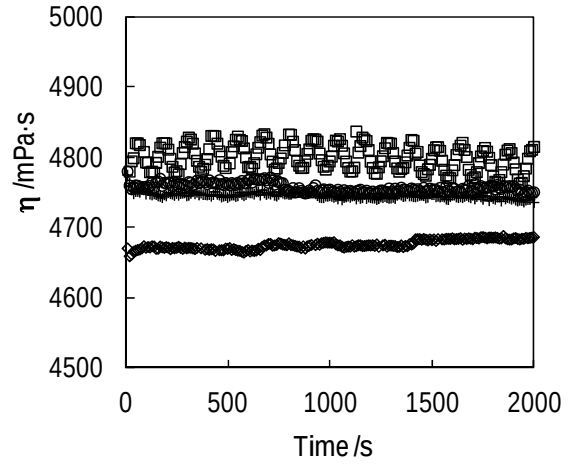

Figure 1. Steady state test for polybutene H8 at 303.15 K and 750 bar, at different shear stresses: (□) 40 Pa, (○) 60 Pa, (+) 80 Pa, (◇) 150 Pa.

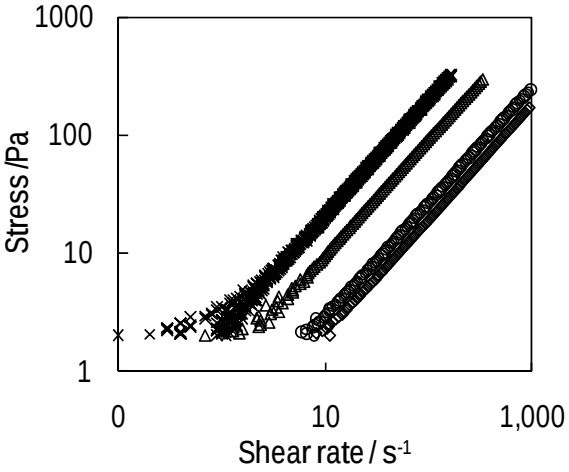

Figure 2. Flow curve for Polybutene H8 at 313.15 K. (×) 750 bar, (△) 500 bar, (○) 100 bar, (◇) 1 bar.

In the studied temperature, pressure and shear rate ranges we can deduce a Newtonian behaviour for polybutene H8. As an example, Figure 2 shows the flow curves for polybutene H8 at 313.15 K. It can be observed that at the lowest stress (2 Pa), that corresponds to the minimum torque, the inertia of the equipment increases with pressure.

In table 1 experimental dynamic viscosities from flow curves are presented. We have correlated our experimental viscosity values by means of the Comuñas et al. equation [20]:

$$\eta(p,T)=A\left(\frac{p+E}{p_{ref}+E}\right)^{F}\exp\left(\frac{B}{T-C}\right) \tag{1}$$

where

$$E=E_0+E_1T+E_2T^2 \tag{2}$$

obtaining an absolute average deviation of 4.4 %. Parameters of the correlation are presented in table 2, whereas in Figure 3 experimental viscosities are presented along with this correlation.

Table 1. Polybutene H8 experimental viscosity data (mPa·s)

***T* / K**	***p* / bar**		
	100	**500**	**750**
298.15	696.1	3071	6868
303.15	444.7	1982	4715
313.15	227.4	886.2	1929
323.15	122.3	433.3	880.4
333.15	74.79	238.4	460.4

We have compared the obtained viscosity data from 303.15 K to 333.15 K in the whole pressure range with data obtained from the correlations published by Bair [18, 19], obtaining an absolute average deviation of 10.6 % and 9.7 %, respectively. It is important to note that even at atmospheric pressure, we have obtained an absolute average deviation of 6.6 % and 8.3 % between Bair correlations [18, 19] and values measured with our rotational Stabinger viscometer, being the uncertainty of this last technique 1%. In Figure 4 relative deviations between viscosity data measured in this work and data from Bair [18, 19] are plotted.

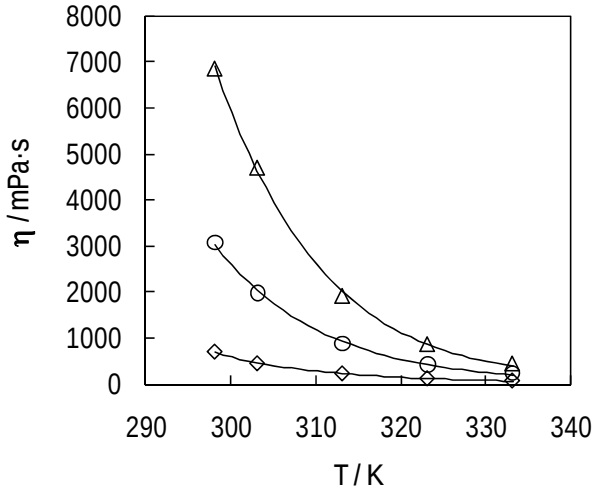

Figure 3. Experimental viscosity values as a function of temperature.
(△) 750 bar, (○) 500 bar, (◇) 100 bar, (–) Comuñas et al. correlation.

Table 2. Parameters of Eqs. (1, 2).

***A*/ mPa·s**	0.0165
***B*/ K**	1330.4
***C*/ K**	168.04
F	9.92
E_0**/ MPa**	7334.0
E_1**/ MPa·K^{-1}**	-47.664
E_2**/ MPa·K^{-2}**	0.08003

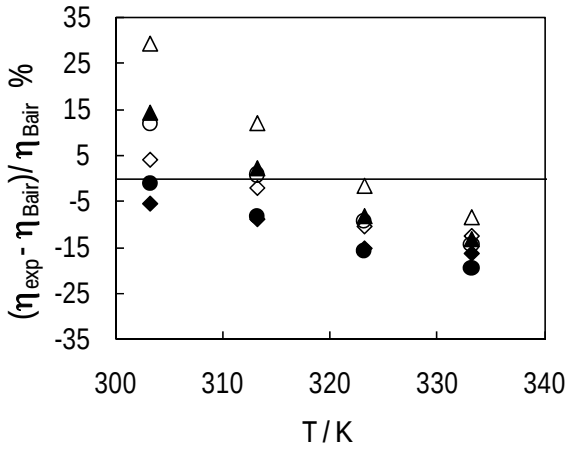

Figure 4. Relative deviations between viscosity data obtained in this work and those from literature. Bair [18] (empty symbols) and Bair [19] (filled symbols). (△) 750 bar, (○) 500 bar, (◇) 100 bar.

Conclusions

In this work we have implemented a new device for rheometric characterization at high pressure based on a commercial rheometer and characterized the rheological behaviour of polybutene H8 in the temperature range from 298.15 K to 333.15 K and pressures up to 750 bar. Flow tests up to 1000 s^{-1} or 350 Pa were performed, obtaining a Newtonian behaviour in the whole experimental range. Furthermore, we have compared our viscosity values with those obtained from the correlations published by Bair [18, 19], obtaining and absolute average deviation of 10.6 % and 9.7 %, respectively.

Acknowlegments

We express our gratitude to Prof. Martínez-Boza (University of Huelva, Spain) for his useful advice and to Ineos Oligomers for providing the polybutene sample. This work is being supported by Spanish Ministry of Science and Innovation and the UE FEDER Program under CTQ2008-06498-C02-01/PPQ project. L.L. acknowledges the financial support of the University of Vigo and the Ramón y Cajal Program from the Spanish Ministry of Science and Innovation and T.R. the financial support provided by the FPU program.

References

1. Kulisiewicz, L., and Delgado, A. (2010). Appl. Rheol. 20, 13018-1-13018-15.
2. Garratt, G. W., Rand, B., and Whitehouse, S. (1988). Fuel 67, 238-241.
3. Khandare, P. M., Zondlo, J. W.; Stansberry, P. B., and Stiller, A. H. (2000). Carbon 38, 881-887.
4. Bair, S. (2007). High Pressure Rheology for Quantitative Elastohydrodynamics, Elsevier, Amsterdam.
5. Khandare, P. M., Zondlo, J. W.; Stansberry, P. B., and Stiller, A. H. (2000). Carbon 38, 889-897.
6. Parris, M. D., MacKay, B. A., Rathke J. W., Klingler R. J., and Gerald, R. E. (2008). Macromolecules 41, 8181-8186.

7. Hwang, Y., Kim, M., Ahn, Y., and Lee, J. W. (2010). Annual Technical Conference - Society of Plastics Engineers 68th, 933-936.
8. Martínez-Boza F., Fernández-Latorre, F., and Gallegos C. (2009). Fuel 88, 1595–1601.
9. Martín-Alfonso, M.J., Martínez-Boza, F.J., Navarro, F.J., Fernández, M., and Gallegos, C. (2006), Fuel 86, 227–233.
10. Martín-Alfonso, M.J., Martínez-Boza, F., Partal, P., and Gallegos, C. (2006), Rheol. Acta 45, 357-365.
11. Larsson, R P, Larsson, O., Eriksson, E., Sjöberg, M., and Höglund, E. (2000). Proc. Instn Mech. Engrs, Part J: J Engineering Tribology. 214, 17-27.
12. Pettersson, A. (2003). Tribol. Int. 36, 815–820.
13. Pettersson, A. (2007). Tribol. Int. 40, 638–645.
14. Bair, S., and Winer, W. O. (1993). Tribol. Trans. 36, 721 – 725.
15. Bair, S. (2002), Proc Instn Mech Engrs Part J: J Engineering Tribology 216, 139-149.
16. Briscoe, B., Luckham, P., and Zhu, S. (1996). Macromolecules 29, 6208-6211.
17. Regueira, T., Comuñas, M.J.P., Lugo, L., Paredes, X., and Fernández, J. (2011). 19th European Conference on Thermophysical Properties, Thessaloniki, Greece.
18. Bair, S. (2000).Tribol. Trans. 43, 91-99.
19. Bair, S. (2001). J. Non-Newtonian Fluid Mech. 97, 53-65.
20. Comuñas, M.J.P., Baylaucq, A., Boned, C., and Fernández, J. (2001). Int. J. Thermophys. 22, 749-768.

7.2. Rheometric characterization of 1-ethyl-3-methylimidazolium n-hexylsulfate and trihexyl(tetradecyl)phosphonium tris(pentafluoroethyl)trifluorophosphate up to 75 MPa[*]

[*]T Regueira, L. Lugo, M.J.P. Comuñas, J. Fernández, to be submitted.

Abstract

Ionic liquids have been broadly studied in the last decade for being used as lubricants or lubricant additives. The rheometric characterization of these fluids is very important in this context because it determines to a great extent their performance for different lubricants applications, such as hydraulic or gear lubricants. Thus, in this work we have performed the rheometric characterization of two ionic liquids, 1-ethyl-3-methylimidazolium n-hexylsulfate and trihexyl(tetradecyl)phosphonium tris(pentafluoroethyl)trifluorophosphate, in the temperature range from 298.15 K to 353.15 K up to 75 Pa and shear rates of $1000s^{-1}$. Moreover the pressure-viscosity and temperature-viscosity coeffitients of these ILs have been calculated.

Introduction

Nowadays high pressure rheometry is gaining growing interest in several areas such as high-pressure treatment and processing of foods, basic research in chemistry, physics and geophysics, fuels for diesel engines, high-pressure extraction processes using supercritical fluids, high-pressure impregnation and coating, innovative solvent technology based on ionic liquids and semiconductor and nanoparticle industries [1].

Additionally, the lubrication field high pressure rheometry comprises an important area because this technique allows accurate determination of the pressure-temperature-viscosity relationship [2]. Thus, in elastohydrodynamic lubrication (EHD), one of the main parameters governing the global contact behaviour is the fluid film thickness, which separates the solids under contact, and is controlled to a great extent by the lubricant high pressure rheology. It is important to mention that the lubricant film thickness was the first parameter studied in EHD contacts [3]. The classic formulas for the calculation of the film thickness require the knowledge of the pressure-viscosity coefficient, which can be determined from measurements of the low-shear viscosity as a function of pressure up to moderate pressures. Additionally, other interesting parameter to be considered in an EHD analysis is the temperature-viscosity coefficient [4].

On the other hand, studies of ionic liquids (ILs) as potential lubricants have greatly increased during the last decade, due to their main properties such as low volatility, high thermal stability and conductivity, low melting point, broad liquid range and low temperature fluidity [5-7]. Thus, in this work we have selected two ILs, 1-ethyl-3-methylimidazolium n-hexylsulfate and trihexyl(tetradecyl)phosphonium tris(pentafluoroethyl) trifluorophosphate, which have a ISO viscosity grade slightly higher than VG100 [8], as potential gear lubricants. We have performed the rheometric characterization of these two ILs up to 75 MPa over the temperature range from 298.15 K to 353.15 K. Moreover, we have calculated the local and universal pressure-viscosity

coefficient, as well as the temperature-viscosity coefficient, comparing the obtained results with those of some reference lubricants.

Materials and methods

Two ILs are studied in the present work, i.e. 1-ethyl-3-methylimidazolium n-hexylsulfate, $[C_2C_1Im][C_6SO_4]$, and trihexyl(tetradecyl)phosphonium tris(pentafluoroethyl) trifluoro-phosphate, $[P_{6,6,6,14}][(C_2F_5)_3PF_3]$. Prior to their use, samples were degassed under vacuum and agitation at least during 48 h, and the water content was after measured through a Karl Fischer method using a Mettler Toledo DL32 coulometric titrator. Purity of the IL samples as well as the water content are presented in table 1.

Table 1. Purity and water content (ppm) of IL samples.

Ionic Liquid	Mole-fraction purity	Water content
$[C_2C_1Im][C_6SO_4]$	>0.999[a]	16.39
$[P_{6,6,6,14}][(C_2F_5)_3PF_3]$	0.98[b]	10.74

[a]HPLC
[b]NMR

The core of the experimental device is a Reologica StressTech HTHP concentric cylinder, which is connected to a computer and works along with the RheoExplorer software. The rheometer relies on Couette flow and the geometry of the concentric cylinder is defined by a standard DIN53019. The inner cylinder rotates on a low friction air bearing and is suspended by a magnetic coupling. It has a diameter of 25 mm and the sample is confined in a gap of 1 mm between a stationary cup and a rotating bob. The maximum shear stress is around 350 Pa. Temperature is controlled through an electrical resistance heating aided by a cooling thermostatic bath and is measured with a thermocouple, which was calibrated from 288.15 K to 363.15 K with an uncertainty of ±0.5 K. A pressure line, comprised of a piston screw pump and a pressure transducer, was coupled to the rheometer in order to generate and measure pressure on the system up to 100 MPa with an uncertainty of ±0.02 MPa.

The equipment is calibrated for each liquid and temperature taking into account the viscosity values at atmospheric pressure measured with a precise rotational viscometer Anton Paar Stabinger SVM 3000. This viscometer has a cylindrical geometry and is based on a modified Couette principle with a rapidly rotating outer tube and an inner measuring bob. More details of this technique have been previously given [9].

The accuracy of determination of high pressure Newtonian viscosity has been previously checked by means of the measurement of this property of a PAO40 [10] and also of polybutene H8 [11] as it was reported in the previous section. For the PAO40 and AAD% of 7% in the temperature range from 298.15 K to 353.15 K up to 75 MPa with correlated data from Bair [12]

was obtained. Moreover, for the polybutene H8, Newtonian viscosity values were also compared with correlated data from Bair [12,13] obtaining an absolute average deviation of 10.6 % and 9.7 %, respectively.

Flow tests of the IL samples were performed at 0.1 MPa, 10 MPa, 50 MPa and 75 MPa in the temperature range from 298.15 K to 353.15 K.

Results

Rheological flow tests were performed up to shear rates of 1000 s^{-1} for both ILs at 298.15 K, 313.15 K, 323.15 K, 333.15 K, 343.15 K and 353.15 K up to 75 MPa. As example, a flow test is presented in Fig.1 for both ILs at 298.15 K for the different pressures. A Newtonian behaviour was found for the studied ILs in the temperature and pressure range analysed in this work.

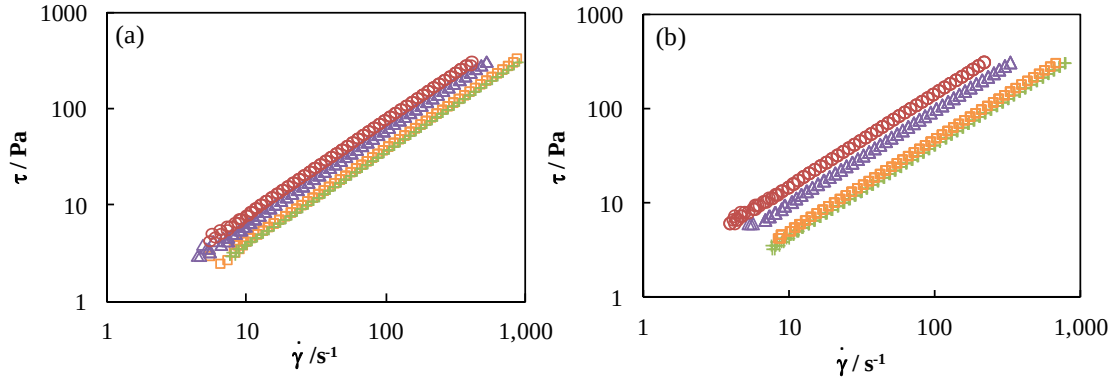

Fig.1. Flow tests at 298.15 K for (a) $[C_2C_1Im][C_6SO_4]$ and (b)$[P_{6,6,6,14}][(C_2F_5)_3PF_3]$ at 0.1 MPa (+), 10 MPa (□), 50 MPa (△) and 75 MPa (○).

The reference viscosity values at atmospheric pressure employed for calibration were taken from Gaciño et al. [9] and the obtained viscosity values at high pressure are presented in table 2. The viscosity values of $[P_{6,6,6,14}][(C_2F_5)_3PF_3]$ are higher than those of $[C_2C_1Im][C_6SO_4]$.

Table 2. Viscosity values, η (mPa·s) of the ILs measured in this work.

	T / K					
p / MPa	298.15	313.15	323.15	333.15	343.15	353.15
	$[C_2C_1Im][C_6SO_4]$					
10	354	154	94.0	63.8	44.5	31.4
50	571	238	142	94.8	65.9	46.0
75	737	304	186	120	82.1	56.9
	$[P_{6,6,6,14}][(C_2F_5)_3PF_3]$					
10	413	189	114	78.1	53.5	37.9
50	913	401	223	159	112	76.3
75	1417	615	364	232	162	109

Viscosity values were correlated as a function of temperature and pressure by means of the Comuñas et al. [14] correlation, employing for the adjustment of viscosity at atmospheric pressure the data published by Gaciño et al. [9]:

$$\eta(p,T)=A\left(\frac{p+E(T)}{p_{ref}+E(T)}\right)^{D}\exp\left(\frac{B}{T-C}\right) \tag{1}$$

where

$$E(T)=E_0+E_1T+E_2T^2 \tag{2}$$

Coefficients of this adjustment are presented in table 3. Moreover, correlated values are plotted along with the experimental ones as a function of temperature for the different pressures in Fig. 2. It can be observed that the influence of pressure on viscosity is stronger for $[P_{6,6,6,14}][(C_2F_5)_3PF_3]$.

Table 3. Parameters of the Comuñas et al. [14] correlation for the ILs studied in this work.

	$[C_2C_1Im][C_6SO_4]$	$[P_{6,6,6,14}][(C_2F_5)_3PF_3]$
$10^2 \cdot A$/ mPa·s	9.265	3.588
B/ K	1074.7	1423.6
C/ K	166.13	142.93
D	4.125	7.971
E_0/ MPa	-828.4	684.3
E_1/ MPa·K^{-1}	5.879	-2.745
$10^3 \cdot E_2$/ MPa·K^{-2}	-6.69	5.837
AAD%	1.0	2.2

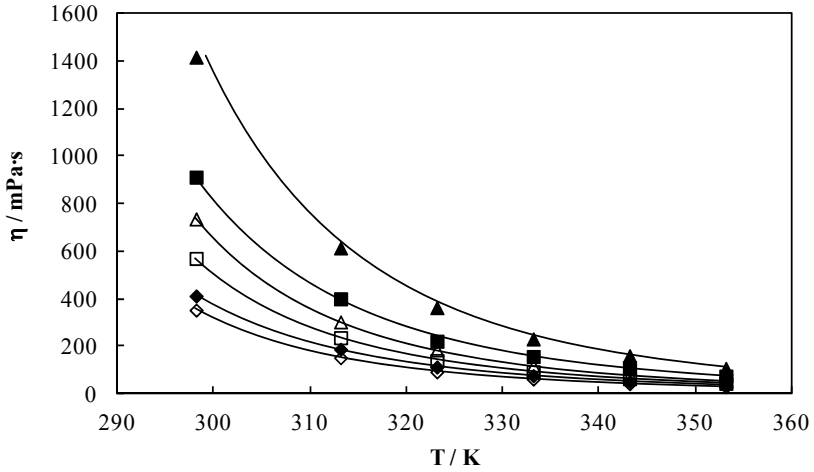

Fig.2. Viscosity values of $[C_2C_1Im][C_6SO_4]$ (empty symbols) and $[P_{6,6,6,14}][(C_2F_5)_3PF_3]$ (filled symbols) as a function of temperature for different pressures. 10 MPa (◇, ◆), 50 MPa (□, ■) and 75 MPa (△, ▲).

We have performed a comparison between the experimental viscosity values for $[C_2C_1Im][C_6SO_4]$ and $[P_{6,6,6,14}][(C_2F_5)_3PF_3]$ and some data previously published [15] for mineral and synthetic gear lubricants with an ISO viscosity grade of 100. This comparison is depicted as a function of temperature at 50 MPa in Fig. 3. It is important to notice that the viscosity of $[C_2C_1Im][C_6SO_4]$ is very close to those for the polyalkylene glycol 992.PG.100 [15]. The AAD% in the whole experimental temperature and pressure range is 11%.

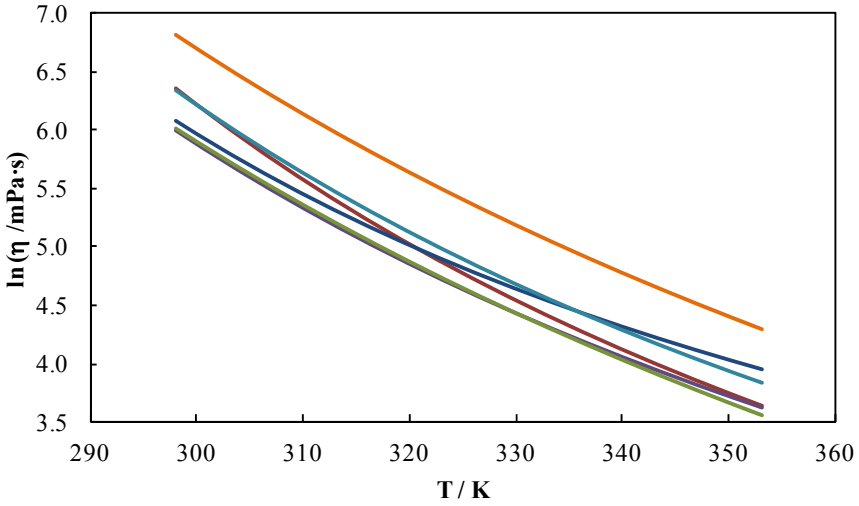

Fig.3. Viscosity values as a function of temperature at 50 MPa. $[P_{6,6,6,14}][(C_2F_5)_3PF_3]$ (—), $[C_2C_1Im][C_6SO_4]$ (—), mineral oil 923.M.100 [15] (—), biodegradable synthetic ester 1.ES.100 [15] (—), polyalphaolefin 971.PAO.100 [15] (—), polyalkylene glycol 992.PG.100 [15] (—).

The local pressure-viscosity coefficient, α, is employed for the characterization the viscosity pressure dependence of lubricants and it is defined by means of the following equation:

$$\alpha(p) = \frac{1}{\eta}\left(\frac{\partial \eta}{\partial p}\right)_T \tag{3}$$

This coefficient quantifies the EHL film-generating capability of a lubricant [16]. We have calculated this property by differentiation from the $\eta(T,p)$ correlation and it is plotted in Fig. 4 for the two ILs studied in this work. It can be observed that α diminishes both with temperature and pressure and that $[P_{6,6,6,14}][(C_2F_5)_3PF_3]$ has higher values of this property than $[C_2C_1Im][C_6SO_4]$. It must be mentioned that Gaciño et al. [17] have previously found that ILs with the anion $[(C_2F_5)_3PF_3]^-$ present also higher pressure viscosity coefficients than those with the anion $[NTf_2]^-$.

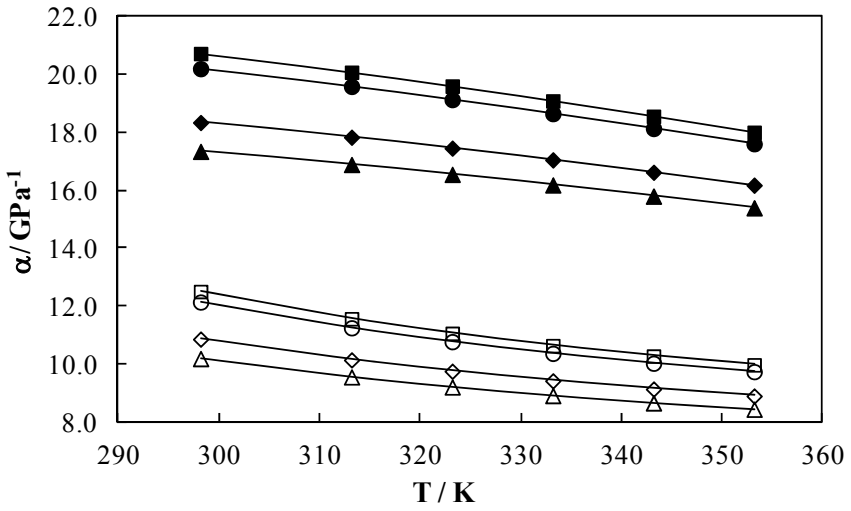

Fig. 4. Local pressure-viscosity coefficient, α, of $[C_2C_1Im][C_6SO_4]$ (empty symbols) and $[P_{6,6,6,14}][(C_2F_5)_3PF_3]$ (filled symbols) as a function of temperature at 0.1 MPa (■, □), 10 MPa (●, ○), 50 MPa (◆, ◇), 75 MPa (▲, △).

Additionally, we have performed in Fig. 5 a comparison between the local pressure-viscosity coefficient of the ILs studied in this work with other fluids from literature at 313.15 K, an IL based on $[(C_2F_5)_3PF_3]^-$ anion, a polyalkylene glycol (PAG3) [18] and also squalane [19]. It can be observed that the pressure-viscosity coefficient of $[C_2C_1Im][C_6SO_4]$ is the lowest and also that $[P_{6,6,6,14}][(C_2F_5)_3PF_3]$ and squalane present quite similar values of this property.

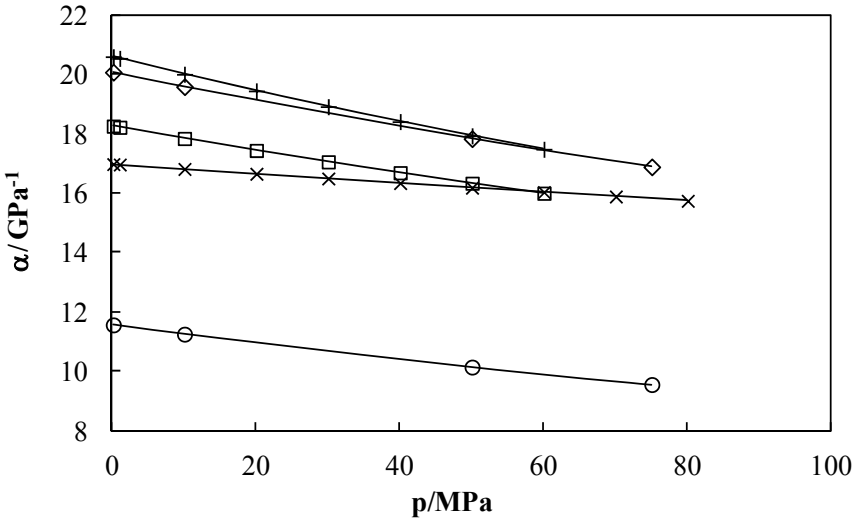

Fig. 5. Local pressure-viscosity coefficient, α, of squalane [19] (+), $[P_{6,6,6,14}][(C_2F_5)_3PF_3]$ (◇), PAG3 [18] (□), $[C_1OC_2C_1Pyrr][(C_2F_5)_3PF_3]$ [17] (×) and $[C_2C_1Im][C_6SO_4]$ (○).

Another interesting parameter for characterizing fluids for lubricant applications is the universal pressure-viscosity coefficient, $\alpha_{film,}$ which is independent of pressure and it is given by the following equation [20]:

$$\alpha_{film} = \frac{1-\exp(-3)}{p_{iv}(3/\alpha^*)} \tag{4}$$

where p_{iv} (isoviscous pressure) and α^* (piezo-viscous coefficient) are defined as follows:

$$p_{iv}(p) = \int_0^p \frac{\eta(p'=0)dp'}{\eta(p')} \tag{5}$$

$$\alpha^* = \frac{1}{p_{iv}(\infty)} = \left[\int_0^\infty \frac{\eta(p=0)dp}{\eta(p)}\right]^{-1} \tag{6}$$

The universal pressure-viscosity coefficient was calculated for the ILs studied in this work and is depicted in Fig.6 for the different temperatures. It is observed that the α_{film} values of $[P_{6,6,6,14}][(C_2F_5)_3PF_3]$ are near the double of those of $[C_2C_1Im][C_6SO_4]$.

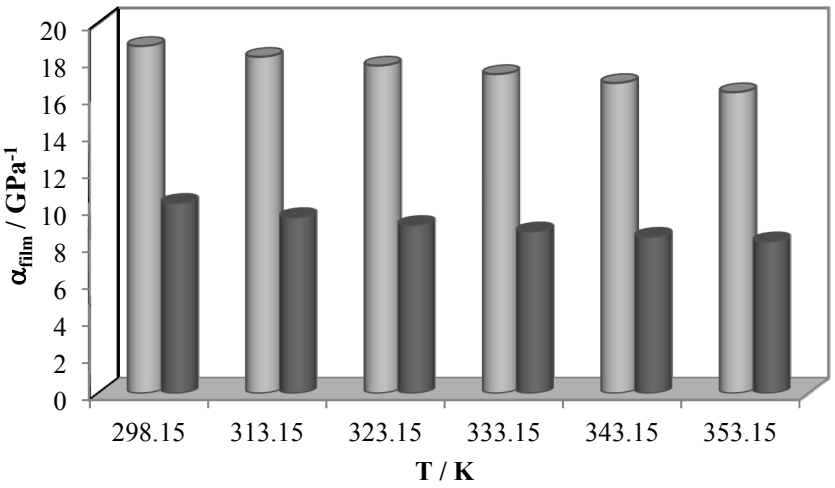

Fig. 6. Universal pressure-viscosity coefficient, α_{film}, of $[C_2C_1Im][C_6SO_4]$ (dark grey) and of $[C_1OC_2C_1Pyrr][(C_2F_5)_3PF_3]$ (light grey).

The pressure-viscosity coefficient was employed by Hamrock and Dowson [21] for calculating the central film thickness (h_c) at isothermal conditions in a rolling element with speed U under EHL conditions, according to the following expression:

$$h_c = k\eta_0^{0.67}\alpha_{film}^{0.53}U^{0.67} \tag{7}$$

where η_0 is the viscosity at atmospheric pressure and k is a parameter that depends on surface geometry, the applied load and the elastic parameters of the rolling elements. Moreover, the American Gear Manufactures Association (AGMA) has proposed an equation similar to those of Hamrock and Dowson [21] for calculation of h_c, which is given by the following equation [16]:

$$h_c = k\eta_0^{0.69}\alpha_{film}^{0.56}U^{0.69} \tag{8}$$

If geometry, elastic properties, speed and loads are fixed, EHL film thickness varies with the pressure-viscosity coefficient and the absolute viscosity, as follows [16]:

$$h_c \propto \alpha_{film}^{0.56}\eta_0^{0.69} \tag{9}$$

Thus, we have plotted in Fig.7 $\alpha_{film}^{0.56}\eta_0^{0.69}$ against temperature for the studied ILs, finding that under the same EHL conditions, $[P_{6,6,6,14}][(C_2F_5)_3PF_3]$ would have a thicker central thickness than $[C_2C_1Im][C_6SO_4]$.

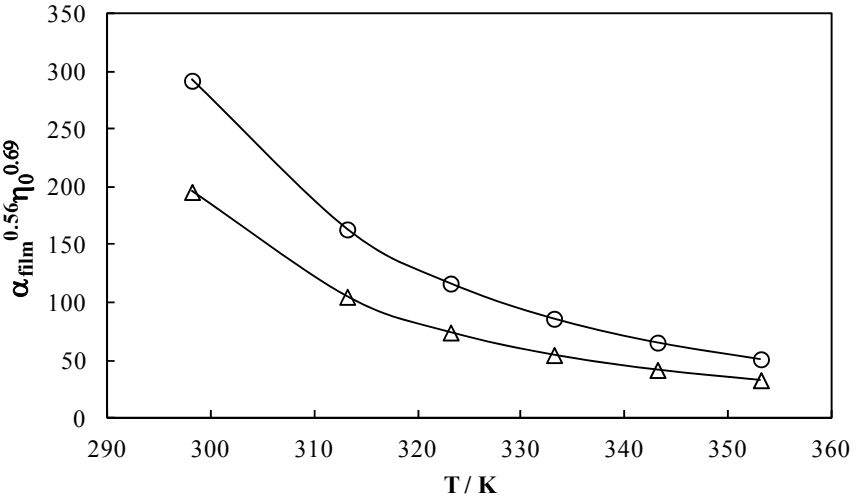

Fig. 7. $\alpha_{film}^{0.56}\eta_0^{0.69}$ against temperature for $[C_2C_1Im][C_6SO_4]$ (△) and $[P_{6,6,6,14}][(C_2F_5)_3PF_3]$ (○).

Finally, we have calculated the temperature-viscosity coefficient, β, which is given by the following equation:

$$\beta = -\frac{1}{\eta}\left(\frac{\partial \eta}{\partial T}\right)_p \tag{10}$$

The obtained values of the temperature-viscosity coefficient are presented in Fig. 8. This property depends highly on temperature, decreasing with the temperature increase, whereas the dependence on pressure is rather smooth. It can be observed that the values of this property, as well as the viscosity index (136 for $[C_2C_1Im][C_6SO_4]$ and 128 for $[P_{6,6,6,14}][(C_2F_5)_3PF_3]$ [9]), are very similar for both ILs, the AAD% between their values is 3.9%.

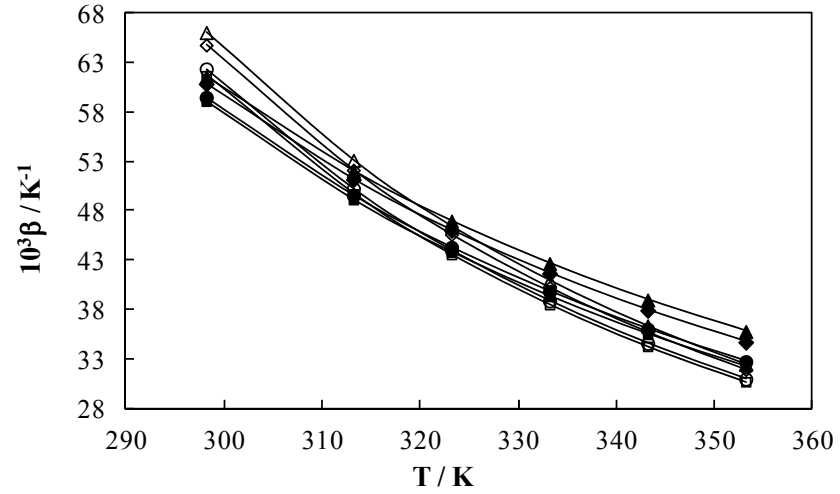

Fig. 8. Local temperature-viscosity coefficient, β, of $[C_2C_1Im][C_6SO_4]$ (empty symbols) and $[P_{6,6,6,14}][(C_2F_5)_3PF_3]$ (filled symbols) as a function of temperature at 0.1 MPa (■, □), 10 MPa (●, ○), 50 MPa (◆, ◇), 75 MPa (▲, △).

Conclusions

A rheometric characterization of $[C_2C_1Im][C_6SO_4]$ and $[P_{6,6,6,14}][(C_2F_5)_3PF_3]$ was performed in the temperature range from 298.15 K to 353.15 K up to 75 MPa and shear rates up to $1000s^{-1}$. It was found a Newtonian behaviour for both ILs under the studied conditions, finding viscosity values higher for $[P_{6,6,6,14}][(C_2F_5)_3PF_3]$ than for $[C_2C_1Im][C_6SO_4]$. Moreover, these viscosity values were compared with those of different reference oils for gear applications, finding that viscosity values of $[C_2C_1Im][C_6SO_4]$ are close to those of a polyalkylene glycol with VG of 100.

Additionally we have calculated the viscosity derived properties $\alpha(p)$ and β. For the first of them, it was observed that values for $[P_{6,6,6,14}][(C_2F_5)_3PF_3]$ are of the same order than literature values for squalane [19] and also higher than those for $[C_2C_1Im][C_6SO_4]$. As regard the temperature-viscosity coefficient, very similar values were found for the studied ILs (AAD% = 3.9%). Finally, α_{film} values of $[P_{6,6,6,14}][(C_2F_5)_3PF_3]$ were found to be near double than those of $[C_2C_1Im][C_6SO_4]$.

Acknowledgements

Authors acknowledge the advices and samples provided by Merck KGaA. This work was supported by Spanish Ministry of Science and Innovation and FEDER Program through CTQ2008-06498-C02-01 and CTQ2011-23925 projects. L.L and T.R. acknowledge financial support under the Ramon y Cajal Program and the FPU program, respectively.

References

[1] L. Kulisiewicz, A. Delgado, High-pressure rheological measurement methods: A review, Applied Rheology 20 (2010) 13018-13011-13018-13015.
[2] F.J.M. Boza, C. Gallegos, High pressure rheology, Encyclopedia of chemical sciences, engineering and technology resources (Encyclopedia of life support systems), 2009.
[3] D. Berthe, P. Vergne, High pressure rheology for high pressure lubrication: A review, Journal of Rheology 34 (1990) 1387-1414.
[4] S.S. Bair, High-pressure rheology for quantitative elastohydrodynamics 1st ed., Elsevier, Amsterdam, 2007.
[5] N.V. Plechkova, K.R. Seddon, Applications of ionic liquids in the chemical industry, Chemical Society Reviews 37 (2008) 123-150.
[6] M. Freemantle, New frontiers for ionic liquids, Chemical & Engineering News 85 (2007) 23-26.
[7] H. Zhao, Innovative applications of ionic liquids as 'green' engineering liquids, Chemical Engineering Communications 193 (2006) 1660 - 1677.
[8] T. Regueira, L. Lugo, J. Fernández, Ionic liquids as hydraulic fluids: comparison with conventional oils, Lubrication Science in press (2013)
[9] F.M. Gaciño, T. Regueira, L. Lugo, M.J.P. Comuñas, J. Fernández, Influence of molecular structure on densities and viscosities of several ionic liquids, Journal of Chemical & Engineering Data 56 (2011) 4984-4999.
[10] T. Regueira, Comuñas, M.J.P., Lugo, L., Paredes, X., and Fernández, J., Implementation of a concentric cylinder rheometer for high pressures 19th European Conference on Thermophysical Properties, Thessaloniki, Greece., 2011.

[11] T. Regueira, L. Lugo, M.J.P. Comuñas, J. Fernández, High pressure rheometric characterization of a polybutene, Caparica, Portugal, 7-9 September 2011, pp. 313-316.
[12] S. Bair, Pressure-viscosity behavior of lubricants to 1.4 GPa and its relation to EHD traction, Tribology Transactions 43 (2000) 91-99.
[13] S. Bair, The high-pressure, high-shear stress rheology of a polybutene, Journal of Non-Newtonian Fluid Mechanics 97 (2001) 53-65.
[14] M.J.P. Comuñas, A. Baylaucq, C. Boned, J. Fernández, High-pressure measurements of the viscosity and density of two polyethers and two dialkyl carbonates, International Journal of Thermophysics 22 (2001) 749-768.
[15] P.W. Gold, A. Schmidt, H. Dicke, J. Loos, C. Assmann, Viscosity–pressure–temperature behaviour of mineral and synthetic oils, Journal of Synthetic Lubrication 18 (2001) 51-79.
[16] R. Errichello, Selecting Oils with High Pressure-Viscosity Coefficient - Increase Bearing Life by More Than Four Times, Machinery Lubrication http://www.machinerylubrication.com/Read/586/viscosity-coefficient-bearing (2004)
[17] F.M. Gaciño, X. Paredes, M.J.P. Comuñas, J. Fernández, Pressure dependence on the viscosities of 1-butyl-2,3-dimethylimidazolium bis(trifluoromethylsulfonyl)imide and two tris(pentafluoroethyl)trifluorophosphate based ionic liquids: New measurements and modelling, The Journal of Chemical Thermodynamics 62 (2013) 162-169.
[18] X. Paredes, O. Fandino, A.S. Pensado, M.J.P. Comunas, J. Fernandez, Pressure-viscosity coefficients for polyalkylene glycol oils and other ester or ionic lubricants, Tribology Letters 45 (2012) 89-100.
[19] M.J.P. Comuñas, X. Paredes, F.M.Gaciño, J. Fernández, J.P. Bazile, G. Galliero, C. Boned, J. Pauly, J.L. Daridon, K.R. Harris, M.J. Assael, Journal of Chemical & Engineering Data to be submitted for publication
[20] S. Bair, L. Yuchuan, Q.J. Wang, The pressure-viscosity coefficient for Newtonian EHL film thickness with general piezoviscous response, Journal of tribology 128 (2006) 624-631.
[21] B.J. Hamrock, D. Dowson, Isothermal elastohydrodynamic lubrication of point contacts: Part III—fully flooded results, Journal of tribology 99 (1977) 264-275.

Chapter 8

Conclusions

This PhD Thesis was carried out under the framework of three research projects funded by the Spanish Science and Innovation Ministry. The BIOVESIN project, whose aim was the generation of new environmentally friendly lubricants based on vegetable oils, the LUBIONIC project, which analysed the influence of the ILs structure on thermophysical and tribological properties and the RENELUBIL project which tries to develop lubricants based on biodegradable base oils and ILs. The following conclusions were drawn:

- Several reference, base and developed oils were characterised in terms of viscosity index and also of density and viscosity at atmospheric pressure in the temperature range from 278.15 K to 373.15 K through an Anton Paar Stabinger SVM 3000 apparatus. Viscosity values were successfully correlated by means of the VFT equation. Vegetable based lubricants present higher viscosity index than reference oils, therefore, their viscosity changes with temperature are lower for the vegetable lubricants. In the case of gear lubricants, the formulated oils present the lowest viscosity values at low temperatures, becoming more suitable for machinery cold start.
- Two high pressure vibrating tube densimeters were calibrated and employed to determine density values of eight reference oils, two vegetable base oils and eleven biodegradable developed oils in the temperature range from 278.15 K to 398.15 K and pressures up to 120 MPa. It was found that, at the same temperature and pressure conditions, density of biodegradable lubricants and high oleic sunflower oils is higher than those of the mineral and synthetic reference oils for every application. Thus, according to the Sieder-Tate equation, the latter will have poorer heat-transfer coefficient than the vegetable base and developed biodegradable oils. Density data of each oil were correlated as a function of temperature and pressure through a modified Tammann-Tait equation with standard deviations lower or equal to 0.05%.
- Density of seven ILs, ($[C_1OC_2C_1Pyrr][NTf_2]$, $[C_4C_1Pyrr][NTf_2]$, $[C_2C_1Im][C_2SO_4]$, $[C_2C_1Im][C_6SO_4]$, $[C_1OC_2C_1Pyrr][(C_2F_5)_3PF_3]$, $[C_4C_1Pyrr][(C_2F_5)_3PF_3]$, and $[P_{6,6,6,14}][(C_2F_5)_3PF_3]$) in the temperature range from 278.15 K to 398.15 K up to 120 MPa was also reported. A correction of density data due to the viscosity of the ILs was applied to four of them. The measured data were correlated as a function of temperature and pressure through the Tammann-Tait equation with an AAD% lower than 0.02%. The lightest of the studied ILs was $[C_2C_1Im][C_6SO_4]$. Densities of the studied ILs are higher than those of the reference, base and developed oils for the different applications. Additionally, a literature study of IL density values was performed, finding that density decreases with the increase of the cation alkyl chain length, and among the ILs containing the $[NTf_2]^-$ anion, the one with the lowest density is $[P_{6,6,6,14}][NTf_2]$. Furthermore, concerning anion, density decreases

according to the following trend: $[(C_2F_5SO_2)_2N]^- > [NTf_2]^- > [PF_6]^- > [CF_3SO_3]^- > [ClO_4]^- > [CF_3CO_2]^- > [C_1SO_4]^- > [BF_4]^- > [C_1(OC_2)_2SO_4]^- > [NO_3]^- > [C_8SO_4]^- > [N(CN)_2]^- > [CH_3CO_2]^- > [C_4C_4PO_4]^- > [C(CN)_3]^-$.

- Density data at high pressure for the gear mineral and developed oils were predicted with AAD% lower or equal to 0.4% by means of Dowson and Higgison and Zhu and Wen EoS. Extrapolation of density values by means of these two equations up to pressure values of 4 GPa gives rise to lower values (8%) in comparison with the extrapolation performed through the Tammann-Tait equation. Moreover, when these equations are used to extrapolate compressibility values up to 4 GPa, Dowson and Higgison and Zhu and Wen EoS predict lower values than those obtained through the Tammann-Tait equation.
- Density of the six ILs studied was predicted, in the whole experimental temperature and pressure range, through the Gardas and Coutinho prediction method with an AAD% lower or equal to 1.5 %. Moreover density values of $[C_4C_1Pyrr][NTf_2]$ and $[C_2C_1Im][C_2SO_4]$ were also predicted with the method proposed by Jacquemin et al. with an AAD% of 0.46 % and 2.5%, respectively.
- Isothermal compressibility, κ_T, of the reference, vegetable base and biodegradable developed oils and ILs was calculated by differentiation from the Tammann-Tait equation. It was found that compressibility of vegetable base oils and biodegradable developed oils for hydraulic applications is lower than those of the hydraulic mineral reference oils. This fact means that the vegetable and the biodegradable hydraulic oils have better power transfer properties. Concerning gear oils, it was found that reference and developed lubricant have similar compressibility values (within 5%), which means that regarding this property, they are suitable for substituting mineral oils. Furthermore, ILs present low isothermal compressibility values, thus, at 313.15 K and 50 MPa, compressibility of the studied ILs, except $[P_{6,6,6,14}][(C_2F_5)_3PF_3]$, is lower than those of the mineral, base and biodegradable lubricants for hydraulic applications. A literature search concerning κ_T values of ILs was performed finding that this property increases with the alkyl chain length of the cation and for ILs with the same cation, it decreases according to the following sequence $[(C_2F_5)_3PF_3]^- > [NTf_2]^- > [C(CN)_3]^- > [C_2SO_4]^- > [C_1SO_4]^- > [PF_6]^- \approx [BF_4]^-$.
- Isobaric thermal expansivity, α_p, was obtained for the studied reference, based and developed oils, as well as for the ILs, by differentiation from the correlated experimental density data. The studied ILs present lower thermal expansion coefficient than synthetic, mineral and vegetable oils, and a non monotonous behaviour of this property with temperature was found for the ILs.

- Solubility of CO_2 in a reference semi-synthetic oil (SYN-2T) and in a developed biodegradable oil (BIO-2T-03) was determined in the temperature range from 283 K to 348 K and pressures up to 9 MPa through an isochoric technique. These results were modelled by means of the PC-SAFT EoS with a smooth linear dependence of k_{ij} with temperature, yielding average deviations, expressed in CO_2 mass fraction of 0.006 and 0.015 for CO_2+SYN-2T and CO_2+BIO-2T-03, respectively.
- Solubility of CO_2 in three vegetable base oils, HOSO-B1, castor oil and rapeseed oil was determined in the temperature range from range 298 to 363 and up to 75 MPa through a visual synthetic technique in the PATh laboratory from the University of Aveiro. It was found that HOSO-B1 and rapeseed oil present similar CO_2 solubilities in all the studied composition range. For CO_2 mass fractions higher than 0.2 solubilities start to increase slower, especially for castor oil, due to the hydroxyl groups of the ricinoleic chains. Moreover, crossovers between the isotherms of the diagrams p-w_{CO2} were found for all the systems. Results were described through the SRK EoS with two binary interaction parameters for each temperature and system, with mole fraction global average deviations lower than 6%.
- A new visual synthetic technique for determination of high pressure phase equilibria was implemented in the Thermophysical Properties Laboratory. Solubility of the system CO_2+HOSO-B1 was determined finding and AAD% of 2.2% in CO_2 mole fraction with the results previously determined in the University of Aveiro. Moreover, solubility of CO_2 in the biodegradable developed oil BIO-2T-05 was determined with this technique in the temperature range from 298 K to 363 K up to 53 MPa. VLLE for this last system was observed at T=298 K and p=6.5 MPa for $w_{CO2}\geq$0.36. Crossovers among the isotherms of the p-w_{CO2} diagrams were found for both systems. These solubility results were correlated through a modification of the Gordillo et al. correlation, with an AAD% for CO_2 mole fraction lower than 1.5%.
- CO_2 solubility results in the reference oil for two stroke engines and in the oils based in HOSO were compared. It was found that the lowest CO_2 solubility is in the reference SYN-2T oil, due to its low polarity. Among the biodegradable oils, solubility in HOSO-B1 and in BIO-2T-03 are the highest, due to the polarity of the ester groups, whereas solubility in BIO-2T-05 is close to those in HOSO-B1 and in BIO-2T-03 but slightly lower due to the PAO2 contain of the base oil of BIO-2T-05, which reduces its polarity.
- Carvalho and Coutinho correlation was employed for prediction of solubility for all the studied systems. Good results were found for the vegetable based oils up to molalities of 5

mol·kg^{-1}, with AADs% ranging from 8% for the CO_2+ BIO-2T-03 system to 17 % for the CO_2 + castor oil system.

- A high pressure rheometer was implemented in the Thermophysical Properties Laboratory for operating in the temperature range from 298.15 K to 333.15 K and pressures up to 75 MPa. This technique was verified by measuring the rheological behaviour of a PAO40 and a polybutene. AADs% in viscosity values over the whole temperature and pressure range of 7% and 11% were obtained with data previously published by Bair for PAO40 and a polybutene, respectively.
- Rheological behaviour of the ILs $[C_2C_1Im][C_6SO_4]$ and $[P_{6,6,6,14}][(C_2F_5)_3PF_3]$ was determined in the temperature range from 298.15 K to 353.15 K up to 75 MPa and shear rates up to 1000s^{-1}. A Newtonian behaviour was found for both ILs. Values of the local pressure-viscosity coefficient, $\alpha(p)$, are higher for $[P_{6,6,6,14}][(C_2F_5)_3PF_3]$, whereas values of the temperature-viscosity coefficient, β, are similar for both ILs (AAD% = 3.9%). Moreover, the values of the universal pressure-viscosity coefficient of $[P_{6,6,6,14}][(C_2F_5)_3PF_3]$ are near double than those of $[C_2C_1Im][C_6SO_4]$.

Appendix

Appendix A

Ionic liquids treatment

As ILs are highly hygroscopic, prior to measurements, they are dried and degassed under vacuum for at least 48 h, under agitation and using a vacuum system with a rotary pump Edwards RV3 (Fig. A.1) in order to eliminate water and volatile compounds. Vacuum is measured with a vacuometer Edwards Pirani 501 obtaining values around 8 Pa.

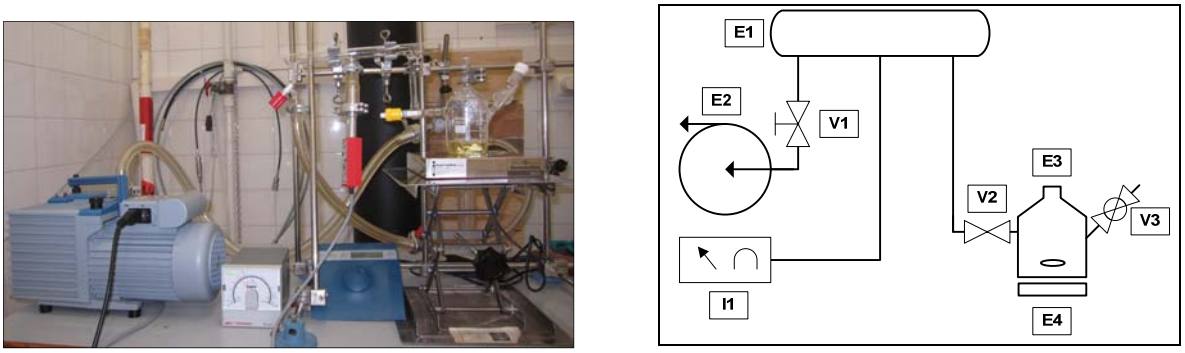

Fig.A.1. Picture and scheme of the vacuum line. (E1) Glass line, (E2) vacuum pump, (E3) sample flask, (E4) magnetic stirrer, (V1, V2, V3) valves, (I1) vacuometer.

A sample of the IL is analysed with a Karl–Fischer coulometric titrator (Mettler Toledo DL32) in order to measure the water content in the samples before and after density measurements. This titrator can determine water content in the range from 1 ppm to 5% and it is based on the standard reaction equation for the Karl Fischer reaction:

$ROH + SO_2 + RN \rightarrow (RNH)\cdot SO_3R$

$(RNH)\cdot SO_3R + RB + \mathbf{I_2 + H_2O} \rightarrow (RNH)\cdot SO_4R + 2\,(RNH)I$

In coulometry, however, the iodine is generated electrochemically by anodic oxidation:

$2\,I^- \rightarrow I_2 + 2\,e^-$

The anode compartment contains the anolyte that consists of sulphur dioxide, imidazole and iodine. Methanol or ethanol is used as solvent. At the anode, iodine is generated from iodine anions. The iodine reacts with water, whereas at the cathode, the positive hydrogen ions are reduced to hydrogen that is the main product formed. An ammonium salt is added to the catholyte in order to promote hydrogen production.

$2\,RN[H]^+ + 2\,e^- \rightarrow H_2 + 2\,RN$

In the global reaction, two iodine ions are converted to iodine, therefore, 2×96485 C are needed for 1 mole of water, thus, the amount of water that has reacted with the iodine can be calculated by measuring the current and the time.

Finally, in order to avoid contact between the ILs and the atmosphere, they are transferred to the evacuated densimeter through a Hamilton valve, HV Standard PTFE, connected to a glass syringe.

Appendix B

Experimental density data obtained in densimeter verification

Table B.1. Density data of n-hexane in g·cm^{-3}, measured with the densimeter DMA 60/512P.

	T/K				
p / MPa	278.15	293.15	313.15	333.15	353.15
0.10	0.6738	0.6597	0.6409	0.6216	0.6013
1.00	0.6746	0.6606	0.6420	0.6230	0.6029
5.00	0.6782	0.6647	0.6468	0.6288	0.6099
10.00	0.6824	0.6694	0.6523	0.6353	0.6176
15.00	0.6864	0.6738	0.6574	0.6412	0.6245
20.00	0.6901	0.6780	0.6621	0.6467	0.6307
30.00	0.6971	0.6856	0.6707	0.6564	0.6418
40.00	0.7035	0.6926	0.6784	0.6650	0.6514
50.00	0.7094	0.6990	0.6854	0.6728	0.6599

Table B.2. Density data of toluene in g·cm^{-3}, measured with the densimeter DMA 60/512P.

	T/K				
p / MPa	278.15	293.15	313.15	333.15	353.15
0.10	0.8813	0.8668	0.8477	0.8285	0.8091
1.00	0.8820	0.8675	0.8485	0.8295	0.8102
5.00	0.8847	0.8705	0.8519	0.8334	0.8146
10.00	0.8879	0.8741	0.8559	0.8380	0.8198
15.00	0.8911	0.8775	0.8598	0.8424	0.8247
20.00	0.8942	0.8809	0.8635	0.8465	0.8294
30.00	0.9000	0.8872	0.8705	0.8543	0.8380
40.00	0.9055	0.8931	0.8770	0.8614	0.8459
50.00	0.9107	0.8987	0.8831	0.8682	0.8532
60.00	0.9157	0.9040	0.8889	0.8744	0.8600

Table B.3. Density data of n-decane in g·cm^{-3}, measured with the densimeter DMA HPM.

	T / K						
p / MPa	278.15	298.15	313.15	333.15	348.15	373.15	398.15
0.10	0.7410	0.7263	0.7149	0.6994	0.6876	0.6680	0.6475
1.00	0.7416	0.7270	0.7156	0.7003	0.6886	0.6687	0.6482
10.00	0.7475	0.7338	0.7230	0.7085	0.6977	0.6794	0.6609
20.00	0.7535	0.7407	0.7305	0.7167	0.7067	0.6897	0.6726
40.00	0.7643	0.7527	0.7434	0.7308	0.7218	0.7066	0.6914
60.00	0.7738	0.7632	0.7545	0.7428	0.7345	0.7206	0.7067
80.00	0.7822	0.7726	0.7643	0.7533	0.7455	0.7325	0.7196
100.00	0.7898	0.7811	0.7732	0.7627	0.7554	0.7430	0.7309
120.00	0.8001	0.7903	0.7825	0.7728	0.7660	0.7544	0.7417

Table B.4. Density data of bromobenzene in g·cm^{-3}, measured with the densimeter DMA HPM.

	T / K						
p / MPa	278.15	298.15	313.15	333.15	348.15	373.15	398.15
0.10	1.5153	1.4880	1.4675	1.4404	1.4199	1.3855	1.3502
1.00	1.5162	1.4889	1.4685	1.4415	1.4211	1.3864	1.3509
10.00	1.5242	1.4977	1.4780	1.4520	1.4324	1.3994	1.3657
20.00	1.5327	1.5070	1.4880	1.4629	1.4442	1.4126	1.3806
40.00	1.5486	1.5242	1.5063	1.4828	1.4654	1.4362	1.4070
60.00	1.5634	1.5400	1.5230	1.5007	1.4842	1.4568	1.4295
80.00	1.5771	1.5546	1.5382	1.5170	1.5013	1.4754	1.4497
100.00	1.5899	1.5682	1.5524	1.5321	1.5171	1.4923	1.4679
120.00	1.6019	1.5811	1.5658	1.5462	1.5317	1.5079	1.4845

Appendix C

Resumen

Resumen

Las ventajas del uso de lubricantes se conocen desde hace milenios. Su principal función consiste en reducir la fricción y el desgaste que existe entre dos superficies en contacto, aunque llevan a cabo otras funciones secundarias tales como la refrigeración de las superficies, la eliminación de las partículas producidas por el desgaste o el aporte de resistencia frente a la corrosión, entre otras. Los principales lubricantes que se empleaban en la Edad Media eran grasas animales y aceites vegetales. Posteriormente, con el inicio de la industria del petróleo en 1859, los aceites minerales empezaron a usarse en lubricación ya que tenían diversas ventajas con respecto a los vegetales, como por ejemplo su estabilidad térmica. Dos décadas después, comenzó una exitosa búsqueda de alternativas sintéticas a los aceites minerales y, finalmente, entre 1910 y 1940 se popularizó el uso de aditivos químicos para mejorar las prestaciones de las diferentes bases lubricantes existentes.

Desde hace un par de décadas, la creciente preocupación por la conservación del medio ambiente y la búsqueda de procesos y productos más sostenibles, ha hecho que factores como la biodegradabilidad, la toxicidad y el impacto sobre el medio ambiente se tengan en cuenta en el diseño de nuevos productos, hecho que incluye a los lubricantes. Así, por ejemplo, la etiqueta europea Ecolabel que ayuda a identificar productos con reducido impacto ambiental a lo largo de todo el ciclo de vida, desde la extracción de las materias primas hasta el fin del ciclo de vida del producto seleccionado, establece una serie de criterios para ser otorgada a lubricantes para diferentes aplicaciones.

En este contexto se ha tratado de recuperar, en los últimos tiempos, el uso de bases vegetales buscando la aditivación más adecuada para obtener unas óptimas prestaciones en las diferentes aplicaciones y que puedan mejorar la estabilidad térmica y química así como la fluidez a bajas temperaturas (que son las principales desventajas de estos aceites). Las principales ventajas con respecto a los lubricantes minerales son mayor índice de viscosidad, mayores puntos de inflamación, baja volatilidad y excelente lubricidad. Además, también representan un ahorro de costes con respecto a las bases sintéticas.

Por otra parte, durante la última década se ha tratado también de buscar fluidos alternativos para su uso como lubricantes o aditivos de lubricantes, que puedan satisfacer las crecientes exigencias que conlleva el rápido desarrollo tecnológico. El desarrollo de nueva maquinaria, que alcance elevados niveles de producción bajo condiciones severas de operación, supone una enorme exigencia en la formulación de nuevos lubricantes. De esta forma los líquidos iónicos (LIs), que son sales con puntos de fusión por debajo de la temperatura ambiente, comenzaron a estudiarse hace una década para su uso como lubricantes debido a que poseen

propiedades muy adecuadas para esta función, tales como, una volatilidad despreciable, elevada estabilidad térmica, bajo punto de fusión, fluidez a baja temperatura, elevada polaridad y alta conductividad térmica y eléctrica. Otra característica que cabe destacar de los LIs es que, mediante la selección adecuada del catión y del anión, se pueden obtener líquidos con las propiedades más favorables para cada aplicación.

En esta Tesis Doctoral se estudian algunas propiedades termofísicas en amplios rangos de temperatura y presión de lubricantes de referencia minerales y semisintéticos, aceites vegetales y lubricantes biodegradables desarrollados, así como LIs, para su uso como fluidos hidráulicos, lubricantes de engranajes y lubricantes para motores de dos tiempos. Los lubricantes minerales de referencia, así como los aceites base y los desarrollados han sido proporcionados por los socios del proyecto BIOVESIN, un proyecto singular y estratégico que ha desarrollado lubricantes de base vegetal para distintas aplicaciones, mientras que los LIs han sido seleccionados y suministrados por Merck KGaA, Alemania.

Los sistemas hidráulicos se emplean en aplicaciones en las cuales es necesaria la conversión de energía mecánica en hidráulica y de nuevo en mecánica. Estos sistemas transmiten energía y permiten aplicar grandes fuerzas con alta flexibilidad y control, y constituyen una forma más precisa de transmitir energía que los sistemas eléctricos. Por su parte, los engranajes controlan el movimiento y transmiten potencia mecánica de un eje rotante a otro o de un eje rotante a un elemento reciprocante. Finalmente los motores de dos tiempos se suelen emplear cuando se requiere una alta potencia específica, un bajo peso y un bajo precio.

Una de las propiedades que se ha estudiado en esta Tesis Doctoral es la *densidad* en un rango de temperatura desde 278.15 K hasta 398.15 K y presiones de hasta 120 MPa. El conocimiento de esta propiedad en función de la presión y la temperatura es necesario para la determinación experimental de la viscosidad dinámica, entre otras. Además, los datos volumétricos son fundamentales para el desarrollo de ecuaciones de estado, que se usan para la predicción de propiedades termofísicas y también en diseño de procesos. La medida de la densidad se ha llevado a cabo en dos densímetros de tubo vibrante de la casa comercial Anton Paar (Graz, Austria), el primero de ellos es el densímetro DMA 512P, que fue calibrado en el rango de temperaturas desde 278.15 K hasta 353.15 K y presiones de hasta 60 MPa siguiendo el método propuesto por Lagourette et al., que emplea como fluidos de referencia agua y vacío. Con esta técnica se llevó a cabo la determinación experimental de densidades, en el citado rango de presión y temperatura, de *un aceite base girasol alto oleico y seis aceites biodegradables desarrollados* para su aplicación como fluidos hidráulicos. El segundo densímetro utilizado es el densímetro DMA HPM, que fue empleado en dos configuraciones distintas durante la realización de esta Tesis Doctoral. Inicialmente las medidas se realizaron en un modo manual y

posteriormente en un modo automatizado. En la configuración manual, la calibración y las medidas se realizaron en el rango de temperatura de 298.15 K a 373.15 K y hasta 60 MPa. Se caracterizaron mediante esta configuración las propiedades volumétricas de *tres aceites minerales y uno semisintético de referencia, un aceite base de girasol alto oleico y un aceite biodegradable comercial*. En cuanto a la configuración automatizada, la calibración del equipo y las medidas se realizaron en el rango de temperaturas entre 278.15 K y 398.15 K y hasta 120 MPa. Esta calibración se realizó siguiendo el procedimiento de Lagourette et al. modificado por Comuñas et al., que emplea como fluidos de referencia, agua, vacío y decano, y se midieron las densidades de *tres aceites minerales de referencia*, *cinco biodegradables desarrollados y siete LIs*.

El efecto "amortiguación" presente en los densímetros de oscilación mecánica debido a la viscosidad de las muestras se ha tenido en cuenta empleando un factor de corrección que depende del modelo de densímetro, siempre que los datos de viscosidad a alta presión de las muestras se encontrasen disponibles en la bibliografía.

Los datos de densidad de cada líquido fueron correlacionados en función de la presión y la temperatura por medio de la ecuación de Tammann-Tait, y para algunos de los lubricantes estudiados también mediante una ecuación de Tait modificada. A partir de dicha correlación se han calculado, mediante derivación, los valores de las propiedades derivadas de la densidad, la compresibilidad isotérmica, κ_T, y el coeficiente de expansión térmica isobárica, α_p. El conocimiento de la compresibilidad isotérmica de los lubricantes en lubricación elastohidrodinámica es necesario, ya que los picos de presión y el espesor de la película en el centro del contacto se ven influenciados por esta propiedad. Además, la compresibilidad isotérmica es un parámetro esencial en la elección de un fluido hidráulico, ya que determina la eficiencia de la trasferencia de potencia, una compresibilidad baja da lugar a tiempos de respuesta rápidos, alta velocidad de transmisión y pequeñas pérdidas de potencia. Por otra parte, el coeficiente de expansión térmica isobárica es útil en la determinación de la cuña térmica, que es una generación de presión provocada por cambios en la densidad y la viscosidad debido al incremento de temperatura en una película elastohidrodinámica.

Dentro de los fluidos estudiados los LIs son más densos que los aceites minerales, base y desarrollados mientras que la densidad del aceite de girasol alto oleico y de los lubricantes desarrollados es más alta que la de los aceites minerales y semisintéticos de referencia. En cuanto a la compresibilidad, el aceite de girasol alto oleico y los aceites biodegradables desarrollados como fluidos hidráulicos presentan valores más bajos que los aceites minerales de referencia para esta aplicación. En cuanto a los lubricantes de engranajes, la compresibilidad de los aceites de referencia es similar a la de los biodegradables desarrollados. La compresibilidad

de los LIs estudiados, excepto el $[P_{6,6,6,14}][(C_2F_5)_3PF_3]$, es menor que la de los lubricantes hidráulicos de referencia, base y desarrollados. Finalmente, en cuanto al coeficiente de expansión térmica isobárica, los LIs presentan un comportamiento no monótono con la temperatura, y también valores más bajos de esta propiedad que los aceites minerales, vegetales y sintéticos para aplicaciones hidráulicas.

Con los valores de densidad experimentales se ha analizado también la capacidad predictiva de la densidad a presión atmosférica del modelo '*Fragment-based approach'*, propuesto recientemente por Zong et al. para estimar propiedades termofísicas de grasas y aceites vegetales. La verificación se realizó para el aceite de girasol alto oleico y el aceite de colza. Además se ha determinado el valor de los parámetros del fragmento ricinoleico necesarios para la estimación de la densidad, ya que Zong et al. no los habían incluido en su trabajo. Además también se ha evaluado el método propuesto por Anand et al. para estimar la densidad de aceite de girasol alto oleico a partir de su composición en ácidos grasos. Por otra parte, los valores de densidad a alta presión de algunos de los lubricantes de engranajes estudiados, se han utilizado para evaluar la capacidad predictiva de las ecuaciones de estado de Dowson and Higginson, Zhu y Wen y Jacobson y Vinet. De esta forma se ha comprobado que las ecuaciones de Dowson y Higgison y Zhu and Wen predicen los valores experimentales de densidad de lubricantes de engranajes con un AAD% menor o igual que 0.4%. Por otra parte, cuando estas dos últimas ecuaciones se emplean para extrapolar los valores de compresibilidad isotérmica hasta 4 GPa, predicen valores de esta propiedad menores que los obtenidos mediante la ecuación de Tammann-Tait.

Respecto de los LIs, se ha comprobado la capacidad de predicción de su densidad en amplios rangos de presión y temperatura usando los métodos propuestos por Gardas y Coutinho y por Jacquemin et al. El método de Gardas y Coutinho predice los valores de densidad de los siete LIs estudiados con un AAD% menor o igual que 1.5%, mientras que el propuesto por Jacquemin et al. predice densidades de $[C_4C_1Pyrr][NTf_2]$ y $[C_2C_1Im][C_2SO_4]$ con un AAD% de 0.46% y 2.5%, respectivamente. Asimismo, se ha realizado un amplio estudio bibliográfico de la densidad de LIs con objeto de establecer secuencias para esta propiedad en función del catión y del anión constituyentes de los mismos. De esta forma se ha encontrado que la densidad de los LIs disminuye con el aumento de la cadena alquílica del catión. En cuanto al anión se ha encontrado que la densidad decrece de acuerdo con la siguiente secuencia: $[(C_2F_5SO_2)_2N]^- > [NTf_2]^- > [PF_6]^- > [CF_3SO_3]^- > [ClO_4]^- > [CF_3CO_2]^- > [C_1SO_4]^- > [BF_4]^- > [C_1(OC_2)_2SO_4]^- > [NO_3]^- > [C_8SO_4]^- > [N(CN)_2]^- > [CH_3CO_2]^- > [C_4C_4PO_4]^- > [C(CN)_3]^-$.

Otra propiedad objeto de estudio en esta Tesis Doctoral es el equilibrio de fases a altas presiones de CO_2 en lubricantes de referencia, aceites base y lubricantes biodegradables

desarrollados para motores de dos tiempos. La solubilidad de gases en lubricantes puede afectar a diferentes propiedades tales como viscosidad, espumabilidad, compresibilidad, cavitación, transferencia de calor, oxidación y corrosión, entre otras. Así, por ejemplo, el oxígeno disuelto puede causar oxidación en los lubricantes y corrosión de las superficies. En fluidos hidráulicos, el gas disuelto puede causar una disminución abrupta de la compresibilidad. En los motores de dos tiempos los gases se mezclan con el lubricante y la gasolina en la cámara de combustión, y el estudio de la solubilidad de gases en los lubricantes de referencia nos permite realizar una comparación con los lubricantes biodegradables desarrollados.

Las medidas de *solubilidad* a alta presión de esta Tesis Doctoral se han llevado a cabo mediante dos técnicas experimentales diferentes, de tipo sintético que evitan la toma de muestra de las fases en equilibrio, un método isocórico y otro visual. Respecto de la técnica isocórica, ésta es similar a la empleada por Wahlström y Vamling y se basa en el cálculo de la cantidad de gas absorbida en una cantidad determinada de disolvente mediante la determinación de la caída de presión que se produce durante el proceso de absorción en un sistema de volumen conocido. Esta técnica se puede aplicar siempre y cuando la presión de vapor del disolvente sea despreciable. Esta técnica se había instalado en el Laboratorio de Propiedades Termofísicas con anterioridad al inicio de esta Tesis Doctoral y se ha llevado a cabo la determinación experimental de *solubilidades de CO_2 y O_2 en un lubricante semisintético de referencia y uno biodegradable* desarrollado en el rango de temperatura de 283 K a 348 K y presiones de hasta 10 MPa.

Respecto del método visual, es importante mencionar que la nueva técnica de *equilibrio de fases* fue *implementada* en el Laboratorio de Propiedades Termofísicas en el desarrollo de esta Tesis Doctoral para trabajar en el rango de temperaturas de 298.15 K a 363.15 K y presiones de hasta 100 MPa. Esta técnica está constituida por una célula de alta presión de volumen variable (de 8 a 30 cm^3) que consta de dos ventanas de zafiro que permiten observar el interior de la misma, una de ellas se utiliza para iluminar la celda mientras que a través de la otra se observa el cambio de fases que se produce en los sistemas objeto de estudio con ayuda de una cámara de video. A la célula de volumen variable se le ha añadido una línea de presión conectada a una botella de gas, que permite el llenado de la misma. Por otra parte se ha instalado también una unidad de adquisición de datos que permite recoger en un ordenador los datos de presión y temperatura a la vez que se observa en la pantalla el interior de la célula. Asimismo, se ha realizado una estancia en la Universidad de Aveiro, Portugal, en el grupo de investigación Process and Product Applied Thermodynamics, para llevar a cabo la determinación experimental de la solubilidad con una técnica análoga. En estos dos últimos equipos se han realizado ensayos de *tres sistemas CO_2 + aceite base vegetal (girasol alto oleico, colza y ricino)* así como *un sistema formado por CO_2 y un aceite biodegradable desarrollado* para su uso en motores de dos

tiempos. Es importante mencionar que la verificación del equipo instalado en el Laboratorio de Propiedades Termofísicas se realizó comparando los resultados de solubilidad de CO_2 en un aceite de girasol alto oleico con los obtenidos en el laboratorio de la Universidad de Aveiro Process and Product Applied Thermodynamics. La solubilidad de CO_2 en el aceite semisintético de referencia para motores de dos tiempos es menor que en los aceites base de girasol alto oleico y biodegradables desarrollados, debido a la baja polaridad del aceite de referencia.

Las solubilidades a alta presión obtenidas en esta Tesis Doctoral han sido modeladas con éxito mediante el uso de las ecuaciones de estado PC-SAFT (*Perturbed-Chain Statistical Associating Fluid Theory*) y SRK (Soave-Redlich-Kwong). Para la aplicación de estos modelos se ha empleado el software Phase equilibria (PE 2000) y el cálculo de las propiedades críticas de los aceites se ha llevado a cabo aplicando el método de Constantinou y Gani. Así, la solubilidad de CO_2 en el aceite semisintético de referencia para motores de dos tiempos (SYN-2T) y en el aceite biodegradable desarrollado (BIO-2T-03) se modeló con PC-SAFT con unas desviaciones absolutas expresadas en fracción másica de CO_2 menores o iguales que 0.015. En cuanto al modelado mediante SRK-EoS, se obtuvieron desviaciones absolutas menores del 6% para los tres sistemas constituidos por CO_2 y aceite de girasol alto oleico, colza y ricino.

Además se ha analizado la capacidad de predicción del modelo propuesto por Carvalho y Coutinho para la solubilidad de CO_2 en disolventes poco volátiles y se ha propuesto una modificación de la ecuación de Gordillo et al. para correlacionar los resultados experimentales de solubilidad de CO_2 en un aceite base y uno desarrollado. La ecuación de Carvalho y Coutinho predice la solubilidad de CO_2 en los aceites base vegetales y desarrollados para motores de dos tiempos hasta molalidades de 5 $kg \cdot mol^{-1}$ con AADs% menores o iguales que 17%.

Durante esta Tesis Doctoral se ha determinado la *viscosidad* a presión atmosférica y el *índice de viscosidad* (VI) de los lubricantes *de referencia, base y biodegradables desarrollados* y la viscosidad de dos *LIs* hasta 75 MPa. La viscosidad es una propiedad importante de los lubricantes ya que influye en la formación de la película lubricante, en la fricción y el desgaste, en la generación de calor, en el sellado, en el arranque en frío y en el eficiencia energética, entre otros. Además, los lubricantes se clasifican mediante un estándar en función de su viscosidad cinemática en grados de viscosidad ISO. En cuanto al índice de viscosidad, es una propiedad que cuantifica la tasa de variación de la viscosidad con la temperatura, y cuanto mayor sea el VI, menor es el efecto de la temperatura en la viscosidad. Por otra parte, la caracterización reológica de los aceites lubricantes en función de la presión, temperatura y velocidad de cizalla es básica para determinar su capacidad de formar una película lubricante en las diferentes condiciones o regímenes de utilización.

La técnica empleada para la caracterización de la viscosidad a presión atmosférica es un viscosímetro rotacional de tipo Couette Anton Paar Stabinger SVM 3000. El principio de medida se basa en la rotación a velocidad constante de un tubo lleno con la muestra cuya viscosidad se quiere medir en el que flota un rotor de medida. Este equipo posee además un densímetro de tubo vibrante que consiste en un tubo de vidrio en forma de U y permite realizar medidas de densidad a presión atmosférica. Por último el equipo también calcula el valor del índice de viscosidad de acuerdo con el estándar ASTM D2270-04. Los índices de viscosidad más bajos se obtuvieron para los aceites minerales y semisintéticos de referencia así como para el aceite de ricino y los más altos para los demás aceites base y los aceites biodegradables desarrollados. Por otra parte se usaron los valores experimentales de dos aceites base girasol alto oleico y colza para evaluar la capacidad predictiva del 'Fragment-based approach' propuesto por Zong et al. Además, se han propuesto parámetros para el fragmento ricinoleico para la determinación de viscosidad mediante este método.

Finalmente, durante esta Tesis Doctoral se llevó a cabo la *implementación* de un *reómetro de alta presión*, modelo StressTech HTHP de Reologica, para operar hasta 75 MPa. Se trata de un reómetro Couette de geometría cilíndrica (CC25) especificada en la norma DIN53019. La muestra está confinada en el hueco existente entre el cilindro rotante interior y el cilindro estacionario exterior, que posee 1 mm de espesor. El control del funcionamiento del reómetro se realiza por medio del software RheoExplorer instalado en un ordenador conectado al mismo. Además, se ha añadido una línea de presión que consta de un transductor y un pistón para generar presión. El reómetro se ha instalado para operar en el rango de temperaturas desde 298.15 K hasta 353.15K y presiones de hasta 75 MPa. La calibración del reómetro se realiza para cada sistema a medir mediante la comparación de los resultados obtenidos a presión atmosférica con los obtenidos en el Stabinger SVM 3000.

La verificación de este equipo se ha hecho mediante la comparación de los resultados de viscosidad obtenidos con esta técnica para dos lubricantes, una polialfaolefina (PAO40) y un polibuteno (H8), con los obtenidos previamente por Bair. Asimismo, los resultados obtenidos fueron correlacionados mediante la ecuación de Comuñas et al.

Además, durante esta Tesis Doctoral se realizó la caracterización reológica de dos LIs, *$[C_2C_1Im][C_6SO_4]$ y $[P_{6,6,6,14}][(C_2F_5)_3PF_3]$*, con un grado de viscosidad ISO mayor que 100. Los ensayos de flujo se llevaron a cabo en el rango de temperaturas de 298.15 K hasta 353.15K, presiones de hasta 75 MPa y velocidades de cizalla de hasta 1000 s^{-1}. Se encontró un comportamiento Newtoniano para ambos fluidos, y los valores de viscosidad fueron correlacionados en función de la presión y la temperatura mediante la ecuación de Comuñas et al. Además, se calcularon, para estos dos LIs, las propiedades derivadas de la viscosidad, el

coeficiente de viscosidad–temperatura, β, y el coeficiente local de viscosidad-presión, α. Por otra parte, también se calculó el valor del coeficiente universal de viscosidad-presión, α_{film}, que es independiente de la presión y ha sido empleado para cuantificar el efecto de estos dos LIs en el espesor central de película, h_c, en condiciones isotermas bajo lubricación elastohidrodinámica.